TM-100369

RESEARCH AND TECHNOLOGY 1989

ANNUAL REPORT OF THE MARSHALL SPACE FLIGHT CENTER

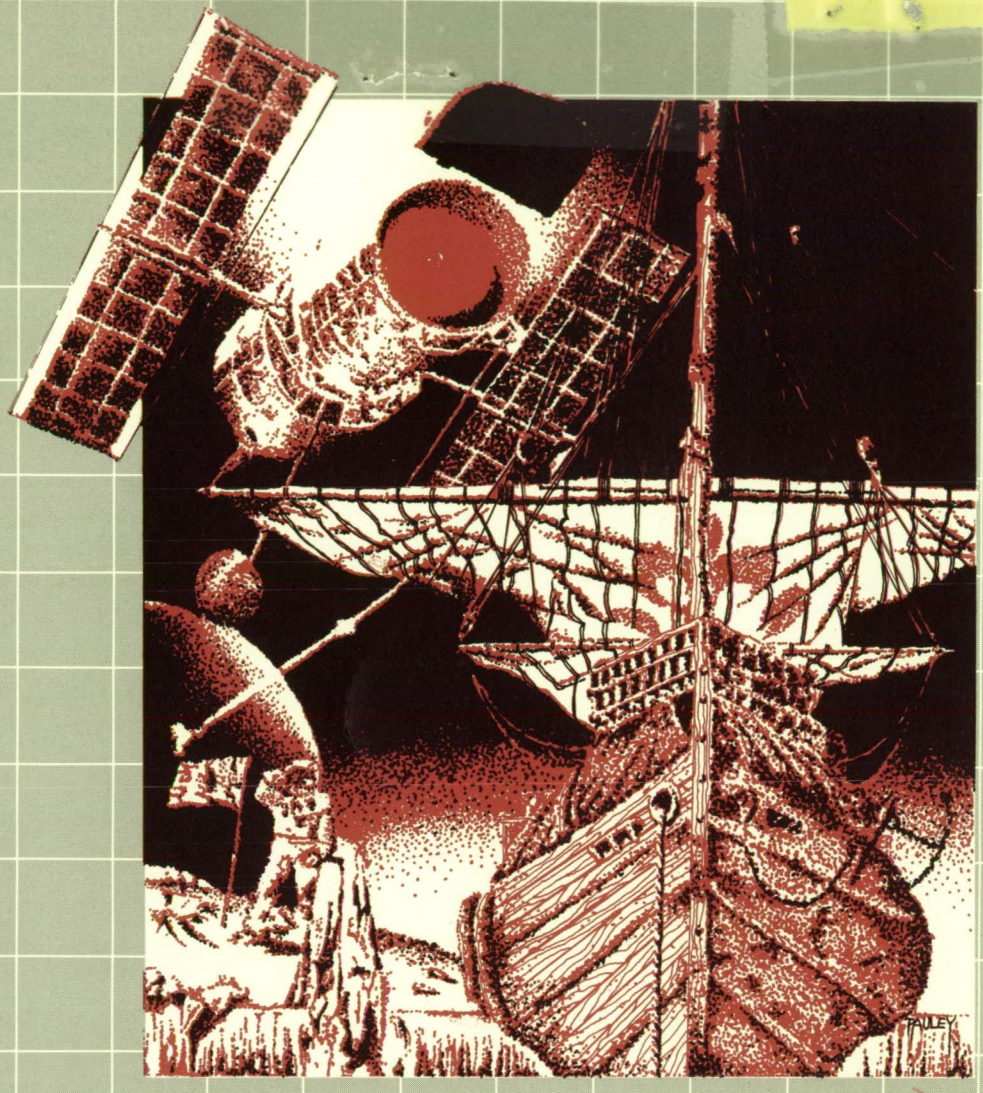

TRADITION OF DISCOVERY

Research and Technology 1989

Annual Report of the Marshall Space Flight Center

NASA TM – 100369

NASA
National Aeronautics and
Space Administration

George C. Marshall Space Flight Center
Marshall Space Flight Center, Alabama 35812

Tradition of Discovery

Once the world was believed to be flat. Each horizon ended in a treacherous ocean, ending in huge water falls dropping into a dark abyss. Over time, our knowledge of the world and the universe has evolved. The sky is no longer the limit, and new discoveries await us. Research and technology, the key to our future, continues to unlock the doors of knowledge, and provide new insights into the universe that today we can only dream of.

Join us for a report on tomorrow, by those who are leading us there.

Director

Acknowledgements

The point of contact and coordinator at MSFC for this report is P.Y. Potter [ER01/(205) 544-5723]. She was assisted by an editorial committee consisting of E.A. Tandberg-Hanssen, G.R. Wallace, G.F. McDonough, C.R. Chappell, W.C. Snoddy, and T.W. Moorehead. Detailed editorial support and production assistance was provided by MSI, a division of the Bionetics Corporation. The work at MSFC is a cooperative effort, but because of space restrictions, it is impossible to list all those involved in the projects described in this report.

To assist the reader, the MSFC contact, office code, telephone number, and sponsoring agency are included at the end of each article. An alphabetical index of all contacts is presented at the end of this report.

Table of Contents

Advanced Studies

Research Programs

Earth Science and Applications

Technology

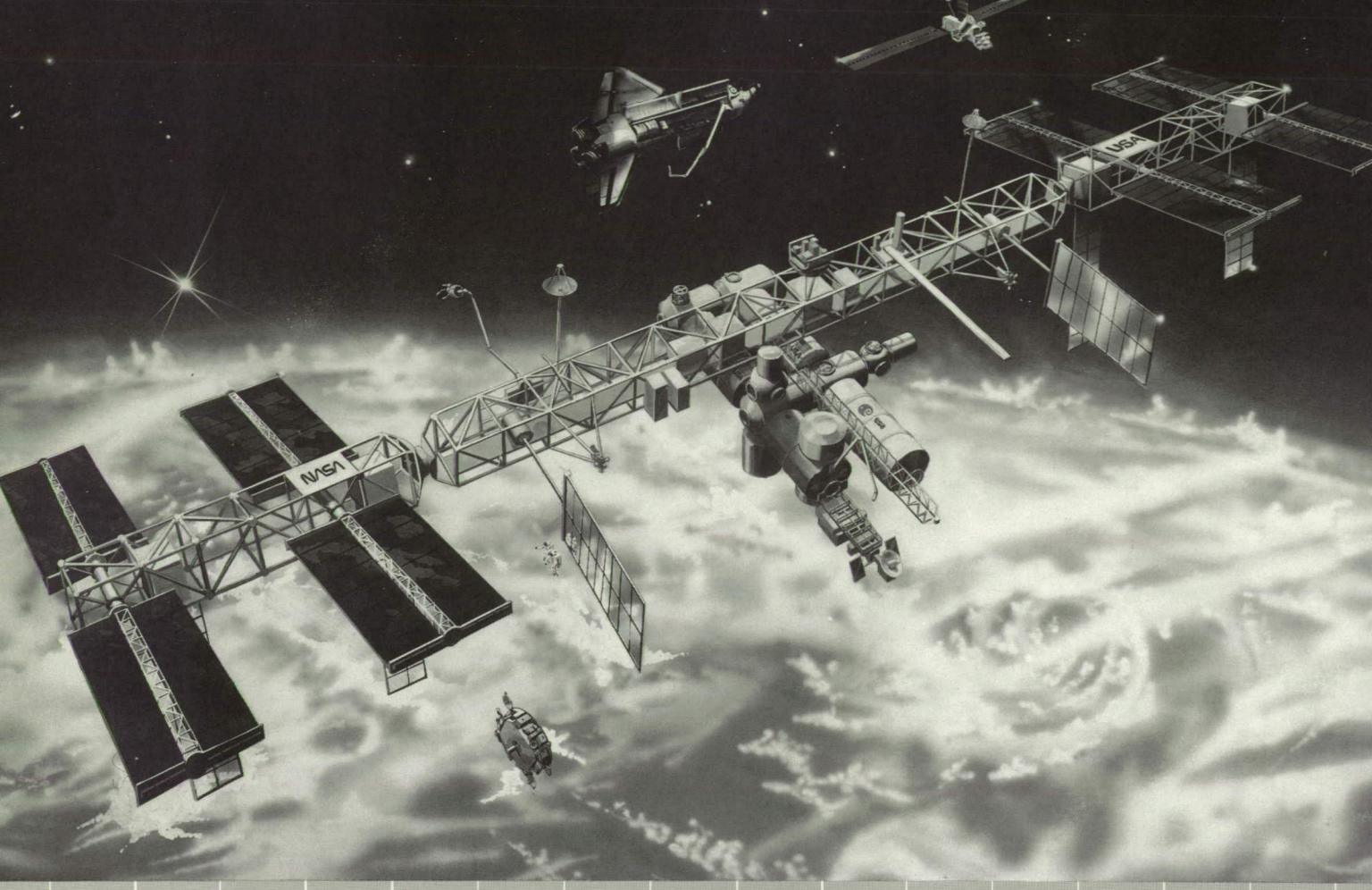

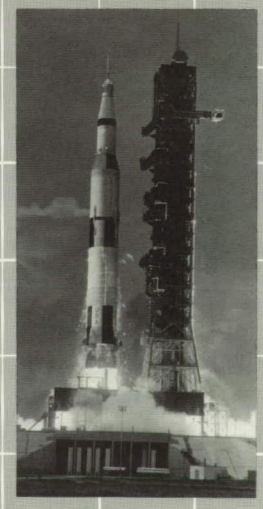

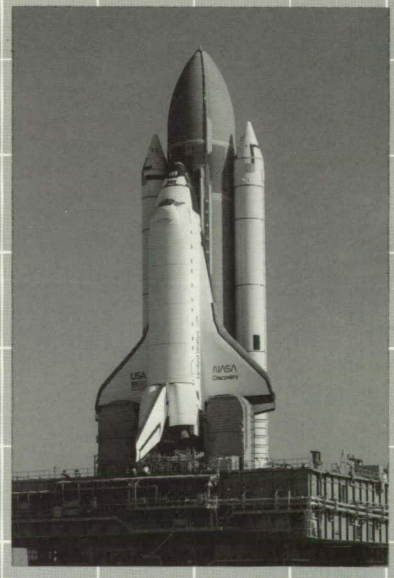

Advanced Studies

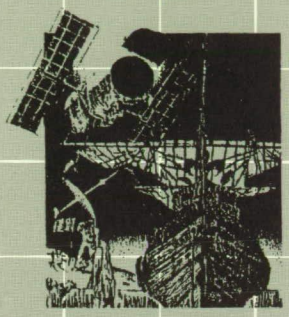

The past quarter century of space exploration has witnessed a revolution in the discovery and understanding of the Earth, our solar system, and the universe. Advanced studies provide both a foundation and a passageway to the future as we further push back the frontiers and carry on this revolution into the next century.

The future depends in a fundamental way upon those systems that give us access to space. MSFC continues to support these vital areas with studies that include the evolutionary development of near-term space transportation systems, and transportation elements that will provide the means for human expansion beyond Earth orbit into the solar system.

The future will include intensive and comprehensive investigations of our home planet. To support this critical need, we are conducting advanced studies of missions and geostationary and instrument platforms that will provide the means to obtain a wide range of Earth science data.

The first of the four Great Observatories, the Hubble Space Telescope, is nearing launch. Even more powerful facilities now being planned will be assembled on-orbit during the 21st century to succeed the Great Observatories. While the development of Space Station *Freedom* proceeds, we are planning beyond the baseline facility, including its role as a base for the expansion of human presence to the Moon and on to Mars.

Transportation Systems

Shuttle-Cargo Vehicle

The unmanned shuttle cargo vehicle (Shuttle-C) proposed for first launch in 1994 will deliver a variety of payloads including payloads that are too heavy [up to 77,100 kg (170,000 lb)] and too large to be launched with current capabilities, or that are not compatible with manned launch vehicle constraints, thereby complementing the National Space Transportation System (NSTS). Missions that require multiple launches and on-orbit assembly can also benefit from a heavy lift launch vehicle which could minimize on-orbit assembly requirements.

The core of the Shuttle-C design philosophy is product improvement, a technique used by several space launchers (notably the U.S. Delta, Titan, and Saturn missile families). These demonstrate that a "new" launch capability can be provided over a period of years by constant upgrades to existing systems rather than development of a new system with its attendant research, development, and facility costs. Shuttle-C is a logical outgrowth of the designs and infrastructure available in the "baseline" space shuttle which is now flying (Fig. 1). It will

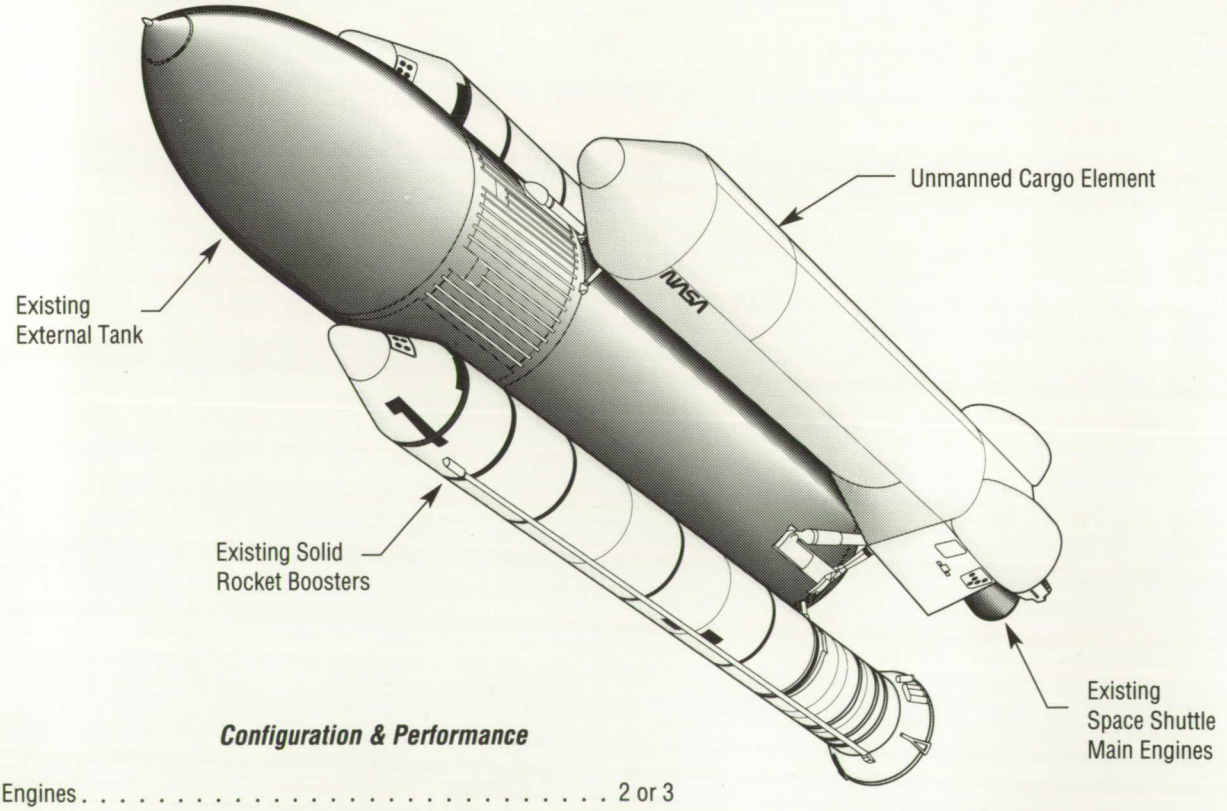

Configuration & Performance

Number of Engines	2 or 3
Engine Thrust Level	100%
Payload Lift Capability (To 220 nmi)	77,100 kg (170,000 lb)
Payload Bay Size	25 m by 5 m (82 ft by 15 ft)

Figure 1. Shuttle-C Arrangement

allow the existing NSTS to grow with and support space programs well into the 21st century.

The competitive price of Shuttle-C compared with other currently available launch vehicles will help meet foreign competition, while providing synergistic cost benefits for the NSTS, and increasing the availability of equipment spares. With an appropriate upper stage such as Centaur, Shuttle-C can place a 9,100-kg (20,062-lb) payload in geosynchronous orbit. More ambitious planetary missions such as those with shorter trip times, larger payloads, etc., will be possible with the greater lift capability (Fig. 2). Shuttle-C will also provide increased design flexibility, margin, and growth potential for payloads planned for smaller and more constraining vehicles, as well as providing flexibility for assembly of Space Station *Freedom*, and functioning as a flying test bed for new or modified hardware.

The Shuttle-C reference configuration has been defined as an STS-type vehicle consisting of two standard four-segment solid rocket boosters, a standard expendable external tank, a minimally-modified orbiter boattail, standard Space Shuttle Main Engines, and a new payload carrier. This configuration has been selected because of early availability; a reduced design, development, testing, and evaluation cycle; synergism with STS; efficient utilization of STS infrastructure; and low development risk. Phase II of the Shuttle-C Systems Definition studies, currently underway, is directed at refinement of the Shuttle-C reference configuration and trade studies to further the design definition of the vehicle.

J. Walker/PF24
(205) 544-3963
Sponsor: Office of Space Flight

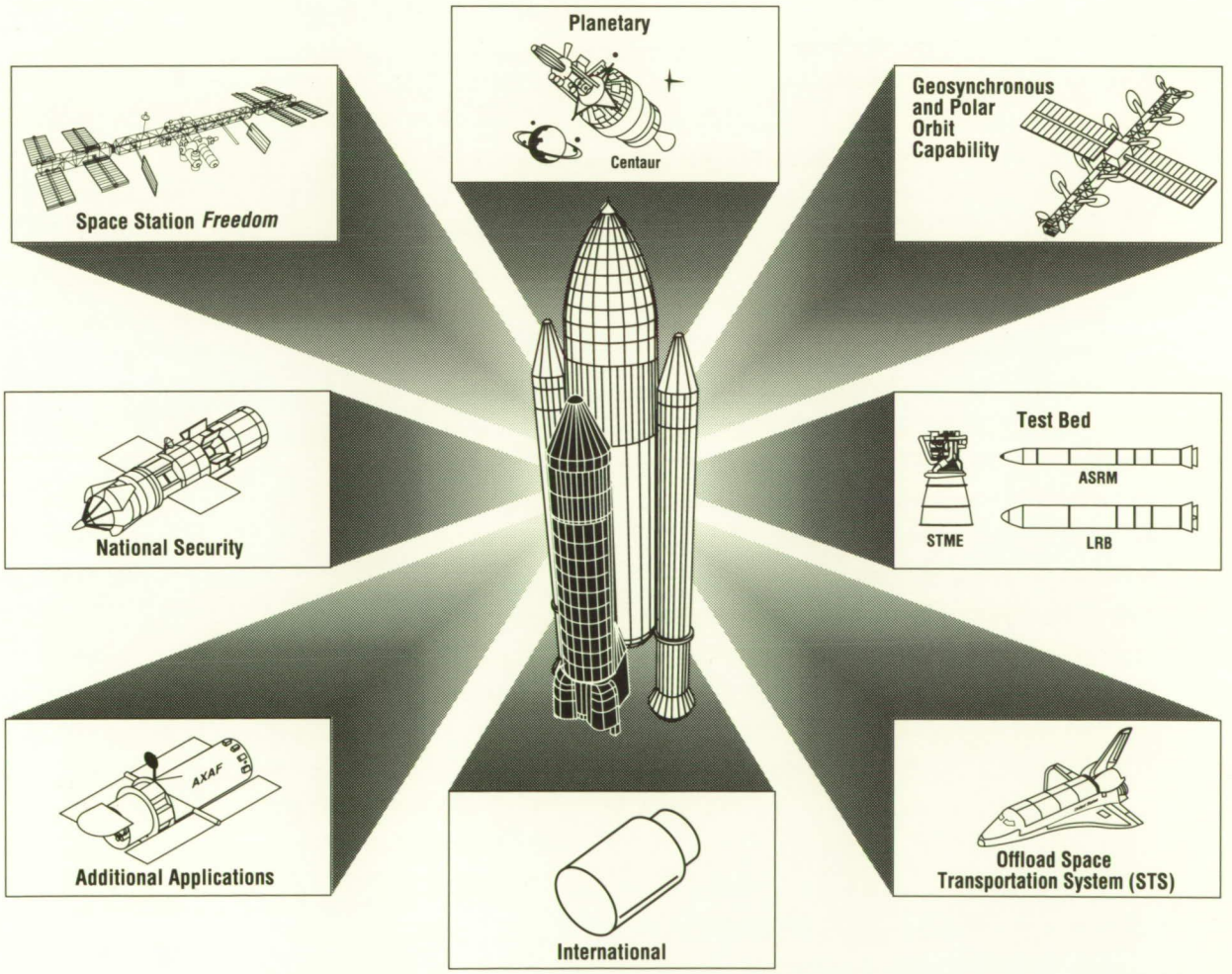

Figure 2. Shuttle-C Applications

Advanced Launch System

The Advanced Launch System (ALS) is a joint venture of the U.S. Air Force and NASA. It will consist of a family of unmanned cargo vehicles planned to meet the Nation's payload needs into the 21st century. The family is conceived to provide optimal launch capability at minimal cost over a range of payload weights from 500 kg (1,100 lb) to 100,000 kg (220,000 lb) to low Earth orbit. The design objectives of each member of the family of vehicles are low cost, high reliability, and operability. To meet the cost and robustness goals, tradeoffs will be made in the areas of weight and performance. The primary goal of the program is to reduce today's cost per pound of payload delivered to low Earth orbit by an order of magnitude. Overall responsibility for the program is vested in a Joint Program Office attached to the Air Force Space Division and supported by the Aerospace Corporation in Los Angeles, CA.

Authorization to proceed with Phase I was given in the first quarter of 1987. Phase I, concept and definition, included a strategic design review in mid-1988 and ended in October 1988.

The Phase II contracts were signed December 27, 1988, with the three prime contractors: Boeing, General Dynamics Space Systems, and a team comprised of Martin Marietta Aerospace Group and McDonnell Douglas Corporation. The three prime contractors are cooperating and sharing information in an advanced development program in order to focus the technology needed to meet the ALS goals of reliability, producibility, operability, and cost reduction. Simultaneously, each of the three prime contractors will develop a vehicle systems design concept in a highly competitive atmosphere. One contractor will be selected to continue the program after Phase II. Advanced development program tasks have also been assigned by the Joint Program Office to NASA and Air Force laboratories to capitalize on a knowledge base accumulated from many years of experience.

Phase II is planned to be a 25-month effort, with an option for extension of up to 2 years. Existing and proposed funding through FY92 provides $319 million for the prime contractors, $572 million for the NASA and Air Force laboratories, and $82 million for Aerospace Corporation and other support. The cost of the optional 2-year extension is estimated at $110 million for the prime contractors, $388 million for the Government laboratories, and $48 million for support activities.

Major milestones ahead are Defense Acquisition Board (DAB) Milestone I in mid-1990, DAB Milestone II in mid-1992, Phase III development starting in 1992, first launch in 1998, and DAB Milestone III, production start, in late 1998.

The mission model for ALS includes the mission needs of all authorized users (the Strategic Defense Initiative Organization, NASA, DOD, and universities). The two basic scenarios are the normal mission model and the expanded mission model. The normal mission model is based on DOD and civil payloads similar to those being launched by today's launch vehicles. The expanded model includes a deployment of either a Strategic Defense Initiative system or a Mars or lunar program being considered for the Civilian Space Leadership Initiative. Each of the scenarios involves a different mission which drives the design of the ALS. For Scenario I, the ALS will be sized to deliver a cargo mass of between 36,400 kg (80,000 lb) and 54,500 kg (120,000 lb) to the reference orbit of 28.5 degrees inclination. The lift capability to a corresponding polar orbit (90 degree inclination) is at least 29,500 kg (65,000 lb). For Scenario II, the ALS will deliver between 54,500 and 100,000 kg (120,000 and 220,000 lb) to a 28.5 degree inclination. Polar mission capability will be

72,200 kg (160,000 lb). For Scenario I, the ALS will be designed for a sustained launch rate of 20 flights per year. For Scenario II, the ALS will be capable of delivering 2,300,000 kg (5 million lb) per year. Some other requirements are:

- *Initial launch capability in 1998*
- *Initial operational capability in 2000*
- *Design reliability greater than 98 percent*
- *Launch call-up capability of 30 days or less*
- *Payload substitution within 5 days of launch*
- *Launch-on-schedule probability of 95 percent*
- *Surge capability of seven missions in 5 days*
- *Life-cycle cost competitive across payloads of 453,500 – 2,300,000 kg (1–5 million lb) per year*
- *Clean pad (no tower) and simple payload interfaces*

An advanced development program (ADP) is being implemented by the prime contractors and Government laboratories to address propulsion, avionics/software, structures/materials, aero/thermo, and ground and flight operations/manufacturing.

L.O. Wear/PF23
(205) 544-3215
Sponsor: U.S. Air Force

Space Transportation Main Engine

The Space Transportation Main Engine (STME) will provide Earth-to-orbit main propulsion for the next generation of U.S. launch vehicles (Fig. 3). STME Phase A concept study began in 1986 to support joint NASA/U.S. Air Force space transportation architecture studies. Current STME Phase A studies are providing engine designs and program plans to support the joint NASA/Air Force Advanced Launch System (ALS) Phase II studies. The STME has followed a revolutionary approach to rocket engine concept definition leading to high reliability, low cost, producible designs.

Results show that the STME is a key to the ALS family of vehicles building block approach which allows a broad range of economical payload capability. The STME building block will provide reliable, economical, core propulsion across the family. With the STME and other building block elements, various combinations of the ALS will be able to launch payload masses from 22,000 to 200,000 kg (48,000 to 440,000 lb) per mission. The versatile STME can also provide economical boost propulsion for heavy lift two-stage parallel burn ALS config-urations with a 30,000 – 200,000 kg (66,000–440,000 lb) payload capacity, and can be utilized in a variety of additional applications including shuttle liquid rocket boosters and Shuttle-C.

STME parametric cost and performance data have been developed for use in ALS design trades. Based on trade results, a baseline gas generator cycle engine configuration, which can be applied to either expendable or reusable vehicle configurations, was selected to allow thorough investigation of design features and program plans. The baseline engine concept fits well within the reliability, cost, and performance guidelines required by ALS vehicle concepts. Upon determination of detailed vehicle requirements, STME designs can be adjusted to provide an optimum system configuration.

The STME will set new standards for high reliability, low cost, and robust features in a high-performance liquid rocket engine system utilizing

Categories	Space Transportation Main Engine (STME)	Space Transportation Booster Engine (STBE)
Propellants:	LOX/Hydrogen	LOX/Methane
Cycle:	Gas Generator	Gas Generator Derived From STME Hardware
Demonstrated Reliability:	99% @ 90% Confidence	99% @ 90% Confidence
Thrust:	2,580 kN (580K lb_F) (VAC)	2,669 kN (approx. 600K lb_F) (Sea Level)
Application:	Expendable or Reusable (15 Mission Life) Core or Booster	Expendable or Reusable (15 Mission Life) Booster
Chamber Pressure:	2,250 psia	Approx. 2,250 psia
Control:	Dual Positiion Thrust Open Loop	Dual Position Thrust Open Loop

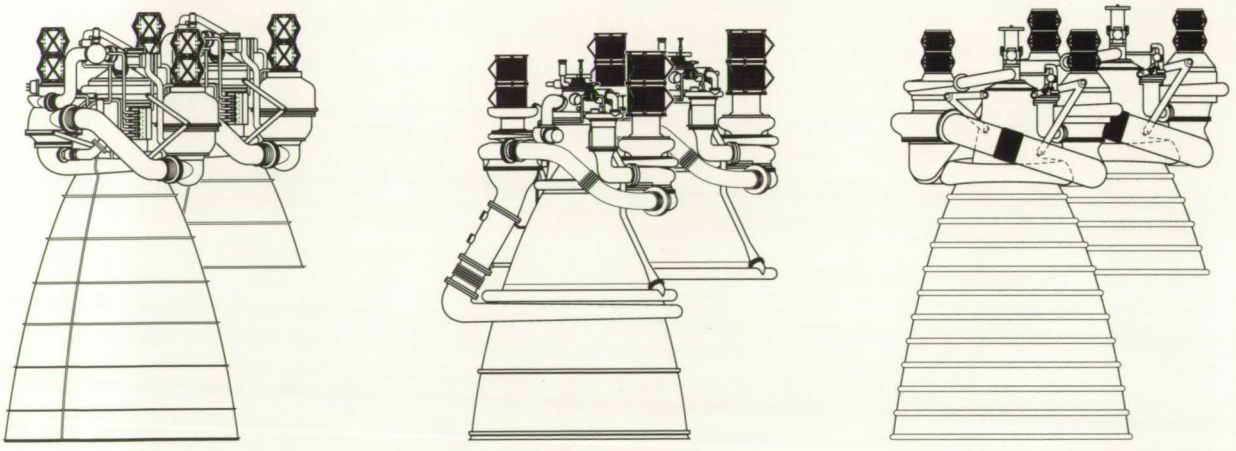

Figure 3. Space Transportation Engine Program

liquid hydrogen fuel and liquid oxygen. The revolutionary design approach embraces the best technology and management techniques to design for high quality and producibility at the expense of conservative thrust/weight and I_{sp}. Engine features include dual-thrust capability to provide engine-out failure coverage throughout the mission. Total quality management techniques such as simultaneous engineering, quality function deployment, and variability reduction, combined with new processes such as investment castings, plasma-spray metal application, automated joining, automated assembly, and advanced materials exemplify technologies under consideration to help make program goals a reality.

To develop, verify, and validate these manufacturing and design technologies, an extensive advanced development research and technology program has been established in support of STME studies. Full-scale turbopumps, a thrust chamber, and control hardware will be built and tested to provide confidence in the results of STME Phase A studies. Test facilities at the Air Force Astronautics Laboratory and MSFC will be upgraded to perform thrust chamber firings, and a new Component Test Facility (CTF) is under construction at Stennis Space Center (SSC) to provide turbopump testing.

Engine system and major component testing during full-scale development and production will be performed at SSC. The SSC CTF will be expanded to meet full-scale development requirements, current propulsion test facilities will be converted for STME use, and a new dual-position single-engine stand will be constructed. The development program will be a 90-month effort which will include research and development testing of engine components and systems, followed by a complete, rigorous verification and certification program. Studies in support of ALS have identified non-engine propulsion hardware as a major contributor to reliability. Therefore, STME testing will include parallel development of many traditional vehicle hardware elements such as flexible interface lines, thrust-vector control hardware, heat shields, and flight configuration feedlines. This integrated development approach will culminate in core and booster cluster tests at SSC, followed by two development flight tests. These development features, along with design concepts and management approaches defined in Phase A, will give the program unprecedented confidence in reliability and cost as production and operation program phases are entered.

STME primary performance characteristics are:

- *Thrust: 2,580 kN (580,000 ft•lb)*
- *Specific Impulse (Vacuum): 438 s*
- *Chamber Pressure: 153 atm (2,250 psia)*
- *Mass: 3,539 kg (7,800 lb)*
- *Area Ratio: 62:1*

H.A. Cikanek/HA31
(205) 544-1461
Sponsors: Office of Space Flight
U.S. Air Force/Space Division
Strategic Defense Initiative Organization

Space Transportation Booster Engine

The Space Transportation Booster Engine (STBE) is planned to provide Earth-to-orbit boost propulsion for the next generation of U.S. launch vehicles. STBE Phase A study began in 1986 to support joint NASA/U.S. Air Force space transportation architecture studies. Current STBE Phase A studies are providing engine designs and program plans to support the joint NASA/Air Force Advanced Launch System (ALS) Phase II studies.

Extensive trade studies resulted in the selection of methane as the engine fuel to be combusted with liquid oxygen for hydrocarbon booster application. The studies showed unique advantages to methane in that a baseline gas-generator cycle engine configuration derived from Space Transportation Main Engine (STME) hardware could result in a highly capable engine for a fraction of STME development cost. Thus, to take best advantage of methane, the derivative concept has been baselined. The derivative STBE can be designed to provide a range of thrust capability (depending on which option is selected) to fit well within the requirements of the ALS vehicle booster concepts currently under study. Upon determination of detailed vehicle requirements, the STBE designs can be adjusted to provide an optimum system configuration. Thus, the STBE provides an attractive alternative to the STME for booster application in the ALS. It will also have potential for upgrading propulsion in current expendable launch vehicles, in liquid rocket booster application for the shuttle, and as a growth path to a national fly-back booster.

STBE designs will provide high reliability, low cost, and robust design features derived from the STME. It will have dual-thrust capability to provide engine-out throughout the mission, and will employ the same modern design methods, advanced manufacturing technologies, and advanced materials that will be utilized in the STME. To develop, verify, and validate these technologies, an extensive advanced development research and technology program has been established to support STBE studies. Since the STBE is a derivative of the STME, the STBE and STME advanced development tasks support both engine designs, and allow exploration of a broader range of technologies and design concepts than are possible in the STME program alone.

A full-scale fuel turbopump and thrust chamber are the cornerstones of the advanced development effort supporting the STBE. The turbopump will use test cells in the same Stennis Space Center test facilities that will be used for advanced development supporting the STME. The thrust chamber will be tested in a MSFC facility currently undergoing an upgrade for that purpose. STBE full-scale development will be integrated with STME development, requiring one additional dual-position single-engine test stand.

STBE primary performance characteristics are:

- *Thrust (Sea Level): 2,224–2,891 kN (500,000–650,000 ft•lb)*
- *Specific Impulse (Sea Level): 297 s*
- *Chamber Pressure: 153 atm (2,250 psia)*
- *Mass: 3,181 kg (7,000 lb)*
- *Area Ratio: 35:1*

H.A. Cikanek/HA31
(205) 544-1460
Sponsors: Office of Space Flight
U.S. Air Force/Space Division
Strategic Defense Initiative Organization

Advanced Launch System Propulsion Advanced Development

Advanced development research and technology activities to support Advanced Launch System (ALS) propulsion definition studies were initiated in 1988. Efforts covered by the program are divided according to the nature of each task into the five following categories: liquid oxygen (LOX)/hydrogen engine, LOX/hydrogen-LOX/methane engine, hydrocarbon engine, booster/core propulsion subsystem, and solid propulsion. The primary emphasis of the tasks is to support definition studies with demonstration and validation of design concepts, manufacturing processes, materials, and design techniques, which will be employed to enable ALS propulsion to meet the program goals of high reliability, low cost, and operability. Particular effort is concentrated on producibility to allow dramatic cost reduction and quality increases compared to conventional propulsion systems. Testing is conducted at the MSFC Pressure Fed Test Facility (Fig. 4) and other test facilities at Stennis Space Center and the U.S. Air Force Astronautics Laboratory.

LOX/liquid hydrogen (LH_2) activities include conduct of detailed trade studies, detailed design, fabrication, and testing of major engine components to fully investigate low-cost manufacturing processes, low-cost/producible/high-quality design concepts, and advanced manufacturing techniques. Emphasis will be placed on materials and materials fabrication processes which will support the selected approaches. The total effort will include the design, fabrication, and test of an LH_2 turbopump, LOX/LH_2 thrust chamber assembly, LOX/LH_2 gas generator assembly, an electromechanical propellant valve flow control system, and a brass board controller/sequencer.

LOX/LH_2-LOX/CH_4 activities include conduct of detailed trade studies, and design, fabrication, and testing of major engine components to fully investigate low-cost manufacturing processes, low-cost/producible/high-quality design concepts, and advanced manufacturing techniques. Emphasis will

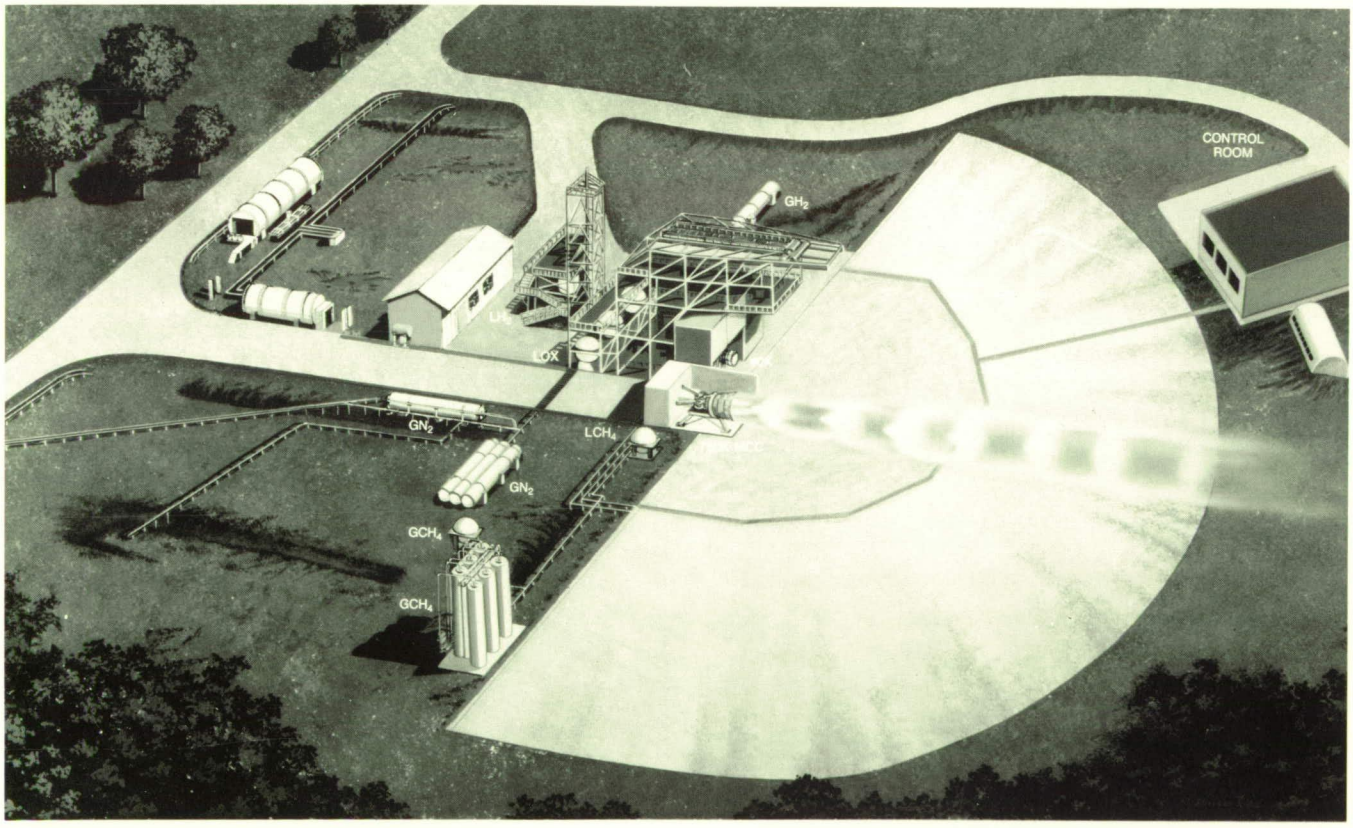

Figure 4. MSFC Test Cell 116 Pressure Fed Test Facility

be placed on evaluation of materials and materials fabrication processes which will support the selected approaches. The total effort will include the design, fabrication, and test of the LOX/LH_2-LOX/LCH_4 turbopump, thrust chamber assembly, and gas generator assembly.

LOX/hydrocarbon activities are focused on detailed technical investigations in support of low-cost, producible hydrocarbon engine candidates. Specific tasks include study and hardware demonstrations in LOX/hydrocarbon injector stability, tri-propellant thrust chamber stability/efficiency, and critical thrust chamber technologies (e.g., compatible materials, fuel cooling limits, gas side heat flux, and advanced cooling concepts).

Booster/core propulsion subsystems technology activities will provide definition of system architecture for low-cost auxiliary propulsion systems, definition of ALS design requirements and design criteria, design and validation of a prototype LOX tank pressurization system remote from the engine, and demonstration of control authority and stability.

Solid propulsion activities center on technologies that support a monolithic case, fixed nozzle, clean-propellant booster concept selected by ALS studies as the candidate to best meet ALS goals of high reliability and low cost. Specific tasks are grouped into the categories of clean propellants, nozzle/case technologies, and motor element integration technologies. Clean propellant work will demonstrate high-rate, low-cost processing of low hydrochloric-acid content propellants. To support the demonstration, a pilot scale plant will be built, continuous processing methods will be operated, and moderately large-scale demonstration firings will occur. Hardware concepts which will improve the reliability and costs of nozzles, cases, insulation, etc., will be selected, designed, and demonstrated on a small-scale basis to verify that the new concepts can meet ALS goals. A task investigating castable nozzles is also being pursued.

H.A. Cikanek/HA31
(205) 544-1460
Sponsors: Office of Space Flight
U.S. Air Force/Space Division
Strategic Defense Initiative Organization

Advanced Recovery Systems

Many studies of advanced launch vehicles including new designs, space shuttle derivatives, and more recently, the joint U.S. Air Force/NASA Advanced Launch System, have shown the potential economic and operational advantages of recovering main engines and other high-cost equipment for reuse. By incorporating the main propulsion and avionics into a single package, generally referred to as the propulsion/avionics (P/A) module, the launch vehicle's most expensive and complex components are combined into a relatively compact package for expeditious recovery, refurbishment, and reuse. This approach, enabling rapid reuse of the components, at the same time maximizes launch vehicle payload performance above that of a totally reusable manned vehicle. The P/A module is being considered in two basic configurations (Fig. 5). The high lift-to-drag (L/D) ratio configuration has the advantage of using wheels for a conventional aircraft-type landing, while affording increased landing opportunities when returning to the launch site from orbit. The ballistic, or low L/D configuration is relatively less complex, lighter in weight, and costs less. Weights range from about 25,500 kg (56,000 lb) for a low L/D configuration to almost 30,000 kg (66,000 lb) for a high L/D module.

The high L/D P/A module features a delta platform shape approximately 15 m (50 ft) long, 15 m (50 ft) wide, and 6 m (20 ft) tall. Advanced carbon/carbon material is needed for the short radius leading edge. Otherwise shuttle thermal protection is adequate. This shape provides a cross range of 2,897 km (1,800 mi), which allows more than 10 return orbit opportunities per day to Kennedy Space Center (KSC) and Edwards and Vandenburg Air Force bases. The low L/D P/A module has a blunt shape of approximately 22 ft diameter and is 20 ft long. Cork is the preferred ablator for the expendable nose heat shield. The shuttle thermal protection system is used for the remaining areas of the body, including the base. This vehicle has only two return landing opportunities per day to KSC. It lands on a circular, grass-covered site 1 to 2 km (0.5 to 1 mi) in diameter, depending on whether a lifting or ballistic parachute is used. Final impact attenuation is provided by airbags.

The current P/A module effort centers on refinement of subsystem description, advanced development, integration into specific applications, and programmatic definition (a significant aspect being costing). Scale-model wind tunnel testing of the

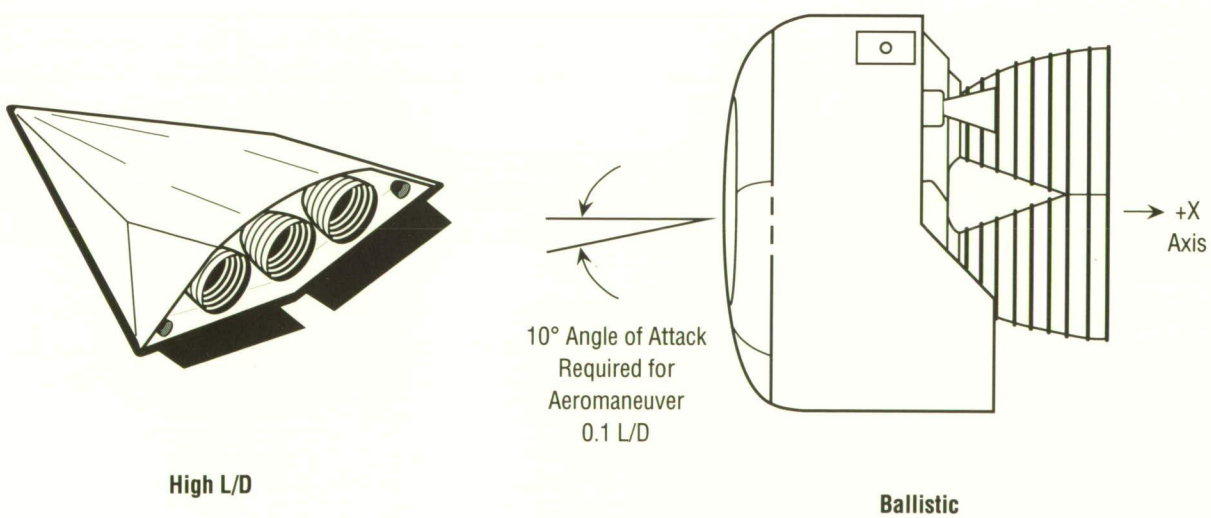

Figure 5. Propulsion/Avionics Module Concepts

high L/D configuration has been conducted up to Mach 5 speeds. High speed (up to Mach 20) heating and force-model testing are planned for this year. For the ballistic vehicle, a full Mach range of aerodynamic testing is planned for this year, including heating tests at Mach 8. Drop tests for the ballistic configuration are planned for this year to confirm the airbag design to attenuate terminal landing loads.

In concert with the P/A module effort, a precision recovery gliding parachute system for soft touchdown of the P/A module at the launch site is being developed. This system, termed the Advanced Recovery System (ARS), with a target landing capacity of more than 27,000 kg (60,000 lb), represents a significant advance in the weight-carrying capability of deployable ram-air gliding parachutes with a potential touch-down descent velocity of only 4.5 m/s (15 ft/s). To provide a precision return capability to the ballistic P/A module (and potentially other applications such as space station crew return), studies have been made of various systems ranging from ballistic parachutes to advanced gliding deployable wings to be used for land recovery. Benefits of a land touchdown, as opposed to ocean splashdown, include elimination of salt water corrosion, simpler recovery logistics, avoidance of cross country transportation of large objects (if recovered at the launch site), simpler refurbishment operations, and a potentially smaller inventory of modules because of faster ground processing operations.

Phase I of the ARS for the Advanced Launch Vehicle program examined a broad range of candidate recovery concepts, and ultimately defined a system using a 985 m^2 (10,600 ft^2) ram-air gliding parachute (also known generically as the parafoil) for soft landing the module at a prepared area near the launch site.

Phase II extends the effort to include a scaled demonstration of this concept. This program, currently underway, includes wind-tunnel tests in the 24.4- by 36.6-m (80- by 120-ft) test section at the National Fullscale Aerodynamic Complex at Ames Research Center. Two similar model parafoil systems, including 3.05- by 9.15-m (10- by 30-ft) and 6.1- by 18.3-m (20- by 60-ft) canopies, were used to establish scaling effects. Figure 6 shows the larger model in the wind tunnel. Data collected included basic aerodynamic parameters, control forces, and deflections. These wind tunnel tests were conducted in September 1988, and additional tests to establish a parafoil aerodynamic data base using different size models, airfoils, and aspect ratios are scheduled for October 1989.

The other portion of the program includes a series of 11 aircraft drop tests with weights ranging from 4,500 to 9,000 kg (10,000 to 20,000 lb). The parafoil and weights being used are about one-third scale, so the tests represent wing loadings of a full-scale module. Man-in-the-loop controls for steering and flare to landing will be incorporated into later stages of the program.

Reliable, controlled deployment of any parachute is critical for successful recovery. The deployment method used in this program is unique in that the cells are folded much like an accordion and allowed to open in a controlled manner to minimize opening shock loads. Three stages of controlled opening will be incorporated. The basic objectives of the drop-test program are to demonstrate reliable deployment of the parafoil; demonstrate stability, direction control, and flare to soft landing; and establish a data base to be used for further parafoil research and provide the basis for development of autonomous control systems. To date, four drop tests have been conducted with weights up to 4,500 kg (10,000 lb), and plans are to continue through the remaining nine tests with weights up to 9,000 kg (20,000 lb). A phase III program is planned to demonstrate automatic controls with heavier weights. This program will begin after the conclusion of the current program and will continue for about 3 years.

G.W. Johnson/PT01
(205) 544-0636
Sponsors: Office of Space Flight
Advanced Launch Systems Joint Program Office

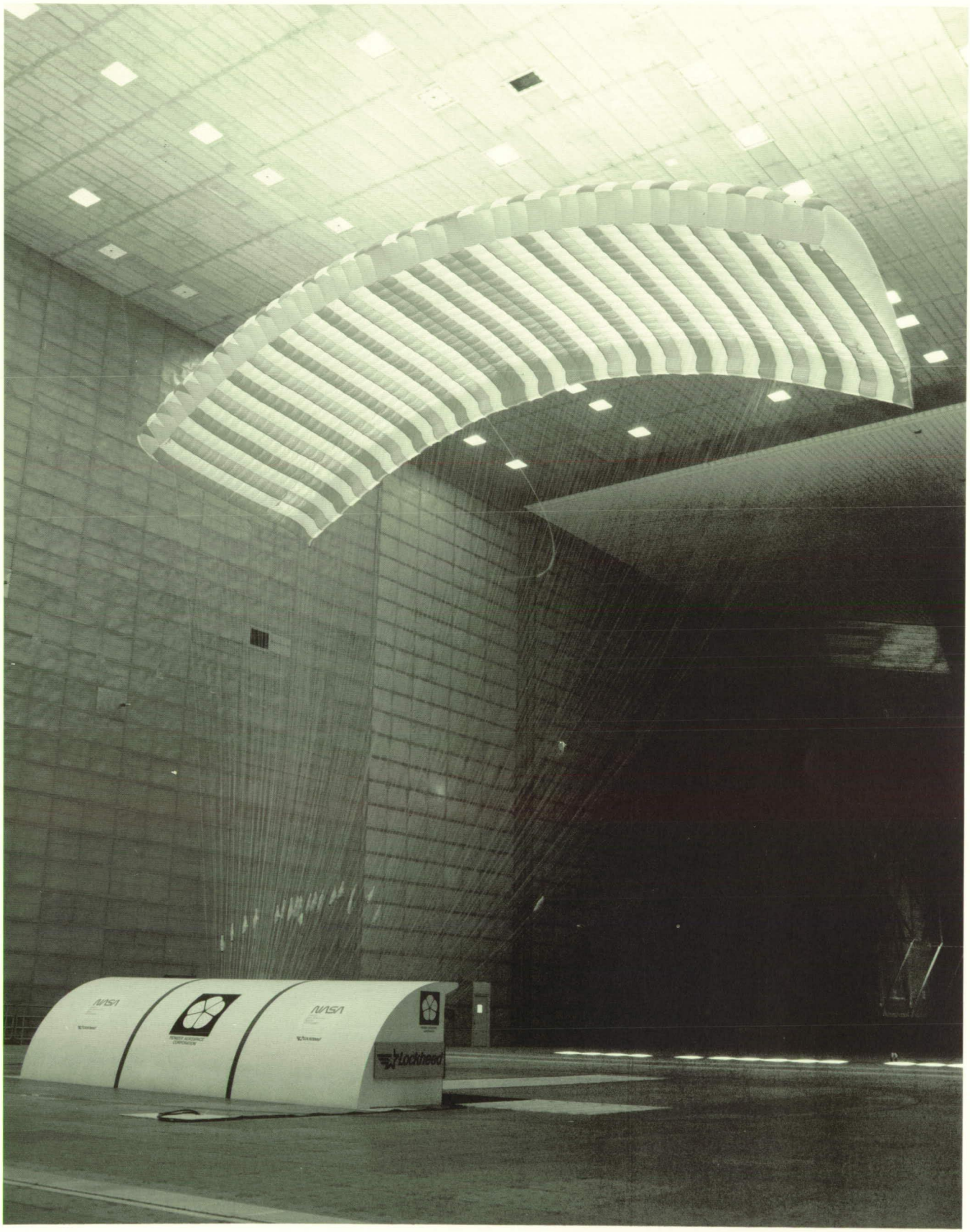

Figure 6. Large Ram-Air Gliding Parachute Model

ORIGINAL PAGE
BLACK AND WHITE PHOTOGRAPH

Liquid Rocket Boosters for Space Transportation System

Design studies of liquid rocket boosters (LRB's) have been conducted by a joint MSFC, Kennedy Space Center (KSC), and Johnson Space Center (JSC) team. The studies, under the direction of MSFC, were structured to provide independent system design studies by both Martin Marietta and General Dynamics. Aerodynamic analysis and wind tunnel support was provided by the MSFC Structures and Dynamics Laboratory. Ground and flight operations design and evaluation support were provided by KSC and JSC, respectively. The latter two centers were supported by the Lockheed Corporation.

Design studies were structured to evaluate two primary concepts, pressure- and pump-fed LRB's, and associated ground and flight operations for two specific payload cases. The contracts were structured to develop a definition of each booster concept. Principal design requirements were:

STS Program Requirements

- *JSC 07700 – Volume X System Specification*
- *JSC 08934 – Operations Data Book*

Payload Requirements

- *Case 1: 31,979 kg (70,500 lb) at 104 percent Space Shuttle Main Engine power level (SSME P.L.)*
- *Case 2: 28,350 kg (62,500 lb) at 104 percent SSME P.L. (109 percent SSME P.L. for abort in both cases)*

The studies evaluated various potential fuel systems for an LRB, but focused on the use of LOX/RP-1 for both pressure and pump-fed systems and LOX/H_2 for pump-fed systems. The former system was attractive due to low cost, prior experience, and density considerations. The latter system was attractive due to advantages of a common propellant system with the space shuttle, and due to synergism with planned engines for the Advanced Launch System (ALS).

The study concluded that LRB's are indeed a viable alternative for the Space Transportation System. Significant advantages for the LRB system that were identified included: engine verification prior to lift-off, engine-out capability during all flight phases, intact abort capability, increased payload capability [29,484 kg (65,000 lb) to space station 220 nmi orbit], streamlined process flow at KSC (20-day booster flow reduction), and elimination of hazardous propellants from the Vehicle Assembly Building.

Studies are continuing in FY89 to refine the analyses and to examine synergism with other vehicle systems including the ALS.

L.O Wear/PF23
(205) 544-3215
Sponsor: Office of Space Flight

Next Manned Space Transportation System

NASA is currently analyzing alternatives to establish the desired path for future manned launch vehicles. The next manned transportation systems (NMTS) could follow one or more of the following three paths: National Space Transportation System (NSTS) evolution, the Personnel Launch System (PLS), and the Advanced Manned Launch System (AMLS). Figure 7 shows some conceptual configurations for each of the different paths. These NMTS studies will be conducted over the next several years to ascertain the best path to follow from both a technical and programmatic point of view. The NSTS evolution study is currently in preliminary design, whereas both PLS and AMLS are in conceptual design.

Shuttle evolution deals with major block changes to the NSTS, as opposed to the NSTS improvements currently underway. One potential block change being considered is the introduction of liquid rocket boosters (LRB's). The LRB's would improve reliability by providing engine-out capability, and would also allow improved emergency escape capability for the crew by permitting booster throttling and/or engine shutdown. Additionally, the LRB's would provide an increase of 9,000 kg (20,000-lb) lift capability over the current SRB's.

The PLS study includes the feasibility of separating man from cargo, and the potential of carrying either a manned capsule or a cargo return vehicle (CRV) on existing and/or new launch vehicles. One option being investigated is an LRB with a second stage, potentially a derivative of the LRB. Other options could be manned versions of either Titan missiles or Advanced Launch System vehicles. The manned capsules to be studied are both low and high lift-to-drag configurations. The primary function of the CRV is to provide the ability to return unmanned payloads from Space Station *Freedom*. The PLS is being looked at as both an augmentation to the STS or an intermediate evolution step between NSTS and an AMLS.

The AMLS, formerly known as Shuttle II, will be the next generation reuseable manned transportation system to replace the existing NSTS. Technology from the mid-1990's will be used to provide the most reliable, safe, robust, and efficient vehicle possible. The vehicle will be capable of transporting both crew and cargo to low-Earth orbit. However, its cargo-carrying capability may be less than the current NSTS since alternate unmanned vehicles will be available for heavier payloads.

U. Hueter/PT21
(205) 544-8492
Sponsor: Office of Space Flight

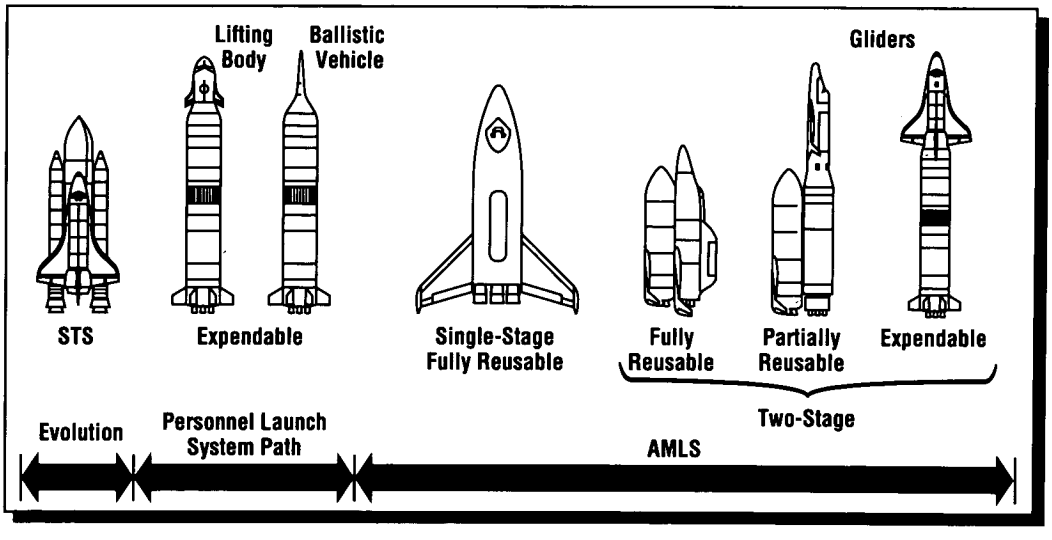

Figure 7. Next Manned Transportation System Concepts

Manned Lunar and Mars Exploration

In February 1988, President Reagan announced a comprehensive space policy intended to insure U.S. leadership in space. One of the three main goals of this policy was to establish a long-range goal to expand human presence and activity beyond Earth orbit into the solar system. Dr. Sally Ride's report, "Leadership and America's Future in Space," set goals for the establishment of manned bases on the Moon and Mars during the 21st century. These initiatives will require new and advanced concepts and propulsion systems.

During FY89, MSFC has continued studies in transportation vehicle design and propulsion systems to support both lunar and Mars missions. One emphasis of these studies has been to assess mission scenarios and develop transportation element requirements and concepts, including spacecraft and landers, to support the missions. Figure 8 depicts one concept for a Lunar Transfer Vehicle as it would appear in lunar orbit. The Lunar Transfer Vehicle, which operates to carry crew and cargo between Space Station *Freedom* and lunar orbit,

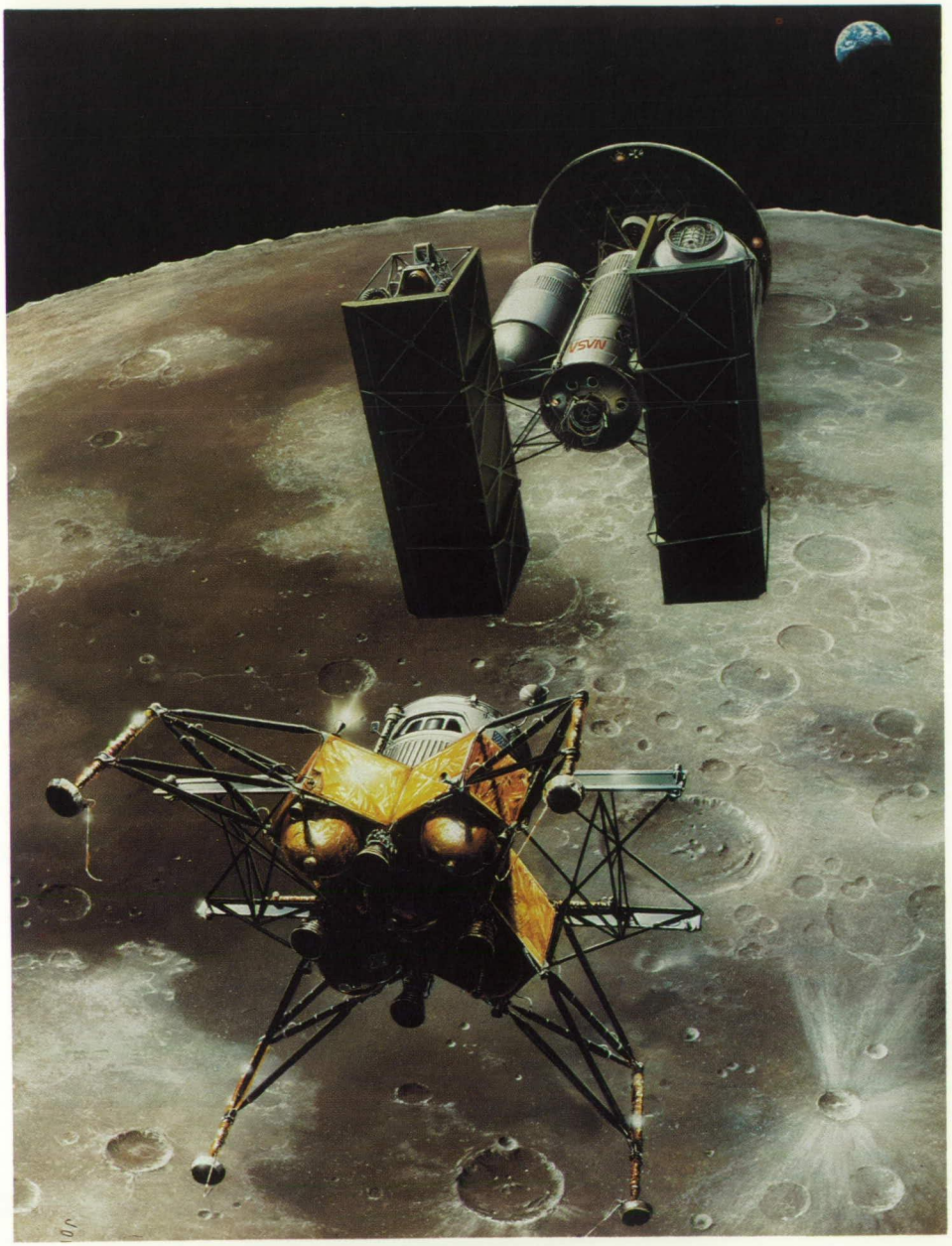

Figure 8. Lunar Transfer Vehicle and Lunar Excursion Vehicle in Lunar Orbit

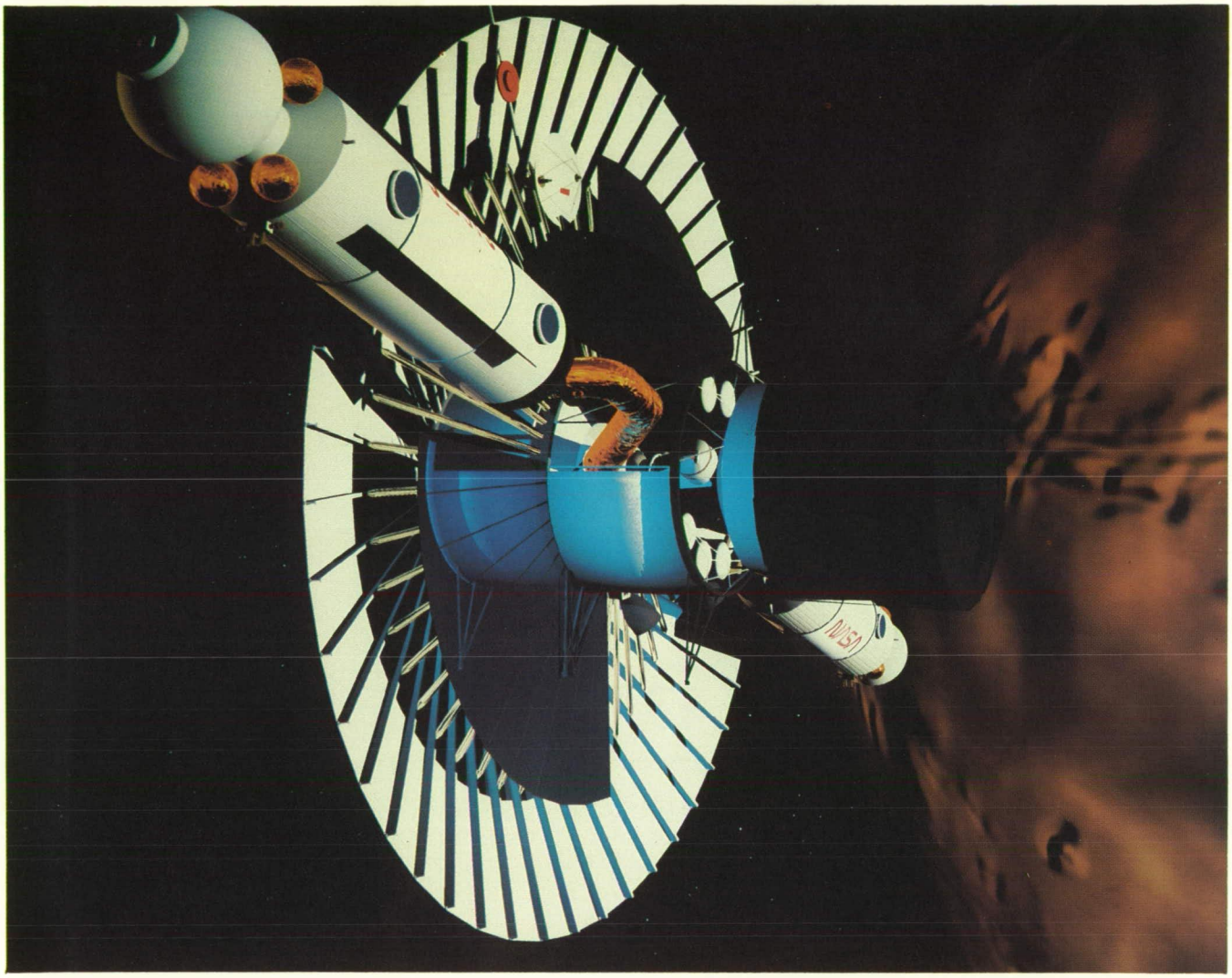

Figure 9. Mars Transfer Vehicle Prior to Mars Arrival

utilizes aerobraking for Earth orbit capture upon return from the moon. The Lunar Exursion Vehicle operates between lunar orbit and the surface. Each vehicle has its own crew module, and both vehicles feature cryogenic propulsion.

Figure 9 shows a preliminary concept for a Mars Transfer Vehicle, required to support a Mars mission in the post 2000 time frame. The integrated spacecraft includes a habitation module to support the flight crew during the transfer from Earth orbit to Mars orbit, and the return to Earth orbit; an aerobrake for Mars orbit capture and later for Earth orbit capture; the lander which will descend to the planetary surface; and a trans-Earth injection stage for Mars orbit departure. Additional study in this area includes identification and evaluation of feasible transportation concepts for the mission scenarios, along with trade and sensitivity analyses.

Investigations underway include analysis of current propulsion systems and their applications to mission scenarios. Propulsion systems investigated have included both high-thrust chemical and nuclear-thermal concepts, as well as low-thrust nuclear-electric and solar-electric concepts for exploration missions. Trade studies are being conducted based on current predictions of propulsion advancements over the next two decades to determine the impact of these advancements on mission scenarios.

J.P. Sumrall/PT41
(205) 544-8491
Sponsor: Office of Exploration

Space Transfer Vehicle

Space transportation requirements have been identified from analyses of NASA's long-range planning in science, applications, and technology, and from assessments of future manned exploration needs. Analyses of these various sources support the need for a high-performance upper stage transportation system known as the Space Transfer Vehicle (STV). A representative concept is shown in Figure 10.

A broad spectrum of STV concepts has been studied to determine the best method of meeting future mission requirements. The final phase of these conceptual studies will begin this year with the primary goal of defining an evolutionary family of vehicles that can grow with mission needs and have the flexibility to be launched by more than one launch system.

Candidate STV concepts will be developed against the latest version of the Civil Needs Data Base national mission model, augmented by current planning from the Office of Exploration relative to advanced manned missions. These new mission model data provide significant implications concerning system requirements for the STV in terms of performance requirements for various scenarios and potential evolution schemes.

Candidate STV's are being defined and evaluated which are compatible with the current space transportation system (with new launch constraints and safety policies), Shuttle-C, Titan IV, and the Advanced Launch System.

The results of these studies will be combined with earlier studies and in-house investigations to identify the most promising concepts and approaches, to document alternative trades, and to determine areas requiring technological advancement.

An advanced development program has been underway for several years, devoted to such areas as cryogenic fluid management, atmospheric modeling, aerobrake structural dynamics, avionics, and cost modeling. System definition (Phase B) is currently scheduled to start in FY92.

D.R. Saxton/PT31
(205) 544-5035
Sponsor: Office of Space Flight

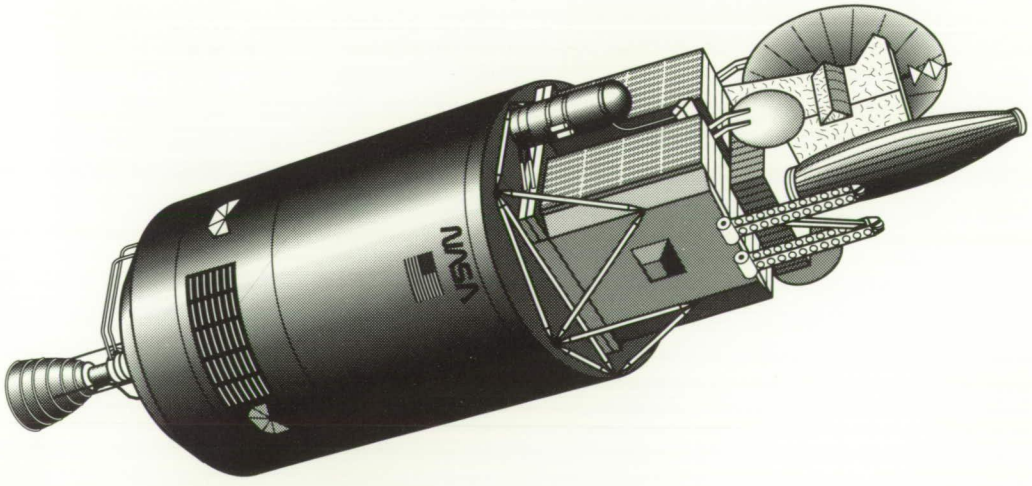

Figure 10. Space Transfer Vehicle Concept

Space Systems

Gravity Probe-B

Gravity Probe-B (GP-B) is a fundamental experiment in gravitational physics. It will measure the effects of the Earth's mass and rotation on the surrounding gravitational field to experimentally verify Einstein's theory of General Relativity. It is a spacecraft containing a system of four orbiting, ultraprecision, cryogenically cooled gyroscopes designed to detect extremely small changes in the structure of space and time over a 1-year period.

The project has been approved for an engineering development phase consisting of two distinct, but complementary, efforts — the Space Test Unit (STU) and the Ground Test Unit (GTU). The present focus is on the First Integrated Systems Test (FIST) of the Ground Test Unit.

The FIST will use a laboratory dewar with a well, neck tube, and magnetic shielding of the same design as the science mission. The probe, quartz block, and gyros will be prototypes of the science mission (Fig. 11). The test will demonstrate that the entire multigyro system can be operated in the required ultralow magnetic field, ultralow vacuum, cryogenic environment.

Milestones scheduled and accomplished during FY89 included prototypical gyro manufacture and testing, composite alumina dewar neck tube fabrication, laboratory dewar delivery, quartz block fabrication, and completion of clean room facilities and procedures for cleaning and assembly of the experiment. Recent gyro testing has demonstrated high-speed spin (at room temperature) with excellent Superconducting Quantum Interface Device read-out quality and long spin-down rates (at low temperature) which indicate a flight-quality rotor and very low disturbing torques.

Major milestones scheduled for FY90 include completion of FIST and initiation of Phase B science mission spacecraft studies. Preliminary design will also be started on the flight telescope and electronics.

The experiment is being developed for NASA by Stanford University.

R. Ise/JA51
(205) 544-1962
Sponsor: Office of Space Science and Applications

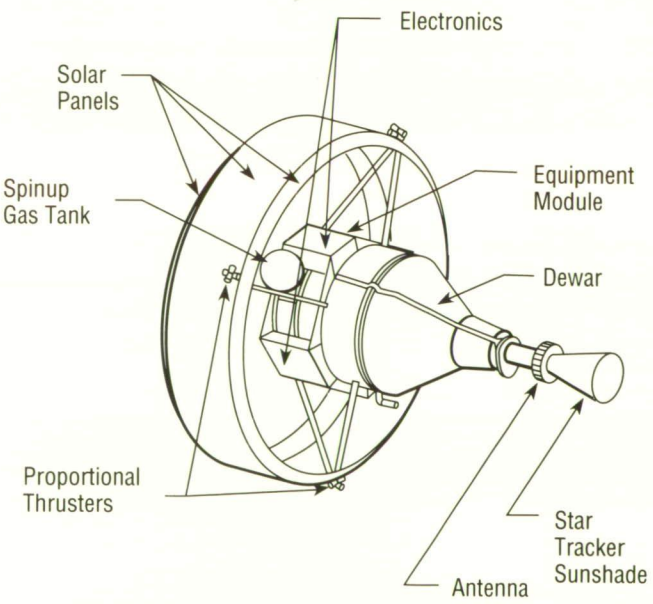

Figure 11. Gravity Probe-B

Superconducting Gravity Gradiometer

During the past three decades, measurements and observations from space have stimulated a major revolution in Earth science. Fundamental new knowledge of the Earth, its continents, oceans, atmosphere, biosphere, and ice covers has revealed a complex and dynamic Earth system that could only have been imagined before the era of space observations. This scientific revolution has in turn increased the need for new and more accurate observations and data in order to better understand this complex system. Fundamental to Earth science is knowledge of the Earth's gravitational and magnetic fields. An instrument that holds great promise for sensitive gravity measurements is the Superconducting Gravity Gradiometer (SGG).

Since 1980, the University of Maryland, under NASA sponsorship, has made significant advances in the development of an SGG. This instrument, planned for a satellite mission in the year 2000, would measure the global gravity field to a precision of 2–3 mgal (1 gal = 10^{-2} m s^{-2}) with a resolution of 50 km (31 mi). Besides this primary objective, SGG will also present opportunities to test Newton's inverse square law of gravitation, and could offer an independent experimental test of the Lense-Thirring effect of General Relativity.

The Superconducting Gravity Gradiometer Mission (SGGM) will include a three-axis SGG integrated with a Superconducting Six-Axis Accelerometer (SSA) to map the Earth's gravitational field. The required sensitivity for space geodesy is:

$3 \times 10^{-4}\ E\ H_z^{-1/2}$ (1 Eötvös = 1 E = 10^{-9} sec^{-2}).

A study team, managed by MSFC and consisting of representatives from NASA centers and headquarters, the U.S. Air Force, the U.S. Army, and universities, has developed preliminary concepts of a free-flying science mission (Fig. 12) and a precursor orbital flight test of the instrument. During Phase II of the instrument development (ending April 1989), a three-axis SGG of improved design (Model II) has been assembled and is undergoing tests. This device has an intrinsic noise level of $5 \times 10^{-3}\ E\ H_z^{-1/2}$. Also during this phase, groundwork has been laid for construction of a three-axis SGG with even higher sensitivity (Model III). With further technological innovations, Model III is expected to meet the mission sensitivity requirements.

Major research and technology areas that will be pursued during the coming year include the continued test of a single-axis, Model III SGG; the construction and test of a three-axis Model III SGG; the integration of the Model III SGG with the SSA; and the investigation of platform stabilization. Additional tasks include software development, electronic automation of the SGG instrument, thin-film coil development, and a feasibility study of the precursor flight test.

Moody, M.V., Chan, H.A. and Paik, H.J.: Superconducting Gravity Gradiometer for Space and Terrestrial Applications. J. of Appl. Physics, Vol. 60, No. 12, pp. 4308–4315, 1986.

Morgan, S.H. and Paik, H.J., ed.: Superconducting Gravity Gradiometer Mission. Vol. I, Study Team Executive Summary, NASA TM, in press.

S.H. Morgan/PS02
(205) 544-0614
Sponsor: Office of Space Science and Applications

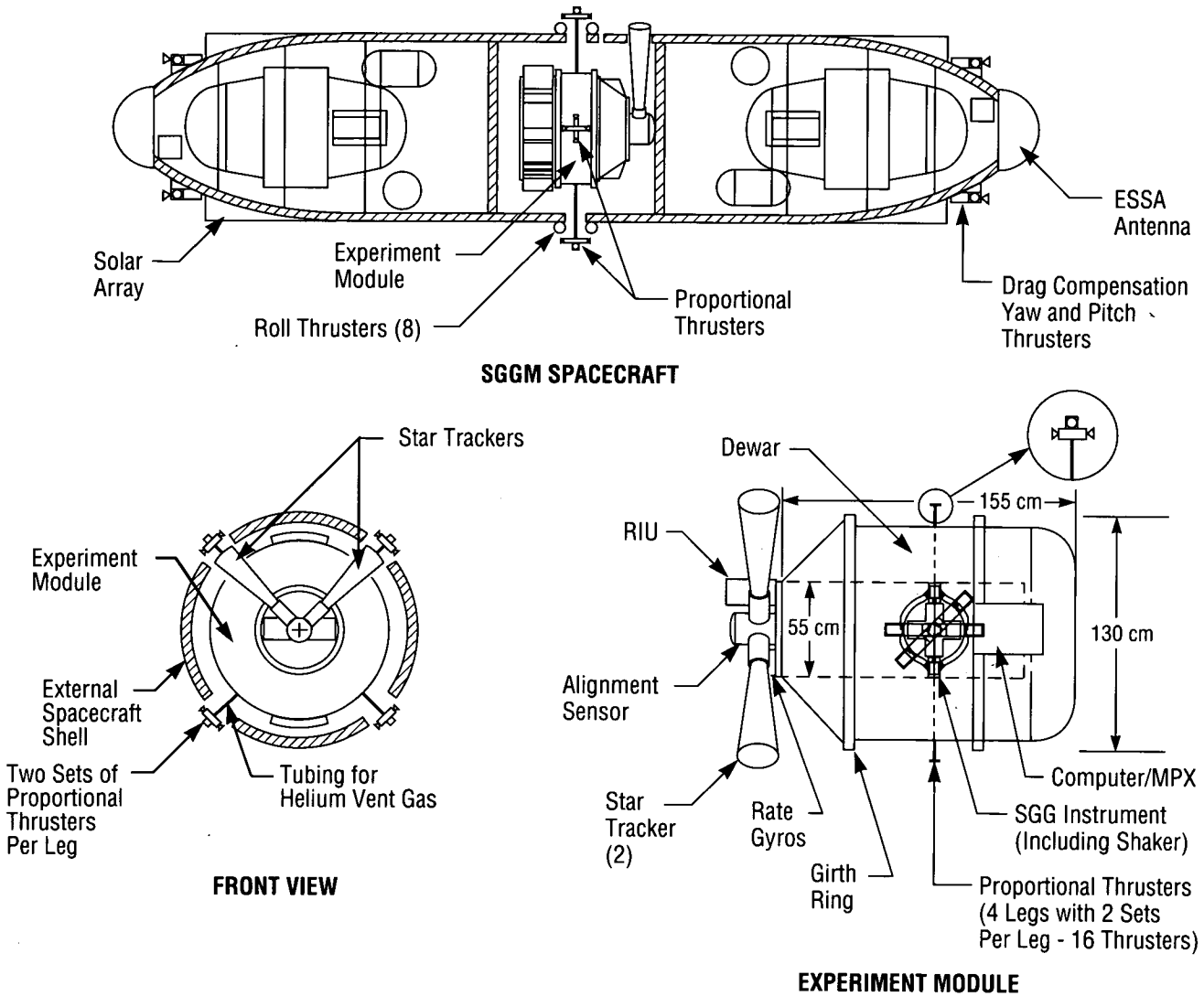

Figure 12. Free-Flying Superconducting Gravity Gradiometer

Tether Applications in Space

Tether Applications in Space (TAS) studies and experiments are aimed at defining and developing ways to use tethers in space. These activities have been underway for about 6 years and some, like the Small Expendable Deployer System (SEDS), have reached the hardware stage.

SEDS is a lightweight spinning-reel type of system designed to deploy a payload attached to the end of a 20-km (12-m) long tether, which is cut and discarded after use. First flight objectives are to validate the design concept and study the dynamics of tether deployment. SEDS weighs about 39 kg (85 lb), including the tether weight of 7 kg (15 lb). The tether is made from a high-strength, low-density, polyethylene fiber called SPECTRA. SEDS will fly on a Delta II launch vehicle in 1991. Hardware development was completed in 1989. Analysis and physical integration of SEDS into a Delta II is expected to be accomplished by the end of 1990.

During flight the payload, weighing 23 kg (50 lb), will be deployed toward the Earth. The experiment will last about 2 hours, ending when the tether is fully deployed and has swung to a near-vertical position, pointing toward the Earth. The tether is then cut, allowing it and the payload to re-enter the Earth's atmosphere. The SEDS concept is shown in Figure 13.

An interesting application of SEDS is the routine de-orbiting of Space Station *Freedom* waste materials, packaged in lightweight containers that can be folded for easy storage during shuttle trips to the station. A shuttle-based Tether Initiated Space Recovery System (TISRS) experiment is being planned that would use SEDS to re-enter an existing re-entry capsule. Preliminary design work is going on now to modify, for tether use, some of the key features of the capsule. The TISRS experiment is a joint project with the Italian Space Agency, which

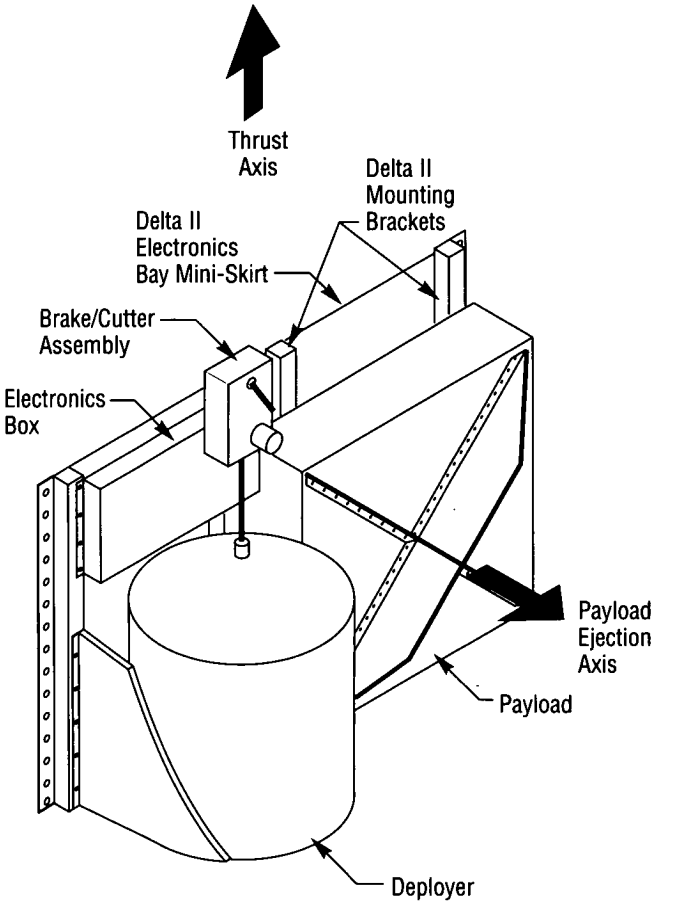

Figure 13. Small Expendable Deployer System Components and Configuration

is defining the data and instrumentation system, and may develop these systems later on if the necessary international agreements and arrangements can be satisfactorily worked out.

Another TAS activity is the development of a laboratory prototype of a Getaway Tether Experiment (GATE). This laboratory system consists of a miniature reel mechanism to control the tether, a tensiometer, control electronics, and a television-based tracking system. The purpose of this laboratory equipment is to develop prototype tether control mechanisms for possible flight use. A typical flight experiment would be a mother-daughter pair of satellites connected by a 1-km (0.62-mi) tether. Control techniques can be tested during flight to enhance the damping of tether vibrations. Long-term measurements of micrometeoroid damage could be made and used to predict survival of similar systems. Redesigned key hardware components (reel, motor, and tension sensor) were built in 1989 for the laboratory prototype and for the test support equipment, a television system that tracks the tether position during deployment. Laboratory tests of GATE are planned for mid-1990.

J.K. Harrison/PS04
(205) 544-0629
Sponsor: Office of Space Flight

Materials Processing in Space

The weightlessness of space reduces buoyancy forces, hydrostatic pressure, sedimentation, and thermally-induced convection flows, and eliminates the need for contact with containers. Flight results indicate novel effects on a wide spectrum of important materials including inorganic crystals, biological fluids, and many others. Space experiments will provide critical insights into terrestrial materials processes and will possibly produce unique high-value-added products in space.

Work sponsored by the Office of Space Science and Applications has resulted in a body of science and technology that forms the technical basis for materials processing in space activities. The Office of Commercial Programs, supported by MSFC, has established policies and procedures for making business and legal arrangements with commercial firms and for providing technical assistance to their research and development work aimed at commercial applications of materials processing in space.

MSFC ground-based microgravity activities provide accessibility to short-term, low-gravity periods and are used to test concepts that will be developed for use in space. For example, the High-Temperature Containerless Aircraft Furnace is used in an aircraft which provides up to 20 s of low gravity during parabolic flight. This furnace processes conductive materials. The Zirconia Furnace is another aircraft furnace being developed to accommodate materials with a high melting point and low surface tension. Other apparatus have also been developed for ground-based use.

MSFC is involved in microgravity space apparatus development. Modular design is emphasized to allow a variety of experiments and in-orbit flexibility. Advancements have been made in heater technology, temperature control, insulating materials, and sample containers. Some of this flight hardware will fly in the upcoming United States Microgravity Laboratory (USML) series. The Crystal Growth

Furnace (CGF, Fig. 14) will utilize USML to grow electronic crystals or photonic materials. The CGF will process large samples and allow sample change-out in orbit.

In FY89 on the STS-29 flight, the Protein Crystal Growth apparatus provided crystals of high quality and uniform morphology; analyses are in process to determine the complex molecular structure of these proteins. The satellite tobacco mosaic virus was also crystallized for the first time, and the gamma interferon crystals produced were of higher quality than any grown on Earth.

The Advanced Automated Directional Solidification Furnace is being developed for U.S. microgravity payload missions. It will provide precision control of the melt growth of electronic materials and

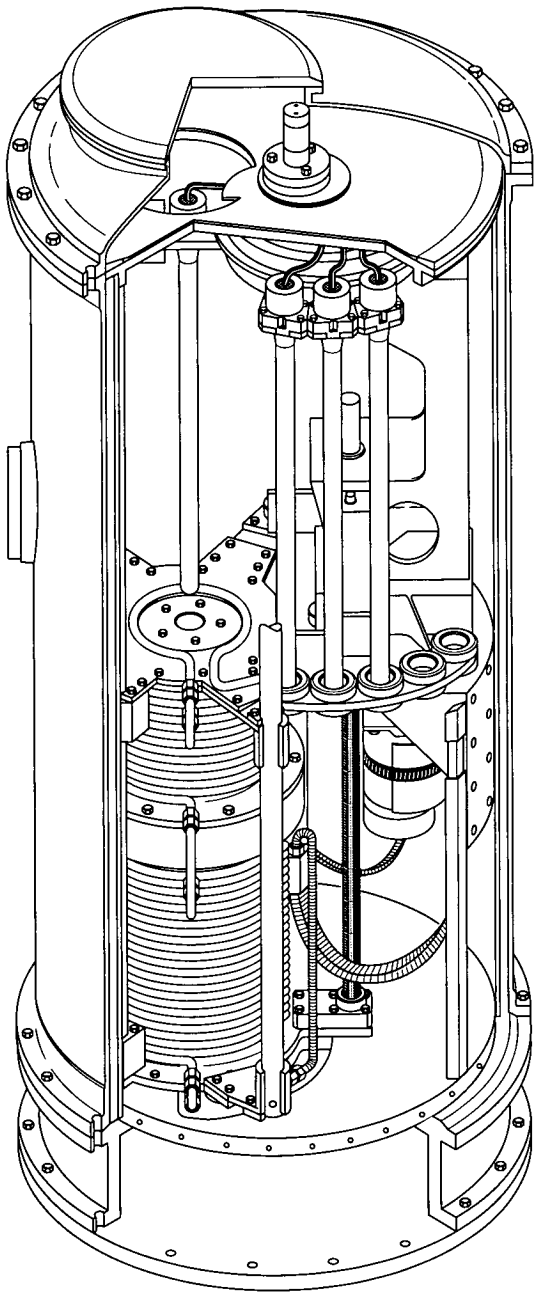

Figure 14. Crystal Growth Furnace

continued research of the effects of thermal- and density-driven convection on these materials.

Another experiment device, the Fluid Experiment System (FES), is being prepared for the International Microgravity Laboratory-1 mission. This apparatus is used for studying fluid convection, phase transition, surface tension, immiscible fluids, and bubble behavior.

Conceptual designs have begun for two systems to be used on Space Station *Freedom*: the Space Station Furnace Facility (SSFF) and the Advanced Protein Crystal Growth (APCG) Facility. The SSFF will include advanced furnaces such as a hot-wall float-zone furnace and a large-bore Bridgman furnace. The APCG will allow growth of large protein crystals which can then be analyzed to determine how these proteins control the key mechanisms involved in biological processes.

The Centers for the Commercial Development of Space (CCDS) Program was instituted by the Office of Commercial Programs to provide a focus for industrial, academic, and governmental elements to advance from pure research to commercial applications. Sixteen CCDS's, with 128 industrial and 48 university participants, have been established. Seven of these CCDS's are associated with MSFC, and five of these specialize in materials processing in space activities.

The CCDS at the University of Alabama in Huntsville sponsored the March 29, 1989, Consort 1 suborbital mission. It provided 7 min of microgravity for seven materials processing experiments which produced 152 experiment specimens. These experiments included demixing of immiscible polymers, elastomer-modified epoxy resins, organic foam processing, powdered metal sintering, electrodeposition, and a materials dispersion apparatus. Additional suborbital missions are planned.

Research by the CCDS at Vanderbilt University has resulted in a patent application for a platinum-cobalt magnet alloy. Also, a high-temperature [2,800 °C (5,072 °F)] directional solidification furnace is being developed for research on platinum-group refractory metal alloys.

The CCDS located at the University of Alabama at Birmingham flew two sets of protein crystal growth experiments (on STS 26 and 29) during this period. Protein crystals were selected for their importance in researching diseases such as cancer, emphysema, and high blood pressure.

MSFC, under the Office of Commercial Programs, is working on 13 joint agreements with commercial users for potential applications of materials processing in space. As a result of these efforts, the 3M Company experiment, Physical Vapor Transport of Organic Polymers, flew for the fourth time in September aboard Space Shuttle Discovery. 3M has filed several patents and is preparing for another shuttle flight. The Rockwell International Corporation Fluids Experiment Apparatus also flew this year on STS-30 with the Indium Corporation of America as a co-investigator.

MSFC is supporting the planning for S.S. *Freedom* by providing materials processing technical data and analyses, and by developing requirements for potential commercial users. Fourteen strawman payloads have been conceived to define a typical set of accommodations that would be needed to support them.

C.M. Davis/PS05
(205) 544-0645
Sponsors: Office of Commercial Programs
Office of Space Science and Applications

Space Station Transition Definition

The "transition" period for Space Station *Freedom* is the time period after it becomes operational, and includes growth and/or evolution of the initial space station. "Growth" generally implies increase in size or capability of an existing concept, whereas "evolution" connotes some change in the basic approach, direction, or broad use of a facility, including its growth. Some evolution options assume that only one space station is available, and evolution is accomplished by converting the original station to one having a different application. Other options involve multiple space stations (or derivatives) having different emphases.

MSFC's 1989 activities in the area of space station growth/evolution included systems studies and advanced development tasks as part of an intercenter effort sponsored by the S.S. *Freedom* Project Office at NASA Headquarters. One principal thrust in this work has been to provide preliminary identification of potential "hooks and scars" which would have to be implemented early on the baseline S.S. *Freedom* to allow subsequent growth/evolution with minimum impact. One concept of an evolutionary space station is provided in Figure 15. This concept is an R&D-emphasis space station; other concepts emanating from the current overall effort have more of a transportation node emphasis. Each type of space station is responsive to different types of user requirements, and it is not yet clear which trend will predominate in the early time-frame after the initial S.S. *Freedom* becomes operational. Thus, one goal of the transition definition activity is to identify the potential modifications to the initial S.S. *Freedom* which would allow maximum growth/evolution flexibility.

Systems studies have examined logistics systems evolution, Environmental Control and Life Support System (ECLSS) evolution, and the implications of accommodating space transfer vehicles at S.S. *Freedom* (as part of lunar and Mars manned exploration initiatives). In these studies, various concepts of each of the systems, encompassing a range of differ-

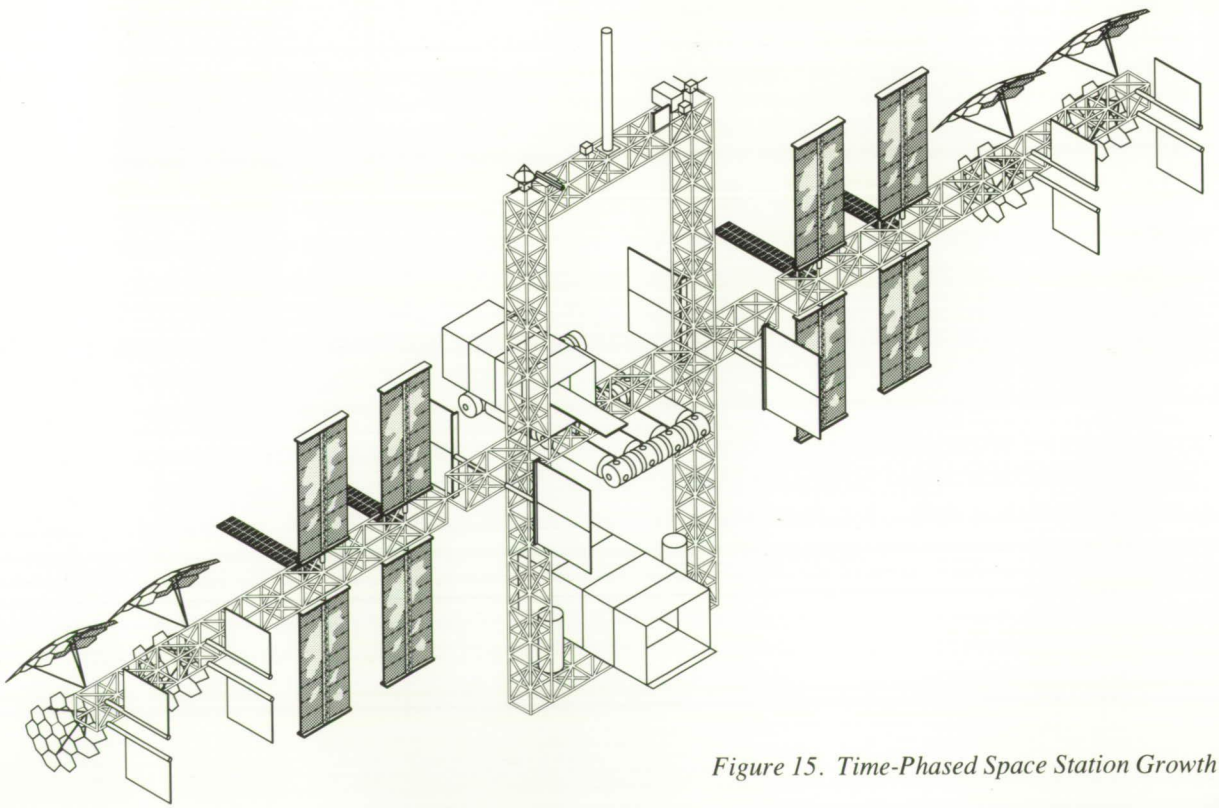

Figure 15. Time-Phased Space Station Growth

ent sizes, technologies, and capabilities, were examined. Several versions of the growth/evolutionary space station, embodying increases in size, technology level, mission accommodation, capability, and/or quantity, were considered in these assessments, and implications of such evolution were defined. Potential hooks and scars were identified in each area of study.

Another area of study has been the evolution of manned modules. Various types of modules were examined, including resource nodes and pocket labs. Extension of resource node lengths will be necessary to allow the adequate intermodule clearances that were assessed in this study. Concepts of pocket labs, providing volume for discipline-peculiar research, were assessed. A limited assessment of user requirements was made, and resource requirements for different concepts were determined.

Advanced development work was done in the areas of advanced automation of the ECLSS, the Power Management and Distribution system, and space station housekeeping functions. Work was also done in the area of potential utilization of design/engineering knowledge from the Hubble Space Telescope to augment space station design knowledge capture. The work done in these advanced development tasks involved implementation of preliminary hardware/software concepts into test beds, models, and simulation equipment to verify concepts. The size and complexity of space systems is increasing dramatically. Effective use of automation and robotics will be necessary for the S.S. *Freedom* program and other related projects to ensure effective systems management and to conserve scarce crew time.

J.M. Butler/PS04
(205) 544-4833
Sponsor: Office of Space Station

Cryogenic Storage Facility

Accomplishment of projected NASA objectives into the 1990's and beyond will require large quantities of liquid cryogenic propellants (hydrogen and oxygen) to be accessible on-orbit. The long-term storage and efficient transfer of these cryogens are essential to support the Space Transfer Vehicle, planetary probes, and lunar and Mars missions.

The Cryogenic On-Orbit Liquid Analytical Tool (COOLANT) has been developed to analyze the thermodynamic processes required in maintaining and utilizing a cryogen depot tank in a microgravity environment. COOLANT's architecture is modular in design, allowing the program algorithms and data bases to be upgraded and expanded as required (Fig. 16).*

The COOLANT code contains four major analysis modules, a tank geometry module, and a fluid and material properties data base. The No-Vent Fill Module performs receiver tank chill-down and non-vented fill. Analytical predictions include cryogen mass needed to chill a warm tank, the time required to perform the chill/fill, and the pressure history of the receiver tank during the fill process. Long-term storage boil-off losses are predicted by the System Performance Module. This module allows parametric studies on a variety of thermal control insulation systems including foam, multilayered insulation, vapor-cooled shields, and combinations of these systems, as well as the coupling of an externally mounted hydrogen vapor-cooled shield on the liquid oxygen tank. The System Performance Module can read heat rate versus time data from the Thermal Radiation Analysis System (TRASYS) program output file. Analysis of supply tank expulsion and re-equilibration times along with transfer losses are calculated by the Tank Outflow Module by modeling the thermodynamics of an autogenous pressurization system. In addition to the on-orbit analyses modules, the program contains a Settled Fill Module which allows the simulation of a vented tank

chill-down and fill under 1-g conditions for the study of ground loading of propellants onto the launch vehicle.

The Tank Geometry Module supports the analysis modules by calculating various geometry parameters for spherical and cylindrical tanks with spherical or elliptical end caps. At present, COOLANT has a fluid properties data base containing five fluids (helium, hydrogen, nitrogen, oxygen, and Freon 113), and has the capability to add additional fluids. An extensive material properties data base and several component performance modules used to model storage system penetrations and subsystems can be selected as options.

The model outputs can be represented in file format or graphically, and can be characterized by time history of quantified (boil off, pressure, flow rate, etc.) variables.

COOLANT is coded in FORTRAN 77 for a VAX VMS 11/785 operating system.

*General Dynamics Space Systems Division: The Cryogenic On-Orbit Liquid Analytical Tool User's Manual, Vol. 1, NAS8-36612.

S.P. Tucker/PD22
(205) 544-0500
Sponsor: Office of Space Flight

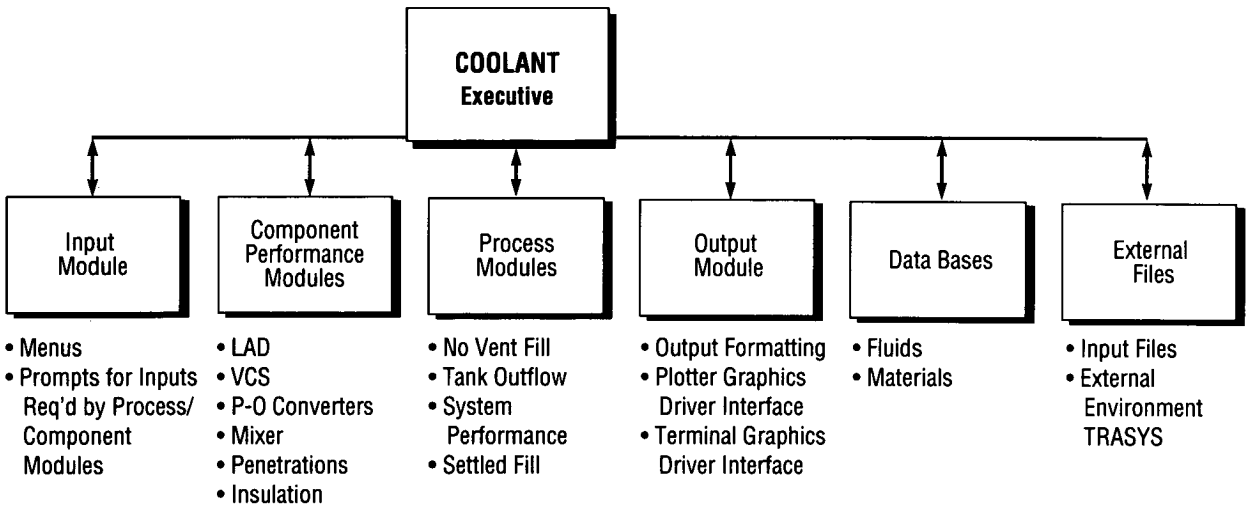

Figure 16. COOLANT Program Top Level Architecture

Tumbling Satellite Recovery

In the next few decades, NASA will be launching expensive satellites and space platforms that will require an on-orbit system to perform recovery missions to repair initial malfunctions, perform servicing and repairs, and for end-of-life retrieval. The satellites and the space platforms will be so costly that recovering them becomes an economical alternative to leaving them in space and launching a replacement system. The need for this less costly alternative, together with growing concern over space debris removal, mandates a dedicated effort to create a satellite retrieval capability as part of the U.S. space infrastructure.

With the emergence of the Orbital Maneuvering Vehicle (OMV), projected for the early 1990's, the potential for retrieving satellites will be greatly enhanced. The OMV can access satellites at orbital altitudes not otherwise achievable, and can provide the necessary maneuvering and impulse to effect capture and recovery of the satellite in a stable control mode. OMV spacecraft recovery capability

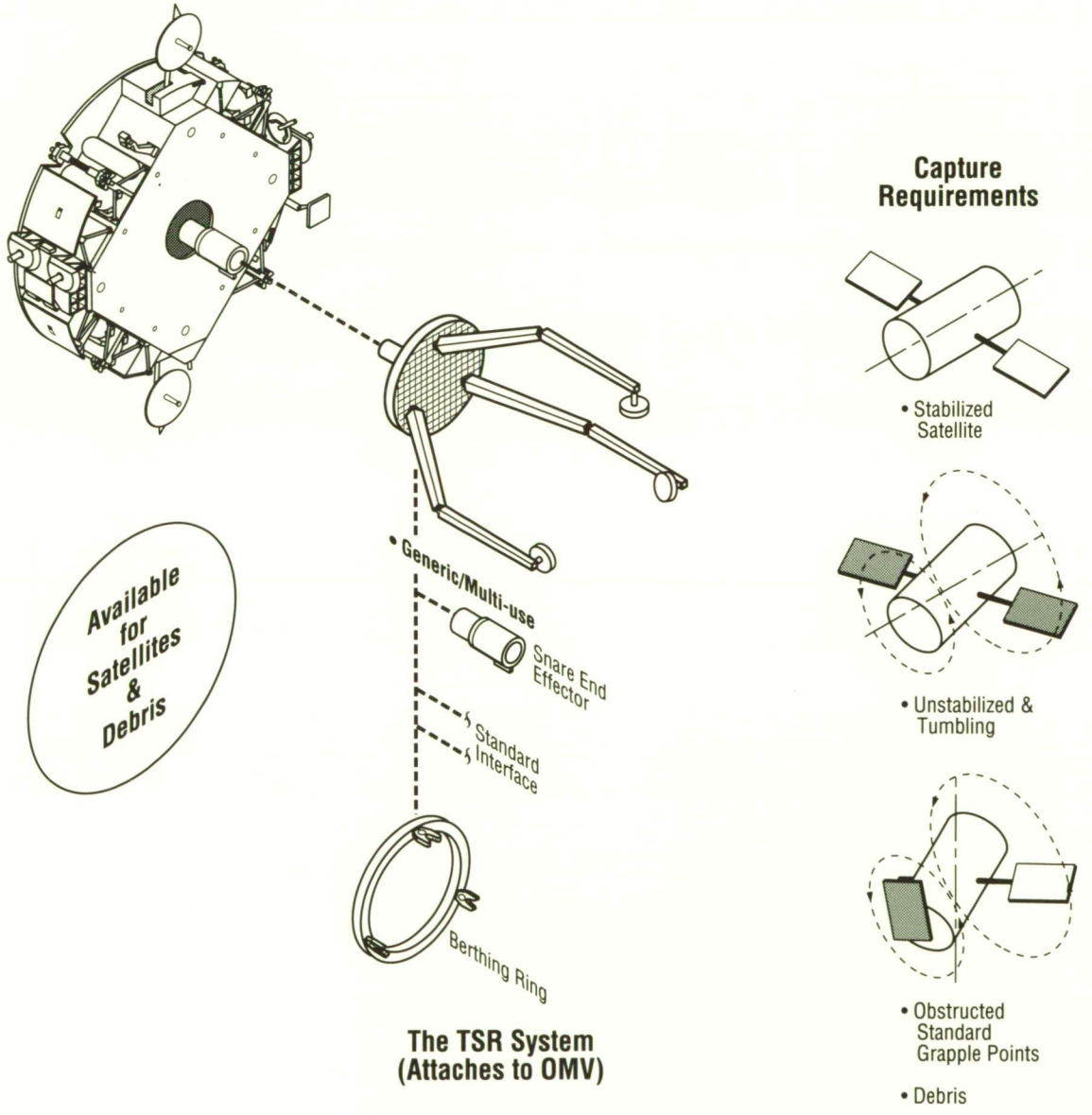

Figure 17. Tumbling Satellite Retrieval

can be extended to include unstable spacecraft and certain classes of orbital debris by the addition of special purpose mission kits. Such a kit has been under study at MSFC for several years. The work performed resulted in design and fabrication of a Tumbling Satellite Retrieval (TSR) test article and plans for initial simulation tests.

The current contracted study is being conducted in two phases. The first phase, which was completed in August 1988, defined the system concept. In the current phase, the ground test articles are being fabricated. Physical system demonstrations will be conducted in contractor and MSFC facilities. The general concept is pictured in Figure 17; however, there are many variants and areas of investigation, study, and simulation which must be performed prior to the final concept. Figure 18 reflects several approaches to resolving system requirements including analysis, ground simulation, and flight experiments.

Successful completion of these studies and demonstration activities will allow development of a TSR kit when program funds become available.

J.R. Turner/PS01
(205) 544-0617
Sponsor: Office of Space Flight

Issues	Resolution Approaches		
	Analysis	Ground Simulation	Flight Experiment
Debris characteristics (physical and dynamic)	√		
SAT characteristics (physical and dynamic)	√		
• Capture interface and mechanism design	√	√	
• Capture technique	√	√	√
• Capture object transport technique	√	√	√
• Spin/despin interface design	√	√	
• Extension arm(s) design	√	√	
• OMV thrust vector and control authority	√	√	
• OMV protection approach	√	√	
• Retrieved capture subject handoff approach	√	√	√
• Time delay operations	√	√	√
• Autonomous versus tele-op control mix	√	√	
• Control system design and integration	√	√	
• Viewing and lighting requirements	√	√	√
• Number/variety of kits	√		
• Kit modularity level	√		
• Reconfiguration capability during flight	√	√	
• Hazards handling and avoidance	√	√	
Abort capabilities and methods	√		
• Deorbit techniques and systems	√	√	√

Figure 18. Flight Systems Issues

Controls, Astrophysics, and Structures Experiment in Space

The Controls, Astrophysics, and Structures Experiment in Space (CASES) addresses critical controls and structures interaction (CSI) problems, such as stabilizing and pointing large flexible structures in space. The control of a large structure, in this case consisting of the orbiter plus a deployable 32-m (105-ft) boom, will be implemented using small cold-gas thrusters for pointing, and angular momentum exchange devices for active damping to suppress vibration. Since the boom is rigidly attached to the orbiter, the orbiter/boom system will be pointed at a predetermined target for periods of tens of minutes. In addition, tracking and slewing of the orbiter at small angular rates will be demonstrated. A significant side-effect is that during the periods of time that CASES is controlling the orbiter, disturbance levels will be very low and possibly benign for materials science experiments.

CASES will provide very accurate pointing for the Astrophysics/Solar Hard X-Ray Imaging experiment. This experiment will address important issues in high-energy astronomy, in particular the identification and characterization of the energy source seen at the galactic center, and the energy release mechanism in solar flares. Imaging of hard x rays is accomplished by aperture plates placed at the tip of the boom. This provides both coded-aperture and Fourier-transform imaging on position-sensitive proportional counter arrays placed in the cargo bay at the base of the boom. The large separation between masks and detectors makes high spatial resolution possible.

CASES astrophysics experiments enhance CSI technology demonstration experiments by providing a clear mission focus which is technically challenging with respect to the CSI problem, by generating synergism between the CSI progenitor group (technology) and a CSI user group (science), and by establishing a requirement to perform sub-arc-minute inertial pointing of space shuttle orbiters and payloads. Of these three, the mission focus enhancements are perhaps the most beneficial since these elements provide hard performance requirements and system capabilities which can only be met with CSI technology. The exceptional feature of this combined CASES science and technology mission is compatibility between science instrument requirements and the CSI technology demonstration experiment requirements. In this way, clear criteria is provided against which the success of the mission can be measured.

Science mission requirements tend to enhance CSI experiment requirements rather than override them. The quality of the science data will provide a completely independent assessment of how well the structure satisfied the requirements established for pointing, stability, twisting, and alignment.

Accomplishments in FY89 include significant progress on the ground test facility and completion of an in-house preliminary definition study. Experiment definition study contracts were awarded in mid-1989. CASES is currently manifested for launch in mid-1995.

Program Development Directorate: CASES, Preliminary Definition Study. MSFC internal document, November 1988.

J.R. Dabbs/PS02
(205) 544-0623
Sponsor: Office of Aeronautics and Space Applications

Pinhole Occulter Facility

Hard x-ray imaging of the Sun in the range 10–100 keV is very important in understanding energetic processes such as solar flares of the active Sun. The Pinhole Occulter Facility (POF) is a novel instrumentation concept which uses a 32-m (105-ft) deployable boom to position a mask, which provides occultation for coronal telescopes. It also provides coded array and Fourier-transform apertures for hard x-ray imaging. The purpose of the facility is to image the solar disk in the x-ray spectrum at higher energies than previously possible and to study the solar corona with greater sensitivity, to lower limb heights, and with greater angular resolution. It also has the capability of imaging celestial sources in hard x rays.

High-resolution hard x-ray observations of the Sun, and high-resolution, wide dynamic range observations of the corona from very near the solar limb to the outer corona are considered of major importance in the modeling of initial energy-release mechanisms in a solar flare, and also for studies of energy transport mechanisms in the low corona. The availability of the POF as a high-resolution x-ray imaging tool and as a high-resolution, wide-scale white light and ultraviolet coronal facility provides the technological advance necessary for the next generation of solar studies.

In the next phase, POF studies will continue the modeling and analytic analysis of science instruments, continue development of breadboards of critical facility subsystems to refine the mathematical models used, and study the interface and accommodation requirements for POF as a space station payload.

The POF mathematical model will be upgraded and matched to a space station simulation to simulate pointing and other accommodation problem areas. The characterization and preliminary design of an aspect and alignment system will be continued with emphasis on testing of a breadboard which will eventually be integrated into the ground-based Large Space Structure Control Verification Facility for system testing and verification. Work will continue with the POF Science Working Group to define instrument requirements and facility interfaces.

J.R. Dabbs/PS02
(205) 544-0623
Sponsor: Office of Space Science and Applications

Advanced Solar Observatory

The Advanced Solar Observatory (ASO, Fig. 19) is a comprehensive long-duration solar space observatory. It will provide solar astronomers the observational power (spectral, spatial, and temporal resolution, sensitivity, and breadth of wavelength coverage) necessary to address fundamental problems relating to: the solar convection zone and activity cycle; thermal and nonthermal processes which control the transport of energy, mass, and magnetic flux in the solar atmosphere; generation of the solar wind; and the dynamics of the inner heliosphere. The ASO was recommended as the highest priority solar physics program for the 80's in the Astronomy Survey Committee report. The ASO Science Working Group has developed an exciting concept for the evolutionary development of the ASO which encompasses four instrument ensembles: the Orbiting Solar Laboratory (OSL) which includes visible and ultraviolet telescopes; the High Resolution Telescope Cluster, which includes extreme ultraviolet, soft x-ray, and gamma-ray telescopes, and global dynamics instrumentation;

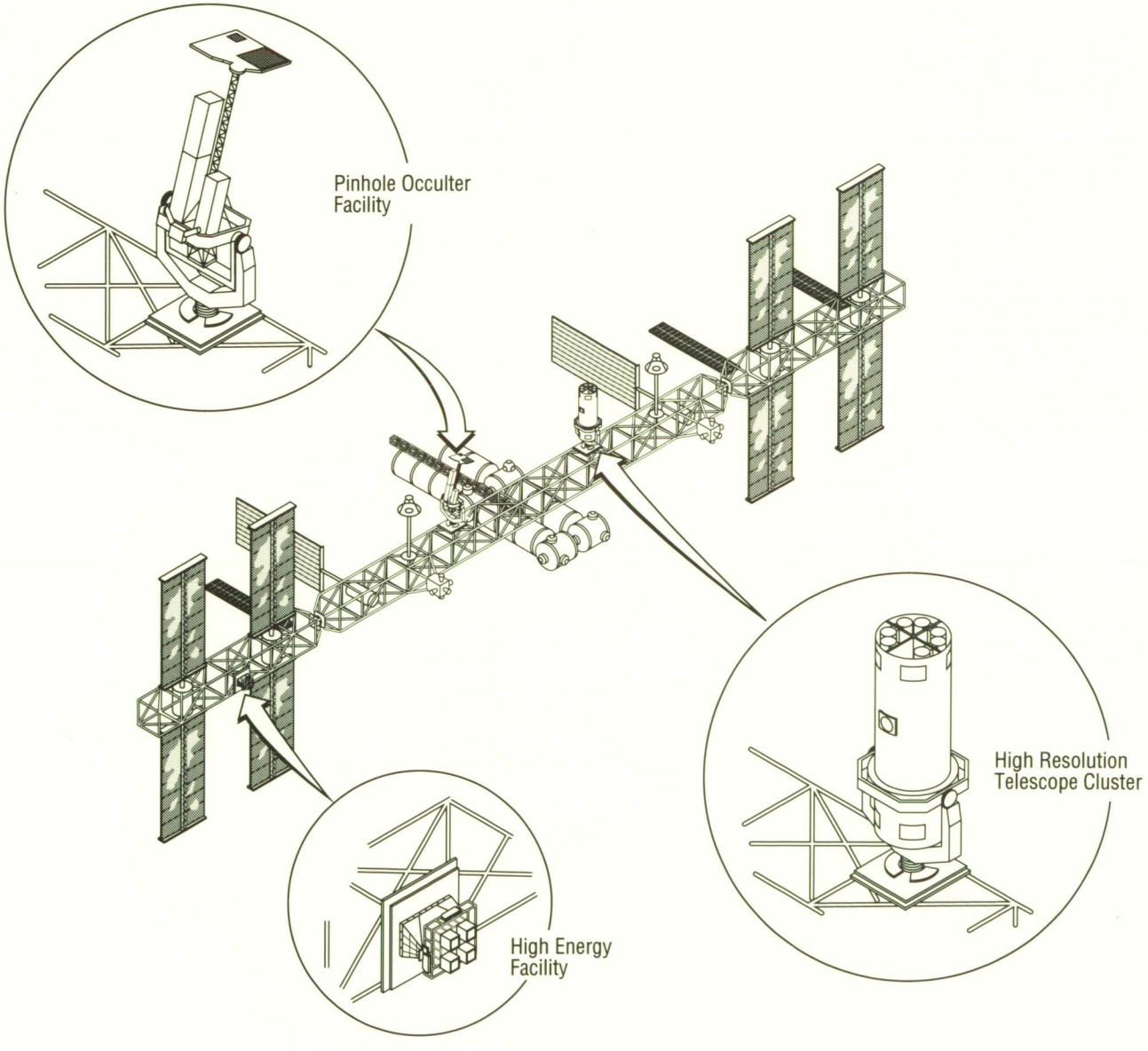

Figure 19. Advanced Solar Observatory

the Pinhole Occulter Facility, which includes Fourier transform and coded-aperture x-ray and gamma-ray telescopes and occulted ultraviolet and visible light coronagraphs; and the High Energy Facility that contains neutron, gamma-ray, and low-frequency radio spectrometers. OSL is currently the highest priority moderate mission candidate within the Office of Space Science and Applications. The ASO Science Working Group (ASOSWG) has recommended the deployment of the remaining ASO instrument ensembles on Space Station *Freedom*. The ASO will be available to the entire astronomical community.

Instrument concepts which incorporate innovative new technologies have been developed by ASOSWG and others; however, detailed scientific analysis, comprehensive engineering studies, and an assessment of the relevant technologies critical to these updated instrument concepts is essential to the further development of ASO. Preliminary results of an ongoing accommodation study have confirmed the assessment of the ASOSWG that the ASO can be accommodated on S.S. *Freedom*. However, in-depth studies are required to address critical accommodation issues, notably pointing, data handling, command, and control. A major goal of the concept study proposed herein is to carry out these detailed analyses, studies, and assessments.

The ASO is especially well suited for implementation on S.S. *Freedom* as it requires a pointing system, and power, thermal, and data rates of the magnitude that S.S. *Freedom* is designed to provide. Other unique resources that are available from S.S. *Freedom* are the ability to coordinate observations from multiple instruments, maintenance and servicing functions, and the capability of periodic replacement and upgrading of instruments on-orbit.

A contracted study defining the accommodation requirement of the ASO on S.S. *Freedom* was concluded earlier this year. Preliminary results of this study indicate that the ASO is very adaptable as an attached payload on S.S. *Freedom*.

W.T. Roberts/PS02
(205) 544-0621
Sponsors: Office of Space Science and Applications
Office of Space Station

Geostationary Lightning Mapper

A geostationary-based instrument called the Lightning Mapper Sensor (LMS) is currently under development. This sensor will be capable of detecting and locating up to 90 percent of all lightning flashes that occur within its field of view. The proposed spatial coverage includes all of the continental United States and Latin and South America as far south as the Amazon Basin, the Caribbean, and parts of the Pacific and Atlantic oceans.

The LMS uses an innovative optical design that has been optimized for the unique signal from lightning. Lightning is accompanied by the sudden release of electrical energy which is converted into rapid heating in the vicinity of the channel, the generation of a shock wave, and electromagnetic radiation ranging from extremely low-frequency radio waves to x rays. One of the strongest radiation regions is at visible wavelengths, which accounts for almost 1 percent of the total energy releases: 100 to 1,000 MW of light. These optical emissions result from the dissociation, excitation, and subsequent recombination of atmospheric constituents which are primarily affected by electron bombardment and the sudden heating of the lightning channel. The heating is so intense that emissions occur primarily at discrete atomic lines, with some continuum at shorter wavelengths. The strongest emission lines are produced by neutral oxygen and neutral nitrogen, and occur in the near-infrared from 7774 Å to 8683 Å.

With present technology, the two viable approaches for the detection and location of lightning events are either optical or radio frequency (RF) techniques. For ground-based operations, RF approaches have been preferred because optical systems suffer from obscuration, attenuation, and limited range (line of sight). Conversely, for remote sensing from space, optical techniques offer many advantages. Light is not affected by the ionosphere or magnetosphere. The relatively short wavelengths of light permit accurate direction-finding with small detectors. The large signal strength of the lightning event at optical wavelengths provides usable signals from a geostationary orbit. But radio signals at longer wavelengths are strongly attenuated or refracted by the ionosphere, and thus are unsatisfactory for accurate lightning direction-finding from orbit. At high RF, the lightning source strength is weaker than the cosmic ray background noise at geostationary altitudes; therefore, lightning detection would be extremely difficult.

A space-based sensor for the optical detection of lightning is conceptually a simple device. It is basically a staring imager that is optimized to detect and locate lightning events. The LMS images a scene in much the same manner as a television camera; however, because of the transient nature of lightning, its spectral characteristics, and the difficulty of daytime detection, actual data handling and processing differs vastly from that required by simple images. The heart of the lightning mapper consists of a very large mosaic-array, focal-plane assembly, tightly coupled to high-speed processing electronics. This signal processor performs real-time discrimination between lightning events and the background, compressing the total data rate by approximately a factor of 1 million. A request for proposals for the lightning mapper has been released to industry. The resulting contract requires a detailed design for the LMS and contains a hard option, which, if exercised, will cover the final design and fabrication of the instrument. The LMS is scheduled to fly aboard the National Oceanic and Atmospheric Administration's Geosynchronous Operational Environmental Satellite-M.

H.J. Christian/ES43
(205) 544-1649
Sponsor: Office of Space Science and Applications

Laser Atmospheric Wind Sounder

The Laser Atmospheric Wind Sounder (LAWS) moved a step closer in FY89 to its eventual position as one of the primary instruments in the Mission to Plant Earth initiative — the Earth Observing System (EOS). Two contracts were initiated with aerospace industry teams for Phase I/II feasibility and preliminary design studies. The contractors will study the feasibility of placing the LAWS instrument on one of the EOS polar orbiters (Fig. 20) or on Space Station *Freedom* (Fig. 21). The LAWS facility instrument will join five other major facility instruments as the NASA contribution to the multiagency, international EOS orbiting observatory.

During FY89, a science panel was formed to direct the development and operation of the LAWS instrument. The initial meeting of this panel at the EOS "All Hands" meeting revealed the breadth of panel membership, which includes atmospheric scientists, weather forecasters, laser technologists, and signal processing experts. An additional meeting in late FY89 will be held to continue close cooperation

Figure 20. The Laser Atmospheric Wind Sounder Mounted on a Free-Flying Orbiting Platform

between the LAWS science panel, study contractors, and MSFC in the development of this crucial instrument.

The system technology in the LAWS instrument will be a coherent Doppler lidar operating in the eye-safe infrared region. The space-based system will be similar to instruments that have been successfully used in ground-based and airborne experiments for a number of years. The system as currently envisioned consists of a pulsed, frequency-controlled CO_2 laser transmitter, a continuously-scanning transmit-and-receive telescope, a heterodyne detector, and a signal processing system. Initial studies have shown that this instrument can be accommodated on the EOS polar orbiting platform or S.S. *Freedom*.

D.E. Fitzjarrald/ES43
(205) 544-1651
Sponsor: Office of Space Science and Applications

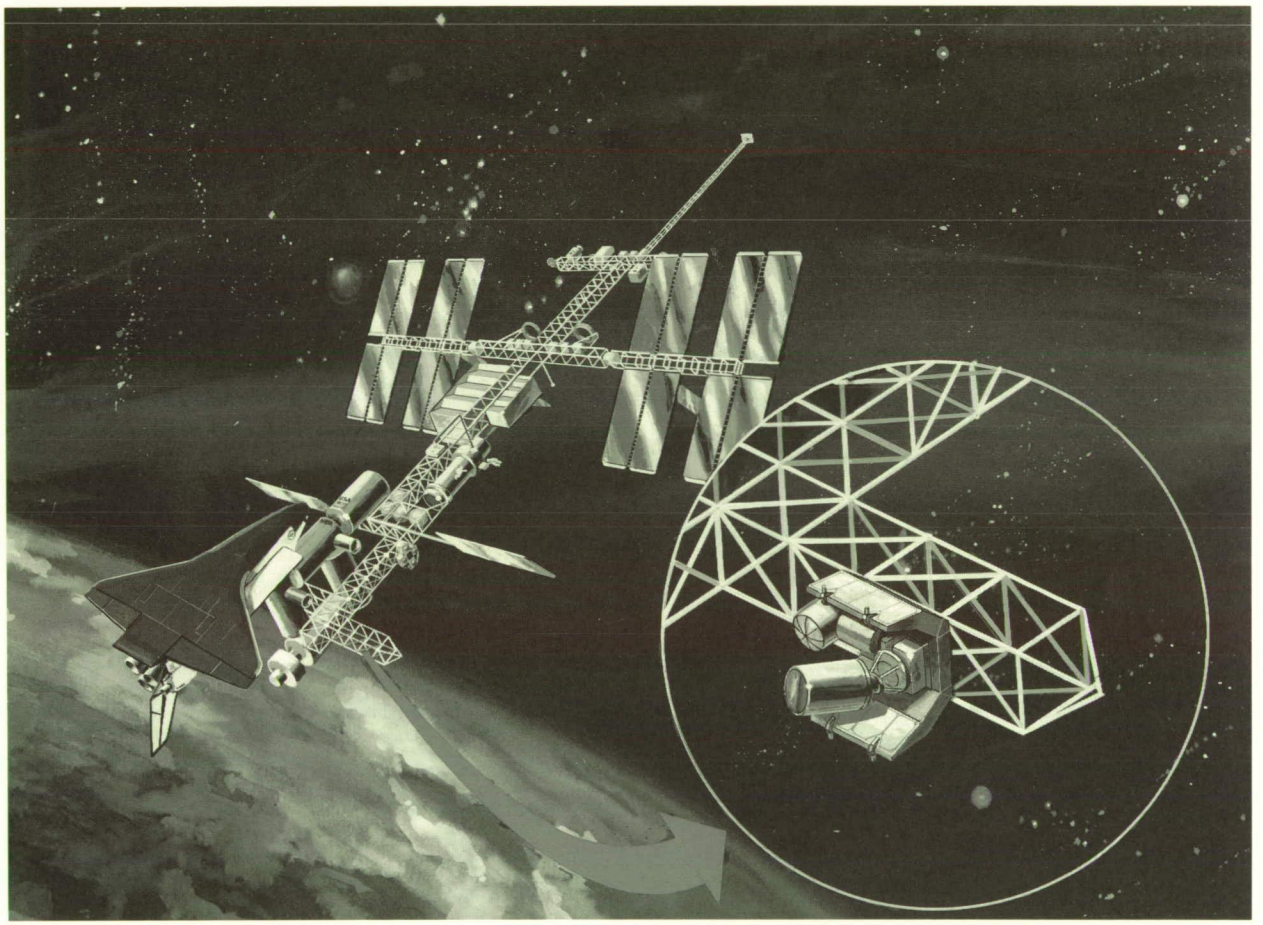

Figure 21. The Laser Atmospheric Wind Sounder Mounted on S.S. Freedom

Earth Science Geostationary Platforms

Earth Science Geostationary Platforms (ESGP) are large geosynchronous-orbit platforms that will be used to track global environmental change and provide data concerning the complex interactions among the land, sea, and atmosphere. ESGP is an integral part of the Mission to Planet Earth (MPE) initiative. This program calls for large new Earth-monitoring spacecraft to be internationally developed and launched by the late 1990's. Three of the five ESGP platforms would be developed by the United States; the others will be provided by Japan and Europe. Unlike polar-orbit platforms, ESGP will provide the advantage of continuous environmental data coverage of the entire Earth hemisphere; current polar orbiters can only see some parts of the globe at intervals of several days. Data collected from MPE spacecraft could provide an integrated model of the Earth which may allow prediction of the future course of the global environment.

In 1988, MSFC was designated as the lead center for the advanced study of the initial ESGP platform. During FY89, an in-house study team was established to develop a baseline ESGP concept, review studies on previously contracted systems, and perform platform subsystem trade analyses. Several concepts for the initial ESGP have been explored based on preliminary strawman science instrument payload complements. The instrument complement will provide data allowing the Earth to be viewed as a total system. Instruments are grouped into three classes based on their application. The first class is facility instruments which will provide observations that are multidisciplinary. Some of these instruments are similar in measurement capability to those on the Earth Observing System polar platform. The second class of instruments will support operational requirements for Earth, atmospheric, and solar measurements. The third class consists of principal investigator instruments which will allow unique measurements of Earth system processes.

Figure 22 shows a typical platform concept in deployed on-orbit configuration that will accommodate the current science instruments being discussed by the ESGP science steering committee. This present configuration weighs 4,654 kg (10,260 lb) and carries 17 payload instruments with a total weight of 1,645 kg (3,627 lb). Platform electrical power and propellant capacity is sized for a 10-year life. Over the lifetime of the platform, all of the instruments are assumed to operate continuously, while providing their own means of thermal control. As more details of the payload complement and the individual science instruments become known, ESGP concepts will be refined. Since the initial ESGP geosynchronous orbital emplacement and activation will not require crew support, the platform is a candidate for launch on an expendable launch vehicle. The Titan IV with Solid Rocket Motor Upgrade and Centaur G-Prime upper stage is the current baseline launch vehicle for the initial ESGP. In the future, payload instruments may grow in weight and perhaps in dimension. As an alternate launch vehicle, Shuttle-C could be used in place of the Titan IV. The Shuttle-C with an appropriate upper stage would increase significantly both the volume and payload delivery capability. Platform guidance, navigation, and control (GN&C) is a major design driver and has a significant effect on current stringent instrument pointing and stability requirements. Platform GN&C system operation may determine whether some of the instruments

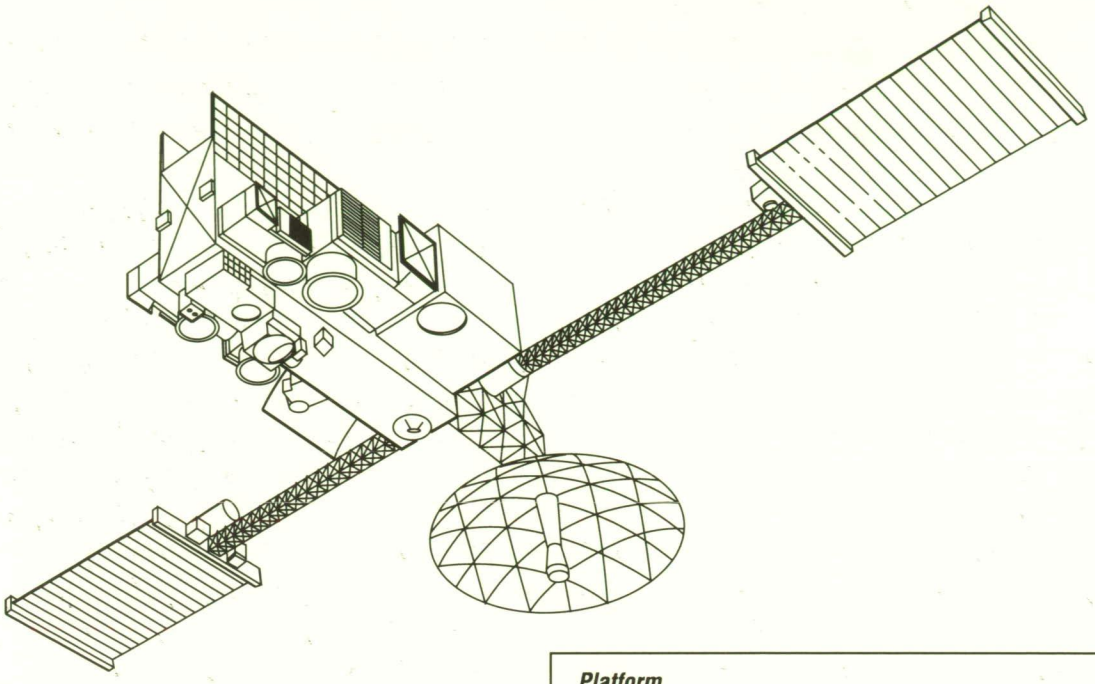

Platform	
Dimension	23 m x 12 m x 4 m (74 ft x 38 ft x 14 ft)
Bus Weight (+30%)	4,644 Kg (4,536 lb)
Total Weight (BOL)	2,057 Kg (10,239 lb)
Total Power (BOL)	2.7 kW
S/C Life	10 years
Payload	
Payload Weight	1,642 Kg (3,620 lb)
No. Instruments	17
Launcher	
Vehicle	Titan IV/SRMU
Max. Payload to Geo	5,216 Kg (11,500 lb)

BOL: Beginning of Life

Figure 22. Earth Science Geostationary Platform Typical Concept

will have to be equipped with their own pointing mounts or image motion compensation devices.

One of the major challenges of the MPE program is to integrate and manage the flow of data from all sources such as the ESGP, planned polar platforms, space station instruments, and Earth probes. Since this is an international program, information must be disseminated to scientists around the world in a timely manner. Presently, the ESGP data system is being sized to handle a high data rate of at least 100 megabits per second. The ESGP platforms may also be interconnected by optical communication data links to facilitate large data flows.

J.A. Lee/PS04
(205) 544-9290
Sponsor: Office of Space Science and Applications

Advanced X-Ray Astrophysics Program

The Advanced X-Ray Astrophysics Program (AXAF, Fig. 23) progressed during 1988-89 in the development of critical technology required to support mission objectives. The technology area receiving the greatest emphasis this year was preparation for fabrication and test of the largest mirror pair of the High Resolution Mirror Assembly (HRMA). As a specific criterion for assuring continued AXAF approval by Congress, it is NASA's plan to complete the grinding and polishing of this largest mirror pair to the required resolution of 0.5 arc-sec no later than June 1, 1991, followed by comprehensive x-ray validation testing of these mirrors later the same year in the X-ray Calibration Facility located at MSFC. To accomplish this goal, TRW and its subcontractor Perkin-Elmer are performing analyses and putting in place the necessary tooling and metrology to grind and polish the x-ray mirrors.

As a technology base, the Technology Mirror Assembly (TMA) program reached a successful conclusion with the x-ray testing of a scaled-down version of the HRMA inner mirror pair. The TMA demonstrated the techniques required for meeting HRMA performance requirements, verified the accuracy of the analytical model for predicting x-ray performance from optical surface parameters, and provided direct experimental data on the effect of particulate contamination on mirror performance.

In the area of science instruments, important progress was made in both of the instruments which have been identified with technology challenges. In the AXAF Charge Coupled Device (CCD) Imaging Spectrometer program, continued improvements in CCD performance by Lincoln Laboratories have virtually eliminated the development of a satisfactory CCD as a program concern. Chips are now available which meet the minimum performance requirements for the instrument. Future efforts will concentrate on obtaining improved performance. In the X-ray Spectrometer program at Goddard Space Flight Center (GSFC), three of the five milestones identified by the Peer Review Committee as prerequisites for Phase C/D approval have already been met. The final two milestones must be met by the end of January 1990. A significant achievement by GSFC this year was attainment of a spectral resolution of 12 eV — a value very close to the requirement of 10 eV.

C.C. Dailey/TA71
(205) 544-0571
Sponsor: Office of Space Science and Applications

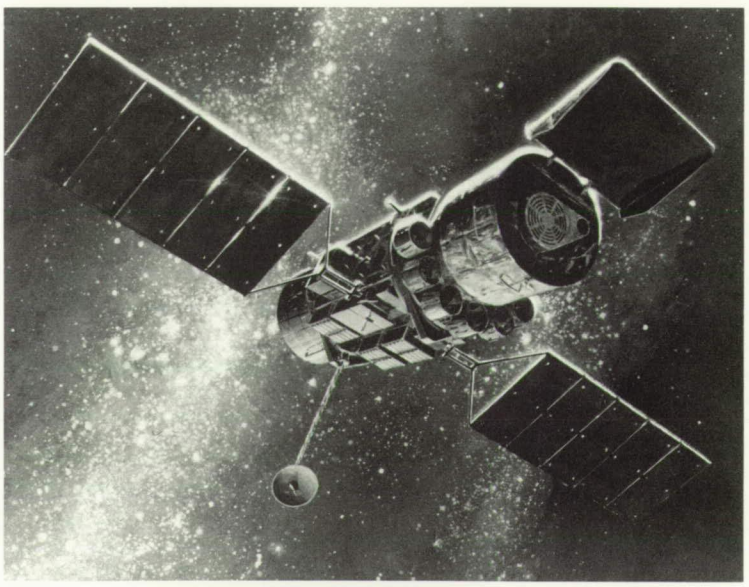

Figure 23. The Advanced X-Ray Astrophysics Facility

Gamma Ray Imaging Telescope

A potential follow-on mission to the Gamma Ray Observatory (GRO) currently under study is a Gamma Ray Imaging Telescope (GRIT) using the shuttle external tank (ET). The telescope (Fig. 24) will be configured on-orbit inside the LH_2 tank of the ET. A deployable 8.2-m (27-ft) diameter mirror that can fit through the 91-cm (36-in) diameter manhole will be used. Subsystems for telescope control and avionics will be mounted inside the intertank. The telescope, which could be launched in the late 1990's, has been under investigation at MSFC and the Smithsonian Astrophysical Observatory. It would have a collecting area of 2.5×10^5 cm^2 (3.9×10^6 in^2) and provide about 10 times the resolution of the GRO. MSFC has conducted extensive studies to solve technical problems which were identified during systems studies. These concerns include protection of the pressurized tank from micrometeoroid penetration and containment of secondary space debris caused by existing space debris and micrometeoroid impact with tank insulation, de-orbit of the tank, thermal control, reboost, and packaging of subsystem components inside the intertank.

These areas were studied this year and are now better understood. A more thorough analysis of the on-orbit thermal conditions of the tank and the telescope within the tank was made. These analyses proved that a thermal environment that is adequate for ET-GRIT operation can be maintained. Analysis of the atmospheric drag revealed a timeline for

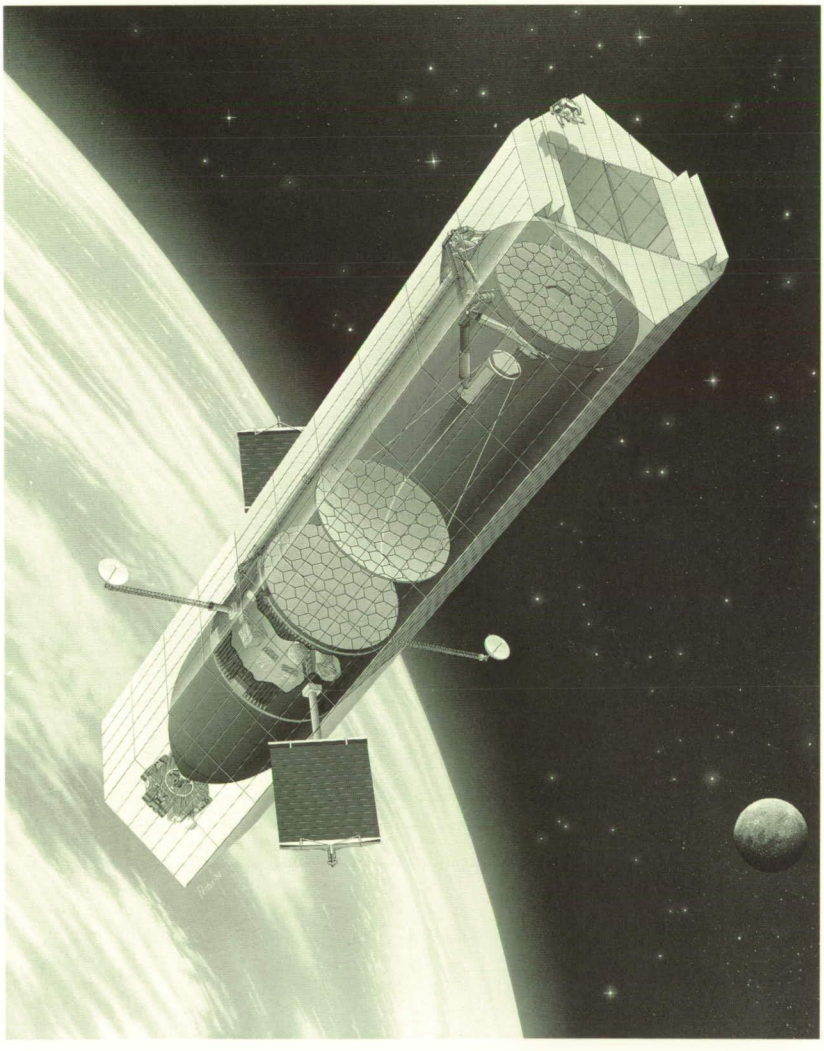

Figure 24. Gamma Ray Imaging Telescope Using Shutttle External Tank

reboost that the telescope will have to follow to accomplish the 5-year mission requirement. An analysis of placement of subsystem components inside the intertank was also accomplished. An intertank at MSFC was utilized and full scale models of the subsystems were placed inside. Placement of the components proved feasible and optimum positions were identified.

Using information prepared during last year's experimental studies in the MSFC Light Gas Gun Facility, four options for a micrometeoroid and debris penetration and containment shield were developed. These options were evaluated, and the most advantageous option was selected based on a set of criteria that included complexity, weight, and cost. The winning option (Fig. 25) weighs 7,260 kg (16,000 lb) and uses space station truss construction. Another area that is being evaluated is a GRIT de-orbit system. Design of a simple, light-weight de-orbit system that can be installed while on-orbit is currently underway. The de-orbit system is necessary to ensure that telescope re-entry is safely accomplished. This information will also be useful to anyone interested in utilizing ET's on-orbit.

In FY89, MSFC continued the development of thin-film mirror technology, which will be required for development of this telescope.

M.E. Nein/PS02
(205) 544-0619
Sponsors: Office of Space Flight
Office of Space Science Applications

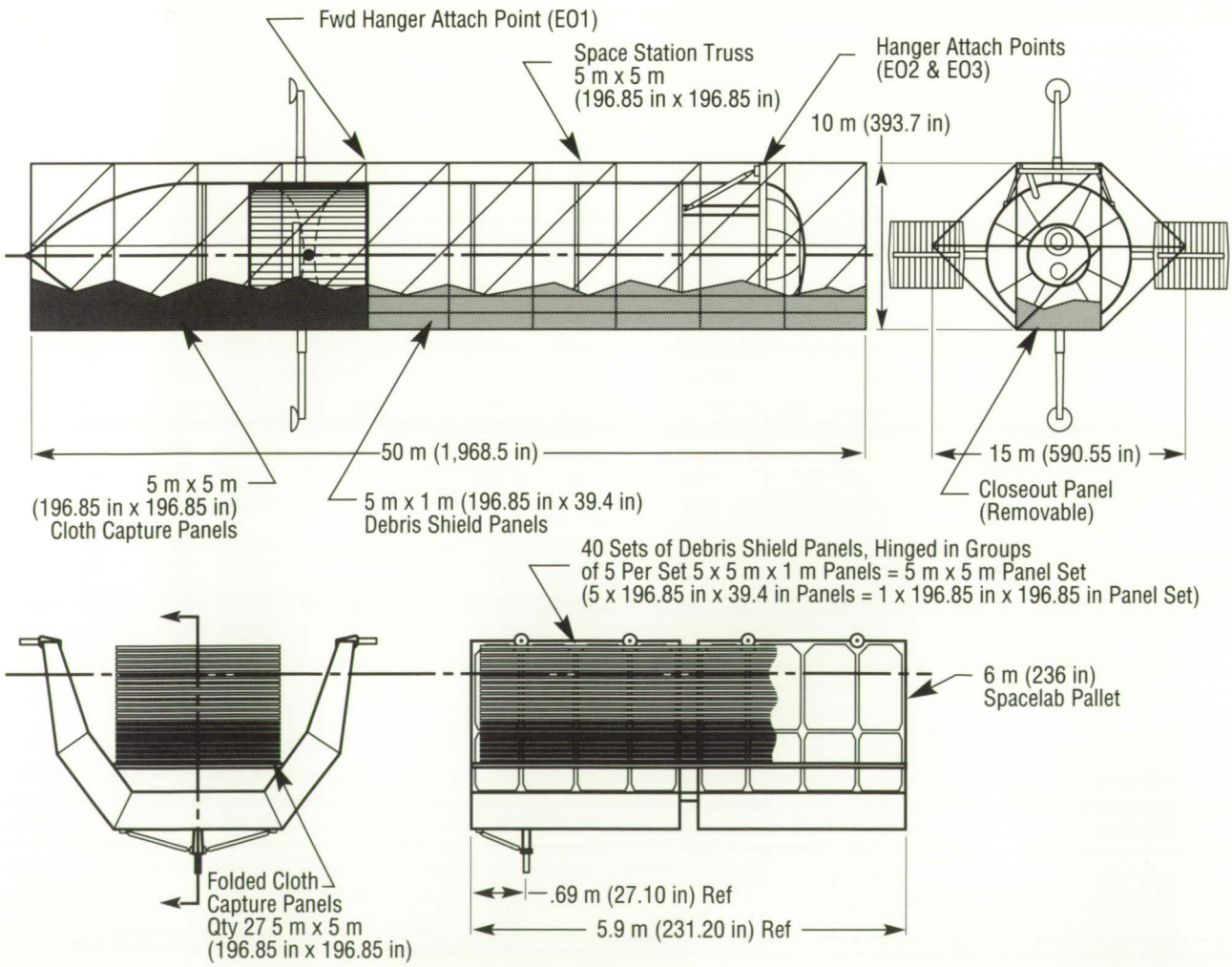

Figure 25. Micrometeroid Protection System

Data Systems

The Marshall Archival and Retrieval System

The Marshall Archival and Retrieval System (MARS) is a research and development project to develop the technology required for a high-speed large-capacity ground-based data base management and archive system. The performance criteria was to design a system that could accept data from multiple external sources at an aggregate data rate of 50 million bits per second (mbps), archive the data on-line, and make it available to the users in near real-time. The initial phase provided on-line storage capacity of 2×10^{13} bits on 125 platters. The second development phase will have the same data rate, but will have virtually unlimited on-line storage capacity.

Three major components in MARS provide the basic systems capability. A 16-port fiber-optic data bus with a passive star coupler moves the data within the system at 100 mbps. The second major component is a laser optical disk that records and reads data, using write-once read-many (WORM) media, at a sustained rate of 50 mbps. Data is recorded on the glass dual-sided 35.5-cm (14-in) WORM platter at a spot size of 0.4 μm. Encoding algorithms provide a bit error rate of 10^{-9}. The laser optical disk unit in the initial phase has an internal "jukebox" that holds 125 platters, each having a capacity of 1.6×10^{11} bits, which is equivalent to 140 fully-loaded 6250 magnetic tapes or 64 magnetic disks (300 million bytes per disk). Once recorded, the data will have an archive life of 15–20 years with no data degradation. Worst-case access time to any data in the archive is 6 s with a nominal access time of 0.5 s. The third class of components consists of four computers (Fig. 26). Three VAX 11/780's are used to monitor and control the configuration and to maintain the archive directory. VAX No. 1 executes

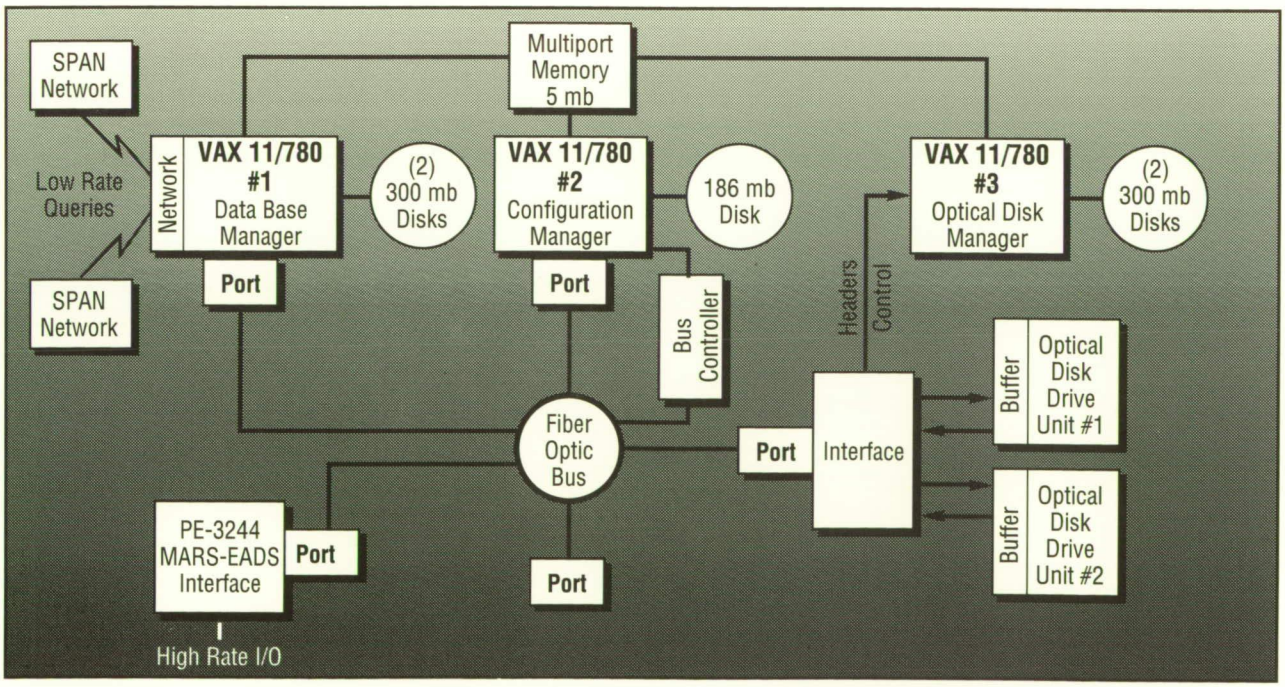

Figure 26. Marshal Archival and Retrieval System Configuration

the relational software ORACLE, which interfaces with users and generates and maintains the directory of all data in the archive. VAX No. 2 is the configuration monitor while VAX No. 3 provides the interface and controls the laser optical disk subsystem. A Perkin-Elmer 3244 is used as the interface between MARS and the high-speed data link.

A key element in the system is the use of autonomous data packets. Each packet has a header appended to the front that contains all the information required by ORACLE to make an entry in the directory. ORACLE does not look at the data itself, only the header (Fig. 27). This allows packets from totally different sources and applications to be interleaved onto disks. All users then remotely query the directory for their data with the physical location of the data being transparent.

Currently, MARS is being interfaced to the Engineering Analysis Data System (EADS) network at MSFC. The EADS interface will allow engineering test and flight data from sources such as the Space Shuttle Main Engine to be archived or retrieved, along with science data or any other data that can be logically packeted.

A second laser optical disk is also being developed. Development of the second disk will provide recording redundancy and more basic capability. This unit will have two turntables. Data packets can be recorded on one turntable while other packets are being read from a disk on the other turntable. Dual read/write heads at each turntable allow data to be recorded on a disk while other data is being read from the same disk simultaneously. The system is designed so that when a platter has been completely filled, the incoming data stream is directed to the second disk on the other turntable. This is done without any reduction in the continuous recording rate. To support continuous recording, a "mailbox" has been added to this unit. An operator can command the unit to remove a full platter from the jukebox and put it in the mailbox for external storage. The operator can then place a blank disk in the mailbox and command the system to load the platter into the blank slot in the jukebox left by the full platter just removed. All mailbox activity is done without interfering with any recording or reading activity that may be in progress. This in effect provides a continuous high-rate recording capability for an indefinite period with an unlimited storage capacity. Users will have immediate access to their data while recording is still in progress, provided the recording process is not using the entire 50 mbps bandwidth (recording has priority over reads).

Future activity will include interfacing to a higher-rate communication link that will allow MARS to be driven at its full bandwidth capacity.

B.L. Beabout/EB32
(205) 544-3611
Sponsor: Office of Aeronautics and Space Technology

Field	PL	DT	MID	SID	SSC	Time	Subsec	User	Data
# Bits	32	8	16	16	16	32	32	104	

PL = Packet Length DT = Date Type to Uniquely Identify User

Figure 27. Packet Header Keys Accessed by ORACLE

WetNet: a NASA Earth Science and Applications Data System Prototype for Global Moisture Cycle Studies

WetNet is a NASA-sponsored prototype Earth Science and Applications Data System tool that attempts to optimize the scientist's ability to conduct research and applications tasks. This involves the acquisition, management, archival, distribution, analysis, and display of meteorological data relevant to the study of the global moisture cycle. The development of WetNet is based upon the meshing of satellite and terrestrial data communication links, mainframe and personal computer workstations, optical disk technology, and interactive data base management software. Investigative teams located in the United States and the United Kingdom are focusing their research on passive microwave studies of precipitation, water vapor, near-surface ocean wind speed, ice type and concentration, and other topics relevant to the global moisture cycle. The interactive nature of this system permits sharing of algorithms for verification, inter-comparison, and modification. The results of these algorithms are derived data products which are available at MSFC for distribution to the various investigative teams.

The primary data source for the WetNet project is the Special Sensor Microwave/Imager (SSM/I) onboard the polar-orbiting Defense Meteorological Satellite Program F8 satellite. The SSM/I instrument is a passive microwave imaging radiometer which scans in four frequencies (19, 22, 37, and 85 GHz). Raw data is collected at the Fleet Numerical Oceanography Center and reduced to temperature data records which are calibrated, Earth-located data expressed as equivalent black-body temperatures. The data are then sent to the National Environmental Satellite Data and Information Service (NESDIS) for archival.

It is at this point that WetNet distributes data to a group of selected investigators (Fig. 28). The purpose of WetNet is not to circumvent or replace the data gathering and distribution process described above, but to provide a common system for data visualization and scientific analysis. The first step in WetNet data flow is for Remote Sensing Systems, Inc., to perform quality control and compact the SSM/I data. The compacted data tape is sent to MSFC for placement onto the IBM 4381 computer running the Man-Computer Interactive Data Acquisition System (McIDAS) software package. In the future, this data ingest at MSFC will be streamlined so that MSFC will ingest SSM/I data electronically into the MSFC computer directly from the NESDIS computer.

The SSM/I data is converted to image format and placed in the WetNet data base. Derived SSM/I data products are generated by applying algorithms to the data. Possible derived products include precipitation over land and ocean, integrated water vapor over the ocean, soil moisture categories, vegetation index, and sea ice type and concentration. Supplementary Geosynchronous Orbiting Earth Satellite and Advanced Very High Resolution Radiometer satellite imagery, ingested from the University of Wisconsin–Madison, are also added to the WetNet data base.

A 2-week rotating data base is maintained on the MSFC computer. This data base is available for electronic file transfer over telephone lines through high-speed modems. Remote users dial up the MSFC computer and browse through the WetNet data base to select the desired images. The selected images are then transferred to the user and displayed on a local workstation. Each of the individual principal investigators is outfitted with a workstation. The WetNet workstation is composed of a modem, a display monitor, an optical disk drive, and an IBM PS/2 Model 70 running the PC-McIDAS software package under the OS/2 operating system. The workstations perform image display, enhancement, and modification using a variety of different research algorithms.

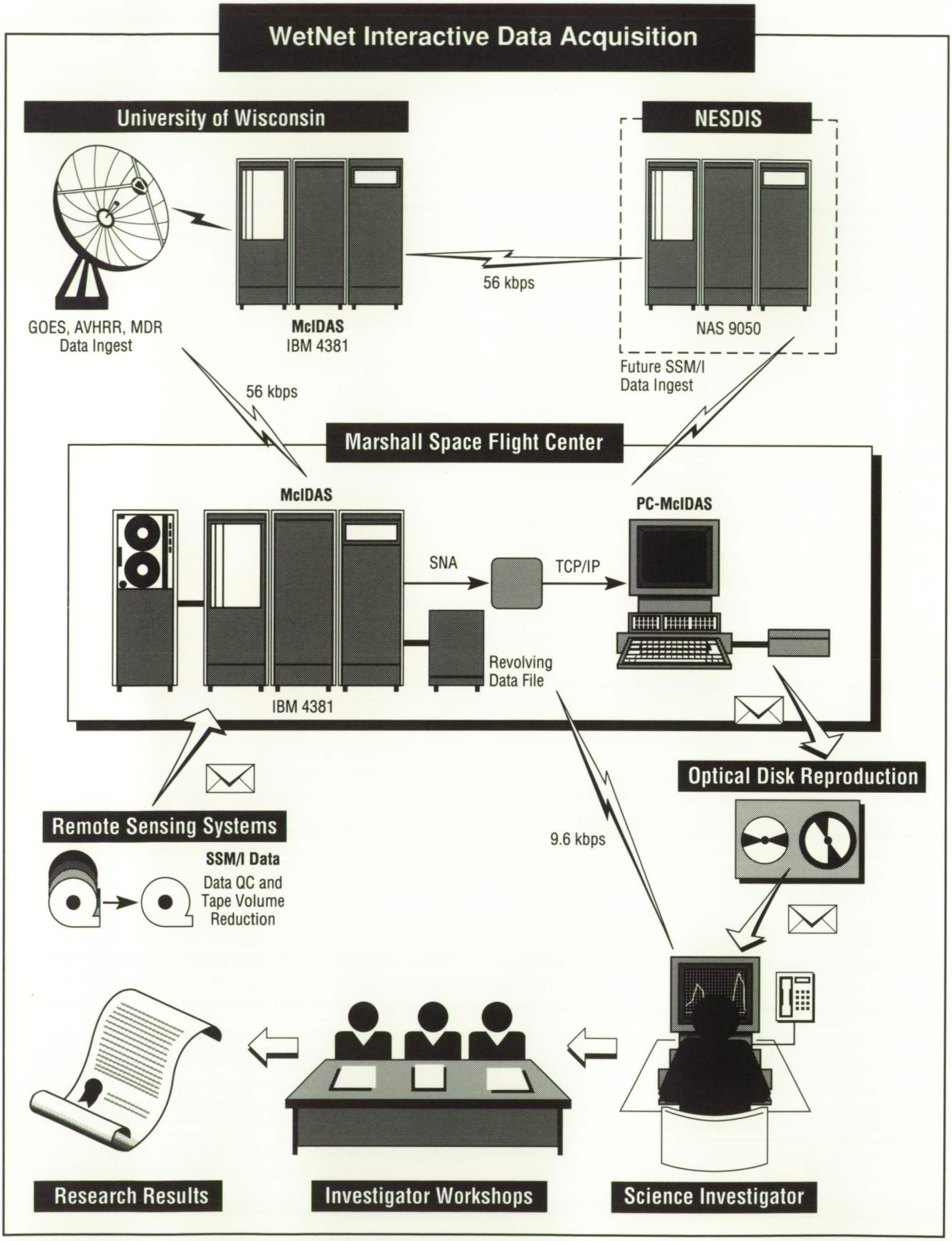

Figure 28. WetNet Interactive Data Acquisition

An alternative method for receiving WetNet data is through optical disk distribution. The daily SSM/I data stream, derived products, and supplementary satellite imagery are written to optical disk. Approximately 2 weeks of data can be placed on the optical disks and sent to investigators. This retrospective aspect of WetNet ensures that investigators receive the entire WetNet data base for their studies. WetNet is a complete package and as such all the computer equipment, data stream, browse, and image display software is provided.

The emphasis of WetNet is not on the data distribution, although this certainly is a fundamental aspect of the project. The emphasis is on providing a system which enhances the research environment and promotes a cooperative atmosphere for sharing and developing algorithms dedicated to understanding the global moisture cycle. To achieve these goals, participants are encouraged to work collegially on algorithm improvements, to contribute their results to the WetNet data base, and to evaluate the overall system in terms of interactive computer networking, image browse and data base management, and optical disk technologies.

H.M. Goodman/ES44
(205) 544-8006
Sponsor: Office of Space Science and Applications

Four-Dimensional Man-computer Interactive Data Access System Technology

The Man-computer Interactive Data Access System (McIDAS) has been under development at the Space Science and Engineering Center (SSEC) of the University of Wisconsin–Madison for 19 years. During this period, the software and data bases have grown extensively. The system has been used for the analysis and display of two-dimensional meteorological data, e.g., satellite imagery, temperature contours, etc. Under support from MSFC during FY89, SSEC has been developing a four-dimensional (4-D) analysis and display tool. Since the Earth-atmosphere system is a volume which is evolving in time, a tool is needed that will allow scientists to visualize various and multiple parameters from varied viewing geometries.

The eventual goals of this effort are to design and implement a 4-D data management system within McIDAS and design and develop the software and hardware necessary for interactive display of Earth-systems data. This should provide tools which will render complex 4-D fields of environmental data sets interactively, allowing rapid integration of interdisciplinary Earth science data sets into one display. The system will be used for qualitative and quantitative interpretation.

Toward these goals, the following tasks were accomplished during FY89: the software was utilized to visualize water drainage through soils and the three-dimensional structure of a cave system; a decision was made as to which commercially available hardware to purchase as the new video system — the Stellar GS-1000 series machine was chosen due to its ability to render graphics rapidly, yet still maintain generic computational capabilities; and portions of the McIDAS system have now been ported to the Stellar device allowing for the data management and display of 4-D data sets. Figure 29 is representative of McIDAS output on the GS-1000. It depicts several properties of a mature thunderstorm. Cyan represents the 0.5 gm cm^{-3} water

vapor isosurface, which in this case is indicative of the outer cloud boundary. Red represents the vertical velocity field of 10 m s^{-1} (33 ft s^{-1}). Also included are wind trajectories showing the source and destination of air parcels. The Stellar device has allowed the rendering of complex views such as Figure 29 in near real-time. It allows interactive change of viewing angle or time animation of the data sets. Note the use of transparency to visualize the vertical velocity field contained within the outer cloud shell. Another powerful aspect is the ability to interactively change the analysis level of an isosurface. For example, if one were viewing the 273 K temperature surface, the current view could be switched to a 290 K surface with the click of a button. Within seconds, a new view is generated. The new hardware has greatly increased efficiency. What used to take 8 hours of computation using standard McIDAS on an IBM mainframe is now performed in approximately 3 minutes on the GS-1000. This should allow scientists to ask new and more insightful questions about the interactions of Earth science parameters.

Planned activities for FY90 include greater generalizations of McIDAS software to operate under the Unix and X-Windows environment. Improved utilization of the GS-1000 may allow the blending of real-world versus modeled results in one display. Work remains to be done on obtaining a quantitative understanding of these data volumes. The Stellar GS-1000 will be upgraded to a model which is approximately 2 times faster. Porting the McIDAS code to the Cray supercomputer at MSFC will also be explored.

Hibbard, W.L.: Visualizing Large Data Sets. Preprints, Fifth Conf. on Interactive Information and Processing Systems for Meteorology, Oceanography, and Hydrology, Anaheim, CA, American Meteorological Society, pp. 172–174, 1989.

P.J. Meyer/ES43
(205) 544-1654
Sponsor: Office of Space Science and Applications

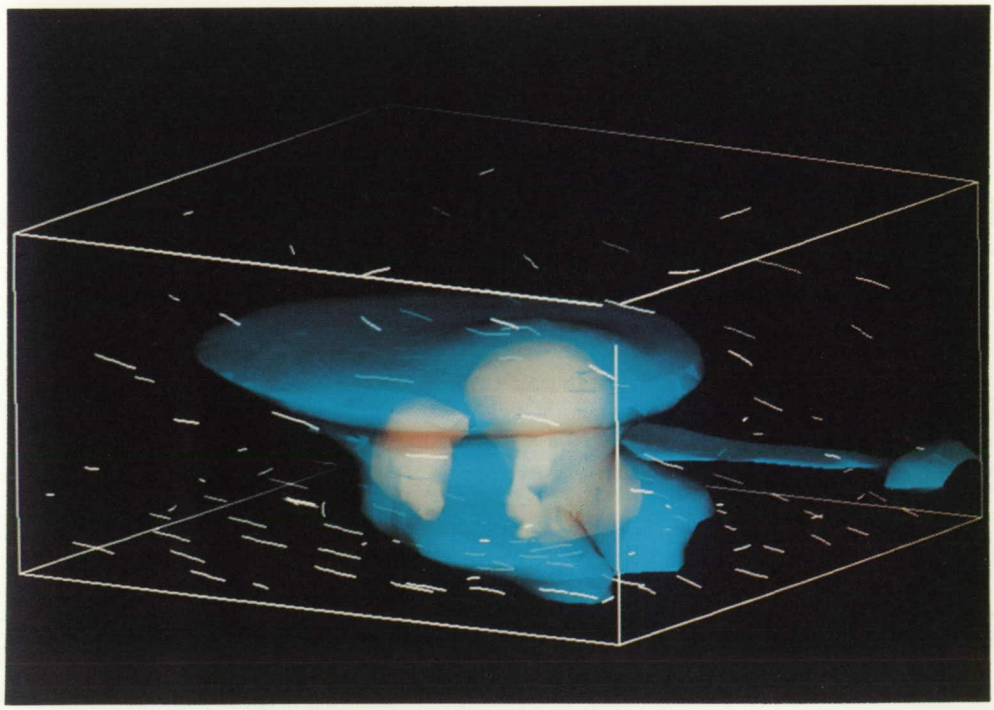

Figure 29. Thunderstorm as Visualized by McIDAS

Personal Computer Man-computer Interactive Data Access System

The University of Wisconsin's Man-Computer Interactive Data Access System (McIDAS) has been in use at MSFC since the late 70's. Since then, the software and the hardware have both evolved enormously, and the software is now running on an IBM 4381 mainframe, and on personal computers (PC's) using PC-McIDAS. There are two mainframe workstations, but anyone with PC-McIDAS has access to most of the mainframe's imaging, graphics, and computing capabilities. Currently, about half the personnel in the Earth Science and Applications Division are capable of using PC-McIDAS at their desks.

PC-McIDAS was first used at MSFC in 1987 on PC's with the MS-DOS operating system. In 1989, the University of Wisconsin released a version for IBM's new OS/2 operating system. With the source code available, existing McIDAS programs can be altered and new ones can be created on the PC. The mainframe code is also portable to the PC, allowing old programs to take advantage of the PC's small but "dedicated" processor.

There are currently two major division projects involving PC-McIDAS: the Multispectral Atmospheric Mapping Sensor (MAMS) Quick View System and WetNet (MSFC's prototype data network for precipitation process research). The MAMS project will use PC-McIDAS to provide researchers quick results of instrument performance in the field. Without this capability, it would be hours before it was known whether or not each flight was a success. The WetNet project is just getting underway and will involve about 30 principal investigators around the country using pseudo real-time microwave data from the Special Sensor Microwave/Imager. Each investigator will have a personal computer (IBM PS/2 with 80386 processor) and interactive access to MSFC's mainframe McIDAS, as well as the means to communicate with other principal investigators.

P.J. Meyer/ES43
(205) 544-1654
Sponsor: Office of Space Science and Applications

Image Processing and Computer Graphics

The Integrated Computer-Aided Design (CAD)/ Image Processing System is a dedicated computer graphics system built around the Digital Equipment Corp. VAX-11/785 superminicomputer. An International Imaging Systems Model 75 image processing system and an Intergraph CAD workstation, along with image translation software, provide the VAX with a powerful graphical analysis capability. Both remotely-sensed imagery and manually-digitized photographs can be viewed, enhanced, manipulated, and overlaid with two- or three-dimensional graphic designs. The digital image can also be warped to match control points in the design file. Hidden-surface rendering of a design model can be transported to the image processing station for further enhancement and frame loop animation. Images can also be transferred to a Stellar GS-1000 graphics workstation, which can manipulate extremely large images.

The system is used for image analysis and data visualization tasks associated with sensor development and atmospheric phenomena studies, and also supports mission projects in phases from conceptual design to flight support. The integration of image processing and CAD has resulted in more generalized approaches to the solutions of a wide variety of research and development problems.

J.V. Parker/ES43
(205) 544-1526
Sponsor: Office of Space Flight

Low-Gravity Fluids and Materials Processing Data Base

A data base identifying more than 600 fluids and materials processing experiments performed in low gravity is maintained and updated in the Space Science Laboratory. The compilation has been separated into two parts, designated as version 1 and version 2. Version 1 represents a complete listing of experiments performed during the Apollo, Apollo-Soyuz, Skylab, and U.S. space shuttle missions. This version also includes a listing of sounding rocket experiments performed under the programs of the United States (Space Processing Applications Rocket), West Germany (TEXUS), Japan (TT-500A), and Sweden (MASER). Version 2 represents only a partial listing of experiments performed under the Soviet space program. Within this version, research efforts completed during sounding rocket, Soyuz, Salyut, and MIR missions have been identified. Together, versions 1 and 2 reflect scientific contributions and technology from more than 25 countries.

Although hundreds of experiments have been completed in the space environment, fluid response related to low-gravity acceleration is still not well understood. Thus, creation of the data base was motivated by the need to highlight basic flow processes which govern most low-gravity fluids experiments. It is expected that by categorizing research efforts by similar flow physics, fluid dependence on system parameters and low-gravity disturbances will be more efficiently identified. Flexible computational models which can examine the fluid response of several classes of experiments may then be more effectively employed to achieve improved experimental control.

A typical experiment within version 1 is represented in Figure 30. General information is available concerning principal and co-investigators, mission, launch date, etc. Short descriptions outlining experiment goals, setup, and space results are being prepared. Experiments are categorized by major and minor subject titles (key words) identifying similar flow and system parameters. A thesaurus

Principal Investigator(s): Schafer, C.F.
From: NASA Marshall Space Flight Center, Huntsville, AL

Co-Investigator(s): None

Experiment Origin: USA
Mission: SPAR 1
Date: Dec. 1975
Launched From: White Sands Missile Range, NM
Payload Type: Sounding Rocket Experiment
Processing Facility: Temperature Control Unit (TCU) Furnace: Heaters, Sample Cartridges, Water Quench System, Sample Monitoring Thermistors
Builder of Processing Facility: Developed by NASA Marshall Space Flight Center, Huntsville, AL

Experiment: Characterization of Rocket Vibration Environment by Measurement of Mixing Two Liquids (74-18)

The first of a series of two experiments, designed to illustrate the nature of the SPAR rocket acceleration environment and its effect on diffusion controlled fluid systems was performed on SPAR 1. Three cylindrical samples, each composed of a section of indium joined to a similar section of indium-lead, and each aligned differently with respect to the rocket longitudinal axis and accelerometer axes, were melted and solidified during the low gravity coasting phase of the rocket. The density differences of the two molten materials were chosen to allow convective mixing to occur if sufficient residual gravity was present. Post flight, In-(In-Pb) interfaces were examined. The sample "...(oriented parallel to the payload longitudinal axis) experienced interface motion near that of expected from diffusion...<the> sample (aligned parallel to the accelerometer x-axis) experienced a small amount of interface motion...which might be slightly more than that expected by diffusion...<and the> sample (aligned parallel to the accelerometer y-axis) experienced flow down one side of the container." (1, p. IV-27) Both experimental and computational correlation of fluid motion with acceleration environment was performed. It was observed that the "...magnitudes of the flow experienced by the three samples...were consistent with the acceleration arising from the rotation of the payload about its longitudinal axis..." (1, p. IV-36) and that convective motion is possible in the low gravity environment.

Key Words
Melt and Solidification,* Water Quench, Convection, Alloys, Density Differences, Mixtures, Alloys, Rotation of Payload, Effects of Spacecraft Microaccelerations

Materials
3 Indium/Indium-Lead Alloy Samples were processed: (80 wt% In, 20 wt% Pb) In*Pb*. Shape, size and kinematic viscosity of employed samples were representative of systems of interest to other investigators. Cylindrical aluminum sample containers housed "...a 7/16 in. long by 1/4 in. diameter solid cylinder of indium joined to a cylinder of In-Pb of the same size, forming cylinders 7/8 in. long by 1/4 in. in diameter..." (1, p. IV-4)

Experiment Applications
It is expected that the low gravity experiment will reduce convective flow in systems with density gradients. This experiment illustrates the need to characterize the acceleration environment and to consider the effects of possible fluid motions even at low acceleration levels.

Publications
1) Schafer, C. F.: Liquid Mixing Experiment. In Space Processing Applications Rocket Project, SPAR I Final Report, NASA Technical Memorandum TM X-3458, pp. IV-1 – IV-37, December 1976 (Post Flight)

2) Schafer, C.F., and Fichtl, G.H.: SPAR 1 Liquid Mixing Experiment. 15th AIAA Aerospace Sciences Meeting, 15th, Los Angeles, CA, Jan. 24-26, 1977, 8p. (Post Flight)

3) Toth, S., and Frayman, M.: Measurement of Acceleration Forces Experienced by Space Processing Applications, Goddard Space Flight Center, Contract No. NAS5-23438, Mod. 23, ORI INC, Technical Report 1308, March 1978 (Acceleration Measurements, SPAR 1-4)

Contact: C.F. Schafer
EP55
Marshall Space Flight Center
Alabama 35812

Figure 30. Typical Version I Experiment

listing these titles is being prepared and will enable users to search quickly for subjects of interest. An excerpt from the key words thesaurus can be seen in Figure 31. Each bold-faced word in Figure 30 represents a field for which information can be searched, and each has its own thesaurus. For example, the Materials Thesaurus lists the fluids or processed materials implemented in the space investigation.

Data base information has been obtained by a number of methods, mostly via extensive literature searches. Thus, the status of the information available on each experiment depends greatly on the amount of documentation available describing the experiment. Publications often do not contain specifics such as principal and co-investigator designations, processed sample identifications, or even ground-based versus reduced gravity research distinctions. Because data concerning past experimental space efforts have proved so difficult to resolve and obtain, the Center for Space Advanced Technology has been contracted to aid in the verification, acquisition, and completion of experiment-related information. Principal investigators are being asked to review the available data base information for accuracy and to make additions/corrections where appropriate. Investigators are also given the opportunity to write an experiment summary paragraph describing their objectives, setup, and results. After response (or lack thereof) from the principal investigators is documented, experiment information still incomplete is summarized as much as available documentation permits. A hard-copy release of version 1 discussing experiments performed prior to February 1986 is targeted for late 1990. Lack of principal investigator response is an uncontrollable variable in the preparation of the document and unfortunately delays the final publication.

Currently, the compilation is maintained in a commercially available data base software package. The data entry panel was designed at MSFC. The menu-driven system is easy to use, and searching and sorting capabilities are, for the most part, extremely efficient. Computational data base release options are still being reviewed.

C.A. Winter/ES42
(205) 544-1695
Sponsor: Office of Space Science and Applications

Key Words Thesaurus Excerpt

Fluids

Aqueous Solutions	Capillary	Eddies
Benard Cells	Chemical Potential Convection	Evaporation
Binary Fluids	Condensation	Floating Zones
Boiling	Contact Angle	Fluids
Bubble	Convection	Fluid Transfer
Bubble Distribution	Critical Point	Free Surface
Bubble Drop Migration	Cryogenics	Homogeneity
Bubble Formation	Diffusion	Hydrodynamics
Buoyancy-Driven Convection	Drops	Immiscible Fluids
Buoyancy Effects	Drop Vibration	Interfacial Energy

Materials Processing

Acoustic Positioning	Coatings	Dopants
Acoustics	Composites	Electrophoresis
Alloys	Containerless Processing	Emulsions
Axial Segregation	Crytallization	Epitactic Layers
Binary Alloys	Dendrites	Eutectics
Brazing	Deposition from the Gas Phase	Ferromagnetic
Bridgman Growth	Direct Crytallization	Films
Catalysts	Directional Solidification	Foams
Cellular Morphology	Dispersion	Glasses
Chemical Vapor Transport	Dispersion Alloys	Growth from Melt

Figure 31. Key Words Thesaurus Excerpt

Specialized Field Program Data Base Concepts

MSFC Earth science and applications field program data base activities include work in the following field programs: Cooperative Huntsville Meteorological Experiment (COHMEX), Global Backscatter Experiment, Mauna Loa Aerosol Backscatter Intercomparison Experiment, sensor development support data, and preliminary work in the Kennedy Space Center Airborne Field Mill Study. Data base structure design and implementation for these field program data sets are progressing with both mainframe and PC/AT computers.

ORACLE, a commercial relational data base management system, was chosen as the kernel to manage the field program data. A PC/AT version of ORACLE was installed to begin design work of a generic field program data base system using the COHMEX data as a prototype. COHMEX was selected because of its diverse data types and data formats. Due to the virtual size of the actual data, only catalog information could be stored and retrieved on the PC/AT. However, the PC/AT proved to be a good data base design and development tool, including the installation and testing of a menu selectable system. Also, data base tables could be uploaded to a mainframe version of ORACLE. Initial work on integrating PC-ORACLE and PC-McIDAS (Man-computer Interactive Data Access System) in the DOS environment began, but was abandoned due to random access memory conflicts between the two programs. This integration will be continued under the Operating System (OS)/2 environment with the release of OS/2 ORACLE in September 1989.

A mainframe version of ORACLE was installed on an IBM 4381 computer to continue development work and provide a link between the actual data and the catalog/directory information. The concept is to archive/retrieve data directly from the Masstor storage system, as well as to transfer files directly with McIDAS using ORACLE as the data manager. All operations will be transparent to the user, and ORACLE will perform all catalog file transfers and update the archive catalog accordingly. Again, COHMEX data sets were chosen as a prototype because of the previous data base design work completed on the PC/AT and the accessibility of COHMEX data stored on the Masstor archive. Menus have been designed to provide access to ORACLE from the Earth Science and Applications Division, and COHMEX directory information has been uploaded to the mainframe. Preliminary work has commenced to provide "hooks" from ORACLE to the Masstor data archive.

A standardized naming convention for Masstor archive files was designed to work with the ORACLE manager. Existing Masstor file names were converted, and all new data are presently archived accordingly. This standardization will permit ORACLE to name and archive Masstor files automatically, as well as search and retrieve existing files. Work is continuing to archive new data from all field program activities using this convention for future data base needs. In the interim, an Earth Science and Applications Division satellite data base of images archived on Masstor is currently maintained on PC/AT's for use by researchers.

J.E. Arnold/ES43
(205) 544-1646
Sponsor: Office of Space Science and Applications

Global Backscatter Experiment Data Base Development

As part of specialized field program data base activities, development of a Global Backscatter Experiment (GLOBE) data base has started. The purpose of GLOBE is to determine typical values and the spatial/temporal variability of aerosol backscatter at carbon dioxide wavelengths in clean background air masses on a global scale. This information is critical to simulation and design studies for the Doppler Laser Atmospheric Wind Sounder (LAWS), which MSFC will develop as a facility installation on NASA's planned Earth Observing System in the 1990's. To facilitate GLOBE data transfer from worldwide sources to LAWS design contractors, a central data base will be maintained by MSFC.

Current GLOBE field activities include routine measurements taken on a global scale by various countries and agencies, such as the Mauna Loa Aerosol Backscatter Intercomparison Experiment (MABIE) held in Hawaii, November 1988, and the upcoming GLOBE first survey flight over the Pacific Ocean in November 1989. The GLOBE data base was designed for the IBM PC/AT (due to the relatively small size of the data base) using existing GLOBE data sources. Figure 32 shows the proposed GLOBE data base structure and the data flow from the principal investigators (PI's) to the PC/AT. Considerable effort is underway to standardize compatible formats from individual PI's. Data sets collected from MABIE are being used as the initial "test" input into the data base.

Preliminary work is underway in the planning of the GLOBE first survey flight to create a real-time data base for inclusion into the central data base as a partitioned data set. Other data sets collected from other GLOBE investigators will be added to the data base as they become available. Networking requirements of the GLOBE data will be evaluated as needs dictate.

J.E. Arnold/ES43
(205) 544-1646
Sponsor: Office of Space Science and Applications

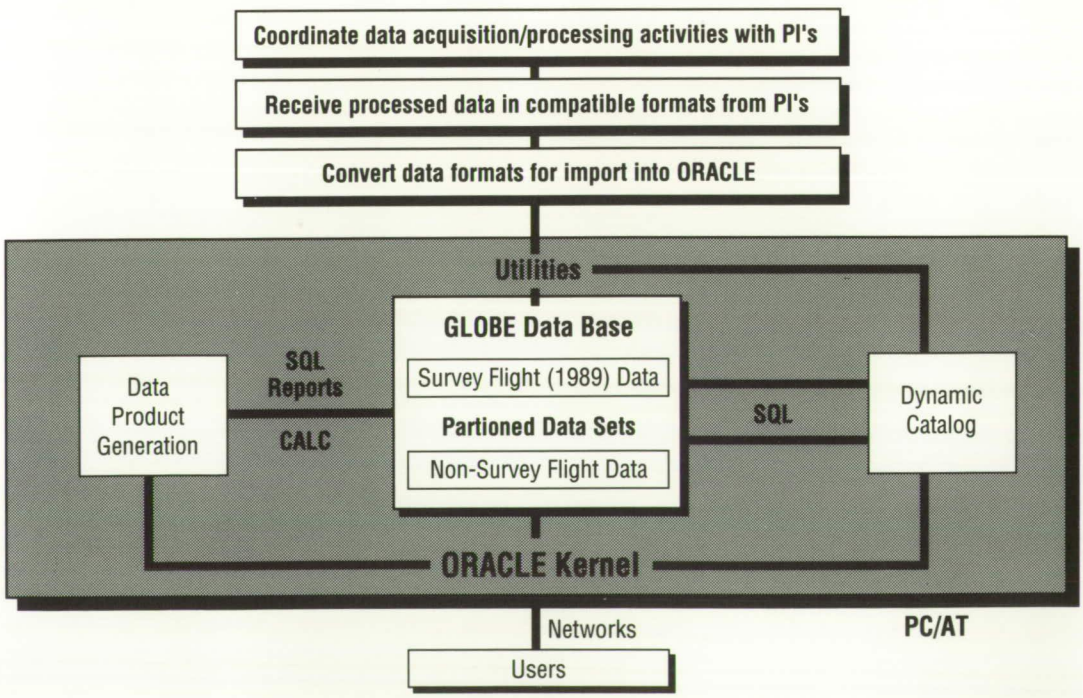

Figure 32. Proposed GLOBE Data Base Structure

The Process Development Advisor — Information Management for Process Development and Control

The necessity for integration of information and experimental data required for development of new chemical systems and automated processes for the Thermal Protection System of the Space Shuttle External Tank (ET) project has lead to the development of a generic information management system for engineering development of processes.

Information about chemical processes exists at multiple levels of complexity. The process engineer uses information from the heuristic level ("rules of thumb"), from the empirical level generated by experimentation, and from the causal level where rigorous mathematical treatments may be available. A constant dialogue among materials engineers, process engineers, equipment designers, and controls engineers is necessary to understand the trade-offs and arrive at an optimum balance of physical properties, processability, and consistency in any chemical processing scenario.

To meet these needs, a Process Development Advisor (PDA) has been designed by Martin Marietta and MSFC to organize process characterization and allow process optimization. The PDA is a "coupled" software system of both numerical and symbolic computer processing methodologies for representing process knowledge at multiple levels of complexity.

The PDA provides a contextual language for describing process relationships which cross traditional engineering boundaries by treating all process knowledge as a continuum of discrete, yet interrelated components. This software tool supports the porting of processes from laboratory development to implementation on the production floor. The PDA provides the capability to acquire and refine knowledge of machine performance and processing characteristics of foam materials targeted for use as thermal protection on the ET.

A key objective of PDA development is the implementation of statistical experimental design methods to capture, understand, and enhance development of process data. Knowledge gained from statistically designed experimentation will be stored in the form of empirical models. The techniques of response surface modeling are employed to design the experiments, produce models, and analyze the information to determine relationships between factors and responses. Contour plots will be generated to aid the visualization of response and factor interactions.

The objective of response surface investigations is the empirical determination of functional relationships between variables and their interactive effects. The use of balanced, orthogonal experiments greatly increases the likelihood of determining and quantifying the relationships between measurable variables. In both material formulation and equipment development, contour plots will be generated and maintained within PDA. The combination of models from both the material and equipment components of processing will allow a complete definition of processing windows and clearly present the ranges of producibility for the desired product.

Figure 33 shows the architecture of the PDA system. The user interface provides access to statistical design and analysis modules. Empirical models of machine controls, reaction mechanisms, intermediate process parameter effects, and their relationship to the requirements and desired properties of the product are stored in the case memory. Once the limits of producibility are established during process development within PDA's Experiment Design and Analysis modules, system parameters and their appropriate processing ranges may be set for process control. Problems detected with a process can flag specific development cases for recall, reasoning, and diagnosis of the process.

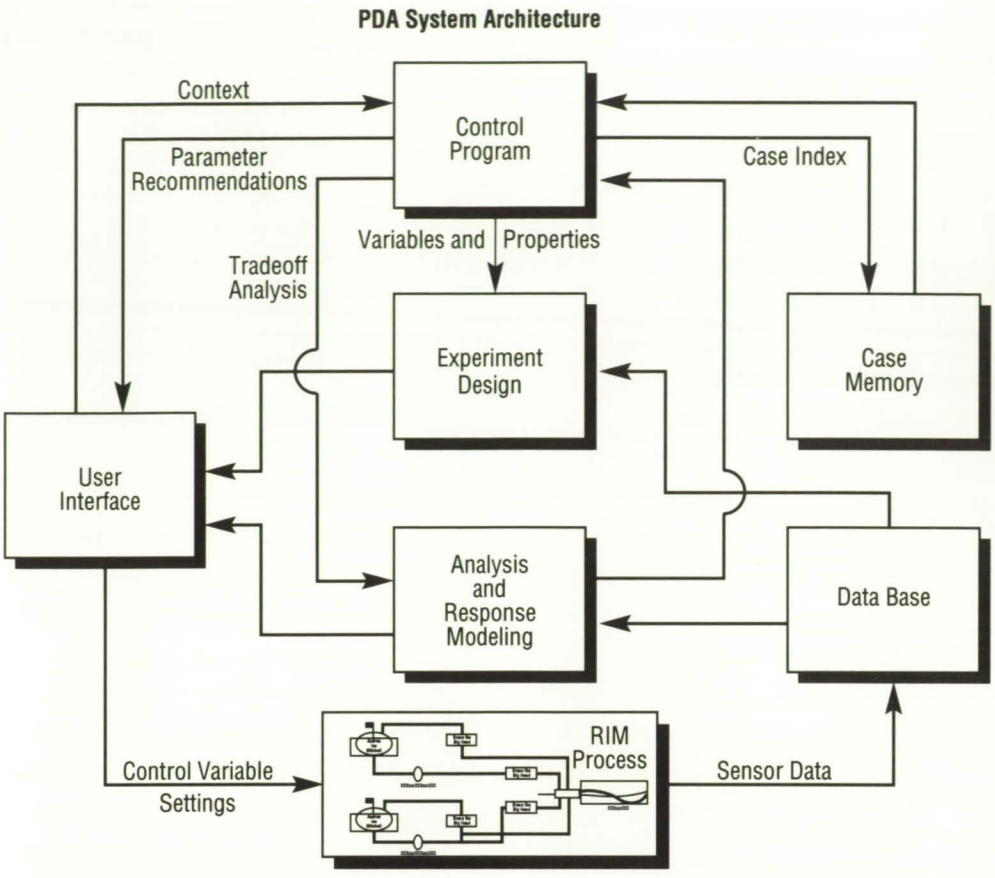

Figure 33. Process Development Advisor System Architecture

Figure 34 shows the Data Flow Model for process control implementation of the PDA. Sensor data will allow the process to be statistically monitored with real-time analysis of sensor readings with respect to the control and specification limits that are centered about optimal values. Significant parameters will be monitored during production operations. Variables found to be out of the prescribed processing range will initiate a dialogue with the operator. This dialogue will alert the operator to the presence of trended variables that are straying from the prescribed operating region. The early detection of a potential problem will permit PDA to make suggestions for restoration of normal processing. An operator receiving an error message will have the opportunity to pursue background information abstracted during process development. The communication of process knowledge reduced to empirical models is essential information that will allow operators to make educated decisions and processing adjustments in order to restore the producibility of a quality product.

Knowledge acquisition for PDA involves statistical design and analysis of experiments in both material and equipment development. Experiments have been conducted with this software for chemical foam formulations in order to optimize catalyst levels, determine the effects of various polyol levels, and study the effects of surfactant on the final and intermediate properties of cured experimental foams. Process equipment and environmental settings have been studied in the process characterization of alternate vendor materials for backups to flight-qualified materials.

The ability of the PDA approach to reduce the amount of experimentation required for materials and process development, while expanding the data manipulation and representation capability to maximize the interpretation of results, has been the most significant aspect of current work.

Continued development of PDA during 1990 will concentrate on a foam material data base and the development of a new generation of processing equipment for spray-on foam insulation for the ET. The PDA has been used for experimental design to determine acceptability of prototype equipment designs and will be used for process control of the new system at the Productivity Enhancement Center at MSFC.

E. Martinez/EH43
(205) 544-2724
Sponsor: Office of Space Flight

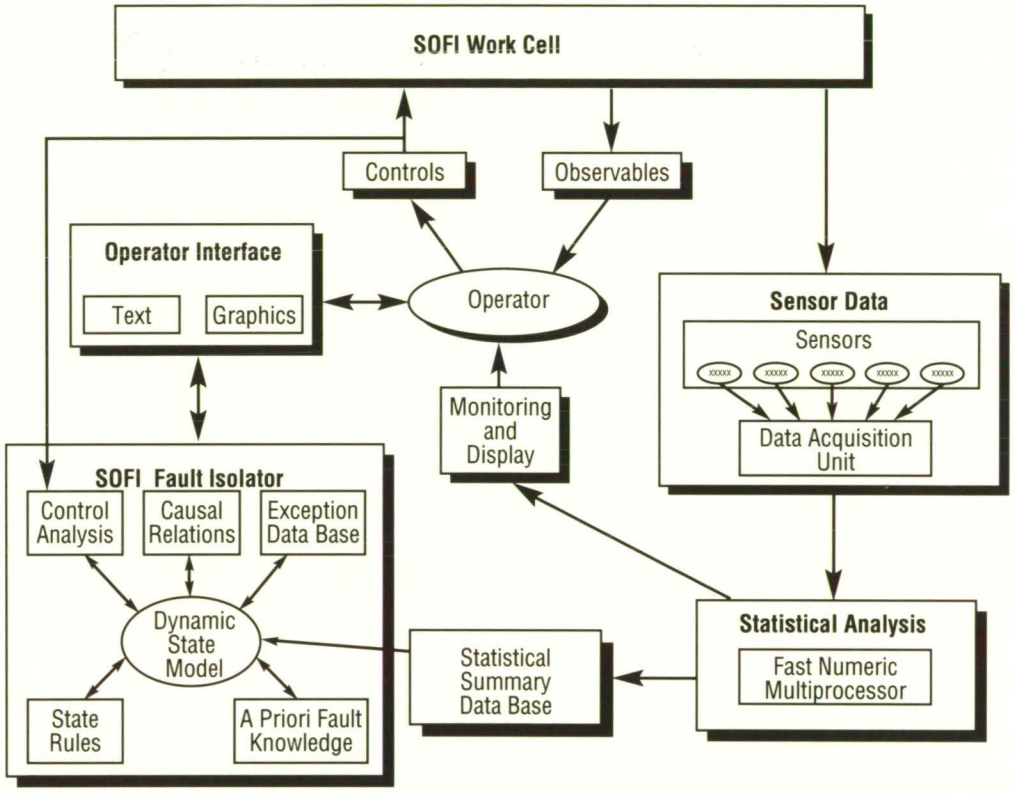

Figure 34. Process Control Data Flow Model

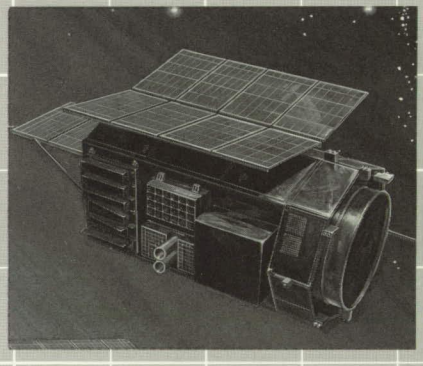

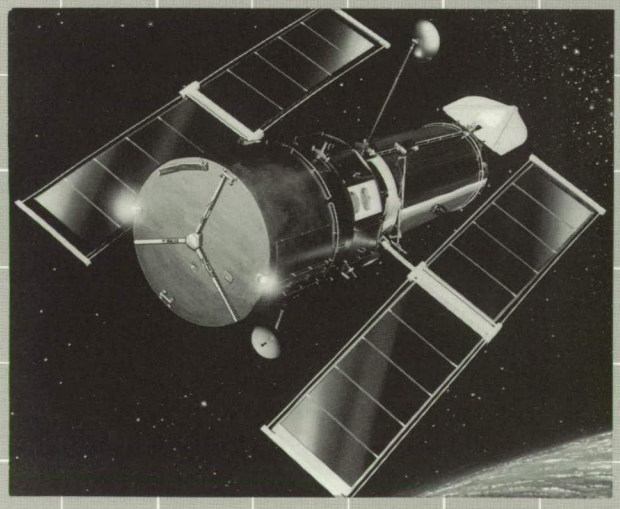

Research Programs

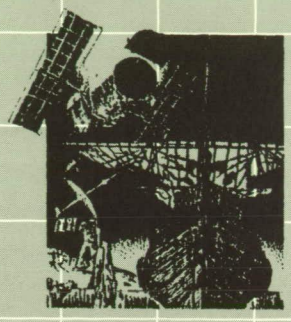

For over three decades, beginning with the launch of the Nation's first satellite, Explorer I, MSFC has been involved in many space science missions and programs that have helped increase our understanding of the universe. The Apollo Telescope Mount on Skylab changed our notion of the importance of magnetic fields in solar physics; the High Energy Astronomy Observatory-2 (Einstein) gave us the first x-ray images of celestial sources; data from the numerous experiments on Spacelabs 1, 2, and 3 profoundly deepened our understanding in microgravity and atmospheric research, and in many other areas as well.

The Hubble Space Telescope, developed by MSFC, is being prepared for launch and will yield visions of the universe that will surpass anything previously obtained from astronomical observations. Even greater expectations await the Center's future involvement in the development of the Advanced X-Ray Astrophysics Facilty, which will use the most sophisticated techniques and instruments ever applied in the study of x-ray objects. In the coming years, fundamental microgravity research will be conducted aboard Space Station *Freedom*, and we will participate in a comprehensive program to understand the Earth System.

Microgravity Science

In preparation for using flight experiments to study the influence of weightlessness on basic physical processes, a number of ground-based microgravity research programs are continuing at a high level of activity. MSFC scientists and engineers are heavily involved in research using the MSFC Drop Tube/Drop Tower and the NASA KC-135 aircraft. More than 25 principal investigators have had contracts selected as a result of peer review in MSFC-managed microgravity ground-based disciplines.

Our scientists and engineers are preparing state-of-the-art experiments for a number of flight programs aimed at the U.S. Microgravity Laboratory (USML), the International Microgravity Laboratory (IML), the Materials Science Laboratory, Space Station Freedom, *and other shuttle flight opportunities. The result of these efforts has been the selection of three MSFC scientists as principal investigators for the USML/IML series of Spacelab flights commencing in 1991. Such experiments will clarify how the absence of, for example, gravity-driven convection can beneficially influence solidification and crystallization processes.*

Advanced Technology Materials

Research is being conducted in the development of materials for use in advanced technology applications and more specifically in satisfying NASA-unique needs and requirements.

This effort involves work in two areas of extreme importance to our technology and the use of new materials in device and process applications: organic substances that possess nonlinear optical properties, and high-temperature superconducting materials (HTSC).

L-arginine phosphate (LAP) is a very promising material for nonlinear optical applications. It has very efficient second harmonic generation capabilities and a very high damage threshold. It will find future use in laser conversion and nuclear fusion technologies. The solution growth of large LAP crystals is now in progress and has produced large crystals [2 by 1 by 0.5 cm (.8 by .4 by .2 in.), Fig. 35] of excellent optical quality. Growth parameters for the process have been determined, and further trials are in progress to obtain crystals with reproducible properties. Physical and optical characterization is also in progress. A flight experiment proposal has

Figure 35. Crystals of LAP Grown from Aqueous Solutions

been submitted to NASA Headquarters in response to an announcement of opportunity for the crystal growth of LAP in the microgravity environment.

In the area of HTSC, work on these materials is being actively pursued, with two goals in mind: improving the critical current (J_c) properties of the bulk materials, and searching for new materials with possible higher transition temperatures (T_c) and higher J_c. The Yb-Ba-Cu-O system was investigated by studying the heat treatment parameters, resulting in excellent 123-type ($YbBa_2Cu_3O_7$) ceramic material with $T_c > 90$ K and $J_c > 70$ A/cm^2 (Fig. 36).

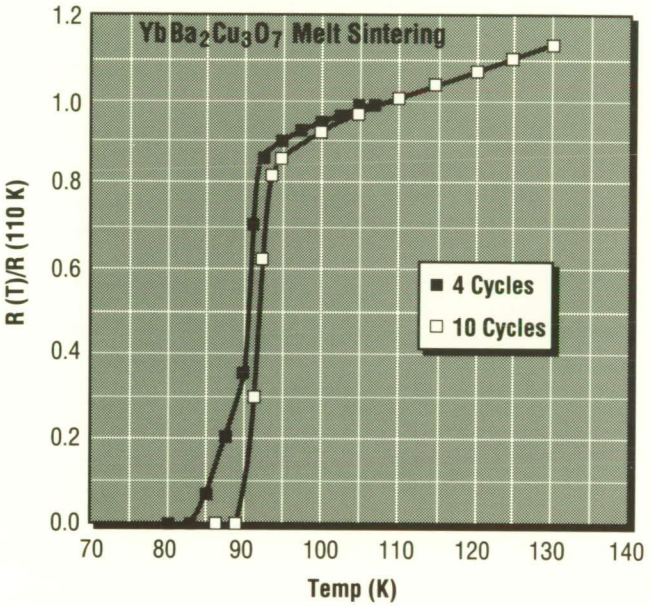

Figure 36. Resistivity vs. Temperature Plot for $YbBa_2Cu_3O_7$ Presenting Thermal Cycling

Experiments were performed in the Bi-Sr-Ca-Cu-O system by substituting Pb for Bi and controlling the Sr/Ca ratio in the hope of obtaining the 110 K phase (2–2–2–3 — numbers indicating the atomic ratios) pure, free of lower T_c phases. The temperature and the time of the heat treatment were optimized to obtain the 110 K phase. Material was obtained with $T_c = 105$ K containing only small traces of other phases. In parallel, efforts continue to increase the J_c of bulk ceramics, which up to the present have been rather low. The preparation of composites of Ag and superconducting phases in the Bi- and Yb-based systems also continues. This work will allow the preparation of more ductile materials.

The powder x-ray diffraction facility for characterization of HTSC samples has now been installed and structural study of HTSC materials has begun.

A number of tasks have been written and submitted to NASA Headquarters dealing with the application of new HTSC substances to endeavors specific and unique to NASA. This will establish MSFC as a leading center for the use of HTSC materials for applications such as propulsion, shielding, levitation, devices, etc.

M. Vlasse/ES75
(205) 544-7781
Sponsors: Center Director's Discretionary Fund
Office of Space Science and Applications
Office of Aeronautics and Space Technology

Protein Crystal Growth

Protein crystallography is currently the most powerful method for determination of the three-dimensional (3-D) structure of proteins and other macromolecules. This method usually requires crystals which are relatively large (0.5–1.0 mm) and which possess a reasonably high degree of internal order. Consequently, protein crystal growth has become the subject of an increasing number of fundamental studies, including several ongoing microgravity experiments. The knowledge of the 3-D structure of macromolecules is of fundamental importance to the field of molecular biology, and is presently receiving considerable attention from the biotechnology industry based on its promising potential for rational drug design and protein engineering.

One of the proteins extensively studied at MSFC is human serum albumin (HSA). HSA is the most abundant protein of the circulatory system, contributing significantly to colloidal osmotic blood pressure. HSA is a large protein comprised of 585 amino acids. One of the outstanding properties of this molecule relates to the transport of many important biological and pharmaceutical molecules in the blood stream. As a class of proteins, the serum albumins are among the most studied and applied in biochemistry.

Using a new tetragonal crystal form of HSA (Fig. 37) and x-ray diffraction methods, the 3-D structure of this molecule has recently been determined at MSFC for the first time. The molecule (Fig. 38) is predomi-

Figure 37. Tetragonal $P4_12$ Crystal Form of HSA Grown in Microgravity

ORIGINAL PAGE
COLOR PHOTOGRAPH

Figure 38. Molecular Configuration of HSA at 6 Å Resolution. Transport Binding Sites are Illustrated as Red Spheres

nantly alpha helical and spans an ellipsoidal area of approximately 140 by 35 Å. The molecule is formed by six subdomains, each of which is comprised of a three- to four-helix bundle. Preliminary binding studies have shown that most of the important biological and pharmaceutical compounds are transported within the first and fifth subdomains.

The determination of the positions of all 585 amino acids to a resolution of 3.0 Å is currently in progress.

Carter, D.C., He, X.M., Munson, S.H., Twigg, P.D., Gernert, K.M., Broom, M.B. and Miller, T.Y.: Three-Dimensional Structure of Human Serum Albumin. Science, Vol. 244, pp. 1195–1198, 1989.

Delucas, L.J., Smith, C.D., Smith. H.W., Senadhi, V.K., Ealick, S.E., Carter, D.C., Snyder, R.S., Weber, P.C., Salemme, R., Ohlendorf, D.H., Navia, M.A., McKeever, B.M., Nagabhushan, T.L., Nelson, G. and Bugg, C.E.: Protein Crystal Growth in Microgravity. Science, submitted,1989.

D.C. Carter/ES76
(205) 544-5492
Sponsor: Office of Space Science and Applications

Alloy Directional Solidification Experiments

Metal alloy and composite solidification is strongly influenced by buoyancy-driven convective and Stokes flow in the melt. Commonly used metal alloys are multiphase, multicrystalline, are often solidified with complex solid/liquid interfacial morphology and cast into complex three-dimensional geometries. Because of the commercial and strategic importance of metals and alloys, their solidification processes have been intensely studied by both the commercial and academic communities. However, because of the complexity of the solidification processes and the largely uncontrollable influence of gravity-driven flows, few models of alloy solidification are advanced enough to be utilized extensively in commercial processes. Consequently, commercial processing of metal alloys is still largely an empirical science.

Research conducted in low gravity has the advantage of greatly simplifying the solidification process. Buoyancy-dependent variables can be isolated, quantified, and incorporated into solidification models. Because of the geometrical and physical complexity of alloy solidification, castings with unique microstructure and properties can be made in low gravity that are impossible to duplicate on Earth.

Directional solidification of alloys during continuous KC-135 low-gravity maneuvers provides useful data, since convective and Stokes flow damping time is within the first quarter of the low-gravity period. Research this year on Fe-C alloys has shown, for the first time, that convective flow contributes (about 20 percent) to graphite nucleation. Such information is of critical importance to the foundry industry, since mechanical strength is a strong function of graphite grain size. Experiments with metal matrix composites have shown that Einstein's viscosity relation must be incorporated into the particle engulfment theory. High-temperature superconducting oxide particles have been solidified in a silver matrix (to improve critical current, flux pinning, and mechanical toughness) in aircraft low gravity with increased dispersion homogeneity. Superalloy dendritic spacing (which strongly influences mechanical properties) has been shown to be a function of dendritic orientation to, as well as the magnitude of, the gravitational field.

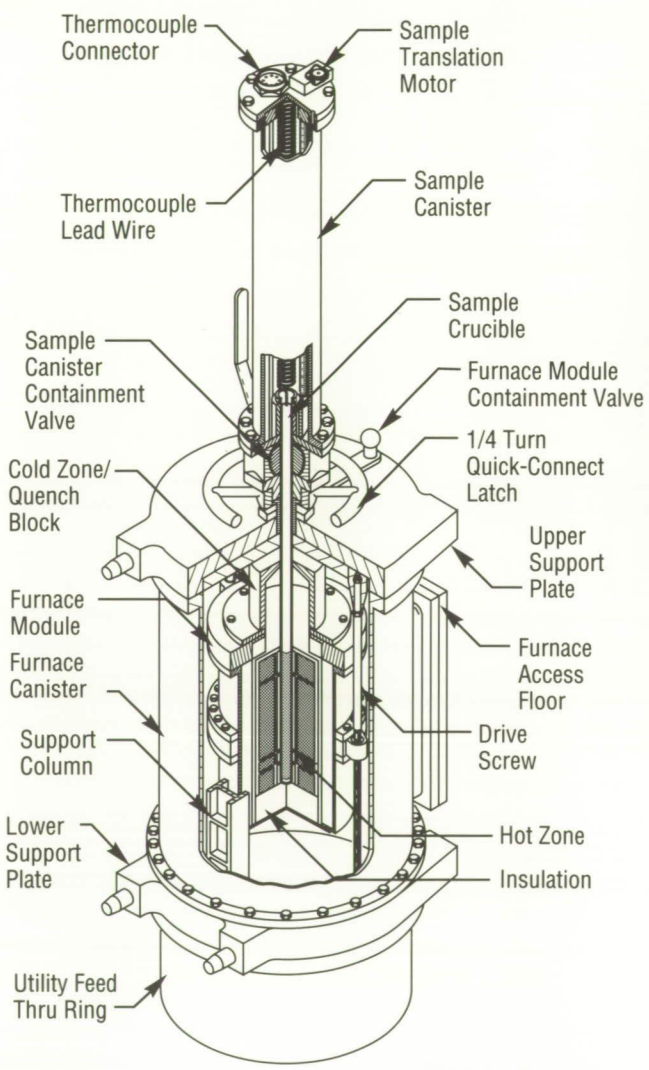

Figure 39. The Metal and Alloys Solidification Apparatus

Despite much progress, only a very limited number of processes critical to metal alloy and composite solidification can be studied effectively in the KC–135 or on sounding rocket flights. Most experiments in immiscible alloys, eutectic alloys, or metal matrix composites for the quantitative study of cell nucleation, dendritic spacing, arm coarsening, and complex casting geometry have time constants dictating that they be conducted in space. To facilitate these studies, the prototype Metal and Alloys Solidification Apparatus is being developed (Fig. 39). The furnace is multiuser (20 samples per flight). Science requirements have been defined with input from the commercial, government, and academic metallurgical communities. The furnace, with planned enhancements, could provide for a vigorous research program in solidification of alloys in orbital low gravity which will lead to the use by the metallurgical community of Space Station *Freedom*.

P.A. Curreri/ES74
(205) 544-7763
Sponsors: Office of Space Science and Applications
Office of Commercial Programs

Particle Motion in a Rotary Reactor

The basic objective of this effort is to perform calculations and verify them with experimental data, in order to determine the motion of latex microspheres and other chemical or biological particles while they are held in suspension in a rotating system. This will allow operational parameters of the rotary reactor to be optimized, with specific application to the ground-based production of monodisperse polystyrene microspheres similar to those manufactured aboard the space shuttle.

During polymerization of large particle-size monodisperse latexes, the growing microspheres must be held in suspension in an extremely low-shear environment without touching the reactor walls for long periods of time, generally 20 hours or more. It is expected that the fluid and particle motion data from this effort will result in improved production of these microspheres, and will also be applicable to many other chemical and biological processes where buoyancy and sedimentation cause difficulties.

A description of the Monodisperse Latex Reactor space processing space shuttle flight experiment was published in the 1985 MSFC Research and Technology (R&T) Report, and a description of the first-generation Rotary Reactor for Latex Production was published in the 1986 MSFC R&T Report. The current report describes the advanced second-generation rotary reactor, which is designed primarily for fluid-motion studies. Now in operation at MSFC, it is an important example of technology transfer from microgravity space processing to Earth-based processing, using a slowly rotating environment to simulate microgravity.

This new rotary reactor (Fig. 40) features a horizontal cylindrical pyrex glass sample chamber of 250 mL volume, which is rotated about its long axis within a constant-temperature water bath. Rotation rates can be varied between 0.5 and 23 rpm. The

reactor chamber is basically a piston dilatometer, and is filled completely with the test fluid to eliminate all bubbles which would interfere with fluid motion. A piston at one end of the chamber transmits any fluid volume changes through a linear variable differential transducer to a strip-chart recorder. Three thermistors within an extendable probe detect any temperature changes within the chamber and transmit this data to the same recorder. A stir-rod containing a syringe needle projects through the face of the piston and, with rotary seals, allows a test fluid or a suspension of particles to be injected or withdrawn from the chamber at any time during a test run, without disturbing chamber rotation. The other end of the chamber consists of an optical glass window. A rotoscope is mounted just outside this window to allow observation of particles during rotation. The rotoscope is an optical device which subtracts angular movement. It consists of a dove-tail reversing prism which is geared to the reactor chamber to rotate at exactly half the rotation rate of the chamber. The object is viewed through the rotating prism and the image appears at rest. This allows individual particle spirals to be clearly observed while the chamber is rotating. An argon-ion green-light laser (5145 Å) is currently being used to illuminate the suspended particles. The laser beam is refracted by a cylindrical lens into a vertical sheet about 1 mm wide, and projects through the side of the water bath and test chamber to illuminate a vertical slice of the chamber. Only those particles within the illuminated slice scatter light and are visible through the rotoscope or from the side for photography. A 35-mm still camera is used to record particle concentration through the rotoscope, and a video camera is used to record particle motion from either the side or end of the chamber.

A computer model has been developed which includes all known forces that are acting on the suspended particles during rotation, and a paper has been submitted for publication to the Journal of

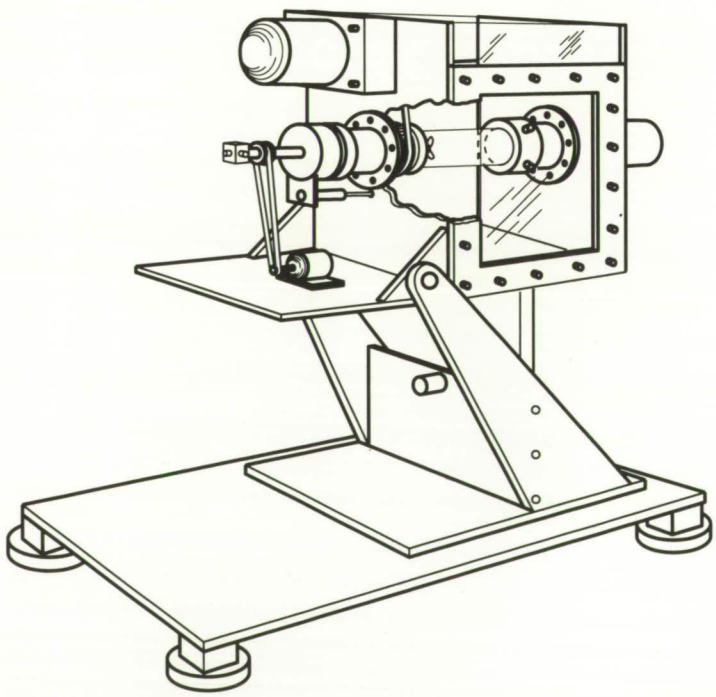

Figure 40. Advanced Rotary Reactor for Fluid and Particle Motion Studies

Fluid Mechanics describing the mathematics used in preparing the model. Particle motion as predicted by the computer model is now being checked against experimental results, as monodisperse microspheres are suspended within the test chamber. The motion of these particles is recorded photographically at various rotation rates, as particle batches from submicron to 100 μm in diameter are tested. Early results indicate that at low rpm, secondary flows appear at high particle concentrations and cause significant deviation from uniform solid body rotation. Once the approximate theories and the computer code have been checked against experimental results, they will be formulated in such a way that they can be easily used by nonspecialists in fluid dynamics and computer methods to ascertain maximum suspension times and optimum rotation rates for a wide range of particle sizes and densities in this type of rotating system.

U.S. Patent No. 4,247,434; issued January 27, 1981: Process for Preparation of Large-Particle-Size Monodisperse Latexes. Inventors: Vanderhoff, J.W., Kornfeld, D.M., Micale, F.J. and El-Aasser, M.S.

Vanderhoff, J.W., El-Aasser, M.S., Kornfeld, D.M., Micale, F.J., Sudol, E.D., Tseng, C.M. and Sheu, H.R.: The First Products Made in Space: Monodisperse Latex Particles. Mat. Res. Soc. Symp. Proc., Vol. 87, pp. 213–223, 1987.

Kornfeld, D.M.: Rotary Reactor Makes Large Latex Particles. NASA Tech Briefs, Vol. 12, No. 3, p. 76, May 1988.

D.M. Kornfeld/ES76
(205) 544-7808
Sponsor: Technology Utilization Program

Phase Partitioning

Phase partitioning is a separation technique for the isolation of biologicals such as proteins, DNA, subcellular particles, and cells. It is unsurpassed as a separation technique in certain biotechnical/biomedical applications. Its usefulness for cells is of particular interest because the need to retain cell viability and function limits the use of many separation techniques for cell separation. This gentle and cost-effective technique uses two-phase systems which are created by dissolving two types of polymers, such as dextran and polyethylene glycol, in buffered isotonic aqueous solutions above certain low concentrations. Each of the resulting two immiscible phases is enriched with one of the polymers. The material to be separated is partitioned either between the two phases or between one of the phases and the interface. Separation efficiency can be enhanced by multiple step partitioning in a counter-current distribution apparatus.

On Earth, the partitioning of cells is affected by cell sedimentation. In addition, convection occurring during demixing of the phases may also reduce separation efficiency. By performing experiments which exclude these gravity-derived effects, the advantages of carrying out partitioning in space can be ascertained, design of Earth-bound partition apparatus can be improved, and improved apparatus and protocols for space bioprocessing can be designed. In preparation for cell separation experiments in space and to provide information on the determinants of demixing of immiscible phase systems, the Phase Partitioning Experiment (PPE) was conducted on shuttle mission STS-26 (Fig. 41). Effects of interfacial tension, phase viscosities, phase volume ratio, container geometry, and wall-wetting characteristics were studied in 18 separate experimental chambers.

Data from the STS-26 experiment are being analyzed by a method developed in-house at MSFC. Photographs of the demixing phases taken at various times between 5 seconds and 2 hours after

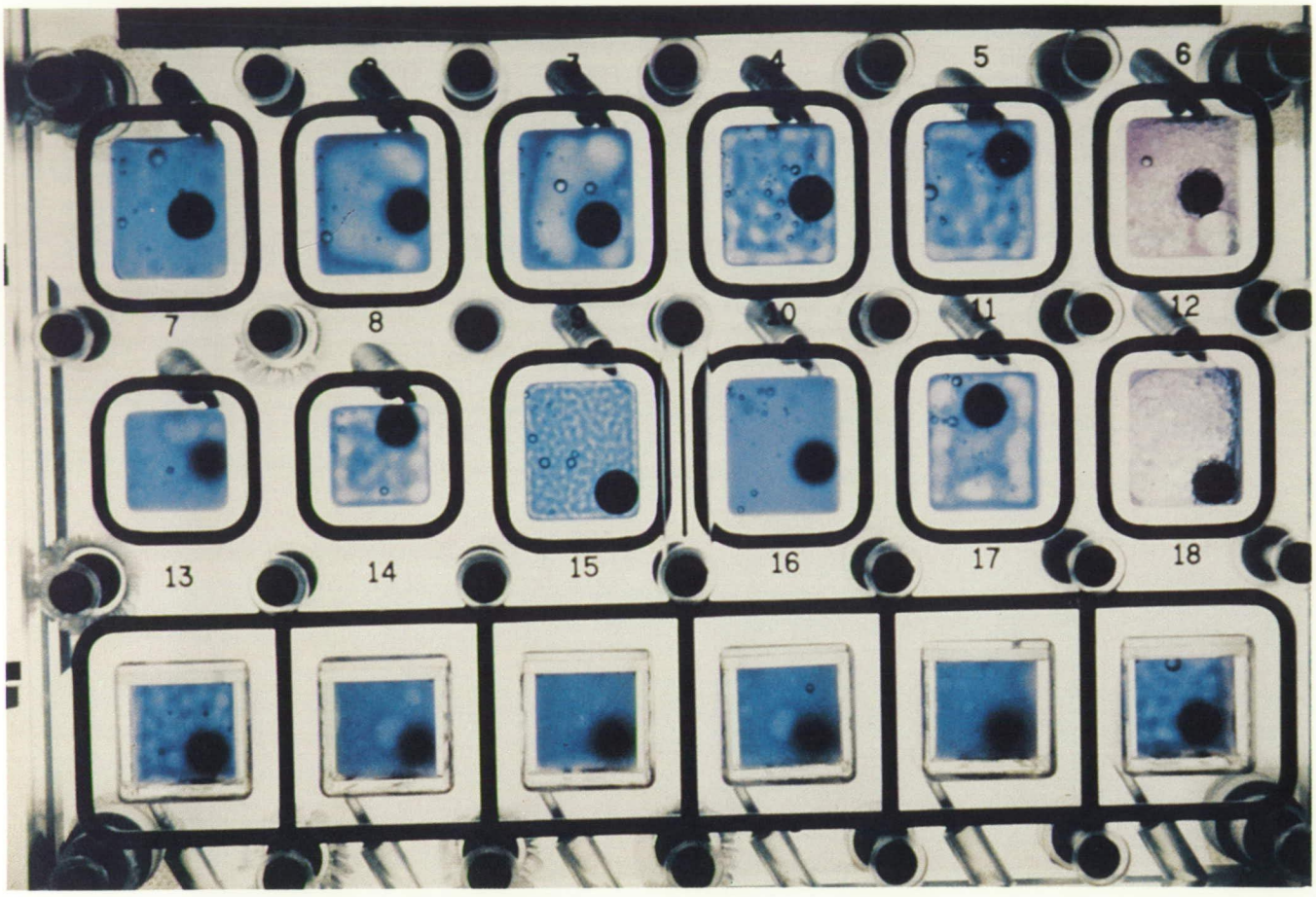

Figure 41. Phase Partitioning Experiment Results

mixing are digitized, and subsequent data are subjected to two-dimensional Fourier transformation. The average distance between adjacent domains of the same phase is then determined from the maximum intensity of the Fourier frequency distribution. Preliminary results indicate that demixing rates are consistent with shear-induced coalescence. Phase wall-wetting and chamber geometry effects were as predicted from Earth-bound contact angle measurements. Increasing viscosity or interfacial tension reduces the demixing rate. This method will be useful for the analysis of future flight experiments and for study of the initial coalescence stage of 1-g demixing. In addition, it is applicable to analysis of the kinetics of segregating phases that occur in independent studies involving critical phenomena and alloy formation.

Van Alstine, J.M., Karr, L.J., Harris, J.M., Snyder, R.S., Bamberger, S.B., Matsos, H.C., Curreri, P.A., Boyce, J. and Brooks, D.E.: Phase Partitioning in Space and on Earth. Immunobiology of Proteins and Peptides IV. Atassi, M.Z., ed., Plenum Press, New York, pp. 305–436, 1987.

Bamberger, S., Van Alstine, J.M., Harris, J.M., Baird, J.K., Snyder, R.S., Boyce, J. and Brooks, D.E.: Demixing of Aqueous Polymer Two-Phase Systems in Low Gravity. Sep. Sci. Tech., Vol. 23, pp. 17–34, 1988.

Van Alstine, J.M., Bamberger, S., Harris, J.M., Snyder, R.S. and Brooks, D.E.: Demixing of Immiscible Aqueous Polymer Solutions on Flight STS-26. Hurle, D.T.J., ed., Seventh European Symposium on Materials and Fluid Sciences in Microgravity, ESA Pub. Div., Noordwijk, The Netherlands, 1989.

R.S. Snyder/ES76
(205) 544-7805
Sponsors: Office of Space Science and Applications
Universities Space Research Association
National Research Council

Undercooling Studies in Metals and Alloys

In order to improve present metals and alloys through space processing, it is necessary to first understand the effect of low-gravity processing on the structure and properties of each material. The effect of low gravity coupled with containerless processing is being studied using the 105-m MSFC Drop Tube facility. This environment, achieved in both the drop tube and during a containerless space flight, is conducive to large degrees of undercooling before solidification of the metal occurs. Undercooling studies in the drop tube have primarily centered on niobium-based binary alloys and pure, refractory metals.

In the past year, effort was directed at measurement of the solidification velocities of drop tube samples after large degrees of undercooling. The technique involved makes use of fast silicon detectors and an IBM-based data acquisition system capable of 10^6 readings per second for the 4.6 s of free-fall time achieved during drop tube processing. Solidification velocities have presently been measured for niobium-platinum alloys ranging in composition from 6 to 35 atomic percent platinum. Results have been compared to current dendritic solidification velocity theories. Samples of compositions ranging from 25 to 32 atomic percent platinum revealed solidification velocities which agreed very closely with theory. However, solidification velocities measured for samples of lower platinum content are an order of magnitude less than theory predicts. This difference is caused by the formation of a metastable platinum-deficient A15 phase in the undercooled samples of 16 to 19 atomic percent platinum. Investigation of these alloys continues.

In addition to alloy research, study of the solidification velocities for pure refractory metals was begun. In particular, pure niobium was studied. It was found that the solidification velocities measured for pure niobium are considerably less than the theoretical predictions. Research is continuing.

The solidification velocity measurements just discussed have been helpful in understanding the extensive study of structures and properties previously completed. Through this research, a better understanding of low-gravity containerless processing, and the resulting undercooling and solidification phenomena has been obtained.

Hofmeister, W.H., Bayuzick, R.J. and Robinson, M.B.: Noncontact Temperature Measurement of a Falling Drop. International J. of Thermophysics, Vol. 10, pp. 279-292, 1989.

Robinson, M.B., Hofmeister, W.H. and Bayuzick, R.J.: Undercooling Studies on Nb-Si Alloys using the 105-Meter Drop Tube. Advances in Space Research, Vol. 8, No. 12, pp. 321–330, 1988.

Hofmeister, W.H., Bayuzick, R.J. and Robinson, M.B.: Experiments in Long Drop Tubes. Proceedings, Third International Colloquium on Drops and Bubbles, Jet Propulsion Laboratory, Monterey, CA, September 18–21, in press, 1988.

M.B. Robinson/ES74
(205) 544-7774
Sponsor: Office of Space Science and Applications

Solution Crystal Growth

Research is continuing on the growth of crystals from solution. This effort includes both ground-based laboratory studies and proposed flight experiments. An experiment to grow single crystals of triglycine sulfate (TGS) was successfully carried out on Spacelab 3 using the Fluids Experiment System (FES). The crystals were grown from seeds, and holograms were taken to record the growth process. Design modifications to the FES cells are being developed to facilitate the study of new materials and growth techniques.

Crystal growth initiated by nucleation instead of from a seed is now being investigated. A prototype cell has been built and is being used in ground-based research on nucleation from solution, which includes the evaluation of techniques for initiating nucleation. Several prototype devices for retrieving nucleated crystals from the growth cell in low-gravity have been designed and built. These designs are being evaluated for further development.

Ground-based research areas include studies of crystal properties as a function of growth conditions using a reciprocating rotary crystallizer, and the development and use of optical techniques for the study of growth processes and crystal properties. A unique technique of shadowgraph imaging has been developed and is being used for the precise determination of the equilibrium temperatures of growing crystals in known solution concentrations. A second-generation solubility measuring system of this kind was also built. It is used to generate solubility curves for aluminum potassium sulfate, L-arginine phosphate (LAP, Fig. 42), and other materials being considered for flight experiments. A laser-scattering technique used in conjunction with a microscope, a detector, and a computer system, collectively termed a laser-scattering ultramicroscope, has been developed. An enhanced ultramicroscope system with greatly improved sensitivity and data handling capabilities has been built and tested. The performance of this system is being upgraded further by hardware and software modifications. The

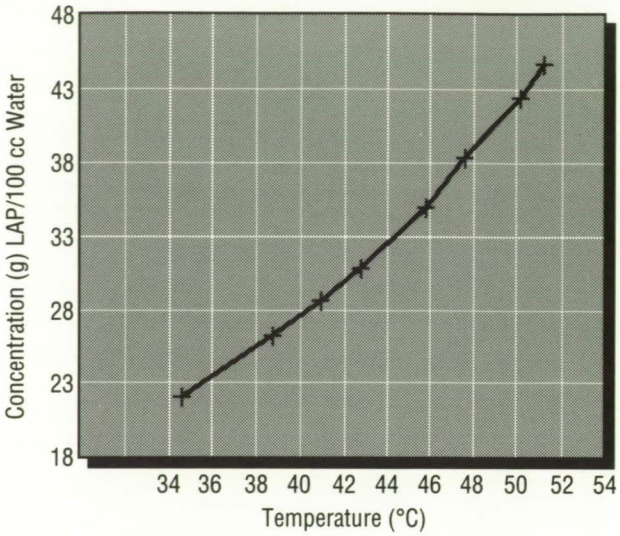

Figure 42. LAP Solubility in Water

system is being used to produce three-dimensional maps of the distribution of scattering centers (Fig. 43), such as voids and inclusions, within crystals of a limited number of materials, including TGS and LAP. The possibility of using it on proteins is being investigated. The density and distribution of inclusions can strongly affect the optical and electrical quality of crystals. Therefore, the laser-scattering technique will be useful in the characterization of crystals grown in planned flight experiments.

Ground-based research, focused on the growth of crystals with interesting physical properties, such as ferroelectric, nonlinear optical, and electro-optical materials, has identified LAP as a candidate material for a space flight experiment. It is of interest because its nonlinear optical properties exceed those of materials currently in use in industry, and because it can be grown from low-temperature aqueous solutions. The physical properties of crystals and growth solutions are being investigated to determine the possible effects of a low-gravity environment on the growth of LAP.

Two new techniques for nucleation and growth of crystals from solution have been developed. One technique uses a rotating growth chamber in which small crystallites are maintained suspended in the

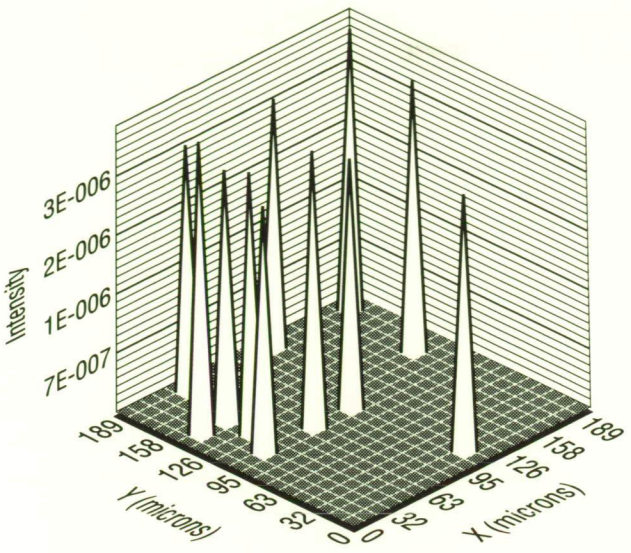

Figure 43. Three-Dimensional Map of the Distribution of Scattering Centers in a LAP Crystal

solution. The other technique uses a forced-convection cell in which the flow of solution pumped through a nozzle holds a large crystal suspended where it cannot contact the cell walls. These techniques have been used to nucleate and grow materials such as Rochelle salt and TGS. The flow technique has been used to grow protein crystals. Modification of the rotating chamber technique for this purpose is in progress.

Lal, R.B., Aggarwal, M.D., Batra, A.K., Kroes, R.L., Wilcox, W.R., Trolinger, J.R. and Cirino, P.: Growth of Triglycine Sulfate Crystals Aboard Spacelab 3. Spacelab 3 Mission Science Review, NASA Conference Publication 2429, 1987.

Reiss, D.A., Kroes, R.L. and Anderson, E.E.: Growth Kinetics of the (001) Face of TGS Below the Ferroelectric Transition Temperature. J. Crystal Growth, Vol. 84, No. 1, pp. 7–10, 1987.

Kroes, R.L. and Reiss, D.A.: Development of New Techniques for the Characterization of Crystals and Their Growth Solutions. NASA TM-100371, 1989.

R.L. Kroes/ES76
(205) 544-7770
Sponsor: Office of Space Science and Applications

Estimation of the Initial Equilibrium Constants in the Nucleation of Tetragonal Lysozyme Crystals

Knowledge of solution aggregate composition in both undersaturated (prenucleated) and oversaturated (nucleated and crystal-growing) solutions is important to the eventual understanding of protein crystal nucleation and growth processes. Using relative light-scattering intensity measurements, estimates of the initial equilibrium constants in the formation of tetragonal lysozyme nuclei have been made.

Assuming "ideal" behavior, and making several other assumptions, the light-scattering equations can be manipulated into the form:

$$\frac{Is2}{Is1} = \frac{\sum_i i^2[M_i]}{[M_1]}$$

The $Is2/Is1$ ratio is then equal to the average molecular weight ratio of the aggregated material to the original monomeric molecular weight. Data are collected as 90-degree light-scattering intensities over a range of concentrations for a system known to be monodisperse ($Is1$) versus one believed to be polydisperse ($Is2$). The data are plotted as the intensity ratios $Is2/Is1$ versus concentration. The data in this form are then readily amenable to parameter estimation by fitting calculated model curves.

While the aggregation pathway is not known, it is assumed that the first step is dimer formation ($K_1 = [M_2]/[M_1]^2$). Current experiments at 3.0 percent NaCl, 0.1 M acetate buffer, pH 4.0, 22 °C (72 °F) indicate $K1$ values of 1–3 x 10 $L*mol^{-1}$. Estimation of subsequent equilibrium constants will be dependent upon the aggregation model chosen. For a 1 -> 2 -> 4 pathway, K_2 values are estimated to be 2–8 x 10^3 $L*mol^{-1}$, while for a 1 -> 2 -> 3 pathway, values of 8–15 x 10^3 $L*mol^{-1}$ are estimated.

While this technique cannot unambiguously determine the correct nucleation pathway, and probably cannot accurately estimate equilibrium constants past the second or third level, it has still yielded valuable information concerning the lysozyme nucleation and crystal growth process. Equilibrium values of this magnitude, especially the $K1$ value, essentially "fix" the monomer concentration by the saturation concentration point with only the higher order aggregates showing appreciable concentration increase with increasing total protein concentration. This strongly suggests that tetragonal lysozyme crystal growth is by addition of aggregates preformed in the bulk solution, not by monomer addition. This is independent of a screw dislocation or surface nucleation type mechanism. Currently, an octameric growth unit is favored as a working hypothesis in this laboratory, based upon electron microscope photographs showing unit cell (octamer) step heights, and from aesthetic considerations.

M.L. Pusey/ES76
(205) 544-7823
Sponsor: Center Director's Discretionary Fund

Vibration Sensitivity of Selected Fluids and Materials Processing Experiments to Low-Gravity Disturbances

The expected benefits (and trials) of materials processing and fluid control in space have driven the initiation of hundreds of experiments in the reduced gravity environment. As one example, research efforts related to float zone technology have sought to benefit from the expected reduction of buoyancy-driven convection within the zone melt, while also being challenged by the presence of surface tension-driven convection along the cylindrical zone-free surface. Resultant low-gravity fluid response of an experiment is related to several factors, including the system's dependence on gravity, thermal and solutal distributions, fluid characteristics, etc. While deleterious effects attributed to strong gravitational forces may be suppressed in the low-gravity environment, the mere reduction in the magnitude of the imposed gravity does not necessarily correspond to an elimination of all gravity-induced effects. The space environment does not represent a true "zero g" situation, as it is composed of a quasi-steady acceleration component and a myriad of additional alternating acceleration components.

During past space investigations, many experiments have been suspected to be dependent on the imposed acceleration environment. There are few experiments, however, which correlated the sensitivity of the fluids experiment to measured time-dependent low-gravity disturbances. Therefore, because several experiments appear susceptible to the low-gravity environment, efforts are being made to determine acceleration effects, and possibly reduce the disturbances experienced by the fluid system. For example, if fluid sensitivity could be characterized in a computational, quantitative way, vibration isolation systems might be tuned to filter bandwidths expected to produce adverse effects.

In an effort to determine if low-gravity experiments might benefit from vibration isolation techniques, MSFC and the University of Alabama in Huntsville

(UAH) are computationally investigating the vibration sensitivity of a group of selected fluids and materials processing experiments. This effort is part of the Vibration Isolation Advanced Technology Development Program sponsored by NASA Headquarters. During the 3-year program, several classes of fluid systems expected to be sensitive to low-gravity disturbances will be examined (Fig. 44). In the interest of time, highly detailed modeling of each fluid class is not the objective; determination of the overall fluid response to imposed gravitational disturbances is the goal.

A review of related fluids experiments which were performed in the low-gravity environment has been completed. Fluid characteristics and system parameters of these past space investigations are being implemented in current analysis efforts. Order of magnitude estimates of fluid sensitivity as a function of acceleration, amplitude, and frequency have been completed by UAH. Such estimates permit only single disturbance input, but serve as a preliminary guide for more detailed computational analyses which involve both single and multiple disturbance input.

Containerless Liquid Bridges

- Computational Analysis of Bridge Shape Deformation and Breakage

Thermocapillary Convection of Open Cavities and Float Zones

- Computational Analysis of Buoyancy and Marangoni Driven Convection
- Computational Analysis of Thermal and Solutal Distribution
- Effects of Rotation and Encapsulation on Resultant Convective Flow

Diffusion Coefficient Calculations

- Computational Analysis of Convective Transport Contributions Arising from Buoyancy Forces

Figure 44. Classes of Fluids Systems Selected for Sensitivity Analysis

In-house modeling of enclosure and thermocapillary problems have been initiated. The detailed expansion of a finite volume code has been completed allowing computation of the resultant fluid flow in open and closed cavities, float zone, rotating float zone, and encapsulated float zone systems. Information on the numerical scheme can be obtained.* The computations consider realistic vibration isolation disturbance filtering limits and examine fluid response at, below, and above these limits. In addition, acceleration magnitudes and frequencies typical of those which might be encountered on the space shuttle or Space Station *Freedom* are being imposed over fluid systems.

A sample of results for a germanium melt float zone is shown in Figure 45. A sinusoidal g-jitter variation with a frequency of 10^{-3} Hz and an amplitude of $10^{-4}g_o$ is considered, where g_o is terrestrial gravity. The magnitude of the surface tension force acting on the free surfaces is given by the Marangoni number (Ma) and is taken to be equal to -1 (representative of an encapsulated float zone situation) in the calculations. The flow field (represented by the velocity vectors) and the temperature distribution (represented by color) are shown over one period of g-jitter. As can be seen from the figure, g-jitter modifies the flow field by strongly driving the upper cell during the first half of the cycle, and then driving the lower cell during the other half, before reverting to the almost symmetrical situation at the end of the cycle. The temperature field, on the other hand, shows no effect of the g-jitter or the surface tension forces. Although not pictured, for float zones without encapsulation, the Marangoni number is much larger (about -10^4 for this case), and significant isotherm distortion due to a stronger flow field is noticed. This type of information is useful in the growth of crystals where the flow field might affect the dopant distribution in the melt, and where the temperature field determines the shape of the growing crystal interface.

In addition to order of magnitude calculations, UAH supports this effort with isothermal zone sensitivity analysis. Currently, zone deformation and breakage

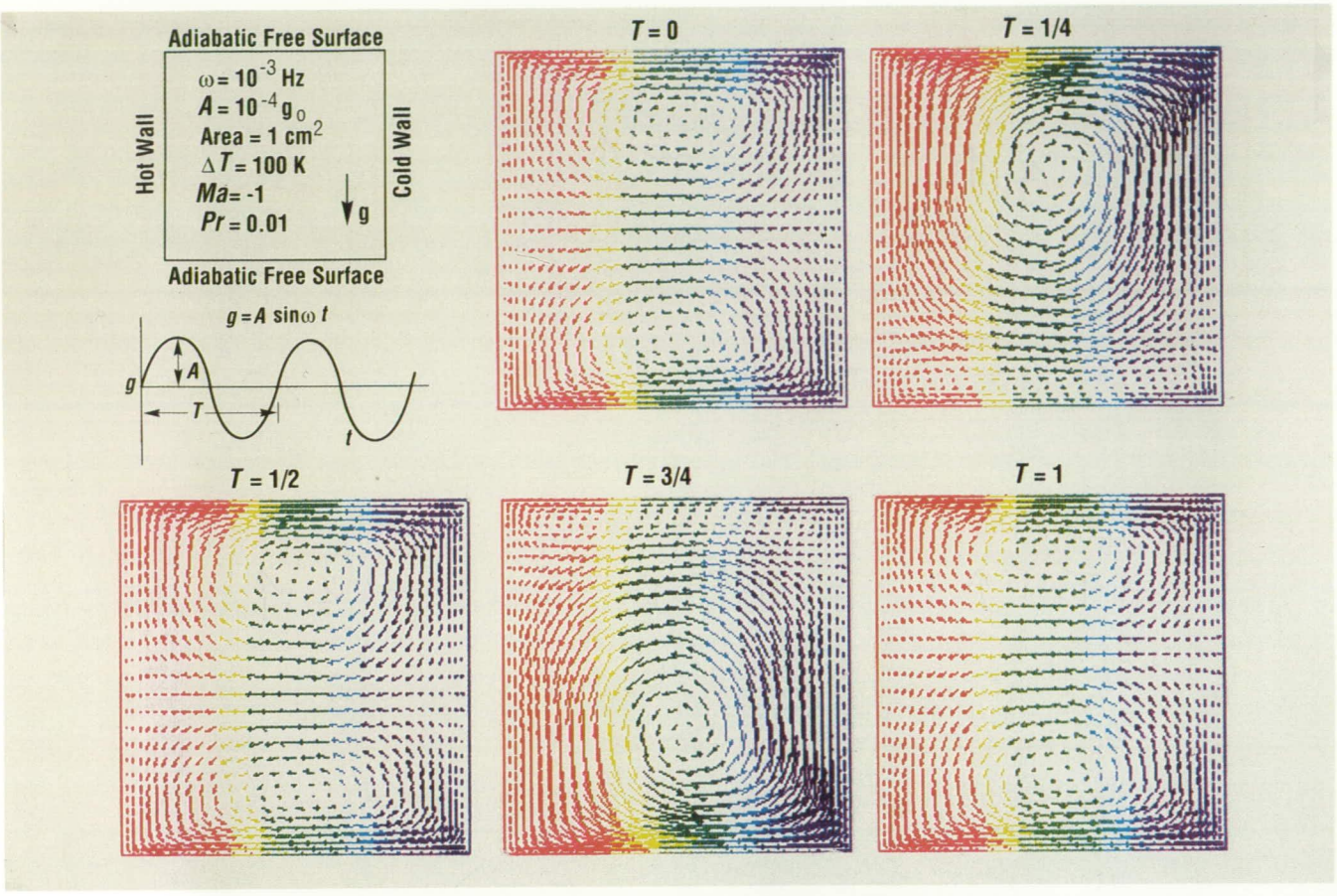

Figure 45. Sample of Germanium Melt Float Zone Results

as a result of a single axial disturbance is being examined. UAH is also adapting a spectral code to model thermocapillary convection, and to compute diffusion coefficient calculations.

Resultant sensitivity analysis may be verified with experimental research on the Lewis Research Center Lear jet low-gravity aircraft.

*Ramachandran, N. and Schafer, C.F.: Numerical Simulation of Forced Convection in a Two Fluid Layered System in a Floating Zone Configuration. Paper No. AIAA-89-0071, AIAA 27th Aerospace Sciences Meeting, Reno, NV, Jan. 9-12, 1989.

C.A. Winter/ES42
(205) 544-1695
Sponsor: Office of Space Science and Applications

The Spacelab-J Mission

A Spacelab mission (SL-J) is planned for launch in mid-1991. The mission will have 35 experiments from Japan aboard, and will also carry six U.S. experiments. The SL-J payload requires an extended microgravity and cosmic ray environment for materials science research of crystal growth, solidification processes, drop dynamics, free surface flows, gas dynamics, metallurgy, combustion processes, and semiconductor technology. The same environments are needed for research in life sciences including cell development, human physiology, radiation-induced mutations, vestibular studies, embryo development, and medical technology.

Through an international agreement with the National Space Development Agency of Japan, NASA is preparing to fly the First Materials Processing Test. The hardware consists of two double racks of materials science experiments and one double rack of life science experiments. Complementing the mission will be U.S. hardware including a life science single rack, a Shuttle Middeck Experiment double rack, a double rack containing the General Purpose Workstation for handling samples under containment, and three racks for holding refrigerated and nonrefrigerated samples and stowage. The Space Acceleration Measurement System, consisting of three triaxial accelerometer heads, will record Spacelab acceleration levels at various intervals and frequencies. All of the acceleration data and orbiter timing data will be stored on optical disks with a capacity of 200 megabytes each. Each investigator has provided requirements regarding position of the sensor heads, data rates, acceleration range, and data acquisition times. The data derived from this mission will be used to characterize the microgravity environment.

Some of the materials experiments onboard include the Continuous Heating Furnace, which can process four metal samples simultaneously (two heating and two cooling) up to 1,300 °C (2,372 °F); the Large Isothermal Furnace, used for materials processing studies with larger samples up to 1,600 °C (2,912 °F); the Gradient Heating Furnace, designed to study directional solidification by imposing a temperature gradient along the axis of the sample of up to 60 °C cm^{-1} and as high as 1,200 °C (2,192 °F); the Image Furnace, which uses an elliptical mirror around two halogen lamps to heat float zone samples at the foci up to 1,400 °C (2,552 °F); the Acoustic Levitation Furnace, which uses a single-axis acoustic levitator to position and hold the samples; the Liquid Drop Facility, which is used to excite oscillations in drops and induce rotations; the Crystal Growth Experiment Facility, which operates up to 1,450 °C (2,642 °F), and is capable of growing a single spherical crystal of Si-SiO_2 to investigate its electrical properties; the Bubble Behavior Unit, which will examine the motion of bubbles in response to acoustic vibrations and a temperature gradient of 10 °C cm^{-1} to 60 °C cm^{-1}; the Marangoni Convection Experiment Unit, which will impose a temperature gradient across a liquid column to investigate the surface-driven convection and heat-transfer effects which often plague microgravity materials processing; the Gas Evaporation Experiment Facility, which will be used to study the spherical transport of silver from a heated filament and its deposition on a surrounding sphere in microgravity where natural convection is suppressed; and finally, the Organic Crystal Growth Experiment Facility, which will grow large and high-quality single crystals of organic metal by diffusion.

The life sciences complement of the mission includes the Free Flow Electrophoresis Unit, which will be used to separate biogenic material; the Vestibular Function Experiment Unit, which is a life support system for two carp which will be used to investigate visuo-vestibular interactions; the Egg Rack, which will be used to house 30 chicken eggs fertilized preflight, will be used to examine the suppression of bone growth that has been observed in humans and monkeys exposed to extended microgravity; the Enzyme Crystallization Kit, which will be used to grow large single crystals of protein so that diffraction techniques may be used to determine their structure;

the Protein Crystal Growth experiment, a complement to the previous experiment, will grow another class of proteins using a different technique; the Cell Culture Kit, which will grow a variety of cells in microgravity and fix them at various stages of development; the Fly Container, which holds about 100 fruit flies to be used to assess the space radiation environment's influence on inducing wing hair mutations in offspring; the Radiation Monitoring Device, which will be used in the development of radiation protection technology and for noting biological effects on living specimens; and the Fungi Growth Chamber, which will study the circadian rhythm of a common fungus.

Other life science missions include the Physiological Monitoring System, which will record the physiological status of the Japanese crewman during the mission; the Urine Monitoring System, which will complement the above study by investigating endocrine and metabollic changes in association with exposure to microgravity; the Light Stimulation Experiment System, which is designed to investigate eye movements and motor functions (in an effort to design better man-machine interfaces for space flight, subjects will also manually track a random light pattern using a hand controller); the Frog Embryology Experiment, which will examine the low-gravity development of frog eggs fertilized on-orbit; the Autogenic Feedback Experiment, which will collect data on the effectiveness of using standard biofeedback techniques to control the onset of space motion sickness among crewmembers; the Lower Body Negative Pressure experiment, which will apply a negative pressure to the lower trunk of the subject crewman to counter the headward fluid shift observed in space flight crewmembers which could affect cardiac performance; Magnetic Resonance Imaging, which will be performed on crewmen before and after the flight to examine physical changes resulting from exposure to microgravity; and finally, the Fluid Therapy System, which is an element of the planned space station health maintenance facility. The apparatus will generate sterile water from onboard potable water, reconstitute intravenous solutions from the sterile water, and validate the action of the pump for intravenous injections into a simulated arm.

The mission is well into its design phase and integration of the hardware will begin soon. Afterward, the mission will progress into the operations phase. Crew training on experiments and integrated simulations will begin about 2 years before launch. The standard crew size of five (commander, pilot, and three mission specialists) will be augmented by a Japanese payload specialist and a U.S. payload specialist. The shuttle will be placed in a 160 nmi orbit at an inclination of 44 degrees and will have continuous payload operations for 7 days.

F.W. Leslie/ES42
(205) 544-1633
Sponsor: Office of Space Science and Applications

Astronomy and Astrophysics

Astronomy and astrophysics are interdependent with the space program, since many observations in these fields can only be made above the atmosphere. MSFC had project responsibility for early experiments in gamma rays (SO15) and x-ray astronomy (on the Saturn V instrument unit). Starting with Skylab, MSFC has had an increasing role in managing, developing, and performing astrophysics experiments in diverse areas such as infrared astronomy, relativity, and the elemental composition of cosmic rays. MSFC has managed or performed the development of major astrophysics observations and many experiments including the Apollo Telescope Mount on Skylab, the three High Energy Astronomy Observatories, the Hubble Space Telescope, Spacelab astrophysics experiments, and major experiments on the Gamma Ray Observatory.

Responsibility for future missions includes the Astro Mission on the space shuttle and the Advanced X-Ray Astrophysics Facility (AXAF). The Space Science Laboratory is engaged in experimental and theoretical research in x-ray astronomy, gamma-ray astronomy, astrophysics, infrared astronomy, and cosmic rays. New detector systems, instruments, and experiments for future space flight missions are under development. Balloon-borne experiments and ground-based astronomical observations are being conducted. In connection with project management responsibilities such as the AXAF program, an increasing role in astrophysics at MSFC is foreseen.

Experimental X-Ray Astronomy

Development of advanced x-ray astronomy detectors to explore the energy range of 5–100 keV continues to be a primary concern of the X-Ray Astronomy Branch at MSFC. This regime is above that accessible to conventional reflecting x-ray telescopes, such as the type flown on the Einstein High Energy Astronomy Observatory-2 and the European X-Ray Astronomy Satellite, and thus remains ripe for exploration.

The basic requirements for detectors in this energy range are well satisfied by xenon-filled multiwire proportional counters (MWPC), which combine large collecting areas with reasonable energy and spatial resolution. While the standard MWPC has been in use for a long time, several techniques have been developed that dramatically improve the performance of the device. The first of these is multistep operation, wherein the detector is divided into two regions. One region is devoted to measuring the energy of the incoming x-ray photon, and the other is devoted to position sensing. In this way the detector can be simultaneously optimized for both parameters, a condition which is impossible to achieve in a standard MWPC. The second technique is that of fluorescent gating, which makes use of the fact that above the *K* shell in xenon (35 keV), true x-ray interactions predominantly induce fluorescence in the detector gas. By detecting this fluorescence and accepting only those events that produce it, the pervasive cosmic ray background, against which all sources must be measured, is effectively discriminated against.

As part of the development program, recently a full-size single-stage detector was flown to investigate the efficiency of fluorescence gating. The device formed the heart of a coded mask telescope having 7 arc-minute angular resolution and 750 cm^2

(295 in^2) of useful collecting area. This telescope was flown as part of NASA's SN1987A balloon campaign in collaboration with the Harvard-Smithsonian Center for Astrophysics. Data from this flight have yet to be analyzed, but indications are that the instrument performed extremely well during flight, and that the background in the fluorescence-gated mode was lower than expected. Conversely, the efficiency for detecting fluorescence produced by true x-ray interactions was found to be very high; fluorescence pairs from the Crab supernova remnant, used as a calibration source, were clearly visible in 100 s of quick-look data. The results and experience from this flight will be used to fine tune the instrument for stage II of the development work, which will include multistep operation.

In addition to building flight instruments, work continues on developing new instruments and techniques for x-ray astronomy. Typical of these is a recently started investigation of the light produced in proportional chamber avalanches. The goal is to utilize this light for position sensing. If successful, this technique could greatly reduce the complexity of the current generation of instruments, and could provide enhanced spatial resolution and charged particle rejection capabilities.

Ramsey, B.D. and Weisskopf, M.C.: The Performance of a Multistep Proportional Counter for Use in X-Ray Astronomy. IEEE Trans. on Nucl. Sci., Vol. NS-34, p. 672, 1987.

Ramsey, B.D., Weisskopf, M.C. and Elsner, R.F.: A Fluorescent Gated Proportional Counter for X-Ray Astronomy. Proceedings, Second International Symposium on Optical and Electro-Optical Applied Science, SPIE Vol. 597, p. 213, 1986.

M.C. Weisskopf/ES65
(205) 544-7740
Sponsors: Office of Space Science and Applications
Center Director's Discretionary Fund

Observational and Theoretical X-Ray Astronomy

During the past year, research in x-ray astronomy focused on three topics: quasi-periodic oscillations (QPO's) from the galactic bulge and other compact x-ray sources, x-ray polarimetry, and studies of active galactic nuclei.

The study of QPO's is of great interest because of their potential use as a probe of the physical processes taking place in compact x-ray sources. During the past year, various aspects of shot-noise models for QPO's have been explored and related to physical models for these sources. Calculations are underway of the second order auto-correlation function and bispectrum expected for shot-noise models. These functions may provide information on the time structure of the unresolved shots. Studies continue of the physical properties and effects of the electron scattering cloud thought to encase QPO sources. This work entails Monte Carlo simulation and analytical calculation of the scattering process leading to predictions of the relative delays between photons of different energies and for the emergent spectrum. Work also continues on the QPO's previously discovered in European X-Ray Observatory Satellite power spectra for the pulsing x-ray binary Centaurus X-3. These power spectra show complicated structure and time variability, providing valuable probes into the physical processes responsible for QPO's.

X-ray polarimetry is a diagnostic tool for probing important properties of cosmic x-ray sources. It has not yet realized its full potential due to the limitations of available instrumentation. The advent of grazing incidence telescopes, together with new techniques of measuring x-ray polarization, now promise an increase in the number of objects with measurable x-ray polarization from 1 supernova remnant (the Crab Nebula), to around 50. Objects that may be measurable include pulsing x-ray binaries, black hole candidates, and perhaps a handful of active galactic nuclei. The MSFC x-ray astronomy

group is participating in an international collaboration, with Columbia University as the lead institution, to build and fly a sensitive x-ray polarimeter at the focus of one of the XSPECT telescopes on the SPECTRUM-X-Gamma mission. Such measurements of x-ray polarization will provide important constraints on emission mechanisms and geometries. At MSFC, a Monte Carlo code is being assembled in order to provide a complete simulation of the polarimeter. These simulations will assist detailed design of the polarimeter, and will allow the investigation and understanding of instrumental systematic effects.

The most luminous discrete x-ray sources in the universe are quasars and clusters of galaxies. In contrast with the thermal bremsstrahlung emission from the intracluster plasma of galaxy cluster sources, the physical processes occurring in quasars and other active galactic nuclei (AGN's), such as blazars (highly polarized quasars), radio galaxies, and Seyfert I galaxies, are not well understood. It is, however, generally believed that AGN's are powered by accretion onto a supermassive black hole. This frequently leads to the formation of a relativistic jet, which emits nonthermally by way of synchrotron and Compton-scattering mechanisms. In collaboration with Lawrence Livermore Laboratory, a numerical code is being developed to determine self-consistently the structure and emergent spectra of thermal accretion disks, which may account for some of the ultraviolet emission from AGN's. When completed, this code will also be applicable to other thermal accretion disks, such as those in x-ray binaries and cataclysmic variables.

Shibazaki, N., Elsner, R.F., Bussard, R.W., Ebisuzaki, T. and Weisskopf, M.C.: Shot-Noise Cross-Correlation Functions and Cross Spectra: Implications for Models of QPO X-Ray Sources. Astrophys. J., Vol. 331, p. 247, 1988.

Scott, H.A. and O'Dell, S.L.: Spectra of AGN Accretion Disks — Preliminary Results. IAU Symposium No. 134: Active Galactic Nuclei, D.E. Osterbrock and J.S. Miller, eds., New York, in press, 1989.

M.C. Weisskopf/ES65
(205) 544-7740
Sponsor: Office of Space Science and Applications

Infrared Astronomy and Cometary Research

This year, infrared (IR) astronomy at MSFC has focused on two research areas: the extensive observation of comets, protoplanetary disks, and star-forming regions with the previously developed MSFC mid-IR camera; and development of two new IR detector systems. The mid-IR camera, which has been fully operational for 4 years, was developed for astronomical observations at 8–30 μm. The key component is a spatial array of 20 gallium-doped germanium bolometers, which are extremely sensitive in the high-thermal-background environment of ground-based observations. Because of its relatively large spatial coverage, the camera permits many types of observations that are not possible with smaller field of view, single-channel IR photometers.

The unique capabilities of this camera were demonstrated when it was used to obtain the first ground-based thermal-IR image ever made of a comet, Giacobini-Zinner, followed by images of Comet Halley and Comet Wilson (March 1987). After making the first detection (April 1988) of Comet Tempel 2 in the thermal IR, this comet was mapped on three nights in late 1988. Tempel 2 is being studied widely by astronomers. These observations were made at the NASA IR Telescope Facility on Mauna Kea, HI. The IR radiation from comets is emitted by dust grains which have been expelled from the comet nucleus and heated by sunlight. Detailed analysis of the IR images has provided insight into the rate at which particulates leave the nucleus, the types of particles leaving, and their temporal behavior. Because nearby comets rapidly change appearance, the MSFC IR camera is uniquely suited to obtain an image in a short enough time period for the results to be meaningful.

Because of its outstanding sensitivity, in 1988 the MSFC IR camera made the first, and so far the only, spatially-resolved detection in the mid-IR of the famous circumstellar disk around the star Beta Pictoris. This disk was discovered in 1983 with the Infrared Astronomical Satellite (IRAS) and is thought to be one of the best examples of a

protoplanetary dust cloud. The MSFC camera observations showed that the disk may contain a short-lived component of grains that may have to be continuously replenished, possibly by comets in the Beta Pictoris system.

In addition to its application to cometary research and protoplanetary studies, the MSFC IR camera has studied IR radiation from galaxies detected by IRAS. The camera permits detailed maps to be made of these galaxies, which often are strong IR sources. The IR radiation is produced when dust is heated by newborn stars, and currently provides the only means to determine how rapidly stars are forming. The efficiency of the IR camera is demonstrated by the capability to map more than 10 galaxies in an observing night, whereas with previous IR instruments a whole night was needed to map just one galaxy.

In parallel with the observational program using the mid-IR camera, which has moderate spatial resolution (about 4 arc-sec), is the development of a new bolometer array which will have very high spatial resolution (about 0.4 arc-sec). This system, which will be cooled to 0.3 K, will be used to study the 8- to 30-μm emission from extremely distant or very compact sources such as ultraluminous galaxies and quasars. Array construction is nearing completion. Construction is also nearing completion on a unique camera for use in the near-IR, at 1–5 μm. The near-IR camera will contain an integrated array with 4,000 pixels, and will be used for a broad range of projects including the search for newly forming galaxies.

Telesco, C.M., Becklin, E.E., Wolstencroft, R.D. and Decher, R.: Resolution of the Circumstellar Disk of Beta Pictoris at 10 and 20 microns. Nature, Vol. 335, p. 51, 1988.

Telesco, C.M. and Decher, R.: The Infrared Structure and the Origin of the Starburst Disk in NGC 1068. Astrophys. J., Vol. 334, p. 573, 1988.

Campins, H., Lien, D.J., Decher, R., Telesco, C.M. and Clifton, K.S.: Infrared Imaging of the Coma of Comet Wilson. In press, 1989.

C.M. Telesco/ES63
(205) 544-7723
Sponsor: Office of Space Science and Applications

Burst and Transient Source Experiment

The Burst and Transient Source Experiment (BATSE) is one of four experiments on the Gamma Ray Observatory (GRO). The GRO will be the second of the four Great Observatories in space astronomy that NASA intends to place in Earth orbit by the year 2000. During the past year, final assembly, testing, and calibration of BATSE was performed at MSFC. The system was delivered to the mission contractor, TRW, for integration and testing on the GRO. BATSE was designed, assembled, and tested primarily by the in-house engineering and technical staff of the Science and Engineering Directorate of MSFC.

The primary scientific objective of BATSE is the study of gamma-ray bursts. BATSE consists of eight detector modules arranged on the corners of the GRO to provide the maximum unobstructed view of the celestial sphere. Each detector module contains a large-area detector, optimized for sensitivity and directional response, and a spectroscopy detector optimized for broad energy coverage and energy resolution (Fig. 46).

The BATSE instrument will allow the observation and location of hundreds of gamma-ray bursts with unprecedented sensitivity for performing spectral observations and rapid temporal variability studies. In addition, the locations of some stronger bursts will be determined quicker than previously possible, so that longer-lived emission at other wavelengths can be sought. BATSE also provides a gamma-ray burst signal and a solar flare trigger signal to the other experiments on the GRO.

Gamma-ray bursts remain one of the least understood phenomenon in astrophysics. Although many theories of gamma-ray bursts have been proposed, the explanation of them is still quite speculative. Most recent theories propose that gamma-ray bursts are associated with old neutron stars within the galaxy. Initial attempts to identify the bursts with known objects have not succeeded. Recent observa-

tions have confirmed the existence of spectral absorption features in gamma-ray bursts. Other experiments have detected gamma-ray emission up to 80 MeV from many bursts, and have established a new class of repeating bursts with soft spectra.

It is now recognized that there are distinct classes of gamma-ray bursts that probably have different spatial distributions, emission mechanisms, and perhaps different central objects. Some types of bursts may be extragalactic, such as the burst on March 5, 1979. The soft, repeating gamma-ray bursts are associated with the central galactic bulge. The objective of burst classification and the determination of the spatial distribution of the different classes of gamma-ray bursts can be met through the detection and localization of many hundreds of gamma-ray bursts by BATSE. The spatial distribution of bursts in galactic coordinates or the association of certain types of bursts with extragalactic objects such as the Large Magellanic Cloud, M31, or the Virgo Cluster would immediately provide the much sought-after distance scale needed to provide luminosities. Sensitive observations by the BATSE large-area detectors will provide a large population sample along with a single-spacecraft determination of burst locations.

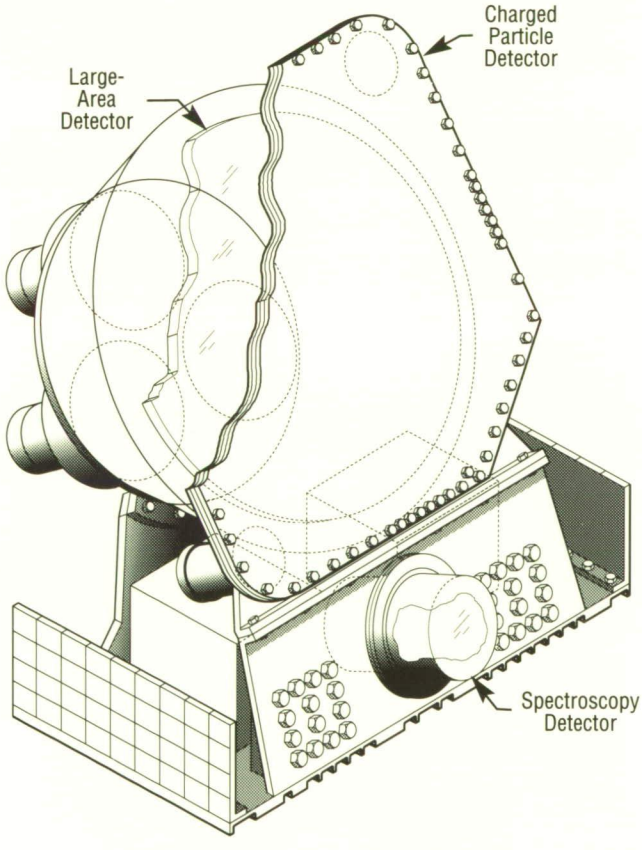

Figure 46. BATSE Module

Many of the observational features of BATSE such as full sky coverage, a wide energy range, and large, sensitive detectors will also permit the simultaneous accomplishment of secondary objectives. These include the nearly continuous monitoring of stronger sources, transient sources, and solar flares within the BATSE energy range. It may also be possible to provide an early detection of explosive phenomena in the galaxy, such as novae and supernovae.

Fishman, G.J., Meegan, C.A., Wilson, R.B., Paciesas, W.S., Parnell, T.A., Austin, R.W., Rehage, J.R., Matteson, J.L., Teegarden, B.J., Cline, T.L., Schaefer, B.E., Pendleton, G.N., Berry, F.A., Jr., Horack, J.M., Storey, S.D., Brock, M.N. and Lestrade, J.P.: BATSE: The Burst and Transient Source Experiment on the Gamma Ray Observatory. Proceedings, GRO Science Workshop, Goddard Space Flight Center (GSFC), to be published, 1989.

Fishman, G.J., Meegan, C.A., Wilson, R.B., Paciesas, W.S., Parnell, T.A., Matteson, J.L., Teegarden, B.J., Cline, T.L., Pendleton, G.N. and Schaefer, B.E.: The Burst and Transient Source Experiment (BATSE) Scientific Objectives and Capabilities. Proceedings, GRO Science Workshop, GSFC, to be published, 1989.

G.J. Fishman/ES62
(205) 544-7691
Sponsor: Office of Space Science and Applications

Solar Physics

The Sun is the nearest star and is the source of energy which controls the environment of the space surrounding the Earth and of the Earth itself. To understand the influence of the Sun on terrestrial systems and the space environment through which man will soon travel to explore the inner solar system, knowledge is needed of the processes that occur in the Sun's outer atmosphere which lead to generation of the high-energy particles and radiation that pervade interplanetary space.

These phenomena are intimately connected to the Sun's magnetic field, which is thought to be generated by a dynamo action arising from the interaction between convective and rotational motions at the base of the convection zone deep within the Sun. As the magnetic field emerges into the solar atmosphere, it heats and concentrates atmospheric material into a wide range of structures. The instability of the structures gives rise to flares and coronal mass ejections whose products propagate through space to Earth and beyond to the boundary between the solar wind and the interstellar medium.

The properties of the solar magnetic field form the basis of the research at MSFC. Through direct observation of the vector field, a capability developed at MSFC and still quite unique, we are attempting to understand how the energy stored in the magnetic field by the convective motions of the Sun's atmosphere is released, and how the products of this release are propagated. We are continuing to develop the technologies needed for future ground- and space-based magnetographs. Of particular interest are advanced polarimeters and large focal plane arrays with high-speed readouts. Our plans include development of a balloon-borne instrument as a precursor to a satellite mission.

We have continued to develop instruments based on normal incidence, multilayer optics for imaging the million-degree plasma that forms the solar corona, and an investigation based on these concepts has been selected for flight on Space Station Freedom. *This investigation will allow us to observe how the influence of the magnetic field extends into the outer solar atmosphere and, coupled with new theoretical and analytical approaches, to understand how the magnetic field is transported through the solar system to the distant boundaries of interstellar space.*

Coronal and Interplanetary Physics

The solar atmosphere, or corona, expands supersonically and becomes the solar wind. The Sun's highly structured magnetic field superimposes a complex pattern on this expansion and is also the source of a large variety of temporal variations. The direct cause of coronal expansion is the million degree temperature of the gas. However, no explanation has successfully been made of why the solar corona is more than 500 times hotter than the surface of the Sun. The magnetic field is somehow involved, but little else is known beyond this.

The earliest ideas for coronal heating invoked sound waves generated by the solar convection zone. Those ideas have failed but have been replaced by a class of new ideas involving magnetohydrodynamic (MHD) waves. The main problem with sound waves is that they do not propagate into the corona. MHD waves are capable of propagating into the corona where they can be trapped or dissipated, or can accelerate the plasma. Present data place only very weak restrictions on theoretical models.

With this background, several scientists at the University of Alabama in Huntsville (UAH) and MSFC (C.-H. An, R.L. Moore, Z.E. Musielak, S.T. Suess, and Y.C. Xiao) have been developing theoretical MHD wave models designed to answer critical questions about wave propagation in the corona and the solar wind. Two general types of problems have been addressed in the past year. One is the trapping of MHD waves in the solar corona and the other is the trapping and reflection of MHD waves at interfaces.

Trapping of MHD waves can occur in the corona because the characteristic speed of the waves, which is small near the surface of the Sun, rises and goes through a maximum within 20 solar radii of the surface. Waves which propagate upward from the solar convection zone are partially reflected so that, for a given wave flux in the interplanetary medium, the wave energy density in the corona will be much larger than would be the case in the absence of trapping. The models developed at MSFC show the trapping being strongly dependent on temperature — becoming important for temperatures less than about 800,000 K. This is just slightly below coronal temperatures, a coincidence that is highly intriguing. Presently, the models are being extended to

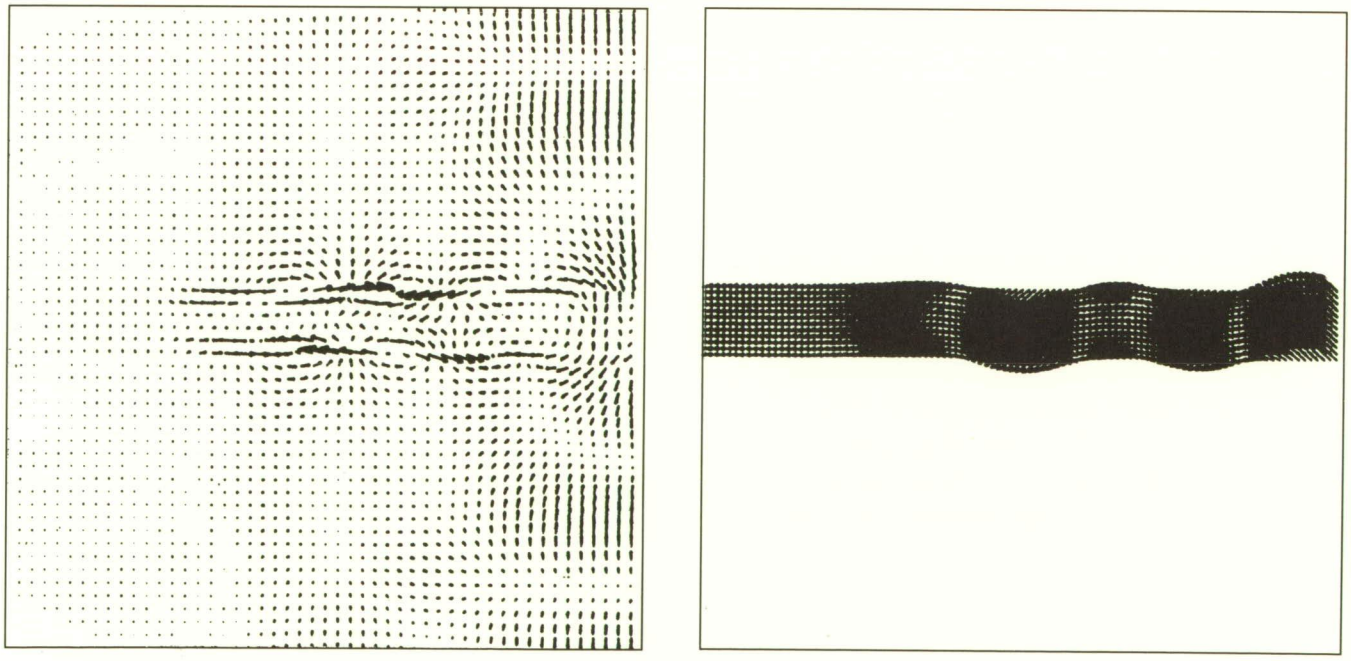

Figure 47. Magnetic Field Vectors (Left) and Velocity Vectors (Right) in a Magnetic Flux Tube Surrounded by a Nonmagnetized Gas and Undergoing a Transverse Displacement at Its Base

include a more realistic description of the complexities of the solar magnetic field.

Observations of the corona made during solar eclipses and from the Solar Maximum Mission, Skylab, and other orbiting solar observatories show that sharp boundaries are abundant in the corona. When the wavelength of a wave is long compared to the thickness of the boundaries, the boundaries can be considered to be infinitely thin interfaces. The theory for MHD waves being trapped or reflected at interfaces is thus applicable. A second major MHD wave project has been to apply numerical and analytic models of waves at interfaces to coronal and interplanetary problems. This work comes back to coronal heating and solar wind acceleration when MHD wave propagation is analyzed through the structured corona, along magnetic flux tubes, and in magnetic loops. Figure 47 illustrates the magnetic field and velocity field in a flux tube during a numerical simulation. The figure shows that an initially transverse wave at the base undergoes mode conversion so that, after a few wavelengths, it becomes a purely longitudinal wave. This result depends on physical parameters such as the field strength and gas density. The simulation is being applied to defining when mode conversion is most effective. Mode conversion is a process that will lead to dissipation once an MHD wave has reached the corona.

The in situ observation of MHD waves in the corona is the prime objective of the proposed NASA Solar Probe mission. This spacecraft is to pass within 3 solar radii of the photosphere and pass through the portion of the corona where MHD waves are suspected of being most important. The present theoretical work will lay a foundation for the interpretation of data to be collected on the Solar Probe mission.

An, C.-H., Musielak, Z.E., Moore, R.L. and Suess, S.T.: Reflection and Trapping of Transient Alfvén Waves Propagating in an Isothermal Atmosphere with Constant Gravity and Uniform Magnetic Field. Astrophys. J., in press, 1989.

S.T. Suess/ES52
(205) 544-7611
Sponsor: Office of Space Science and Applications

Solar Flares and Coronal Mass Ejections

Solar flares and coronal mass ejections are large explosions in magnetic regions of the solar atmosphere. The largest of these events are the greatest explosions in the solar system: the power of the energy burst, about 10^{32} erg in about 10^{3} s, or about 10^{29} erg/s, far exceeds the steady power of the solar wind (about 3×10^{27} erg/s). An example of a coronal mass ejection (observed with the High Altitude Observatory Coronagraph/Polarimeter on the Solar Maximum Mission spacecraft) is shown in Figure 48.

An erupting chromospheric filament often forms the core of a coronal mass ejection, as in this figure. For hours to days before the eruption, the filament is present and traces out a greatly sheared magnetic field in the solar atmosphere. The eruption of the filament marks the eruption of the sheared magnetic field in the region of the filament. If the magnetic field in the sheared region is strong enough (100–1,000 gauss), the field eruption occurs in the midst of a flare marked by intense particle acceleration and plasma heating. If the magnetic field in the sheared region is weaker (about 10 gauss), the

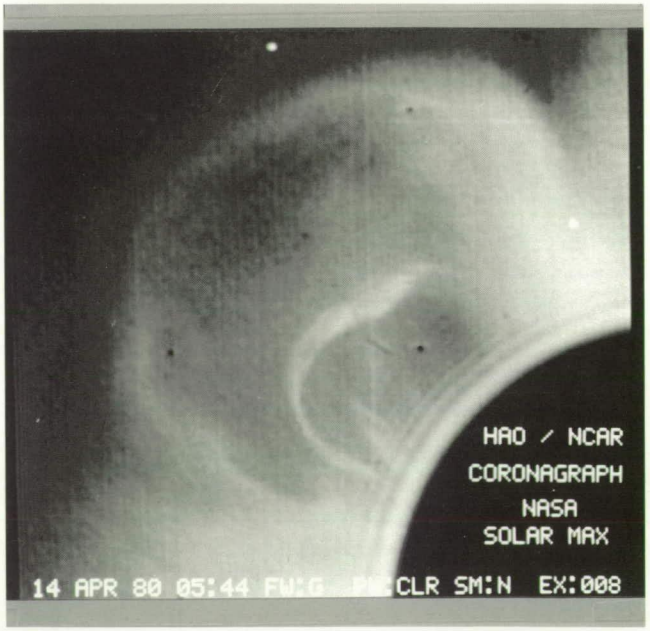

Figure 48. Erupting Chromospheric Filament at Core of Coronal Mass Ejection

particle acceleration and plasma heating are much weaker, but a large coronal mass ejection can still be produced. This raises the question of whether filament eruptions and coronal mass ejections with flares are driven in the same way as those without flares.

This question was investigated by estimating the amount of magnetic energy dumped from the erupting field, using the observed expansion of the filament to gauge the expansion of the field. The energy released by the expansion was found to be ample to drive both the flare and the coronal mass ejection. On this basis, it was proposed that both the flare and the coronal mass ejection are driven by the magnetic expansion that is partially traced by the erupting filament, and that all coronal mass ejections, with or without flares, are magnetically driven in this way.

In a further investigation of this matter, the observed development of filament eruptions from intense flares was examined for evidence of how eruptions of this class are driven. One possibility sometimes adopted as a working hypothesis is that the filament eruption and coronal mass ejection are consequences of the energy release in the flare. They are taken to be ejecta in the explosion resulting from the pressure pulse from the plasma heating in the flare. Evidence was found against this view and in favor of the view that the eruption is driven by magnetic force rather than by the flare plasma pressure.

The evidence is from four flares in which, in high-resolution chromospheric movies, a filament eruption was observed during the impulsive peak in flare energy release marked by a burst of hard x rays. In each of these eruptive flares, the filament eruption began before the onset of the flare impulsive phase, and the eruptive motion was consistent with a smooth evolution through the impulsive phase, accelerating, but showing no new acceleration attributable to the flare impulse. The chromospheric flare brightening in the impulsive phase occurred in compact areas much smaller than the overall span of the erupting filament. These characteristics are consistent with the hypothesis developed at MSFC that the filament eruption is not driven by the flare plasma pressure, but instead marks an eruption of sheared magnetic field driven by a global magnetohydrodynamical loss of equilibrium of the field configuration in the region of the flare. It appears that the filament eruption and the flare energy release are coordinated and driven by a common cause — the eruption of the whole field configuration. In this sense, the flare is an effect of the field eruption, which is a complete reversal of the roles previously attributed to these phenomena.

Moore, R.L.: Evidence that Magnetic Energy Shedding in Solar Filament Eruptions is the Drive in Accompanying Flares and Coronal Mass Ejections. Astrophys. J., Vol. 324, p. 1132, 1988.

Kahler, S. W., Moore, R.L., Kane, S.R. and Zirin, H.: Filament Eruptions and the Impulsive Phase of Solar Flares. Astrophys. J., Vol. 328, p. 824, 1988.

Moore, R.L.: Evidence that Coronal Mass Ejections are Magnetically Self-Propelled. Solar and Stellar Coronal Structure and Dynamics, R.C. Altrock, ed., National Solar Observatory, Sacramento Peak, Sunspot, NM, p. 520, 1988.

R.L. Moore/ES52
(205) 544-7613
Sponsor: Office of Space Science and Applications

Solar Magnetic Fields

The interaction of magnetic fields and plasmas is a common process throughout the universe, and it is the controlling force in the dynamic, high-energy phenomena observed on the Sun. Flares, mass ejections, and eruptive filaments are all examples of energetic processes that are generated by solar magnetic activity. The origin, evolution, and development of the solar magnetic field that produces this activity are central themes in today's solar research. Extensive observational studies are carried out to develop an understanding of just how the solar magnetic field plays this key role in solar activity.

MSFC has a unique instrument for observing the Sun's magnetic field, the MSFC Solar Vector Magnetograph. This instrument measures all three components of the magnetic vector on the Sun's surface, not just the single component that is measured with other operational magnetographs in the continental United States. The additional information derived from observations of the complete vector field has made significant contributions to an understanding of the magnetic Sun. Because of this unique research, MSFC is recognized worldwide as a leader in the study of solar magnetic fields.

In preparation for the next peak of solar activity that is expected to occur in 1991, MSFC scientists have been working to enhance the research capabilities of the magnetograph by making it possible to obtain cotemporal and coaligned observations of the structure and evolution of the solar magnetic field in both the photospheric and chromospheric levels of the Sun. Since these levels represent two different heights in the solar atmosphere, a three-dimensional picture of the solar field can be obtained.

This enhanced capability was made possible by coaligning an Hα telescope with the MSFC solar vector magnetograph (Fig. 49). This pair of telescopes can produce time-lapse digital images of coaligned Hα and magnetograph observations. The magnetograph images provide quantitative data on the vector magnetic field in the solar photosphere. These data are supplemented by the Hα images which delineate the morphology of the magnetic field in the solar chromosphere above the photosphere. By accurately coaligning the two instruments, the location of solar features such as prominences and flares, that are seen only in the Hα image, can be precisely positioned with the underlying photospheric field seen in the magnetograms. The resulting coaligned images will make it possible to study the dynamical changes in the magnetic field during solar flares. The location of the flare will be accurately positioned in the magnetic field image from its position in the Hα image. Knowing the flaring region in the magnetogram, the data can be closely examined for subtle changes in the magnetic field that are associated with the flare process, and real magnetic changes can be identified from among the small uncertain variations that are usually observed. Using video processing, movies can be made from the time-lapse images that allow tracking of these variations, comparison of them with variations seen in areas not affected by the flare, and a determination of whether or not they are real changes using the hindsight provided by following their evolution over the extended time period of the movie.

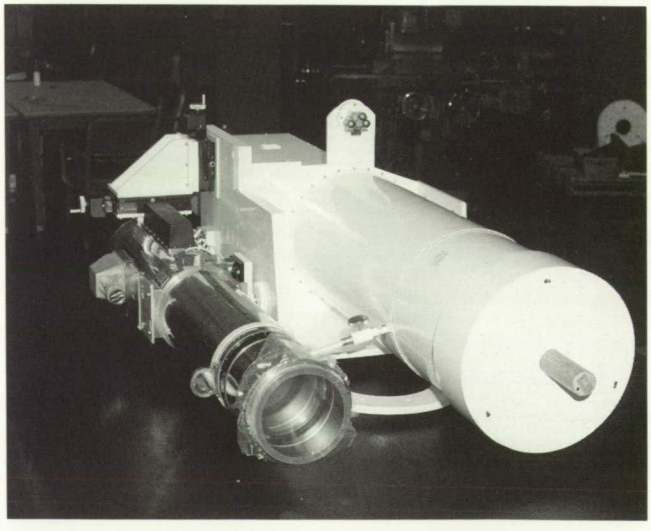

Figure 49. Coaligned MSFC Vector Magnetograph and H-α System

Through a Small Business Innovative Research program, a large-array charge-coupled device (CCD) camera and a data acquisition system (DACS) capable of rapidly processing the large quantities of data generated by the camera have been developed and will be incorporated into an Experimental Vector Magnetograph (EXVM) under development by MSFC scientists. The EXVM is designed to measure the Sun's vector magnetic field more accurately than any other existing magnetograph system. The camera includes four frame-transfer CCD's, each having 1,024 by 1,024 pixels, with half of the pixel area masked. The masked area serves as a temporary storage area where an image from the active area can be rapidly shifted and then read out while another image is formed in the active area. Each of the four CCD's is read out from two serial ports at a rate of 1.2×10^6 pixels s^{-1} at each port. With this design, there is a total imaging area of 1,024 by 2,048 pixels with eight readout ports so that the total array can be read in 0.22 s.

The DACS (Fig. 50) is designed to acquire data from the CCD camera; control instrument functions; perform data reduction, analysis, and storage; and provide host communications. At the heart of the system are eight custom-designed data processing elements (CDPE), one for each of the eight serial ports of the camera. Each CDPE has 0.75 megabytes of internal memory where up to 1,024, 12-bit images can be added. The eight CDPE's can perform block data transfers to four 12-megabyte memories through four subsystem buses. The 12-megabyte memories are linked to a graphics engine to produce high-resolution color graphic displays and to a μVAX computer with an array processor and optical disk storage system.

With the development of the EXVM, MSFC scientists intend to remain at the forefront of research in the study of solar magnetism.

M.J. Hagyard/ES52
(205) 544-7612
Sponsor: Office of Space Science and Applications

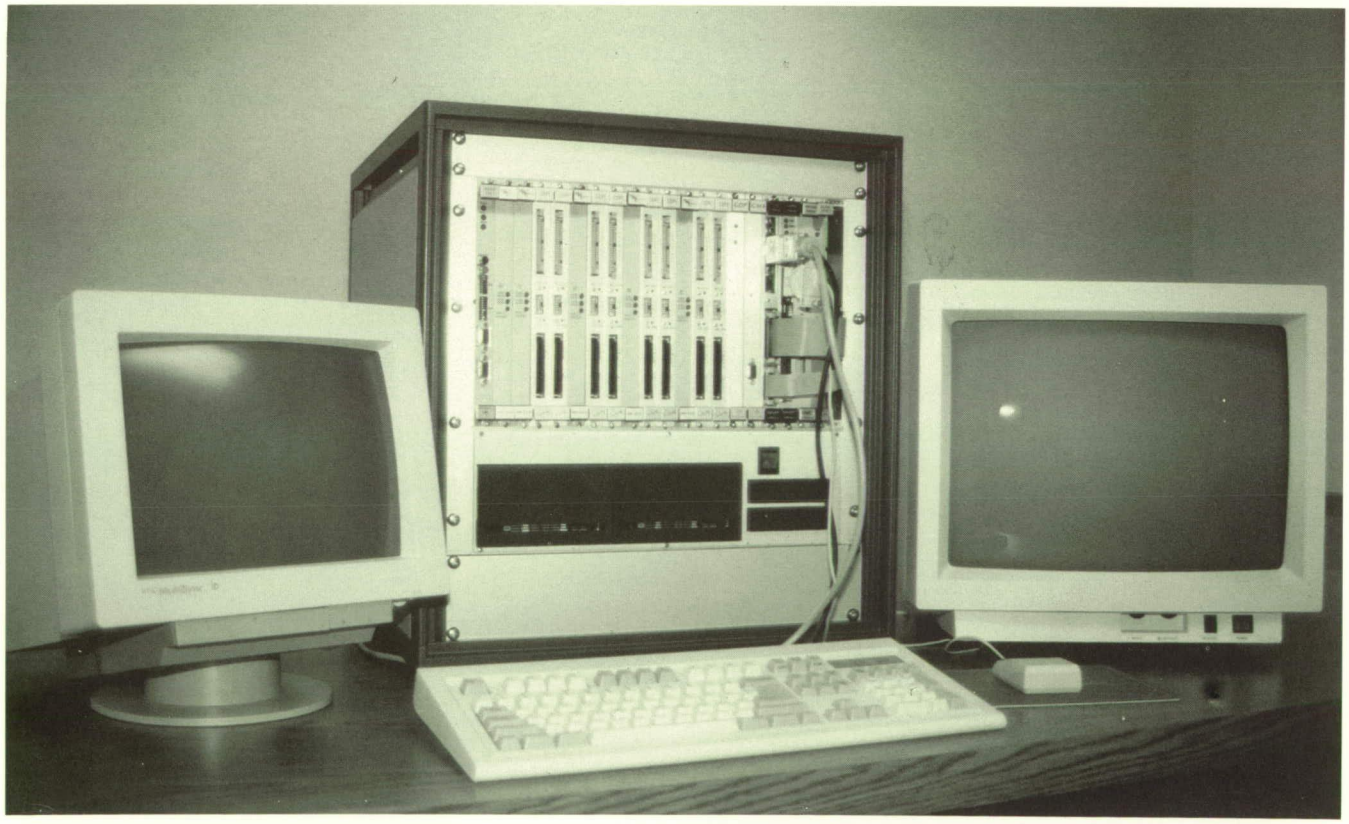

Figure 50. Custom-Designed Data Acquisition System

Schwarzschild Multilayer X-Ray Imaging Microscope Development

The high-resolution, low-scatter, full-disk solar x-ray images produced with the Stanford/MSFC Rocket X-Ray Spectroheliograph conclusively established that doubly reflecting multilayer x-ray imaging systems could be produced. The multilayer mirrors for the 173-Å telescope were made by coating extremely smooth (less than 3 Å RMS) substrates with molybdenum/silicon layers of 36.8-Å and 55.2-Å thickness, respectively.* Since each multilayer mirror reflects effectively in only a relatively narrow bandpass, primary and secondary mirror bandpasses must be accurately matched to assure high system throughput. The flight solar images also demonstrate that aplanatic imaging x-ray microscopes utilizing two spherical multilayer mirrors in the Schwarzschild configuration are feasible. Schwarzschild x-ray microscopes should be ideal for astronomical studies when used in conjunction with grazing incidence or multilayer x-ray telescope systems, and may also have important applications for laser fusion research and biological investigations. During the course of this effort, several Schwarzschild multilayer x-ray microscope optics were designed and analyzed. A 20x Schwarzschild x-ray microscope is being fabricated based upon the results of these studies.

An aplanatic x-ray microscope using two spherical mirrors can be constructed by imposing the Schwarzschild condition on selection of the mirror radii. The Schwarzschild condition can be understood by referring to Figure 51. The mirror surfaces S_1 and S_2 are concentric spherical surfaces of radii R_1 and R_2, respectively. The two mirrors have a common center of curvature. A complete discussion of a ray trace analysis of the Schwarzschild microscope configured for normal incidence multilayer applications has been presented by Hoover, et al.† The Schwarzschild condition for an aplanatic, two mirror imaging system can be expressed:

$$\frac{R_2}{R_1} = 1.5 - \frac{R_2}{Z_o} \pm \left[1.25 - \frac{R_2}{Z_o}\right]^{1/2}$$

where the "+" sign is used for magnifications greater than 5, and the "–" sign for magnifications less than 5.

Grazing incidence x-ray microscopes studied for use in combination with x-ray telescopes have severe limitations due to optical aberrations, strong vignetting, and severe scattering problems. Normal

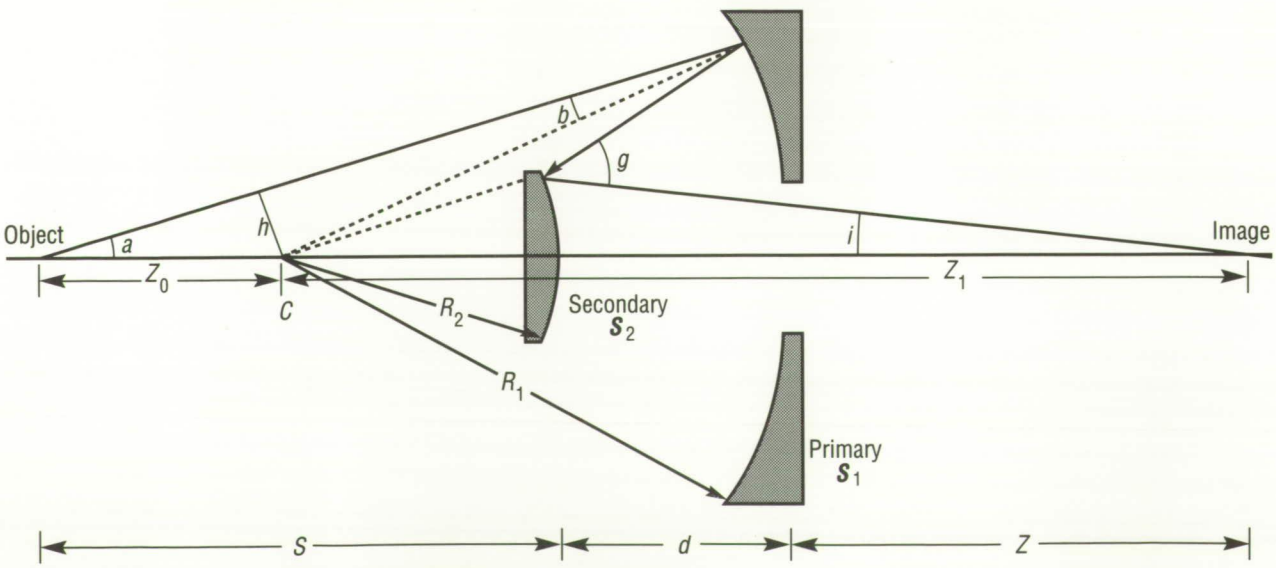

Figure 51. Schwarzschild Configuration for Aplanatic Normal Incidence Multilayer X-Ray Microscope

C-2

incidence multilayer optics can eliminate these problems. During the Spectral Slicing X-Ray Telescope‡ program, it was shown that a single multilayer mirror could be used to magnify the image from a grazing incidence x-ray telescope to produce images superior to grazing incidence optics alone. The Stanford/MSFC Rocket X-Ray Spectroheliograph flight confirmed these predictions as the 44-Å multilayers produced magnified images with noticeably less scattering than observed in the prime focus of the grazing incidence optic. The reduced scattering is due to the fact that multilayer reflectivity is the result of an interference process (Bragg diffraction), so the desired optically reflected intensity is proportional to the square of the amplitude of the diffracted light, but the scattered light adds linearly with intensity. The use of a Schwarzschild x-ray microscope to magnify the image produced by a grazing incidence or multilayer x-ray telescope offers many advantages. The most important advantages are reduced optical aberrations, improved spectral resolution, low vignetting, very low scattering, increased image size, and significantly improved spatial resolution.

A 20x Schwarzschild x-ray microscope was designed for operation at the 125-Å wavelength. To determine system depth-of-field and evaluate improvement in off-axis resolution which can result from intentional defocusing, the RMS blur radius versus object height, as a function of image plane position, was evaluated. In order to determine the diffraction limited resolution that may be achieved with the microscope, a series of point spread functions over the image plane Z_i = 120.016 cm (47.25 in) have been evaluated. This evaluation used Fourier diffraction analysis with the General Laser Analysis and Design code, which was developed at Los Alamos National Laboratory and for use on the Cray X/MP supercomputer. Figure 52 provides three-dimensional point spread functions revealing the intensity versus *X* and *Y* on the image plane for object height of 0, 0.5, and 1.0 mm (0, 0.019, and 0.039 in). These calculations were performed for radiation of 125-Å wavelength. Since the system magnification is 20x, these results imply a spatial resolution of 390 Å in the object plane. For object

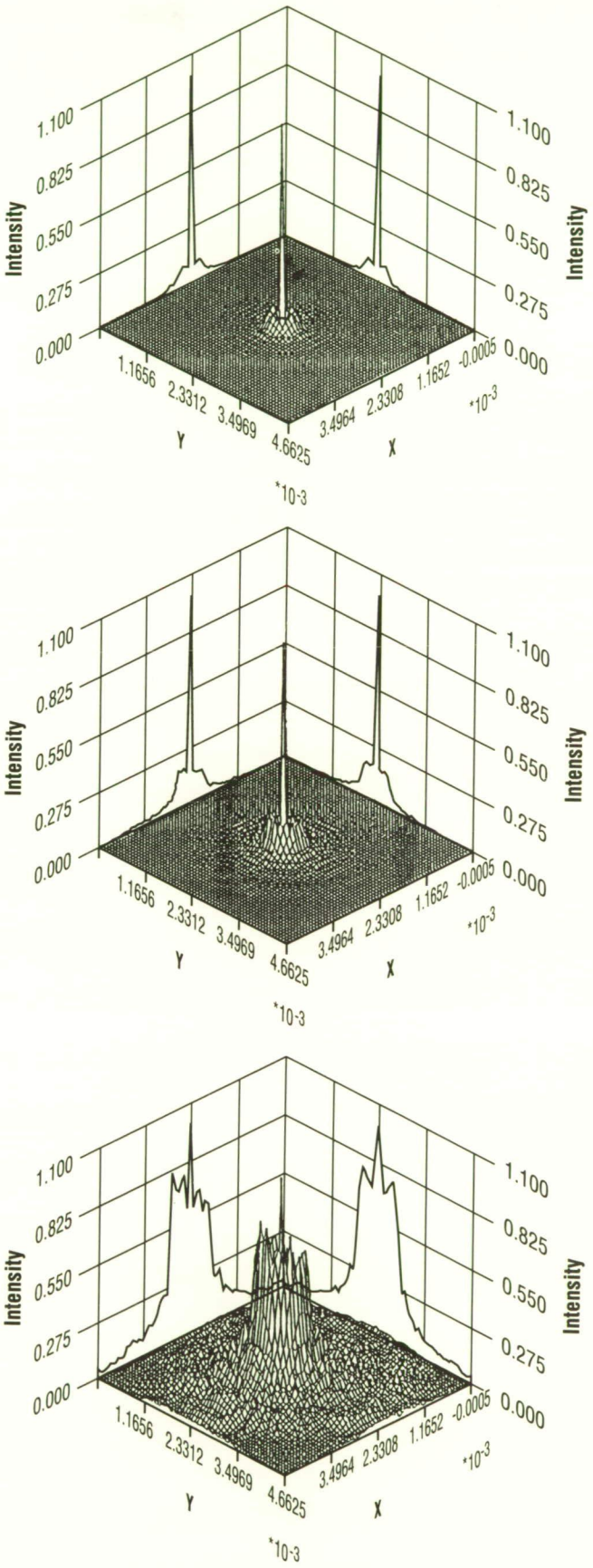

Figure 52. Three-Dimensional Point Spread Functions for the 20x Microscope On-Axis, 0.5mm and 1mm Off-Axis

displacements of 0.8 mm (.031 in) or more, the second- and third-order diffraction wings increase dramatically and the image quality degrades rapidly. In order to take advantage of this high-spatial resolution, photographic emulsions capable of resolving better than 1,300 line pairs/mm will be required. Ultra-high resolution photographic emulsions provided by Eastman Kodak are now being studied at MSFC to determine x-ray/extreme ultraviolet (XUV) sensitivity and establish optimal processing techniques for use with this microscope.

The 20x Schwarzschild x-ray microscope is being fabricated utilizing much of the technology implemented in the Multi-Spectral Solar Telescope Array (MSSTA) program. Dr. Phil Baker of Baker Consulting, Walnut Creek, CA, is fabricating the mirror substrates from Zerodur. The primary mirrors are concave spheres of 8-cm (0.31-in) diameter with a radius of curvature of 23 cm (0.91 in). The convex spherical secondaries are 2 cm (0.079 in.) in diameter with a 8-cm (.31-in) radius of curvature. The optical surfaces will be polished to 1-Å RMS surface smoothness. The multilayer optics will be coated by T. W. Barbee, Jr., at Lawrence Livermore National Laboratory. Dr. Barbee, one of the pioneers of multilayer x-ray optics, also produced the coatings used on the successful Stanford/MSFC Rocket X-Ray Spectroheliograph telescopes.

Microscope tube structures will be fabricated by filament winding methods. Longitudinal fibers will be applied to increase stiffness and to produce microscope tube structures with a near zero coefficient of thermal expansion. The same techniques that were used to fabricate the tube structures for this 12.7-cm (5-in) diameter MSSTA telescope will be utilized to construct the optical bench for the 20x Schwarzschild Multilayer X-Ray Microscope. Images will be recorded on high-resolution soft x-ray/XUV sensitive emulsions transported in 35-mm Canon T-70 cameras used in the rocket flight program.

*Walker, A.B.C., Jr., Barbee, T.W., Jr., Hoover, R.B. and Lindblom, J.F.: Soft X-Ray Images of the Solar Corona with a Normal-Incidence Cassegrain Multilayer Telescope. Science, Vol. 241, pp. 1781–1786, 1988.

†Hoover, R.B., Shealy, D.L., Gabardi, D.R., Walker, A.B.C., Jr., Lindblom, J.F. and Barbee, T.W., Jr.: Design of an Imaging Microscope for Soft X-Ray Applications. Proc. SPIE, Vol. 984, pp. 234–246, 1988.

‡Hoover, R.B., Shealy, D.L. and Chao, S.-H.: Spectral Slicing X-Ray Telescope. Optical Engineering, Vol. 25, pp. 970–978, 1986.

R.B. Hoover/ES52
(205) 544-7617
Sponsor: Center Director's Discretionary Fund

Stanford/MSFC Multi-Spectral Solar Telescope Array

On October 23, 1987, the Stanford/MSFC Rocket X-Ray Spectroheliograph produced the first full-disk, high-resolution soft x-ray/extreme ultraviolet (XUV) images of the Sun using normal incidence multilayer x-ray telescopes. These solar images exhibited lower x-ray scatter and higher spatial and spectral resolution than were previously obtained with grazing incidence x-ray optics. This provided a conclusive demonstration of the value of multilayer optics as a new observational tool for the soft x-ray/XUV regime. The high photographic densities obtained in relatively short exposure times on the photographic emulsions clearly established that excellent x-ray mirror reflectivity could be achieved at normal incidence. The x-ray images also demonstrated that multilayer primary and secondary mirrors with matching bandpasses could be constructed on convex and concave substrates. This rocket flight also established the value of the new tabular-grain (T-grain) photographic film* for astronomical investigations in the soft x-ray/XUV regimes (8–304 Å).

The images of the Sun obtained with these telescopes revealed many interesting and important features of coronal structure, including active regions, magnetically confined loops of hot plasma, coronal plumes, polar coronal holes, filaments, and numerous faint structures on the size scale of supergranulation and smaller (Fig. 53). The 6.35-cm (2.5-in.) diameter Cassegrain multilayer telescope operating in the bandpass peaked at 173 Å, producing the finest images of polar plumes yet obtained in XUV wavelengths. The previous observations in the soft x-ray/XUV regimes from Skylab were limited in resolution to 3–5 arc-sec, and provided data to only 0.4 solar radii above the limb. The multilayer telescope images had spatial resolution of 1 arc-sec and revealed extremely faint coronal features. Analysis of a typical polar plume† in a 200-s exposure permitted the electron density to be determined as a function of height out to 1.7 solar radii.

The 173-Å multilayer telescope will be reflown aboard the Stanford/MSFC Multi-Spectral Solar Telescope Array (MSSTA). This new payload is currently being developed with plans for a November 14, 1989 launch from the White Sands Missile Range, NM, aboard a Terrier-boosted Black Brant sounding rocket. Prof. A.B.C. Walker, Jr. (Stanford University) is the MSSTA principal investigator, with R.B. Hoover (MSFC), T.W. Barbee, Jr. (Lawrence Livermore National Laboratory), and J. Lindblom (Stanford) serving as co-investigators.

In addition to the two Cassegrain multilayer x-ray telescopes previously flown, MSSTA will incorporate seven new ultra-high resolution Ritchey-Chrétien telescopes, eight high-sensitivity Herschelian telescopes, as well as recently developed multilayer x-ray gratings. The payload is housed within the 55.88-cm (22-in) diameter rocket skin. The layout of the front of the MSSTA payload is shown in Figure 54. The 12.7-cm (5-in) diameter

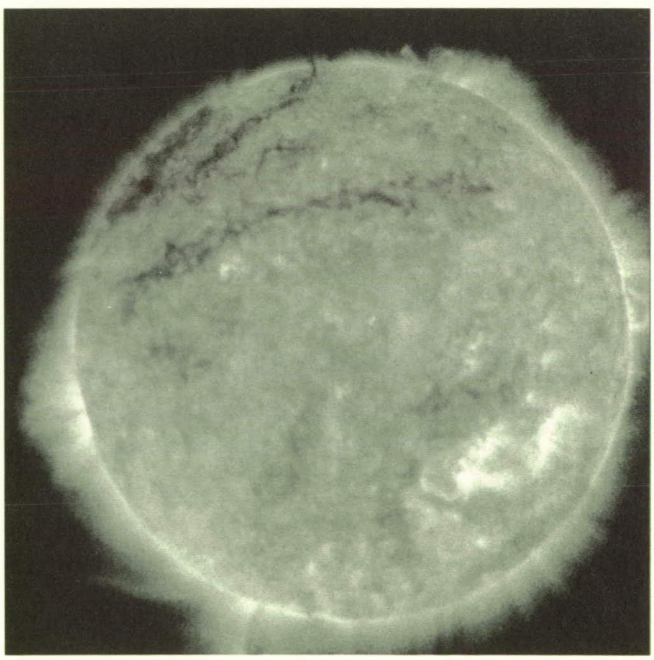

Figure 53. Stanford/MSFC Rocket X-Ray Telescope Image of the Solar Corona, October 23, 1987, 1809 UT (200 s Exposure)

Ritchey-Chrétien telescopes utilize hyperboloidal primary and secondary mirrors to minimize optical aberrations and ensure ultra-high resolution over a wide field of view. These mirrors will be coated to select important solar spectral lines or multiplets in the wavelength range from 150 to 1550 Å.

Since multilayer x-ray/XUV telescopes operate at normal incidence rather than grazing incidence, as did the x-ray telescopes which were flown on Skylab and the Einstein High Energy Astronomy Observatory, and since they are planned for the Advanced X-Ray Astrophysics Facility (in which radiation enters the telescope through one or more very thin annular rings), it is possible to obtain a very large collecting area with an extremely small telescope. Each of the 12.7-cm (5-in.) diameter Ritchey-Chrétien telescopes will have a geometri-

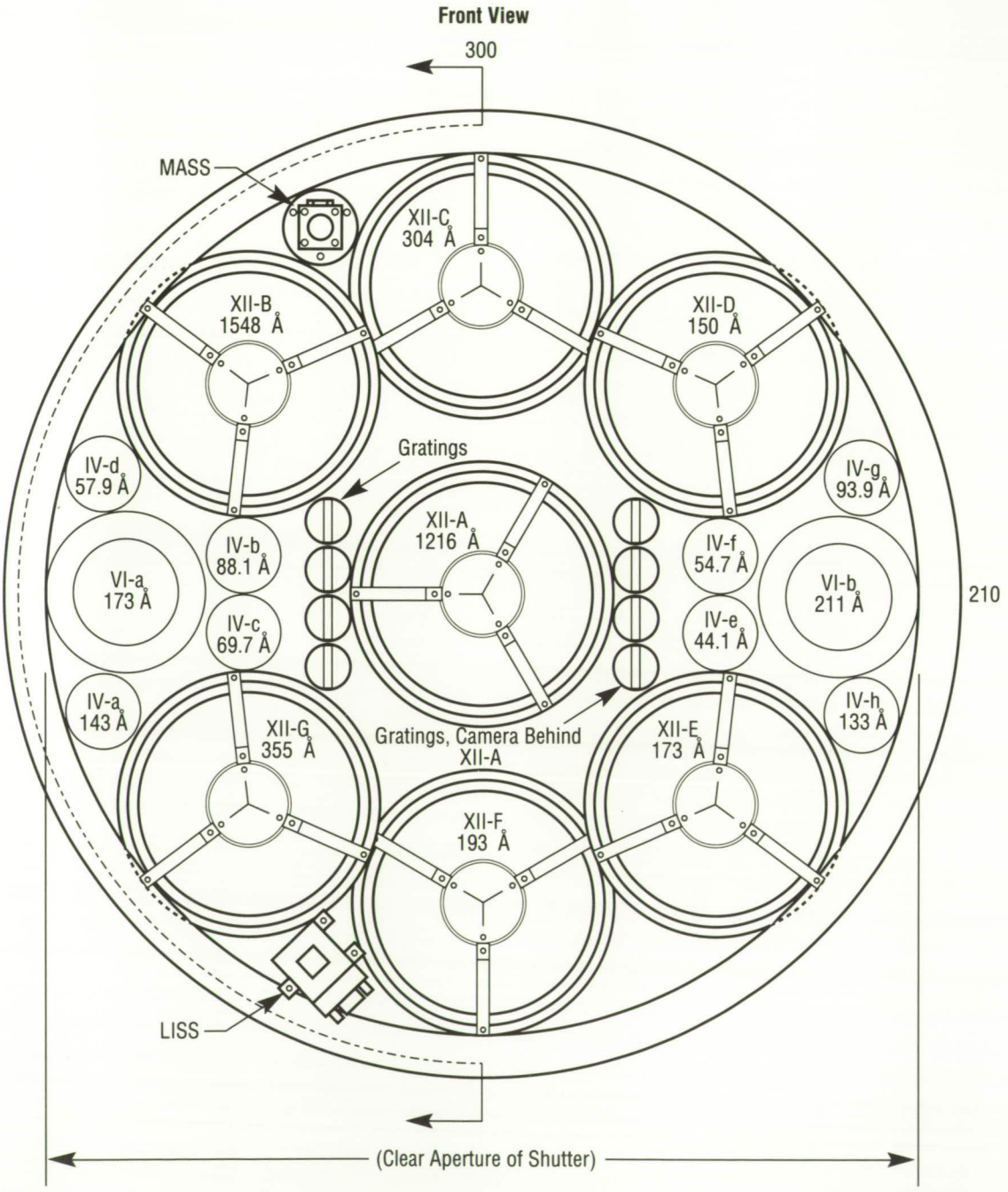

Figure 54. Front of Multi-Spectral Solar Telescope Array Showing Ritchey-Chrétien, Herschelian, Cassegrain Telescopes, and Multilayer Gratings

cal collecting area of 107 cm^2 (42 in^2), an order of magnitude greater than the Skylab S-056 x-ray telescope. The total geometrical collecting area of the MSSTA optical systems is approximately 850 cm^2 (335 in^2), which is over twice that of the Einstein telescope at 100 Å. Since the MSSTA telescopes operate at normal incidence, the severe aberrations and scattering problems encountered with grazing incidence systems are not a problem. It is anticipated that it will be possible to achieve diffraction-limited performance with some of these systems. This is of profound importance, as the diffraction-limited performance of a multilayer Ritchey-Chrétien telescope operating at 150 Å is equivalent to that of a 200-in. diameter Mt. Palomar telescope at 6000 Å wavelength in the visible light regime. The large images of the Sun produced by these systems will be recorded on special 70-mm x-ray/XUV sensitive photographic emulsions transported in Pentax 645 cameras. If pointing stability conditions during the flight are optimal, some of the MSSTA Ritchey-Chrétien telescopes may achieve spatial resolution in the 0.1 arc-sec regime. In addition to the observations in the 150- to 1550-Å wavelength regime with the Ritchey-Chrétien telescopes, MSSTA will also utilize eight single reflection paraboloidal (Herschelian) telescopes for imaging the Sun in selected soft x-ray wavelengths.

The mirror substrates have been polished to 1-Å RMS surface smoothness by Baker Consulting of Walnut Creek, CA. In collaboration with the Center for Applied Optics at the University of Alabama in Huntsville, a detailed ray-trace analysis of the Ritchey-Chrétien telescopes was performed. Three-dimensional diffraction intensity patterns were calculated and optimal focal positions were established to maximize performance over the entire 44 arc-minute field of view. The telescope structures were designed by Professor Walker of Stanford University with design and engineering support provided by MSFC. The telescope structures were fabricated at MSFC in the Filament Winding Facility. The telescope tubes were made by filament winding methods using AS4-12K graphite fiber with an HBRF55A epoxy resin matrix. Longitudinal fibers were applied to achieve a strong tube with a near-zero coefficient of thermal expansion. Detailed soft x-ray/XUV and vacuum ultraviolet (VUV) calibration of the entire MSSTA payload is planned at the SURF II synchrotron facility.

The Stanford/MSFC MSSTA should provide observations of the Sun with ultra-high spatial resolution and good spectral resolution. The many full-disk images recorded simultaneously at selected spectral lines and multiplets in the soft x-ray/XUV and VUV regimes, representing a wide range of chromospheric, transition region, and coronal temperatures within the solar atmosphere, should provide new information of unprecedented value for solar plasma diagnostics.

*Hoover, R.B., Barbee, T.W., Jr., Lindblom, J.F. and Walker, A.B.C., Jr.: Solar X-Ray/XUV Imagery With an Experimental Kodak T-MAX 100 Professional Film. Kodak Tech Bits, pp. 2–6, 1988.

†Walker, A.B.C., Jr., Barbee, T.W., Jr., Hoover, R.B. and Lindblom, J.F.: Soft X-Ray Images of the Solar Corona With a Normal-Incidence Cassegrain Multilayer Telescope. Science, Vol. 241, pp. 1781–1786, 1988.

Walker, A.B.C., Jr., Lindblom, J.F., O'Neal, R.H., Hoover, R.B. and Barbee, T.W., Jr.: The Stanford/MSFC Multi-Spectral Solar Telescope Array. Proc. SPIE, Vol. 1160, pp. 131–144, 1989.

R.B. Hoover/ES52
(205) 544-7617
Sponsor: Center Director's Discretionary Fund

Convection Zone Dynamics

Recent developments in the field of helioseismology have provided solar and stellar astronomers with their first glimpses of the interior of a star — the Sun. By accurately measuring the frequencies of acoustic oscillations (sound waves) at the solar surface, helioseismologists have determined the run of temperature and density throughout much of the solar interior, together with information on the depth of the solar convection zone and the variation of the Sun's rotation rate with depth and latitude. The results of these analyses are most accurate for the region of the solar interior extending from 20 percent of the Sun's radius out to about 95 percent of its radius. The region deep in the Sun's core is difficult to probe with acoustic oscillations because most of the observed oscillations do not extend to that depth. The region just below the surface is difficult to probe because it requires very short wavelength oscillations that are hard to resolve with ground-based telescopes.

During the last year, data from Mt. Wilson Observatory were analyzed to directly measure motions in the surface layers of the Sun. The data were acquired by Dr. Edward J. Rhodes, Jr. and colleagues at the University of Southern California, the Jet Propulsion Laboratory, and the University of California in Los Angeles. The data consist of velocity images of the full solar disk acquired at the rate of one every minute for 8 hours a day during July and August of 1988. While Dr. Rhodes and colleagues were examining the data for information on the acoustic oscillations, Dr. Hathaway at MSFC was examining the same data for information on the nearly steady flows — solar differential rotation, meridional circulation, and convective motions.

This data analysis program takes a series of velocity images and averages them together to remove the signal due to the acoustic oscillations. The resulting velocity image is then mapped onto a longitude-latitude coordinate system fixed with respect to the Sun's rotation axis. The spherical harmonic functions are then used to separate the different flow types according to their characteristics.

Several new results have been discovered from this work. A spectrum for the convective flows was constructed from the results of the analysis (Fig. 55). The spectrum exhibits a peak for convection cells with diameters of about 50,000 km (30,000 mi). The spectrum is broad and continuous and does not indicate the presence of any discrete components. The conventional wisdom for the last 30 years was that there were three or four distinctly different types of convection cells spanning the

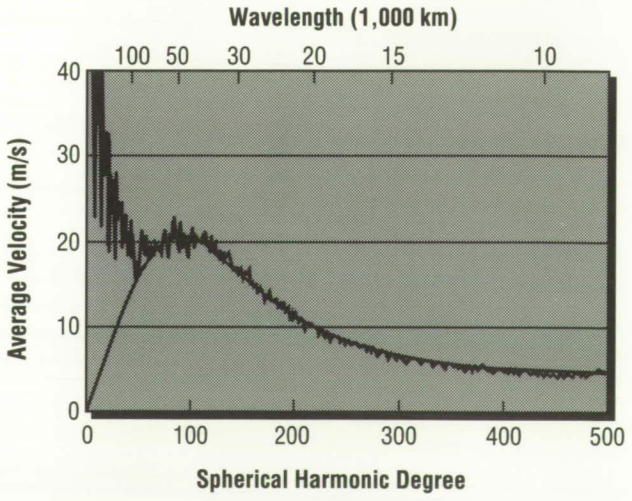

Figure 55. Solar Convection Spectrum

range from the very large giant cells with diameters greater than 150,000 km (100,000 mi) down to the granules with diameters of 1,500 km (1,000 mi). Although the existence of giant cells was never confirmed, there was good evidence for supergranules with diameters of about 30,000 km (20,000 mi) and some evidence for mesogranules with diameters of 7,000 km (4,000 mi). The present study indicates that there is a broad range of convection cell sizes that includes giant cells and mesogranules but is dominated by cells typical of the traditional supergranules.

Discovery of this spectrum suggests several future areas for additional work. It is well known that the supergranule component influences the solar magnetic field elements to produce the chromospheric network and its associated emissions. The giant cell component may influence the larger scale magnetic fields to produce active regions and their associated activity, including flares. This connection between the observed velocity patterns and solar activity may allow us to predict future activity.

Additional analysis with this ground-based data will continue in anticipation of future data from the NASA/European Space Agency Solar and Heliospheric Observatory mission. The Solar Oscillations Imager currently under development for this mission will provide a continuous stream of velocity images with high spatial resolution over the course of several years.

Hathaway, D.H.: Spherical Harmonic Analysis of Steady Photospheric Flows. Solar Phys., Vol. 108, pp. 1–20, 1987.

Hathaway, D.H.: Temporal Filters for Isolating Steady Photospheric Flows. Solar Phys., Vol. 117, pp. 1–12, 1988.

D.H. Hathaway/ES52
(205) 544-7610
Sponsor: Office of Space Science and Applications

Magnetospheric Physics

Magnetospheric physics is the application of continuum mechanics and plasma physics to obtain an understanding of the flow of matter, momentum, and energy near and within the volume occupied by the Earth's magnetic field. The otherwise dipolar magnetic field is compressed on the sunward side and stretched into a long tail on the antisunward side, by the supersonic flow of plasma (the solar wind) emanating from the Sun. As our understanding of this system improves, we are better able to comprehend and anticipate the interactions between solar events, interplanetary conditions, and terrestrial responses. Moreover, our solar-terrestrial environment also serves as the laboratory of opportunity for in situ observations of processes which are of astrophysical importance in such situations as planetary and cometary magnetospheres and stellar atmospheres. Having studied such processes, both remotely and locally, we gain an improved ability to interpret the electromagnetic radiations received from distant astrophysical plasma.

The research emphasis of the Magnetospheric Physics Branch of MSFC continues to be on the observation of low-energy or core plasma which originates in the ionosphere and has been found to supply plasma for the entire magnetosphere. Highlights of our activities during the previous year include discovery of a new low-altitude ion acceleration process in the data from the successful first flight of a fully three-dimensional low-energy plasma instrument, the Superthermal Ion Composition Spectrometer; initiation of the development phase for the Thermal Ion Dynamics Experiment on the International Solar-Terrestrial Physics POLAR spacecraft and continued definition of the Cometary Retarding Ion Mass Spectrometer for the Comet Rendezvous Asteroid Flyby Mission; delivery of the flight unit of the Research on Orbital Plasma Electrodynamics investigation for the Tethered Satellite System; development of a sophisticated software system for computer-aided engineering of charged particle optics systems; modeling of the contribution of ionospheric plasma to the magnetosphere including adiabatic acceleration effects; study of the variability of dayside upwelling ion outflows, including effects of geomagnetic activity and interplanetary (i.e., solar wind) conditions; diagnosis of the induced environment of the space shuttle orbiter using data from the Spacelab 2 Plasma Diagnostics Package/Retarding Potential Analyzer/Differential Ion Flux Probe; study of the statistical properties of polar wind outflows in the polar regions of the Earth's topside ionosphere; further development of the MSFC empirical plasma specification model, including the development of a capability of ray-tracing of plasma waves within the observed distribution plasma in the magnetosphere; and application of data analysis techniques to the interpretation of results from plasma simulation work done by the University of California in Los Angeles.

Plasma Interactions Monitoring System

Space Station *Freedom* will present unprecedented challenges in future U.S. space activities. Allowing large-scale, permanent space operations, S.S. *Freedom* will also provide structural support, electrical energy, data processing, communication, and life support resources. It will serve as a vehicle fueling and repair facility. Traffic will include space shuttles, the Orbital Maneuvering Vehicle, and other space vehicles. Thus, S.S. *Freedom* will be a large, complex, busy structure in space. Its size, the variety of materials and resources, and the many different vehicles and payloads in its vicinity will create significant perturbations in the ambient environment. Additionally, operations on the S.S. *Freedom* will be affected in yet undefined ways by the environment.

Operationally, the large scale of S.S. *Freedom*, the inclusion of many high-current electrical paths, and the large number of simultaneous communications links will produce many environmental perturbations, the nature and magnitude of which are quite uncertain. As a result, the environment of the station will need to be verified as it is constructed, and as operations commence and continue. A comprehensive set of measurements of the resulting environment of S.S. *Freedom* will be needed for the life of the station, to aid in compensating for the perturbations experienced and for design guidance in station growth.

Users of S.S. *Freedom* will have a critical need for knowledge of the actual environment within which measurements will be made. For instance, electrical noise levels may exceed the sensitivity of many instruments at various locations on the station structure. Telemetry and sensor signals may be masked by the noise, leading to false conclusions due to defective data. Thus, a continuous, ongoing data base that characterizes the environmental parameters of and around the station as functions of time and location is critically needed.

In addition to the above needs, there also is a strong need for the monitoring of station "weather." That is, the operators and users will require an ongoing characterization of the environmental conditions within which events occur and are measured. Such a characterization will be required to separate the natural episodic changes at the station from induced changes.

In response to the above needs, a system to provide comprehensive environmental measurements at multiple locations on S.S. *Freedom* is planned. This system, called the Plasma Interactions Monitoring System (Fig. 56), will have at least a twofold function: to monitor the impact of the station on the environment and vice versa, and to supply a data base to users that can be employed to unfold natural from induced changes in environmental parameters at the station.

W.T. Roberts/PS02
(205) 544-0621
Sponsor: Office of Space Science and Applications

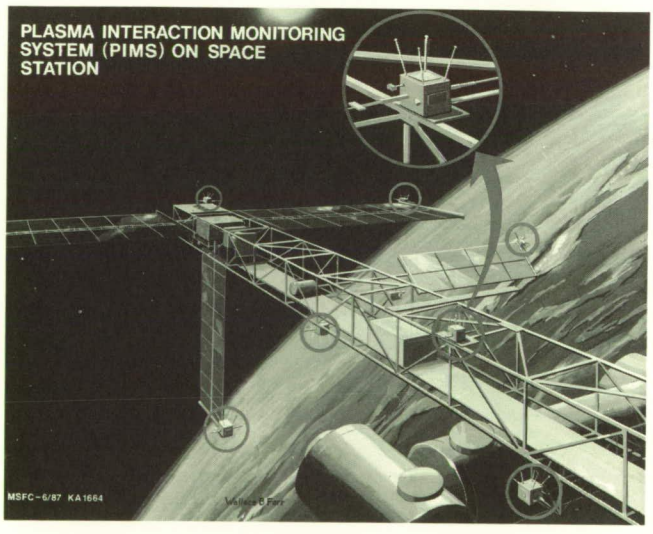

Figure 56. The Plasma Interactions Monitoring System Installed on Space Station Freedom

Discovery of Transversely Accelerated Core Ions in the Ionosphere

Based upon more than 30 years of spacecraft observations, the ionosphere has come to be thought of as a region of relatively well-known plasma properties exhibiting, at most, moderate departures from local thermodynamic equilibrium. Instruments designed to diagnose and document its behavior have been generally based upon the assumption that the thermal and flow speeds of the ionospheric plasma are smaller than typical orbiting spacecraft speeds. While processes by which the solar wind dissipates energy in the ionosphere are known to be active, this assumption has seemed defensible throughout the F region, where temperatures of a few thousand degrees Kelvin prevail, and flow velocities are generally well under 1,000 m s^{-1} (3,281 ft s^{-1}).

In recent years, a wide variety of observations have shown that very energetic phenomena occurring in the auroral zones of the Earth are severely disturbing the auroral zone ionosphere. Observations using instruments that were designed based upon these assumptions about the plasma have clearly indicated violations of those assumptions, in particular extreme temperatures and flow velocities. Other instrumentation designed to view the energetic particle and electromagnetic field environment in the auroral regions also clearly indicate that the ionosphere must be severely out of thermodynamic equilibrium. Ionospheric ions are observed at energies up to several hundred electron volts traveling mainly perpendicular to the local magnetic field, in conjunction with very strong low frequency electric fields indicative of strong plasma turbulence with flow velocities of several kilometers per second.

A rocket payload on the Topside Probe of the Auroral Zone (TOPAZ-2) carrying a new three-dimensional (two angles and energy) scanning mass spectrometer (the Superthermal Ion Composition Spectrometer), designed to observe the auroral ionosphere without making assumptions about its character, has returned exciting new data on the effects of auroral energetic phenomena. Immediately above an active auroral form at 900-km (559-mi) altitude, the mainly O^+ plasma was found to have a velocity distribution which can be described as a "perpendicular beam" or a "ring-shaped" velocity distribution.

Such a distribution can also be described as "doughnut-shaped," with nearly all particles present gyrating at large velocities in circular orbits around the local magnetic field direction. In contrast, a normal or equilibrium velocity distribution has most particles at the very lowest velocities, and fewer and fewer particles at larger and larger velocities, in a "bell-shaped" curve of normal distribution. Recently, incoherent radar observations of the auroral ionosphere have also suggested the presence of ring distributions, but skeptics have argued that the radar data might be misleading due to spatial aliasing of regions with different flow velocities. The rocket observations suffer from no such ambiguities.

Two slices taken at right angles to each other through the ring distribution observed by TOPAZ-2 are shown in Figure 57. Note that the ring is off-center in the frame of reference of the rocket payload, indicating that the plasma as a whole was moving relative to the payload at a speed approximately equal to the ring radius, about 4.5 km s^{-1} (2.8 mi s^{-1}). Independent measurements of the electric field at the payload confirm this very large plasma flow velocity, the dc electric field being an excellent measure of the plasma flow in this part of the ionosphere. Other electromagnetic field observations indicate the presence of strong fluctuations at the O^+ gyrofrequency and at harmonics of the H^+ cyclotron frequency, which are clearly related to the highly unusual plasma characteristics. Such a distribution is known to be highly unstable to plasma waves which would tend to diffuse and thermalize the energy of the ring. The ring feature can be created by infrequent collisions between the rapidly moving ions and the relatively stationary neutral gas atoms.

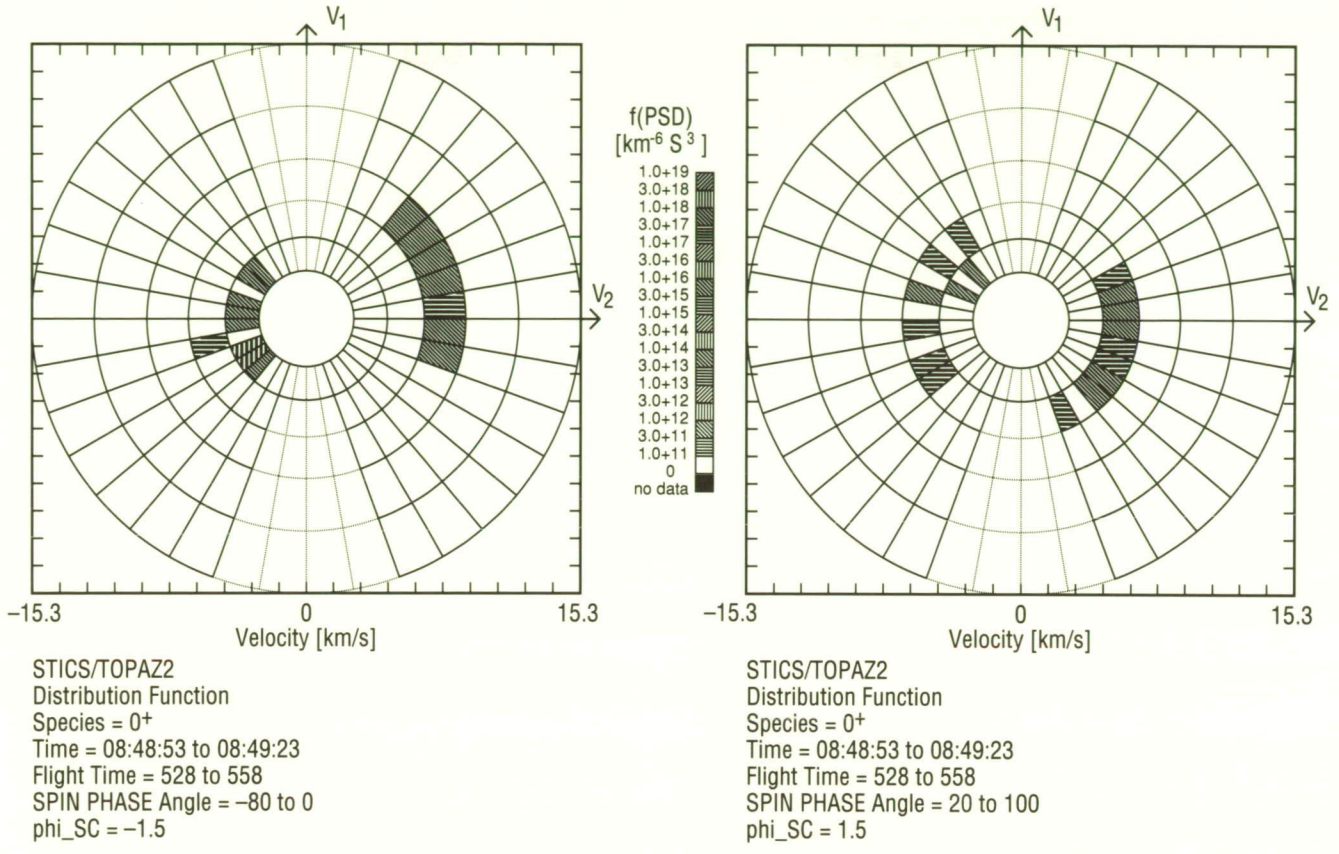

Figure 57. Two Orthogonal Cuts Through the O^+ Distribution Function Observed by STICS on TOPAZ-2

The formation and thermalization of such distributions appears to be a fundamental dissipative process in marginally collisional plasmas, with implications for the condensation of matter which forms planets, the behavior of comets, and the stability of planetary atmospheres over geological time scales, as well as the escape of the terrestrial ionosphere into space from the auroral zones. These observations demonstrate the truth of the aphorism that "we see mainly what we look for." Clearly, future observations of low energy plasma must be capable of measuring the properties of such distributions if accurate assessments of density, "temperature," and flow velocities are to be obtained, and if the actual thermodynamic state of the plasma is to be known.

Moore, T.E., Waite, J.H., Jr., Lockwood, M. and Chappell, C.R.: Observations of Coherent Transverse Ion Acceleration in the Magnetosphere and Ionosphere. AGU Monograph No. 38, T. Chang, ed., p. 50, Washington DC, 1986.

T.E. Moore/ES53
(205) 544-7633
Sponsor: Office of Space Science and Applications

Possible Solar-Terrestrial Control of Upwelling Ions in the Earth's Ionosphere

The study of the physical processes which influence the supply and transport of plasma in the terrestrial magnetosphere is a continuing mission of the Magnetospheric Physics Branch at MSFC. The most recent phase of this mission has been carried out using the Dynamics Explorer satellite which has provided long-term monitoring of the lowest energy ions present in the magnetosphere through observations made by the Retarding Ion Mass Spectrometer (RIMS) built by MSFC.

During the past year, this data base has been used in a study of the factors which control the outflow of ions from the cleft/cusp region. This flow contains both light ions such as H^+ and He^+, as well as heavy ions such as O^+, and the term "upwelling ions" has been used to describe its character. In view of the fact that upwelling ion events are closely associated with the dayside magnetospheric cleft, which is itself in dynamic and electromagnetic communication with the magnetosheath and magnetopause, a question arises regarding the relationship of the ion upwelling phenomenon to interplanetary conditions and to interactions between the solar wind and Earth's magnetopause. It has been suggested that upwelling ion events may be very closely related to phenomena, involving sporadic reconnection of interplanetary and geomagnetic field lines, known as flux transfer events. The idea is that a piece of geomagnetic flux becomes connected to the interplanetary magnetic field and is dragged antisunward at high velocity by the solar wind. This would cause the plasma at the ionospheric end of the geomagnetic flux tube to be dragged through the otherwise stationary ambient ionospheric plasma, resulting in strong local shears in plasma velocity, magnetic field-aligned electric currents, and frictional heating due to ion neutral collisions. These effects would result in ionospheric plasma heating and expulsion and are typical of those observed by RIMS within upwelling ion events.

The hypothesis that some interaction between the interplanetary environment and the dayside magnetosphere gives rise to upwelling ion events can be further investigated by comparing satellite measurements of interplanetary plasma and fields, upstream of Earth, with simultaneous measurements taken by RIMS within the upwelling ion events. Such studies were pursued using plasma and magnetic field data obtained by instruments onboard the International Sun-Earth Explorer-3 and Interplantary Monitoring Platform-8 satellites, in conjunction with RIMS data. Figure 58 shows sample results from such comparisons. In all four panels of this figure, the intensity of ionospheric upwelling is shown as measured by the O^+ outflux [normalized to 1,000-km (621-mi) altitude by an r^{-3} scaling law to take into account magnetic flux tube divergence] plotted against various interplanetary environment parameters. The first example (top left) shows the comparison with B-z, for which negative values are conducive to magnetopause reconnection. The next two examples (top right and bottom left) show the comparison with two measures of interplanetary parameters thought to control the cross-polar-cap magnetospheric potential drop and, therefore, the rate of magnetopause reconnection. These three examples test the association of upwelling ion events with flux transfer events, and each gives a negative result, as shown by the small correlation coefficients. The last example (bottom right) compares

upwelling ion intensity with the solar wind dynamic ram pressure, a measure of the piston force per unit area applied to the magnetopause by the solar wind. This is the only comparison which shows a significant (albeit, not conclusive) correlation. The analysis embodied in the figure indicates that, if upwelling ion events result from interactions between the solar wind and Earth's dayside magnetopause, the interactions involved are mechanical in nature, involving solar wind plasma pressure and are not due to coupling at the magnetopause between the interplanetary and geomagnetic fields.

C.J. Pollock/ES53
(205) 544-7638
Sponsor: Office of Space Science and Applications

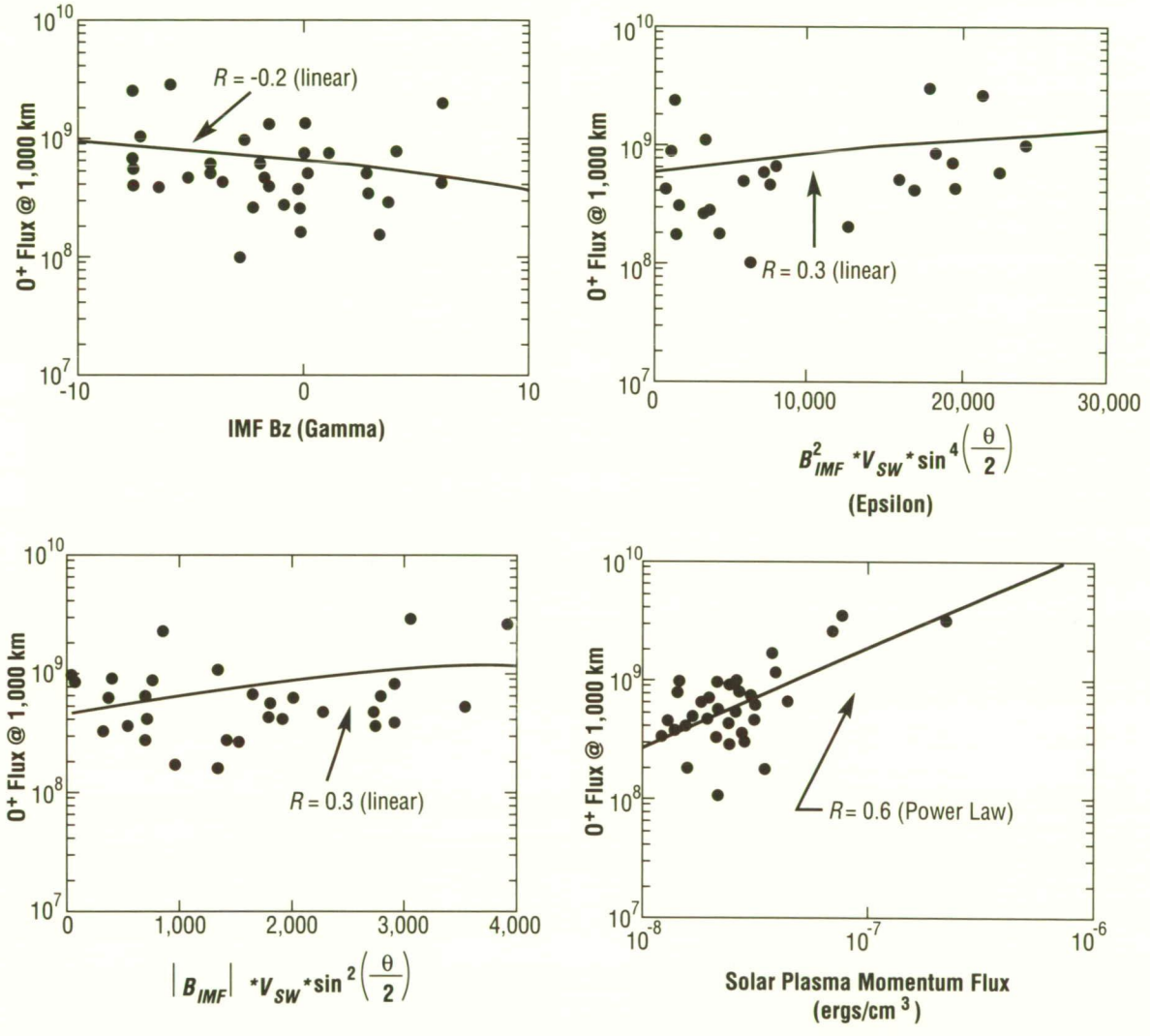

Figure 58. Correspondence Between the O^+ Flux in Upwelling Ion Events and Various Solar Wind and Interplanetary Magnetic Field Parameters

The Influence of Solar and Terrestrial Inputs on the Polar Wind

The continuing mission of the Magnetospheric Physics Branch at MSFC is the study of the dynamics of plasma in the magnetosphere and the factors which control these dynamics. This mission has been pursued both in space with instruments carried aboard spacecraft and on the ground through data analysis and interpretation and theoretical investigations. The Dynamics Explorer (DE) mission has provided a data base of observations of the lowest energy ions present in the magnetosphere through observations made by the Retarding Ion Mass Spectrometer (RIMS) built by MSFC. Such an extended data base makes possible the statistical study of the varying terrestrial and solar processes which modulate the character of these ion populations.

Recently a study has been directed toward the flow of ions from the polar cap region. In the polar cap, ions are accelerated upward from the ionosphere because of the relatively low plasma pressure in the distant magnetosphere, at a rate which is controlled by several factors. For example, even though hydrogen ions are being accelerated upward by the polarization electric field, in the topside ionosphere momentum transfer collisions with O^+ are sufficiently frequent, due to the high O^+ density, that the H^+ is unable to gain significant momentum from the electric field. As the O^+ density decreases with altitude the momentum lost by H^+ in these collisions becomes smaller and at some altitude H^+ begins to accelerate to significantly high velocities. Any factors which influence the O^+ density in the topside ionosphere should, in theory, influence the altitude at which the upward H^+ speed begins to significantly increase. One factor which is known to influence the O^+ density is the level of solar extreme ultraviolet flux – the radiation responsible for photo-ionizing neutral oxygen and producing O^+. As the level of solar output increases more energy is deposited in the neutral atmosphere thereby raising the temperature. This rise in temperature causes more neutral oxygen to be present in the ionosphere and available for ionization. The net result is higher O^+ densities which means that the frictional force on H^+ due to collisions with O^+ is important at higher altitudes. Thus during time of high solar output the location at which H^+ is able to overcome this friction and be accelerated to high velocities should occur at higher altitudes in the ionosphere than during times of low solar output.

This effect has been observed as illustrated in the results shown in Figure 59. These data are taken from the DE/RIMS data base for magnetic latitudes greater than 70°. The data have been divided into two cases based on the level of solar output as

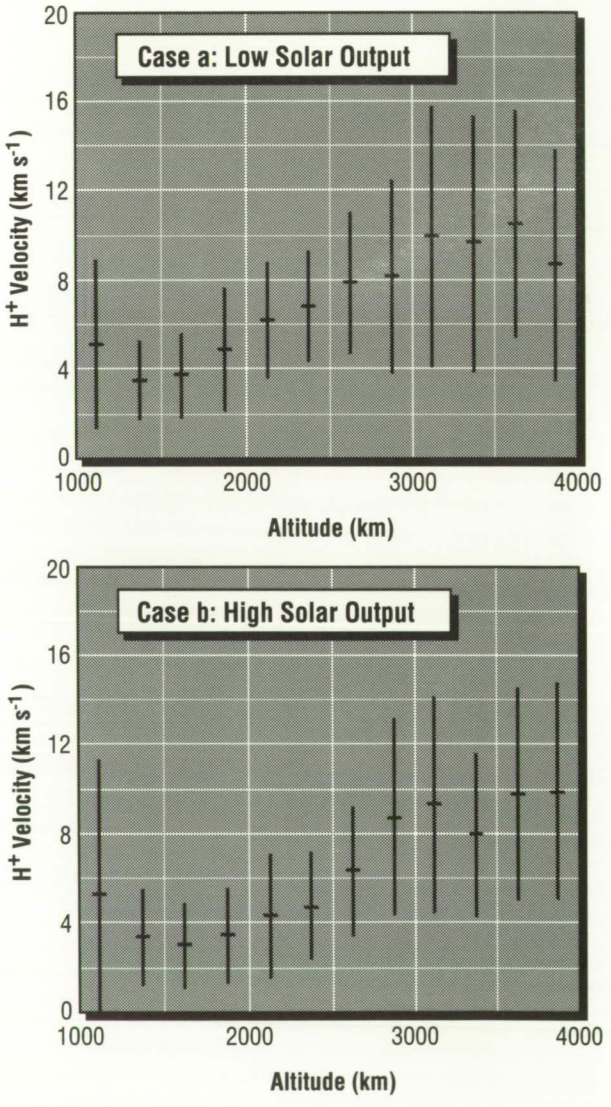

Figure 59. Average Polar Wind H^+ Velocity as a Function of Altitude Observed by DE/RIMS

characterized by the solar flux at a wavelength of 10.7 cm (4.2 in). Notice the large increases in H^+ velocity with altitude, evident in both figures, in the altitude range between 1,500 km and 2,500 km (932 and 1,553 mi). But note that the velocities shown in the bottom graph (high solar output) begin to increase at higher altitudes [by approximately 700 km (435 mi)] compared to those in the top graph (low solar output). It can also be shown, although it is not illustrated here, that the O^+ density is larger in the high solar output case and that similar O^+ densities to those observed in the low solar output case occurred approximately 700 km (435 mi) higher in the ionosphere. This correlation supports the conclusion that the differences in the velocity vs. altitude profiles for these two cases is primarily a result of increased friction on H^+ produced by high O^+ densities.

The results from this study of the processes controlling ion outflows from the polar cap illustrate the importance of large data bases in determining the influence of the solar-terrestrial environment on the supply and transport of plasma with the magnetosphere. The long lifetime of the DE mission has, for the first time, provided scientists with a data base which encompasses both the short- and the long-time-scale variations in the physical processes known to exist in this environment, thereby allowing a quantification of their importance in determining the nature of near-Earth plasma.

M.O. Chandler/ES53
(205) 544-7645
Sponsor: Office of Space Science and Applications

Development of Focusing Electrostatic Mirrors for Charged Particles

Experience with the Retarding Ion Mass Spectrometer (RIMS) of Dynamics Explorer 1 (C. R. Chappell, Principal Investigator) has shown that improvements in the sensitivity of instruments for low-energy space plasma observations pay huge returns in the variety of new phenomena revealed. RIMS achieved a very high sensitivity through the use of electrostatic preacceleration which effectively widened the angular entrance aperture. Moreover, RIMS had an integral response in energy; that is, it responded to ions over a broad energy range above the potential applied to its retarding grid.

In order to improve the quality of low energy plasma measurements, the next generation of instruments should be capable of even higher sensitivity while achieving narrower angular and energy response. Since these goals are mutually inconsistent, it has become necessary to develop an entirely new technical approach to the design of such instruments. In particular, for the past 3 years, application of optical techniques heretofore applied only to photon collection in large telescopes has been pursued. The basic idea is to use focusing particle deflection systems (optics) to transform the small area, wide angle response intrinsic to mass spectrometers using preacceleration, into a very large area but narrow angle response presented to the external particle population. The alternative to this approach is to simply collimate down the desired angular response, which sacrifices sensitivity in a very wasteful way.

The primary approach to this problem is the development of electrostatic mirrors consisting of parallel fine wire mesh grids, suspended from frames with shapes appropriate to create the proper figure

for the mirror shape. The first grid approached by incoming particles is maintained at local chassis potential to provide a field free drift path into and away from the mirror. A second grid is maintained at a variable positive potential to reflect the ions while they are between the grids. This technique has the desirable property that ions with energies larger than a small multiple of the mirror potential are not reflected by the mirror. Thus, an upper energy bandpass can be defined which, in conjunction with a lower bandpass limit set by a conventional retarding potential analyzer, creates a differential energy bandpass of variable width. This provides for a variable sensitivity, with obvious improvements in dynamic range of operability.

Both numerical modeling and prototype fabrication of such mirrors have been undertaken by the Magnetospheric Physics Branch in connection with the Thermal Ion Dynamics Experiment (TIDE) for the International Solar-Terrestrial Physics/POLAR spacecraft, the Cometary Retarding Ion Mass Spectrometer for the Comet Rendezvous Asteroid Flyby Mission, and sounding rocket applications. The proper shape for such mirrors is not a simple parabolic curve due to the finite thickness of the particle reflection region. The correct curve is described by a nonlinear differential equation for which a solution can be found by perturbing from a parabolic shape. Using the numerically determined mirror shape, investigators at MSFC solved for the potential distribution within such a mirror and then computed the trajectories of particles in the overall optics. Sample results are illustrated in Figure 60. The focusing action apparent here is marred by some residual numerical diffusion in the particle pushing code, but the basic correctness of the geometry is apparent.

Two different prototype units have been assembled to investigate the properties of these mirrors directly in the laboratory using the Low Energy Ion Facility. The results are generally consistent with the ray tracing results, to within the accuracy to which the properties of the incident ion beam are known. Figure 61 shows data obtained from the TIDE prototype unit in which the width (transverse to the focal

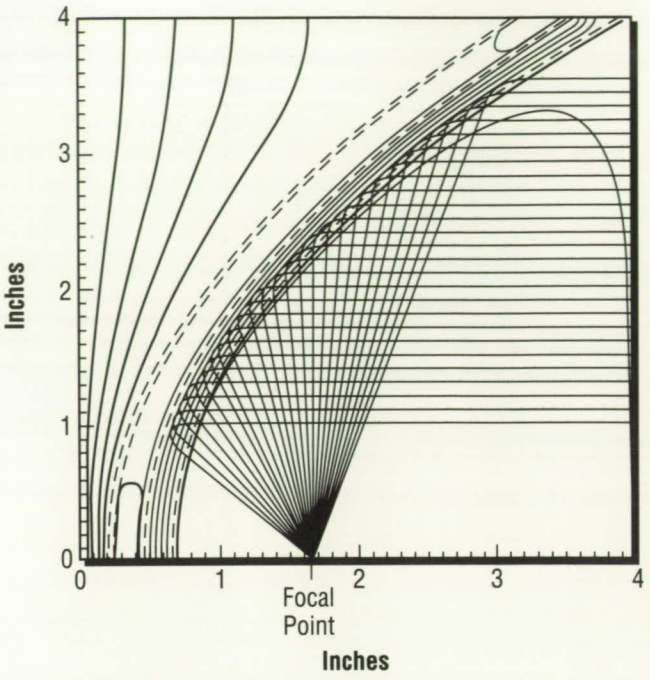

Figure 60. Numerical Ray Tracing of the Trajectories of Parallel Rays Representing 100 eV Ions Incident Upon the Focusing Electrostatic Mirror

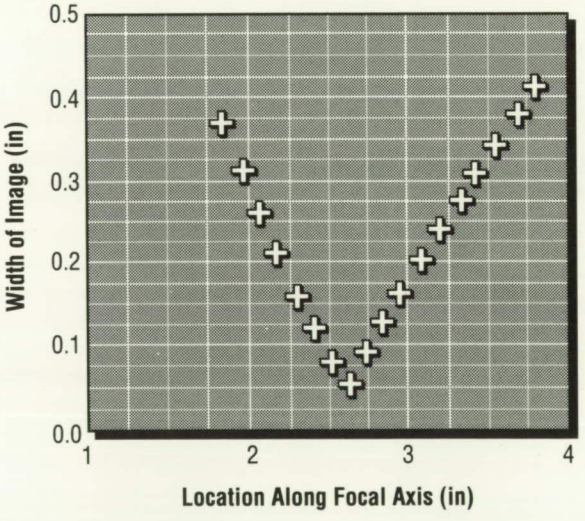

Figure 61. Laboratory Measurements of the Width of an Ion Beam Which is Initially 2.0 in. Wide, Versus Position Along the Focal Axis

axis) of an initially broad and quasi-parallel beam is plotted versus its position along the focal axis. It may be seen that a well-defined focal point exists, at which the beam is compressed from a cross section of some 5 cm (2 in) down to a width of some 1.63 mm (0.064 in), a compression factor of approximately 30.

This type of charged-particle optics technology will make possible huge gains in the sensitivity of space plasma diagnostic instrumentation, with simultaneous gains in angular and energy resolution. At the same time, a mechanism is provided to "stop down" the response of the mirror/retarding potential analyzer (RPA) system by varying the energy bandpass (and also the effective area of the mirror) by programming the mirror and RPA potentials appropriately. This capability will permit such sensitive instruments to function both in unexplored regimes of very low density and in better-known regimes of higher density where the detectors would otherwise saturate.

Pollock, C.J., Chisholm, W.L., Coffey, V.N., Giles, B.L., Moore, T.E., Reasoner, D.L. and Sloan, P.: Focusing Electrostatic Mirror for use in Space Plasma Diagnostics. Rev. of Scientific Instruments, to be submitted, 1989.

C.J. Pollock/ES53
(205) 544-7638
Sponsor: Office of Space Science and Applications

Empirical Modeling of the Earth's Plasmasphere

An accurate empirical model of the plasmasphere and inner magnetosphere is needed for comparison with theoretical models, for use in studies of plasma waves, in studies of other planetary bodies, and in other research areas. No comprehensive empirical model exists for the plasmasphere and magnetosphere even though these regions of space have been the object of study for several years. Empirical or numerical models do exist for some very limited spatial regions. The advantage of empirical over numerical models is that they can provide good quantitative results with only modest requirements of computer time and memory.

An empirical model has been developed for density of the most dominant ion in the plasmasphere, H^+. The model is based on data from the Retarding Ion Mass Spectrometer (RIMS) on the Dynamics Explorer 1 satellite.* The development of the model has been a two-step process. First the data from RIMS has to be reduced to obtain the plasma parameters density, temperature, and flow velocity. The second step involves organizing and analyzing the data in some statistical format to obtain a meaningful representation of each of the parameters.

The reduction of the data obtained from RIMS is accomplished by computer automated software that independently determines density, temperature, and flow velocity for each of the major ion species, H^+, He^+, and O^+, and, when measured, the minor species N^+, O^{++}, and He^{++}. The reduction of all the available and applicable RIMS measurements to density, temperature, and flow velocity is in itself a rather large task that will take about a year.

The empirical model for hydrogen density consists of an analytical expression that can be used to reproduce the average density at arbitrary locations in the plasmasphere for a given range of geomagnetic and solar cycle activity. The principal spatial dependence of plasmaspheric density is on the McIlwain *L*-shell parameter. The functional de-

pendence of hydrogen density on *L*-shell that is currently used in this modeling effort is given by:

$$LOG_{10}(n) = a_1 \cdot F(L) \cdot G(L) \cdot H(L) .$$

Three functions have been derived to represent the density profiles in the ionosphere, inner plasmasphere, and at the plasmapause. Nine free parameters are used to fit this equation to the logarithm of ion density. The free parameters can themselves be functions of magnetic local time, latitude, or *Kp* (a measure of geomagnetic activity).†

The procedure for producing this empirical model is to fit the equation given above to statistical profiles of density versus *L*-shell for various local times and latitudes and then to find analytical representations for the variation in the fit parameters as a function of magnetic local time, latitude, and weight *Kp*. The weighted *Kp* used is one that incorporates *Kp* history and is strictly empirical although there are physical grounds for expecting that the history of geomagnetic activity should be included.

Although still being developed, the empirical model of the plasmasphere has begun to take shape. As the model matures, more ions will be added so that a better picture can be obtained of the compositional characteristics of the plasmaspheric plasma. In addition, other plasma parameters are to be modeled so that ultimately the average state of the plasma under given conditions can be represented by a set of analytic expressions. Such a mature model can serve as the empirical basis for extensions of both theory and empirical modeling to include the more dynamic characteristics of the plasmasphere. The present empirical model is such that other sources of plasmaspheric observation may be included with the RIMS observations in order to extend the spatial coverage and to improve the statistical base for geomagnetic activity and solar cycles.

*Chappell, C.R., Fields, S.A., Baugher, C.R., Hoffman, J. H., Hanson, W.B., Wright, W.W., Hammack, H.D., Carignan, G.R. and Nagy, A.E.: The Retarding Ion Mass Spectrometer on Dynamics Explorer-A. Space Sci. Instrum., Vol. 5, p. 477, 1981.

†Gallahager, D.L., Craven, P.D. and Comfort, R.H.: An Empirical Model of the Earth's Plasmasphere. Adv. Space Res., Vol. 8, pp. (8)15–(8)24, 1988.

D.L. Gallagher/ES01
(205) 544-7639
Sponsor: Office of Space Science and Applications

Atomic Physics and Aeronomy

Aeronomy is the study of the wide variety of physical and chemical processes arising from an interaction of solar electromagnetic and corpuscular radiation with the mixture of gases comprising the upper atmosphere. Solar radiation in the x-ray, ultraviolet, visible, and the infrared part of the electromagnetic spectrum is absorbed, emitted, and scattered by atmospheric gases at various levels. At low energies, mission and absorption processes involve discrete quanta with electronic, vibrational, and rotational transitions resulting in a characteristic spectrum. Photons with sufficiently high energies ionize and dissociate atmospheric molecules, producing reactive species of free radicals which interact with other molecules in a complex set of reactions. The characteristic thermal structure and the composition of the Earth's atmosphere is a consequence of this complex interaction with atmospheric gases.

A quantitative knowledge of this interaction of both solar electromagnetic radiation and the energetic particles with the atmospheric constituents, and the rich array of photochemical and dynamical processes that result, is crucial to an understanding of the nature and balance of this part of the Earth's environment. A great deal of knowledge about the physical state of the atmosphere and the complex photochemical and dynamical processes can be obtained from observation and analysis of atmospheric spectra in the ultraviolet and infrared regions. These studies involve atmospheric observations, laboratory experiments for acquiring molecular parameters, and development of theoretical models and analytical techniques for interpretation of the observations.

Infrared Spectroscopy of the Stratosphere

A research program based on observations and development of analytical techniques for balloon-borne thermal emission spectra of the Earth's stratosphere in the far and the middle infrared (IR) spectral regions has been in progress. An analysis of the observed spectra provides simultaneously determined profiles of temperature and a number of trace gases in the Cl_x, HO_x, and NO_x families, including many isotopic species (Fig. 62).

It is well recognized that knowledge of the isotopic composition of the atmosphere can lead to valuable information about physical and chemical processes involving photochemically related species. Interest in a quantitative understanding of atmospheric isotopic composition has increased in recent years with the observational evidence related to isotopic ozone. Recent results provide substantial evidence that the stratospheric heavy ozone is substantially enhanced with respect to the statistically expected value. This evidence, however, is contradicted by theoretical considerations that predict no enhancement or even a small depletion in the isotopic composition of stratospheric ozone. While efforts for a better understanding of the theoretical basis of isotopic fractionation in the stratosphere continues, information about the distribution of other O_{18} bearing molecules is being obtained from the observed spectra.

A constituent of particular interest is H_2O^{18}. The lower tropospheric concentration of this constituent, measured by both ground-based and aircraft-borne instruments, indicate depletions of O^{18} by 1.5 to 5.0 percent in water vapor and 0.5 to 2.5 percent in precipitation up to the levels above the mixing layer. The O^{18} depletions were also found to be approximately linearly correlated to the D depletions in HDO. No stratospheric measurement of H_2O^{18} has been reported so far.

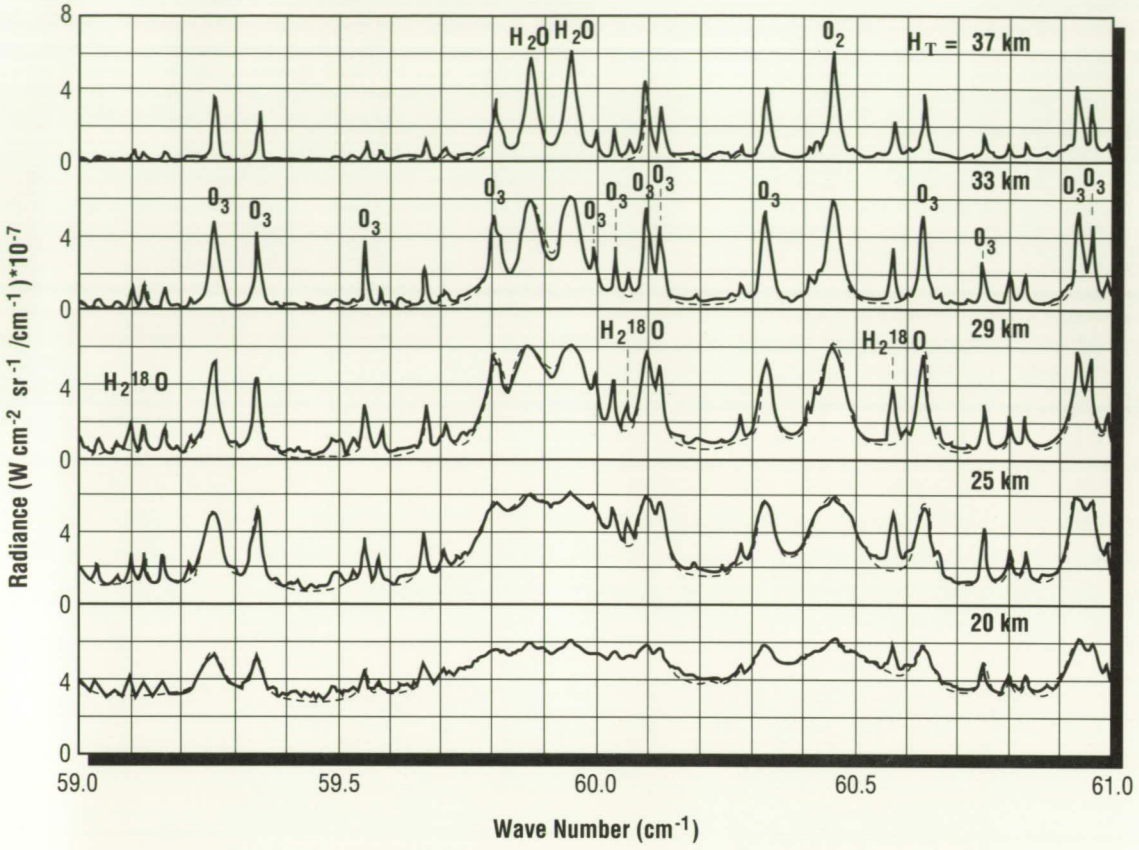

Figure 62. Analysis of Observed Spectra in the Stratosphere

The results presented in this report have been obtained from far IR observations made with a Michelson interferometer on a balloon flight launched from Palestine, TX, on October 5, 1982.*‡ The balloon reached a float altitude of approximately 38.5 km (23.9 mi) and limb thermal emission measurements were made for a period of about 26 hours in the 20 to 100 cm^{-1} (7.9 to 39.4 in^{-1}) range with a spectral resolution of 0.0033 cm^{-1} (0.0013 in^{-1}). The observed spectra in the 46–100 cm^{-1} (18.1–39.4 in^{-1}) range exhibit some 13 isolated spectral lines of H_2O^{18} which are clearly identified.

The IR radiative transfer model used in the analysis is based on line-by-line and layer-by-layer calculations and includes temperature and curvature effects. The molecular spectral data employed were obtained from a combination of the Jet Propulsion Laboratory and HITRAN 1986 compilations. The inversion algorithm for retrieval of the stratospheric H_2O^{18} mixing ratios uses a non-linear least-square fitting technique.

Figure 63 shows the average of some 30 H_2O^{18} mixing ratio profiles retrieved from 9 selected spectra in 4 limb sequences. The statistically expected H_2O^{18} profile, calculated from the normal H_2O profile using the O^{16}/O^{18} ratio of 0.00204, is shown by the dashed curve. The inferred enhancement in the observed H_2O^{18} concentrations compared with the statistically expected values indicate average enhancements of 7.0 percent at 22 km (15.5 mi), 9.1 percent at 25.8 km (16.0 mi), 26.7 percent at 29.5 km (18.3 mi), 34.0 percent at 33.3 km (20.7 mi), and 39.5 percent at 37 km (23.0 mi).

The observed enhancements in stratospheric H_2O^{18} concentrations appear to be similar to the $O^{50}{}_3$ enhancements reported previously† with 18 percent at 25 km (15.5 mi), a minimum of 13 percent at 29 km (18.0 mi), increasing to 45 percent at 37 km (23.0 mi). With the observed depletion in H_2O^{18} concentrations in the lower troposphere, and with a reduc-

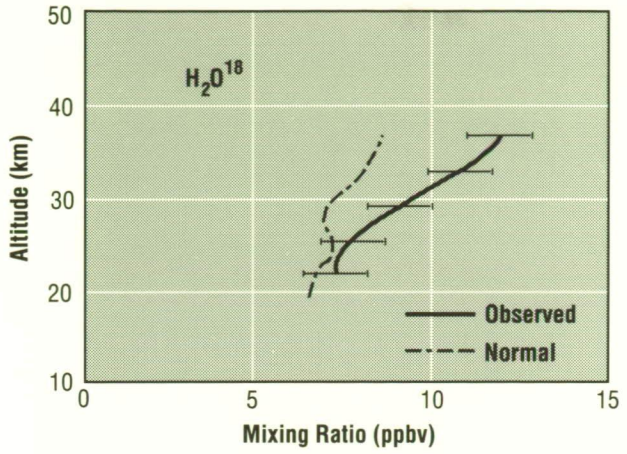

Figure 63. Averaged Mixing Ratio Profile of H_2O^{18} from Nine Spectra

tion in depletion reflecting the atmospheric O^{18}/O^{16} ratio in the water vapor arising from methane oxidation, the stratospheric water vapor is expected to be depleted in O^{18}. The physical basis for the enhancement of H_2O^{18} suggested by far IR observations is not clear. Further work on the distribution of stratospheric isotopic species is continuing.

*Abbas, M.M., Guo, J., Carli, B., Mencaraglia, F., Bonetti, A., Carlotti, M. and Nolt, I.G.: Stratospheric O_3, H_2O, and HDO Distributions from Balloon-Based Far Infrared Observations. J. Geophys. Res., Vol. 92, pp. 8354–8364, 1987.

†Abbas, M.M., Guo, J., Carli, B., Mencaraglia, F., Carlotti, M. and Nolt, I.G.: Heavy Ozone Distribution in the Stratosphere From Far Infrared Observations. J. Geophys. Res., Vol. 92, pp. 13231–13239, 1987.

‡Carli, B., Mencaraglia, F. and Bonetti, A: New Assignments in the Sub-Millimeter Emission Spectrum of the Stratosphere. Int. J. Infrared Millimeter Waves, Vol. 3, pp. 385–394, 1982.

M.M. Abbas/ES55
(205) 544-7680
Sponsor: Office of Space Science and Applications

Global Modeling of the Thermosphere

Space shuttle and satellite-borne instruments allow the acquisition of information on that part of the atmosphere known as the thermosphere [above 120 km (74.6 mi) in altitude]. By making measurements of this region from orbiting platforms, data is obtained that reflects the variability with altitude, latitude, longitude, local time, season, solar cycle, and magnetic activity. The thermospheric variability as a function of these parameters is complex. Such data become difficult to interpret, and their acquisition is difficult to plan without the support of highly developed theoretical models. Correspondingly, the purpose of making the measurements is to refine and place on a quantitative basis our ability to model the region. Thus, a study of the thermosphere and ionosphere requires both experimental and theoretical programs that advance the state-of-the-art and that are developed interactively.

During 1989, a long program of thermospheric modeling achieved the capability to model thermospheric spectral emissions (or indeed any thermospheric species or temperature) on a global scale. A comprehensive set of coupled equations that describe the physics and chemistry of the upper atmosphere is solved on the MSFC Cray supercomputer to provide a grid of results as a function of all of the parameters mentioned above (altitude, local time, geographic coordinates, etc.) The model is unique in several areas, but one worth mentioning is that the equations are solved from 80 km (49.7 mi) in one hemisphere, along the magnetic field line, to 80 km (49.7 mi) in the other hemisphere. This means that artificial upper boundary conditions do not have to be placed on the solution, and that thermal and photoelectron fluxes are free to flow from one hemisphere to the other.

With this capability, the first global maps of thermospheric emissions or species can be generated. As an example, the 7320 Å emission from the long-lived state of the atomic oxygen ion $O^+(P^2)$ was studied. This ion (and its emission) is of interest

because it can be used to infer the atomic oxygen concentration and the solar ionizing flux. Figure 64 shows the production rates of this state for typical midday conditions. The production mechanisms are solar ultraviolet photons and photoelectrons. Figure 65 shows a global map of this emission rate at the peak of the layer. The example shown corresponds to November 30, 1983, a day during the Spacelab 1 mission.

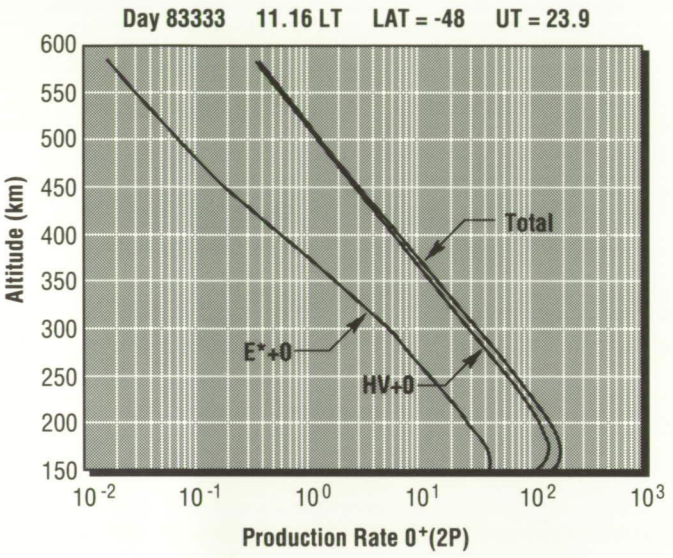

Figure 64. Typical Production Rates of O^+ (2P) for Mid-Day

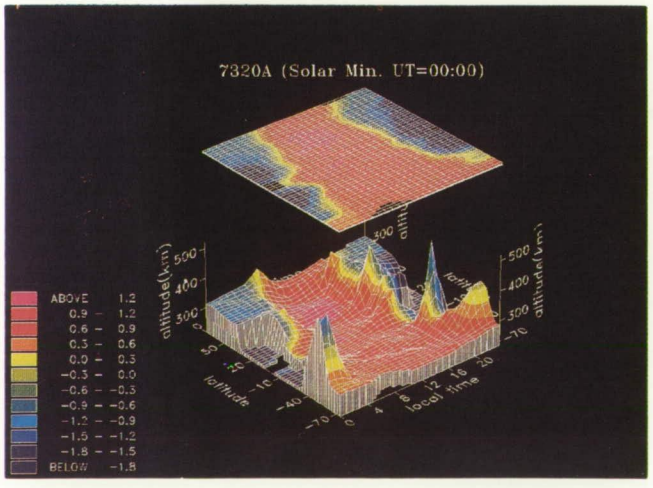

Figure 65. Global Map of the Peak Volume Emission Rate as a Function of Altitude, Local Time, and Latitude for November 30, 1983

For this case, summer is in the southern hemisphere, and the longer periods of sunlight in this hemisphere can be seen as the larger periods of greater emission. With increasingly high southern latitudes, the days are longer. At twilight, the Sun begins to set at the lower altitudes, with the result that the peak of the layer rises sharply in altitude but decreases in magnitude.

At night in the winter hemisphere, one would not expect to find any production of 7320-Å emission. However, significant emission can be seen at the higher latitudes. This is a result of production caused by photoelectrons generated by ultraviolet sunlight at the southern end of the magnetic field lines. The photoelectrons are subsequently transported by electromagnetic forces, along the magnetic field lines to the other hemisphere, where they excite the $O^+(P^2)$ state.

This model represents a most significant milestone in our ability to understand and predict the upper atmospheric behavior.

Torr, M.R., Torr, D.G., Richards, P.G. and Yung, S.: Global Modeling of Thermospheric Emissions. EOS, Vol. 70, p. 411, 1989.

Torr, M.R., Torr, D.G. and Richards, P.G.: A Global Model of the $O^+(P^2)$ Airglow Emission at 7320 Å. Geophys. Res. Lett., submitted, 1989.

M.R. Torr/ES51
(205) 544-7591
Sponsor: Office of Space Science and Applications

Earth Science and Applications

The goal of the MSFC Earth Science and Applications program is to develop and utilize space technology to observe the Earth's atmosphere, land, and ocean from space to gain an improved understanding of geophysical processes and their role in the interactions between various components of the Earth system (atmosphere, hydrosphere, cryosphere, biosphere, and solid Earth), consistent with the emerging concept of Earth-System Science.

Research and development activities are conducted in support of NASA's planned Mission to Planet Earth and Earth Observing System. These programs involve theoretical/analytical model development, remote sensor development, flight payload analyses, laboratory and field experiments, and appropriate information system development. A major area of focus is the hydrologic cycle. Ground- and space-based measurements of Earth parameters are used to develop and verify analytical and theoretical models of global and mesoscale processes to establish remote sensor requirements. Field experiments provide data required to verify the operation of air- and space-borne remote sensing instrumentation. Data derived from observations are used as input to model computer codes for simulation and prediction experiments. Extensive use is also made of interactive data display and access systems to study time-dependent development of Earth system processes on all scales.

Space Applications of Sensor Development

The Remote Sensing Laboratory is currently being outfitted to support development of space sensors. Most recently, airborne activity has been the major emphasis of laboratory programs. With the knowledge gained from airborne programs in design and data analysis, coupled with sensor development efforts, the laboratory will expand to address the needs of spaceborne applications. These space applications will be an extension of current programs and include new areas of sensor development. As a result of the Earth Observing System (EOS) program, a major task of the laboratory will be to develop the Lightning Imaging Sensor (LIS).

The LIS is a calibrated optical lightning imaging sensor that will be flown on the EOS polar platform to acquire and investigate the global distribution and variability of total lightning. The LIS will detect and locate lightning with storm scale resolution over a large region at the Earth's surface along the orbital track of the satellite. The instrument will mark the time of occurrence of the lightning with 1 ms resolution and measure the radiant energy of the detected flash. The LIS will have a nearly uniform 90-percent detection efficiency within the field of view of the sensor, and will detect intracloud and cloud-to-ground discharges during day and night observations. The LIS will view a total area of approximately 640 km by 640 km (397.7 by 397.7 mi) at the cloud top using a 64 by 64 element charge-coupled device (CCD) array to give a 10-km (6.2 mi) pixel resolution. The entire globe will be covered by the LIS instrument every 6 days. The ground-track speed of 6.67 km s^{-1} (4.1 mi s^{-1}) allows the LIS to monitor individual storms and storm systems for about 96 seconds, a period long enough to obtain a

good measure of the lightning flashing rate in these storms while the storm is in the field of view of the LIS.

One of the major areas of development for the LIS is the reduction of data off the focal plane and the difficulty of daytime detection of lightning against the brightly lit background. An approach is being looked at that will combine the CCD array and a real-time data processor for event detection and data compression. On-focal-plane signal processing is being addressed with the Hybrid Mosaic On Stacked Silicon (HYMOSS) technology developed by Irvine Sensors Corporation through the Small Business Innovation Research program sponsored by MSFC. The HYMOSS module contains a transimpedance amplifier, tunable bandpass filter, thresholding, comparing, and one random access multiplexer per channel. A single channel is shown in Figure 66. Sixty-four of these channels are placed on a single silicon die. Sixty-four of these die are stacked to form a cube on which a detector array is bump-bonded to the face of the module using the same technology as planar hybrids. Data rate reduction is accomplished by adjusting the bandpass filter to the expected time rate of a lightning flash. Signal detection is then accomplished by comparison to a background-corrected threshold signal to detect a minimum lightning pulse of 4.7 $\mu J\ m^{-2}\ sr^{-1}$. Pixel location and radiant intensity from the pixel itself are bussed off the module through the multiplexer. The data is then time tagged and passed to platform telemetry formatting as digital words via interface electronics.

An alternate design uses a 64 by 128 CCD element device with 64 output channels. This array is divided into two independently clocked 64 by 64 element sections. The first of these is optically active and is used to image the object, while the second is masked and used for storage of the imaged information. This frame shift architecture allows for rapid image transfers to the masked array, minimizing read time and improving integration time. Image data from the masked array is then clocked out at a reduced rate to the processing electronics. Background averaging circuitry and the background subtraction/event decision circuitry will then be performed off-focal-plane in analog or digital circuitry. Benefits of digital signal processing or analog subtraction techniques to remove the background sunlit scene data clutter will be studied.

M.W. James/ES43
(205) 544-5020
Sponsor: Office of Space Science and Applications

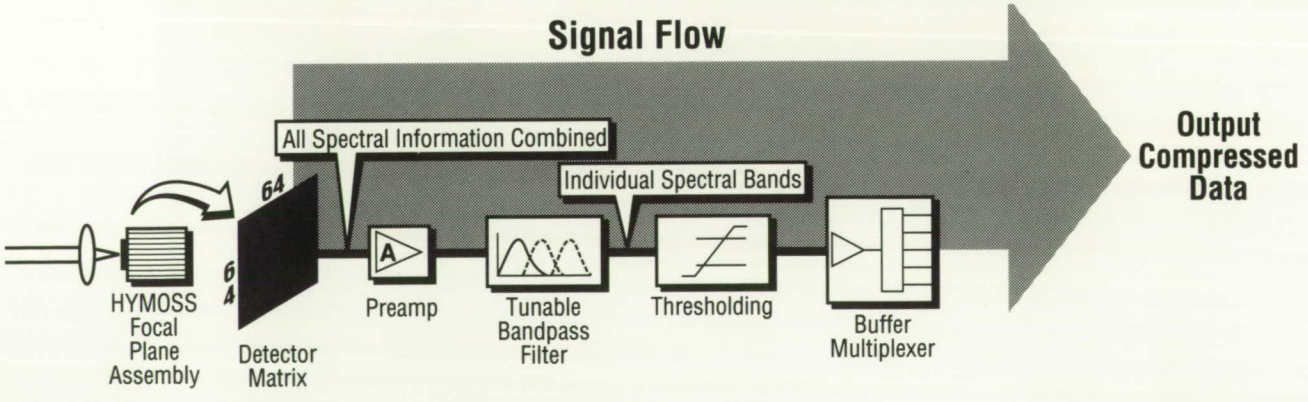

Figure 66. On-Focal-Plane Signal Processing

Aircraft/Field Sensor Development Applications

Research in aircraft/field applications can be divided into three major areas: lightning instrument package updates, surface sensor developments, and airborne sensor development.

The NASA U-2 fleet is being retired in favor of ER-2's, therefore, the U-2 Lightning Instrument Package (LIP) needs to be modified to fly on the ER-2. As part of the process of modification, several instruments were updated. The first such instrument is the Multiple Optical Pulse Sensor (MOPS). This sensor is an outgrowth of two other instruments in the LIP, the Optical Pulse Sensor (OPS) and the Lightning Spectrometer (LS). The basic purpose of MOPS is to have the time resolution of the OPS with the spectral resolution of the LS at several different frequencies. Another instrument being developed for the ER-2 LIP is the Cylindrical Field Mill (CFM). This instrument will augment the electric field measurements of the current Rotating Vane Field Mills (RVFM's) that were used on the U-2 flights. The major advantage of the CFM is that it is nearly immune from aircraft charge, allowing better determination of the electric field, and that it measures two components of the electric field with a single instrument. Combining two CFM's or one CFM and the two current RVFM's results in the ability to determine the total vector electric field at the ER-2 location. Another instrument, the Conductivity Probe, is to be redesigned to fit in a smaller package. With the smaller package, it will be easier to integrate onto the ER-2. One other instrument, the Slow and Fast Electric Field Antenna, will be separated into two units. This way, each antenna can be individually optimized.

The present U-2 recording system incorporates two analog 14-track wide-band tape units. Because most lightning signals are transient in nature, the present system does not use the tape in the most efficient manner. Most of the data recorded on tape is between lightning events, which is of very little use. Actual usable data occupies small, widely-separated sections of the data tapes. Analog tape length limitations restrict data collection flight times to less than 2 hours. To alleviate this problem, a digital system is being designed, employing a transient recorder to digitize events and then write them to 8-mm video cassettes. With proper triggering, all transient data from the whole ER-2 flight can be recorded on one tape. Some of the data associated with lightning, however, is slow and continuous and does not adapt well to a transient recorder system. For this data, a continuous data recorder is also being developed that is based on the same 8-mm video tape technology used in the transient system. The two systems, fast and slow data recorders, will be integrated into a single versatile system that will allow multiple channels of fast and slow data to be recorded on a single cassette.

Several new ground-based instruments are being developed. The first one is the coronasonde; it consists of a Vaisala RS-80-15L radiosonde with an added circuit to measure the electric field aloft. The basic radiosonde uses LORAN-C navigation signals to locate its position on the ground. This allows the launching and tracking of radiosondes from remote and mobile locations. The spare radiosonde transmitter bandwidth was used to add a measurement of the electric field in thunderstorms by using a simple set of corona points. With this system, the charge structure of both summer and winter thunderstorms can be better determined. A related effort involves modification of the present NASA/U.S. Air Force ground meteorological detector system to add digital processing of the ground data. The digital data is more accurate and is available immediately for real-time processing and analysis.

Tests have shown that there are wide variations in the measurement of atmospheric moisture by radiosondes. To use satellite sensors to measure global moisture content, an accurate baseline to calibrate the orbiting sensors is needed. It is not clear which, if any, of the present radiosonde systems accurately measure the amount of water vapor in the atmosphere, especially above -40 °C. The goal of this

project is to use an environmental chamber to test the various humidity sensors and determine which is most accurate. If none are found to be accurate, then the project will try to develop a sensor that is accurate. Once an accurate measure of atmospheric moisture can be determined, the task of calibrating orbital moisture sensors can begin.

Airborne sensor development also consists of adding instruments to a NASA Lear jet for the study of shuttle and expendable launch vehicle launch constraints. Because of recent lightning strikes to launch vehicles, a conservative set of weather-related launch rules was formulated. The launch constraints are believed to be overly restrictive, but current knowledge is insufficient to determine which rules can be relaxed. The goal of this project is to study the cloud and weather formations that have been labeled dangerous to launch vehicles and determine which are not actually hazardous. The measurements that will be made from the aircraft include the vector electric field, the liquid water content, the amount of ice, and the temperature and pressure at the aircraft flight level. Eventually, the project should become a range asset to be used operationally on the day of launch. Between launches, however, the aircraft system will be available for research projects.

M.W. James/ES43
(205) 544-5020
Sponsor: Office of Space Science and Applications

Mosaic Array Imaging Technology

Sensor development activities have increased in importance with the need to support Earth system science. Earth Observing System (EOS) programs have stimulated the need for new generations of remote sensing instrumentation to address the various requirements for improved spatial, spectral, and temporal sensing of Earth system interactions. A number of instrument programs have been developed that will utilize single element detectors and mosaic arrays for visible to infrared detection for such programs as atmospheric moisture mapping, atmospheric electrostatic activities, ocean color and temperature variations, and land vegetation stress. With the need to better understand these processes and their interactions with other global cycles, improving data quality and data rates has required technology development of better sensing detectors and data recording systems.

The Remote Sensing Laboratory is developing the capability to design and build sensors to support EOS platforms. Instruments being built in the laboratory are being utilized for underflights of spaceborne sensors and as test beds for spaceborne versions that will support EOS objectives. In order to support the design and testing of these airborne sensors, the laboratory has expanded to include an optical laboratory outfitted with the test equipment necessary for proper calibration and setup of instruments. The emphasis of the laboratory toward instrument development will require complete end-to-end testing of the sensors. Additional test and scene simulation equipment is being developed for full functional testing before deployment.

The Lightning Imaging Sensor (LIS) is one of the EOS instruments that will use these laboratory resources. The LIS will incorporate a charge-coupled device (CCD) visible array to detect and measure lightning flashes, both count and intensity, seen from polar orbit. Evaluation boards provided by vendors are being used to set a baseline for understanding CCD arrays and to provide a stepping stone for instrument design. For the LIS instrument, both on- and off-focal-plane signal processing are being studied. The current design utilizes a 64 by 64

element CCD array which helps keep the data rates off the focal plane to a manageable number. On focal plane signal processing is being studied for the LIS sensors as a test bed for high density arrays. These larger arrays increase the field of view and resolution of spaceborne sensor applications while also increasing data rates by several orders of magnitude. On-focal-plane signal processing and data compression can be accomplished using technology being developed in a Small Business Innovation Research program sponsored by MSFC. Hybrid technology is being used for preamplification, filtering, detection, and event-driven multiplexing of the data on the focal plane assembly. Data compression is inherent in the on-focal-plane design, because data selection occurs on-focal-plane, so only valid data is read from processing the module to obtain good passivation, metal pad deposition, and indium bumps for bonding to the detector arrays. To process the data off-focal-plane would require digital signal processing or analog signal subtraction to remove background noise from sunlit scenes so the 4.7 $\mu J\ m^{-2}\ sr^{-1}$ lightning pulse is detected. The major difficulty with off-focal-plane processing is that the power and size of the processing electronics increase rapidly for small increases in two-dimensional array sizes.

To complement the increased resolution, high density recorders are being developed to record digital data on compact tape cassettes. These tape systems will extend flight missions due to the high capacity of around 2×10^9 bytes being recorded using the on demand system rather than continuous recording. These tape systems will allow scientific personnel at each deployment to have access to the data in a usable format. Portable work stations for data analysis are being constructed to interface with the formatted data recorded on the aircraft. These quick view systems will allow the preprocessing of data from either analog or serial digital format on multitrack instrumentation recorders to single-user personal computer systems for first look verification of the data quality.

M.W. James/ES43
(205) 544-5020
Sponsor: Office of Space Science and Applications

Lightning Simulator

The purpose of the lightning simulator is to approximate the temporal, spatial, and spectral properties of the in-cloud portion of lightning flashes. The lightning simulator will be used to evaluate the end-to-end performance of the geosynchronous lightning mapper. This is a joint project between MSFC and the University of Alabama in Huntsville.

The most difficult task of the lightning mapper will be to detect daylight lightning flashes over the background of solar reflected light from cloud tops. Even with spectral filtering to a single strong lightning emission line, the background radiation will still be orders of magnitude greater than the lightning signal. This requires temporal filtering to extract the lightning signal. The lightning mapper uses a system of background subtraction and averaging to detect the lightning signal. Because this is a relatively unique analysis approach, the method will need to be tested on the ground under controlled conditions.

The first part of the lightning simulator will be a background simulator that consists of a Lambertian surface of sufficient area to cover the field of view of the laboratory lightning mapper. The second part will be a lightning simulator. The simulated lightning location, brightness, and temporal and spectral characteristics will be controlled by a computer.

The first task of the lightning simulator will be to verify the operating characteristics of the lightning mapper, to see if the lightning mapper electronics and software meet requirements. The final task will be to test the absolute limits of the lightning mapper; to test how small a signal it can detect given a set background level, determination of the maximum signal level it can handle without saturation, and determining how many signals it can process at one time before the lightning mapper system overloads.

M.W. James/ES43
(205) 544-5020
Sponsor: Office of Space Science and Applications

Satellite Sensor Simulations

Accurate modeling of the radiative transfer processes occurring in the atmosphere is important to the evaluation and analysis of aircraft and satellite remote sensing data. With an appropriate model, the radiant energy received by the sensor can be predicted by convoluting the incident energy with the transmission properties of the optical and detector system. This capability allows simulation of current and future sensor systems and their impact on the analysis of the Earth system.

Several radiative transfer software packages have been acquired and modified at MSFC to simulate a variety of infrared sensor systems. These programs are used in conjunction with the analysis of multispectral airborne and satellite measurements for the research tasks described elsewhere in this report. Additional research simulation code is used which involves the simulation of Television Infrared Observation Satellite Operational Vertical Sounder (TOVS) data from numerical weather prediction model output. Initial and forecast fields of thermodynamic parameters from the Limited Area Mesoscale Prediction System (LAMPS) are used as input to the radiative transfer code. Infrared and microwave TOVS channel radiances are generated and converted into image form based on the LAMPS grid domain. These images (in multiple channels and at multiple times) are looped on an image display system to simulate real TOVS observations. Comparisons to real TOVS observations show good agreement, which lends credibility to the numerical model forecast fields and to the radiative transfer simulation code.

Jedlovec, G.J. and Batson, K.B.: Interpretation of Observed TOVS Imagery from Simulated Radiance Fields. Proceedings of the Fourth International TOVS Study Conference, Igls, Austria, CIMSS/SSEC/UW, Madison, WI, pp. 69–84, 1988.

G.J. Jedlovec/ES43
(205) 544-5695
Sponsor: Office of Space Science and Applications

High Spectral Resolution Measurements

This research effort is being monitored in the Remote Sensing Branch at MSFC, with most of the research activities being performed at the University of Wisconsin–Madison under NASA Contract NAS8-36169, which is in its final year of funding.

NASA funded the University of Wisconsin, under a previous contract, to develop a high resolution interferometer for the NASA ER-2 aircraft platform in order to demonstrate the capability to improve vertical resolution of remotely-sensed temperature and moisture profiles from space. The High-resolution Interferometer Sounder (HIS) development was completed in early 1986, and a series of data flights were made in conjunction with other aircraft instruments during the summer of 1986 as part of the Cooperative Huntsville Meteorological Experiment (COHMEX). The data obtained from HIS were of very high quality with noise equivalent delta temperatures of between 0.1 to 0.2 K. Under the current contract, a retrieval algorithm was developed and applied to produce temperature and moisture soundings for 2 COHMEX days. The results of these case study investigations indicate that much-improved soundings of temperature and moisture are possible with the HIS instrument. An improvement in vertical resolution by a factor of 2 was shown to exist in the HIS data over current operational sounders. This improved resolution has lead to improved retrieval accuracies because of the reduced vertical smearing of measured radiance information. Intercomparison of HIS data with Multispectral Atmospheric Mapping Sensor (MAMS) data for the June 15 and 19, 1986, case studies indicates good agreement in absolute calibration of the two instruments (to within 1.0 K) and excellent agreement in horizontal resolution. The sounding capabilities provided by HIS have allowed for a better interpretation of the level of radiance emission sensed by MAMS aircraft data.

The high spectral resolution measurements from HIS (less than 0.5 cm^{-1}) allow for a detailed look at absorption and emission spectrum of various gaseous absorbers. This has allowed evaluation of the way absorption is formulated in radiative transfer models used to simulate satellite data (e.g., FASTCOD2), and to make corrections when necessary. The data can also be used to estimate concentrations and vertical distributions of trace gases in the atmosphere.

G.J. Jedlovec/ES43
(205) 544-5695
Sponsor: Office of Space Science and Applications

Multispectral Mapping

The use of the Multispectral Atmospheric Mapping Sensor (MAMS) continues to be an important aspect of the remote sensing activities at MSFC. A number of instrument flights have been made during FY89 in support of existing and new research efforts. Some of these activities are highlighted elsewhere in this report, including geomorphic mapping, surface thermal flux and emissivity, and soil and snow properties studies. Data were collected in November and March over the Atchafalaya Delta region of Louisiana in support of the geomorphic mapping studies being conducted at MSFC and the University of Wisconsin. These flights captured coastal conditions in various seasons and before and after significant weather events. During June of 1989, three additional MAMS flights were made for Earth System Science investigations. The first two flights were over Seneca County, OH, in order to detect thermal changes which are associated with soil moisture variations. MAMS data were collected at various times on each day. A third flight was conducted over Mount Mitchell, NC, in order to map changes in vegetation associated with an increase in atmospheric pollutants.

Research continues on algorithm development to determine low-level precipitable water variations with MAMS using data from the FY86 and FY88 flight programs. A technique was developed over the last 2 years which utilizes MAMS split-window channels to determine precipitable water at very fine horizontal scales.

Strong moisture gradients were shown to exist over a 10- to 20-km (6.2- to 12.4-mi) region which were associated with the position of the leading edge of a cumulus cloud field which produced isolated thunderstorms. The technique has been refined to produce more accurate estimates of precipitable water. The technique is also being modified for application to current operational weather satellites such as the Advanced Very High Resolution Radiometer for real-time applications.

Jedlovec, G.J.: Precipitable Water Estimation from High-Resolution Split-Window Radiance Measurements. J. of Applied Meteorology, submitted, 1989.

G.J. Jedlovec/ES43
(205) 544-5695
Sponsor: Office of Space Science and Applications

Multispectral Atmospheric Mapping Sensor

NASA's Multispectral Atmospheric Mapping Sensor (MAMS) is a line scanner with eight visible and three infrared (IR) channels. The eight visible channels range from 0.42 μm to 1.05 μm with the IR channels as follows.

Channel	Central Wavelength	Bandwidth (at 50 % Response)
9	3.73 μm	3.47 - 3.86 μm
10	6.54 μm	6.28 - 6.98 μm
11	11.12 μm	10.55 - 12.24 μm
12	12.56 μm	12.32 - 12.71 μm

Only three of the IR bands are available during any configuration and the 6.54 and 3.73 μm cannot be used together. MAMS data are being used to determine atmospheric moisture variability and its importance for cloud formation and storm development at scales not available from satellites. The MAMS instrument is flown aboard NASA's ER-2 high altitude aircraft where data are recorded on a 14-track high-density instrumentation tape recorder. Further detailed information on the data analysis and instrument configurations are available from NASA TM-100352, "Improved Capabilities of the Multispectral Atmospheric Mapping Sensor."

The baseline system flown in 1985 consisted of a 5-mrad aperture which produced a ground instantaneous field of view (IFOV) of 50 m (164 ft). With the scan mirror rotation of 12.5 revolutions per second (rps) the noise equivalent change in temperature (NEΔT) ranged from 0.5 to 0.9 K. The following year, 1986, the configuration was changed to improve the NEΔT down to the 0.3 to 0.5 K range. This resulted from having a larger aperture of 5 mrad which produced a 100-m (328-ft) IFOV at a scan rate of 6.25 rps. The slower scan speed and larger aperture allowed more radiant energy to fall on the detectors and increased the integration period, improving the NEΔT of the thermal channels. The scan head or primary optics used by the MAMS spectrometer is also used by other spectrometers such as the Thematic Mapping Sensor and the

Advanced Ocean Color Imager (AOCI). Several changes which directly affect data quality have been made to the scanner system to accommodate the AOCI spectrometer. These changes have improved data quality in all scanner applications. The axe blade scan mirror was upgraded to a full face mirror. This change increased the amount of energy falling on the detectors, thus increasing the signal-to-noise ratios in all channels. With the improved dynamic range, the digitization resolution was upgraded from 8 to 10 bits for the IR channels. The averaging electronics for the blackbodies were also changed to average over more samples of the blackbodies to reduce the sensitivity of the detectors to noise. With these improvements, sensitivity became less than 0.1 K with a NEΔT of less than 0.2 K. Based on current instrument performance, minimal changes are necessary for the collection of high-quality data in the future.

Recent deployments have demonstrated a deficiency in on-site data analysis capabilities for scientific evaluation of the MAMS data. The Quick View Display (QVD) system (Fig. 67) is being developed to address this deficiency by reading data directly from the instrumentation tape after a deployment. This data will be stored in frame format on a personal computer (PC) and be made available for analysis with various software packages. Existing analysis software developed at MSFC for calibration, presentation, and navigation of the data is being ported to the PC for use at the deployed site.

The QVD system consists of a single PC-AT form factor card which performs the bit and frame synchronization of the incoming single serial Bi-f-L encoded data. Once start-of-frame code is detected, five scan lines are stored in a local buffer before transfer to the PC hard disk drive is performed. Data are recorded in frames of 750 bytes with start-of-frame code, housekeeping data, scene data, and end-of-frame code comprising a single frame. Software drivers developed for the PC will read five line blocks through a direct memory access transfer to a file which is then read by the analysis software for calibration and navigation correction.

M.W. James/ES43
(205) 544-5020
Sponsor: Office of Space Science and Applications

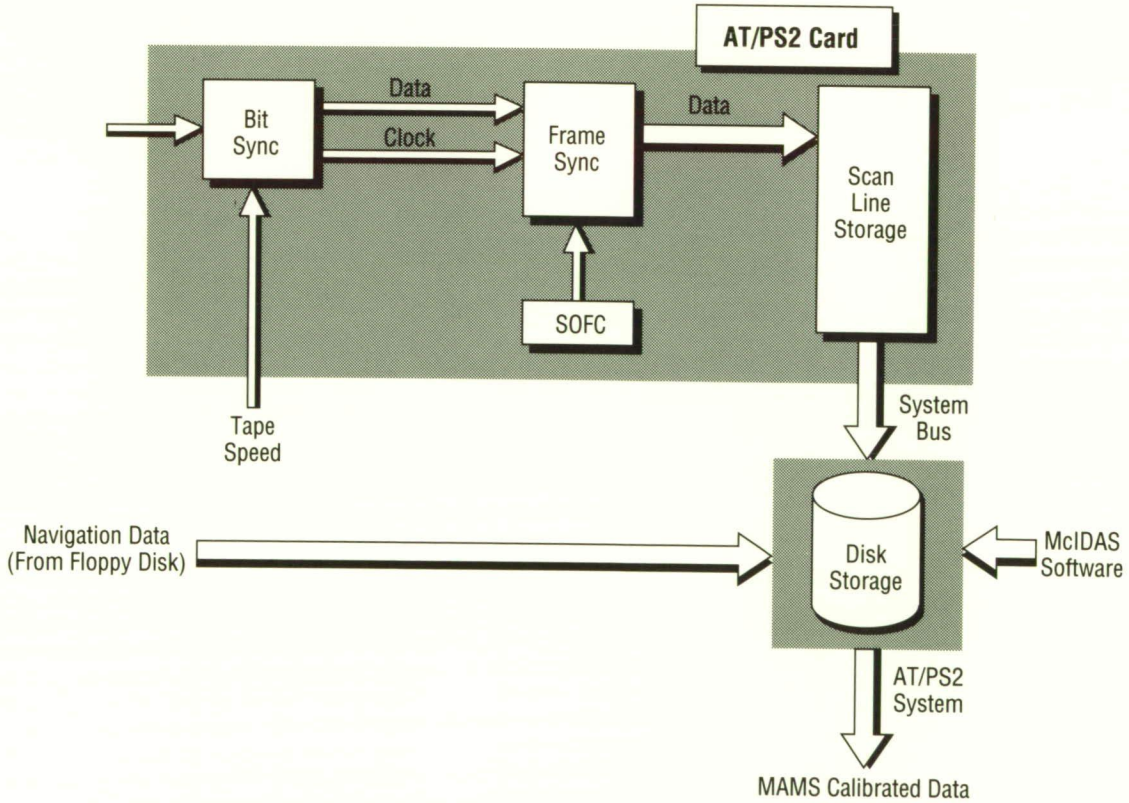

Figure 67. MAMS Quick View Display

Observations of Soil and Snow Properties

This new research activity is still in the planning stage. This research will attempt to make use of high-spatial and temporal resolution data from the Multispectral Atmospheric Mapping Sensor (MAMS) and the Advanced Microwave Precipitation Radiometer (AMPR) to determine the feasibility of mapping geomorphic changes in snow fields and relative variations of soil moisture over agricultural regions from space-based sensors.

A preliminary data set has been collected with MAMS on the NASA ER-2 aircraft over Seneca County, OH, to study soil moisture variations. This region was selected because of its diversity in tillage and drainage properties and because of an ongoing field program to collect in situ measurements of geophysical parameters important to understanding soil moisture variations. MAMS visible and infrared measurements of the region have provided data at multiple times during an experiment day and on multiple days. The days selected were based on variability of soil moisture over the test site and instrument aircraft availability. The diurnal change in MAMS infrared channel data and the multispectral signature variations will be correlated to soil moisture measurements over the region. Aircraft flights in FY90 over the same region will include the AMPR which will provide passive microwave measurements at four different frequencies to provide additional remote sensing measurements in support of the investigation.

The snow geomorphology study is still in the planning stage. Preliminary data collection will begin in the winter season of FY90 with several MAMS and AMPR flights over the basin region of Idaho and Wyoming. Extended periods of cold dry weather induce snow to change into a more crystalline and unstable structure. Snowfall on top of this metamorphosed snow creates a hazardous situation and is the cause of many avalanches in the region. A 1.6-μm channel will be added to the MAMS instrument to help distinguish between various snow and ice types. The AMPR will be used to estimate snow-water equivalents and to provide additional information on snow structure signatures. Both MAMS and AMPR data will be compared to ground truth data collected from snow pits and other routine observations collected during the snow season.

G.J. Jedlovec/ES43
(205) 544-5695
Sponsor: Office of Space Science and Applications

Surface Thermal Flux and Emissivity Studies

The three infrared channels of the Multispectral Atmospheric Mapping Sensor (MAMS) have been used to provide unique thermal measurements over regions where special ground truth data were available. The 100-m resolution of the infrared channels is used to estimate the radiating or "skin" temperature of the Earth's surface at scales not available from satellite sensors. These high-resolution temperature measurements are then used to compute the total flux from the surface of the Earth and at the top of the atmosphere in order to study their role in boundary layer processes. The total flux emanating from the surface is an important boundary condition for mesoscale models which couple the Earth's surface with the atmosphere.

The surface skin temperature is computed via a split window correction scheme traditionally applied to data in the calculation of sea-surface temperatures. In the scheme, the differential absorption between the two split window channels is used to correct the most transparent one for atmospheric water vapor absorption. For MAMS, simple linear regression is used to derive coefficients for the split window correction procedure.

As a result of estimating the skin temperature with the 11- and 12-μm channels, theoretical estimates of the 3.7-μm radiances can be made and compared with observed values. Differences in these values, which exceed those expected as a result of observational and simulation error, can be attributed to a nonunity emissivity at 3.7-μm. This can be observed in Figures 68 and 69, which present a pair of MAMS images at 3.7 and 11 μm during the day and at night. Since solar radiation can have a significant contribution at 3.7 μm, a surface with nonunity emissivity will have a reflected solar component. This reflected component can be quite large and can significantly affect measured radiances with MAMS. The nonunity emissivity in the figure can be inferred by contrasting the 3.7- (left) and 11-μm (right) channels between day (top) and night scenes (bottom). Reflected radiation during the day produces a larger effective temperature (darker image) at 3.7 μm during the day. The opposite situation occurs at night when no solar radiation is present.

Figure 68. Multispectral Atmospheric Mapping Sensor 3.7 and 11.1 μm Day Images

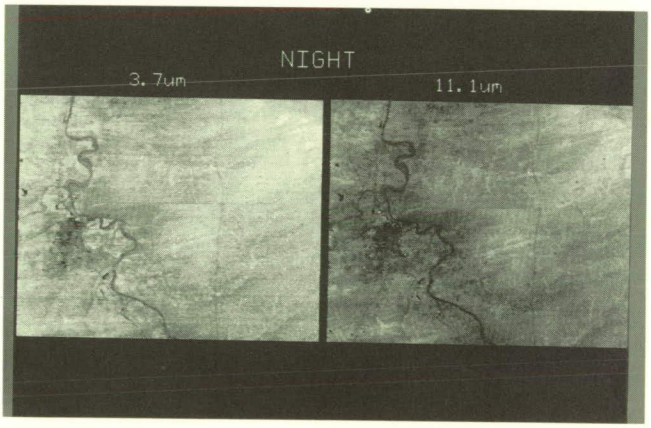

Figure 69. Multispectral Atmospheric Mapping Sensor 3.7 and 11.1 μm Night Images

The 3.7-μm emissivity is calculated as the scaling factor which makes the 3.7-μm effective temperature equal to that of the longwave 11-μm window channel.

Jedlovec, G.J.: Estimation of Thermal Flux and Emissivity of the Land Surface from Multispectral Aircraft Data. Proceedings of IGARSS 89, 12th Canadian Symposium on Remote Sensing, Vancouver, B.C., July 10–14, 1989.

G.J. Jedlovec/ES43
(205) 544-5695
Sponsor: Office of Space Science and Applications

Visible/Infrared Observations and Geophysical Parameter Retrieval

This research is directed toward better use of multispectral visible and infrared measurements from aircraft- and space-based sensors. Most of the work is conducted in-house in the Remote Sensing Branch at MSFC. Measurements are used to derive surface and atmospheric parameters which are useful in the description of processes that govern the Earth's hydrologic cycle. These research activities focus on evaluating the accuracy of the remotely-sensed radiance measurements, the development of parameter retrieval algorithms, an assessment of the accuracy of the derived geophysical parameters, and their application to improving our understanding of various aspects of the hydrologic cycle.

The data utilized in these investigations come from sensors on the current operational satellites used for routine weather observations and several research instruments flown on NASA aircraft. The satellite instruments include the Visible Infrared Spin Scan Radiometer Atmospheric Sounder in geostationary orbit, the Advanced Very High Resolution Radiometer, and the Television Infrared Observation Satellite Operational Vertical Sounder on Sun-synchronous polar orbiting satellites. The aircraft instruments include the High-Resolution Interferometer Sounder built by the University of Wisconsin and the Multispectral Atmospheric Mapping Sensor built by Daedalus and operated by MSFC. The aircraft instruments are prototypes of instruments for future NASA polar and geostationary observing platforms.

A number of geophysical parameters can be derived from these measurements, including temperature and moisture vertical profiles, horizontal maps of perceptible water, stability, and estimates of trace gas concentrations (e.g., ozone, methane, carbon monoxides, and chlorofluorocarbons). Surface parameters include soil moisture and surface temperature, estimates of suspended sediment in coastal waters and rivers, characteristics of surface vegetation over land, surface thermal flux, and emissivity of the surface in the 3.7-μm region.

G.J. Jedlovec/ES43
(205) 544-5695
Sponsor: Office of Space Science and Applications

Satellite-Derived Humidity

This research activity is coordinated by the Remote Sensing Branch at MSFC, with most of the research investigation being performed by Dr. Henry E. Fuelberg at Florida State University under NASA Grant NAG8-653. Activities over the past year have concentrated on two areas of new research. The first task is aimed at acquiring a better understanding of how variations in temperature, moisture, and derived parameters, such as precepitable water and instability, lead to thunderstorm development. The utility of these parameters, derived from remotely sensed radiance observations, is in their increased time and spatial coverage over the more conventional measurements methods. The investigation has focused thus far on one of three planned case studies from a special observing period [the Cooperative Huntsville Meteorological Experiment (COHMEX)] in 1986. The June 17 COHMEX case was selected because of the availability of data and occurrence of isolated thunderstorms centered over the COHMEX ground truth network. Surface dewpoint and time tendency maps indicated an enhanced region of moisture over southern Tennessee which increased in magnitude with time and corresponded to the region of afternoon thunderstorm development. Visible and Infrared Spin Scan Radiometer Atmospheric Sounder (VAS)-derived precepitable water and lifted index fields also isolate this region for potential thunderstorm development. The utility of these parameters in diagnosing favorable regions for thunderstorm development will be further evaluated for the June 17 case by looking at time changes of basic and derived parameters from VAS. The investigation will be extended to the June 15 and 19 COHMEX days.

The second thrust in this research focuses on an evaluation of temperature and moisture profiles derived from VAS data. Previous investigations have presented results of VAS versus rawinsonde comparisons from individual days or case studies and have not focused on an entire season or year. This current effort uses a very large statistical sample covering all VAS retrievals produced operationally during the summer of 1986. Both basic and derived parameters were evaluated and compared to coincident rawinsonde data (Fig. 70). The results suggest that the utility of VAS data may not be as great as originally anticipated. The standard deviations of the difference between rawinsonde and VAS ranged between 1.3 to 2.2 and 3.0 to 5.8

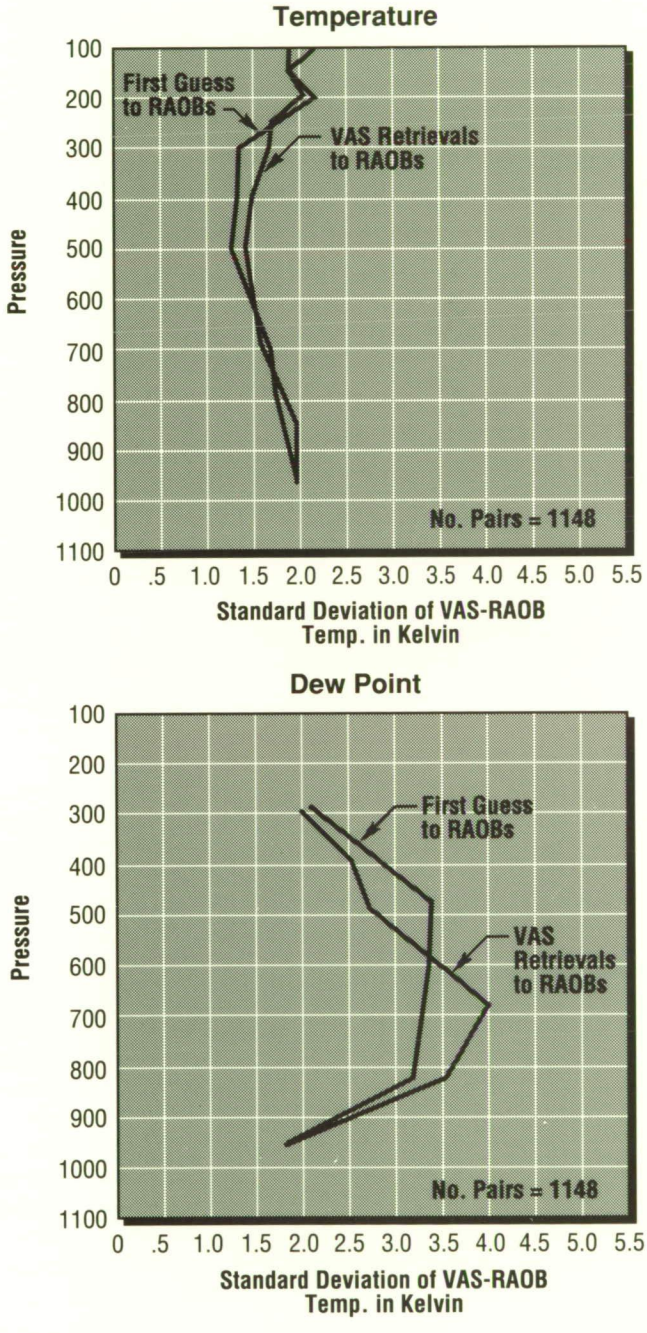

Figure 70. Satellite-Derived Humidity Data Comparisons

for temperature (K) and dewpoint, respectively. Comparisons made with the VAS first-guess data (forecast fields valid at VAS observation times) suggest that VAS retrievals seldom improve on the first guess information, and at some levels (e.g., 300 millibars) VAS-retrieved temperatures are statistically worse than the guess. Future efforts will extend this evaluation to additional data sets and parameters.

G.J. Jedlovec/ES43
(205) 544-5695
Sponsor: Office of Space Science and Applications

Geomorphic Mapping

Interactions between land and water and/or the atmosphere and Earth's surface can produce significant changes in the physical and biological systems of a region. Data from the Multispectral Atmospheric Mapping Sensor (MAMS) have been collected during several periods of significant weather events over lowland and coastal regions to study the processes which are responsible for changes to these regions. The processes under study include sediment transport by rivers and streams, atmospheric forcings such as frontal passages and tropical storms, human influences such as dredging and breakers, and the natural erosion action of tides. This research is coordinated by the Remote Sensing Branch at MSFC and is being conducted by Dr. Paul Menzel under a NASA grant.

Figure 71 presents an example of the MAMS data used in this investigation. Data were collected on January 27, 1988, off the coast of Louisiana, in the Atchafalaya River Delta region. MAMS channels at 0.48, 0.56, and 0.61 μm were used to produce a suspended sediment concentration (SSC) map of the delta region using an approach similar to that for the Coastal Zone Color Scanner satellite instrument. In the SSC image (at left), increasing concentrations of suspended sediment are designated as increasing image brightness. The land regions appear dark in the image. A sea-surface temperate (SST) map was also produced for the same region, using a split-window connection technique for the 11- and 12-μm channels. Both images are centered on the Atchafalaya Bay region. Much structure is present in both the SSC and SST products. The SSC image suggests a high concentration of sediments in the bay associated with flow from the mouth of the Atchafalaya River, with significantly less sediment outside the bay region. The SSC image suggests the origin of the water and that significant amounts of

sediment are transported away from the bay and deposited on the Chenier plain to the west of the region. The SST image also suggests the origin of the sediment, and values are negatively correlated with the SSC values.

These MAMS data represent a typical setting for the transport of suspended sediment from the Atchafalaya River into the Gulf of Mexico. The sediment is transported westward by circulation in the Gulf. This pattern can be redisturbed by the interaction of weather systems with the oceans to change the circulation and deposition of the transported sediment. These atmospheric systems and tidal action can erode the newly deposited sediment from coastal regions, thereby reversing the geomorphic activity of the coastal region.

Moeller, C.C., Gumley, L.E., Strabala, I. and Menzel, W.P.: High Resolution Depiction of SST and SSC from MAMS Data. Preprints, Fourth Conference on Satellite Meteorology, AMS, Boston, MA, 1989.

G.J. Jedlovec/ES43
(205) 544-5695
Sponsor: Office of Space Science and Applications

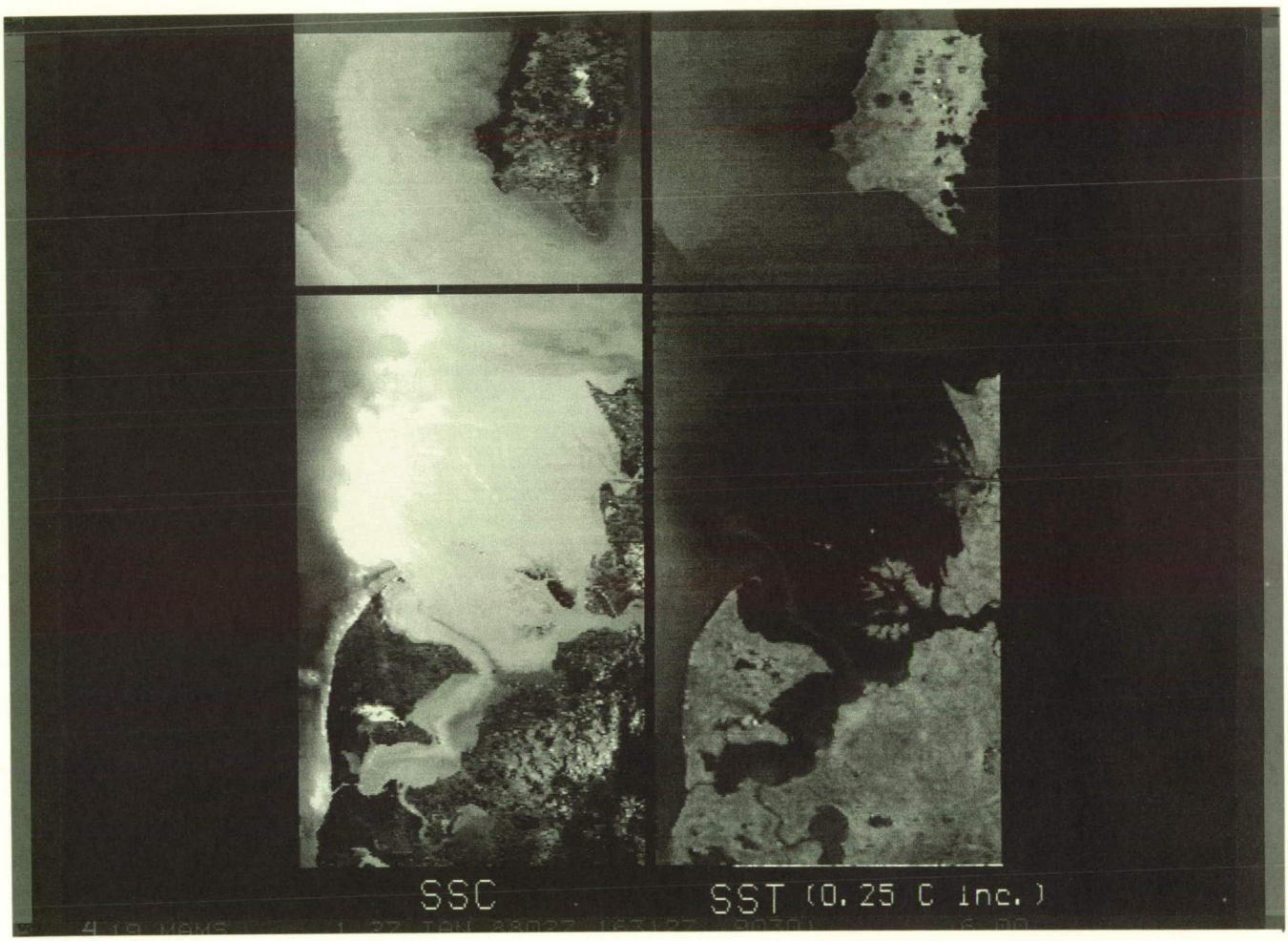

Figure 71. Geomorphic Change in Atchafalaya River Delta, off the Coast of Louisiana

Global Atmospheric Modeling

For several years, MSFC has been actively participating in the Global Scale Atmospheric Processes program. Most research efforts have addressed the dynamics of atmospheric flows using gridded analyses of conventional and remotely-sensed observations. In FY89, a cooperative effort with the National Center for Atmospheric Research (NCAR) was initiated through which the NCAR Community Climate Model (CCM1) would be implemented for use in MSFC science studies. The CCM1 is currently formulated as a global spectral model which predicts atmospheric state variables and the momentum field, and also treats radiative processes, subgrid-scale deep convection, boundary layer processes, and exchanges of energy with underlying land or oceans. Figure 72 shows the model simulated zonal wind component (i.e., the east/west component) averaged over longitude. The two subtropical jet maxima lying at approximately 40° North and South and 150 millibars are similarly observed in nature. Also reproduced are the easterly winds (negative values) in the deep tropics near the surface and above 100 millibars. Access to a global atmospheric general circulation model like CCM1 enables a more comprehensive investigation of global geophysical processes involving atmospheric dynamics, radiation, and land/ocean/atmosphere interactions.

The CCM1 was installed on the MSFC Cray XMP 416 supercomputer in March. Baseline experiments have been run to duplicate results obtained at NCAR

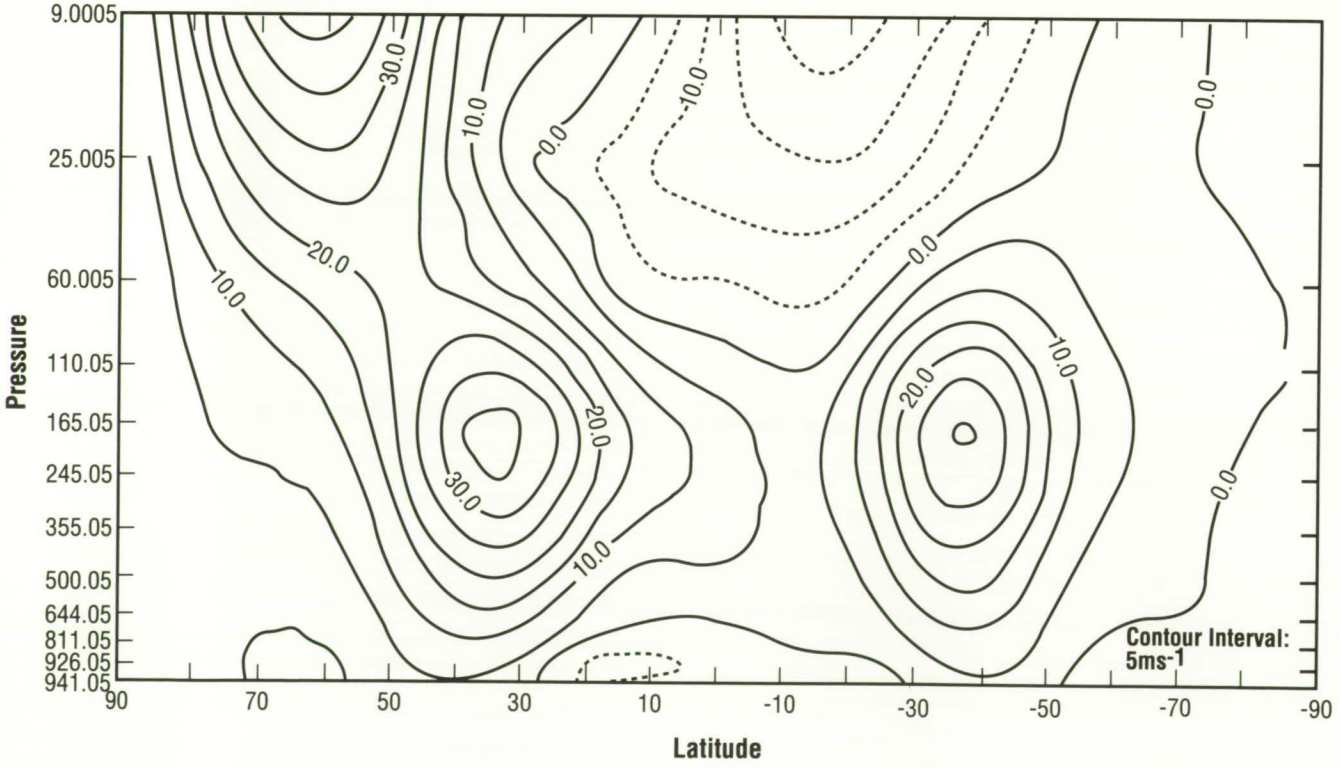

Figure 72. Zonally Averaged, Time Averaged (Dec.-Jan.-Feb.) Zonal Wind Component Simulated by CCM1

to verify operation of the model. One of the first objectives will be to examine the model's hydrologic cycle by comparing the results of model integrations to global determinations of atmospheric water vapor, liquid water, and ice obtained from the Special Sensor Microwave Imager; specifically, to determine how accurately the modeled synoptic, intraseasonal (40–50 days), and seasonal scales of moisture variability compare with observations. In conjunction with NCAR scientists, a series of tests will begin with upgraded physics packages which will assist in developing future versions of the model.

In the context of the Earth Observing System initiative, a variety of model studies will be conducted that examine the sensitivity of short-term climate to interactions between the hydrologic cycle, radiation, and the lower boundary. Remote sensing will play a key role both in evaluating the realism of the model simulations and in specifying forcing mechanisms for model experiments.

F.R. Robertson/ES42
(205) 544-1655
Sponsor: Office of Space Science and Applications

The Global Hydrologic Cycle

The cycling of water through the geophysical environment has long been recognized as crucial to understanding of the Earth's physical climate system and various biogeochemical processes. Space-based remote sensing is rapidly becoming a tool of critical importance for inventorying and understanding the global water cycle. The requirement for a perspective from space results, in part, from the paradox that, while the distribution of water is globally extensive, the processes of phase change between vapor, liquid, and ice, associated Earth radiation budget influences, and interaction with other chemical constituents all occur on scales ranging from global to molecular. While no single observing system or research tool can address the whole problem, space observations make a unique and critical contribution.

For several years, studies at MSFC have involved the atmospheric component of the hydrologic cycle. These investigations have sought to understand how heat sources and sinks induced by condensation and evaporation modify atmospheric thermal structures and wind fields. For example, it has been shown that persistent atmospheric condensation and heating in tropical cloud bands over the South Pacific is important in maintaining the thermal gradient and associated southern hemisphere subtropical jet stream. A more detailed discussion of this was given in the FY88 Research and Technology Report.

Recently, passive microwave measurements of atmospheric water vapor, liquid water, and ice have become available from the Special Sensor Microwave Imager (SSM/I) flying on a polar-orbiting Department of Defense satellite. During the past year, these measurements were analyzed in a number of ways. Global monthly distributions of column-integrated water vapor (precipitable water) have been generated and compared against similar measurements taken from conventional observing networks. This comparative analysis has demonstrated the variability of water in the atmosphere and shown that the conventional observing system, while

describing a significant fraction of this variability, undersamples many important transient features.

The rich structure seen in global moisture distributions attests to the complex dynamical processes which both transport water and determine its sources and sinks. A program of numerical modeling and simulation has been developed to allow controlled experiments which assist in sorting out these processes. The Limited Area Mesoscale Prediction System (LAMPS) numerical code is serving as a tool to investigate mesoscale moist atmospheric dynamical processes. During the past year, this model was used to simulate winter storms off the east coast which owed their rapid development in part to condensation and release of latent heat in clouds. The evolution of these numerically simulated clouds and precipitation has been compared to SSM/I measurements. To address processes on a global domain, a version of the Community Climate Model (CCM1) developed at the National Center for Atmospheric Research was recently acquired. This tool will enable a series of experiments that explore how global land and sea surface characteristics and radiative processes operate on time scales from weeks to months and years in determining the global hydrologic balance. During the past year, research began on verifying the CCM1 moisture balance with SSM/I measurements.

Next year, this research will focus even more strongly on science issues within the framework of the Earth Observing System (EOS) initiative. The research effort proposed by MSFC and selected under the EOS program will build on the remote sensing observations and modeling outlined here and point toward solving issues of the global water cycle that require the space-based observations planned for the 1990's.

Robertson, F.R. and Huang, H.-J.: Atmospheric Moisture and Cloud Structure Determined from SSM/I and Global Gridpoint Analyses. Preprints, Symposium on the Role of Clouds in Atmospheric Chemistry and Global Climate, Amer. Meteor. Soc., January 1989.

F.R. Robertson/ES42
(205) 544-1655
Sponsor: Office of Space Science and Applications

Stratosphere/Troposphere Dynamical Coupling

The troposphere is the lowest layer of the atmosphere. It contains 90 percent of the atmospheric mass, and provides living organisms a suitable environment. The next layer, the stratosphere, extending from about 15 to 50 km (9.3 to 31.1 mi) in altitude, contains 99 percent of the remaining mass of the atmosphere. In recent years, the stratosphere has been the object of considerable scientific interest due to the importance of stratospheric ozone in protecting living things from damaging ultraviolet radiation, and the realization that some human activities threaten the ozone layer.

The stratosphere is not an isolated system, but exchanges mass and energy with the troposphere. The understanding of this interaction is a key part of NASA's mission to develop a better understanding of the planet Earth. In FY89, MSFC initiated a research program involving scientists at Iowa State University (ISU), the University of Alabama in Huntsville (UAH), and Florida State University (FSU), aimed at increasing our understanding of troposphere/stratosphere coupling, with an emphasis on the influence of the stratosphere on tropospheric circulation. Mass exchange between the troposphere and the stratosphere is mesoscale, dominated by extrusions of tropospheric mass in tropical thunderstorms and extrusions of stratospheric mass in long, narrow regions adjacent to extratropical storm systems. Planetary-scale or ultralong waves in the troposphere have a strong influence on middle- and high-latitude motions in the stratosphere. The stratosphere is a reservoir of ozone and of air with high potential vorticity, capable of enhancing cyclonic flow when brought into the troposphere.

A highly idealized model developed at ISU suggests that photochemical heating of stratospheric ozone by ultraviolet radiation from the Sun can destabilize planetary Rossby waves of growth periods of 20–40 days. This study is proceeding with a more realistic model. Internal Rossby waves may be important in

the month-to-month evolution of general circulation, and may be related to persistent anomalies in weather, the local manifestations of which can be floods, droughts, and extremes of temperature.

Total column ozone observed from satellites yields potential insight into the behavior of both the troposphere and stratosphere. Several studies have shown a strong inverse correspondence between the height of the tropopause and the total ozone signature. A lowering of the tropopause is the result, by continuity arguments, of the convergence of mass in the stratosphere, resulting also in a convergence of ozone. The distribution of column ozone is affected, however, by other factors related to the gradients of the ozone mixing ratio, which effects are most pronounced on planetary scales. An effort is underway at UAH to study the relationship between the ozone distribution and the motions of the upper troposphere and lower stratosphere.

A dominant feature of the stratospheric circulation in winter is a strong polar vortex, often centered off the pole by some 20 degrees of latitude. This vortex is subject to the intrusion of tropical air and the subsequent stretching and shedding of small vortices, seen as blobs of potential vorticity which often eventually interact with and are incorporated into developing tropospheric weather systems. The analysis of isentropic potential vorticity computed from atmospheric data is underway at FSU.

Nathan, T.R.: On the Role of Ozone in the Stability of Rossby Normal Modes. J. Atmos. Sci., Vol. 46, pp. 2094–2100, 1989.

T.L. Miller/ES42
(205) 544-1641
Sponsor: Office of Space Science and Applications

Atmospheric Dynamics Modeling

In developing an understanding of the processes which affect global change of the Earth, a component which offers one of the greatest challenges is the fluid system comprised of the atmosphere and oceans. Clearly, understanding this system is important, since the atmosphere, the fluid system in which we live, supplies the land with fresh water and shields life from harmful solar radiation.

Many questions about the future of the atmospheric environment have been identified but remain unanswered, including those relating to human activity. Due to the complex nature of this system and the difficulty of obtaining sufficient observational data, accurately predicting its behavior for all but very short time periods remains an elusive goal. Obtaining the level of understanding required to predict future behavior of the system requires a three-pronged approach which includes observations, idealized theoretical and conceptual modeling, and detailed numerical (computer) modeling. This particular research effort concentrates on the second two aspects through the use of supercomputers and laboratory experiments.

The most fundamental influences upon the atmosphere and oceans which drive their fluid motion are differential solar heating and the rotation of the Earth. A "simple" fluid system which involves these processes alone turns out to have quite complicated behavior. One way to study this behavior is to conduct laboratory experiments in cylindrical annulus containers where a fluid such as water is differentially heated and rotated. Depending upon the strength of the differential heating and the rate of rotation, the flow may be very simple — steady in time and axisymmetric in structure. For other values of the heating and rotation, the flow may be made of steady, regular waves, or it may be quite irregular and chaotic. Such experiments are being conducted in the laboratory, and numerical models are being used to test our ability to predict the type of flow and to assist us in the development of an understanding of such processes as heat and momentum transport.

Understanding a simple system such as this laboratory experiment is a precursor to developing an understanding of more complicated atmosphere and ocean flows. These studies are also being used to help design future space flight experiments using the Geophysical Fluid Flow Cell apparatus.

In addition to using models of a simple fluid system which can be constructed in the laboratory, a complex atmospheric model is being used which considers a domain approximately 2,500 km^2 (1,500 mi^2). This model was developed at the National Center for Atmospheric Research and Drexel University and is used for other research efforts described here as well. It includes the effects of water substance in the atmosphere, of which latent heat release by condensation is particularly important. In this case, interest is in the nonlinear development of a single baroclinic wave (a mid-latitude low-pressure center) and in the ensuing mesoscale [about 100 km (62.1 mi)] phenomena such as rain bands and cold fronts. While the large-scale storm is a result of strong horizontal temperature gradients and acts to reduce those gradients on the large scale, in smaller regions the storm actually increases the gradients—resulting in such important weather-making features as cold fronts and rain-bands. The formation of these smaller-scale features is much enhanced in the presence of air which is only weakly stable to vertical and slantwise motion. A measure of this stability is the quantity called potential vorticity. It has recently been shown that frontogenesis and mid-latitude cyclogenesis is very much enhanced when the updrafts are in regions of small or negative potential vorticity.

The current research effort is studying several aspects of this problem, such as:

- *What is the effect upon large-scale storms of these regions of enhanced activity?*
- *How rapidly do these small-scale features develop, and how strong do they become?*
- *What happens to the weakly stable air after it is drawn through the storm, and does it give rise to other features elsewhere, at a later time?*

The answers to these questions will provide a better understanding of atmospheric processes and the interaction of the atmosphere with the surface below (the source of the instability via heat and moisture fluxes), as well as assisting in the design of new space-based sensors which could provide the necessary data to test theories developed from the atmospheric models.

T.L. Miller/ES42
(205) 544-1641
Sponsor: Office of Space Science and Applications

Climate Dynamics and Forcing Mechanisms

The dynamic processes inherent in the Earth's climate are coming under scrutiny with a variety of tools. Research during the past year within the Earth Science and Applications Division at MSFC has been directed toward the complementary use of simple, spectrally truncated models, global calculations of atmospheric forcing, and experiments with a comprehensive atmospheric general circulation model.

The most exciting new development in applied mathematics is the emergence of a new discipline devoted to the application of nonlinear dynamic systems to a wide variety of problems in physics, medicine, and chemistry. A body of techniques and expertise has been built up that is particularly well-suited to the study of climate with simple, highly truncated models. The latest in a series of these models is capable of describing the ice age fluctuations of the most important of the slow response variables, i.e., the ice amount, atmospheric CO_2, and oceanic state. This work[*†] and the continuing work in progress should help to determine the natural variation of the climate system and its sensitivity to inadvertent change.

Dynamic systems techniques are also useful in looking at faster climate fluctuations with truncated models (Fig. 73) which show a phase plot of a chaotic region of a three-component model.[‡] This three-component model includes baroclinic and thermal-monsoonal forcing and is capable of producing a winter-time limit cycle with vacillatory fluctuations corresponding with those observed. It is of interest that the plot was made on a novel machine, a super-microcomputer that for the first time allows interactive computation of these models, so that the operator can quickly find the nature of the model by scanning through parameter space.

Results from these simple model experiments point to the importance of variable atmospheric heating in short-term climate variability. The differential heating of the atmosphere by condensation, radiation, and turbulent transfer is the primary forcing mechanism of atmospheric motion. The sum of these forcing processes is the net diabatic heating rate which has been diagnosed from atmospheric observations assimilated at the European Centre for Medium-Range Weather Forecasts for the entire globe over a 3-year period. There is conspicuous interannual variability in the areas of heating and cooling, and therefore, year-to-year variability in the forcing of regional and global weather patterns. The nature of this large-scale variability and its impact on circulation patterns is being examined. For example, the difference between 1987 and 1986 in diabatic heating (Fig. 74) shows that in 1987, a major shift in the atmospheric heating rate occurred from north of Australia to the International Dateline. This shift is associated with the 1987 Pacific warming event (El Niño) which altered planetary-scale atmospheric circulation.

To complement the simple models and further interpret observations, a version of the Community Climate Model developed at the National Center for Atmospheric Research was acquired. This numerical code has been implemented on a Cray XMP-416. During the next year, experiments will be conducted in which land and ocean surface boundaries with the atmosphere are controlled. These experiments should help reconcile the vacillatory behavior exhibited by low-order models and the variability in forcing in the form of diabatic heating.

[*]Maasch, K.A. and Saltzman, B.: A Low-Order Dynamical Model of Global Climatic Variability Over the Full Pleistocene. J. Geophys. Res., in press, 1989.

[†]Saltzman, B. and Maasch, K.A.: Carbon Cycle Instability as a Cause of the Late Pleistocene Ice Age Oscillations: Modeling the Asymmetric Response. Global Biogeochemical Cycles, Vol. 2, pp. 177-185, 1988.

[‡]Saltzman, B., Tang, C.M. and Maasch, K.A.: Folded Resonance and Seasonal Vacillation in a Minimum Thermally-Forced Baroclinic Wave Model. In press, 1988.

D.E. Fitzjarrald/ES43
(205) 544-1651
Sponsor: Office of Space Science and Applications

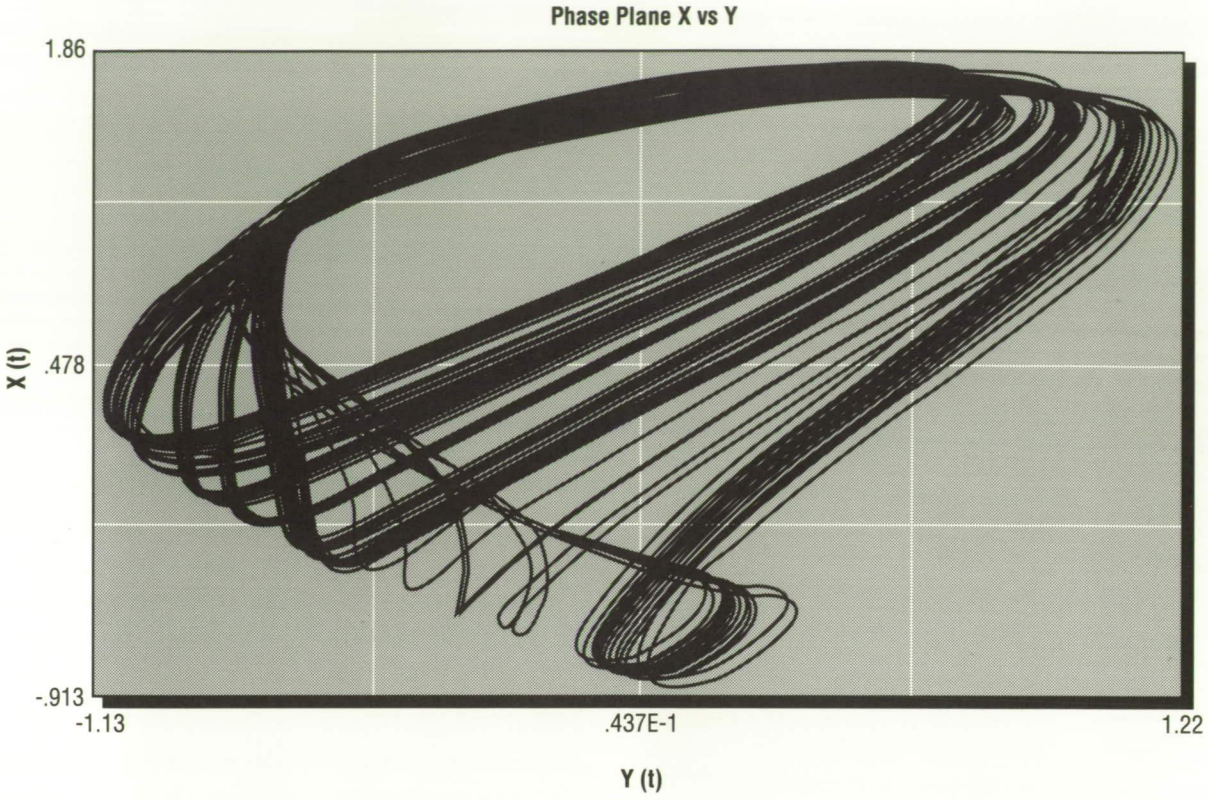

Figure 73. Phase Plot of a Chaotic Region of a Three-Component Model

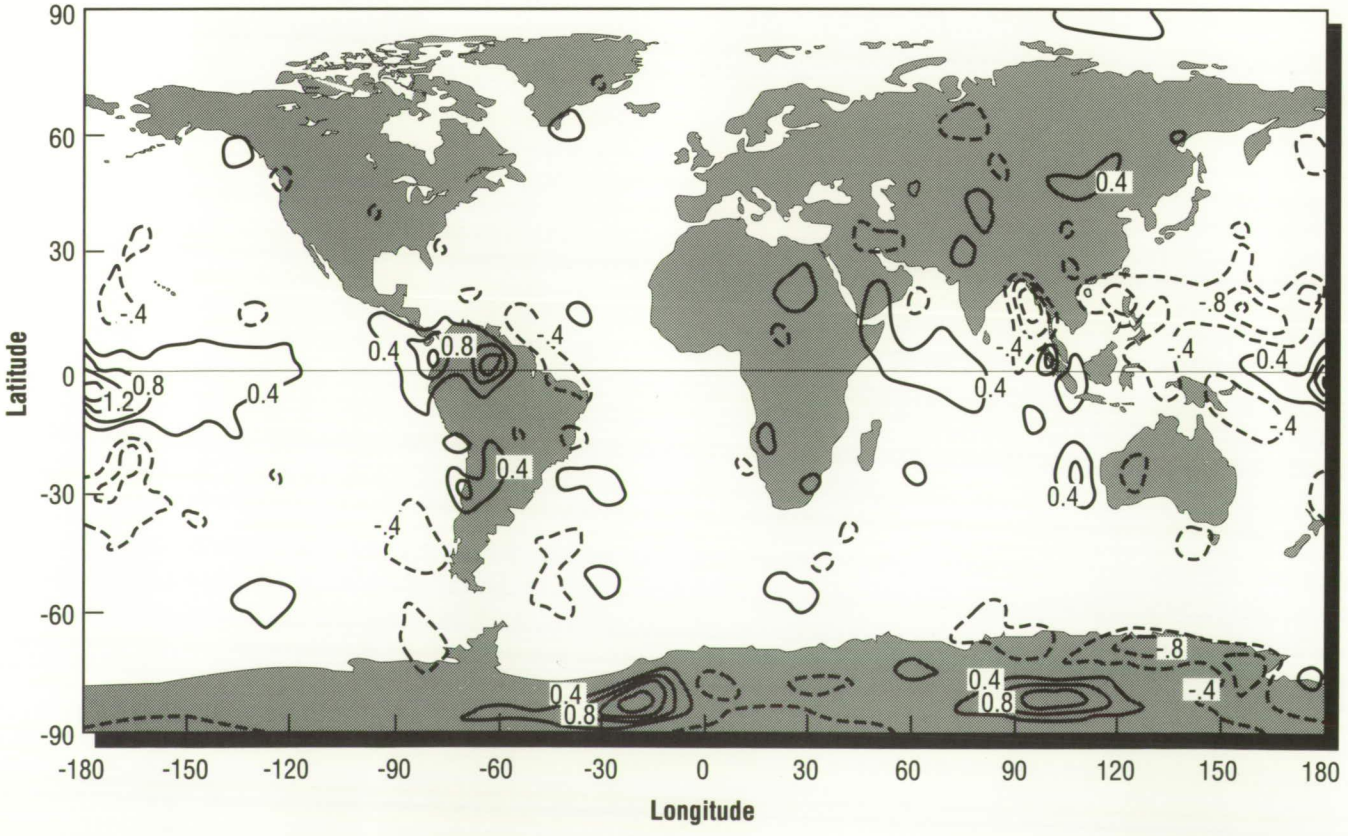

Figure 74. Differences Between 1986 and 1987 in Diabatic Heating

Atmospheric Laboratory for Applications and Science

The Atmospheric Laboratory for Applications and Science (ATLAS) program consists of a series of space shuttle missions utilizing Spacelab pallets which will be conducted approximately annually throughout the 1990's. ATLAS-1 consists of a broad range of experiments which include Earth science, solar physics, space physics, and astronomy. From ATLAS-2 and beyond, there will be a smaller set of experiments with emphasis on Earth science. The core instruments, which are listed in Figures 75 and 76, measure energy output from the Sun (including detailed spectral information) and trace constituents and other properties of the Earth's middle and upper atmosphere. These data will be valuable in monitoring and developing an understanding of the important processes which determine the concentration of stratospheric ozone, which is so important in protecting life from harmful ultraviolet solar radiation. The instruments involve scientific investigators from Europe and the United States.

Name	Acronym	Method
Atmosphere Trace Molecules Observed by Spectroscopy	ATMOS	Measures atmospheric absorption of solar radiation during solar occultations
Millimeter-Wave Atmospheric Sounder	MAS	Measures atmospheric emission of millimeter wave radiation
Co-Manifested with ATLAS:		
Shuttle Solar Backscatter UV	SSBUV	Stratospheric ozone by backscatter of solar UV radiation
Cryogenic Infrared Spectrometers and Telescopes for the Atmosphere	CRISTA	Measures atmospheric emissions in the infrared

Figure 75. ATLAS Atmospheric Instruments

Name	Acronym	Objective
Solar Spectrum	SOLSPEC	Solar spectrum from 170 to 4,000 nm
Solar Constant	SOLCON	Total solar irradiance
Active Cavity Radiometer	ACR	Total solar irradiance
Solar UV Spectral Irradiance Monitor	SUSIM	High resolution solar spectrum from 120 to 140 nm

Figure 76. ATLAS Solar Instruments

One of the major goals of the ATLAS program is to acquire a series of well-calibrated data sets that will provide a reference against which to calibrate instruments on free-flying space platforms that would be in space for extended times, and hence cannot be physically checked for calibration and other performance characteristics. In 1992 and 1993, ATLAS-2 and possibly ATLAS-3 will underfly the Upper Atmosphere Research Satellite, which will have several instruments very similar to some of the ATLAS instruments. In the mid-1990's, ATLAS will provide a set of measurements for NASA's Global Change program, and in the late 1990's, ATLAS will provide calibration data for the Earth Observing System, a set of polar-orbiting platforms and attached payloads on Space Station *Freedom* which will be the first phase of NASA's "Mission to Planet Earth."

T.L. Miller/ES42
(205) 544-1641
Sponsor: Office of Space Science and Applications

The Geophysical Fluid Flow Cell Experiment

Meteorologists and planetary astronomers interested in global planetary and stellar circulations have long recognized the importance of rotation and vertical stratification as strong constraints on dynamical processes. In particular, the effect of latitude-dependent Coriolis forces is thought to play a crucial role in such phenomena as differential rotation on the Sun, cloud-band orientation on Jupiter, and the generation of magnetic fields in thermally driven dynamos. Prior laboratory (and most theoretical) work has treated the curvature effects brought on by sphericity only locally, and the laboratory efforts have only been able to study beta-effects consistently using two-layer quasi-geostrophic models.

The continuous low-gravity environment of an orbiting space shuttle provides a unique setting for conducting geophysical fluid model experiments with a completely consistent representation of sphericity. The Geophysical Fluid Flow Cell (GFFC) experiment constructs its own radial gravity using dielectric forces in a liquid. These are linearly dependent on fluid temperature, and give rise to a radial buoyancy force when a radial electrostatic field is applied. In the GFFC experiment, fluid is held between two rotating hemispheres that are differentially heated and stressed with a large ac voltage. The GFFC flew on Spacelab 3 in May 1985. Image data on convection patterns were obtained in a wide variety of situations: low rotation, rapid rotation, with and without imposed latitudinally-varying temperature fields, etc. Efforts have concentrated on analysis and interpretation of GFFC data and on using results observed in the laboratory to develop models for planetary and stellar circulations by including more realistic processes. For example, having found banana cells in certain parameter ranges in the GFFC, the effects of compressibility, ionization zones, and/or magnetic fields on such global scale convection can be studied to understand under what circumstances banana rolls might be observed at the surfaces of stars.

A low-order model was constructed for the banana cell regime. Since this regime is quasi-two-dimensional, with variations in longitude and radius dominating, the problem can be reduced by an asymptotic expansion off the neutral curve to a set of 12 nonlinear ordinary differential equations. These equations represent the amplitude and phase of the first and second radial eigenfunction for the wave modes, and the first and second radial functions for the zonal flow and radial temperature field. Steady amplitude drift-waves are found for low Rayleigh numbers. These become periodic and then chaotic as the Rayleigh number is raised. Periodicity occurs at higher values than observed in the GFFC, suggesting that periodicity there is a consequence of camera-timing problems, not internal dynamics. The computed periodic regimes are destabilized by weak external time-periodic gravity, as was found for baroclinic waves. These calculations suggest possible experiments for a possible future flight.

Terrestrial laboratory work focuses on two problems. First, because radiative transfer of heat dominates over momentum transfer in many astrophysical fluids, low Prandtl number flows have been of interest. In the GFFC, $Pr = 10$, but global differential rotation appears, based on the relatively few numerical simulations carried out to date, to be favored at lower Pr. Instability and transition to chaos have been studied in a Hadley cell of mercury. At first the experiments are nonrotating to make things simpler. The flow goes to an overstable mode via a super-critical Hopf bifurcation as the Rayleigh number is raised. These oscillations are stable up to a point, then period double into chaos. The effects of rotation and magnetic fields on this instability are under study.

Consideration was given to GFFC-style experiments with application to oceanography. A laboratory configuration using a ferrofluid stratified in its magnetization looks promising. The simplest forcing configuration is periodic, and this led to a study

of the basic properties of oscillatory flow over topography in a rotating fluid.

Deane, A.E., Knobloch, E. and Toomre, J.: Traveling Waves in Large Aspect Ratio Thermosolutal Convection. Phys. Rev. A, Vol. 37, p. 1917, 1988.

Hart, J.E.: Laboratory Experiments on Planetary Scale Instabilities. Nonlinear Ocean Physics, A. Osbourne, ed., Italian Physical Soc., 1988.

Hart, J.E.: Finite-Amplitude Baroclinic Instability with Periodic Forcing. Physica D, in press, 1989.

F.W. Leslie/ES42
(205) 544-1633
Sponsor: Office of Space Science and Applications

Global Backscatter Experiment

The Global Backscatter Experiment (GLOBE) encompassed a large variety of work during FY89, with the operation of a field program in Hawaii, the ongoing analysis of ground-based and airborne data, and preparations for a major NASA DC–8 research program in November 1989. Atmospheric backscatter data from aerosols at laser wavelengths are necessary to support the development of the Laser Atmospheric Wind Sounder (LAWS), under development by MSFC as a facility instrument for the Earth Observing System of the mid-1990's.

A field program was undertaken at the Mauna Loa Observatory, operated by the National Oceanic and Atmospheric Administration (NOAA). Instrumentation included aerosol microphysics and chemistry operated by scientists from the University of Alabama in Huntsville, the University of Hawaii, and the Georgia Institute of Technology. The primary data were taken by a precursor of the space flight instrument, a Doppler lidar (laser radar) operated by scientists from the NOAA Wave Progagation Laboratory. Data were obtained in clean periods characteristic of clean mid-Pacific air and in a time of enhanced backscatter during an Asian dust event. Implications of these data to the LAWS design were discussed, along with other analyses, at a symposium held in Huntsville, Alabama.

Another topic of the symposium was the planning for a major flight program in November 1989 using the NASA DC–8 research aircraft. Two large pulsed lidars for onboard backscatter measurement have been developed, along with a number of smaller instruments designed to make definitive measurements of the aerosol physics and chemistry that affect laser backscatter at infrared laser wavelengths. These efforts are collaborative with scientists from MSFC, the Jet Propulsion Laboratory, Ames Research Center, the University of Hawaii, the Georgia Institute of Technology, the University of Miami, and NOAA. One of the pulsed lidars will be tested during the summer of 1989 and the remainder of the instrumentation will be loaded in time for a

November 1 flight around the Pacific with stops in Fairbanks, AK; Honolulu, HI; American Samoa; Christchurch, New Zealand; Melbourne, Australia; and Tokyo, Japan.

During FY89, effort continued on the design and planning of a GLOBE data base to collect the information being generated by the program into an archive so that it will be readily available for researchers and others associated with the LAWS program. Data from the preliminary experiments have been collected and formats were arranged for the data to be obtained during the research flight.

D.E. Fitzjarrald/ES43
(205) 544-1651
Sponsor: Office of Space Science and Applications

Simulating Observations of Laser Atmospheric Wind Sounder

In order to determine the potential impact of new spaceborne observing systems and to guide the development of hardware, observing system simulation experiments (OSSE's) must be performed. For the Laser Atmospheric Wind Sounder (LAWS) instrument on the Earth Observing System, OSSE studies are in progress by two research organizations. In order to study the effects of variations in the measured quantities, including mesoscale wind variations and variations in aerosol density, a study is underway by scientists at Simpson Weather Associates, Inc. In conjunction with this study, a series of OSSE's particularly concerned with the tropics has been initiated by scientists at Florida State University (FSU).

A computer model has been constructed of the LAWS instrument, which includes the scanning geometry that is used to obtain line-of-sight velocity measurements by the Doppler shift of laser light, and the algorithm by which these velocities are converted into horizontal air motions, i.e., winds. This computer model can operate on the raw data of the OSSE's, much as the real LAWS instrument will operate on the atmospheric motions to determine the winds. This is the technique being used to generate inputs for the FSU tropical circulation model.

It is in the tropics, the energy source for the atmospheric heat engine, that globally measured wind profiles from the LAWS instrument will be most effective. This is because of a lack of data in tropical areas and the importance of tropical motion to the general circulation. The FSU model, which has shown unprecedented success* in predicting tropical weather patterns, will be used to ascertain the effectiveness of increased data from the LAWS instrument. As the simulations are made more realistic during the course of the study, by adding effects of aerosol variations and clouds, this OSSE can be used to guide the development of LAWS hardware.

*Krishnamurti, T.N. and Oosterhof, D.: Prediction of the Life Cycle of a Supertyphoon with a High Resolution Global Model. Bull. Amer. Met. Soc., in press, 1989.

D.E. Fitzjarrald/ES43
(205) 544-1651
Sponsor: Office of Space Science and Applications

Backscatter Properties Aerosol Measurements

In order to adequately understand the response of the Laser Atmospheric Wind Sounder (LAWS) to the distribution and amount of aerosols, it is necessary to obtain a fundamental understanding of the physics and chemistry of these aerosols as it relates to the scattering of laser light. This instrument must operate in the eye-safe infrared region, where stable laser sources are available, but there is insufficient data to confidently predict the signal to be obtained. In conjunction with the MSFC-directed Global Backscatter Experiment, studies of atmospheric aerosol distribution, climatology, physics, and chemistry are being carried out by scientists from MSFC, the National Oceanic and Atmospheric Administration, the University of Alabama, the Georgia Institute of Technology, the University of Hawaii, the University of Miami, the Universities Space Research Association, the University of Arizona, Pennsylvania State University, and Coherent Technology, Inc.

These studies range from climatological measurements of surface-measured dust on remote Pacific islands, to basic physics of scattering from naturally-occurring particles in the atmosphere. The overall goal is to develop a global model of aerosol scattering that can be used in the development of LAWS. Since different instrument concepts may have different wavelengths of operation, the scattering process must be accurately modeled in order to analyze the instrument's operation. Since the scattering depends crucially on the size and composition of the aerosol particles, field measurements must be made to support the research. All of the scientists involved in this effort are combining laboratory and field data with analysis and modeling to develop a knowledge base to predict instrument performance.

The data being obtained in this study are also of prime interest in the study of the Earth's climate. Aerosol distributions figure significantly in the atmosphere's radiation balance and are an important

part of NASA's study of natural and inadvertent climate change. Research results from the work in this area are being published in the scientific literature and presented at appropriate technical conferences.

D.E. Fitzjarrald/ES43
(205) 544-1651
Sponsor: Office of Space Science and Applications

Mars Global Reference Atmosphere Model

The advent of proposed NASA projects, such as the Mars Rover Sample Return mission, the Mars Observer, potential manned Mars missions, and the Mars Aeronomy Orbiter, along with the possible use of aerobrake techniques for aerocapture by Mars, have necessitated the need and construction of a more detailed engineering type of global atmospheric density model for Mars, from 0 to 600 km (0 to 372.8 mi) altitude with similar characteristics to the NASA Earth-based Global Reference Atmosphere Model (GRAM). Small-scale density perturbations and long-term average values are now required in these more complicated engineering Mars aerobrake design studies, as well as density, temperature, pressure, and wind parameters which can be used in aerocapture, orbiter operations, Mars Lander entry/exit (providing lander/rover operational environments on the Mars surface), and in providing environments for design and planning of balloon measurement systems (considered on the Soviet Mars 1994 mission).

After a comprehensive Mars atmospheric data and model literature search was conducted, all available information and data were assembled. The Mars Culp-Stewart ionospheric model was chosen as an excellent upper atmosphere model to use. The lower atmospheric structure will be added later. The call-up procedure was altered to be similar to that used in Earth-GRAM. Monthly mean thermodynamic statistics are produced, as well as Monte Carlo realistic atmospheric generation schemes (similar to the Earth-GRAM). A realistic modeling of a Martian dust storm and its effects on the thermodynamic and wind structure of the Mars atmosphere can be obtained.

The initial Mars-GRAM was assembled for NASA checkout and use in May 1988. Over the last year, Mars-GRAM has been updated with lower atmospheric data bases [less than 100 km (62.1 mi) altitude], along with some theoretical calculations in order to give the model a wide variation in

thermodynamic results at the lower altitudes, guided by realistic parameterizations of height, and latitudinal and seasonal variations of temperature determined from a survey of published measurements from the Mariner and Viking programs (pressure and density were inferred from the temperature by making use of the hydrostatic and perfect gas law relationships). This phase was completed in July 1989 with further improvements and enhancements planned for the future.

B. James/ES44
(205) 544-6985
Sponsor: Office of Exploration

Tropical Atmospheric Density Perturbation Data Program

Small-scale atmospheric density perturbations such as those detected by the shuttle orbiter on reentry at mesospheric altitudes can play a large role in space vehicle design analyses. NASA projects, such as the Aeroassist Flight Experiment and Space Transfer Vehicle, will use the Earth's atmospheric density down to 60 km (37.3 mi) as a brake for change of orbit maneuvers. Detailed atmospheric density and density perturbation measurements are lacking at these altitude levels. Therefore, improvements in the climatology of mesospheric density will have direct benefits for vehicle design and performance.

Since these projects will use a tropical trajectory, NASA is assembling all current data and is funding specific observations by partial reflection drifts (PRD) radar in Hawaii and very-high frequency (VHF) radar in Taiwan.

The radars do not directly measure atmospheric density, but rather the wind field. Since wind fluctuations in the mesosphere are largely due to propagating internal gravity waves (or buoyancy waves) and relationships between wind and density fluctuations are well known for gravity wave processes, it is possible to infer density perturbation magnitudes from the wind measurements. The radars do not provide global coverage but do operate continuously allowing determination of seasonal changes of density fluctuation magnitudes. The VHF radar has enough power to obtain mesospheric echoes sporadically during periods when the mesosphere overhead is sunlit and the electron density has been increased by photoionization. The PRD radar operates at high frequency, which permits day and night observation of 80–110 km (49.7–68.4 mi) winds and daytime observations at heights of 60–80 km (37.3–49.7 mi). The PRD radar is scheduled to begin operation before an intensive, Pacific-wide observation campaign in March 1990.

Work is in progress to assemble such data in an updated version of MSFC's Global Reference Atmosphere Model. This empirical model will aid research into global changes of the Earth's atmosphere as well as provide the more detailed knowledge required by various vehicle projects.

S. Smith/ES44
(205) 544-5971
Sponsor: Office of Space Flight

NASA/Marshall Engineering Thermosphere Model

The Marshall Engineering Thermosphere (MET) model is the most recent version of a series of empirical upper atmospheric models which are all based on satellite drag data. The MET model, by using a more up-to-date and flexible computer code, is numerically faster and its output more reliable than that of its most recent predecessor, the J70 model. The MET model provides global atmospheric composition, temperature, density, and various other thermodynamic quantities between altitudes of 90–2,500 km (56–1,553 mi) for any time and day of the year. The primary purpose of the MET model is to provide engineers with total density values of the orbital environment for calculations concerning orbital lifetimes, stability, guidance, and control. It has been baselined for Space Station *Freedom*, and is also used in other NASA programs including the Hubble Space Telescope, the Orbital Maneuvering Vehicle, and the Tethered Satellite System.

MET also computes the thermospheric and exospheric atmospheric constituent number densities for atomic oxygen, molecular oxygen, molecular nitrogen, argon, helium, and atomic hydrogen versus altitude and time of year. One example for the use of a constituent is in the NASA engineering application which uses atomic oxygen in the degradation studies of spacecraft materials in orbit.

The MET model has also been given to the ENVIRONET data network at Goddard Space Flight Center, so that users can call it up from their computer and obtain results via telephone/communication hookup.

The model is currently being evaluated and improved by comparing output with other upper atmospheric models and with published data, and by incorporating a number of "add-on" subroutines which will model the effects of gravity waves and the semi-diurnal tide, as well as improving the already-modeled diurnal tide and geomagnetic storm effects.

D. Johnson/ES44
(205) 544-1665
Sponsor: Office of Space Science and Applications

Global Reference Atmosphere Model

The NASA Global Reference Atmosphere Model (GRAM) was instituted 15 years ago. For the past 3 years, it has been undergoing a major revision by MSFC's Environmental Analysis Branch of the monthly mean and variability statistics within its stratospheric/mesospheric regions. The most current satellite and radar measurements, that infer atmospheric density and temperature, have been obtained and analyzed and are currently being modeled to reside within an updated GRAM for early 1990. The model will be called the NASA/MSFC GRAM-90. Radar measurement of mesospheric density perturbations taken over semitropical sites in Hawaii and Taiwan are currently being analyzed (using gravity wave analyses) for future modeling into GRAM. Currently, research into the thermospheric orbital regions is also being done so that the most current orbital density model can be included within GRAM.

With the advent of the space shuttle program in the early 1970's, it was perceived that individual site-based reference or standard atmospheres would not fulfill all the demanding engineering studies needed to stimulate design work on the vehicle. Shuttle reentry analyses on a world-wide basis were the key reasons for the construction of GRAM initially. Over the years, the GRAM engineering model has been used in various other projects, such as Shuttle-II, Shuttle-C, Orbital Transfer Vehicle, Aeroassist Flight Experiment, Advanced Launch System, the National Aerospace Plane, and others. Many modifications to GRAM have occurred over the years, with the latest being made in November 1988, giving the current model the identity of GRAM-88.

GRAM is a three-dimensional, world-wide, monthly atmospheric engineering model. It consists of the parameters of pressure, temperature, density, and winds from the Earth's surface to 2,500 km (1,553 mi) altitude. Monthly mean values, along with the daily variability of the parameter about the monthly mean, can be output from any latitude/longitude/altitude location. Vertical profile as well as trajectory outputs are available from GRAM. A Monte Carlo simulation of any output parameter can also be produced from GRAM that would represent a random realization of the atmosphere in a vertical path, or along a trajectory path. Many different realizations of GRAM via Monte Carlo techniques can be produced for engineering analyses.

It is the goal of MSFC to compile a realistic atmospheric model that includes large- and small-scale effects which can be easily accessed by computer for engineering design studies of various space vehicles.

D. Johnson/ES44
(205) 544-1665
Sponsor: Office of Space Flight

Atmospheric Electricity Research

Today there is little doubt that electrical processes in a storm are intimately coupled to its concurrent dynamical and microphysical development. For instance, research conducted at MSFC has shown that there appears to be an almost direct proportionality between total rain volume and the number of lightning flashes (Fig. 77). Similarly, a linear relationship has been found in the total lightning flashing rate and the total electric (i.e., Maxwell) current generated by a thunderstorm (Fig. 78). Establishing such relationships that could employ lightning data derived from satellite observations of optical lightning emissions as the independent variable is a primary focus of atmospheric electricity research at MSFC.

Present research objectives include establishing lightning-precipitation and lightning-storm relationships, determining electrical current output and the energy balance of thunderstorms from topside optical measurements, and investigating the detailed physical properties of lightning discharges and cloud microphysics. Other areas of interest involve using spectral observations to study both the concentration and production of NO_x above cloudtop, and optical pulse data to study the radiative transfer properties of thunderclouds.

This research requires the need to obtain correlated ground-based, airborne, and satellite data sets. Measurements of the optical and electrical emissions of lightning and the electrical environment above thunderstorms have been obtained from a high altitude NASA U-2 aircraft. In the future, these measurements will be obtained using a NASA ER-2 aircraft. Data sets acquired in conjunction with the U-2 lightning measurements include Doppler and conventional radar, ground-based and in situ electricity and microphysical observations, detailed precipitation measurements, ground strike lightning mapping, and visible and infrared Geosynchronous Operational Environmental Satellite (GOES) images.

As previously noted, atmospheric electricity research at MSFC is particularly motivated by the desire to develop the understanding needed for the effective utilization and interpretation of data from the satellite-based lightning detection systems ex-

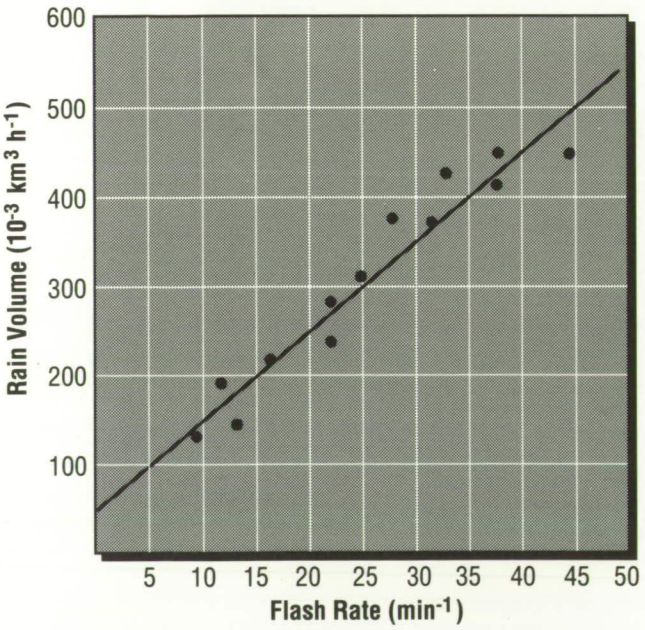

Figure 77. Proportionality Between Rain Volume and Lightning Flash Rate for Mesoscale Convective Systems from the Central United States

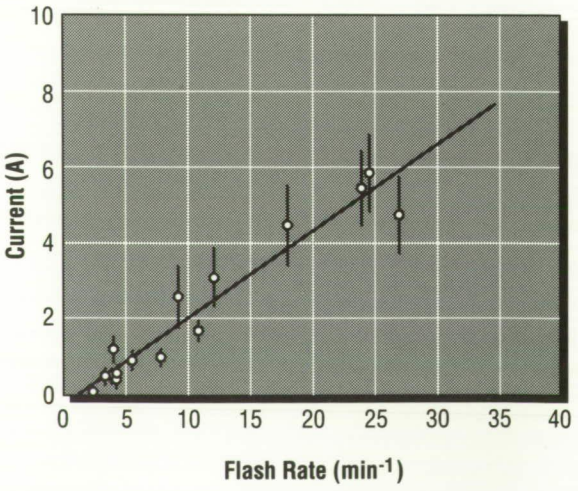

Figure 78. Linear Relationship Between Maxwell Current and Total Lightning Flashing Rate Generated by a Thunderstorm

pected to be in Earth orbit in the mid-1990's. These satellite lightning detection systems will be characterized by high detection efficiencies (i.e., 80–90 percent) and the capability to detect both intracloud and cloud-to-ground discharges during day and night. One such instrument, the Lightning Mapper Sensor, is presently under development by NASA and will be placed in geostationary Earth orbit on a GOES satellite.* Another instrument called the Lightning Imaging Sensor is being developed for the Earth Observing System polar platform and Space Station *Freedom*. A lightning detector system with significantly improved detection capabilities can be expected for the geostationary platform. These satellite lightning detection systems will support Earth System Science studies in the next decade and beyond.

*Christian, H.J., Blakeslee, R.J. and Goodman, S.J.: The Detection of Lightning from Geostationary Orbit. J. Geophys. Res., accepted for publication, 1989.

R.J. Blakeslee/ES43
(205) 544-1652
Sponsor: Office of Space Science and Applications

Lightning/Rainfall Relationships

Radar and lightning data from the Cooperative Huntsville Meteorological Experiment (COHMEX) are being analyzed in an attempt to define a relationship between lightning and rainfall production in convective storm systems. COHMEX was a multiagency sponsored field program conducted in the northern Alabama/central Tennessee region of the southeastern United States during June and July 1986. Establishment of a successful relationship would allow large-region rainfall estimations from a space-based lightning detection system.

Lightning and radar-derived rain rate histories for a small storm were observed on July 20, 1986, during COHMEX (Figs. 79 and 80). This storm produced a strong microburst (dangerous wind shears hazardous to aircraft) and small hail. The lightning and rain rates both exhibit an exponential growth/decay, with the peak lightning activity preceding the maximum rain rate by about 2 minutes. The sudden decrease in lightning rates is associated with storm

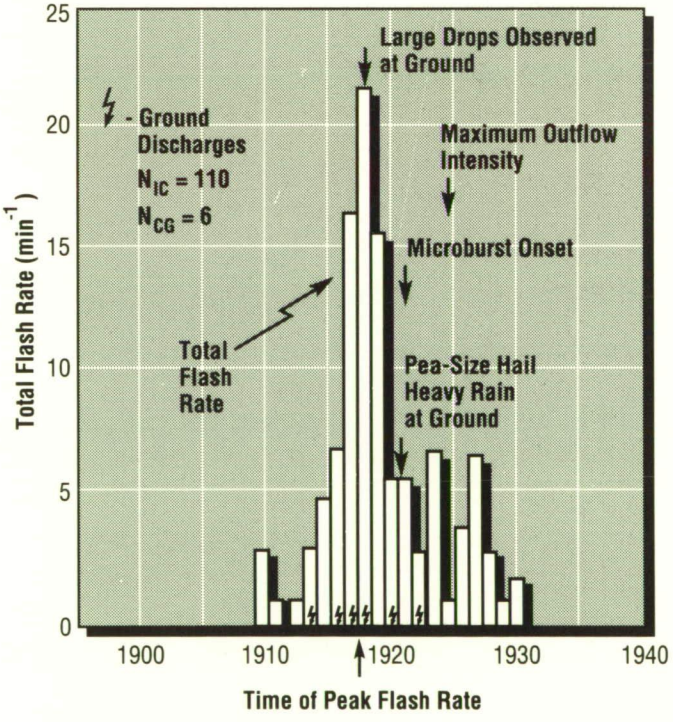

Figure 79. Lightning History of the July 20, 1986, Microburst-Producing Storm

collapse, which explains the lag between the peak lightning and precipitation rates and the time it takes the main precipitation core to descend to the surface. This also suggests that a lightning/rainfall estimation scheme should incorporate the life cycle stage of the storm.

To examine lightning and rainfall production in larger scale systems, hourly cloud-to-ground lightning rates and observed rain volumes from a number of mesoscale convective systems from the central United States were composited. The results exhibited a linear relationship between rain volume and cloud-to-ground lightning rates with a correlation coefficient of 0.96. For a smaller scale system occurring during COHMEX, comparisons between radar-derived rain rates and cloud-to-ground lightning were analyzed every 10 minutes. This system also displayed a high correlation coefficient of 0.9, but with a different slope compared to the central United States systems. This indicates that the environment and/or the size of the system may play an important role and must be considered when devising a rainfall/lightning relationship.

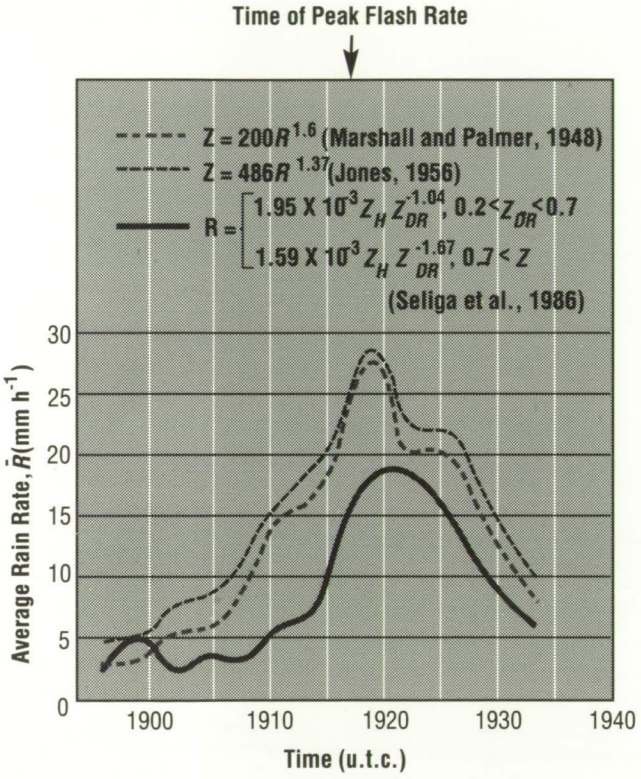

Figure 80. Precipitation History of the July 20, 1986, Storm

Currently, additional systems from COHMEX and the Great Plains that occurred during PRE-STORM (Preliminary Regional Experiment for STORM-Central) are being analyzed using radar-derived rain rates to refine some measurements based on environmental factors. In addition, the utility of using storm top heights derived from radar and/or satellite measurements will be investigated since tall storms typically produce more lightning, although not necessarily more rain. Other data sets from Florida and Darwin, Australia, will also be examined.

Goodman, S.J., Buechler, D.E., Wright, P.D. and Rust, W.D.: Lightning and Precipitation History of a Microburst-Producing Storm. Geophys. Res. Letters, Vol. 15, 1988.

S.J. Goodman/ES44
(205) 544-1683
Sponsor: Office of Space Science and Applications

Optimization Methods for Lightning Location Networks

The ability to forecast microbursts, determine cell growth and decay, and improve rainfall estimates are some of the potential uses of lightning data. The proper location of a lightning flash is important in determining which lightning flashes correspond to which storm cells. Therefore, it is important to determine the best technique or combination of techniques to reduce lightning flash location error to a minimum. One type of lightning location network that detects cloud-to-ground lightning uses magnetic direction-finding (DF) receivers to determine the most likely flash location. The quality of this flash location is a function of random and systematic errors. Magnetic DF networks for locating lightning strikes to ground require that two or more receivers detect the characteristic radio signal produced by the return strokes. Once the signal is detected, an estimate of the most probable flash position and a confidence region can be constructed. The spatial distribution (or clustering) of the lightning flashes, however, is a function of the dimension and vigor of the storm, the characteristics of the lightning channel and its radiation field, and the errors (both random and systematic) associated with the technique.

An eigenvector algorithm called FFIX (Figs. 81 and 82), based on techniques for finding radio transmitter locations anywhere on Earth from multiple DF bearings, has been adapted to the lightning location problem.

The input data consist of "n" station bearings and their respective standard deviations (random plus systematic errors). The random bearing error for each DF is about 1 degree. Attempts by MSFC and others to iteratively remove the systematic errors have not wholly eliminated them. These techniques reduce the total bearing error (BPE) (i.e., the standard deviation) to a value approaching 2 degrees at best. This standard deviation impacts both the BPE calculation and the confidence ellipse.

Sines of the bearing errors are assumed to be independent, normally distributed random variables with zero means, but some bearings may be "wild." A "wild" bearing can be thought of as a bearing that deviates by more than a prescribed number of standard deviations, say $\pm 3\ \sigma$, from the mean of a large number of bearings to a target. The "wild" bearing in this case could be just a chance occurrence or it could be due to a systematic error that has not been corrected for.

"Wild" bearings are rejected by a process where all combinations of bearings are exhaustively evaluated until a consistent subset of bearings is obtained. A set of "n" bearings is "consistent" if the associated sum of squared bearing errors from the best point estimate is less than the 80 percent values of χ^2_{n-2}.

The BPE and confidence ellipse are computed from the largest "consistent" subset of bearings. The algorithm employs two approaches for rejecting the "wild" bearings. The first approach, called the "exhaustive method," is invoked when 10 or fewer bearings are submitted for a BPE. If the submitted bearings lack sufficient consistency to form a BPE, then all subsets of "n" bearings are taken $(n\text{-}j)$ at a time, where $j = 1, 2, 3...$, until an acceptable solution is identified or a lower limit on the number of bearings is reached, in which case there is no solution. The lower limit is the greater of $n/2$ and 3. Thus, the largest subset of consistent bearings forms the BPE. A "sequential method" is employed when more than 10 bearings are submitted for a BPE. If all "n" bearings fail the consistency test, then the bearing that is more "inconsistent" with the bearing set is rejected (i.e., the wild bearing). The remaining set of $(n\text{-}j)$ bearings is examined as before. In this way the most "wild" bearings are rejected sequentially.

In the event that the χ^2 consistency test fails, the "best solution" is chosen as the intersection of the bearing pair having the minimum semimajor axis in

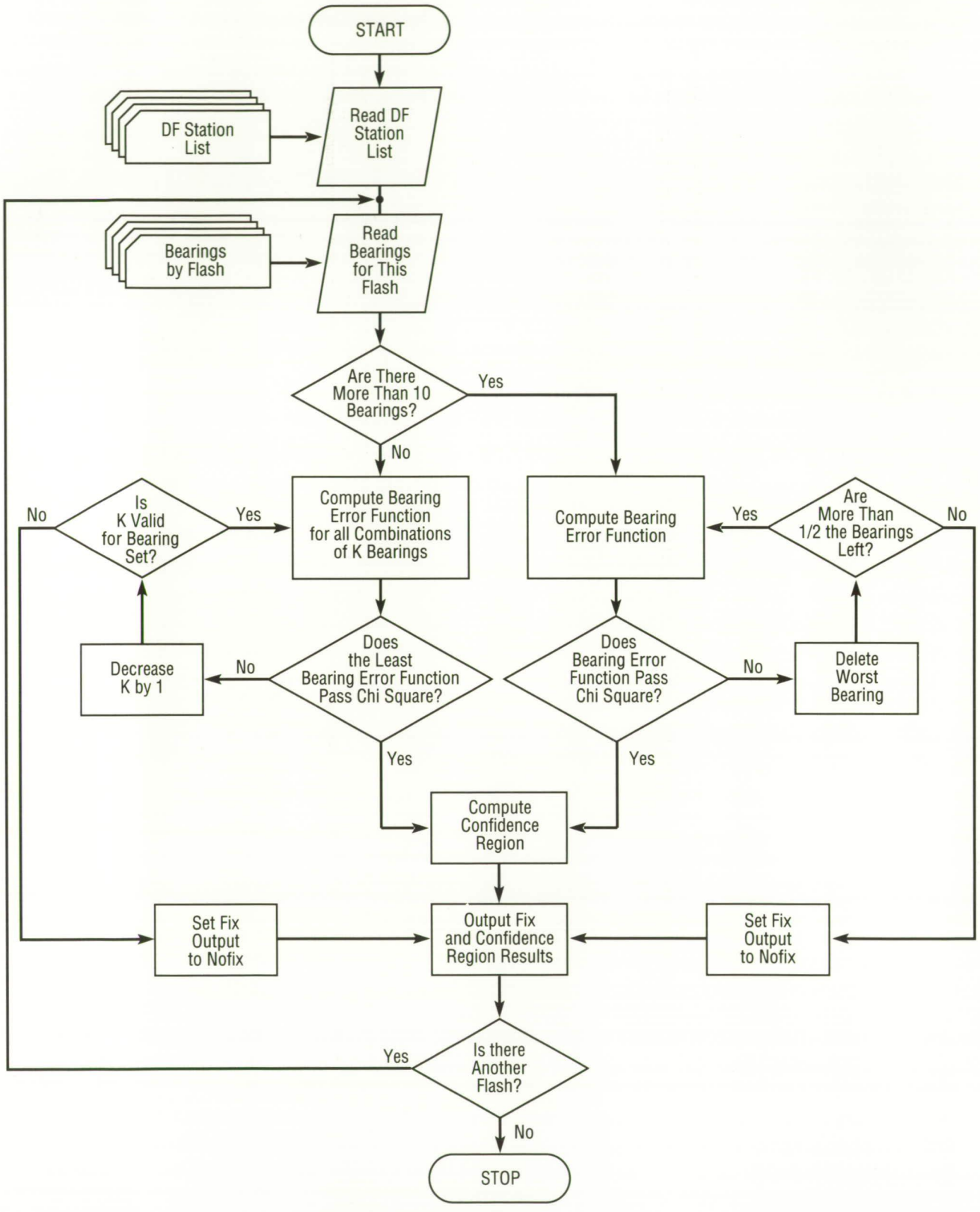

Figure 81. FFIX Algorithm Flowchart

its confidence ellipse. This argument assumes the best network geometry also gives the best solution, all other factors being equal. This approach is supported by earlier work in this field. This final iteration is necessary in a small network such as MSFC's (four DFs) because nearly 50 percent of all flashes are seen by only two DFs. The probability of detection for the network as a whole would be significantly poorer without this last iteration process.

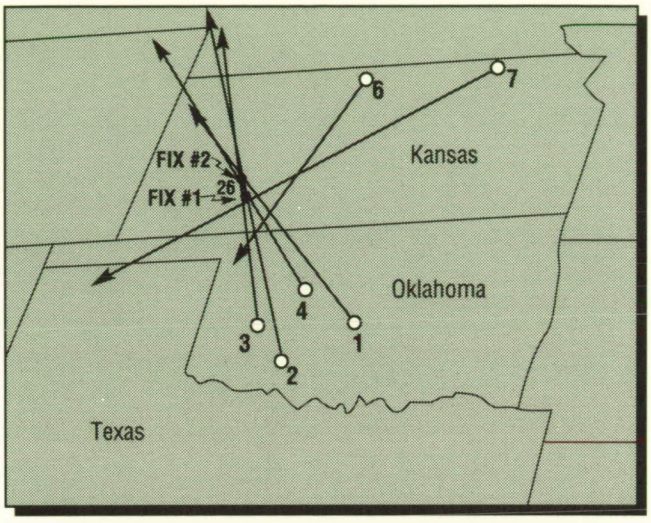

Figure 82. Bearings and Best Point Estimate for Flash Detected by a Six-Direction-Finder Network

The BPE is calculated by the method of maximum likelihood, which is equivalent to the method of least squares in this case. The confidence region is calculated from a linear approximation in which the target location errors are linear combinations of the bearing errors, and therefore have a bivariate normal distribution. Thus, the confidence region with minimum area is an ellipse.

Goodman, S.J.: Optimization Methods for Locating Lightning Flashes Using Magnetic Direction Finding Networks. Preprints, AIAA Aerospace Sciences Meeting, Reno, NV, Jan. 9–12, 1989.

S.J. Goodman/ES44
(205) 544-1683
Sponsor: Office of Space Science and Applications

Multiparameter Radar Studies of Electrified Clouds

The purpose of this study is to improve understanding of the relationship of cloud electrical development to cloud microphysical structure. Data used in this study were collected during the Cooperative Huntsville Meteorological Experiment (COHMEX) in the summer of 1986. A mobile van operated by the National Severe Storms Laboratory collected electrical measurements, while a Doppler radar was used to determine storm structure.

Results from the investigation show that the formation of ice is an important element in the electrification of storms. In addition, ice is shown to be an influence in the development of a vigorous downdraft. Figure 83 shows the vertical cross section of radar reflectivity Z_H and differential reflectivity Z_{DR} for the 19 July storm during its growth and decay phases, respectively. $Z_{DR}(\text{dB}) = 10\log(Z_H/Z_V)$ is defined by the ratio of S-band reflectivity factors at horizontal (Z_H) and vertical (Z_V) polarizations. The additional parameter Z_{DR} can be used as an aid in interpreting the presence of frozen precipitation particles or raindrops. For example, falling raindrops are oblate with a larger horizontal axis, so Z_{DR} is positive in rain. In fact, the oblateness of the raindrops, as measured by Z_{DR}, can be directly related to the median drop size, D_o. Additionally, positive Z_{DR} values above the melting level indicate regions having supercooled water droplets. Graupel and hail have Z_{DR} values near zero because the particles are spherical or tumble as they fall and, thus, have no preferred orientation. Therefore, hail regions within the cloud can be identified by high values of Z colocated with low values of Z_{DR}. From 2302–2306 coordinated universal time (u.t.c), liquid water, shown by high values of Z_H and Z_{DR}, is lifted above the freezing level at 5 km (3.1 mi), and by 2308 u.t.c. this supercooled water begins to freeze, shown by the smaller values of Z_{DR}. Foul weather fields were observed at 2308 u.t.c. showing good agreement with the glaciation.

The electrical life cycles of two microburst producing storms have been documented. In both cases ice phase precipitation particles played an important role in the strong electrification of the storm, leading to the first lightning discharge and in the formation of the strong downdraft leading to the microburst event. The vertical distribution and movement of mass appears to be very important in determining the total lightning activity and the type of flashes (IC or CG) that are dominant during certain phases of the storm life cycle. Although decreasing flash rate trends may not always precede the onset of those microbursts accompanied by heavy rain, some form of lightning will often occur well in advance of the maximum outflows and wind shears.

Goodman, S.J., Buechler, D.E., Wright, P.D., Rust, W.D. and Nielsen, K.E.: Polarization Radar and Electrical Observations of Microburst-Producing Storms During COHMEX. Preprints, 24th Conf. on Radar Meteorology, Tallahassee, FL, Amer. Meteor. Soc., pp. 108–112, 1989.

Goodman, S.J., Buechler, D.E., Wright, P.D. and Rust, W.D.: Lightning and Precipitation History of a Microburst-Producing Storm. Geophysical Research Letters, Vol. 15, pp. 1185–1188, 1988.

S.J. Goodman/ES44
(205) 544-1683
Sponsor: Office of Space Science and Applications

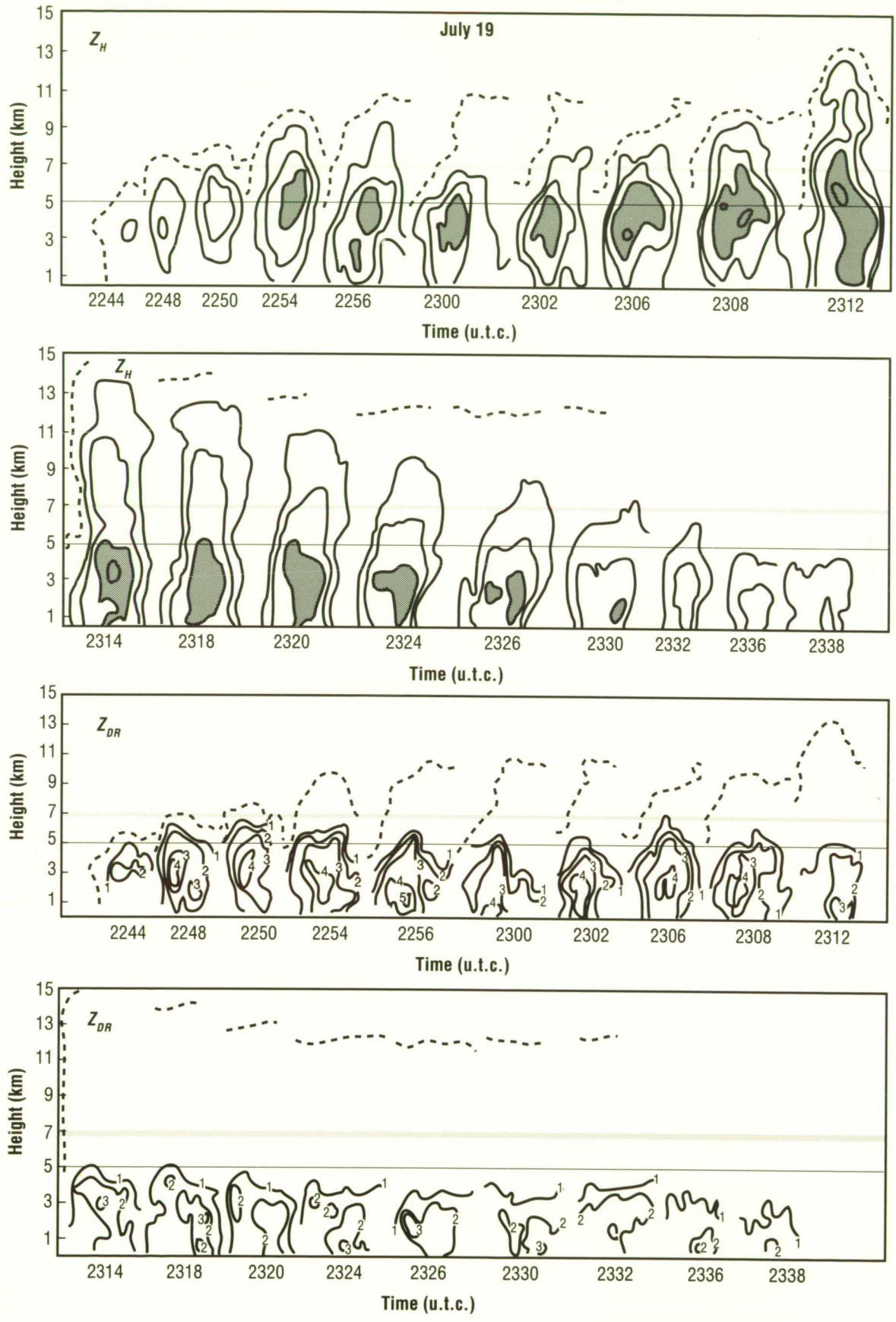

Figure 83. Vertical Cross-Section of Horizontally Polarized Radar Reflectivity (Z_H) and Differential Reflectivity (Z_{DR})

Multisensor Cloud Characterization

New sensors are continually adding to the wealth of meteorological data taken on a daily basis. Computers are routinely processing a wealth of meteorological data from sensors having a broad range of spatial and temporal resolutions. There will be an increased need for and a greater emphasis placed on extracting and displaying the relevant information contained in these multiple datasets. Attention still tends to be focused on displays of single sensor measurements (e.g., blackbody cloud-top temperatures, radar reflectivities, rainfall rates, and lightning flash locations). With the Man-computer Interactive Data Access System, the Program for Regional Observing and Forecasting Services, and the future Advanced Weather Interactive Processing System meteorological workstations, it will be possible for operational forecasters to overlay radar and lightning data with satellite imagery, surface, and upper air data.

How will analysts and forecasters find the relevant information buried under a mass of (colored) contours, dots, shapes, and numbers? To improve the human factor of meteorological displays (i.e., the man-machine interaction), an effort must be directed at maximizing the information content in the products which are examined to form a conceptual picture of what is occurring in the atmosphere. As these more advanced workstations become available, new methods of cataloging, processing, and displaying meteorological information will follow.

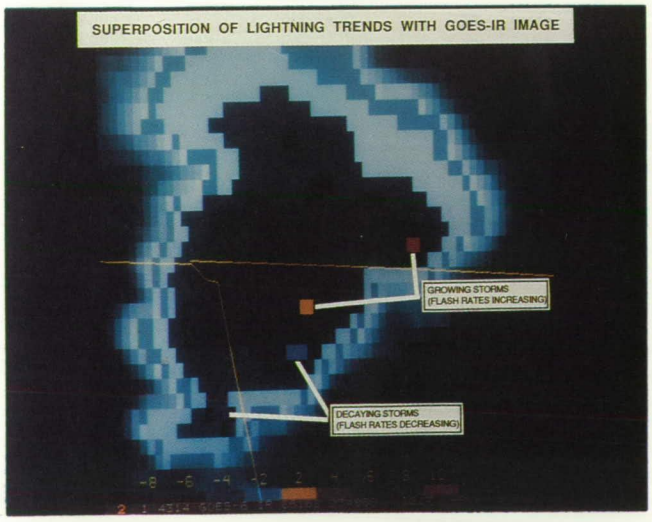

Figure 84. Convective Tendency Satellite Product

To focus on these issues, this work describes a technique for generating trend or convective tendency images. These images are produced by using a combination of Geostationary Operational Environmental Satellite imagery and cloud-to-ground lightning observations made with a ground-based lightning detection network operated by MSFC. Currently, cloud-to-ground lightning measurements are used, but more useful total lightning (intracloud and cloud-to-ground) measurements over large areas are anticipated from a lightning sensor in geostationary orbit in the mid-1990's.

The infrared (IR) sensor detects cloud-top temperatures with the highest (and generally strongest) storms exhibiting the coldest temperatures. However, problems can arise in identifying cells that are obscured by cirrus debris or cells with dimensions below the resolution of the IR sensor. The addition of lightning data provides information on the location, growth, and decay of electrical activity accompanying thunderstorms. It thus supplies an indication of the convective state of storms with increasing or decreasing rates associated with growing or decaying storms.

Lightning trends are computed by taking the difference in flashing rates at two successive 5-minute intervals. The superposition of lightning trends with the IR image (Fig. 84) shows the location of lightning activity and convective cores, the spatial distribution of convective rainfall, the extent of the remaining stratiform and cloud areas, and the growth and decay of storms.

Goodman, S.J., Buechler, D.E. and Meyer, P.J.: Convective Tendency Images Derived from a Combination of Lightning and Satellite Data. Weather and Forecasting, Vol. 3, pp. 173–188.

S.J. Goodman/ES44
(205) 544-1683
Sponsor: Office of Space Science and Applications

Next Generation Weather Radar Algorithm Evaluation and Analysis

The identification of storms prior to the onset of lightning is important for efficient ground processing and launch operations at Kennedy Space Center. A next generation weather radar system (NEXRAD) to be deployed in Melbourne, FL, is expected to be useful because it has a number of algorithms designed to automatically characterize and track individual storms. These algorithms work well on large storms that frequently cause severe weather in the Great Plains. However, it was found that electrically active air mass storms that commonly occur over Cape Canaveral may not be identified by the algorithms due to their small horizontal dimension. The shape of small echoes in conjunction with the radar viewing angle was found to have a significant impact on NEXRAD storm identification.

The NEXRAD storm identification process begins by searching along each radial for storm "segments," defined as contiguous reflectivity values above a threshold (NEXRAD default value is 30 dB) spanning a threshold distance [the NEXRAD default is 5 km (3.1 mi)]. A "dropout" criteria allows lower reflectivity values (25–30 dB) to exist in the interior of a segment. Located segments are then grouped together if sufficient overlap with adjacent segments is found. Finally, grouped segments that correlate vertically are identified as storms. However, to be identified as a storm, a group of adjacent segments must be found in the lowest elevation scan. Current research is concerned only with the low-level aspect of these storms.

To determine the probability of detection of a storm, an idealized echo shape is used in the form of an ellipse (fractal dimension, $D = 1$). Larger storms tend to have a slightly more complicated structure with fractal dimension $D = 1.36$.

A radar viewing a storm along its long axis (Fig. 85, Radar A) will be identified sooner than an echo observed across its short axis (Radar B). The probability of detection of elliptically shaped echoes based on random storm/radar orientations is shown in Figure 86. A detection probability of 100 percent is achieved only when the short axis of the echo is at least 5 km (3.1 mi) in length. The probability of detection drops rapidly with a reduction in size of the short axis. Lightning-producing storms with short echo axes of 3 km (1.9 mi) occur frequently, and have less than a 35-percent chance of being detected.

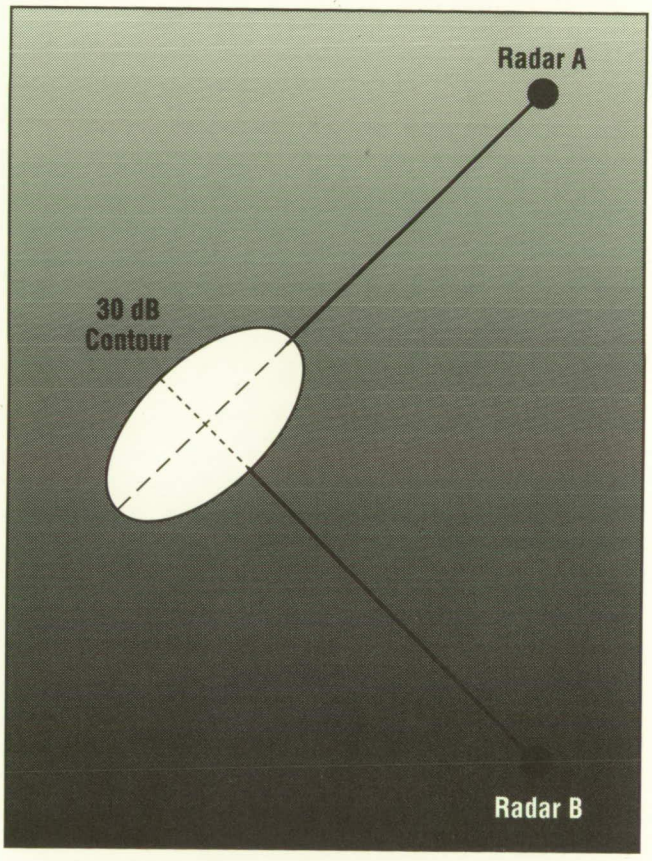

Figure 85. Effect of Radar Viewing Observed Segment Length of a Simulated Elliptical Echo

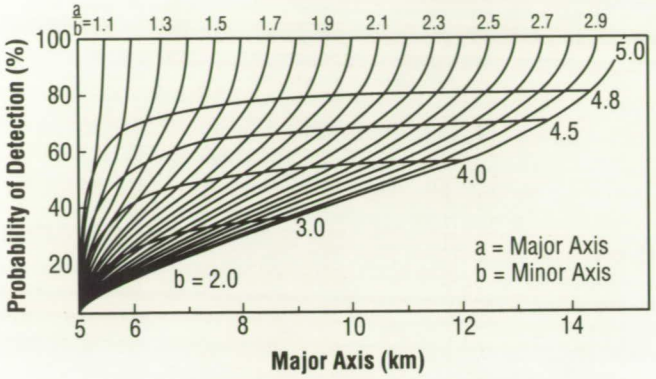

Figure 86. Probability of Detection of Small Elliptically Shaped Echoes from Random Radar Viewing Angles

Methods to detect these smaller storms within the current framework of the NEXRAD system are being reviewed. For example, it may be possible to key on the vertical growth of clouds and the enhancement of reflectivity at the -10 °C (14 °F) level (the height of the main negative charge region in the thunderstorm central dipole) or by using the NEXRAD echo tops product to identify storms tall enough to produce lightning. However, neither of these methods is automated.

Beuchler, D.E. and Goodman, S.J.: Echo Asymmetry and Its Impact on NEXRAD Storm Identification. Preprints, 24th Conference on Radar Meteorology, Tallahassee, FL, March 1989.

S.J. Goodman/ES44
(205) 544-1683
Sponsor: Universities Space Research Association

Doppler Radar Studies and Storm Energetics

Doppler radars were used to collect wind information from storms during the Cooperative Huntsville Meteorological Experiment (COHMEX), which was conducted in northern Alabama during the summer of 1986. The use of multiple Doppler radars allowed reconstruction of the three-dimensional wind fields inside a storm. From these data, retrievals are made of the deviation perturbation pressure, the deviation perturbation density, and deviation perturbation temperature fields. The reflectivity field of the radars is used to determine the liquid water variation for a storm.

Latent heat release has been estimated for small COHMEX storms and found to be on the same order (10^{11} J) as the latent heat release of typical isolated storms and an order of magnitude less than the thermodynamic energy of severe storms. The latent heating is computed as a residual from the water budget equation:

$$\frac{dM}{dt} = G-R-E,$$

where, M is the total radar-detectable liquid water content (i.e., storm mass), E is the evaporation rate which is parameterized in terms of the rainfall rate, R, and G is the condensation rate in the updraft which is are proportional to the latent heating rate (Figs. 87 and 88). The total kinetic energy of the

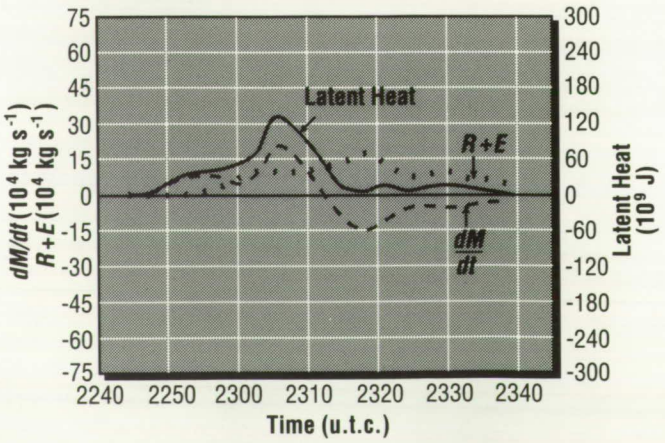

Figure 87. Latent Heat Release, July 19, 1986

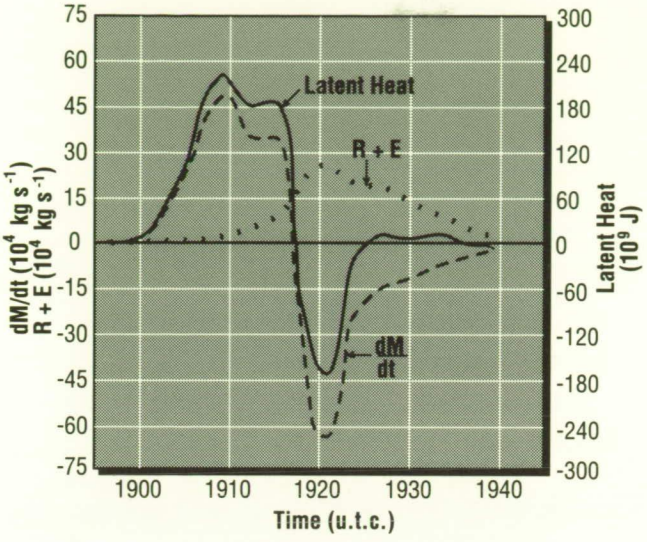

Figure 88. Latent Heat Release, July 20, 1986

system (10^{12} J) is an order of magnitude less than a larger, decaying Colorado storm used as a reference. Currently, kinetic energy budgets are being studied to better understand the physical processes occurring in small storms.

Goodman, S.J., Buechler, D.E., Wright, P.D., Rust, W.D. and Nielsen, K.E.: Polarization Radar and Electrical Observations of Microburst-Producing Storms During COHMEX. Preprints, 24th Conference on Radar Meteorology, Tallahassee, FL, Amer. Meteor. Soc., pp. 108–112, 1989.

S.J. Goodman/ES44
(205) 544-1683
Sponsor: Office of Space Science and Applications

Observations and Modeling of Mesoscale Convective Systems

This work has two primary goals, each of which has eventual applications to remote sensing from space: observational investigation of the kinematic structure and precipitation distribution within a mesoscale convective system (MCS), including the stratiform and convective components of such systems; and examination of the physical processes associated with the upscale growth of convective systems, from an initial structure consisting of disperse convective elements to a final configuration consisting of closely interacting convective and stratiform regions. Work under both categories includes Doppler radar, satellite, and surface observational analyses in conjunction with results from numerical simulations that replicate observed behavior of such systems.

Three particular case studies obtained from the Cooperative Huntsville Meteorological Experiment (COHMEX) data set have been examined in some detail. The July 13 COHMEX case has received the most attention to date, since it satisfies both objectives defined above. This MCS formed and reached maturity over the COHMEX network, within range of Doppler radars and the surface mesonet. A conceptual mode of the initial and mature stages of this system is shown in Figure 89. At maturity, the MCS cloud shield exhibited an east-west major axis of 250 km (155.3 mi) and a north-south minor axis of 150–200 km (93.2–124.3 mi). It was composed of a convective leading edge and an adjacent region of stratiform precipitation extending up to 100 km (62.1 mi) to the rear of the convective leading edge. Rainfall amounts were widespread but variable, averaging about 15–20 mm (0.59–0.79 in) over an area of about 50,000 km^2 (31,070 mi^2). Lightning was prevalent within this system, and positive discharges were common during the mature stage within the trailing stratiform precipitation. Many aspects of the mature structure of this system are thus similar to those reported in the literature.

The three-dimensional precipitation distribution within this MCS has been analyzed using reflectivity from the C-band CP-4 radar. The expansion of precipitation within the western portion of the MCS is illustrated by a series of vertical cross sections in which the reflectivity factor has been averaged over a 70-km (43.5-mi) east-west segment. Such composite pictures covering the time period 2049–2349 universal time are shown in Figure 90. The expansion of precipitation within the MCS was accomplished by both discrete propagation and advection produced by mesoscale flows within the anvil. In addition, there is evidence that appreciable in situ precipitation growth took place within the trailing anvil region. It is interesting to note that a general decrease in echo top was analyzed in the second figure, while the expansion and growth of the stratiform precipitation region occurred. A similar trend was observed in the cloud top infrared temperature pattern. This relationship and physical connection will be examined in the future with additional analysis and numerical modeling efforts.

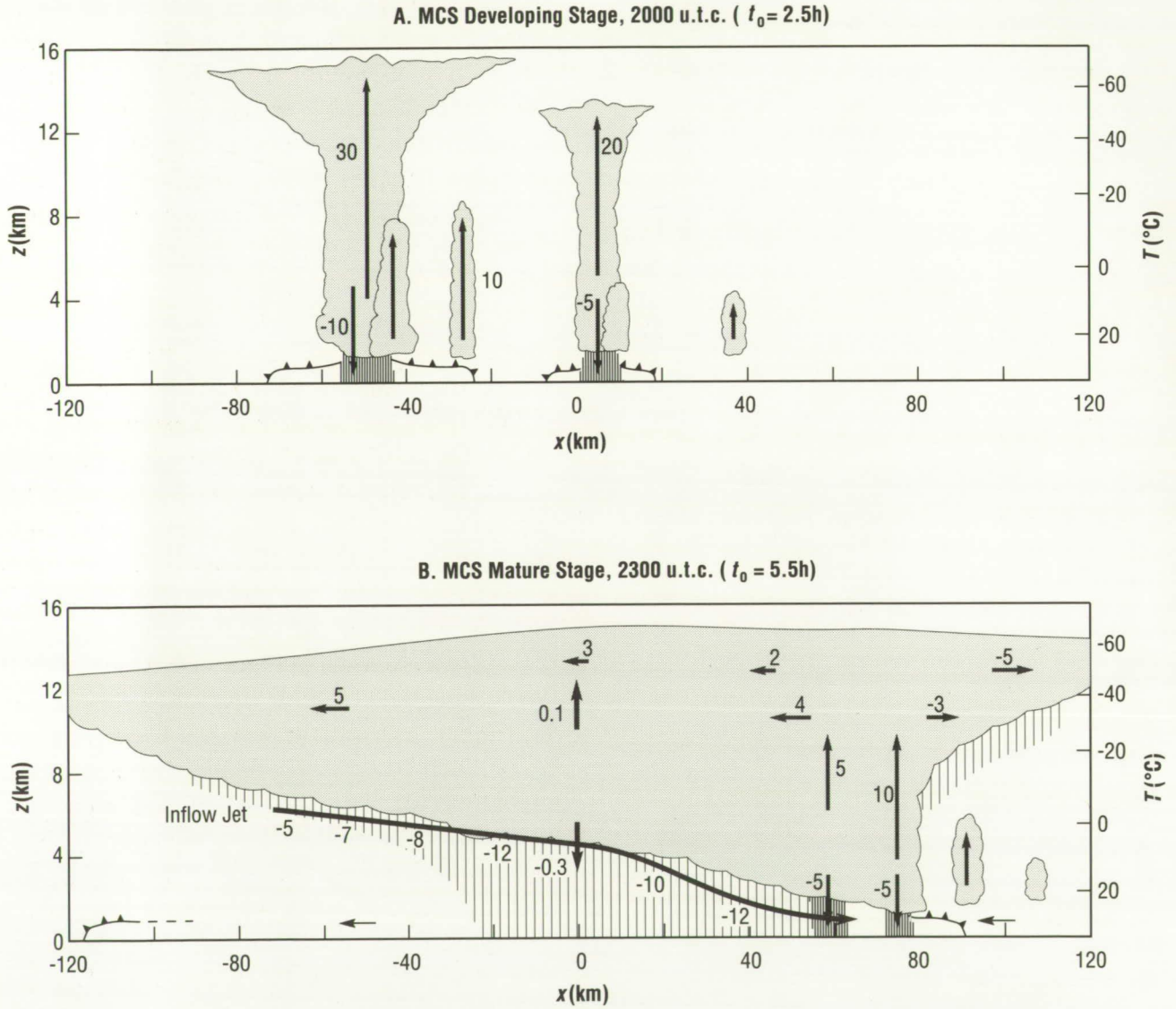

Figure 89. Conceptual Model Illustrating the (a) Developing and (b) Mature Stages of the July 13, 1986, Mesoscale Convective System. Numbers Represent Wind Vector Magnitude in m/s

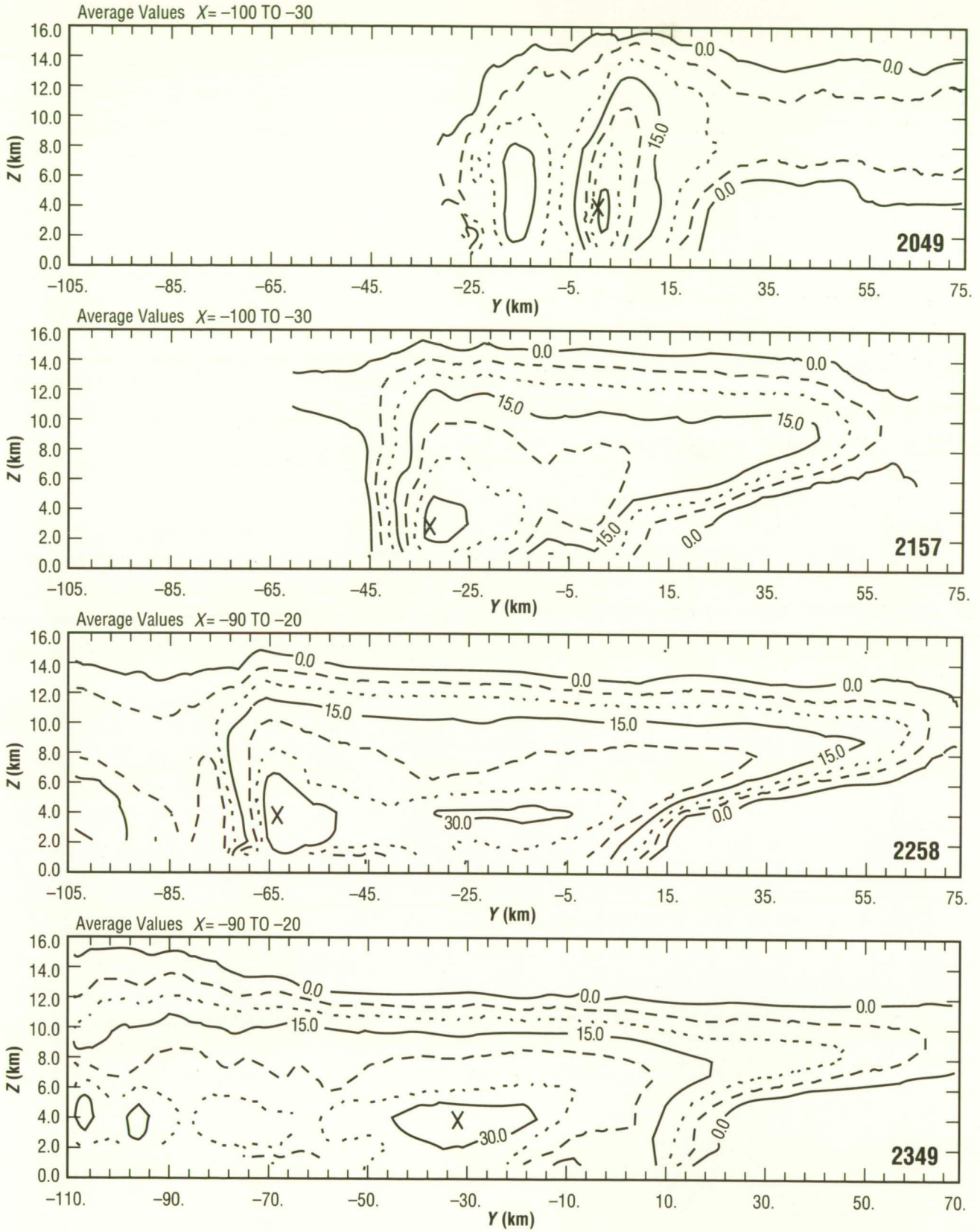

Figure 90. East-West Averages of CP-4 Reflectivity Factor at 2049, 2157, 2258, and 2349 u.t.c. Contours are drawn at Every 5 dB, Starting at 0 dB

Analysis of Doppler velocity data show the development of an inflow jet whose appearance closely corresponded to the development of stratiform precipitation. Other appreciable mesoscale flows, whose effects include both development and advection of precipitation within this system, have been documented with Doppler radar. These include upper-level outflow associated with anvil expansion and associated vertical motion fields (derived from velocity-azimuth display analyses) showing mesoscale ascent of 10–20 cm s^{-1} above 6 km (3.7 mi), and mesoscale descent of approximately 10 cm s^{-1} below 6 km (3.7 mi).

Future work on this case will expand on the precipitation and kinematic analyses presented above. In addition, numerical simulations will further investigate the mature precipitation and kinematic structures, in addition to further defining processes associated with the upscale growth of the system.

Knupp, K.R.: Observed Structural Variability of Deep Moist Convection with a Mesoscale Convective System. Preprints, 24th Conference on Radar Meteorology, AMS, Tallahassee, FL, pp. 467–470, 1989.

S.J. Goodman/ES44
(205) 544-1683
Sponsor: Office of Space Science and Applications

Radar Remote Sensing and Cloud Dynamics

This research is attempting to document the observed structure, and variability in structure, of deep precipitating convection within low-shear subtropical environments. Included are such specific items as precipitation growth and distribution within deep convection and their relation to internal cloud flows. This work involves both observation (radar and Doppler radar) and numerical modeling. Items of interest include an examination of environmental parameters that influence the distribution of precipitation within deep convection. Detailed observations of clouds within low-shear environments generally show a wide variety of cloud structures (e.g., cloud horizontal dimension, cloud top, precipitation intensity, and kinematic characteristics). Such variability may be hypothesized to result from variations in the magnitude of convergence within the atmospheric boundary layer, and from spatial variations in moisture within and above the boundary layer.

The July 13 Cooperative Huntsville Meteorological Experiment case is being investigated in detail so that individual cloud structures can be related to the structure of a mesoscale convective system observed on this day. Several cloud systems observed by multiple Doppler radar displayed a variety of characteristics. The purpose of this study is to quantify the similarities and differences in terms of kinematics, precipitation characteristics and distribution, and lightning production, and then attempt to explain some of the differences. Figures 91 and 92 characterize the structure of one cloud system that was observed. Numerical simulations will play a key role in examining the factors which influence cloud structure and longevity. Cases from other days will be examined in the future to provide further clarification on the cloud structure under low-shear conditions in general.

Knupp, K.R.: Observed Structural Variability of Deep Moist Convection with a Mesoscale Convective System. Preprints, 24th Conference on Radar Meteorology, AMS, Tallahassee, FL, pp. 467–470, 1989.

S.J. Goodman/ES44
(205) 544-1683
Sponsor: Office of Space Science and Applications

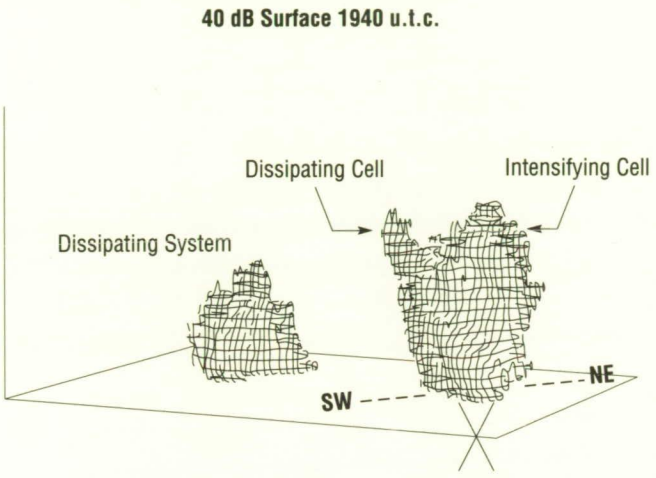

Figure 91. Three-Dimensional Depiction of the 40 dB Surface of a Vigorous Cloud Within a Developing Mesoscale Convective System

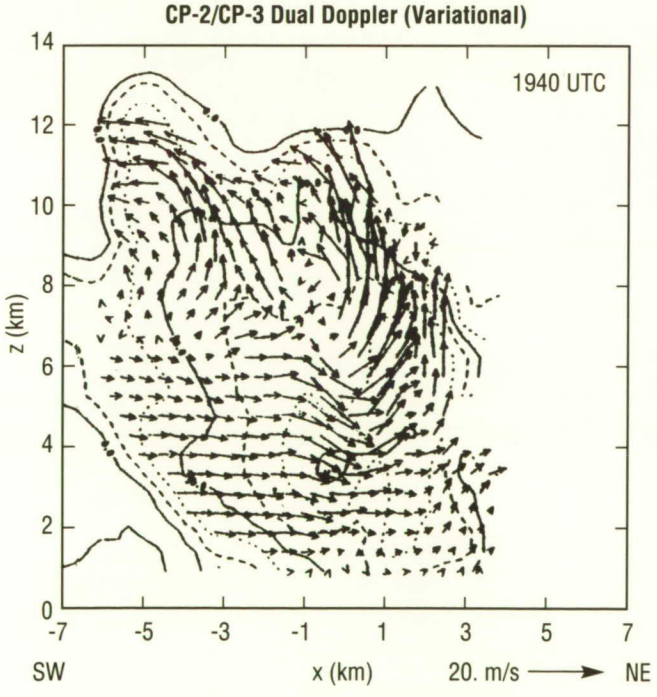

Figure 92. Cell-Relative Flow Within a Vertical Plane Defined by the Line in Figure 91, Derived From a Dual CP-2/CP-3 Doppler Analysis

Doppler Radar Wind Profiler

A 50-MHz Doppler radar wind profiler has been installed at Kennedy Space Center (KSC) along the shuttle runway approximately 9 km (5 mi) from the shuttle launch pads. The current system is operating at reduced power while the high power components are being assembled and tested. The high power system is expected to be operating by fall of 1989. In the meantime, the limited capability system (LCS) is continuously outputting hour-averaged wind profiles in two modes: the high resolution mode which measures the winds from 2 to 9 km (1.2 to 5.6 mi) at 150-m (492-ft) increments, and the low resolution mode which measures winds from 7 to 16 km (4.3 to 9.9 mi) at 600-m (1,969-ft) increments. In the low resolution mode, data dropouts are prevalent above 11 km (6.8 mi). However, these data dropouts are to be eliminated with the inception of the final system. The final system will also measure the winds in a single mode with 150-m (492-ft) resolution from 2 to 16 km (1.2 to 9.9 mi).

With the installation of the LCS in November 1988, several qualitative comparisons between profiler and jimsphere data have been implemented with good results. The profiler data have also been used in an experimental mode to monitor the upper-level winds during the launches of STS-27 and STS-29. The profiler will continue to be used experimentally for future launches until more stringent statistical comparisons with jimsphere data and other measurement systems are performed.

Along with assessing profiler accuracy, work is currently being undertaken to make profiler data accessible to the research community. By midsummer, profiler data will be ingested into the Meteorological Interactive Data Display System which has nodes at MSFC, Johnson Space Center, and KSC. Other plans for the profiler data are to supplement the current wind variability data base, and to assess the usefulness of the data as input to launch loads simulation algorithms.

C.A. Carlson/ES44
(205) 544-2755
Sponsor: Office of Space Flight

Water Balance Dynamics from Local to Regional Scales

Scientific research into the hydrologic response within catchments was initiated during FY89 in conjunction with other Earth Observing System (EOS) activities undertaken by MSFC. One EOS program objective is to understand the interrelationship between land surface and atmospheric processes at different spatial and temporal scales.* This understanding is crucial for modeling of the global hydrologic cycle (Fig. 93).

Central to this problem is defining the rates and pathways of subsurface water movement and catchment runoff production. Field studies have been carried out in various locations to determine the physical controls on runoff production. Analyses of water chemistry and isotopic concentration have been made along with detailed soil physics studies to examine specifically the role of macropores on groundwater-streamflow interactions.

Within storm rainfall, deuterium variations were high (4/100 to 94/100), reflecting changes in air mass trajectory and rainfall intensity.† Soil water and groundwater deuterium concentrations showed a dampened response to the rainfall input, and mean residence time varied from approximately 12–100 days. For monitored storm events, the volume fraction of groundwater, or pre-event water, averaged 90 percent of stormflow volumes. New water contributions could be accounted for by saturation

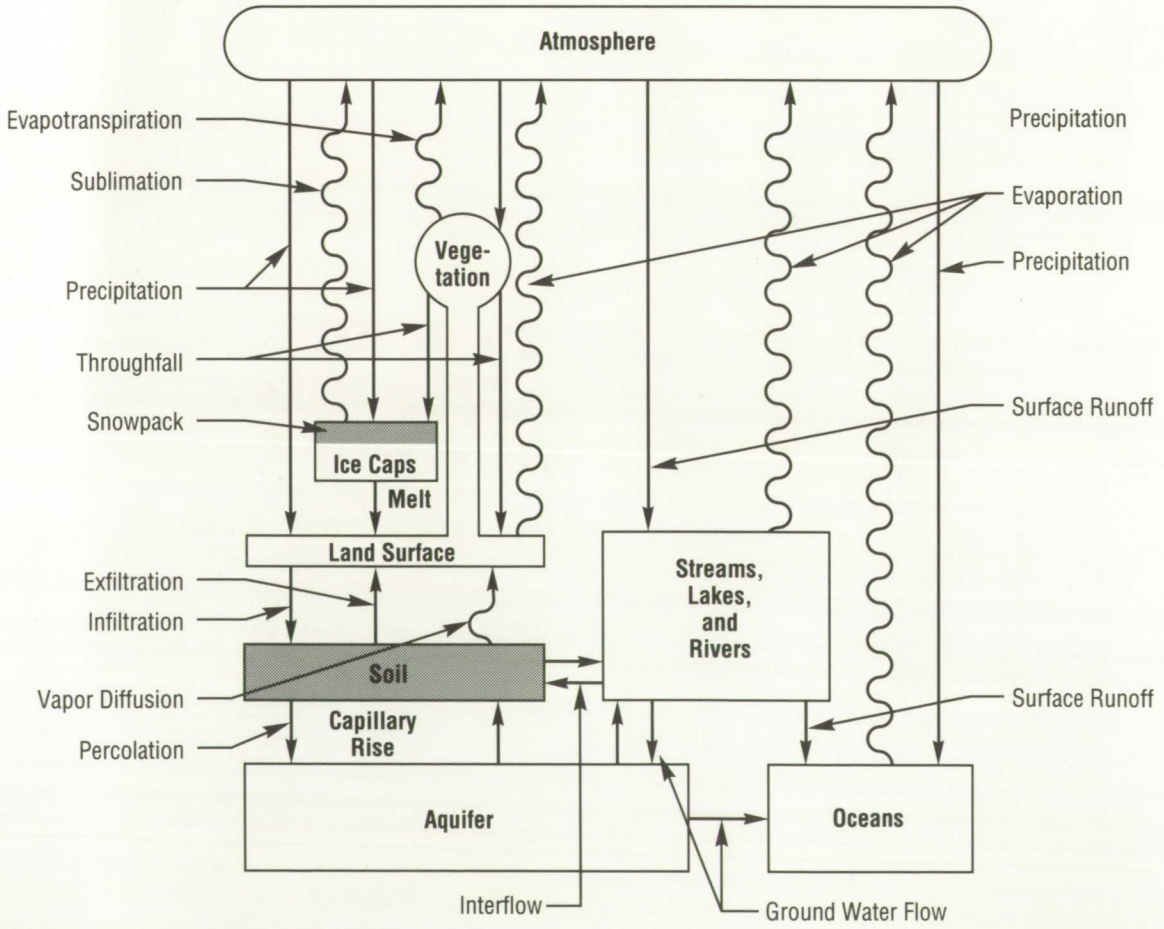

Figure 93. Schematic Diagram of Hydrologic Cycle

overland flow and headwater subsurface flow. Hillslope flow water dominated by old water contributions of between 70 and 100 percent increased the downslope.

Soil physics analyses conducted in various catchment positions have shown that the unsaturated zone overlying nearstream groundwater can be rapidly changed to positive matric potentials due to a disequilibrium between the micropore-macropore system. Such response produces an early and steady increase in old water exfiltration into the stream along the channel margin. As rainfall depth increases above 10 mm (.39 in), contributions from midslope and upslope hollows dominates channel stormflow, and most of the subsurface water is delivered to the first order channels via a continuous system of pipes at the soil-bedrock interface.

The field data will be incorporated into catchment hydrologic models in cooperation with scientists from the U.S. Geological Survey[‡] and Pennsylvania State University. This work will transform the detailed catchment-based data into local and regional estimates of hydrologic response, utilizing remotely sensed information.

*Costes, N.C., Gillette, D.A., Illangasekare, T.H., Leavesley, G.H., Nichols, W.D., Verstraete, M.M., et al.: Land-Surface and Atmospheric Interactions in Semi-Arid Regions and Their Relationship to Climatic Variability. Interdisciplinary investigation proposal submitted to NASA Headquarters in response to AO OSSA-1-88: The Earth Observing System, MSFC, June 1988.

†McDonnell, J.J., Bonell, M., Stewart, M.K. and Pearce, A.J.: Deuterium Variations in Storm Rainfall: Implications for Stream Hydrograph Separations. Water Resour. Res., submitted, July 1989.

‡Leavesley, G.H., Lumb, A.M., and Saindon, L.G.: A Microprocessor-Based Watershed Modeling and Data Management System. Proceedings, Western Snow Conference, Vancouver, British Columbia. Published by Colorado State University, Fort Collins, CO, pp. 108–117, 1987.

N.C. Costes/ED42
(205) 544-1637
Sponsor: Office of Space Science and Applications

Water, Energy, and Biogeochemical Cycles in Arid and Semi-Arid Regions

Interdisciplinary investigations of the water, energy, and biogeochemical cycles in arid and semi-arid regions have been initiated at MSFC.* These regions were selected for study in connection with Earth Observing System (EOS) activities, because: they cover one third of the continental areas; they are quite sensitive to climatic variability and change; and significant changes of albedo, surface soil moisture, and other parameters in these regions have been shown to affect the climate at least marginally. These areas are characterized by a strongly seasonal and highly variable hydrological cycle, and support almost a billion people.

There is ample evidence that the Earth's climate has changed over time, and also that it is changing rapidly as a result of human activity. Among the many effects of such changes, three are of direct concern: the global increase in temperature, the space and time distributions of precipitation, and the composition of the atmosphere. The nature and severity of these changes is a direct function of the intensity of the "forcing", and also of the sensitivity of the biosphere to such changes.

Figure 94 shows the latitudinal distribution of an index of water availability (*P-ET*, annual and zonal mean value of precipitation minus evapotranspiration), as well as the annual and zonal mean distribution of temperature *(T)*. These two variables are by far the most important factors in determining the primary productivity of an ecosystem. The figure demonstrates that semi-arid regions bordering the subtropical deserts are among the regions most sensitive to climate change.

Detailed ground-based micrometeorological studies at selected field sites are being carried out by D. Nichols of the U.S. Geological Survey to accurately define energy and water fluxes. Results of these studies will be used to develop methods and techniques that can be applied at regional and global

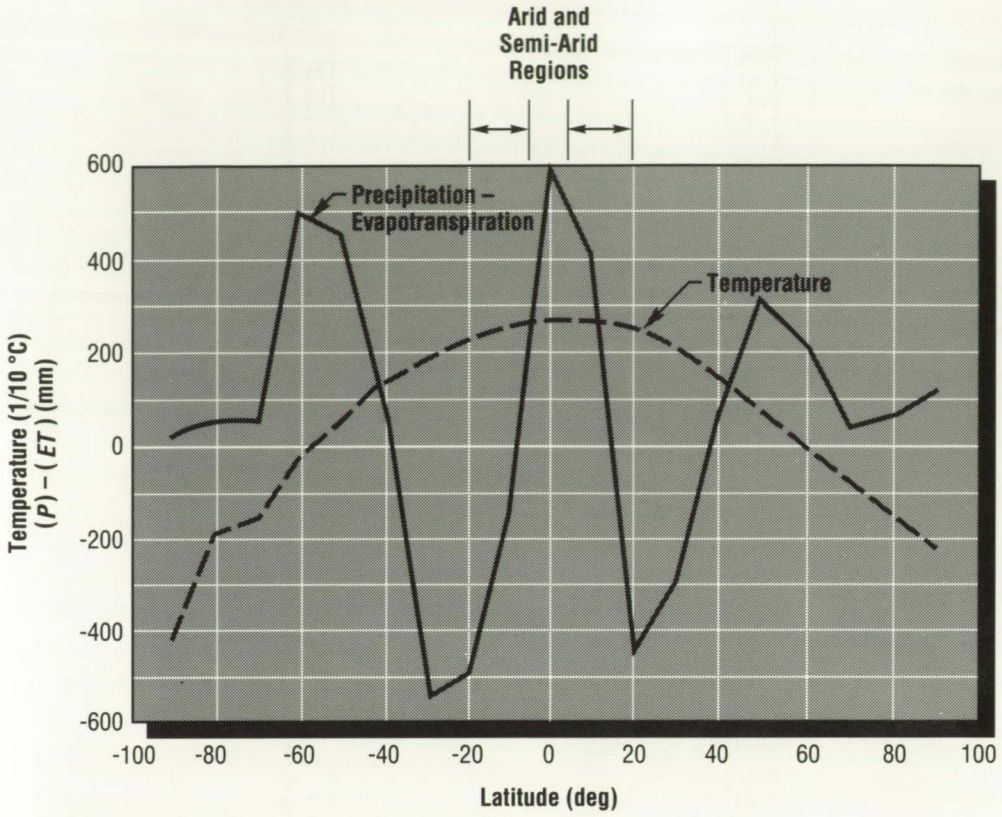

Figure 94. The Sensitive Relationship Between Latitude, Temperature, Precipitation (P), and Evapotranspiration (ET)

scales using remotely sensed data provided by MSFC. By acquiring measurements of radiation and hydrologic flux from representative sites in different seasons, these data are used to develop equations and algorithms for use with satellite data. In addition, land-vegetation-atmosphere interactions are being investigated by Dr. M. Verstraete of the National Center for Atmospheric Research† to document and understand the role of arid and semi-arid region biota in the water, energy, and biogeochemical cycles.

Complimentary humid region work was initiated in FY89 by Dr. J.C. Luvall, Stennis Space Center,‡ in order to extend the results of the semi-arid and arid work and to link the full continuum of water, energy, and biogeochemical cycles. In this context, remotely sensed data are linked to important forest canopy structural and functional attributes which control evapotranspiration. By collecting detailed information on humid region forest cover type, leaf area index, soil moisture and depth, terrain, and hydrologic parameters, remotely sensed data can be calibrated to provide a basis for assessing the spatial variability of water, energy, and biogeochemical fluxes from local to regional scales.

*Costes, N.C., Gillette, D.A., Illangasekare, T.H., Leavesley, G.H., Nichols, W.D., Verstraete, M.M., et al.: Land-Surface and Atmospheric Interactions in Semi-Arid Regions and Their Relation to Climatic Variability. Interdisciplinary investigation proposal submitted to NASA Headquarters in response to AO OSSA-1-88: The Earth Observing System, MSFC, June 1988.

†Verstraete, M.M. and Dickinson, R.E.: Modeling Surface Processes in Atmospheric General Circulation Models. *Annales Geophysicae*, Vol. 4, Ser. B-4, pp. 357-384, 1986.

‡Luvall, J.C., Welch, R.A., and Swank, W.T.: An Approach to Estimating Regional Forest Evapotranspiration Using Remotely Sensed Data. Joint proposal by Stennis Space Center, University of Georgia, and U.S. Forest Service, Coweeta Hydrologic Laboratory, in response to NASA NRA-88-OSSA-11, December 12, 1988.

N.C. Costes/ES42
(205) 544-1637
Sponsor: Office of Space Science and Applications

Mechanics of Aeolian Processes — Wind Erosion and Dust Production

A comprehensive program of fundamental research focused on the mechanics of wind erosion and dust emission is underway at MSFC.* Wind erosion and transport, which are active geologic process, occur as a result of atmosphere/land surface interactions. Such processes occur mainly in arid and semi-arid regions because of prolonged droughts and/or other environment degradation factors. Arid and semi-arid areas suffering from desertification undergo destruction of native vegetation which is quickly followed by excessive soil erosion. The present rate of fertile soil loss in the United States may be as high as 100 tons per acre per year in half a dozen major agricultural regions, including the corn-belt states of Iowa, Missouri, and Illinois. Furthermore, the Council on Environmental Quality estimates that about 10 percent of the U.S. land mass is in a state of severe or very severe desertification.

On a global scale, dust also originates from arid and the surrounding semi-arid lands which cover 36 percent of the Earth's land surface. It is transported thousands of kilometers by wind, and a portion of the transported mass may travel around the globe (Fig. 95). Desert dust has many serious environmental consequences. These include its effect on climatic change, crop growth, ocean sedimentation, air pollution, and acid/base balance of atmospheric deposition. Dust storms cause disease, suffocation of cattle, development of static electricity, disruption of transportation, and destruction of property.

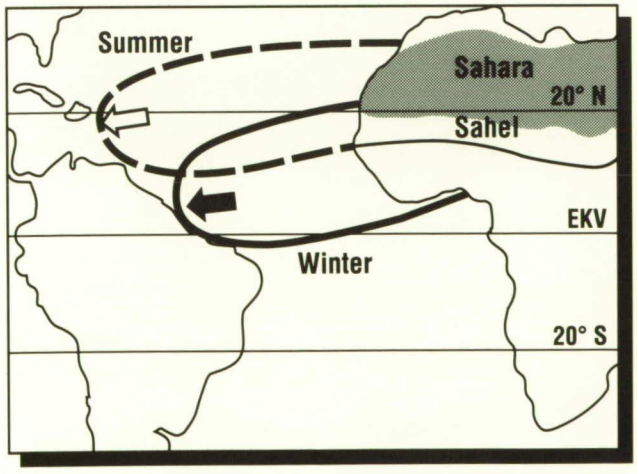

Figure 95. Major Paths of Airborne Soil Dust from West Africa and North Africa

Transport of dust, sand, and other particulate materials by wind takes place mainly in the form of surface creep, saltation, suspension, and deposition.† At present, no comprehensive quantitative analysis of these processes is available.

Gravity is another driving force in the transport of sand and other granular materials. In particular, the movement of sand dunes is due to the combined action of wind on the trailing edge and gravity on the leading edge of the dune. Gravity-driven sand is modeled as an aggregate of dry, smooth, inelastic particles bouncing against each other and moving relative to each other. Methods based on the kinetic theory of dense gases have been modified to derive the governing equations of sand-dune motion. Steady and unsteady numerical solutions are being sought using slip and no-slip boundary conditions at the base.‡

Dust production is generally due to mechanical weathering processes. In turn, these processes may include random collisions of granular particles or particle clods, leading to size reduction of the particle (Fig. 96). The mechanics of grain size reduction due to particle collisions will be developed and may explain the sorting of particles.

One of the specific goals of this research is the formulation and validation of a model for particle saltation and mass flux (per unit land area per unit time) due to the above transport mechanisms. Data obtained from existing data banks, or generated from laboratory experiments, ground-based networks of geometeorological stations, airborne, and spaceborne remote sensors (mounted on Earth Observing System (EOS) or other Earth-orbiting platforms), will be used as appropriate during the validation stage of this effort.

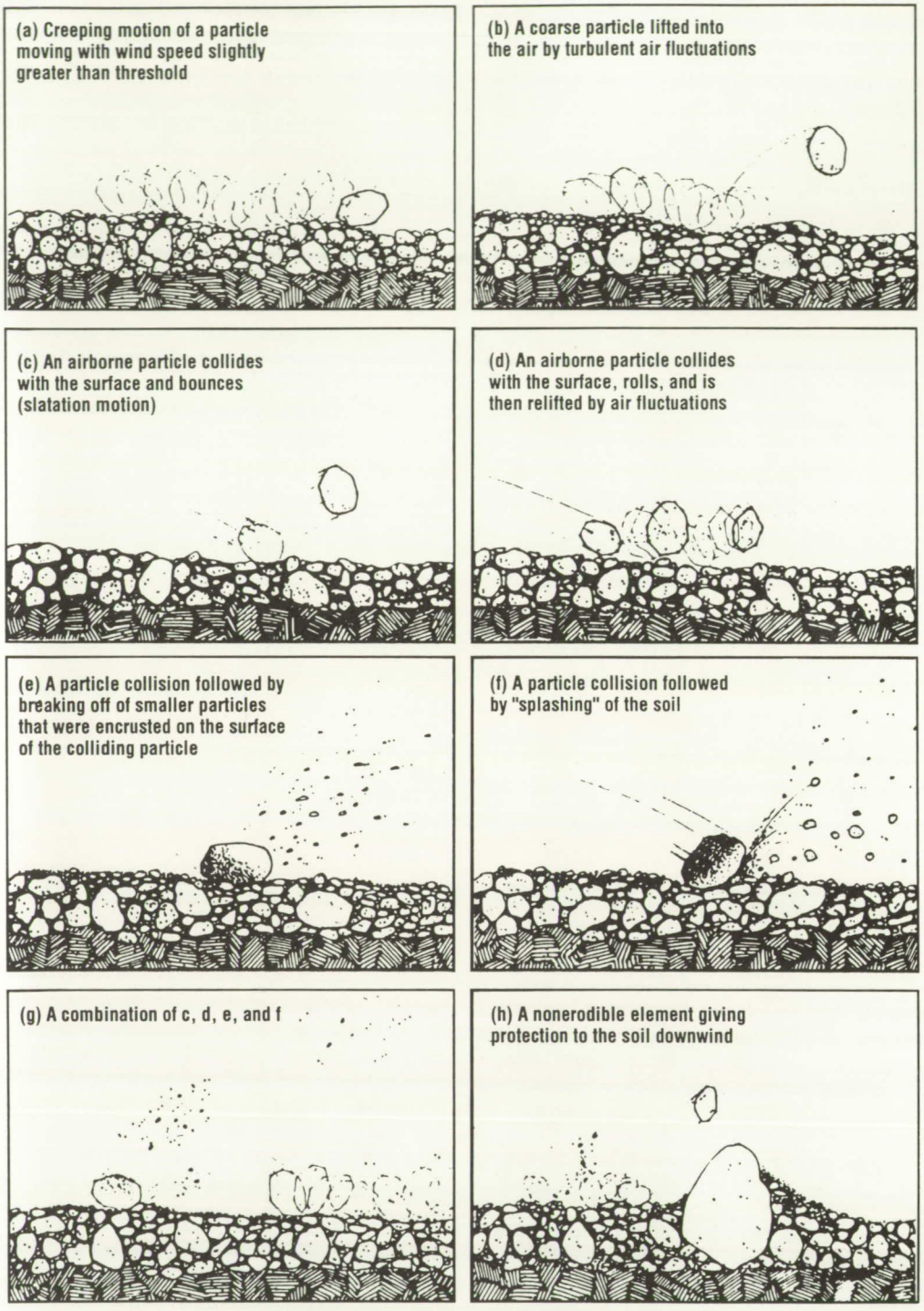

Figure 96. Soil Particle Motions During Wind Erosion

*Costes, N.C., Gillette, D.A., Illangasekare, T.H., Leavesley, G.H., Nichols, W.D., Verstraete, M.M., et al.: Land-Surface and Atmospheric Interactions in Semi-Arid Regions and Their Relation to Climatic Variability. Interdisciplinary investigation proposal submitted to NASA Headquarters in response to AO OSSA-1-88: The Earth Observing System, MSFC, June 1988.

†Gillette, D.A.: Modeling Dust Emission Caused by Wind Erosion. J. of Geophys. Res., Vol. 93, No. D11, pp. 14233–14242, November 19–21, 1989.

‡Oyediran, A.A., Richman, M.W., and Costes, N.C.: Numerical Solutions to the Flow of Granular Materials Down Bumpy Inclines. Presented at 42nd annual meeting of the Division of Fluid Dynamics of the American Physical Society, Ames Research Center, November 19–21, 1989.

N.C. Costes/ES42
(205) 544-1637
Sponsor: Office of Space Science and Applications

Dynamics of Soil Moisture and Heat Transfer as Related to the Hydrologic Cycle

Below the surface of an unconsolidated soil sediment, there are two main regions. One region is located below the ground water level, also known as the ground water table or phreatic line. The other extends from the ground surface to the ground water level (Fig. 97). Within the first region, the pore spaces of the soil mass are completely filled with water, and the mass is said to be saturated. This lower region plays the role of a stationary reservoir to the region above, although in reality, the ground water level may change in time and in space, and the liquid phase within the same region may not be at rest. Within the region between the ground surface and the ground water level, the interconnected pore spaces within the soil mass are partially filled with liquid water, which may or may not contain air bubbles. The remaining pore space is filled with water vapor and air, as shown in Figure 98. The mixture of liquid water and water vapor is also referred to by the generic term "soil moisture".

The unsaturated zone plays a very important role in land/atmosphere interactions which are directly related to the hydrologic cycle at both local and regional scales. Several important processes associated with the hydrologic cycle occur in the unsaturated zone. Among others, these include: evaporation from the soil surface; infiltration and deep percolation caused by precipitation, snow melt, and surface runoff; and transpiration from vegetation extracting water from the unsaturated zone.

All of the processes that take place in the unsaturated zone involve mass transport of the liquid and the gaseous (water vapor, air) phases through the interconnected pore spaces of the soil mass and/or plant roots. This process is driven by hydraulic and/or capillary pressure gradients; phase changes between the liquid and water vapor phase; and heat transfer through the soil mass, including the solid particles. The latter two processes result from thermal

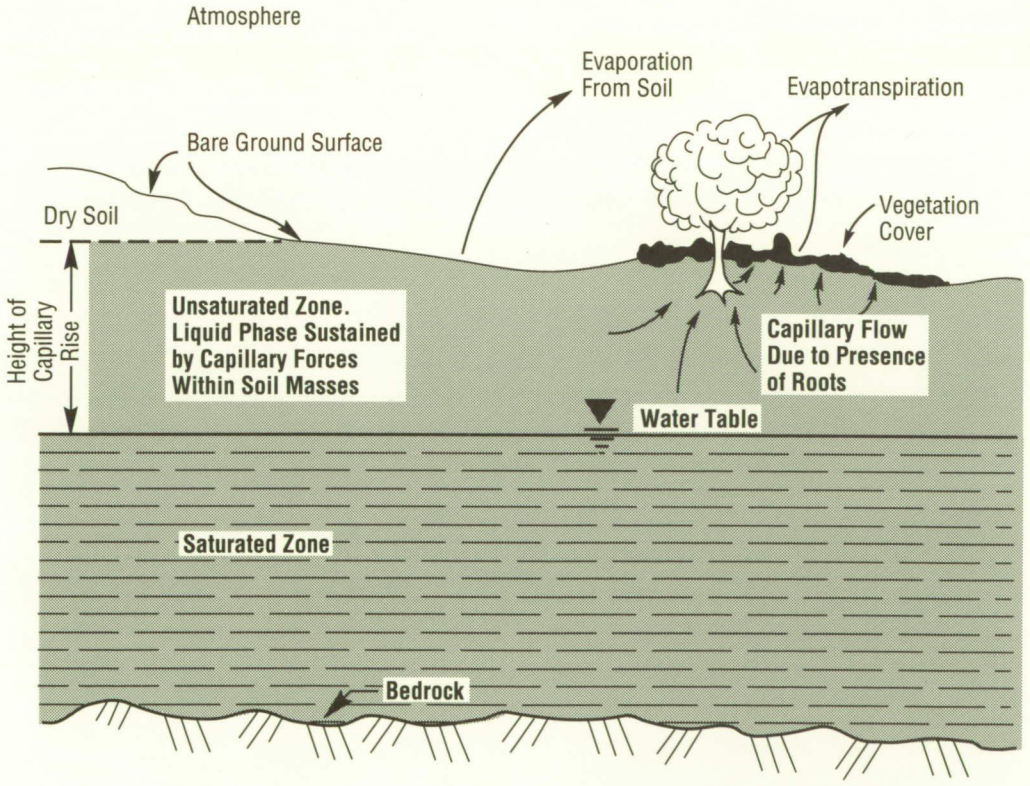

Figure 97. Moisture Conditions in an Unconsolidated Sediment

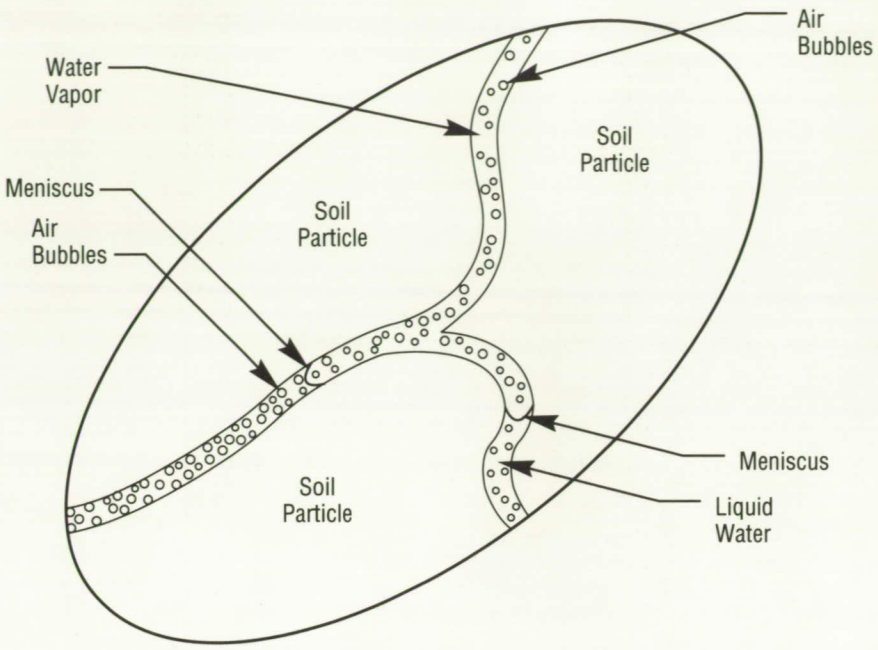

Figure 98. Microscale Structure in Unsaturated Zone

gradients within the unsaturated region. Chemical gradients caused by electrolyte concentrations within the liquid phase, and electric charges at the surface of the soil particles may also be present. However, for the purpose of this discussion, such gradients are not taken into account.

In view of these considerations, a research effort has been initiated by a team of scientists from MSFC,* the Universities Space Research Association,† and Professor T. Illangasekare‡ of the University of Colorado, Boulder, which consists of:

- Theoretical investigations and numerical analyses to model the subsurface dynamics of soil moisture and heat transfer at different spatial scales from known surface boundary conditions.

- Laboratory testing on soil columns and in a soil tank, under various soil conditions and ground covers, to verify the theoretical investigations on a microscale.

- Remote sensing data acquisition and analysis on surface distributions of soil moisture and skin temperature from controlled test sites to provide boundary conditions on local and regional scales.

- Development of a numerical simulation model that can predict dynamics of soil moisture and heat transfer on a regional scale from ground surface data obtained through remote sensing measurements. For this purpose, the physical decomposition model will be used in conjunction with the "continuum model" and "inverse problem" approaches. With these models, the regional scale domain will be decomposed into several different subdomains which will be small enough to be considered as local-scale regions.

Computations will be optimized using the parallel and vector processors of the Cray X-MP supercomputer currently available at MSFC.

Through this modeling, the role of subsurface hydrology on the hydrologic cycle can be assessed by computing surface fluxes, such as evaporation/evapotranspiration rates and thermal fluxes, resulting from subsurface soil moisture and heat transfer. Such information will considerably enhance the usefulness of data obtained through remote sensing.

*Costes, N.C., Gillette, D.A., Illangasekare, T.H., Leavesley, G.H., Nichols, W.D., Verstraete, M.M., et al.: Land-Surface and Atmospheric Interactions in Semi-Arid Regions and Their Relation to Climatic Variability. Interdisciplinary investigation proposal submitted to NASA Headquarters in response to AO OSSA-1-88: The Earth Observing System, MSFC, June 1988.

†McDonnell, J.J, Owens, I.F., and Stewart, M.K.: Effect of Macropores on Groundwater-Streamflow Interactions. Proceedings, 26th Congress of International Geographic Union, Sydney, Australia, p. 369, August 1988.

‡Illangasekare, T.H., and Morel Seytoux, H.J.: Design of a Physically Distributed Parameter Model for Arid-Zone Surface-Groundwater Management. *J. of Hydrology*, Vol. 74, pp. 233–257, 1984.

N.C. Costes/ES42
(205) 544-1637
Sponsor: Office of Space Science and Applications

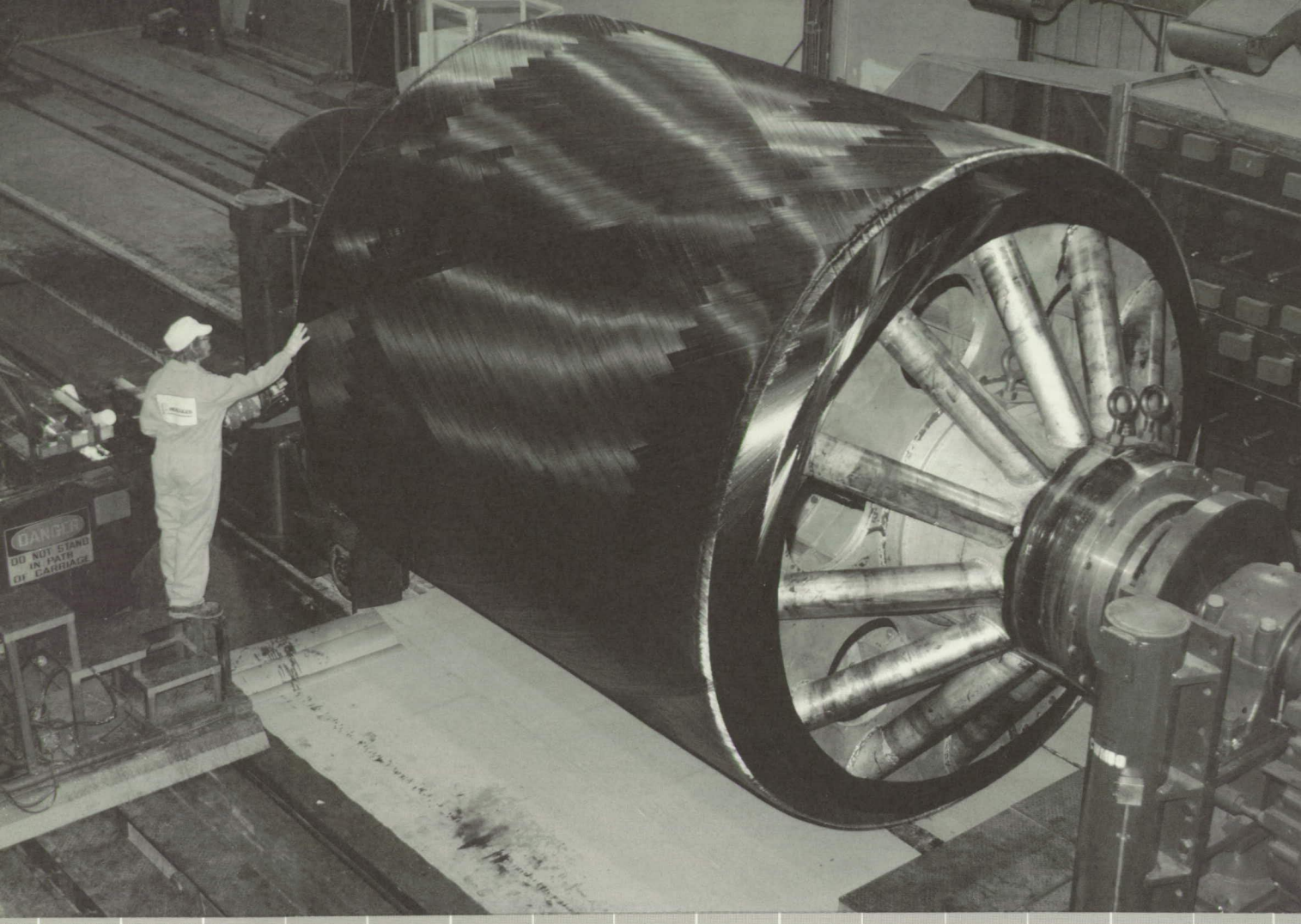
DANGER
DO NOT STAND
IN PATH
OF CARRIAGE

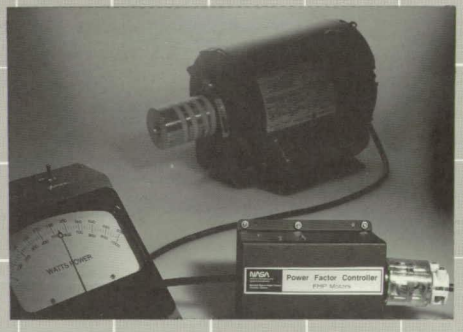
Power Factor Controller

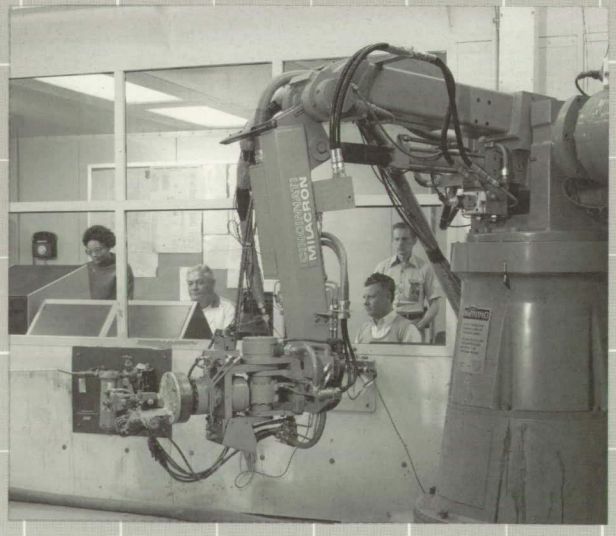
MILACRON

Technology Programs

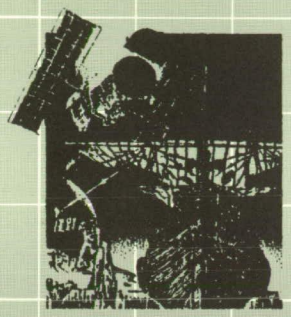

In a very real sense, technology development reflects both our recognition of the need to strive for new discoveries, and the resolve to attain them.

As a strong statement of our commitment to achieve new discoveries through technology development, valuable Center resources, both manpower and funding, are devoted with the certain knowledge that such expenditures must be made to enable MSFC to be preeminent in the development and application of space transportation and propulsion systems. These resources will allow the Center to develop, manage, and utilize major new programs such as Space Station *Freedom;* help plan and develop space exploration systems to expand human presence in the solar system; advance the Center's role as NASA's primary development center for large space observatories; and develop payloads and experiments. It is equally clear that technology development is a key ingredient, necessary to enhance and sustain a highly skilled and motivated work force in the dynamic technological environment in which we live, and to maintain excellence within the Center.

The technology activities depicted in this section have been grouped under the categories of Propulsion, Materials and Processes, Structures and Dynamics, Automated Systems, and Space Systems, and Avionics.

Propulsion

Solid Rocket Booster High Temperature Sealant Qualification/Application

Major improvements in the process of sealing thousands of subsidiary booster areas against saltwater are being introduced by material and system developments collectively called the High Temperature Sealant Project. Work underway at MSFC will qualify and develop a sealant that demonstrates superior properties and lends itself to crucial labor-saving automation.

At present, fasteners, faying surfaces, and interface seams of specified Solid Rocket Booster system components are sealed with a polysulfide called PR-1422. But flight temperatures at these surfaces require an extraneous thermal overcoating for this sealant which is limited to 135 °C (275 °F).

Replacement by a thermally and physically enhanced sealant may eliminate the need for extra insulation, while expanding sealant usefulness in general. As of mid-1989, 12 characterization tests have identified 6 prime HTS candidates: PR-1750, PR-812, PR-1770, PR-1770FR, PR-1826, and PL425 Epoxy. The extensive test series has covered environmental studies (simulated and actual ocean/beach exposures), mechanical studies (lap shear, T-peel, tensile strength, elongation), thermal studies (thermal analyses, flammability), and compatibility with adjacent insulative materials. Durability and radiant heat evaluations will complete the candidate screening process in the fourth quarter of 1989, which is expected to yield more than one qualifier.

Studies in 1989 also began the technology for automating each type of sealant application, which to date requires labor-intensive hand-troweling to seams and faying surfaces, and the hand encapsulation of each bolthead fastener, an estimated 26,400 of the latter per flight set. Each fastener receives its quotient of sealant within a hand-fitted plastic cap, the use of which requires separate insulation operations for flight. Splashdown typically dislodges numerous caps, sending components through a cycle of selective recapping.

As a fundamental step to eliminating sealant cap complexities, automation calls for volume-controlled dispensing. In 1989, preliminary evaluations have been concerned with identifying two-component mixing and metering equipment to sustain beginning robotic studies on the crucial dispensing and placement parameters. Profiled panels, representing several sized fasteners, have been employed in application runs with a robot arm, to the extent that trial designs of dispenser end tooling have been fabricated. Robotic manipulations include tracking studies to determine the use of vision system technology that identifies targeted fasteners and other surfaces.

Eventually, a prototype system designed to the characteristics of the selected sealant will form the basis for optimized mixing, system pressurization, and robot dispensing in a large-scale production environment. Accelerated sealant application, derived from the elimination of manual capping and from the use of a thermally independent sealant, is expected to produce dramatic savings in manpower, processing time, and material costs.

J.B. Thaxton/EH43
(205) 544-2786
Sponsor: Office of Space Flight

Rocket Engine Combustion Device Design and Demonstration

As with other components of the Advanced Launch System (ALS), Space Transportation Booster Engine (STBE) combustion devices must be designed with high reliability, low cost, and maintainability as primary considerations. Emphasis on liquid oxygen (LOX)/methane as a propellant mix for the STBE has shifted to LOX/hydrogen; however, the engine must retain the capability to operate with methane fuel. Development of a thrust chamber assembly and a gas generator which meets the above criteria requires technology development in several key areas. Technology studies critical to the success of ALS which will be conducted during this program include the implementation of state-of-the-art low cost fabrication techniques for the engine main chamber, nozzle, and injector; evaluation of the effectiveness of nozzle cooling with methane; and demonstration of a gas generator which produces a uniform exit temperature profile.

Supporting analytical and experimental investigations will be conducted as is appropriate to verify the suitability of design concepts or materials, select among design options, and develop fabrication

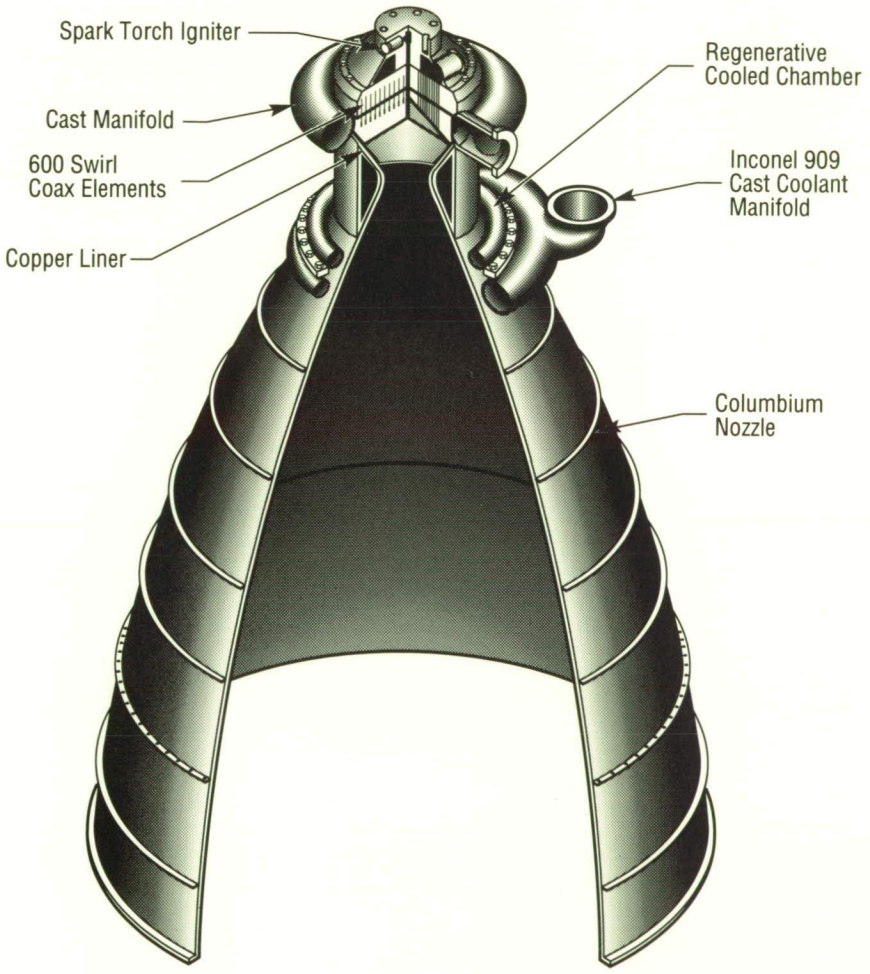

Figure 99. Thrust Chamber Assembly Baseline Design

processes emphasizing low cost and high reliability during all phases of the program. Contract deliverables will include two full-size LOX/hydrogen, methane-compatible thrust chamber assemblies (Fig. 99), each consisting of the injector, combustion chamber, igniter, and nozzle which will be delivered to MSFC for integrated testing in Test Facility 116. These tests will be used to verify that the reliability, cost, and performance goals for the combustion devices have been achieved. The design, fabrication, and delivery of workhorse gas generator assemblies (Fig. 100) will also be provided under this contract to Stennis Space Center for use during advanced development program turbopump testing. Additionally, the evaluation and design of a low-cost flight-type gas generator and validated cost model will be provided to MSFC to enhance further Space Technology Experiment Platform development and cost analysis.

D.L. Sparks/EP62
(205) 544-7111
Sponsors: Office of Space Flight
Strategic Defense Initiative Organization
U.S. Air Force/Space Division

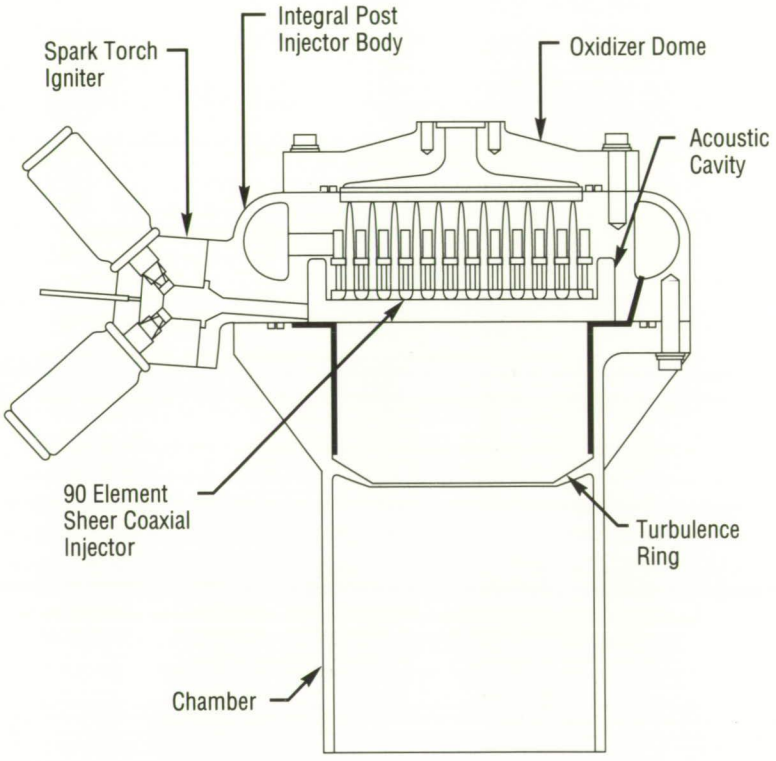

Figure 100. Baseline Gas Generator Assembly

Redesigned Solid Rocket Motor Composite Material Testing

Routine acceptance testing , similar to tests used on the Redesigned Solid Rocket Motor (RSRM) nozzle carbon-phenolic components, is an integral part of flight qualification. Tape wrapped carbon-phenolic rings are typically made oversized to provide for tape wrap angles, contour machining, and acceptance test specimens. The acceptance test specimen (tag end samples) are extracted from excess material and are tested for selected properties. The data obtained from the testing of these samples are used to verify component compliance to established limits, and are added to the historical data base of the process and materials. A statistical analysis of the tag end acceptance test data conducted by Morton Thiokol Inc., Wasatch Division, indicated significant variability in the test results. Subsequent to this finding, a research program was initiated to explore procedural approaches to enhance reproducibility and to investigate improved test methods. Two mechanical property tests, across-ply tension (APT) and double notch shear (DNS), were identified as potential improvements to the existing compression

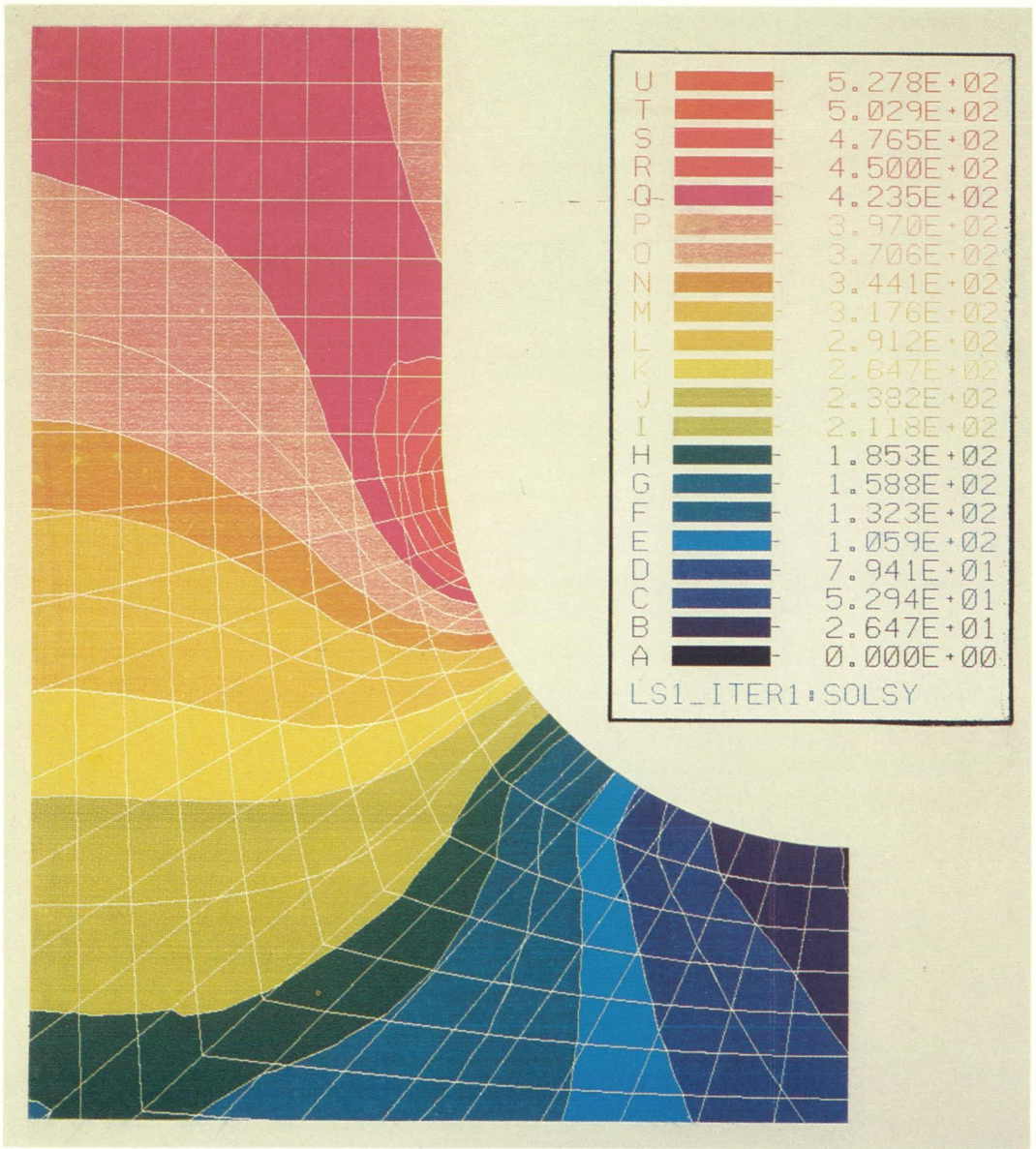

Figure 101. Stress Gradients in Across-Ply Tensile Specimen Transition Region/Original Design

test. The development of these tests is summarized in this report. Assessment of the physical property tests and results of changes implemented to reduce variability will be presented in a later report.

Acceptance test specimen design is governed by the geometry of the component tag end. The industry "standard" double notch shear specimen utilized by Southern Research Institute (SRI) is small enough to be easily adaptable to tag ends. However, the SRI standard APT specimen is too large to be accommodated by available tag end sections and, further, requires a significant amount of time to machine. APT tag end test specimens are limited to approximately 1.9-cm (0.75-in.) length by material geometry. This restriction must be balanced against the requirement for a representative cell size in the specimen gauge section. The result of these competing requirements can be the creation of a significant stress concentration in the transition region (Fig. 101). Design iterations using the finite element method (ANSYS) have aided in the design of an optimal configuration which minimizes this concentration (Fig. 102). Initial testing of carbon cloth phenolic APT test samples produced tensile failures in the ANSYS model predicted stress concentration area. Failure stress values were in reasonable agreement with test data generated by SRI.

To enhance the APT test, an improved test fixture was designed to assure uniaxial loading. This was accomplished by modifying a chain and clevis setup recommended by SRI which minimized off-axis loading. Other improvements made to the APT sample include the development of a sample bonding fixture, a bonding process specification (NMD-P-002), and special tooling for machining the APT sample test gauge section.

Initial DNS tests of carbon-phenolic material yielded interlaminar shear values approximately 40 percent higher than accepted SRI properties. The investigation of this disparity revealed that tighter tolerances

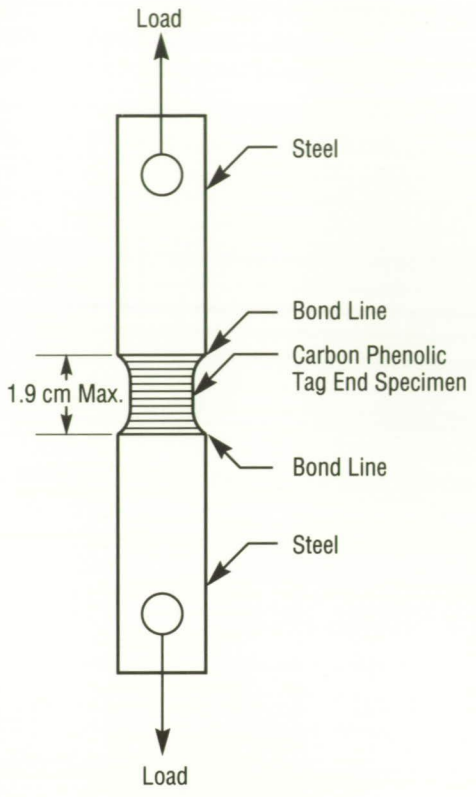

Figure 102. Across-Ply Tensile Test Specimen

on the test fixture were required to prevent off-axis loads. It was analytically determined that across-ply compressive stresses produced by a buckling mode contributed to the higher failure loads. The test fixture has been redesigned to eliminate out-of-plane loading. Qualification tests are in progress.

Development efforts for both mechanical tests include time span and cost analyses for specimen preparation and testing, reproducibility, data quality assessment, and data base generation on RSRM nozzle component tag ends.

Ellick, C.L. and Kitchen, G.N.: Space Shuttle SRM Project SRM Capability Study of Tag End Properties. TWR 16132, MTI/W, February, 1987.

R.G. Clinton/EH34
(205) 544-2682
Sponsor: Office of Space Flight

Solid Rocket Booster Internal Flow Analysis by Adaptive Computational Methods

The eroding of solid propellant boundaries and development of localized burning pockets, as detected in space shuttle solid rocket boosters, are known to have a significant influence on the flowfield structure and overall performance of the system. The modeling of such phenomena couples a dynamic structural analysis with a transient nonlinear fluid analysis for which the computational domain is continuously changing due to structural deterioration. New modeling and computational techniques are being developed to simulate these types of fluid-structure interactions in order to factor such effects into design considerations.

The first phase of this effort has been devoted to the development of testing of various simple adaptive techniques for dynamically updating a computational domain to reflect the erosion of a solid propellant boundary. Two approaches have been investigated, both based on an arbitrary Lagrangian-Eulerian finite element model for the fluid and a background Eulerian grid in the solid propellant. The first approach consists of collapsing the elements in the solid propellant region adjacent to the eroding boundary and allowing them to expand as the boundary erodes. When elements in the solid region are traversed, they are incorporated into the fluid domain, and new bounding elements in the solid region are again collapsed. The second approach is the converse of "flattening" elements in the solid region. Here, elements in the fluid domain adjacent to the solid boundary are "expanded" into the propellant region and subsequently envelop the Eulerian background grid.

Both approaches have been used in the solution of preliminary test problems using an explicit two-step Lax-Wendroff flow solver and a specified maximum burning velocity ranging from Mach 0.0001 to 1.0. An example of the results obtained using the "expansion" method is shown in Figure 103 where the time history of the density contours for a uniform Mach 1.0 inflow and a quadratic convex burning boundary (Mach 0.001 maximum burning velocity) are presented. In this example the flow is from left to right with the lower boundary taken as a symmetry plane and the upper burning boundary as a no-slip boundary.

G.A. Wilhold/ED31
(205) 544-2651
Sponsor: Solid Rocket Booster Project Office

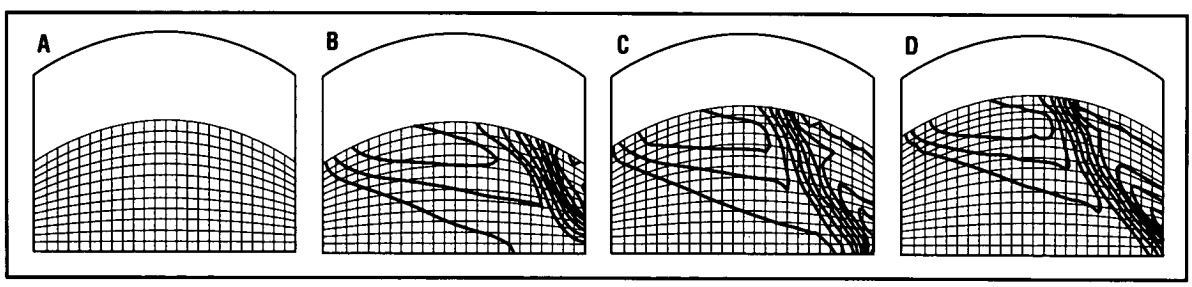

Figure 103. Evolution of Density Contours for Convex Receding Boundary Using "Expansion" Method

Space Transportation Engine Thrust Chamber Technology

The Space Transportation Engine Program is being conducted to provide propulsion for the Advanced Launch System. Engine program requirements specify a Space Transportation Main Engine (STME) as a gas generator cycle engine which uses oxygen and hydrogen propellants and operates at 2,250 psia chamber pressure. A Space Transportation Booster Engine (STBE) using oxygen and methane propellants is now limited in design to a derivative of the STME. The engine is intended to be used initially with hydrogen fuel, then later used with methane fuel after only minimal modifications. These engines will be designed and developed with emphasis on low cost, simplicity, and robustness, as opposed to design sophistication and maximum specific impulse.

Design and operation of the main injector with either fuel represents challenges from the standpoint of combustion efficiency, thrust chamber heating rates, and, particularly, combustion stability. Although extremely high combustion efficiencies are not required for these engines, good injector performance is necessary to prevent combustion chamber wall "streaking" or "blanching," and to control chamber nozzle throat temperatures. Obtaining good injector performance is made much more difficult by the motivation to use simple, large injection elements to reduce fabrication costs. Thrust chamber heating rate profiles must be accurately known for both chamber cooling circuit design and engine cycle flow balancing. Combustion stability is a concern for operation with either fuel. Combustion data using methane are very limited but have shown general tendencies toward instability. The combustion data base with hydrogen is much better defined and indicates a potential instability problem at the fuel injection temperatures projected for the STME.

Injector technology programs are underway at Aerojet TechSystems, Pratt & Whitney, and Rocketdyne to address and solve these technical concerns. Each contractor has structured a technology program which complements and addresses their own baseline STME/STBE designs. Each program is structured to assess and improve applicable analytical codes and procedures, obtain experimental data during subscale thrust chamber testing, and to design, fabricate and deliver to MSFC full-scale injectors to be test evaluated using a government-furnished combustion chamber. Full-scale injector testing, scheduled to commence mid-1991, will include the use of explosive charges for stability ratings.

C.R. Bailey/EP62
(205) 544-7079
Sponsor: Advanced Launch System Joint Project Office

Plume Temperature Measurements

Research is being conducted to measure the exit plane properties of the Space Shuttle Main Engine (SSME) and other engine systems for determination of performance code accuracy and to provide data to guide development of future computational fluid dynamics codes. Nonintrusive techniques are being developed which are based on measurements of the emission and absorption of infrared (IR) and ultraviolet (UV) radiation from the plume gases. The two techniques which are being utilized are IR emission/absorption spectroscopy and hydroxyl radical (OH) resonance line absorption spectroscopy.

The IR emission/absorption technique is being used to determine the temperature profile and species concentration in the exit plane of the SSME using available IR transitions of the H_2O molecule at 2.7 μm. A band model for radiative transport* in the plume is utilized to compute the distribution and temperature of emitting molecules in each assumed axially symmetric zone of the plume gases (Fig. 104). The solution is obtained from a best fit of the emission/absorption data and from experimentally determined band model parameters for the H_2O molecule. Subscale experiments conducted using a hydrogen-air hot gas generator have demonstrated the accuracy of the technique by comparison with thermocouple measurements. A test stand system for full-scale demonstration of the measurement technique on the SSME has been designed and will be utilized to characterize the SSME exit plane on the MSFC Technology Test Bed (TTB). Preliminary tests of the detector system have already been conducted on the TTB.

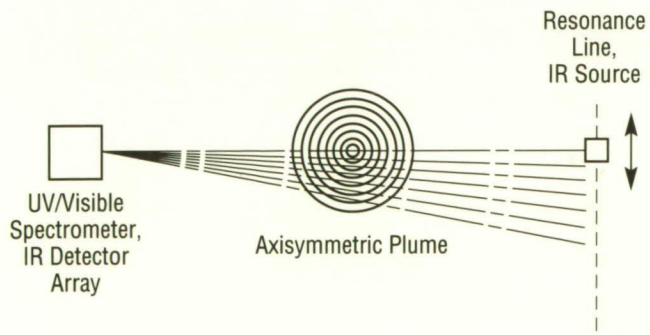

Figure 104. Exit Plane Temperature Measurements

The OH radical resonance line absorption technique is based on the use of a microwave-pumped discharge to produce characteristic OH radical radiation which is transmitted through the plume to determine rotational temperature and species concentration of OH. The OH concentration is of particular interest due to its impact on the kinetics of the rocket engine combustion and expansion process. Such data will provide an excellent check for chemical kinetic models which are currently being used. The OH absorption data will be acquired with an optical multichannel analyzer and a 0.5-meter UV spectrograph which captures the (0-0) band OH radiation from 306 to 320 nm. The UV detector system has been under evaluation on the MSFC TTB since January 1989. The OH data reduction technique is based on early work by Neer† and more recent advances at Langley Research Center.‡

Installation of the translating source system for both the IR and the UV techniques is projected for the spring of fiscal year 1990.

*Brewer, L.E.: A Non-Interference Method for Determining Temperature and Water Vapor Concentration Profiles in Cylindrically Symmetric Combustion Systems. AEDC-TR-71-80, 1971.

†Neer, M.E. and Burde, D.H.: The Advanced Development of a High Frequency Response Spectroscopic Probe for Analysis of Supersonic Combustor Flowfields. NASA CR 145363, 1978.

‡McCullough, R.W.: Improvements to the NASA OH Temperature Measurement System. ARAP Report No. 548, Contract NAS1-14853, 1985.

R.H. Eskridge/EP55
(205) 544-7119
Sponsor: Office of Aeronautics and Space Technology

Injector Diagnostics

Research is being conducted to characterize injector properties (i.e., droplet size distribution, droplet breakup, and gas/fluid stripping phenomena) for single element injector configurations. New instrumentation and visualization techniques are being developed in support of this research. A pressurized atomization test facility (Fig. 105) is also being designed for hot/cold fire testing of candidate injectors.

This research is composed of a measurement effort for hot and cold flows in order to gather data for computational fluid dynamics code validation and development. A Phase Doppler Particle Analyzer is currently being procured to support droplet sizing efforts. Optical diagnostics are also being developed for hot fire applications. These diagnostics will include a laser Raman temperature/species probe and a resonance-line molecular absorption technique.

The cold flow facility is intended to provide a test capability for simulated sprays at chamber pressures to 2,000 psig using liquid nitrogen and gaseous nitrogen as the test fluids. A multipurpose injector plate is being designed to allow installation of several kinds of single-element injectors including the SSME preburner liquid oxygen (LOX) post. The plate is porous to provide for a coaxial flow and prevent recirculation zones from developing in the chamber. Initial cold flow tests are scheduled for the first quarter of FY90.

The hot fire test article will be capable of testing multiple injector elements into a two-dimensional configuration. Facilities will be provided for "bombing" the chamber to test for instability effects. The initial test fluids will be LOX and gaseous methane. The test article will be equipped with quartz windows for access to ultraviolet and visible light imaging and spectroscopy. Preliminary testing of the hot-fire chamber is scheduled for late FY89.

This effort will support Space Transportation Booster Engine development and influence future design changes in Space Shuttle Main Engine injector configurations. Testing will be conducted in the MSFC Combustion Physics Laboratory and on MSFC Test Stand 115.

R.H. Eskridge/EP55
(205) 544-7119
Sponsor: Office of Aeronautics and Space Technology

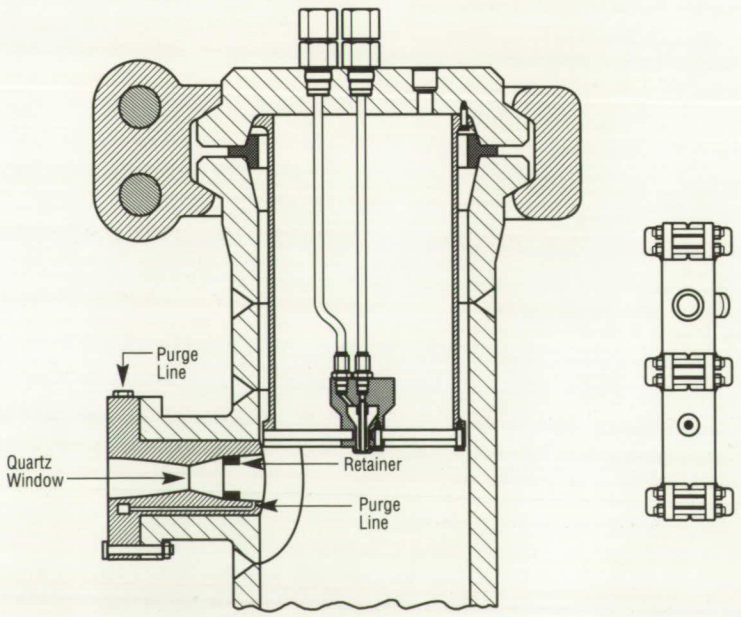

Figure 105. High Pressure Cold Flow Spray Chamber with SSME LOX Post

In-Flight Optical Leak Detection

Presently, no real-time propellant leak detection capability exists for implementing closed-loop control during flight, and ground-based propellant leak detection for flight readiness firings (FRF) is performed with no leak location ability.

Current leak test procedures of the Space Shuttle Main Engine (SSME) are limited to ground-based, low-pressure inspections, post-flight analysis of sampling bottles mounted in the shuttle engine compartment, and mass spectrometer readings taken during FRF. These procedures could be considerably enhanced by a propellant leak imaging system. By this means, full-pressure propellant leaks occurring in flight or during FRF could be detected and located as they occur. The need for post-test or post-flight repairs could thereby be more rapidly and accurately identified, and furthermore, a redline signal for engine safety measures could be provided in real time.

Three general criteria should be met in the design of a propellant leak detection system for the SSME. The system must first of all reliably detect, locate, and measure leaks with sufficient accuracy, thoroughness, and speed so that timely and reliable redline signals and/or maintenance instructions can be generated. Second, the system must operate reliably under high vibration levels and other environmental extremes to which an in-flight engine monitoring system would be subjected. Third, the system design should minimize added weight to the engine and be free of hazards to hardware or personnel.

Most technologies for leak detection require the use of a probe which is sensitive to leaking gas only in its immediate vicinity. An in-flight system based exclusively on such a technology would require a large number of probes to detect and locate leaks with adequate assurance and speed. Such a system would create a serious weight penalty to the vehicle, and would most likely be difficult to maintain and operate reliably. Optical methods exist which eliminate these concerns for ground-based leak inspections, and show promise for adaption to in-flight measurements. Rapid remote inspections are accomplished by rendering leaking gas visible and by obtaining images of large sections of the engine. In this way, foreknowledge of potential leak locations is not required, and only a few remotely mounted sensors are required to detect any leak emerging from the entire engine.

The method envisioned, based on experimental work, would utilize absorption exhibited by gaseous propellants in the far ultraviolet. Information on the absorption curves of gases and propellants of interest was gathered during this work, and a laboratory test was conducted to determine the system's ability to detect oxygen in nitrogen at atmospheric temperature and pressure (Fig. 106). This method shows great promise for the imaging of leaking oxygen, hydrogen, and water vapor both in-flight and for FRF firings. Although oxygen is present in air at levels that would quite possibly make such a propellant detection method difficult to implement, the space shuttle's engine compartment is purged with nitrogen, thus alleviating this difficulty.

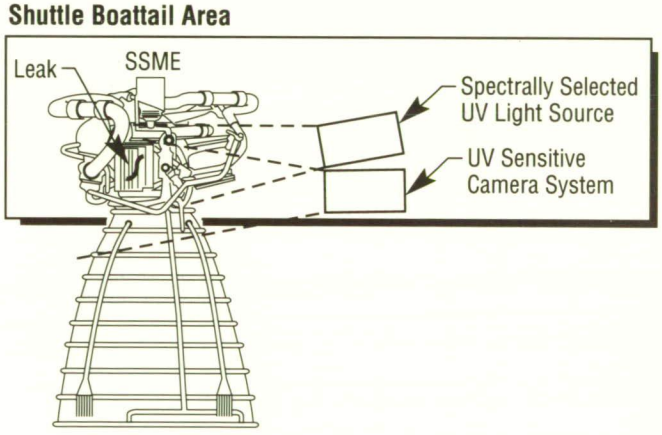

Figure 106. Propellant Leak Imaging System

The ultimate objective of this program is to develop an engine propellant leak detection system for use on the space shuttle during flight and FRF ground tests. The specific objectives of this effort are to select, evaluate, and demonstrate leak detection systems of promise for rapid, thorough, and reliable FRF and in-flight SSME leak detection.

W.T. Powers/EB22
(205) 544-3452
Sponsor: Office of Aeronautics and Space Technology

Optical Leak Detection for Ground-Based Operations

During factory and test stand operations involving Space Shuttle Main Engines, leak testing at the many joints is necessary to assure a tightly fitted assembly. Currently used methods involve pressurizing the assembly, or subassembly, and using a bubbling-type leak test fluid or, when small leaks are sought, using a totally enclosing bag and a mass spectrometer. A method which is faster, easier to use, and possibly more sensitive is being developed for use in the factory and on test stands under purged, nonoperating conditions. This technology (Fig. 107), originally developed under a U.S. Air Force contract, involves pressurizing the configuration under test with a gas containing a selected "seed" gas, illuminating the configuration with light which can be absorbed by the pressurant, and imaging the result with a video camera. Any leaking gas in the vicinity will then be visible in the image and can be quantified and located with automated digital image processing.

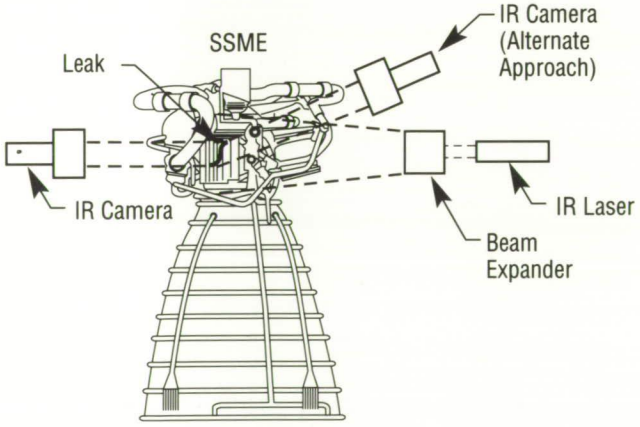

Figure 107. Optical Leak Detection System

This system is to be immune from vibration and other normal environmental effects. The ultimate goal will be preflight inspection of entire engines. To that end, the program will investigate the use of the system as a subassembly inspection tool, allowing assembly personnel to assure proper fit of all involved parts. It will be used for larger assemblies up to and including entire engines, and will eventually be used on test stands (i.e., Technology Test Bed) for normal inspection operations while the engine is in protective purge status.

The major efforts of this task will be to ascertain inertness of the "seed" gas, and therefore its compatibility with the target assemblies, and construct a system which is sufficiently easy to use, requiring only a low level of user skills, so that any operating personnel may use it with minimum impact on schedules.

Maram, J.M. and Deleher, R.C.: Rocket Engine Optical Leak Detection. Rocketdyne Division/Rockwell Int. final report to AFRPL TR-87-006, Air Force Astronautics Laboratory.

W.T. Powers/EB22
(205) 544-3452
Sponsor: Office of Aeronautics and Space Technology

Vortex Shedding Flowmeter for Space Shuttle Main Engine

In order to measure the actual propellant flow in the Space Shuttle Main Engine (SSME), a meter of sufficient ruggedness to withstand the extremely high velocities encountered is required. Meters with moving parts are generally unacceptable and low pressure loss and meter weight are desired. Vortex-shedding flowmeters were examined as candidates. They offer no moving parts, an output which is linear with flow (making them potentially more accurate at low flows than venturis) and are physically short. Their geometry is such that fewer modifications are required for installation.

Several designs have been built and flow-tested with water and air at velocities encountered within the SSME ducts. Most testing was done in ducts of 4.06 and 5.84 cm (1.6 and 2.3) inch internal diameter; testing is done in actual SSME ducts. Meters to be used with LOX are tested with water drawn from a high-head system owned by the City of Boulder, CO. Large heads are necessary to achieve the required velocities. Meters to be used with GH_2 are tested in high pressure air systems provided by a testing laboratory. Correlations to GH_2 from the data obtained with air are computed for these tests.

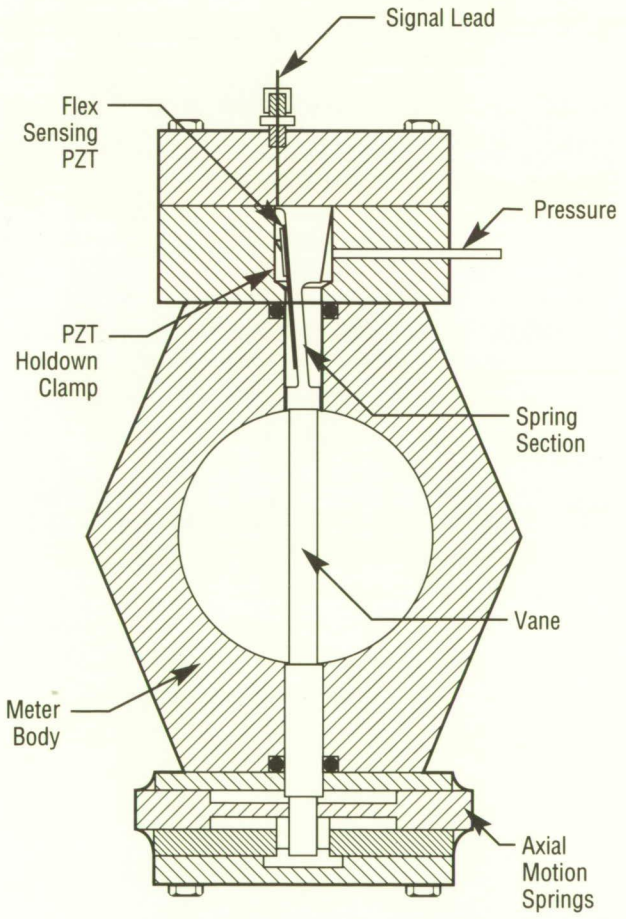

Figure 108. Scale Drawing of Vane 88-6-1

One design criterion is to prevent tieing the sides of a duct directly together with a solid structure such as a shedder vane in order to prevent introducing mechanical stresses due to thermal factors. An early design to circumvent that problem employed dual cantilevered beams, but it was found to be overly sensitive to the gap between the beams. The current design (Fig. 108) uses a beam fastened to the duct at one end and to a "spring" beam (or "washer" assembly) at the other. These latter designs work well, yielding a very clean output, making it easier to interface detecting electronics to the system. The method of sensing the vibration is Lead Zirconate Titanate pickups.

The meters for use in LOX are essentially fully designed. The meters for use in GH_2 still require minor refinement but the overall configuration (vane design, sensor mounting, vane mounting) is defined. Units are being built for use on the Technology Test Bed Engine.

Siegwarth, J.D.: NIST/Boulder: Vortex Shedding Flowmeter for Measurement of Liquids at High Flow Velocities. International Journal of Heat and Fluid Flow, 1988.

Siegwarth, J.D.: Vortex Shedding Flow-meter Performance at High Flow Velocities. NBS Tech Note 1302, October 1986.

Siegwarth, J.D.: Vortex Shedding Flow-meters for Space Shuttle Main Engines. Presented at 1988 Conference on Advanced Earth-to-Orbit Propulsion Technology, MSFC, May 12, 1988.

W.T. Powers/EB22
(205) 544-3452
Sponsor: Office of Aeronautics and Space Technology

Space Shuttle Main Engine Exit Diagnostics

With continued improvements and upgrades planned for the Space Shuttle Main Engine (SSME), it would be beneficial to have a diagnostic system capable of measuring pertinent flow variables, such as temperature, species concentration, and velocity in the exhaust plume. A map of these variables measured in a plane at the nozzle exit would be invaluable for anchoring engine performance codes or for monitoring the performance of individual engines. Physical probes cause perturbations in the flow stream; this problem, combined with the need to correct data, makes a nonintrusive measurement technique desirable.

A number of possible approaches were considered during the study phase of this project. The requirement, that the technique used not require seeding the flow, eliminated many of the better known methods of measuring flow. An approach was selected that does not require seeding of particles of trace molecules — enhanced oxygen hydrogen (OH) flow tagging by ultraviolet-laser photodissociation of H_2O (Fig. 109). A system using a narrowband injection-locked excimer laser (KrF at 248 nm) focused into a sample area produces a small photodissociation of H_2O, which results in a large local enhancement of the OH radical concentration. In order to measure velocity, a time-delayed, pulsed dye laser beam at 308 nm excites fluorescence from OH, and the location of the supersonic, convected, enhanced-OH zone is measured above the background with an optical multichannel detector set. The Raman radiation from the initial excimer pulse yields the information needed to determine the temperature and specie OH concentration.

Laboratory feasibility experiments verified the usability of the technique. Velocities have been measured in a laboratory flat-flame burner to about ±2 percent of full scale. Effort has been concentrated on understanding the possible interferences which could confound the signal. A characterization of the excimer beam was necessary to assure the purity of the excitation pulse. Work is now being done on the optical design of the telescope system which is required for the two-dimensional sweep of the intended subject, an SSME exhaust plume. The assembly is being designed to withstand the environment of the SSME Test Bed Engine Stand (which is generally open to the atmosphere).

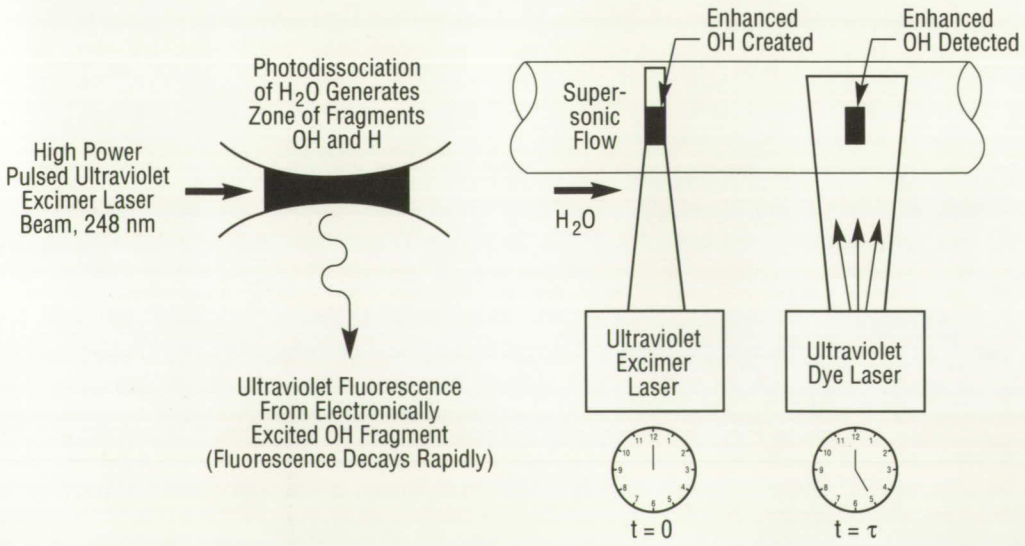

Figure 109. Flow Testing for Velocity Determination

Shirley, J.A. and Boedecker, L.R.; United Technologies Research Center: Nonintrusive Space Shuttle Main Engine Nozzle Exit Diagnostics. Presented at 24th Joint Propulsion Conference, Boston, July 12, 1988.

Boedecker, L.R. and Shirley, J.A.; United Technologies Research Center: Nozzle Exit Plane Measurement Instrumentation. Presented at 1988 Conference on Advanced Earth-to-Orbit Propulsion Technology, MSFC, May 12, 1988.

Shirley, J.A.; United Technologies Research Center: UV Raman Spectroscopy of H_2/Air Flames Excited with a Narrowband KrF Laser. A paper in the Optical Letters.

W.T. Powers/EB22
(205) 544-3452
Sponsors: Office of Aeronautics and Space Technology
Office of Space Flight

Space Shuttle Main Engine Preburner Temperature Profiler

A diagnostic system for nonintrusive temperature profiling in the fuel preburner of the Space Shuttle Main Engine (SSME) has been developed. The approach is based on the measurement of laser-excited, Raman-shifted, backscattered radiation and employs optical fibers for use in the hostile SSME environment. A breadboard system has been completed and tested using a heated cell containing high pressure hydrogen.

The light energy from an argon-ion laser is transmitted through a multimode optical fiber [at lengths of up to about 50 m (164 ft)] to an optical transceiver head, mounted on the engine, which focuses the radiation into the measurement volume and collects the returned radiation, which is transmitted through a second fiber to remotely located instrumentation for spectral analysis (Fig. 110). The hydrogen gas temperature is determined from the distribution of radiation scattered from hydrogen Q-branch nonvibrational transitions. Measurements in the pressure cell indicate that accuracies on the order of 20 to 25 K can be expected, with the probe volume less than 1-cm (0 39-in) long and 0.5 mm (0.02 in.) in diameter, having a time response of 10 ms. Response time and accuracy can be traded off against each other. The system will be mounted in the hard core of the SSME Technology Test Bed

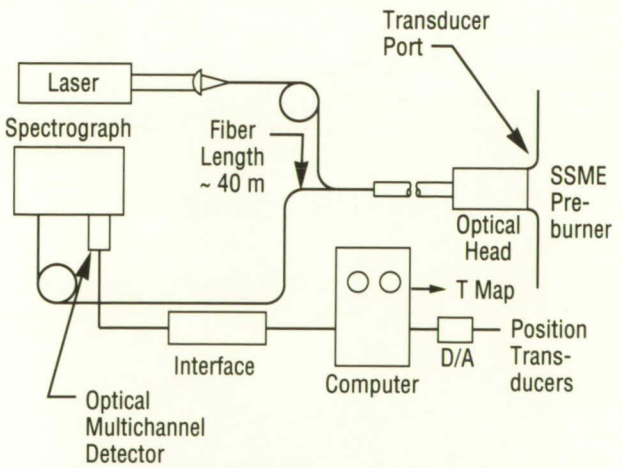

Figure 110. Raman Diagnostic System

Stand with the fiber-optic cable routed to the engine. The transceiver head will be mounted to the fuel preburner body by way of an existing port with an appropriate window added. Evaluation of candidate materials for the window and design of the window assembly is underway (Fig. 111). The design of the access window (fused quartz) and the mounting hardware associated with it, has been prototyped and will be tested in subscale before being mounted on an SSME.

A variation of this system has been designed and built for use in the Advanced Turbopump Development (ATD) program. This version will view the interior of a turbopump combustion chamber through a quartz quarter-dome window, thereby having access for a three-dimensional scan of the combustor interior. The assembly carrying the optical scan head replaces the assembly using the turbine blades with an orifice plate to maintain normal pressures. Tests using this system were run during the summer of 1989. Except for the scanning head, the equipment and software will be the same for both versions, thus the ATD tests were the first use of the system.

Shirley, J.A.; United Technologies Research Center: Fiber Optic Raman Thermometer. Presented at 1988 Conference on Advanced Earth-to-Orbit Propulsion Technology, MSFC, May 12, 1988.

Shirley, J.A.; United Technologies Research Center: Investigation of Breadboard Temperature Profiling Systems for SSME Fuel Preburner Diagnostics. 24th Joint Propulsion Conference, Boston, MA, July 12, 1989.

W.T. Powers/EB22
(205) 544-3452
Sponsor: Office of Aeronautics and Space Technology

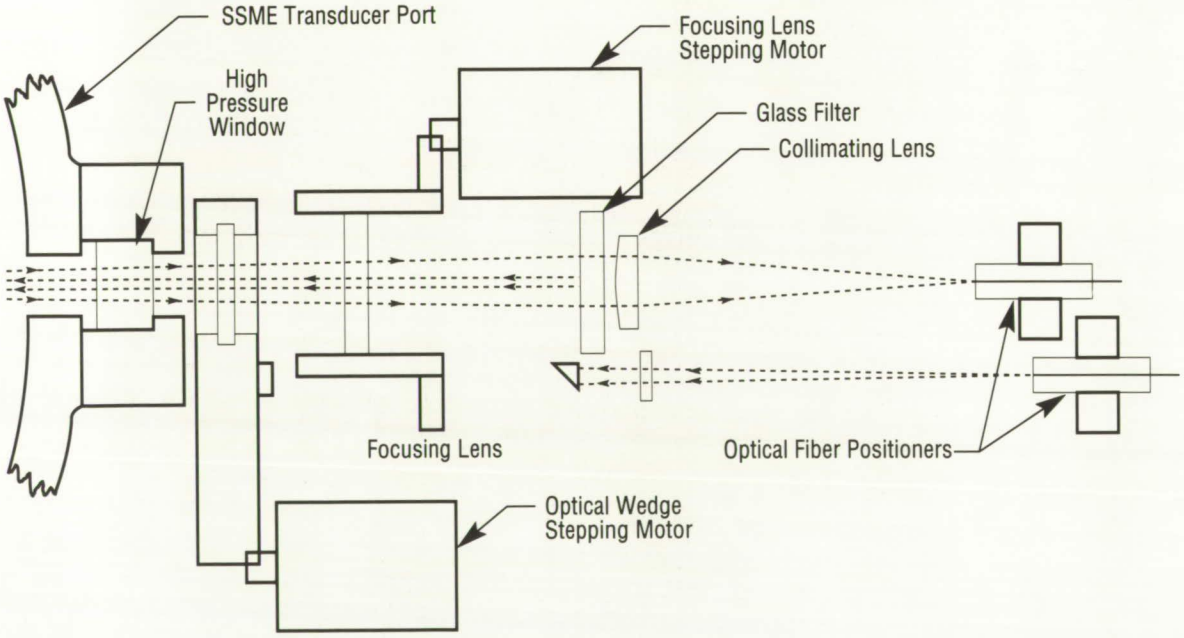

Figure 111. Interior Design of Fiber Optic Raman Thermometer Optical Instrument Head

Space Shuttle Main Engine Turn-Around Duct Simulation

A two-dimensional wind tunnel simulation of the flow in the turn-around duct (TAD) of the Space Shuttle Main Engine (SSME) has been performed at Ames Research Center (ARC). The test supports turbulence model and Navier-Stokes (NS) code development at MSFC for internal flows with extreme curvature. Measurements include profiles of mean and turbulence velocities with a Laser Doppler Velocimeter, including static pressure and skin friction. Comparisons have been made with NS calculations of the flow using several widely-used algebraic turbulence models. They show that unmodified algebraic turbulence models are not capable of calculating many important features of this flow. For example, Figure 112 shows that the theory seriously underpredicts the amount of separation which occurs on the TAD inner wall at the end of the bend. By analogy, these same turbulence models probably cannot accurately predict the flow in the actual SSME TAD.

Using the experiment as a guide, zero-, one-, and two-equation turbulence models will be modified for strong curvature and pressure gradient effects, and their accuracy compared. If successful, the improved code will be applied at MSFC to design a variable-area TAD that does not have any separation. The final shape will be tested in the ARC TAD test section to verify code prediction.

Monson, D.J., Seegmiller, H.L. and McConnaughey, P.K.: Comparison of LDV Measurements and NS Solutions in a Two-Dimensional 180-Degree Turn-Around Duct. Paper No. AIAA-89-0275, 27th AIAA Aerospace Sciences Meeting, Reno, NV, January 1989.

G.A. Wilhold/ED31
(205) 544-2651
Sponsor: Office of Aeronautics and Space Technology

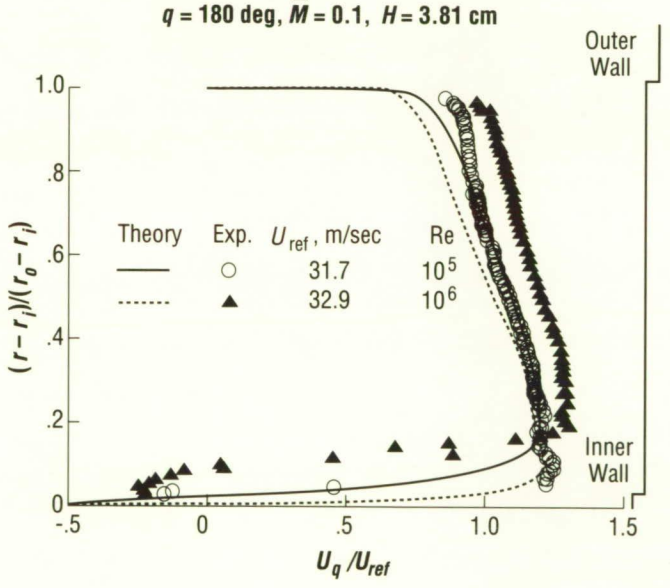

Figure 112. Longitudinal Velocity in Turn-Around Duct of Space Shuttle Main Engine

Space Shuttle Main Engine Turbine Disk Coolant Flow

Turbine disk cavity aerodynamic and heat transfer experiments are being conducted to define the nature of the flow and mixing within each of the disk cavities and about the blade attachments of the Space Shuttle Main Engine fuel turbopump. The experiments are being conducted with a large-scale (2X), well-instrumented model (Fig. 113) which provides close geometric simulation of the entire multidisk cavity flow region and the ability to simulate the sources and sinks for each cavity flow (Fig. 114). These experiments will explore each of the various important aerodynamic driving mechanisms including flow between the main gas path and the disk cavities, flow within the disk cavities, leakage flows through the blade attachments and labyrinth seals, and the role that each of these various flows has in determining the adiabatic recovery temperature at all of the critical locations within the cavities.

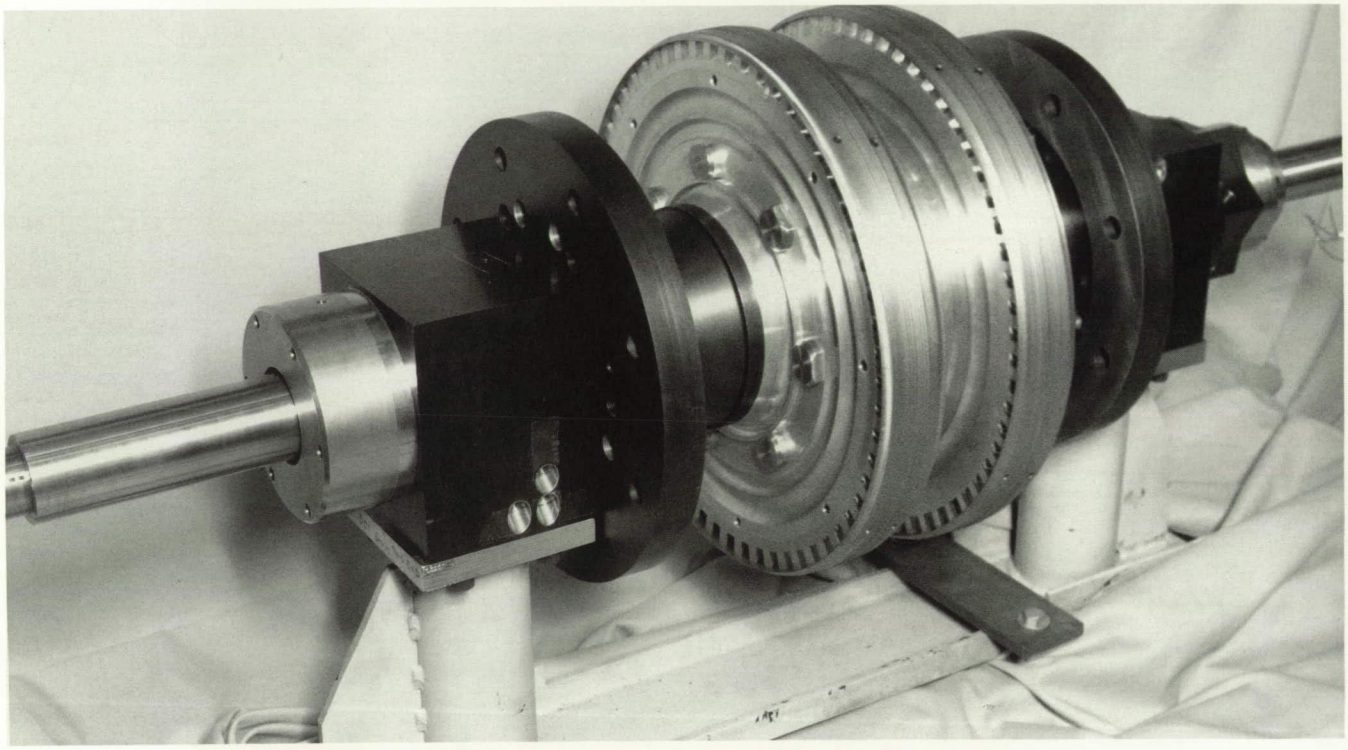

Figure 113. Large-Scale Model Rotor

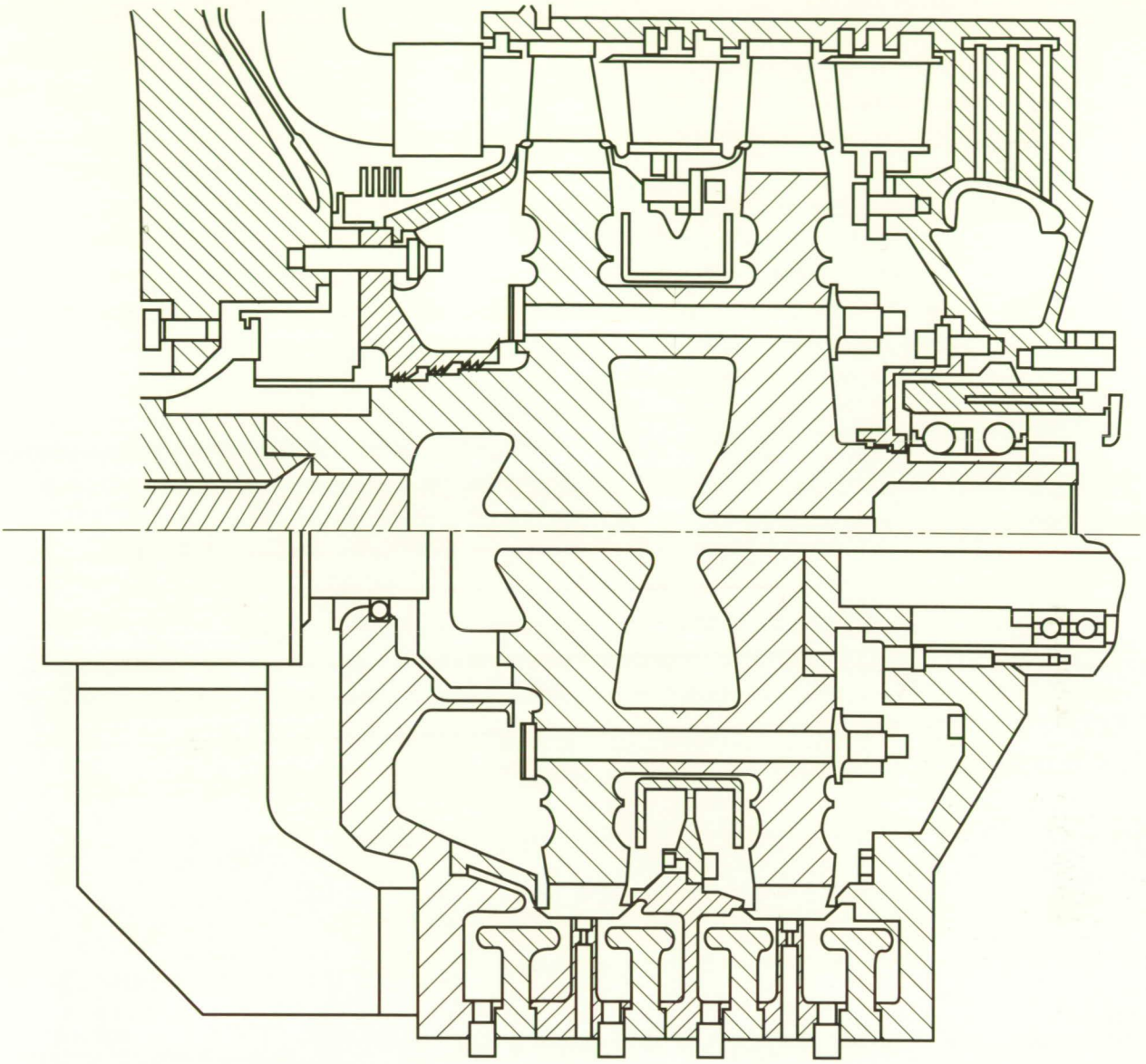

Figure 114. Comparison of Full-Scale Space Shuttle Main Engine Turbine Disk with Large-Scale Model

Although the current computational fluid dynamics (CFD) codes predict well many of the aerodynamic characteristics of flow around rotating disks, the mixing of swirling, variable-density flows, and the mass transport through rotating seals are not well predicted. The deficiencies are attributed to phenomena in the mixing process not included in the current *K*-turbulence model. The first experiments in this program will quantify the fraction of the flow from each of the sources (i.e., coolant injection location or gas path ingestion location) at many locations on the disk and cavity walls. Results from these experiments can be used to evaluate the CFD predictions of flow in the disks and heat transfer to the turbine disks.

G.A. Wilhold/ED31
(205) 544-2651
Sponsor: Office of Aeronautics and Space Technology

C-3

Engine Electromechanical Propellant Control Effector System

The propellant control effector system (Fig. 115) is defined as an electromechanical actuator, control electronics, and a propellant valve. The propellant control effector system shall be sized for the maximum control authority required for the Space Transportation Main Engine (STME). The control system, including the controller and actuators, must have sufficient precision to achieve engine start and to provide continuous throttle of the engine in 10-percent increments from 50- to 100-percent thrust levels. The actuator shall be a bolt-on unit to the valve to allow actuator commonality for all valves. The system shall be designed to operate using 28-volt direct current power to be supplied from an external source. The system shall be designed to prevent a single point electrical failure from rendering the system inoperative or causing an engine failure. Serviceability, maintainability, low cost, and reliability are features that should be reflected in the design. Mechanical component reliability may be achieved through conservative design or redundancy.

The objective of this program is to demonstrate the feasibility of a low recurring cost, highly reliable, electromechanical fuel and oxidizer control system applicable to the STME and Space Transportation Booster Engine system. The use of electromechanical propellant control systems will negate problems and cost associated with conventional hydraulic contamination, hardware change out, and extensive servicing requirements inherent with hydraulic systems. Enhancement in the solid state switching technology can make the high performance electromechanical control system competitive with the conventional hydraulic system and will eliminate the necessity for expensive, complex hydraulic power units. The reliability of electromechanical control systems can be enhanced with respect to conventional hydraulic systems by the elimination of contamination-induced failure modes. Demonstration and validation will be accomplished through the fabrication and test of a large-scale prototype system.

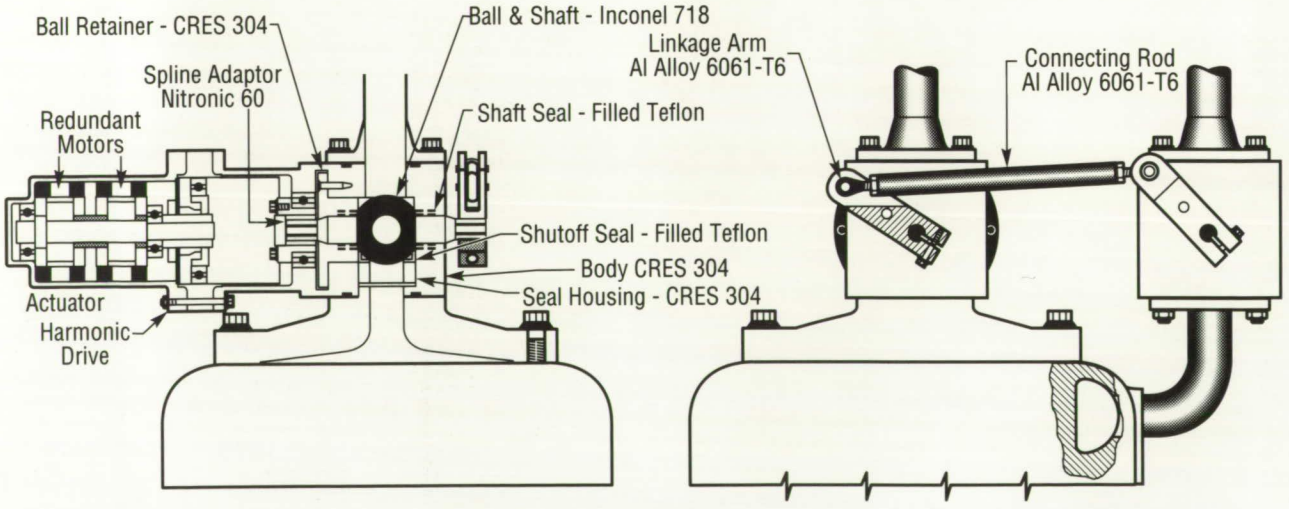

Figure 115. Propellant Control Effector System Hardware

Design simplicity and robust components are features that make the electromechanical actuator a low-cost, reliable, maintenance-free unit. Brushless direct current motors are selected to drive the actuator because of the following superior characteristics:

- *High torque capability*
- *High reliability*
- *Competitive cost*
- *Reduced EMI generation*

The motor drive electronics consist of two identical electrically isolated channels. Each channel is a three-phase, six-step, full-wave closed-loop controller. Power metal oxide semiconductor field effect transistor switches will be used instead of bipolar transistors because of their extremely fast switching capability and low on-resistance. The harmonic drive gear unit is preferred over multistage epicyclic spur and worm gearing because of its high single-stage speed reduction ratio, compact size, efficiency, and low parts count.

Performance, cost, and reliability studies are augmented by test results to ensure that the selected designs are the lowest cost approach that will meet performance and reliability requirements. Performance studies provide guidance in the areas of flow characteristics, forces, leakage, component sizing, positioning, and stability in support of the design evolution. Typical configuration studies involve evaluation of options by a combination of qualitative and quantitative inputs and design layouts. The fabrication and process studies are focused primarily on components. Alternatives regarding material selection, forming methods, joining methods, and tolerances fall into this category.

M. Cash/EP64
(205) 544-4282
Sponsors: Office of Space Flight
Strategic Defense Initiative Organization
U.S. Air Force/Space Division

Three-Dimensional Turbopump Flowfield Analysis

The overall objective of this program is to develop, implement, and verify a computational fluid dynamics (CFD) code which will predict the transient, three-dimensional (3-D), viscous flow in the Space Shuttle Main Engine turbopumps. An unsteady, 3-D, thin-layer, Reynolds-averaged Navier-Stokes code developed at Ames Research Center by Dr. M.M. Rai* to simulate unsteady flow in a turbine stage is being used as the core CFD code for the present application. The unsteady flow prediction capabilities of this code have been demonstrated by Rai* through comparisons against the unsteady and the time-averaged loadings on airfoil surfaces in a turbine stage. The viscous flow prediction capabilities of this code are being verified and enhanced as a part of this program. A steady cascade version of this code (RAI2DC) has been developed to permit evaluation of the viscous flow prediction capabilities against available benchmark quality data. The cascade version also permits the development of new turbulence models for this code in a cost-effective manner.

The turbulence model in this code was modified to simulate transitional flows on the airfoil surface and to account for the effects of high free-stream turbulence level on the turbulent viscosity.

The effect of the turbulence model on the airfoil surface static pressure distribution is shown in Figure 116. Theoretical calculations were conducted for a high-turning airfoil by assuming both a transitional and a fully turbulent flow on the airfoil surfaces. These predictions are compared to the measured experimental data in Figure 117. The transitional calculation indicates the presence of a separation bubble on the airfoil pressure side and yields better agreement with the airfoil surface static pressure distribution data than the turbulent calculation. The results presented in the first figure show the importance of modeling transition accurately, even to acquire good estimates of airfoil loadings.

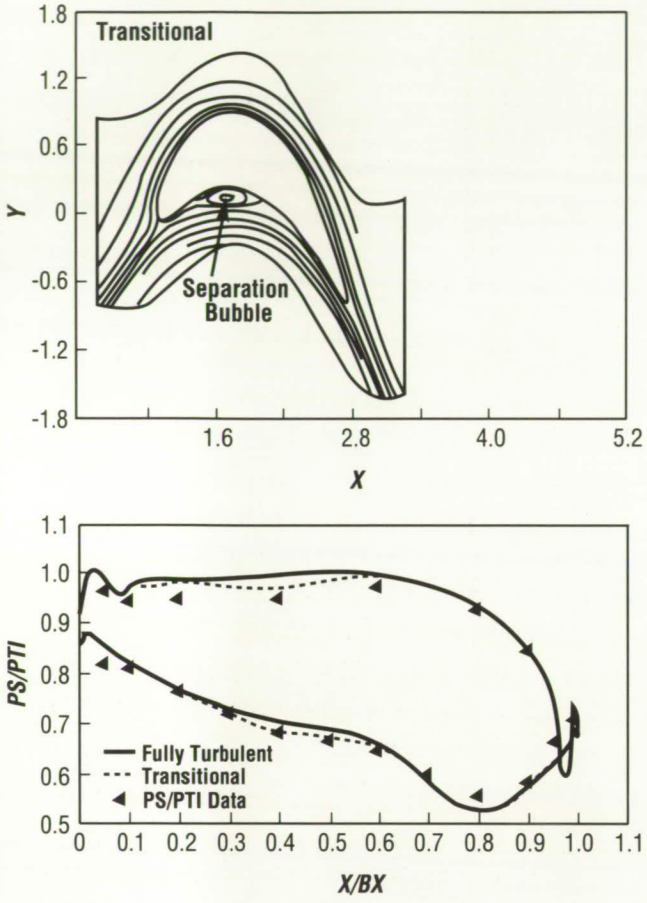

Figure 116. Effect of Turbulence Model on an Airfoil

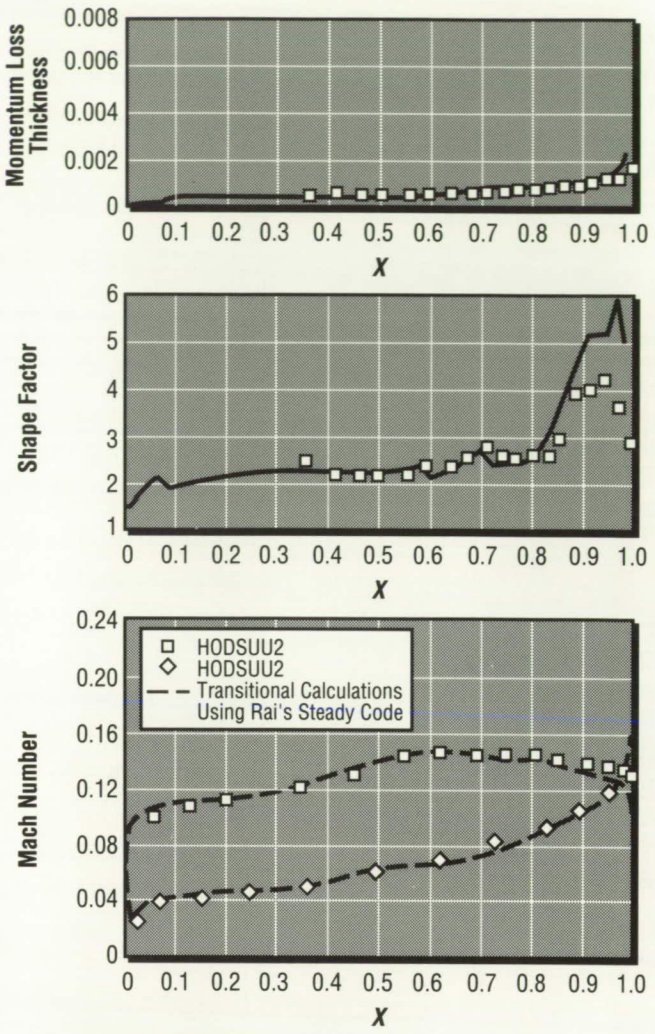

Figure 117. Viscous Transitional Flow Prediction Capabilities of RAI2DC Code

The viscous transitional flow prediction capabilities of this code are demonstrated in the second figure. Measured distributions of boundary layer momentum-loss thickness and shape factor on the suction side of the airfoil and the free-stream velocity on both the pressure and the suction side of the airfoil, tested in a cascade configuration†, are compared with theoretical predictions made by using the RAI2DC code. The code yields good estimates of both airfoil loads and boundary-layer characteristics, indicating that it has the potential of predicting aerodynamic losses generated on the airfoil surface. Measured data for surface static pressures and Stanton number on the midspan of the stator‡ were compared against theoretical predictions of the RAI2DC code. Both airfoil loadings and Stanton number distribution are well predicted by the code, indicating that it has the potential of predicting heat loads well, provided the transition can be predicted in a reliable manner.

The turbulence viscosity in the RAI2DC code was modified to account for the effects of high free-stream turbulence levels. Theoretical predictions conducted for the midspan of the rotor‡ were compared against the experimental data for the distribution of airfoil surface static pressures and Stanton numbers. The experimental data are shown to be in

good agreement with theoretical predictions which indicates that some time-averaged phenomenon (airfoil loadings, heat loads) may be fairly well modeled by using steady-flow prediction codes.

*Rai, M.M.: Unsteady 3-D Simulations of Turbine Rotor Interaction. AIAA Paper No. 2058, 1987.

†Hodson, H.P.: Unsteady Boundary Layers on an Axial-Flow Turbine Rotor Blade. Ph.D. thesis, Cambridge University, Cambridge, U.K., 1983

‡Dring, R.P., Joslyn, H.D., Hardin, L.W. and Wagner, J.H.: Turbine Rotor-Stator Interaction. J. of Engineering for Power, Vol. 104, Oct. 1982.

G.A. Wilhold/ED31
(205) 544-2651
Sponsor: Office of Aeronautics and Space Technology

Transient Fuel Preburner Operation

Several problems remain with the Space Shuttle Main Engine (SSME) fuel preburner (FPB) operation, such as cracking of the first and second stage blade shanks, of the blade root fillets, and under the blade platform. It is postulated that the extreme thermal environment during the start-up transient produces the initial blade cracks; severity of the cracks will depend on the specific transient operations the engine experiences. The cracks can continue to grow due to both high- and low-cycle fatigue as the number of turbine load cycles accumulates.

A computational fluid dynamics (CFD) model with finite-rate chemical reactions (FDNS2DR) has been developed to study the start transient of the SSME fuel preburner operation. FDNS2DR was benchmarked with three well-documented experiments: a confined swirling coaxial jet, a nonreactive ramjet dump combustor, and a reactive ramjet dump combustor. Excellent comparisons were obtained for the benchmark cases.

The code was then used to study the start transient of an axisymetric SSME FPB. At the start command, the initial flowfield of the fuel preburner was filled with atmospheric nitrogen purge gas. After the start command, the transient inlet flow properties were obtained from the Digital Transient Model. The transient FPB thermal flowfield calculation was carried out for 1 second and for a nominal start. A comparison of the calculated FPB start-up transient temperature history at the FPB exit with the measured turbine inlet temperature history is shown in Figure 118. Calculated temperature transients are given at two locations: the middle of the exit line and at the exit on the Kaiser-hat wall. The measured turbine inlet temperature is represented by thermocouples located near the inboard side of the turbine inlet and is between the baffles, so that three-dimensional effects are minimized. Both the calculation and the measurement showed a peak at about 0.5 seconds, and a second peak at about 0.7 seconds. The temperature was greatly reduced as the time approached 1 second. Excellent agreement was

obtained for the temporal occurrence and magnitude of the temperature spikes. Also, it was found that an appreciable amount of unburned oxygen entered the turbine stages. These results cannot be obtained from a steady-state CFD thermal flowfield simulation.

The significance of this study is that a time accurate CFD design tool has been developed to accurately predict the severe thermal gradients which are impressed upon the fuel preburner and turbine during the start transient. Previously, various factors were suspected of causing the ignition temperature spikes, such as the collection of unreacted propellants, a mismatch of the fuel and oxidizer supply rate, and a mixture maldistribution prior to and during ignition. These factors can now be studied with numerical experiments performed with FDNS2DR to alter both the ignition and shutdown characteristics in order to attenuate thermal loads.

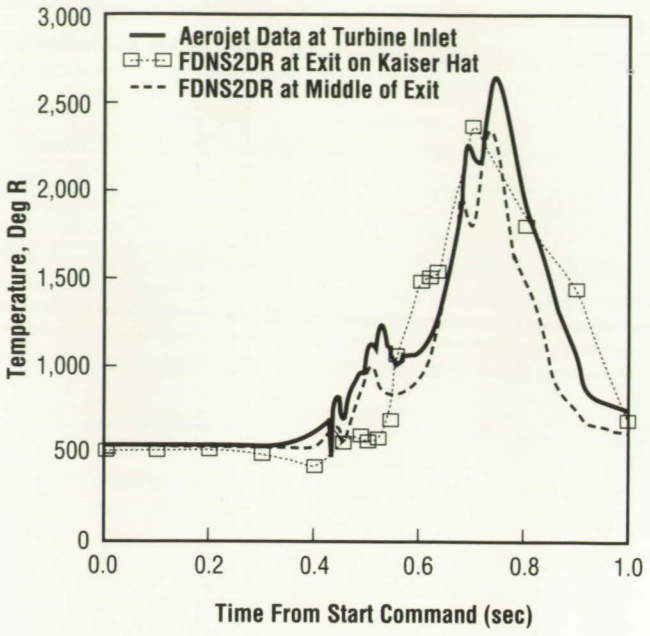

Figure 118. Comparison of Temperature History at Calculated Fuel Preburner Exit and Measured Turbine Inlet

Wang, T.S., Chen, Y.S. and Farmer, R.C.: Investigation of the Transient Fuel Preburner Manifold and Combustor. Final report, Contract NAS8-37461, Report No. SECA-89-10, SECA, Inc., June 1989.

G.A. Wilhold/ED31
(205) 544-2651
Sponsor: Space Shuttle Main Engine Project Office

Turbine Rotor-Stator Interaction

An implicit Navier-Stokes procedure using a single deforming mesh is being developed for analysis of the unsteady rotor-stator interaction problem. Details of the flow pattern in the Space Shuttle Main Engine high-pressure fuel turbine may significantly influence the turbine blade structural integrity due to both the unsteady forces produced by relative blade motion and the blade leading edge and platform heat transfer. The present technique uses a deforming mesh region between the stationary (stator) and rotating (rotor) blade rows. The system of partial differential equations representing the conservation of mass, momentum, and energy are written, along with an equation of state and a suitable turbulence model, using a second-order finite difference formulation. The resulting equations are linearized and then solved using a linearized block implicit algorithm. The scheme has been enhanced to permit optional iteration at each time step in both two- and three-space dimensions in order to improve transient accuracy.

Additional solution procedure, boundary condition, and grid generation improvements have been implemented in order to analyze the three-dimensional unsteady rotor-stator flow problem. Two-dimensional computations for a large scale turbine have been completed,* and a representative grid and static pressure contours are shown in Figure 119. The calculated pressure distributions are compared with the available time-averaged experimental data† in Figure 120. The three-dimensional unsteady calculation of the large-scale turbine flow field, including viscous sublayer resolution on the blades and endwalls, is currently in progress.

*Gibeling, H.J., Buggeln, R.C., Chen, S.Y. and McConnaughey, H.V.: An Implicit Navier-Stokes Analysis of Turbine Rotor-Stator Interaction. AIAA Paper, Vol. 88, No. 3090, July 1988.

†Dring, R.P., Blair, M.F. and Joslyn, H.D.: The Effects of Inlet Turbulence and Rotor/Stator Interactions on the Aerodynamics and Heat Transfer of a Large-Scale Rotating Turbine Model. Vol. IV – Aerodynamic Data Tabulation. NASA Contractor Report 179469 (UTRC–R86–956480–4), November 1987.

G.A. Wilhold/ED31
(205) 544-2651
Sponsor: Office of Aeronautics and Space Technology

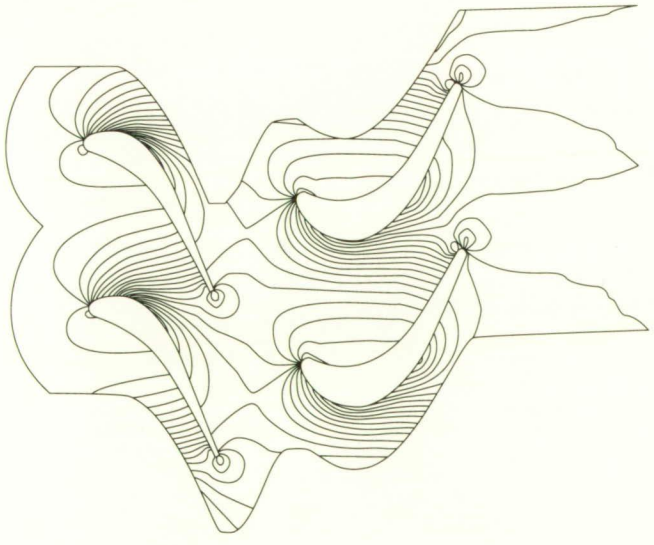

Figure 119. Static Pressure Contours

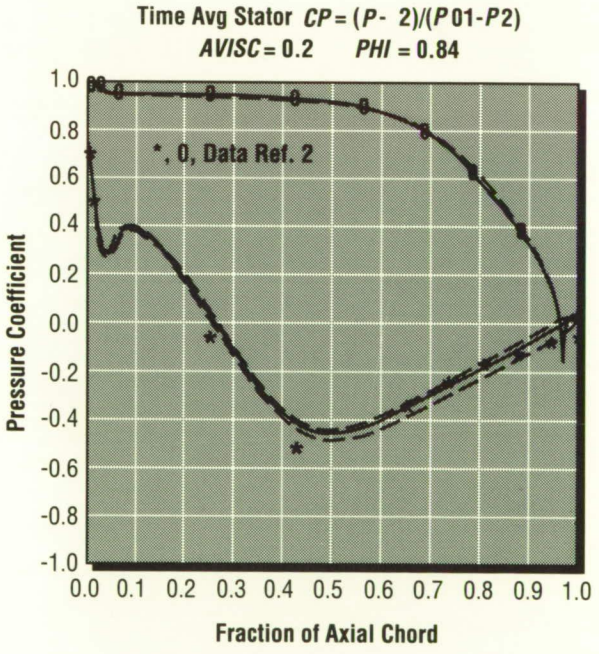

Figure 120. Stator Unsteady Pressure Envelope

Unsteady Wake Flow of a Liquid Oxygen-Tee Vane

Unsteady wake flow (vortex shedding) downstream of the trailing edge of a liquid oxygen (LOX)-Tee vane of the Space Shuttle Main Engine (SSME) can excite the structural vibrations of the vane and other components. This effect is even more pronounced when the vortex shedding frequency is in-phase with the natural frequency of the structural mode.

Numerical study of the unsteady wake flow characteristics was undertaken in FY89 to investigate the effects of flow conditions and boundary geometries on the vortex shedding frequencies downstream of the LOX-Tee vane. A time-accurate finite-difference Navier-Stokes flow solver was employed in this study. This flow solver features a pressure-based predictor plus multicorrector solution method with a time-centered time-marching scheme. To validate the numerical accuracy and computational efficiency of this flow solver, some laminar and turbulent benchmark cases were tested with successful results.

Results of this study (Fig. 121) revealed that the LOX-Tee vane with the original round trailing edge could produce a vortex-shedding frequency very close to the natural frequency of the vane (4,000 Hz) when there was a velocity difference between both sides of the vane at the flow inlet. For the modified trailing edge, a much higher vortex-shedding frequency with less amplitude of the lift oscillations was predicted. To make the analysis complete, application of the present flow solver to a full three-dimensional LOX-Tee geometry is currently under preparation.

Chen, Y.S., Anderson, P.G., Farmer, R.C. and Reske, E.J.: Numerical Simulation of Unsteady Wake Flow Downstream of a LOX-Tee Vane. Seventh SSME Working Group Meeting, MSFC, April 25–27, 1989.

G.A. Wilhold/ED31
(205) 544-2651
Sponsor: Space Shuttle Main Engine Project Office

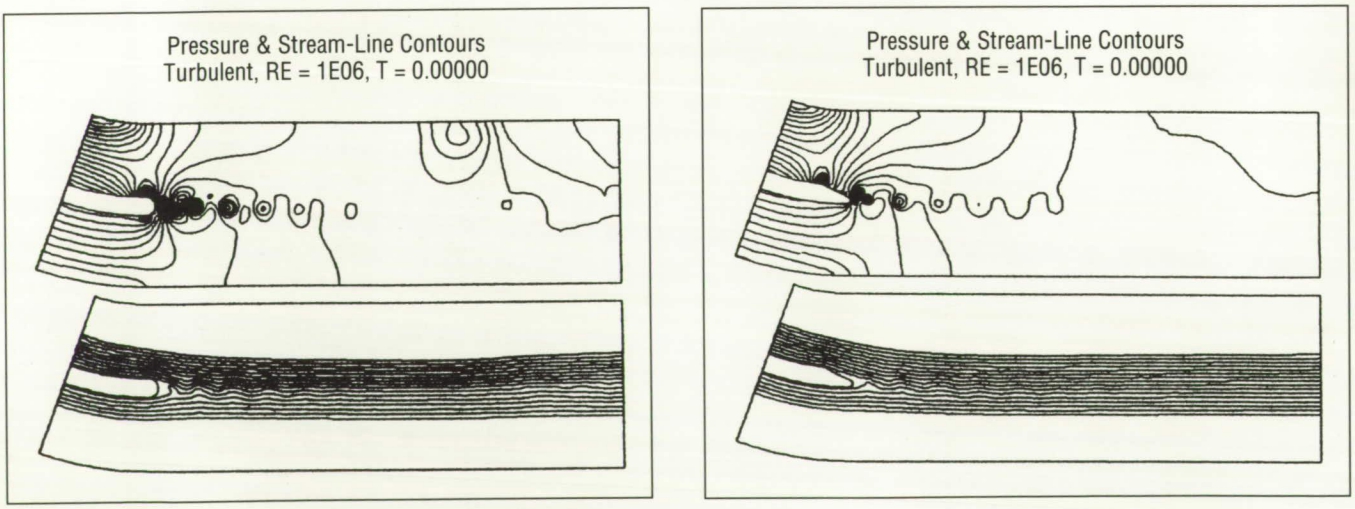

Figure 121. Unsteady Wake Analysis of a LOX-Tee Vane

Variational Principles for Computational Fluid Dynamics Methodology

The concept of this study is to develop accurate and efficient computational fluid dynamics (CFD) algorithms for production-type analyses of viscous/turbulent, multicomponent, combusting flows. Convergence of the solution methods could be accelerated by using criteria developed based on variational principles. Initial investigation revealed that the mechanics of a variational solution involved a predictor-corrector calculation in which a time-advanced approximation is corrected by requiring that certain constraint equations be satisfied to obtain the final solution. It was determined that the time advancement step should most efficiently be accomplished with a rigorous upwind algorithm which evaluated wave propagation along characteristic directions. An upwind, explicit algorithm (GWIND) and an upwind, implicit algorithm (FDNS) were developed and were found to give excellent solutions without requiring additional correction steps.

During FY89, an extensive set of validation cases were run to evaluate these codes. Boundary layers, backsteps, blunt bodies, nozzles, and plumes are being investigated. Typical results of predicted pressure fields compared to experimental data are shown in Figure 122(a) for three-dimensional, Mach 8 flow past a spherical cylinder blunt body, and in Figure 122(b) for three-dimensional, Mach 5.835 flow over an Aeroassist Flight Experiment model. For the nozzle plume problems, results have shown the significant effect of the mass conservation condition on the shape of the Mach disc. Figure 123 shows the solutions of a laminar, 1.25 specific-heat ratio, nozzle flow of a conical nozzle at sea level. Another test case of turbulent flow inside the nozzle of the Space Shuttle Main Engine (SSME) at sea level with variable specific-heat ratio was also studied. Results of the SSME nozzle flow solutions were in good agreement with that predicted by the method of characteristics. Validation cases involving heat transfer and chemical reaction modeling are currently under investigation.

G.A. Wilhold/ED31
(205) 544-2651
Sponsor: Small Business Innovative Research Program

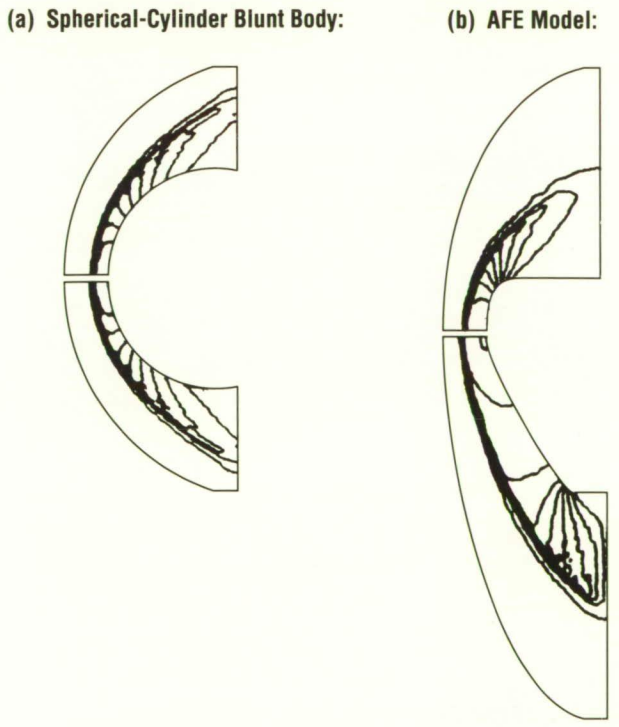

Figure 122. Pressure Contours of Supersonic Blunt Bodies

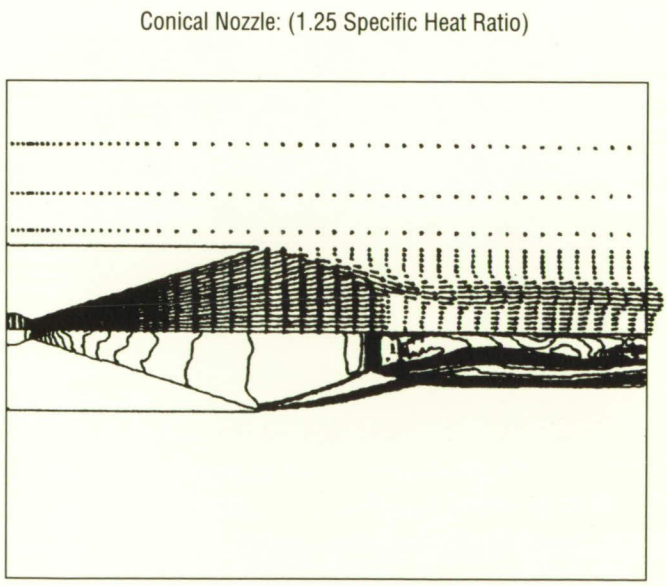

Figure 123. Nozzle Flow Simulation

Turbine Rotor Heat Transfer Studies

Extensive efforts at MSFC and throughout the turbomachinery community are currently underway to improve available techniques for prediction of turbine-passage aerodynamics and heat transfer. Of particular relevance to rocket propulsion is the need to accurately predict thermal load distributions for the unsteady, highly three-dimensional flows that inherently exist in turbine rotor passages. The present study is designed to provide experimental rotor-passage heat-transfer distribution data to be used for evaluation of these newly-developed predictive tools.

The investigation is being conducted in the United Technologies Research Center Large Scale Rotating Rig (UTRC LSRR). This facility (Fig. 124) is a large-scale turbine model which closely matches most of the important dimensionless parameters of the Space Shuttle Main Engine (SSME) High Pressure Fuel Turbopump drive turbine. The large scale of this turbine model permits the measurement of local details of the passage heat transfer that cannot be documented in a hardware-scale test. Both the steady and unsteady aerodynamics of this turbine-passage flow field have been extensively documented with the results available in the open literature.*

Heat transfer data for this program will be obtained using a heated-wall model of one complete rotor passage. The model consists of two instrumented airfoils: one instrumented on its suction surface, and one on its pressure surface and an instrumented hub end-wall. A complete description of the heat transfer measurement technique exists.*

Fabrication and instrumentation of the rotor-passage heat transfer model was completed during FY89. The completed model is shown installed in the UTRC LSRR in Figure 125. Experimental testing started recently with the rotor-passage model in

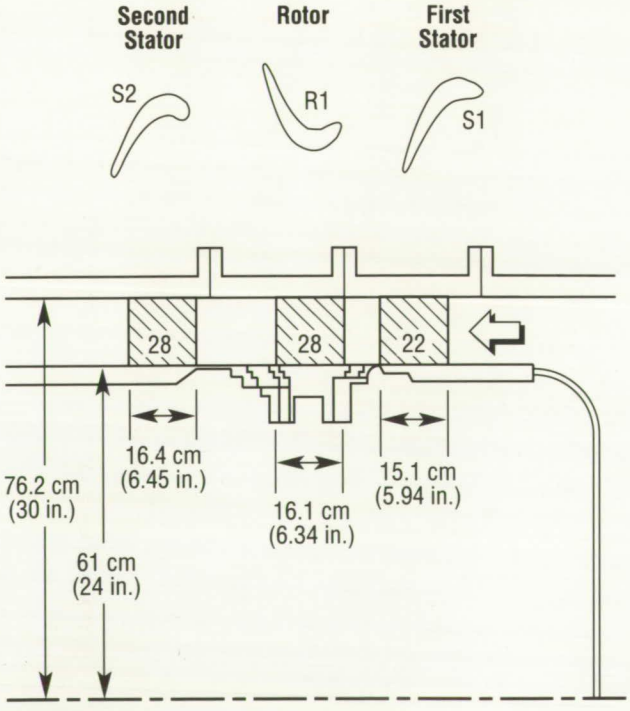

Figure 124. Large Scale Rotating Rig Geometry

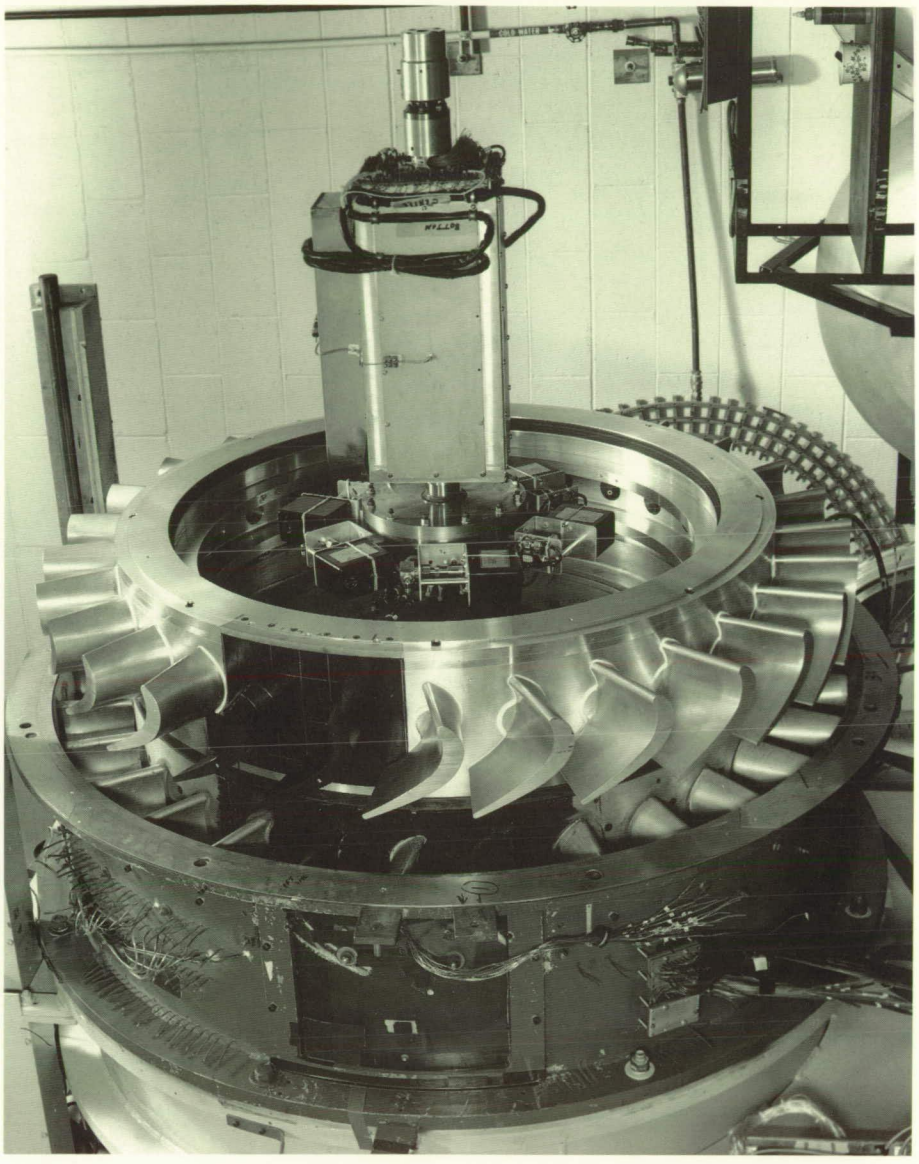

Figure 125. Rotor Passage Heat Transfer Model Installed in Rig

a smooth-wall configuration. For these tests, heat transfer data were obtained using both arrays of thermocouples on the heated model skin and through high-speed photography of liquid-crystal surface temperature patterns. Data were obtained for airfoil Reynolds numbers ranging from 2.2 x 10^6 to 5.7 x 10^6 and for rotor-relative inlet angles from 40 to 57 degrees. Reduction and analysis of the data is currently underway. Additional testing is to be conducted with the model surface roughened to simulate SSME airfoil hardware characteristics.

*Blair, M.F., Dring, R.P. and Joslyn, H.D.: The Effects of Turbulence and Stator/Rotor Interactions on Turbine Heat Transfer: Part 1 — Design Operating Condition, and Part 2 — Effects of Reynolds Number and Incidence. ASME J. of Turbomachinery, Vol. 3, pp. 87–103, January 1989.

G.A. Wilhold/ED31
(205) 544-2651
Sponsor: Office of Aeronautics and Space Technology

Efficient Navier-Stokes Flow Prediction Algorithms

A computational method of increased accuracy and efficiency is being developed for solving the Navier-Stokes equations for steady and unsteady viscous flow in two (2-D) and three dimensions. The investigation is motivated by the need to predict practical internal flows in complex geometries and flows having complex structures with multiple length scales. The overall objective is to develop a method which can meet two different objectives encountered in engineering applications at MSFC. In the first case, an accurate calculation with good viscous resolution is needed, for which a carefully constructed grid is available. In the second case, the objective is to obtain qualitatively accurate results and trends in a short time frame. This may require the use of distorted grids or less than ideal flow resolution. The investigation will develop an efficient, accurate, and reliable computational methodology for the Navier-Stokes equations, and will implement and test these techniques within a modified version of the Scientific Research Associates (SRA) Navier-Stokes code.

Part of this study has employed simple model problems for comparison of numerous spatial differencing techniques on nonsmooth grids, and for matrix analysis of the convergence of several schemes, with and without iteration at each time step. Preconditional artificial compressibility methods have also been developed and tested.

A modified version of SRA's Navier-Stokes code for testing alternative spatial difference procedures and solution algorithms has been completed, and test calculations for a number of different methods are in progress. The spatial differencing techniques being studied include both generalized physical space differencing derived from multidimensional Taylor expansions, finite volume techniques, and techniques based on coordinate transformations. Adjustable matrix dissipation terms based on ideas similar to those used in deriving upwind schemes, have been developed for use with these centered schemes. A number of implicit solution algorithms have now been implemented, including methods based on ADI schemes, line relaxation, and approximate LU factorizations.

Flow calculations have been performed for a test problem (2-D laminar incompressible flow past a rounded leading edge) using two different grids, chosen to test the ability of the solution procedure to meet the differing objectives of high accuracy, or qualitative accuracy, with a nonoptimal grid. The first grid is smooth, carefully constructed, and stretched to provide adequate resolution of both the free-stream, Heimenz layer at the stagnation point, and shear layer development. The second grid is distorted by "wiggles" in the grid lines and has discontinuous variation of cell size. Grid stretching is removed to provide a coarse mesh spacing and inadequate viscous resolution near the wall.

The flow in Figure 126 is adequately resolved using the smooth grid with high wall resolution. By comparison, the flow in Figure 127 has good qualitative accuracy despite the distorted grid and poor wall resolution. Both cases converge rapidly, with three to four orders of residual reduction in about 100 iterations. For flows of the type devised in this test problem, this solution procedure seems well suited for obtaining both accurate results on a carefully constructed grid and also good qualitative results on distorted grids with inadequate resolution.

G.A. Wilhold/ED31
(205) 544-2651
Sponsor: Small Business Innovative Research Program

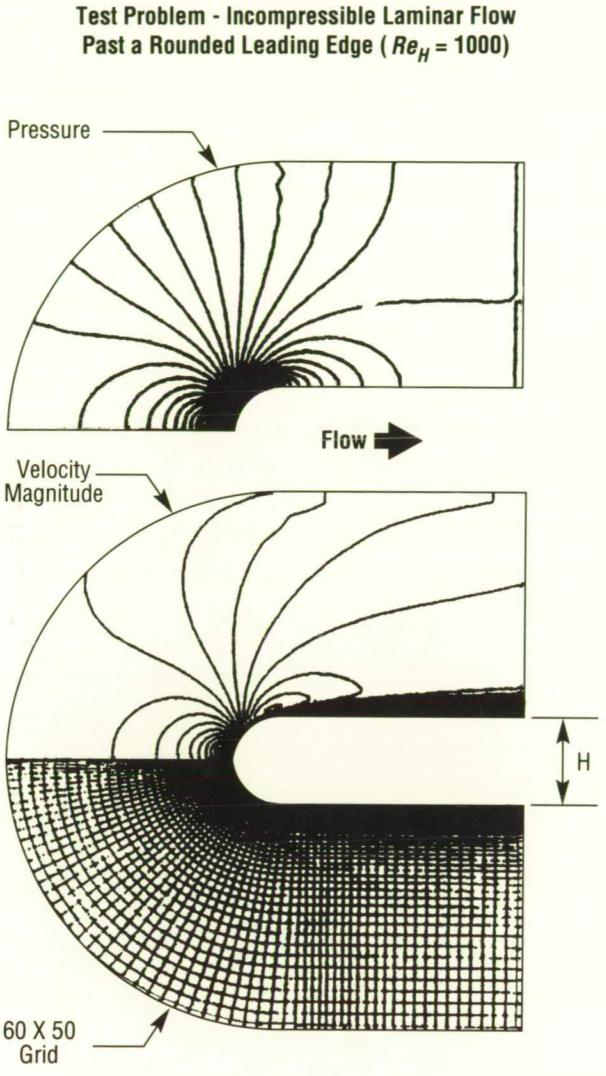

Figure 126. Smooth Grid with Good Viscous Resolution

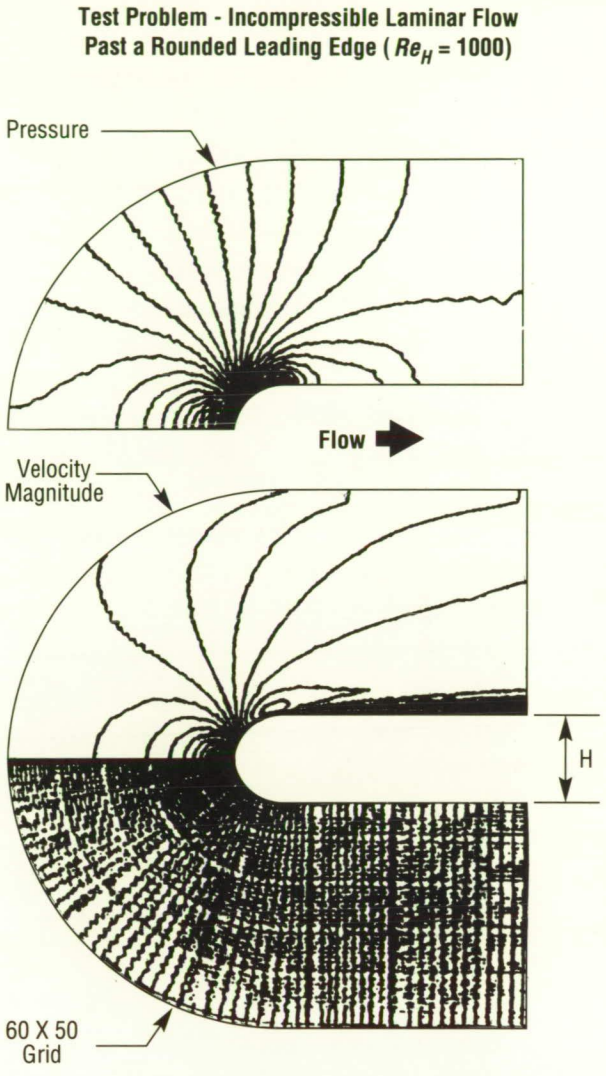

Figure 127. Distorted Nonsmooth Grid with Poor Viscous Resolution

Ball Bearing Coolant Flow Tests

The Space Shuttle Main Engine turbopumps require a unique solution to bearing cooling because of high rotational speeds, high loads, and cryogenic environment. These bearings are cooled by liquid oxygen or liquid hydrogen flowing through them, resulting in a completely submerged bearing. Recent evidence of bearing over-heating prompted questions concerning the cooling effectiveness, fluid dynamic environments, and induced hydrodynamic loads. Two water flow test rigs were designed and fabricated to investigate fluid dynamics inside the liquid oxygen turbine end ball bearing duplex pair.

The first water flow rig (Fig. 128) is a superscale (5.71 X) acrylic rig containing a set of acrylic bearings capable of operating up to 300 rpm and at 284 L/minute (75 gal/minute). This model has been used for flow visualization by injecting dyes and illuminating "cross sections" of the flow with a laser sheet. The rig is currently fitted with pressure taps which are being used to measure differential pressures from the coolant injection jets to the lobe nut area.

The second is a full-scale stainless-steel rig using one actual high-pressure oxygen turbine end ball bearing capable of running up to 5,000 rpm, at 76 L/minute (20 gal/minute), and up to a 455 kg (1,000 lb) axial load. This rig is being used to measure the developed pressure differential or "pumping" generated across the bearing. The rig was purposely designed with symmetrical cavities on either side of the bearing to avoid rig-related pumping effects.

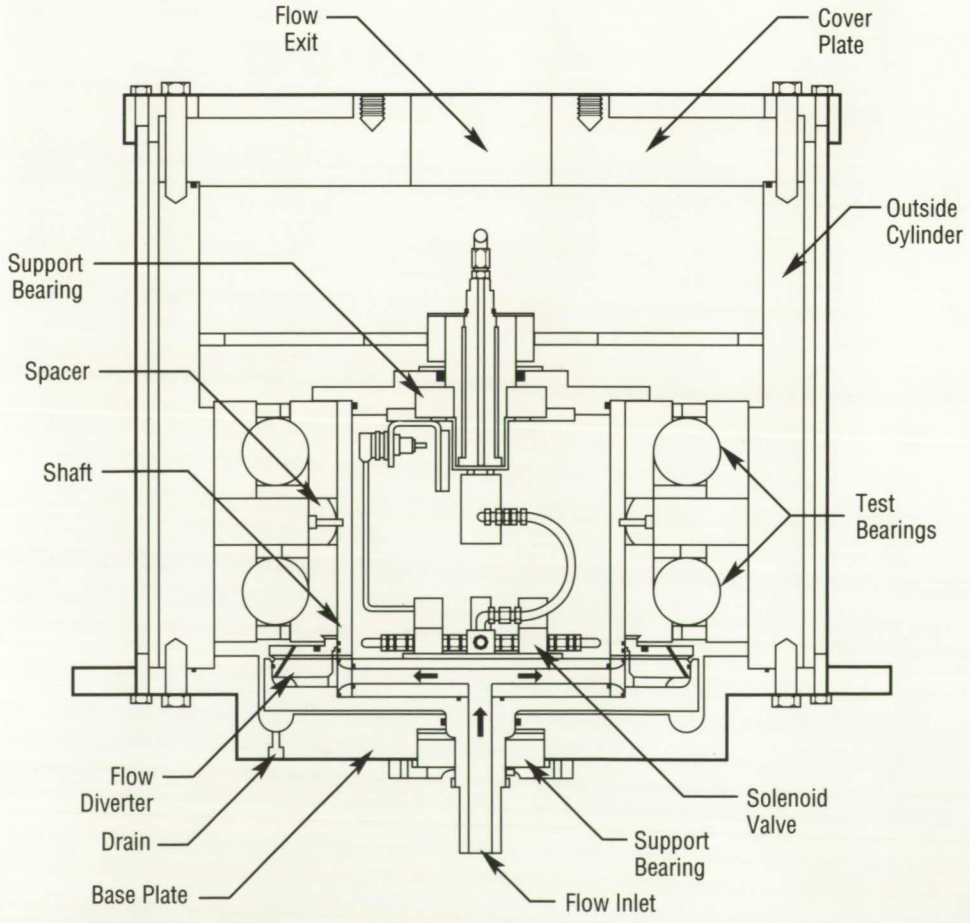

Figure 128. High Pressure Oxygen Turbopump Bearing Coolant Flow Model

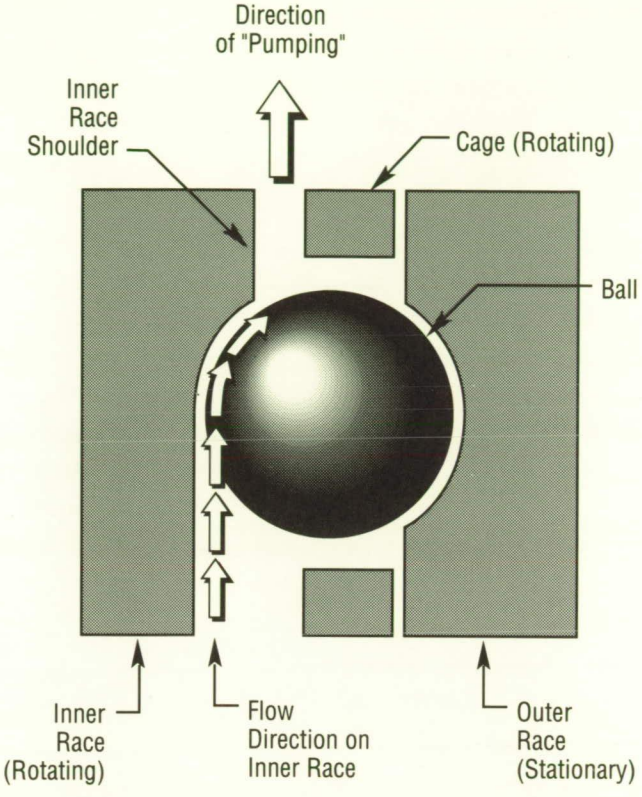

Figure 129. "Pumping" in Angular Contact Bearing

Because actual turbopump bearings operate in cryogenic liquids at high rotational speeds (30,000 rpm), results from water flow tests at low speeds must be scaled to engine conditions. This scaling utilizes nondimensional parameters to ensure geometric, kinematic, and dynamic similarity. For these bearing rigs, the independent nondimensional parameters are the flow coefficient (also referred to as "Q/N" or the Rossby number) and the Reynolds number. The rigs are operated at a flow coefficient equal to that of the engine, but at a lower Reynolds number. Reynolds number effects are currently being evaluated in detail, but results to date indicate insignificant Reynolds number effects (turbulent regime). With a matched flow coefficient and a turbulent Reynolds number, a pressure coefficient is used as the dependent nondimensional parameter to scale the rig measured pressures.

Results from tests conducted with both rigs show that the high-pressure oxygen turbine end bearings do "pump." This "pumping" is in the direction of the inner race shoulder (Fig. 129) and is a function of shaft speed and bearing axial load. Dye injected on the inner race showed that the flow is centrifugally forced radially outward across the inner race shoulder. This unsymmetrical surface is believed to be the major contributor to the "pumping" of these angular contact bearings. With these results and results of continued testing, better predictions of bearing coolant flow rates can be made; ways to utilize the natural "pumping" of the bearings to improve cooling effectiveness can be developed; and cage hydrodynamic loads can be determined.

W.J. Bordelon, Jr./ED33
(205) 544-1579
Sponsor: Space Shuttle Main Engine Project Office

Turbulent Shearing Flow in a Highly Curved Channel

The modeling of turbulent shear flow in a highly-curved channel requires information about the kinetic energy, dissipation, and production of the turbulent flow. More refined modeling will require knowledge of the higher moments of the Reynolds stresses, pressure fluctuations, and surface shear stress fluctuations. This research is directed at the documentation of the flow-field in a highly-curved region. A detailed set of mean and turbulent data was obtained for a 180-degree, small radius of curvature bend. The motivation for the program was to better understand the flow in the Space Shuttle Main Engine turnaround duct.

A special two-dimensional large scale acrylic duct was constructed to attach to a very large water flow facility capable of flowing 100 ft^3/s at a head as great as 61 m (200 ft) of water (6 atm). The duct was a 10 cm by 100 cm (3.9 in by 39.4 in) rectangular section with a 180-degree turn of centerline with a radius of curvature of 10 cm (3.9 in) (Fig. 130).

The mean and turbulent velocity field in the duct has been documented. Effects of Reynolds number, inlet conditions, and exit screens have been evaluated. The duct was operated over a Reynolds number range from 70,000 to 500,000. Detailed measurements of the surface static pressure, mean velocities, flow angles, tangential and radial turbulent velocities, and the turbulent Reynolds stress were made for a number of stations around the duct and over a range of Reynolds numbers. A separation bubble was found near the exit of the turn on the inner surface of the duct. The bubble was found to vary with Reynolds number. However, above a Reynolds number of 300,000, the separation bubble mean flow was insensitive to Reynolds number. The flow along the outer surface developed very large tangential and radial turbulent velocities. Near the exit of the turn the radial turbulent velocity component is approximately two times that of the tangential turbulent velocity.

Sandborn, V.A. and Shin, J.C.: Evaluation of Turbulent Flow in a 180-Degree Bend for Bulk Reynolds Numbers from 70,000 to 160,000. Colorado State University, Res. Memo. No. 51, June 1987.

Sandborn, V.A.: Facility for the Evaluation of Turbulent Flow in a 180-Degree, Small Radius Bend. Colorado State University, Res. Memo. No. 50, December 1986.

Sandborn, et al.: NASA Conference Report, in preparation.

J.P. Heaman/ED35
(205) 544-1642
Sponsor: Office of Aeronautics and Space Technology

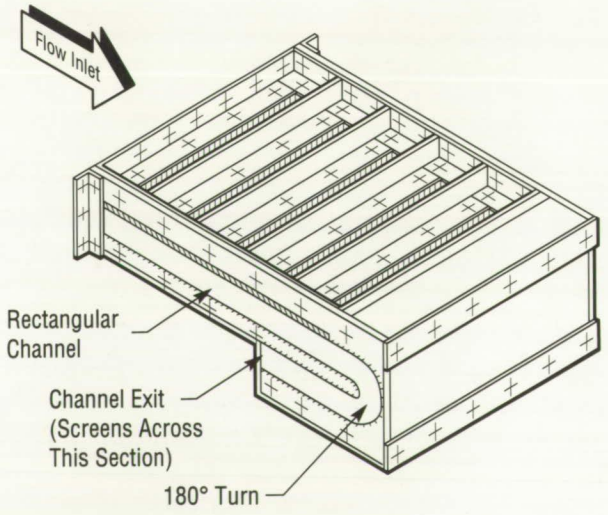

Figure 130. Schematic of the 180-Degree Turn Facility

Turbine Blade/Tip Seal Force Interaction — "Alford" Forces

The only known published test results on turbine blade tip clearance forces, sometimes referred to as "Alford" forces or clearance excitation forces, are those obtained from the test program conducted at the Technical University of Munich (TUM). Test results indicate that the measured forces are significantly larger than the predicted values. Direct correlation of test results with predicted destabilizing forces in the Space Shuttle Main Engine (SSME) turbines, however, is difficult to ascertain because of the difference in operating conditions and geometry of the test and the SSME hardware. The SSME turbopumps appear to be more stable than predicted by the TUM test results. This may be due to the presence of direct damping which theoretical and experimental results do not substantiate. It is, therefore, imperative that a comprehensive investigation be initiated to better define the forces generated at the turbine blade tip seal interface.

The overall objective of this effort is to generate the necessary data base from which a reasonably accurate model for predicting the turbine blade tip seal clearance excitation forces in the SSME turbopumps may be obtained. The first step was the work required under the original contract, NAS8-35018. Included in this effort was a thorough review of literature on turbine blade tip seal clearance excitation forces, the development of an analytical model for predicting these forces for both shrouded and unshrouded turbine blades, and the definition of a test program for measuring stiffness and damping coefficients. The next step was to design, fabricate, and checkout a test article and facility to measure the turbine blade tip seal force interactions. This is being accomplished by an extension to the original contract. The third and final phase is the actual empirical investigation of "Alford" forces.

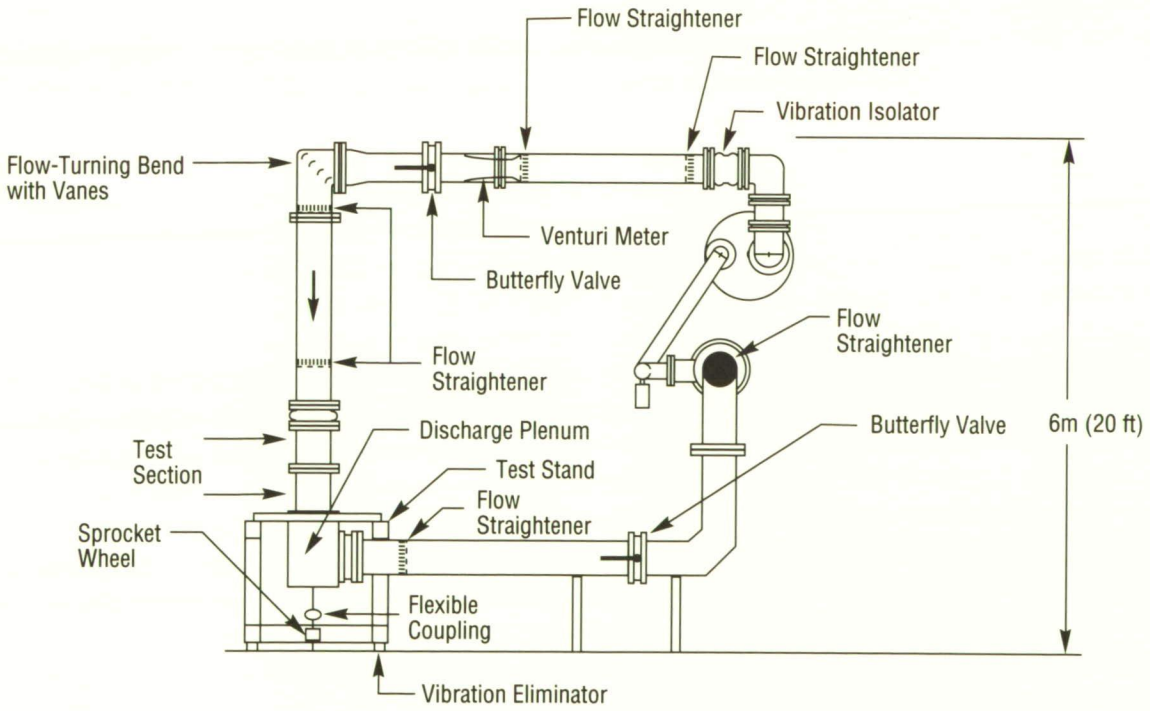

Figure 131. Front View of Test Facility

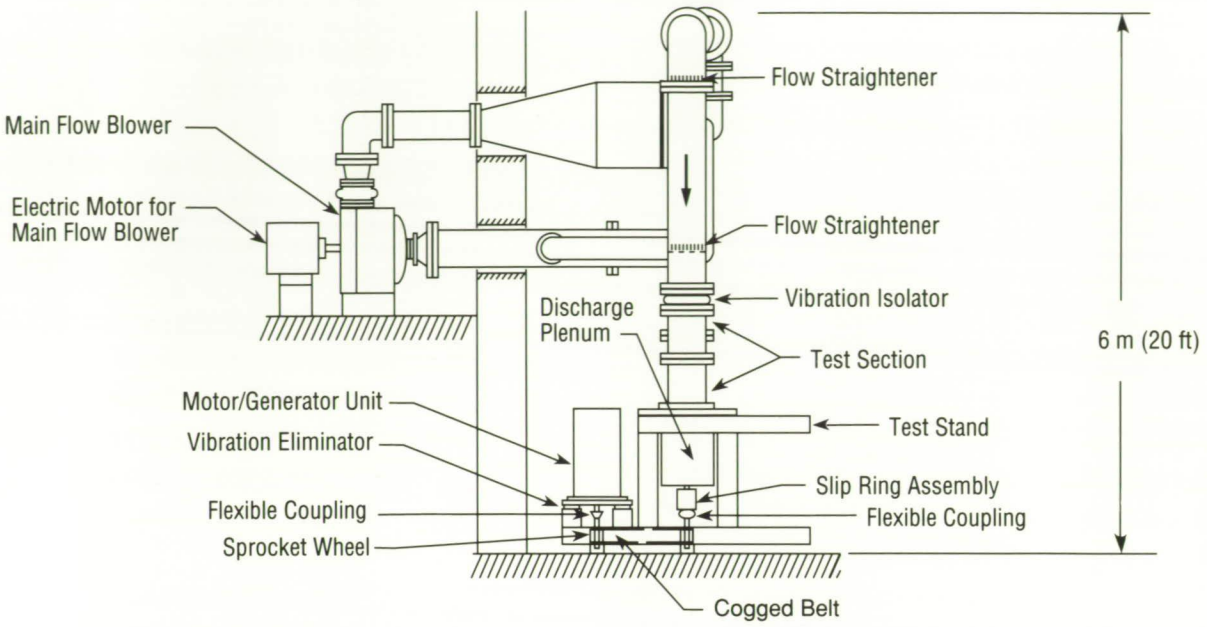

Figure 132. Side View of Test Facility

The first phase of this effort was completed and completion of phase II, the design, fabrication, and checkout of the test article and facility, is in the final construction and checkout stages. The Massachusetts Institute of Technology responded to a procurement request for the third and final phase with a proposal. The final phase contract has been signed and funding initiated. It is anticipated that the actual empirical investigation will begin in FY90.

The test facility (Figs. 131 and 132) and test article, now nearing completion, will be used to investigate the level of "Alford" forces within the SSME high-pressure turbomachinery.

The empirical results will be used to adjust the analytical model to provide a more accurate tool to be used to predict these destabilizing forces within the SSME turbopumps and other similar machines.

G.E. Wilmer, Jr./EP62
(205) 544-7115
Sponsor: Office of Aeronautics and Space Technology

Transpiration Cooling of Hydrocarbon Rocket Engine Nozzle Throats

Hydrocarbon rocket engines employing RP-1 and propane as fuels, and which use these fuels as combustion chamber coolants (regenerative cooling), are limited as to the maximum chamber pressure that can be achieved. As chamber pressure is increased, the chamber wall heat flux to the coolant increases. The limit is reached when the coolant heat flux drives the wall temperature to a value which causes the chemical structure of the coolants (fuel) to change, resulting in the deposition of a carbon layer (coking) on the coolant wall surface. This carbon layer acts as a thermal insulator, preventing the heat from the combustion chamber from reaching the coolant. Since this carbon layer is on the coolant side of the hot wall instead of the hot gas side, it provides no protection for the wall and will drive wall temperatures up to levels at which the wall material strength begins to decrease. If driven far enough, this will result in wall material failure.

Keeping the coolant wall temperature below the coking level requires increasing the coolant velocity, which in turn increases pressure drop in the coolant system circuit. As coolant velocities increase, the coolant pressure drop increases very rapidly to a point which cannot be accommodated by realistic pump supply pressures. When holding coolant velocities constant at the maximum practical level, further increases in chamber pressure will drive the wall temperature above the coolant coking limit and will ultimately reach the wall material strength limit, causing failure of the wall.

One method under investigation for allowing operation at chamber pressures above the regenerative cooling coking limit is to use the fuel as a transpiration coolant in the throat region of the nozzle. Transpiration cooling will cool the throat surface by convective cooling and by forming a film barrier on the throat surface. Analysis has shown that over half of the coolant system pressure drop occurs in the nozzle throat region. Transpiration cooling this region removes it from the regenerative cooling circuit and thus reduces the coolant circuit pressure drop significantly. If this pressure drop reduction is used to increase chamber pressure, additional performance may be achieved.

Figure 133 indicates the results of an analytical study which shows that specific impulse increases may be achieved by the transpiration cooling of various nozzle throat section lengths for engines using the hydrocarbon propellants RP-1 and methane. The analysis indicates that for a nominal transpiration-cooled length of 12.7 cm (5 in), the greatest specific impulse gain (4 s) may be achieved with oxygen/methane propellants using methane as the transpiration coolant. For similar transpiration-cooled section lengths, using RP-1 as a transpiration coolant offers only a very small specific impulse gain. If the oxidizer is used as transpiration coolant instead of the RP-1, considerably more specific impulse gain is indicated. Propane as a transpiration coolant does not offer any specific impulse gain.

F. Braam/EP52
(205) 544-7055
Sponsor: Office of Aeronautics and Space Technology

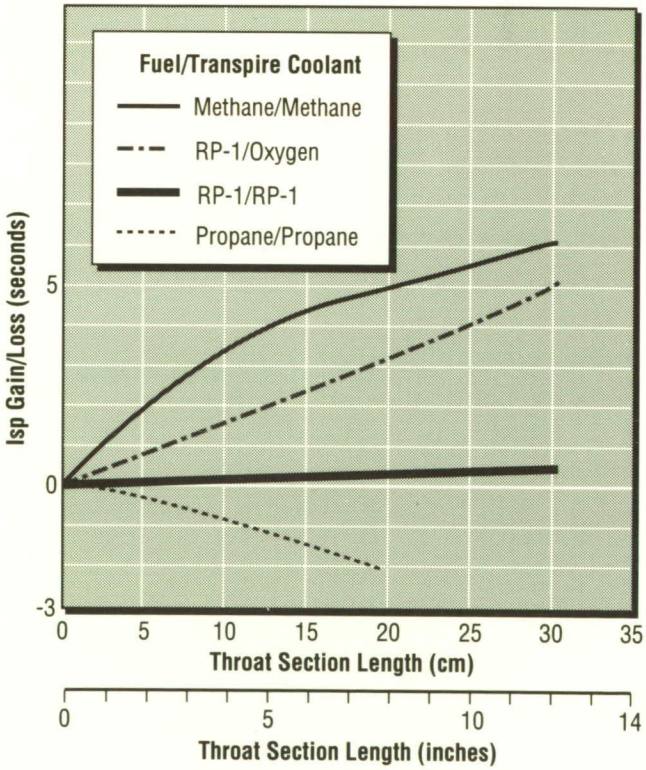

Figure 133. Performance Versus Nozzle Throat Transpiration Cooled Length

Numerical Analysis of Rotor-Stator Interactions

The fluid flow within a turbomachine is extremely complicated. The flow is inherently unsteady due to relative motion between rotor and stator airfoils. To numerically simulate this unsteady flow, the solution method should not only treat the rotor and stator as a single system, but should also be sufficiently accurate in space and time. Recent work in rotor-stator interactions*†‡ uses a zonal approach to discretize the physical domain. Relative movement between different zones is allowed to simulate the relative motion between the rotor and stator.

The current study focuses on the examination of the plurality of spinning modes that are present in rotor-stator interactions and the effect of inlet and exit boundary conditions on the time-varying components of the flow field. In particular, the propagation of the various modes is analyzed and appropriate grid spacing chosen in the upstream and downstream regions to attenuate reflections from the computational boundaries. In addition, radiating boundary conditions are implemented. The derivation of these boundary conditions is based upon the far-field acoustical behavior of the flow field.

Results have been obtained for a low-speed axial turbine configuration.† The variation of the pressure amplitude on a stator airfoil is shown with (Fig. 134) and without (Fig. 135) appropriate grid spacing in the upstream and downstream regions. It can be seen that attenuations of the reflections from the computational boundaries do improve pressure amplitude variation along the airfoil. This essentially reduces the effect of the reflective boundary condition on the solution. The agreement with the experimental data is even better. It was also found that the turbine operating conditions (flow coefficient) were maintained.

In a spectrum of the turbine tones for a three-stator/four-rotor simulation, it is evident that the first two harmonics do not propagate, whereas the third and sixth harmonics propagate. This behavior is expected and conforms with acoustical predictions.‡

At present, the pressure amplitudes and details of the far-field acoustics for the three-stator/four-rotor case with nonreflective boundary conditions are being studied.

*Rai, M.M. and Madavan, N.K.: Multi-Airfoil Navier-Stokes Simulations of Turbine Rotor-Stator Interaction. AIAA Paper No. 88-0361, 1988.

†Dring, R.P., Joslyn, H.D., Hardin, L.W. and Wagner, J.H.: Turbine Rotor-Stator Interaction. J. of Eng. for Power, Vol. 104, October 1982.

‡Tyler, J.M. and Sofrin, T.G.: Axial Flow Compressor Noise Studies. SAE Transactions, Vol. 70, pp. 302–332, 1970.

G.A. Wilhold/ED31
(205) 544-2651
Sponsor: Office of Aeronatics and Space Technology

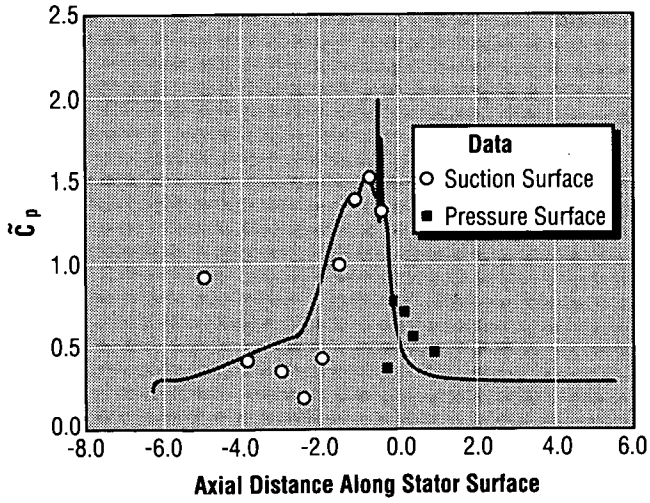

Figure 134. Pressure Amplitude on Stator (With Appropriate Grid Spacing)

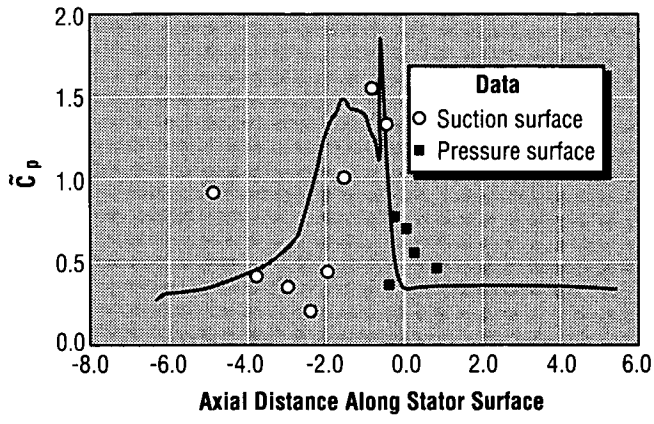

Figure 135. Pressure Amplitude on Stator (Without Appropriate Grid Spacing)

Liquid Turbopump Tasks

The Advanced Launch System (ALS) program objective of reducing the recurring cost of putting an object into low-Earth orbit to $300 per pound requires that the ALS program examine all potential cost savings. The Advanced Development Program has identified those key components that are the most significant cost drivers. Three contracts have been let (Figs. 136, 137, and 138) to address the technology associated with turbopumps which operate in liquid hydrogen (LH_2), liquid oxygen, and LH_2 with conversion options to liquid methane.

The objective of these contracts is to define and demonstrate high-reliability approaches for a low-life-cycle cost and low-recurring-cost liquid turbopump assembly; to validate the approach through design, fabrication, and test of prototype hardware; and to develop a cost model applicable to production hardware. Reliability is to be a quantified design requirement in the same context as cost, performance, and weight. The component-level design reliability requirement should be consistent with and be derived from the engine system-level requirement of 0.99 at 90 percent confidence level.

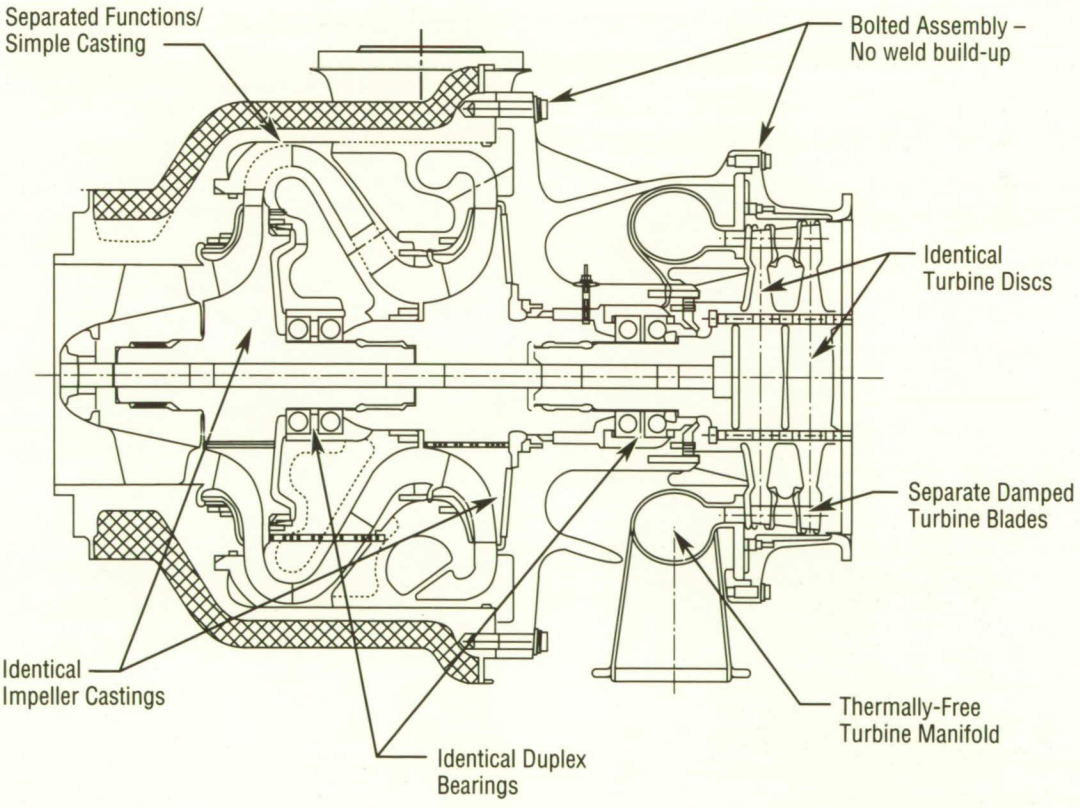

Figure 136. Aerojet LH_2 Turbopump

These contract efforts are structured in two phases. Phase I, or the basic phase, includes preliminary design, trade studies and analyses necessary to support the preliminary design, a technology development program plan, and development of a preliminary cost model. The focus of the studies will be to define low-cost approaches that will potentially make ALS cost goals achievable. The cost model will be used to evaluate the impact of government specifications on the delivered hardware cost and to determine ways of meeting the intent of these specifications at reduced cost.

Phase II is an option. This phase, if exercised, will include detailed design, a detailed cost model, and fabrication and testing of a prototype turbopump.

R.M. Ryan/EP62
(205) 544-4172
Sponsors: Office of Space Flight
Strategic Defense Initiative Organization
U.S. Air Force/Space Division

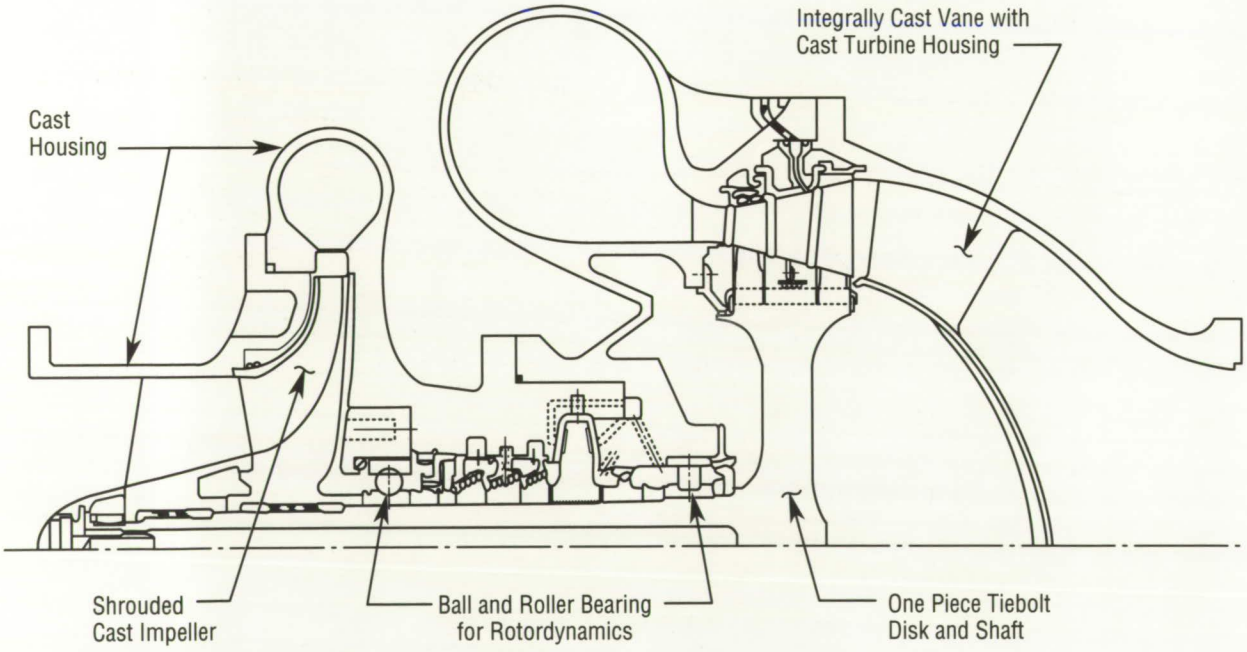

Figure 137. Pratt & Whitney Oxidizer Turbopump

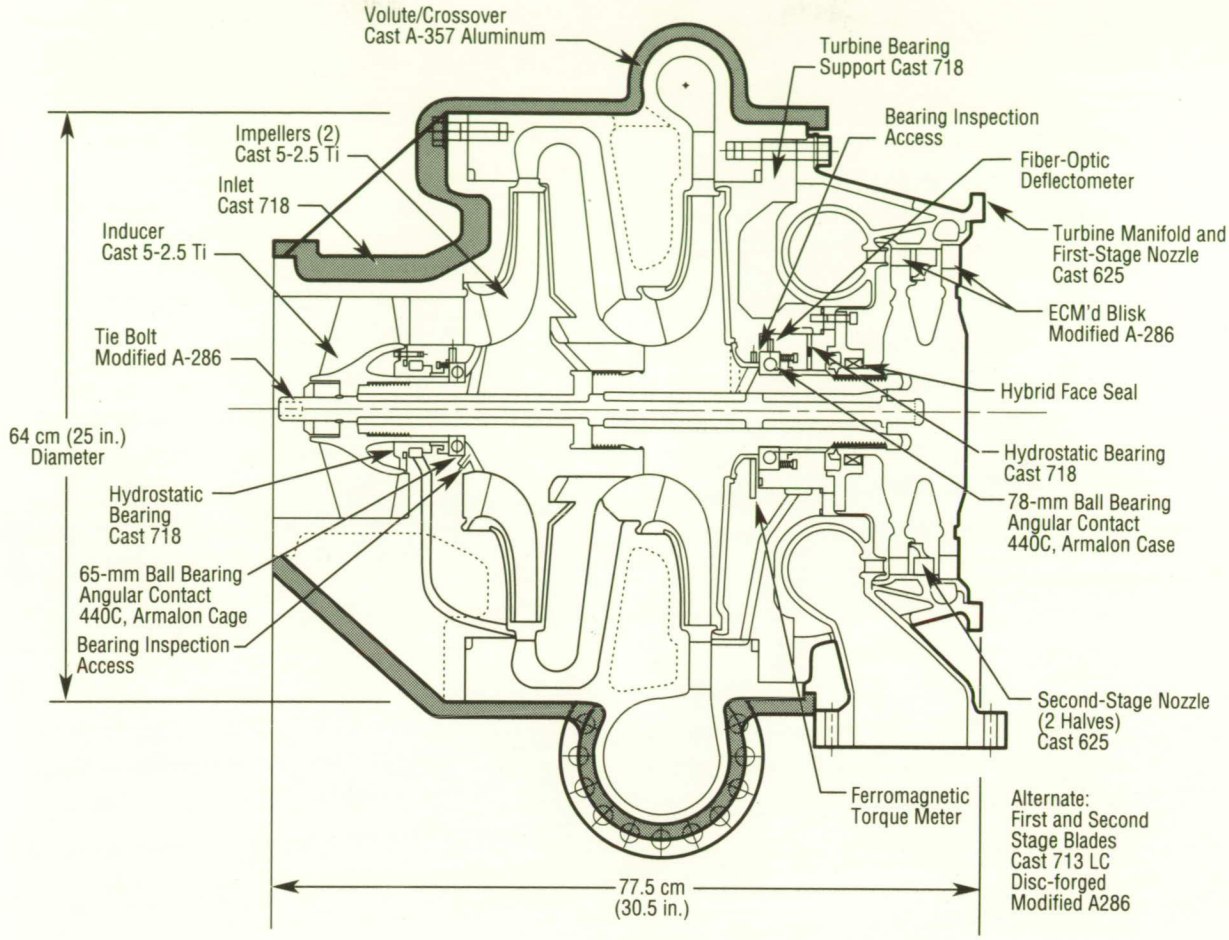

Figure 138. Rocketdyne Liquid Hydrogen/Methane Turbopump

Materials and Processes

Quick Turnaround Bearing Tester

The Quick Turnaround Bearing Tester (Fig. 139) is a cryogenic single bearing tester that was devised to evaluate the performance of one Space Shuttle Main Engine (SSME) high pressure oxidizer turbopump (HPOTP) pump end bearing. The tester was developed because the SSME HPOTP main shaft bearings are not meeting their life requirements of 55 successive flights and 7.5 hours between engine overhauls. In order to meet the life requirements, an improved bearing configuration (i.e., an improved bearing design and/or an improved bearing material) is needed. The Quick Turnaround Bearing Tester was developed so that comparative screening tests of potentially improved bearing configurations could be performed in a timely manner using a simple, easy-to-manage test setup versus the baseline design.

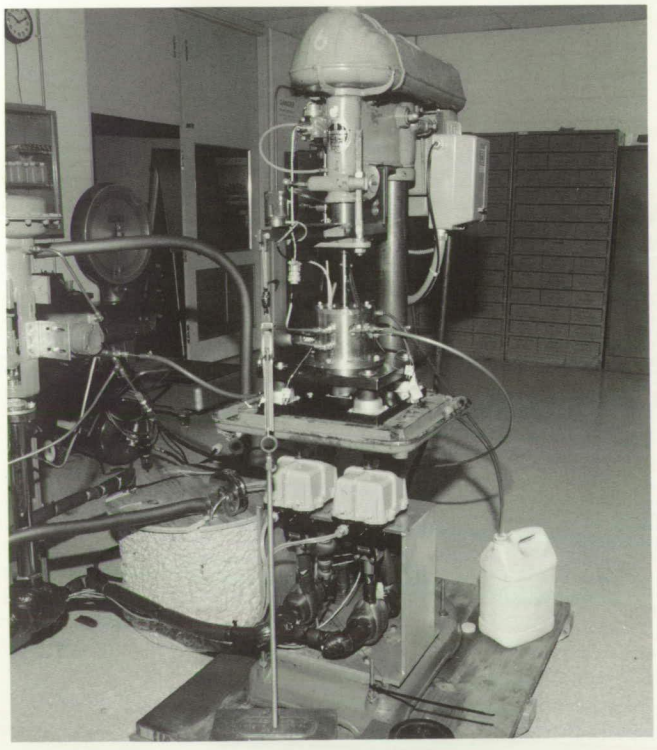

Figure 139. The Quick Turnaround Bearing Tester

ORIGINAL PAGE
BLACK AND WHITE PHOTOGRAPH

The bearing tester was designed and built in-house at MSFC. The basic tester consists of a 304 stainless-steel bearing housing mounted on a modified heavy duty Walker Turner drill press. The inner race of the bearing is press fitted on a drill press arbor adapter, and the outer race is mounted in the bearing housing. The bearing is loaded axially via a simple dead-weight loading mechanism. The tester is designed to use either liquid nitrogen or liquid oxygen as the bearing coolant.

Test parameters include testing of one HPOTP pump end 45-mm (1.772-in) bearing, with a variable coolant flow rate [54 g/s (0.12 lb/s nominal)], up to 227 kg (500 lb) axial load on the inner race, rotation at 10,000 rpm, under variable subcooled conditions.

The tester is instrumented to measure coolant inlet temperature, coolant outlet temperature, coolant flow rate, bearing outer race temperature, and the change in pressure across the bearing. A heat exchanger is used in the coolant supply line to create and control the cryogenic fluid subcooling conditions. During testing, an IBM AT computer and a Fluke Helios data acquisition system are used to control and monitor the tester.

Presently, baseline testing in liquid nitrogen of the present bearing configuration is being performed. After a reliable baseline is determined, improved bearing designs and/or materials will be tested. It is planned to evaluate BG42 stainless steel bearings; CRB7 stainless steel bearings; silicon nitride balls; 440C stainless steel bearings with surface coatings such as titanium nitride, copper, diamond, and gold; and a Salox cage material.

T.R. Jett/EH14
(205) 544-2514
Sponsor: Office of Aeronautics and Space Technology

Weld Process Modeling

Several related studies are underway with the objective of producing a detailed model of the Variable Polarity Plasma Arc (VPPA) welding process, which plays a major role in fabrication of the Space Shuttle External Tank. The model is needed for full automation of the VPPA system and should support system development in general.

A project analyzing heat transfer in the VPPA torch and between torch and workpiece is proceeding. It is expected that a tentative computer simulation of the VPPA process, exhibiting weld geometry as a function of welding parameter inputs, will be available within a year.

Supporting studies include workpiece size, local geometry perturbations, and coupled fixtures representing heat sinks that can affect temperatures and penetration geometry of a weld. Heat sinks are being characterized and related to equivalent weld parameter variations.

Minute quantities of plasma gas contamination, in the 100–500 parts per million range, can cause appreciable voltage, heating, and weld surface appearance changes. These effects are being characterized for simple impurities, e.g. O_2, H_2, N_2, and CH_4. The intent is to gather a data base that will allow analysis of gas purity problems to be carried out by direct observation of VPPA welding characteristics.

Weld strength depends upon the geometry of the weld cross section: weld width, bead reinforcement height, fusion line contour, peaking angle, mismatch, etc. An effort is underway to bring together data from a variety of sources and to synthesize a unified theory of the dependence of the ultimate tensile strength of a weld upon geometry. It may be possible to specify optimal weld cross-sectional geometries.

A.C. Nunes/EH42
(205) 544-2699
Sponsor: Office of Space Flight

Foam Applications Development

Formulation development of polyisocyanurate (PIR) foam systems for use on the Space Shuttle External Tank (ET) was continued at MSFC in FY88. Development of a PIR molding foam has been undertaken in-house because it is not consistently available from vendors. In-house formulations have shown definite promise, although further development will be necessary before one or more of the foams will be qualified for ET use. These foams will be formulated for use in the reaction injection molding equipment and advanced spray application equipment being put into production use at the Michoud Assembly Facility.

Another in-house formulation effort is evaluating alternatives to the chlorofluorocarbon (CFC) blowing agents currently used in all ET foam insulations. These CFC alternatives will provide environmentally safe (i.e., will not contribute to ozone depletion) blowing agents for ET foam insulation systems.

A state-of-the-art formulation laboratory is also being designed and implemented. It will be used for pour and spray foam formulating as well as advanced foam processing equipment development.

An investigation is underway to develop foam processing equipment designed specifically for ET use. Development of an improved spray gun is being investigated because of the additional control needed when spraying specific areas of the ET in automated development activities. This effort is managed under a separate task designed to investigate the development of a foam spray delivery system which will have capabilities for automated control and will incorporate improvements not available on the commercial market. These improvements will allow ET insulations to be applied at variable outputs to meet varying thickness requirements at close tolerances.

J.B. Thaxton/EH43
(205) 544-2786
Sponsor: Office of Space Flight

Tape-Laying Machine Development Software

The Cincinnati Milacron tape-laying machine installed in the MSFC Productivity Enhancement Facility is fully operational. This state-of-the-art system is utilized to develop advanced composite tape-laid parts for the shuttle, Space Station *Freedom*, and future programs. In support of this system, composite engineers have been trained in the use of the end-to-end automated software to create part programs to lay composite tape over complex part surfaces. Technicians have been trained in the operation, maintenance, and quality control of this complex system. This unique software consists of several commercial packages and specially developed programs working together on a VAX 11/780 computer.

The tape-laying machine software consists of four packages: University Computing Company's Automatically Programmed Tool (UCCAPT), a preprocessor (ACRAPATH), a post-processor (ACRAPOST), and a graphics package (ACRAGRAPH), purchased from Cincinnati Milacron. Software developed in-house allows input of complex surface geometries through the use of Computer Vision or Intergraph computer-aided design workstations. The composite engineer inputs the part geometry and ply parameters into the ACRAPATH preprocessor, which optimizes the placement of courses of tape on the part, updates surface geometry for the next ply of tape, and produces an APT program source code. The APT code is com-

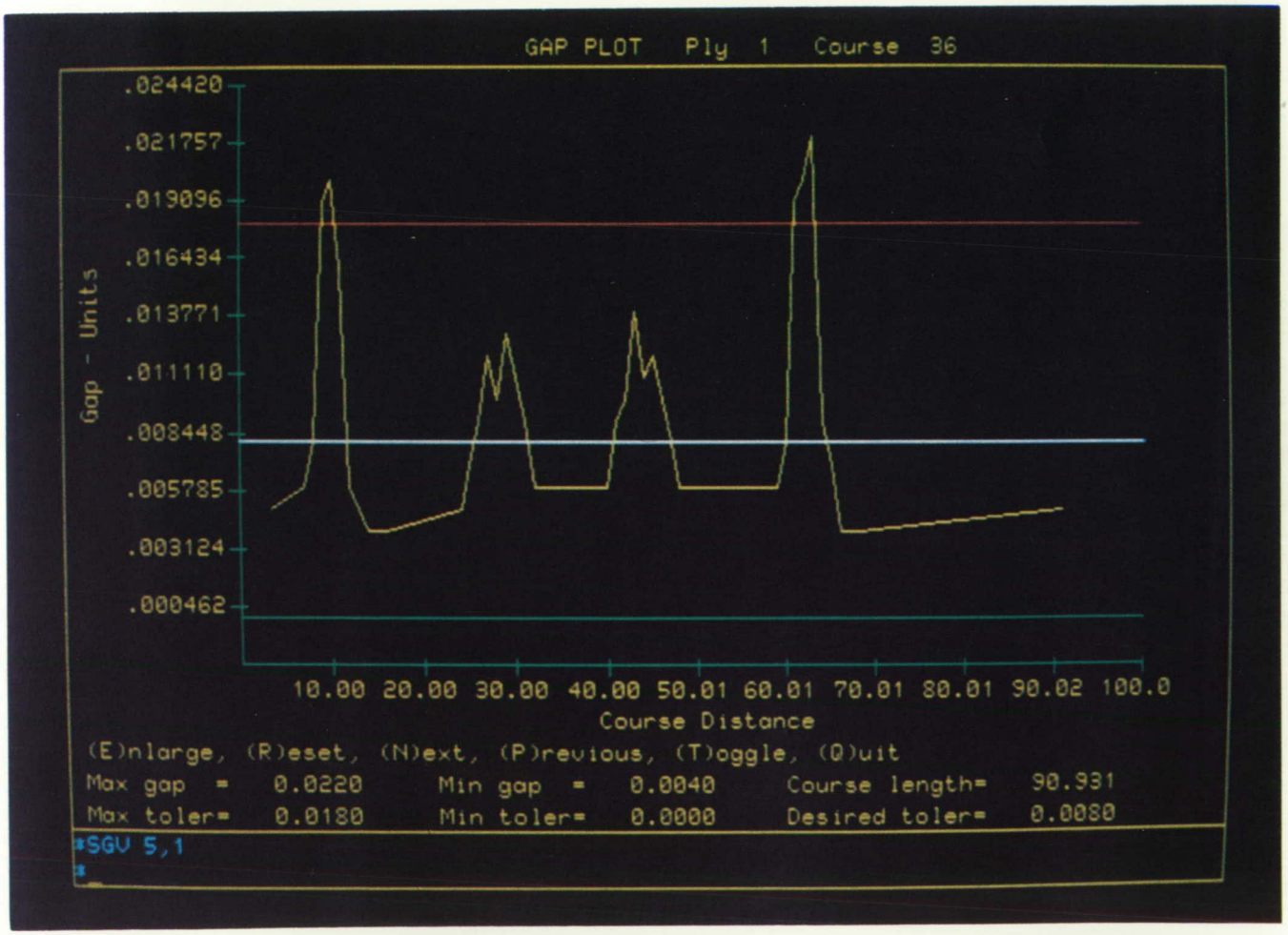

Figure 140. ACRAGRAPH Plot of Tape Gap

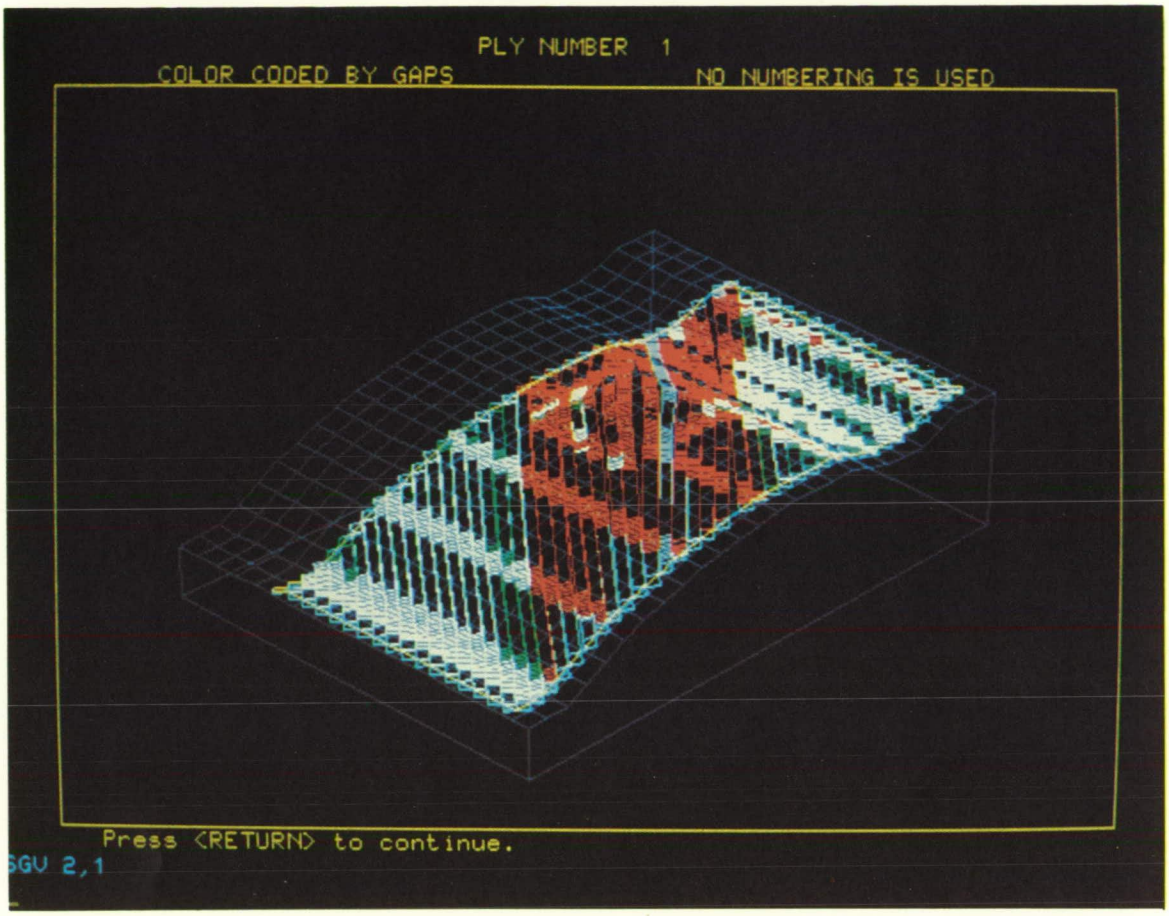

Figure 141. ACRAGRAPH Plot of Overall Geometry

piled and the resulting cutter location file is passed to the post-processor, generating a part program containing machine instructions for the tape-laying machine. The part program is down-loaded from the VAX 11/780 to the tape-laying controller and the optimized part is produced. The tape-laying machine development software can be used to evaluate composite parts in an off-line mode. The ACRAGRAPH software enables detailed evaluation of parameters such as tape gap and fiber orientation. Figure 140 is an ACRAGRAPH plot of the gap between the adjacent tape courses, and Figure 141 is a plot of the overall geometry of the surface with the tape courses indicated. These packages allow engineers to create the best optimized part program, before creating a part, thus saving time, material, and labor. This software provides the composite engineer with a comprehensive tool for developing composite parts without the knowledge of programming languages.

E. Martinez/EH43
(205) 544-2724
Sponsor: Office of Space Flight

Ultrasonic Flowmeter Demonstration

The lack of any on-engine propellant flow measuring equipment handicaps the effective closed-loop control capability of the Space Shuttle Main Engine (SSME), and the internal flow conditions of the SSME make the use of such sensors extremely difficult. This effort provides a comprehensive assessment of the installation of nonintrusive ultrasonic flowmeters on propellant ducts for a technology readiness demonstration on the Technology Test Bed Engine (TTBE) which will allow propellant flow measurements that are presently unavailable. This task provides for the engineering analysis and final design for installation of piezoelectric transducers on a cryogenic propellant duct to provide measurements for control and performance characterization.

The intent of this task is to adapt existing sensor systems to the purpose, not to develop a new system. Normal measurements do not exceed 9.1 m s^{-1} (30 ft s^{-1}) but these must handle flows up to 54.9 m s^{-1} (180 ft s^{-1}) (in liquid oxygen). Tests run at MSFC, using water, have confirmed that measurements are easily made at up to 30.5 m s^{-1} (100 ft s^{-1}). Higher rates could not be obtained due to lack of pumping power. Further testing will be done using LN_2 flowed to the full rate.

If the preliminary tests support the application, the ducts that were prepared for the cryogenic testing, being actual engine ducts, will be used on the TTBE.

W.T. Powers/EB22
(205) 544-3452
Sponsor: Office of Aeronautics and Space Technology

Fracture Mechanics Analysis Technology

Advanced high-pressure O_2/H_2 propulsion components such as the Space Shuttle Main Engine require reusability. This requires critical components to be designed for several hours of life in a myriad of environments and stress fields. Failure of a component is costly — economically, environmentally, and structurally. The prevention of failure by knowledge and control of the fractures (cracks, flaws, defects) present in structures is a major goal of component design.

Fracture mechanics quantifies the conditions under which a structure can fail due to the growth of a crack contained in that body. It provides an analytical tool for assessing defect acceptability; however, it is not a remedy for building poor-quality hardware. Fracture control eliminates or controls the conditions under which cracks are tolerated, and is based on fracture mechanics analysis. Figure 142 shows the fracture control logic sequence.

A state-of-the-art computer code (NASCRAC) was developed for performing fracture mechanics analysis. NASCRAC can perform time- and/or cycle-dependent analysis of subcritical crack growth and evaluate *J* integrals from previously published results.

The NASCRAC code is menu-driven, which makes it very easy for the analyst to input data and obtain results. The code contains a wide variety of stress intensity factor solutions, many of which are based on influence functions. The subcritical crack growth analysis portion of the code is tailored primarily for fatigue crack growth, although time-dependencies, such as introduced by hold times and various cyclic loading frequencies, can also be analyzed. Several fatigue crack growth laws such as Paris, Forman, Walker, Collipriest, etc., are included in the code. Load interactions are accounted for by a variety of user-selected models, including the Wheeler and

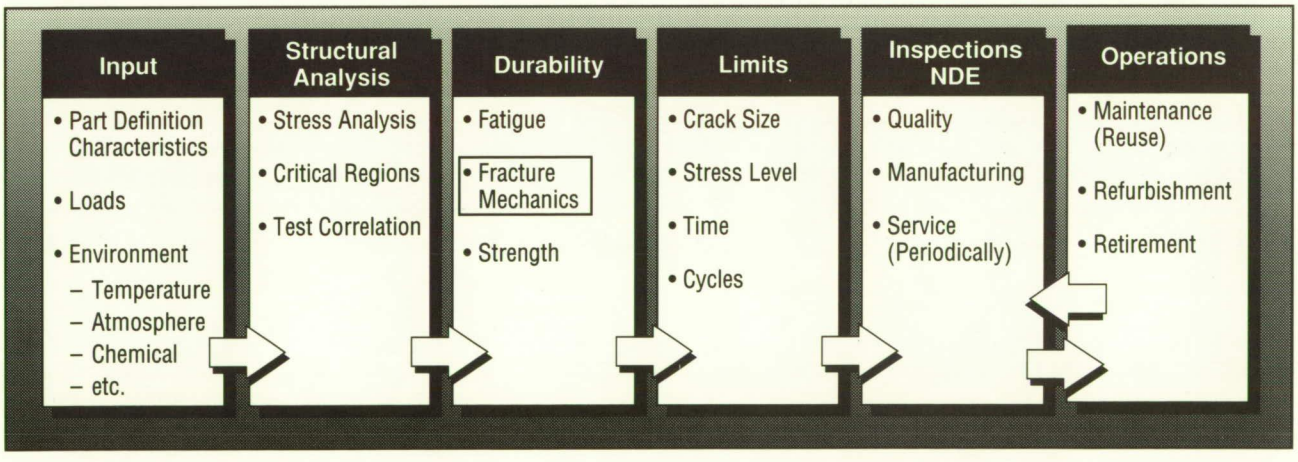

Figure 142. Fracture Control Sequence

Willenborg treatments. Final crack instability is treated by exceedance of a critical value of the stress intensity factor.

Four major classes of input are required to run the NASCRAC program: selection of type of analysis, selection of model crack geometry, material properties, and stresses on the crack plane in the absence of the crack. Figure 143 shows the types of analysis contained in the code.

Ryan, R.J.: Fracture Mechanics Overview, Structures and Dynamics Laboratory Cultural Presentation, MSFC, June 1989.

Failure Analysis Associates: NASCRAC™ NASA Crack Analysis Code, ©1987-1989.

R. Stallworth/ED25
(205) 544-7189
Sponsor: Office of Aeronautics and Space Technology

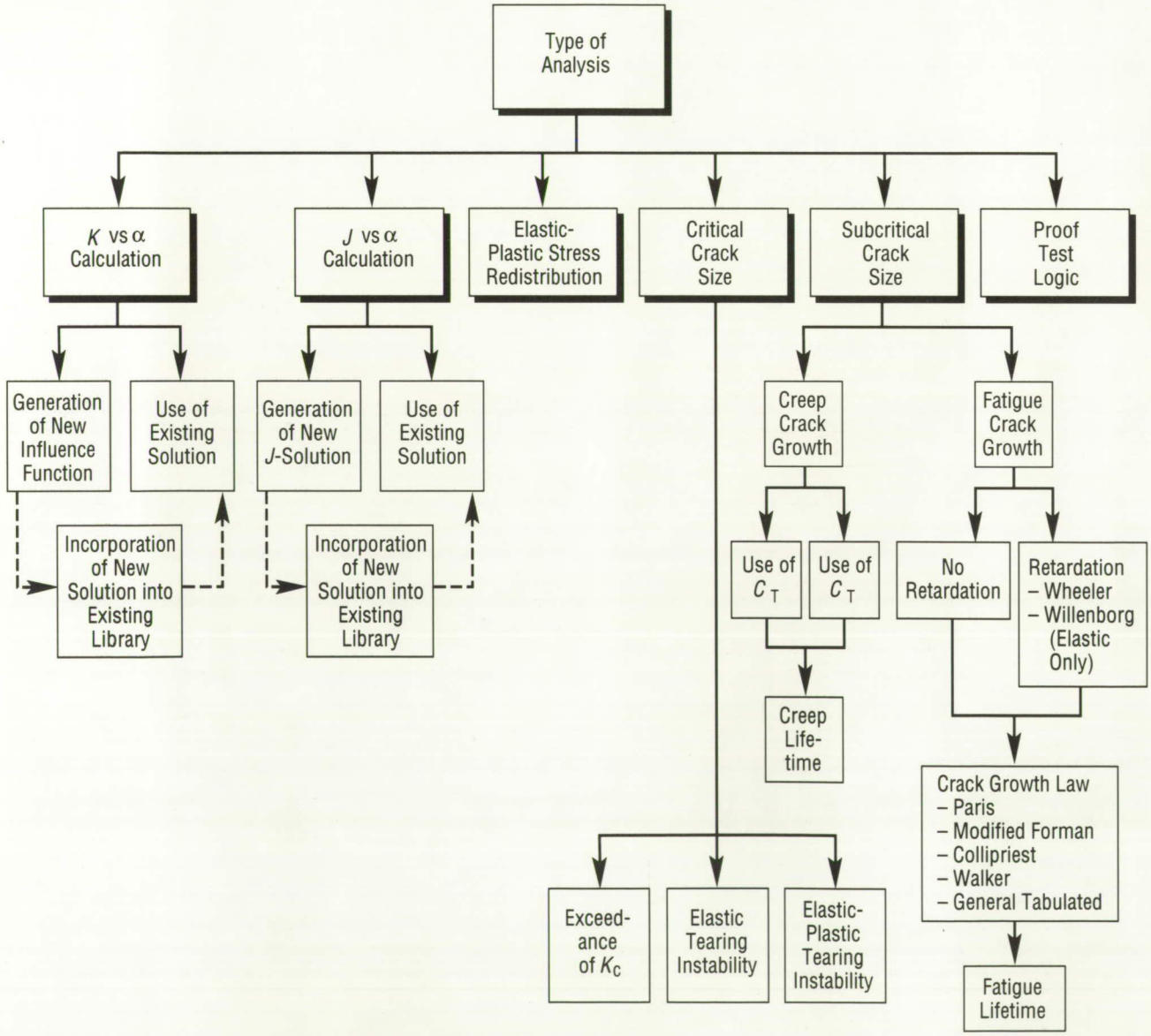

Figure 143. Types of Analysis in the NASCRAC Code

Velocimetry with Refractive Index Matching

The study of internal flows involving complex geometries presents a challenge to both analytical analysis and experimental investigation. Some examples are aircraft engine ducts, heat exchangers, pumps, rocket engine fuel and oxidizer systems, and multiple injector systems. The Laser Doppler Velocimeter (LDV), being nonintrusive and insensitive to fluid properties, is the tool of choice for experimentally studying such flows. However, it requires optical access to the flow and the use of relatively transparent fluids.

Optically flat windows or transparent models may well provide the required optical access, but in many cases the presence of multiple solid boundaries, perhaps with complex surface curvature, introduce additional measurement complications. In a cross-flow tube bundle type heat exchanger, for example, the area of interest may well be between tubes well buried within the tube bundle. A similar situation exists concerning the flow between interior rows of injector posts in the Space Shuttle Main Engine (SSME). Flows within chemical reactor towers, fluidized beds, and absorption columns offer similar problems.

Even if the tubes of the heat exchanger bundle or the injector posts are fabricated of transparent acrylic, their surface curvature would still act as a lens which repositions the LDV laser beams and prohibits beam intersection at the point of interest to form the required measurement volume. If, however, the working fluid and the acrylic model components have the same index of refraction, deflections and defocusing due to refraction at the surfaces vanish, which allows the LDV beams to be positioned anywhere within the model.

The first reported use of this technique,* was followed some years later by more intensive work.† Both of these investigations were for relatively small-scale models at modest Reynolds numbers. Applications of interest in aerospace technology are for larger models and commensurately higher Reynolds numbers.

A Small Business Innovative Research (SBIR) proposal was accepted to bring this matched-index technology from laboratory research apparatus to widely applicable general-purpose engineering test equipment. Extensive research to discover suitable liquids or mixtures to provide the required index of refraction, the control of the value, compatibility with model materials, etc., was performed. A test apparatus using a rod bundle was first constructed for proof-of-concept validation, after which a test apparatus was constructed based upon a one-half scale acrylic model similar to the SSME injector bowl with simplified inlet and outlet geometry. Extensive LDV measurements were made in this model to establish a benchmark data base for computational efforts.

The success of the program led to the award of a phase II SBIR award for development of the technology for commercial applications.

*Drust, F., Keck, T. and Kleine, R.: Turbulence Quantities and Reynolds Stress in Pipe Flow of Polymer Solutions. Proceedings, Sixth Symposium on Turbulence in Liquids, University of Missouri – Rolla, 1979.

†Edwards, R.V. and Dybbs, A.: Refractive Index Matching for Velocity Measurements in Complex Geometries. TSI Quarterly, Vol. 10, No. 4, Oct.–Dec. 1984.

J.P. Heaman/ED35
(205) 544-1604
Sponsor: Small Business Innovative Research Program

Metal Matrix Composite Structural Development

The primary objective of this program is development of thermally stable, open-section structural elements with their associated end fittings, all made using composite construction with aluminum as the metal-matrix material. This is an effort to make use of the high strength of both aluminum and fibers, while gaining the advantage of low distortion due to the thermal conditions which fiber gives to structures. In applications in which thermally stable structures (e.g., trusses for mounting telescopes and pointers) are desirable, metal-matrix composites may be able to replace aluminum as the material. The open sections offer the advantage of being load carriers and also serve as conduits (for cables and wiring) that are easily stackable.

Four strut-end fitting assemblies have been fabricated from each of three cross-sections (Fig. 144). The process of introducing unidirectional P100 graphite fibers into 6061 aluminum is company proprietary; however, the contractor has shown, through previous programs, that the process is reliable. Forming the cross-sections desired proved to be a challenge due to problems in "consolidating" the composite materials, but this was eventually done successfully. The end fittings, made of boron carbide (30 percent by volume) in 6061 aluminum, were machined from billets. Several joining methods (soldering, brazing, adhesion) were investigated before adhesion was chosen.

Tests and calculations have shown the coefficient of thermal expansion (CTE) for graphite-aluminum structures to be about -0.115×10^{-6} cm/cm/°C (-0.207×10^{-6} in/in/°F) which, in effect, indicates that the members contract over a range of -101.1 °C

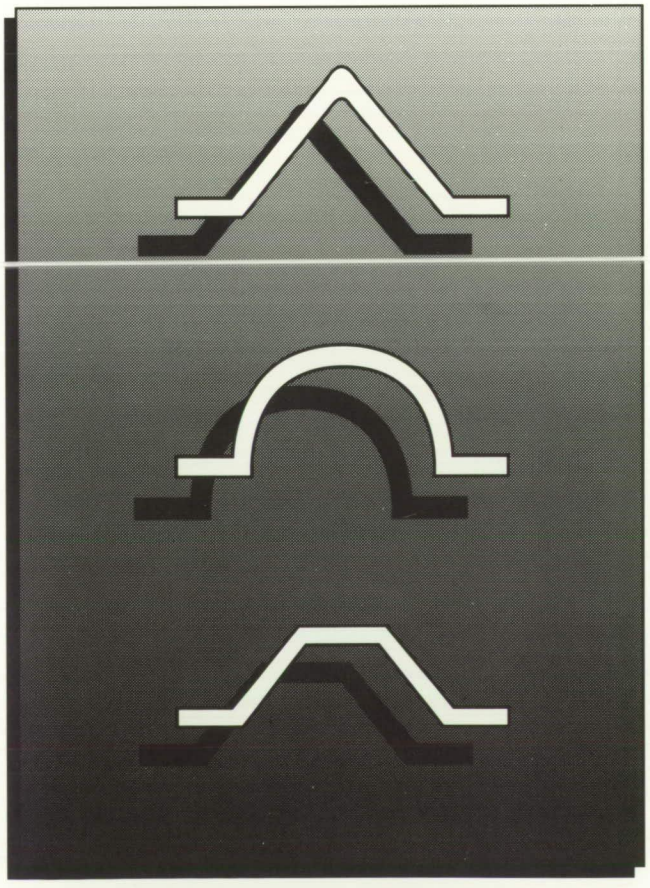

Figure 144. Cross Section of Structural Elements

to 65.6 °C (-150 °F to 150 °F). This phenomena, when coupled with boron carbide in aluminum's CTE of 4.17 x 10^{-6} cm/cm/°C (7.5 x 10^{-6} in/in/°F), is expected to produce an assembly with a CTE of less than 0.278 x 10^{-6} cm/cm/°C (0.5 x 10^{-6} in/in/°F), a number significantly less than aluminum's 7.22 x 10^{-6} cm/cm/°C (13.0 x 10^{-6} in/in/°F) CTE. A series of compression, tension, and torsion tests will be conducted on the strut assemblies at MSFC to measure the material's strength and the bond strength.

Additionally, two structures are being built of particulate-reinforced aluminum extruded sections. One is being made with closed, circular cross-section extrusions, while the other features triangular-section extrusions. The two structures are of a triangular truss type configuration measuring 106.7-cm high by 99.1 cm (3.5-ft high by 3.25 ft) width and depth. Originally, the trusses were to have the same moments of inertia and be made of boron carbide particulate (30 percent by volume) in aluminum, in an effort to make test results more comparative. Due to time limitations and because the tubular extrusions were fabricated during another program, the identical moment of inertia plan was changed. Also, during extrusion of the triangular sections, problems were encountered because of the abrasive nature of boron carbide on the extrusion dies. Conventional lubrication methods failed to work, leading to a decision to use less abrasive silicon carbide in aluminum for the extruded members of the triangular truss. For the tubular element truss, the material used was boron carbide in aluminum. Either spot welding or an adhesion/riveting joining will be used to assemble the truss. Presently, efforts are directed at optimizing a welding technique for particulate reinforced aluminum structures. At this program's completion, the trusses will be delivered to MSFC for torsion and compression testing.

P.E. Thompson/ED52
(205) 544-7017
Sponsor: Small Business Innovative Research Program

Metal Hydrides for Waste Heat Utilization and Long-Term Hydrogen Storage

Utilization of waste energy has always been desirable from an engineering and energy standpoint. Waste energy can take on many forms, but harnessing this energy often requires unique and innovative approaches. The objective of this program is to develop technology to utilize waste energy as a source for driving a refrigeration cycle, and to provide long-term storage of hydrogen in an inert environment. One such approach is a metal/hydrogen technology known as metal hydrides. The utility of the technology lies in the thermochemical interaction between hydrogen molecules with specific metals. Metal hydrides are chemical compounds formed when hydrogen gas reacts with metals. Hydrogen exists within the metal hydride crystal structure as interstitial atoms. Many hydrides absorb and release (desorb) hydrogen at pressures and temperatures that can be useful in spacecraft systems and terrestrial applications (Fig. 145). The phase changes during formation and decomposition of metal hydrides are often accompanied by significant latent heat flows that are useful for thermal energy management. Several concepts were evaluated that would use hydrides to absorb, store, pump, compress, and expand hydrogen. This effort has culminated in the successful development, fabrication, and testing of a hydride freezer and long-term hydrogen storage tank.

Metal hydrides provide a unique opportunity among phase change material for refrigeration. With the exception of a few flow control valves, there are no moving parts, lubrication is not required, and no compressor is required. The resulting ability to operate from a source of low-grade thermal energy reveals development potential for terrestrial and space refrigeration applications. The refrigeration cycle is represented and described in Figure 146. The hydride selected for this particular application was a LaNi compound. The design goal for the thermally-powered freezer unit was to extract heat and provide cooling at -20 °C (-4 °F) while being pow-

ered by a 100 °C (212 °F) heat source. The heat would be rejected to a 4 °C (39 °F) sink. These design conditions were selected based on environments that could be achieved on Space Station *Freedom*. The effort resulted in the successful operation of a hydride freezer that closely achieved its intended goal. A thermocouple located at the hydride heat exchanger indicated that -25 °C (-13 °F) had been achieved; however, the temperature of the storage volume was -19 °C (-2.2 °F). The temperature rise has been attributed to heat losses in the fluid line from the hydride exchanger to the cooling coil at the storage location. Improvements in the design of a hydride-bed heat exchanger could also contribute to improved system performance. Since the primary objective was to demonstrate the technical feasibility of the concept, future development will be required to enhance the system. Future applications for this unique technology could include automotive and commercial carrier vehicles with a hydride exchanger coupled with the engine exhaust or radiator, industrial plants that have high-temperature waste heat, and future spacecraft systems.

Long-term hydrogen storage units utilize metal hydrides' ability to store hydrogen in a solid state over an indefinite period of time. Early studies indicated that metal hydrides could provide an economical long-term storage alternative to liquid hydrogen for certain space vehicles and platforms with long orbit durations (i.e., 24 months). For satellites or other systems that require periodic or gradual attitude adjustments, an electric heat source or alternate heat source could provide slow desorption of the hydrogen supplied to thrusters. Feasibility of the concept was driven by hydrogen/metal compatibility. Several candidate hydride alloys including ultralight metals such as aluminum were considered. A magnesium hydride was selected on the basis of high weight percentage of hydrogen storage (7 percent) and long-term stability of the compound. The goal of 4.53 kg (10 lb) of hydrogen storage in a subatmospheric and room temperature environment was successfully achieved. The hydride must achieve a temperature of approximately 350 °C (662 °F) before desorption of hydrogen begins. At this temperature a constant pressure

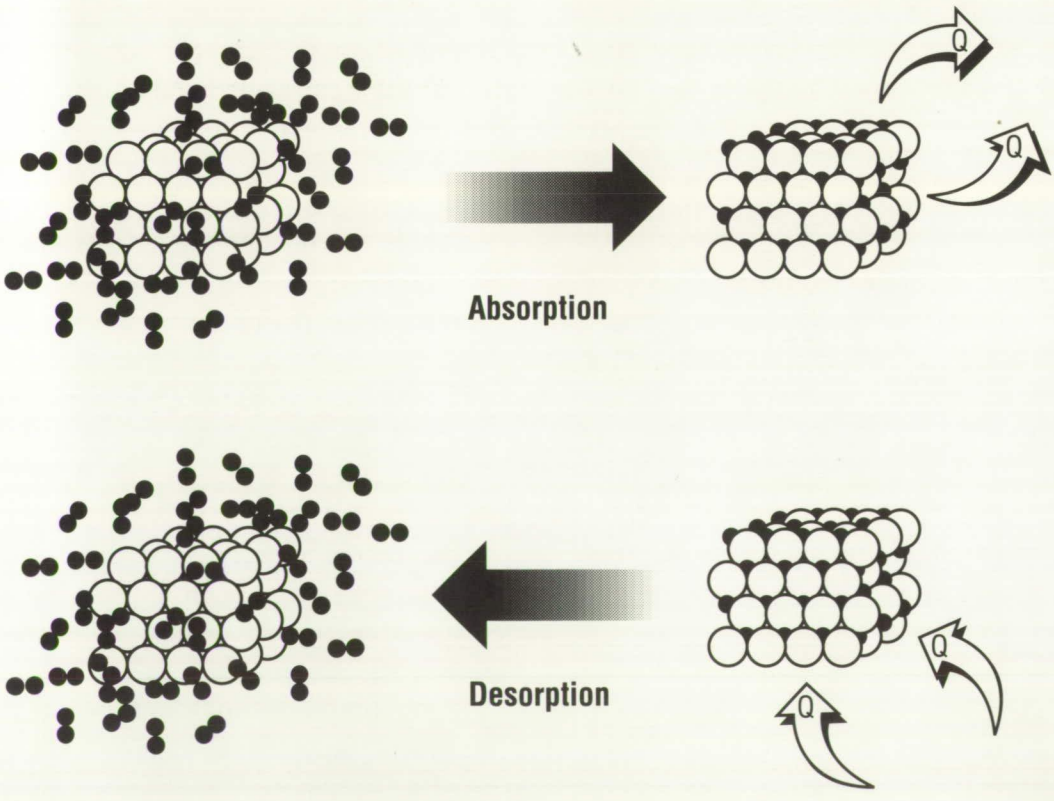

Figure 145. Hydrogen and Metal Interaction

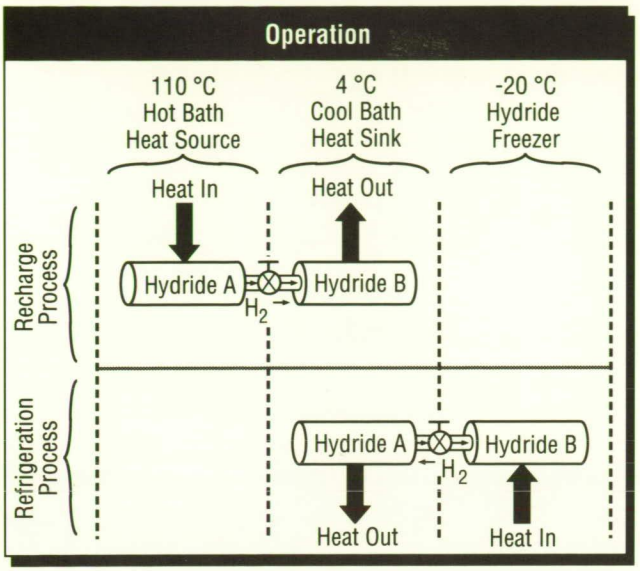

Figure 146. Metal Hydride Refrigeration Process

desorption rate of 5 L/min (0.18 ft^3/min) for about a week was achieved. To provide the necessary power to desorb the hydrogen, studies have indicated that a 1-m^2 (10.7 ft^2) solar array could supply the necessary power over a 1- to 2-month period, or a high-temperature solar collector could possibly be used. This technology is also applicable where residual hydrogen could be captured and stored, such as in the S.S. *Freedom* environmental control system.

C. Horan/ED63
(205) 544-7201
Sponsor: Small Business Innovative Research Program

Evaluation of Polyaryl Acetylene Resin Matrix Composites for Thermal Protection Systems

Recent research in the solid rocket motor industry on development of alternate ablative materials as nozzle insulators has focused principally on fiber reinforcement. The majority of this work is devoted to investigation of potential performance improvements associated with polyacrylonitrile (PAN) versus the standard rayon precursor. Very little research has been devoted to resins. The primary resins for these new material systems have been the industry "standard" phenolics, SC 1008 from Borden and 91LD from Ironsides. The Materials and Processes Laboratory, in cooperation with Dr. W.T. Barry (Aerospace Corp.), recognized the potential advantages in performance offered by polyaryl acetylene (PAA) resin over other ablation systems. These include high char yield, high thermal stability, clean ablation, absence of volatiles, and low moisture absorption. A screening level investigation was conducted, and the preliminary results of the study are summarized in this report.

The PAA resin utilized in the research was produced from materials originally manufactured by Hercules for use in hardened heat shields, commonly referred to as H-resin. The simplified synthesis of PAA resin is represented graphically in Figure 147. The baseline PAA was prepared from a 60:40 meta/para ratio of diethynylbenzenes.

Three composite panels fabricated for the study are described as follows:

Panel 1: T300 PAN-based carbon fabric/75:25 (PAA:PA)
Panel 2: T300 PAN-based carbon fabric/PAA
Panel 3: Low temperature (firing) PAN-based carbon fabric/PAA

PAA denotes the baseline resin previously described. The blend for panel 1 was a mixture of 75-percent baseline PAA with 25 percent of phenylacetylene. The reinforcement for the first and second panels

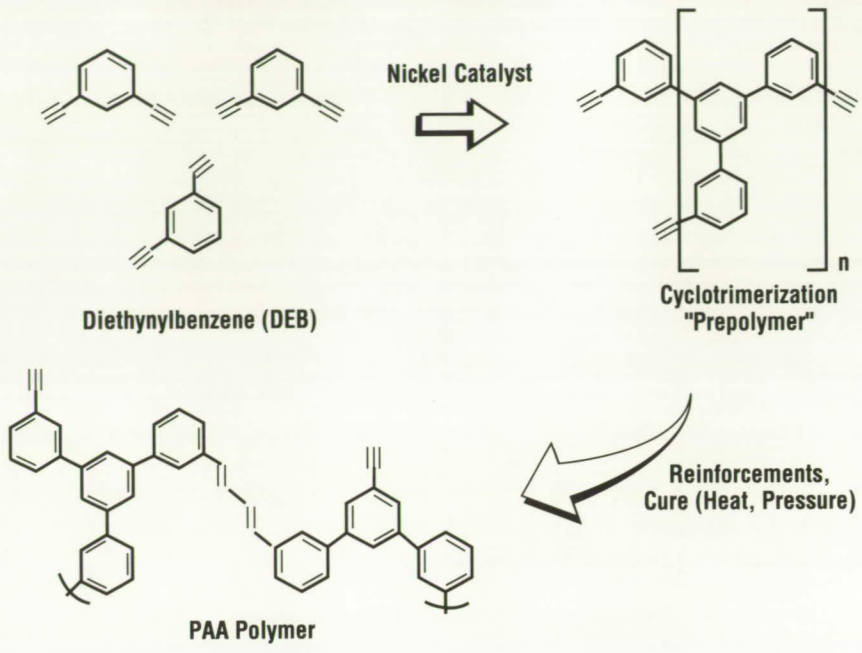

Figure 147. Synthesis of Polyaryl Acetylene

was the standard Amoco T300-3K fiber, woven in eight-harness satin construction. The low-fired PAN was produced by Celanese and was also of eight-harness satin construction.

Cure cycles varied for each of the three panels, but the 200 °C (392 °F) final cure temperature and 100 psi pressure were held constant for all. Reasonably lengthy staging is required early in the cure at temperatures below 140 °C (284 °F) to control exothermic reaction in the 140–150 °C (284–302 °F) temperature range. More research and characterization of cure kinetics will be required to optimize the cure cycle.

As the data base on PAN reinforced phenolics is generally limited, comparisons of mechanical properties may not be made for as many test conditions as is possible for the standard U.S. Polymeric FM 5055 rayon-based carbon fabric reinforced phenolic material. Fill tensile properties of PAA materials at room temperature and 399 °C (750 °F) are comparable to available properties from continuous PAN phenolics. The strength and modulus values are a minimum of 3 times those of the FM 5055 material. This difference in the fiber-dominated property is directly attributable to differences in yarn reinforcement. The across-ply tensile properties at room temperature agree well between the PAN-reinforced standard phenolic and PAA materials. Elevated temperature data at comparable temperatures is not currently available. In comparison to FM 5055, the values are quite low for PAA (3,880 psi versus 765 psi) at room temperature, but improve relatively at 399 °C (750 °F) (348 psi versus 199 psi). Double notch shear properties at room temperature and 1,371 °C (2,500 °F) exhibit the same trend. Both properties are dominated by the fiber/matrix interface bonding which is significantly stronger for the lower-fired rayon-based fibers in the FM 5055 composite. Thermal degradation among the various materials was assessed using thermogravimetric analysis. The PAN phenolics generically retained between 84 to 89 percent of original weight at 1,000 °C (1,832 °F). The PAN/PAA materials 1 and 2 retained 95 percent while FM 5055 generally has only 80-percent weight retention under the same conditions. With respect to across-ply thermal expansion, the PAN/PAA materials did not exhibit the first peak as exhibited in the

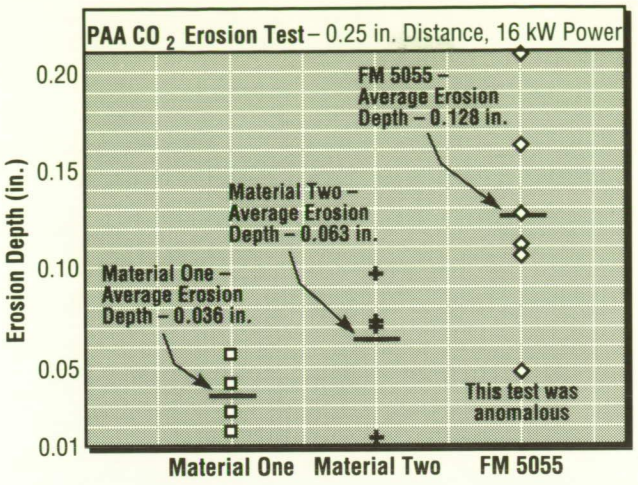

Figure 148. Results of CO_2 Plasma Torch Thermochemical Erosion Tests

classical FM 5055 response and some PAN phenolics. The second, or pyrolysis peak was of the same magnitude of FM 5055 but occurred at approximately 100 °C (212 °F) higher temperature. Further, as the PAN/PAA materials are nonhygroscopic, the thermal expansion responses were not affected by moisture as is FM 5055.

The final critical property tested was performance in a simulated hot fire environment. Preliminary results from CO_2 plasma torch tests (Fig. 148) demonstrate a higher resistance to thermochemical erosion for the PAN/PAA composites. However, differences in reinforcement will affect erosion performance, and data required to uncouple fiber/resin effects is not presently available. Additional research work is planned to further characterize the properties of these promising materials.

Barry, W.T.: Polyaryl Acetylene (PAA) Composites: a New Generation of Thermal Protection Materials.

Southern Research Institute: The Selected Physical, Mechanical, and Thermal Properties of a Polyarylacetylene Composite. SRI-MME-89-207-6526-11, April 1989.

Southern Research Institute: Screening Characterization of Eight Alternative Phenolic Composites. SRI-MME-89-107-6529-I, February 1989.

R.G. Clinton/EH34
(205) 544-2682
Sponsor: Office of Space Flight

Low Mixture Ratio Combustion Carbon Deposition

Rocket engines using hydrocarbon fuels combust these fuels at low-mixture ratios to generate low-temperature gases for driving propellant pump turbines. The low-mixture ratio combustion process for some hydrocarbon fuel candidates results in the deposition of carbon on turbine surfaces. The buildup of carbon as a function of operating time results in narrowing of the turbine drive flow passages causing an unwanted reduction of power to the turbines. This results in a decrease of overall engine power and performance from one mission to the next.

Experimental tests have been conducted to characterize carbon buildup for the hydrocarbon fuels RP-1, propane, and methane. The results of these tests have been reported in previous reports. An additional investigation has recently been completed which evaluated the carbon deposition characteristics of using impure methane with liquid natural gas (LNG) and of injecting LOX/methane propellants into the combustion chamber at 3 times the injection density (propellant weight flow/chamber cross-section area) of previous tests.

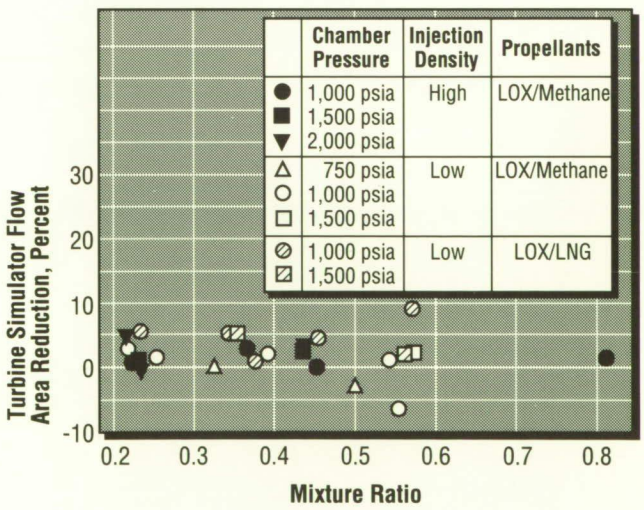

Figure 149. Turbine Simulator Flow Area Change-Versus-Mixture Ratio

The results of these tests, superimposed on the earlier reported methane test results, are shown in Figure149. The figure shows that there was essentially no change in turbine simulator flow area as a function of mixture ratio for either LNG or high-injection-density methane tests, which is consistent with the previous low-injection-density test results. These results further substantiate that the use of methane as a turbine drive propellant will not incur carbon deposition.

F. Braam/EP52
(205) 544-7055
Sponsor: Office of Aeronautics and Space Technology

Carbon/Glass-Phenolic Processing Model

A thermochemical model for carbon-phenolic material processes has been developed. The model will allow optimization of cure cycles as well as prediction of material properties based upon the types of material and the process by which these materials are used to make nozzle components. The model has been developed to employ sophisticated use of computer graphics to demonstrate the change in temperature, degree of cure, viscosity, or any other parameters during the curing process.

The model is unique in that it is three-dimensional with grid generation and graphics capability so that pre- and post-processing of all sizes and shapes of carbon-phenolic parts can be modeled. The model currently includes submodels of heat transfer and thermochemical reactions, moisture generation and diffusion, viscosity and degree of cure with residual stress, and resin flow submodels in work. Results obtained using the model correlate well with actual data for U.S. Polymeric FM5055 carbon cloth phenolic. Chemical kinetic constants for Fiberite MX4926 have also been determined and correlated to actual data so that the optimization of cure cycles of the current Space Shuttle Solid Rocket Motor (SRM) nozzle rings can be determined. This model will be an asset in the development of optimum cure cycles for new materials as well as the current material for SRM nozzles.

The computer-aided cure model is capable of describing the physical and chemical phenomena which occur during the cure of an SRM nozzle part. A flow chart of program capabilities is shown in Figure 150. This math model allows determination of material properties for process variations and material variations with any part configuration.

The model is based on the Systems Improved Numerical Differencing Analyzer (SINDA) heat transfer program, with considerable user programming involved to model other physical phenomena which occur during cure. This programming was

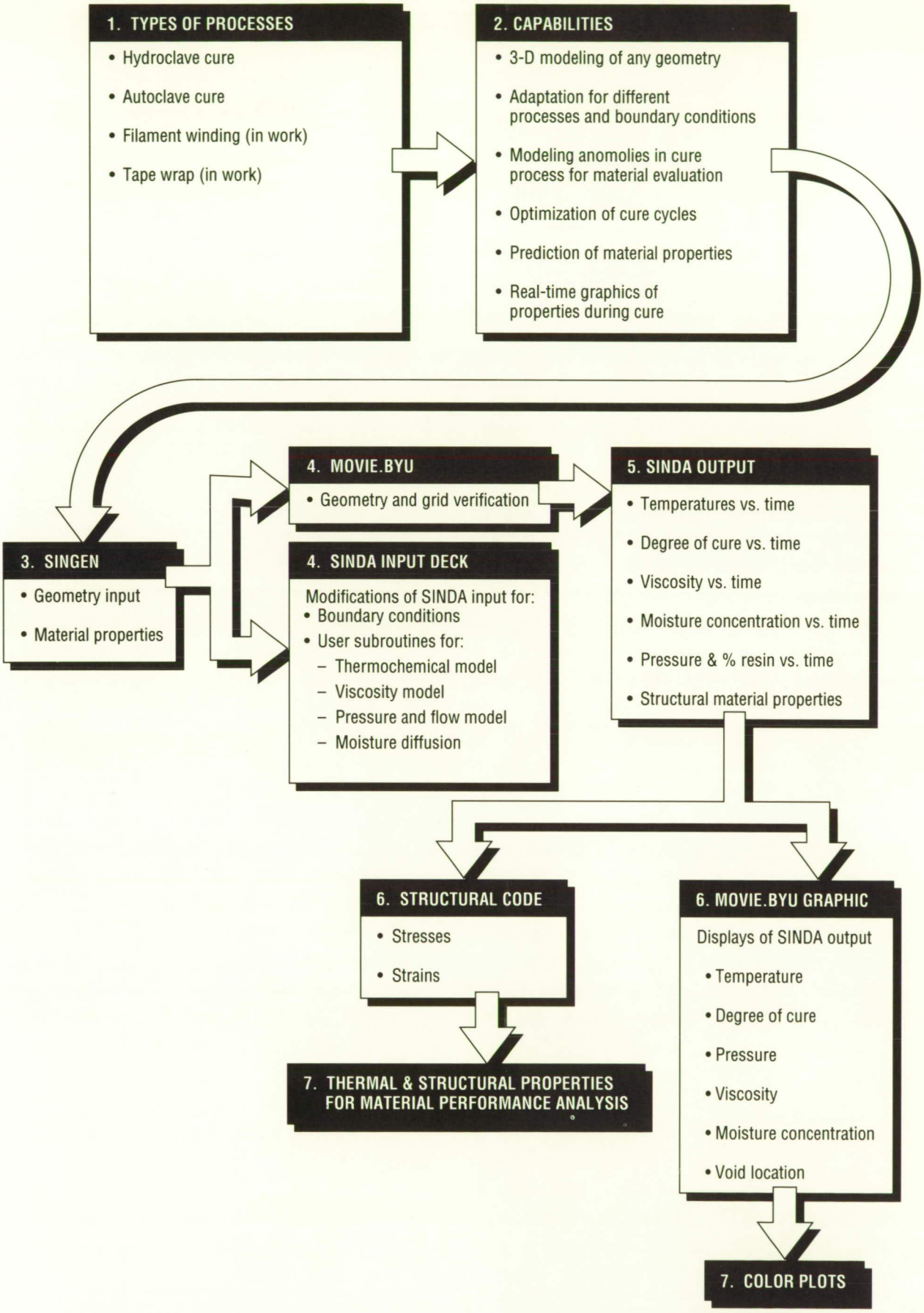

Figure 150. Computer-Aided Process Model Development of Rocket Nozzle Composites

Submodel	Status	Verification	Comments
Thermal Model	Complete	Simulated 504 Ring	SINDA FWDBK
Exothermic Reaction	Complete	DSC and Simulated 504	2 1st Order Reactions in SINDA User Subroutines
Viscosity Model	Complete	RDS Only	2nd Order Polynomial in User Subroutine
Moisture and Volatile Diffusion	Complete	Not Verified	SINDA FWDBK Diffusion Constant Required
Resin Flow	50%	Not Verified	SINDA FWDBK
Residual Stress and Compaction	0%	Not Verified	To Be Determined

Figure 151. Computer-Aided Carbon-Phenolic Processing Model Status

done in the available user subroutines. Submodels have been completed for reaction kinetics, degree of cure, moisture diffusion, and viscosity with resin flow and compaction submodels in work. Figure 151 shows the status of the math models to date. All of the models are independent and must be solved simultaneously. Based upon the computer predictions, the degree of cure, viscosity, moisture content, resin content, and residual stresses and strains versus time and position can be determined.

To date, only the heat transfer and chemical reaction portions of the computer model have been verified. Verification was done by correlation of actual and predicted thermocouple data for a simulated section of a 504 inlet ring in the SRM nozzle. From program output, real-time graphics of properties at time and position are possible. The predicted values compared very well with actual data. In order to accurately predict the exothermic and viscous effects for U.S. Polymeric FM5055 which occur during cure, it was necessary to use a two-series reaction primarily for the exothermic phenomena in parallel with another single reaction to enhance the viscosity model.

Reaction 2 only slightly affects the exothermic reaction and is used primarily for viscosity calculations. Reaction kinetics for U.S. Polymeric FM5055 and Fiberite MX4926 resulted from correlation with differential scanning calorimetry (DSC) and thermocouple data.

Moisture diffusion and viscosity submodels have also been completed using DSC and RDS data for constant evaluation. These models are currently being correlated and verified. Eight 75-degree shingle panels (simulated 504 rings) have been taken to different points of a typical hydroclave cure cycle, then cut into test specimens at key points. These specimens are currently being tested, and the results will be used to verify the models.

The model has been used in several important ways since verification of the temperature model. Several SRM nozzle rings are being analyzed to determine behavior during cure. Considerable effort went into analysis of the SRM throat ring to investigate voids at the carbon-glass interface. Several different cure cycles were investigated to see if an alternate cure cycle would alleviate the problem.

Another capability of the model which is being used is incorporation of anomalies into the cure cycle. This allows discrepancies to be programmed into the model to determine if they are sufficient to make the part unusable. This capability has successfully been put to use on several occasions to make final decisions on the acceptability of actual SRM nozzle parts.

The model has also been used to determine the effects of resin content on cure properties. Results of this study showed that a higher initial resin content results in a higher exotherm and an earlier

total cure for a part. Higher resin content also yields a higher final viscosity throughout the part as well as a higher final moisture content.

A major study was done using the cure model to aid in the selection of cure cycles for new advanced ablative materials. The goal was not only to select the optimum cure cycle but to also choose a cycle which would achieve the least amount of variation between the temperature profiles of each material during cure. Cure cycle selection was done using the 75-degree shingle panel (simulated 504 ring) model. To obtain the least amount of deviation of temperature profiles between the materials, the SRM Throat Ring First Wrap Cure was selected. The use of a -17.5 °C/min (0.5 °F/min) ramp rate reduces the temperature gradient between FM5055 and the hydroclave.

The model has been a useful tool in the determination of material conditions of a part due to the effects of different material and processing parameters. With continuing effort, this model will eventually cut manufacturing costs by eliminating the need for trial and error cure cycles in the laboratory by optimizing the process with the use of a computer.

W.R. Colberg/EH43
(205) 544-2725
Sponsor: Office of Space Flight

Development of Electromagnetic Compatibility Analysis

Research is currently being performed to design, develop, and validate a methodology and the associated computer-aided engineering software for use in the Integrated Space Station Electromagnetic Compatibility (EMC) Analysis System (ISEAS). This analytical tool will enable MSFC engineers to quickly and accurately optimize decisions using the design and performance data obtained at each phase of program development.

The enormous number of potential electromagnetic interference interactions which can occur when equipment and many subsystems are integrated into an overall system can be overwhelming. Modern aerospace systems contain increasing numbers of complex and sophisticated avionics systems and equipment that must operate harmoniously to achieve performance specifications. Achieving EMC, the ability of the equipment to function properly in its intended electromagnetic environment, for such avionics is normally a complex and time-consuming problem. On a program such as Space Station *Freedom*, the problem is also magnified due to components and racks of equipment continuously being replaced on orbit. Under this operational scenario, S.S. *Freedom* system EMC testing, performed at MSFC to verify system compatibility of all S.S. *Freedom* configurations, will not be possible and system-level EMC analysis will be the only option capable of accurately predicting S.S. *Freedom* performance. Methodology incorporated in the ISEAS design will also apply to the various decision-making scenarios that are associated with aspects of the EMC system engineering functions identified in Figure 152.

The approach currently being taken to develop EMC analysis is development of ISEAS. The tasks identified in this effort (Fig. 153) begin with a historical review of existing tools, leading to the selection of a set of coupling equations and analysis program methodologies optimal for use by MSFC in resolving S.S. *Freedom* EMC issues. These selected equations are then transformed into

The methodology incorporated in ISEAS design will permit application to the various decision making scenarios that are associated with the following aspects of the EMC engineering functions:

- Design trade study evaluations
- Participating in design audits and action item resolution
- Monitoring and technical evaluation of contractor analyses
- Review of contractor unit test plans, procedures, and reports
- Evaluation of test procedure change requests
- Evaluation of data adequacy, waivers, and specification change requests
- Trouble shooting during all phases of development and test
- Support to integration and test issues
- Independent prediction of system EMC performance
- Review of contractor EMC system test planning and procedures
- Selection/approval of system critical test points
- Monitoring of EMC system tests
- Buy-off of contractor test results

Figure 152. Applications of ISEAS

engineering models which, together with an engineering data base, are integrated into a complete engineering workstation. A Unix-based VAX 3100 system, utilizing DecWindows software with pull-down menus, meets all of the user requirements and will provide a user-friendly engineering tool.

While there are existing EMC computer programs available, they require that large amounts of input data be tediously organized and input into large computer codes, which in turn generate large amounts of output data which must be digested by EMC engineers to arrive at a conclusion about the integrity of the system. An EMC tool is being developed which allows engineers to interactively configure the system with avionics and flight equipment and to automatically perform an analysis and obtain results in a clear, concise format. The software program has the ability to receive data in several formats (interactive terminal input, other computer files, computer-to-computer, floppy disk, etc.), and to document the output in graphic and/or tabular form. This program will enhance MSFC abilities in EMC engineering, and configure MSFC as the continuing leader in the field of EMC analysis. ISEAS is an innovative tool which will meet current needs, and will also be the state-of-the-art milestone of the 1990's fundamental S.S. *Freedom's* operational success.

S.D. Pearson/EL55
(205) 544-2350
Sponsor: Office of Space Station

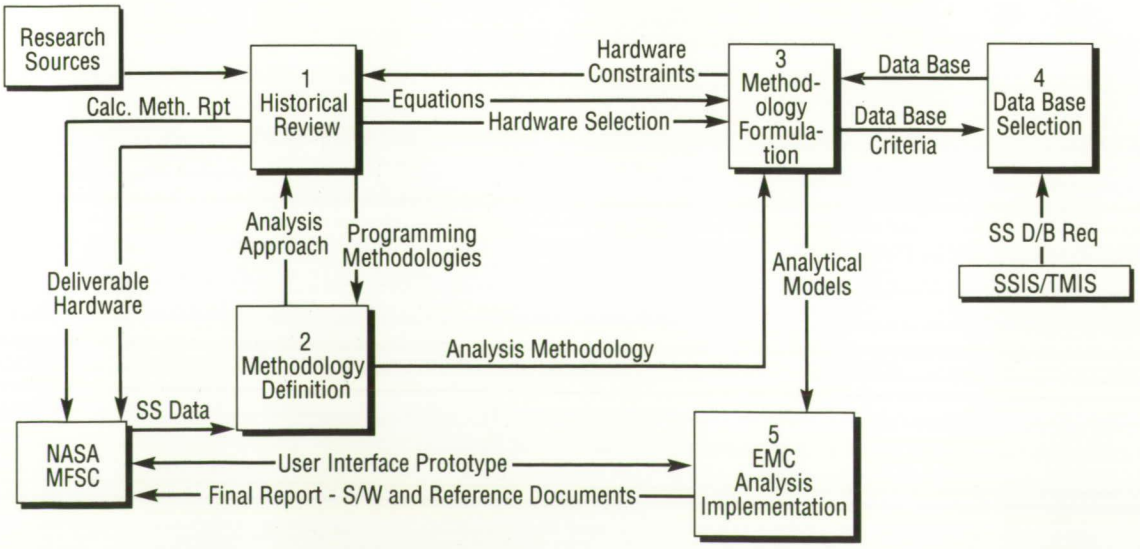

Figure 153. Electromagnetic Analysis Study Task Overview

Alternating Current Impedence Model for Determining Diffusion Polarization

A new equivalent circuit model for calculating the effect of diffusion polarization in alternating current impedence studies of coated metals has been developed during the past year (Fig. 154).

The component Z_w in the figure is given by: $Z_w = sw^{-1/2} - jsw^{-1/2}$, where s is the Warburg coefficient and $w = 2\pi X$ frequency. Z_w is known as the Warburg impedence, with diffusion polarization giving rise to its contribution to the total impedence represented by the circuit illustrated in the figure. The Warburg coefficient s in the previous equation is treated as a parameter, along with all other components of the circuit model, in a least-squares refinement using the Bode magnitude data of the experiment (log impedence versus log w), and its value is thereby obtained. The parameter s can be regarded as a resistance to diffusion of the surrounding medium through the protective coat covering the sample. In general, the higher the value of s, the less is the diffusion of the surrounding medium through the sample coat. If the value of s exceeds that of the charge transfer parameter R_t, corrosion is diffusion controlled. The parameter s has previously been obtained from the Bode magnitude plot by locating the region where the slope of the curve is -1/2 and extrapolating to log $w = 0$. However, contributions from many other components of the equivalent circuit also contributed to the total impedence, resulting in a value of s which is much too large. It has also been obtained from a Nyquist plot (Z'' versus Z', Z'' = imaginary part of impedence and Z' = real part) using a much over-simplified model. The model shown in the figure has been successfully applied to a study of the corrosion protection of aluminum by various anodizing treatments.

Danford, M.D.: The Corrosion Protection of Aluminum by Various Anodizing Treatments. NASA TM, in press.

M.D. Danford/EH24
(205) 544-2612
Sponsor: Office of Space Flight

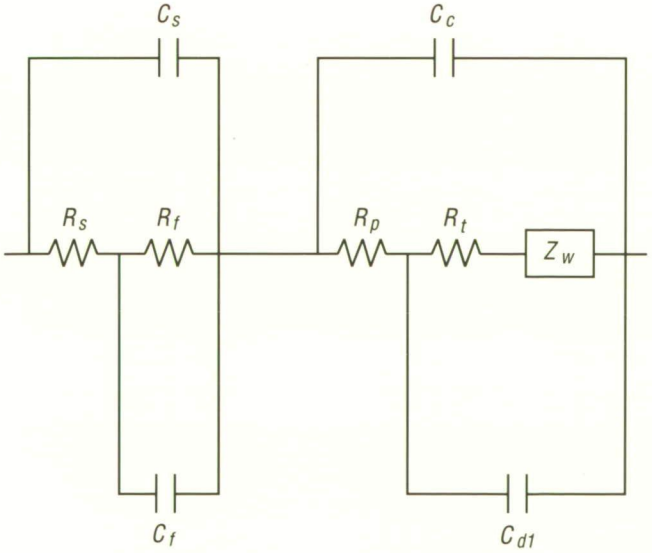

Unit 2 Coating-Solution Unit		Unit 1 Metal-Coating Unit
C_s	Solution Capacitance	
R_s	Solution Resistance	
C_f	Faradaic Capacitance (Coating/Solution)	
R_f	Faradaic Resistance	
C_c	Coating Capacitance	
R_p	Coating Resistance	
R_t	Charge Transfer Resistance	
C_{d1}	Metal/Coating Interface Capacitance	
Z_w	Warburg Impedence (Diffusion Polarization)	

Figure 154. Equivalent Circuit Model Showing Contribution by the Warburg Impedence Z_w

Structures and Dynamics

External Tank – Spray On Foam Insulation Kinematic Simulation System

The External Tank (ET) – Spray On Foam Insulation (SOFI) Research Cell in the Productivity Enhancement Facility is utilized to develop and qualify SOFI materials for use as part of the Thermal Protection System on the ET and other space shuttle flight hardware. The foam is sprayed by a Cincinnati Milacron T3 robot on test panels mounted on a cylinder rotating on a 4.3-m (14-ft) air bearing turntable. A kinematic simulation was completed in 1988 to model and program off-line the operations within the spray booth.

The simulation, developed by MSFC and Martin Marietta, consists of a Silicon Graphics IRIS Model 3120 workstation running a graphics software package known as IGRIP from Deneb Robotics, Inc. This state-of-the-art graphics system provides three-dimensional solid representations of the cell and allows real-time manipulation of these objects (Fig. 155). The robot coordinates are displayed and updated in real-time, emulating the robot controller. This system will detect and alert the operator when the robot arm has reached its travel limits or when

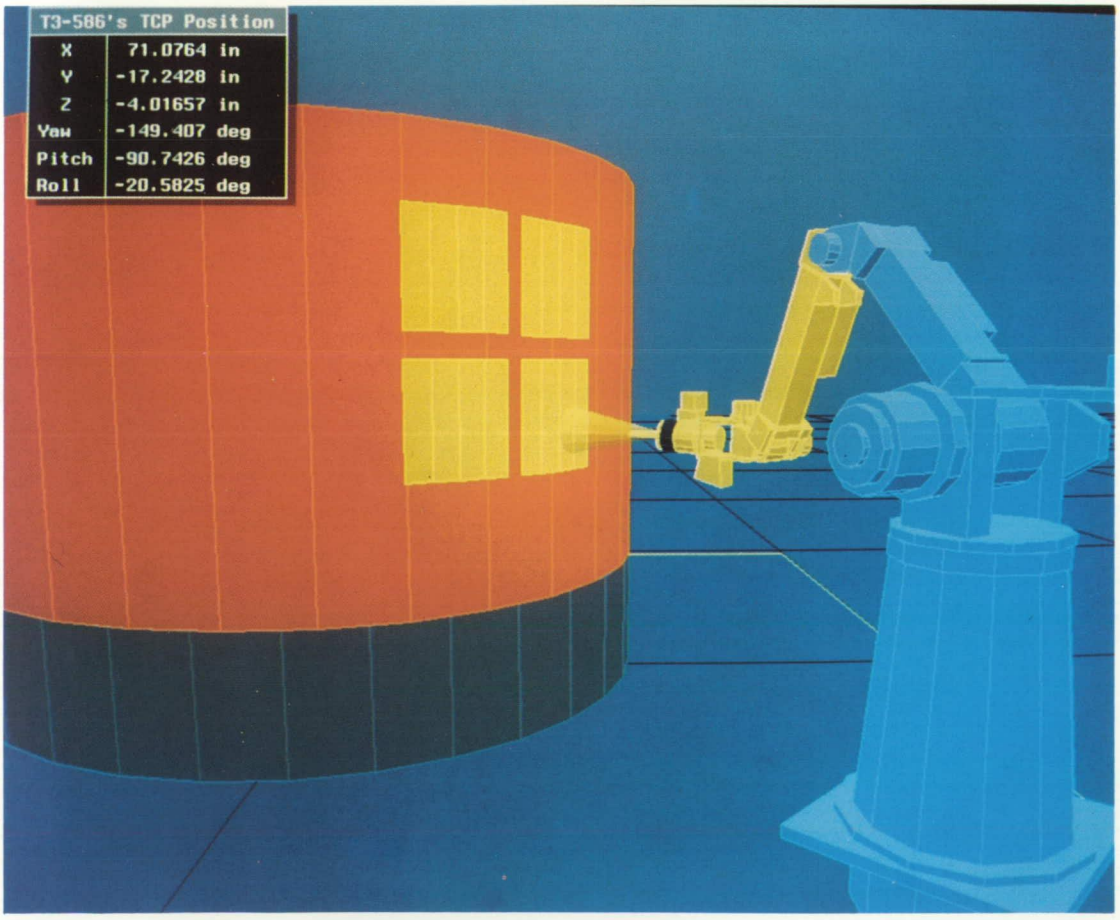

Figure 155. Deneb Model of the Spray on Foam Insulation Research Cell

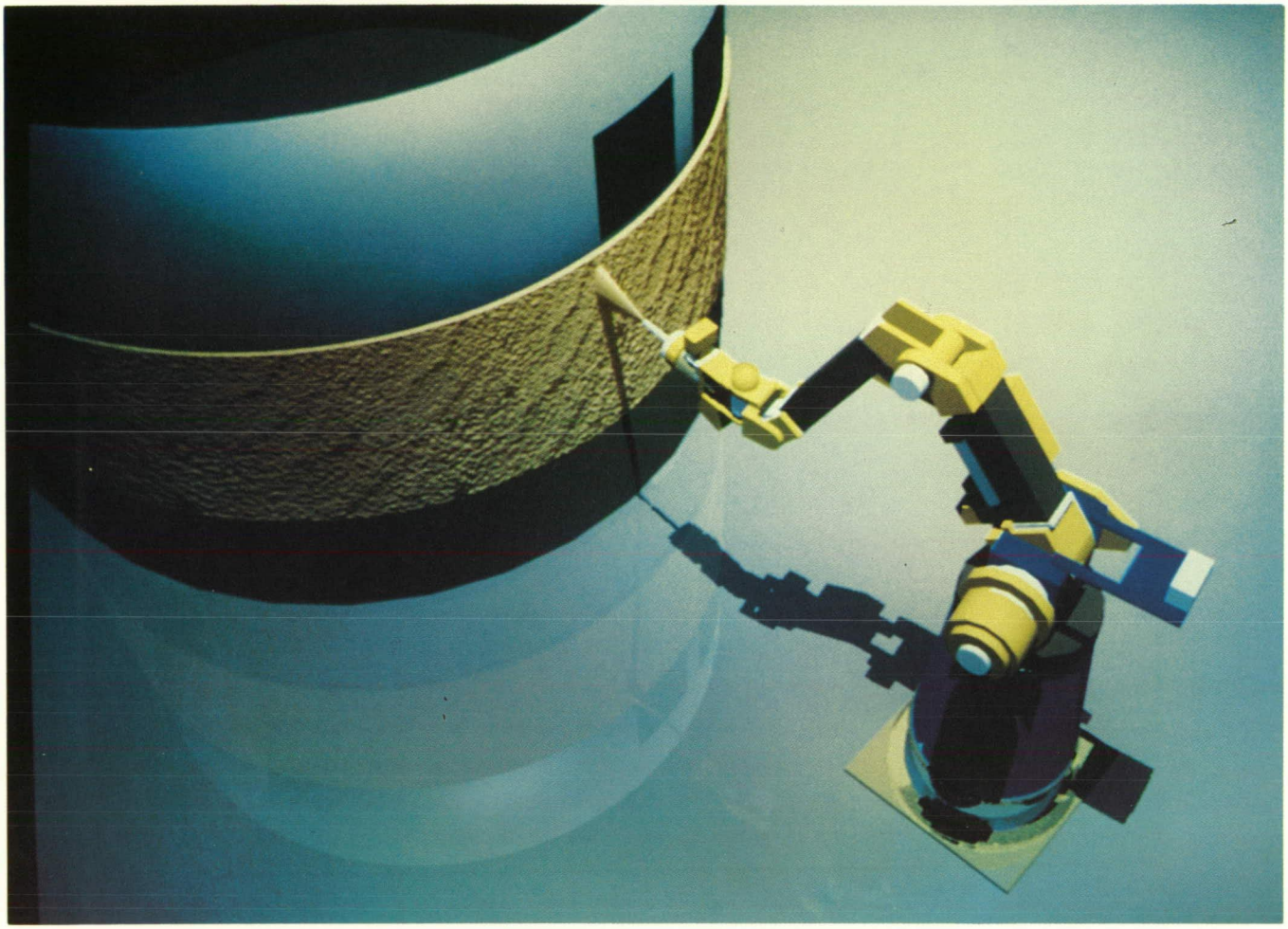

Figure 156. Enhanced Wavefront Image of Kinematic Simulation

there is an impending collision between the robot and turntable. Robot coordinates are optimized off-line on the workstation, translated, and converted into robot-compatible form and downloaded to the robot. The IGRIP kinematic simulation capability results in cost savings to the government by minimizing wasted material and nonproductive labor since the spray parameters are optimized off-line.

A video tape of the simulation is being produced with Wavefront Technologies Animation Software to accurately depict foam spray (Fig. 156). The motion data of the ET-SOFI spray booth kinematic simulation has been translated from Deneb into Wavefront's Dynamic Imaging System. Texture mapping, ray tracing, and materials properties are added to the objects of the simulation allowing the simulation to be displayed as a high-resolution realistic dynamic animation. The frames of the animation are being rendered on a Silicon Graphics 4D 120GTX. Rendered frames are recorded on video tape at a rate of 30 frames per second producing an animation of approximately 1 minute. The Wavefront animation complements the Deneb IGRIP kinematic simulation by providing additional features, not available from Deneb, that allow users to realistically visualize important characteristics such as foam thickness and texture.

E. Martinez/EH43
(205) 544-2724
Sponsor: Office of Space Flight

Nondestructive Evaluation Technology

Nondestructive Evaluation (NDE) data are often ignored or misinterpreted when dealing with solid rocket motor (SRM) components. Few outside the NDE discipline have been able to understand the complexities of the information NDE data provides, or to interpret the effect of NDE-located "defects" on SRM performance. MSFC is learning to provide NDE data in a more meaningful format to manufacturing engineers, analysts, and program managers — particularly those involved with SRM programs.

By using NDE data in a complementary manner, mapping data to a common frame of reference, and equating data to meaningful materials and performance properties, NDE contributes more to overall program goals. MSFC has developed the Integrated NDE Data Reduction System (INDERS) to perform these functions. Digital NDE data from a variety of sources are accepted by the system and mapped to a common frame of reference. Data from different sources are then correlated and matched to material properties.

INDERS also provides a set of statistical validation tools and tools for the quantitative development of mechanical cutting plans. The overall goal of these tools is to reduce the effect of subjectivity in dealing with NDE data. Development of INDERS has continued over the past year. Recent advances have improved the runtime and accuracy of INDERS analyses. Data analysis times have been reduced by almost 400 percent over earlier versions, while simultaneously improving the data's accuracy by more than 50 percent.

Recently, INDERS entered its fourth stage of development. During this phase, the analysis routines have been expanded to incorporate algorithms for handling of data from film radiography, digital eddy current, and video inspections. At the same time, the scope of the program has been broadened to include investigation of the physics of SRM failure modes, the influences of materials properties which have been ignored in the past, and the development of NDE techniques for extrapolating important properties and characteristics such as ply orientation, density, and others. This work has included the design of eddy current probes for measuring the directional conductivity of composites.

Within the past year, INDERS has been distributed to more than a dozen government and industry laboratories for use in establishing correlations between NDE data and motor performance. This broad distribution led to the development of a plan for wide-scale release of INDERS as a multimodality inspection data tool. The release will likely be a joint effort between MSFC and Boeing Aerospace Company.

Also this year, INDERS was selected as the standard framework for performing NDE analyses supporting the Advanced Launch System, SRM, process-optimization studies for the Inertial Upper Stage, and most activities of the Solid Propulsion Integrity Program. Several other programs have expressed a strong interest in applying INDERS.

L.H. Hediger/EH13
(205) 544-2544
Sponsor: Solid Propulsion Integrity Program

Space Debris and Micrometeoroid Testing

Spacecraft designers must anticipate many space environmental factors which affect the success and usefulness of any given mission. Two of the important factors affecting the operating conditions and the survival probability of a spacecraft are the meteoroid and space debris flux. In the last few years, studies by various organizations and individuals have identified the threat of an impact as being of a greater magnitude than was previously identified. Data has been presented which conclude that some experiments flown in Earth orbit to detect meteoroids actually detected mostly aluminum oxide particulates from solid rocket motors, and that the orbital debris flux in certain regions of Earth orbit was either comparable to, or greatly exceeded, the interplanetary meteoroid flux. Therefore, it is evident from the recent studies and papers presented that the orbital debris problem is a real concern for large, long-term spacecraft, and collision probabilities are increasing as the orbital population increases. This increased threat has increased the need for space debris simulation to determine the penetration probability of various spacecraft designs.

Due to the increased threat of collision with meteoroids and principally orbital debris, the Light Gas Gun Facility was reactivated at MSFC to serve as the Meteoroid/Orbital Debris Simulation Test Facility for the Space Station *Freedom* Program. The facility consists of a light gas gun with a 12.7-mm (0.5-in) launch tube capable of launching 2.5- to 12.7-mm (0.098-to 0.5-in) projectiles with a mass of 4 to 300 mg (14×10^{-5} to 10.5×10^{-3} oz) at velocities of 2 to 8 km/s (6,561 to 26,246 ft/s), and three target tanks of 0.607 m^3 (21.437 ft^3), 0.53 m^3 (18.72 ft^3), and 28.5 m^3 (1,006.5 ft^3). Projectile velocity measurements are accomplished via pulsed x ray, laser diode detectors, and a Hall Photographic Station.

Orbital debris impact testing began in July 1985, and approximately 700 samples have been tested to date. Spheres and a limited number of cylinders of 6061 aluminum and 1100 aluminum, ranging in diameter from 3.1275 to 9.52 mm (0.123 to 0.375 in), have been launched at velocities ranging from 2,000 to 7,500 m/s (6,561 to 24,606 ft/s). All cylinders consisted of a length-to-diameter ratio of 1. Test sample configurations included 6061-T6 Al 1-mm thick (0.040 and 0.063 in) and Kevlar single bumpers, and 60-61-T6 Al double bumpers, triple bumpers, and 6061-T6/Kevlar double bumpers. All multiple bumpers were configured to provide an equivalent weight of a single bumper arrangement. Various configurations and materials have been tested with and without multilayer insulation within the 10.16- to 30.48-cm (4- to 12-in) spacing between the bumper and pressure wall. Multiple bumpers were spaced 2.54 cm (1 in) apart within the overall spacing. Candidate window material, and different laminate configurations, and a limited number of pressure bottles have also been tested.

A cursive test program to determine the effects of stress in test panels (simulated module pressure) has been completed, but a more extensive test program is required to further define impact damage.

Predicted debris flux indicates that the majority of the orbital debris will strike the spacecraft at 45- and 60-degree incident angles; therefore, oblique testing was required. Using the same configurations as noted above, tests were performed at incident angles of 30, 45, 60, and 75 degrees from the perpendicular. Although a large number of oblique tests have been completed, more testing is required to quantify the impact damage, including spall and secondary ejecta, to determine the most reliable protection system. Therefore, this test program is still in progress. Of primary importance to long duration spacecraft designers is the ability to launch projectiles at higher velocities; therefore, an effort has been initiated to develop an electric discharge launcher capable of launching lightweight particles at velocities above 10 km/s (6.2 mi/s). This system has been fabricated and is in the development phase, with a projected completion date in the fourth quarter of 1989.

R.A. Taylor/EH15
(205) 544-2554
Sponsor: Space Station Project Office

Load/Recovery Resiliency Testing on Redesigned Solid Rocket Motor Joint Seal Materials

The Space Shuttle Redesigned Solid Rocket Motor (RSRM) field joint may experience a small (9-mil maximum) gap opening resulting from joint deflections during the initial pressurization transient after motor ignition. Joint seal materials must possess sufficient resiliency to track the rapid joint opening without loss of contact with the sealing surface. Two types of tests were conducted to evaluate resiliency characteristics of seal materials: free resiliency, as described in last year's Research and Technology report, and programmed release. This report addresses the programmed release tests in which the sealing surface was moved according to a precise simulation of the worst-case predicted gap opening while the residual sealing load applied by the O-ring material was continuously monitored.

The principal material tested was the fluorocarbon rubber designated V1115, the baseline RSRM O-ring seal material. Two other materials (fluorocarbon V835 and silicone S650) were also tested for comparison data and to complete the documentation of an extensive data base on these alternate materials. The baseline material and comparison materials were tested in the form of an O-ring with 9.208 cm (3.625-in) interior diameter and a cross-section diameter of 1.290 cm ± 0.010 cm (0.290 ± 0.004 in). All test O-rings were formed using a HydraPak splice joint to simulate the actual flight hardware O-rings as closely as possible. The primary focus of the investigation was to validate the use of V1115 fluorocarbon in RSRM field joints. This was accomplished by characterizing the effects of critical factors on load/recovery response. Test matrices were designed to assess influences of each factor, temperature, time under compression, and amount of compression, to the extent present in the motor operational environment. The baseline and alternate materials were evaluated in the primary field joint matrix. Materials were held under 18-percent compression at ambient temperature of 24 °C ± 2 °C (75 °F ± 5 °F) for selected time periods up to a maximum of 360 days prior to testing. Additional tests were conducted on the V1115 material including thermal cycling and an evaluation of reduced compression (16.5, 15, and 12 percent) at ambient temperature for periods up to 180 days prior to testing. The thermal cycling tests involved outdoor storage at MSFC under 18-percent compression for up to 360 days and simulated Kennedy Space Center (KSC) cyclic environment in an environmental chamber under 18-percent compression for periods of 90 and 180 days.

The assembled test fixture is shown in Figure 157. O-ring recovery is measured using an extensometer. Clip gauges provide a measurement of gap opening amount and parallelism, and the load cell determines the residual sealing load applied by the O-ring as the sealing surface is withdrawn. All tests were conducted at 24 ± 1 °C (75 ± 2 °F).

Figure 157. Assembled Test Fixture

ORIGINAL PAGE
COLOR PHOTOGRAPH

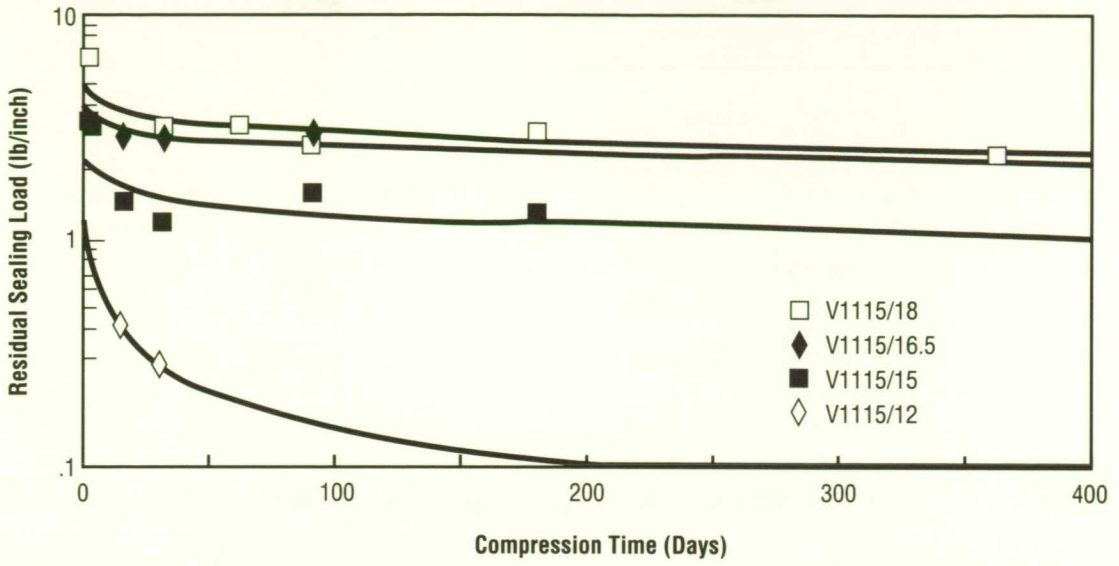

Figure 158. Long Term Load/Recovery for V1115, 75 °F, Various Percent Compressions

The results from tests of the V115 material under the selected levels of compression for extended periods of time are shown in Figure 158. Each data point represents the average of three tests. Reduced compression data have special significance when considering the refurbishment/reuse conditions of RSRM hardware. Pits or scratches in the O-ring gland must be repaired by hand sanding to a smooth surface, which increases the local gland depth and lowers the effective squeeze on the O-ring.

The KSC cyclic temperature environment was a statistically-based simulation of the extreme temperature excursions over the two selected 3-month periods. Results from these tests were in good agreement with the baseline results from 24 °C (75 °F) storage.

The overall results from this test program support the selection of fluorocarbon V1115 for RSRM joint seals in a controlled-temperature environment. Real time data for 360 days at 18-percent compression provide assurance that under this condition, contract end-item specification requirements for field joint assembly times of 180 days can be met. Initial compressions as low as 15 percent will still provide positive sealing loads after 180 days. Reduced compression conditions in this range will likely be encountered in refurbished hardware.

Clinton, R.G.: Load Recovery Resiliency Testing on Shuttle RSRM Joint Seal Materials. Test Report #EH33-34/89-1, Materials and Processes Laboratory, MSFC, June 1989.

St. Aubin, B.K.: RSRM Seal Design Summary Report. TWR-17991 Rev. A, MTI/W, September 1988.

R.G. Clinton/EH34
(205) 544-2682
Sponsor: Office of Space Flight

Catalytic Water Purification

The projected logistics penalties associated with long-term manned space missions make the on-board reclamation of waste water necessary. Existing systems based on distillation, membrane separation, ion exchange, and adsorption are effective at removing the majority of contaminants from spacecraft humidity condensate, waste shower and laundry water, urine, etc. However, spacecraft waste water typically contains significant amounts of low-molecular weight organic contaminants. The high solubility and volatility of these organic contaminants tend to make them difficult to remove from waste water using existing water reclamation systems. Safety concerns relative to a crew's long-term use of recycled drinking and hygiene waters necessitates that technologies be developed to remove these contaminants from water. Three advanced technologies are under development to meet this need. All three are based on the approach of catalytically converting trace organic contaminants to chemical species which are more readily removable from water by existing systems.

The first approach utilizes enzymes which are immobilized to a suitable solid support. The enzymes are selected for the specific organic contaminants to be treated. An example is the enzyme urease which converts urea to ammonium and carbonate ions according to the following reaction:

$$\underset{\text{urea}}{H_2NCONH_2} + \underset{\text{water}}{2H_2O} \xrightarrow{\text{urease}} \underset{\text{ammonium}}{2NH_4^+} + \underset{\text{carbonate}}{CO_3^=}$$

The ammonium and carbonate ions are easily removed using typical ion exchange resins. Other enzymes, such as alcohol and aldehyde oxidases, are also being examined for application to a broader range of contaminants. Immobilized enzymes are an attractive candidate for trace organic contaminant removal since resource penalties associated with their integration into existing filtration systems will be minimal.

The second approach utilizes noble metal and metal oxide catalysts operating at elevated temperatures or in the presence of ultraviolet (UV) radiation. The catalysts enhance the oxidation of trace contaminants by molecular oxygen. For example, ethanol may be converted to carbon dioxide according to the following reaction:

$$\underset{\text{ethanol}}{CH_3CH_2OH} + \underset{\text{oxygen}}{3O_2} \xrightarrow[+\text{ catalyst}]{\text{UV or heat}} \underset{\text{carbon dioxide}}{2CO_2} + \underset{\text{water}}{3H_2O}$$

Depending on the conditions, carbon dioxide may be removed as a gas by a membrane separator or as dissolved carbonates by ion exchange resins. Thermally or UV-enhanced approaches of these types offer the potential of removing a broad range of contaminants, and of commonality with current microbial control devices.

The third approach under investigation utilizes solid-state semiconductor materials which generate hydroxyl radicals from water in the presence of UV radiation. The radicals catalyze the oxidation of organic contaminants. For example, ethanol may be converted to carbon dioxide or to acetate ions according to the following reaction:

$$\underset{\text{ethanol}}{CH_3CH_2OH} + \underset{\text{hydroxyl radical}}{OH\bullet} \xrightarrow[+\text{ catalyst}]{\text{UV}} \underset{\text{acetate}}{CH_3COO^-} + \underset{\text{hydrogen ion}}{4H^+}$$

Acetate can be easily removed by ion exchange resins. Solid state semiconductors offer the potential benefit of eliminating the need for adding molecular oxygen.

Potential space applications of these catalytic technologies include water reclamation systems for Space Station *Freedom*, Mars missions, or lunar bases. Applications in commercial ultrapure water systems in the electronics or pharmaceutical industries are also possible.

R.M. Bagdigian/ED62
(205) 544-7222
Sponsor: Small Business Innovative Research Program

Automated Systems

Robotics

MSFC is committed to a broad-based robotics program for supporting NASA missions involving rendezvous and docking missions as well as in situ servicing of satellites and orbital platforms. The Center's unique facilities include real time full-scale hardware simulators for investigating and testing under conditions as close as possible to those encountered in actual flight.

The Orbital Mobility Hardware Simulator Facility (Fig. 159) contains two independent simulators: a Dynamic Overhead Target Simulator (DOTS), and an Air Bearing Mobility Unit propelled by thrusters over a 1,280 m^2 (4,200 ft^2) precision cast epoxy floor. The DOTS, which spans the entire floor, is an 8 degree-of-freedom (DOF) dynamic simulator capable of positioning a 454 kg (1,000 lb) payload to an accuracy of 12.7 mm (0.5 inch) within the 54,864 m^3 (180,000 ft^3) volume of the facility. Simultaneous operation of both simulators support docking with stable and unstable satellites, formation flight, station keeping, berthing, etc. The floor can also support full scale/weight mocking and simulators for mechanism evaluation with a friction coefficient of 0.00006 (Planar).

MSFC's Robotics Laboratory has the hardware and real time capability for automated satellite servicing

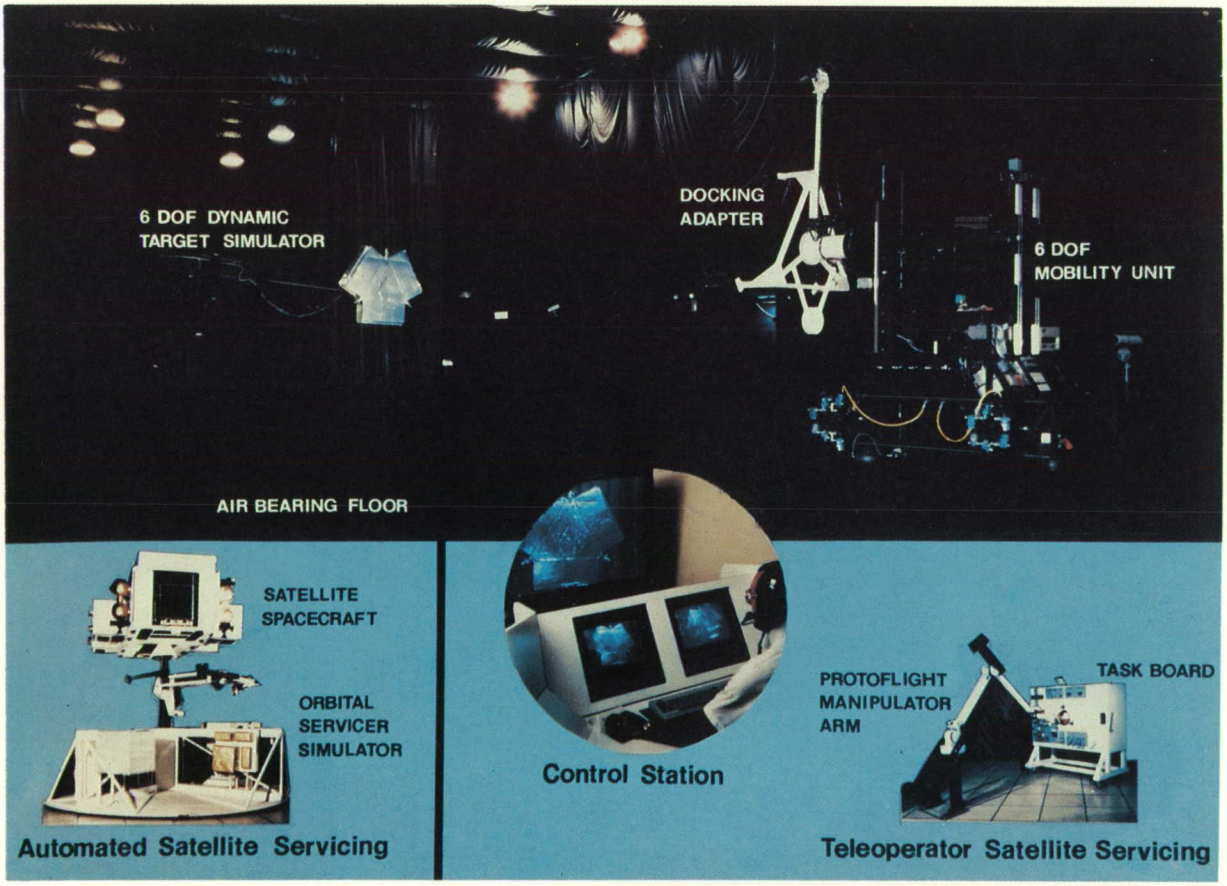

Figure 159. Orbital Mobility Hardware Simulator Facility

ORIGINAL PAGE
COLOR PHOTOGRAPH

with the integrated Orbital Servicer System (IOSS) and for telerobotic servicing with the Protoflight Manipulator Arm (PFMA). The IOSS is used to evaluate mating and demating of various types of orbital replacement unit mechanisms and for demonstrating automated modular servicing of spacecraft. The PFMA, used for supporting studies associated with Space Station *Freedom* and remote satellite servicing, is a 6-DOF manipulator with a range of 25.4 to 243.8 cm (10 to 96 in). Current enhancements include force/torque sensing displayed to operator, automatic force/torque control, and a calibrated task board for quantitative evaluation of manipulators, operators, or computer control schemes. Near-term enhancements include an updated real-time computer system supporting auto motion tracking and compensation, task primitives, automation, and interfaces for either human or artificial operators.

Both the Orbital Mobility Hardware Simulator Facility and the Teleoperator and Robotics Facility support total black-out and simulation of solar illumination for orbital lighting and camera studies. Other features include teleoperator constraints of time delay, video frame rate reduction, gray scale reduction, and resolution reduction.

T.C. Bryan/EB24
(205) 544-3550
Sponsors: Office of Space Flight
Office of Aeronautics and Space Technology
Office of Space Station

Automatic Gore Panel Mapping System

Gore panels are curved metal sections welded together to form domes for use at opposite ends of the hydrogen and oxygen tanks of the External Tank (ET). Using a chemical milling process, the gore panels are reduced in thickness over large areas to decrease the ET's total weight. When the thickness of the panel is reduced, the panel must be inspected to ensure that it meets the required specifications for thickness and uniformity. Presently, gore panels are manually mapped for thickness. Since hundreds of points must be measured to accurately map a panel, the process is extremely tedious and time consuming. Therefore, an Automatic Gore Panel Mapping System that will automatically measure, store, and compute the thickness of gore panels is currently cooperatively under development at the Productivity Enhancement Facility by MSFC, Martin Marietta, and the University of Alabama in Huntsville.

This system consists of a Cincinnati Milacron T3-776 robot, a Krautkramer-Branson WDM ultrasonic thickness measuring device, and a Packard Bell personal computer (PC). In the initial phase of this task, a point-to-point contact ultrasonic sensor was developed. This sensor mounts at the end of the robot arm and must make hard contact with the panel to obtain thickness readings. A hydrosensor is being developed to replace the point-to-point sensor. The hydrosensor utilizes a stream of water to couple the panel surface and offers several advantages over the point-to-point contact sensor. The hydrosensor will allow continuous path scans of the panel. Hard contact with the panel and potential damage is eliminated. The time delay of robot arm in-and-out motion and the associated contact and release times are eliminated. The hydrosensor uses the same ultrasonic instrumentation, scans the panel over the same predetermined grid, and reads and records data with the same accuracy as the point-to-point sensor; however, it performs the operation considerably faster.

Thickness information is stored in the PC and also displayed in a color thickness contour map as can be seen in Figure 160. Several software enhancements were accomplished during this period. One enhancement includes a routine that evaluates the thickness data and identifies areas of the panel that need further reduction. This information is stored in a file, converted to robot-compatible form, and downloaded to the robot. A robot end-effector is being developed to automatically scribe on the panel the contours of the areas requiring rework.

The robot sequence can be programmed and optimized off-line using a Silicon Graphics IRIS Model 3120 workstation and a graphics package from Deneb Robotics known as IGRIP (Fig. 161). The optimized robot coordinates are downloaded to a PC via an RS-232C interface where the coordinate information is converted into robot-compatible form using a software package known as the Remote Off-Line Program System from Cincinnati Milacron. The robot trajectory information is then downloaded to the robot for execution using a HOST

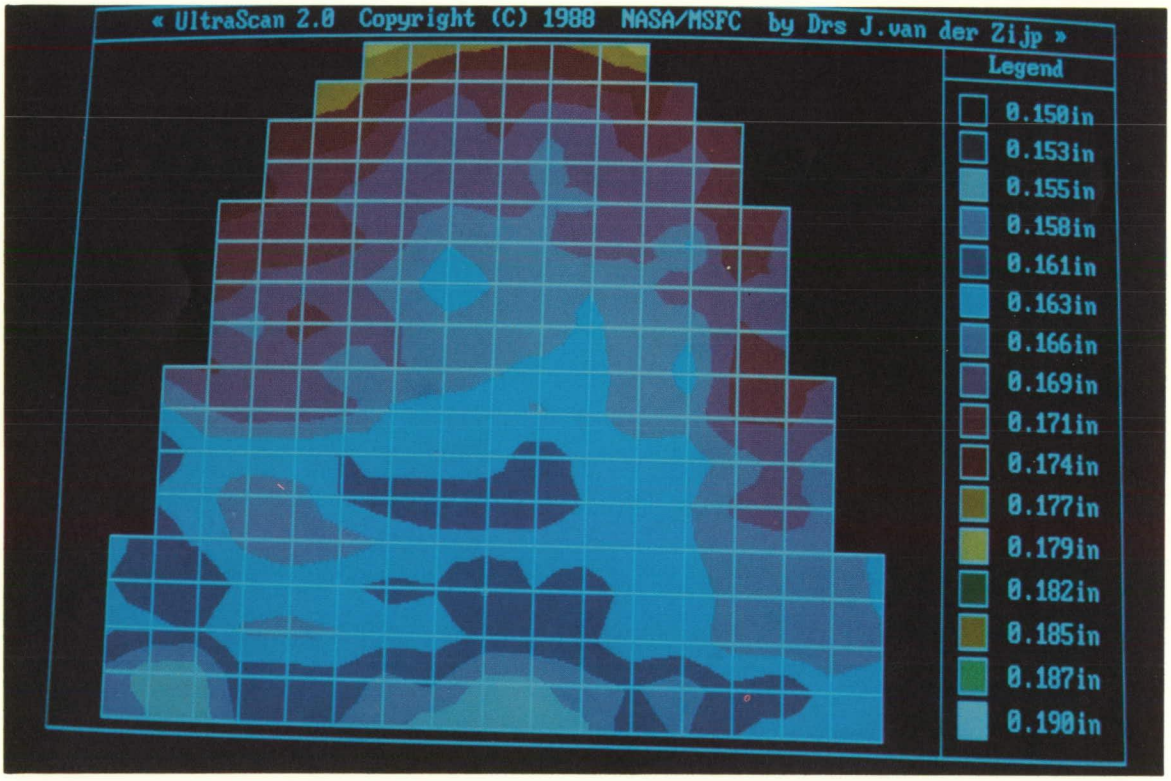

Figure 160. Gore Panel Thickness Contour Map

communications software package. The Deneb IGRIP simulation presently under development is an enhancement over the SILMA simulation reported last year.

The Automatic Gore Panel Mapping System has been successfully integrated and demonstrated. When completed, this system will result in substantial cost savings to the Government. In addition, the quality and reliability of the panels will be enhanced as a result of the improved repeatability and accuracy of this system. Results obtained from this task have shown great potential for the application of this system to other manufacturing processes. Work is presently underway to automate other operations of gore panel processing which include spraying, cutting, and removing the masking on the panels prior to the chemical milling. Transfer of this technology to the production sites is presently being negotiated.

E. Martinez/EH43
(205) 544-2724
Sponsor: Office of Space Flight

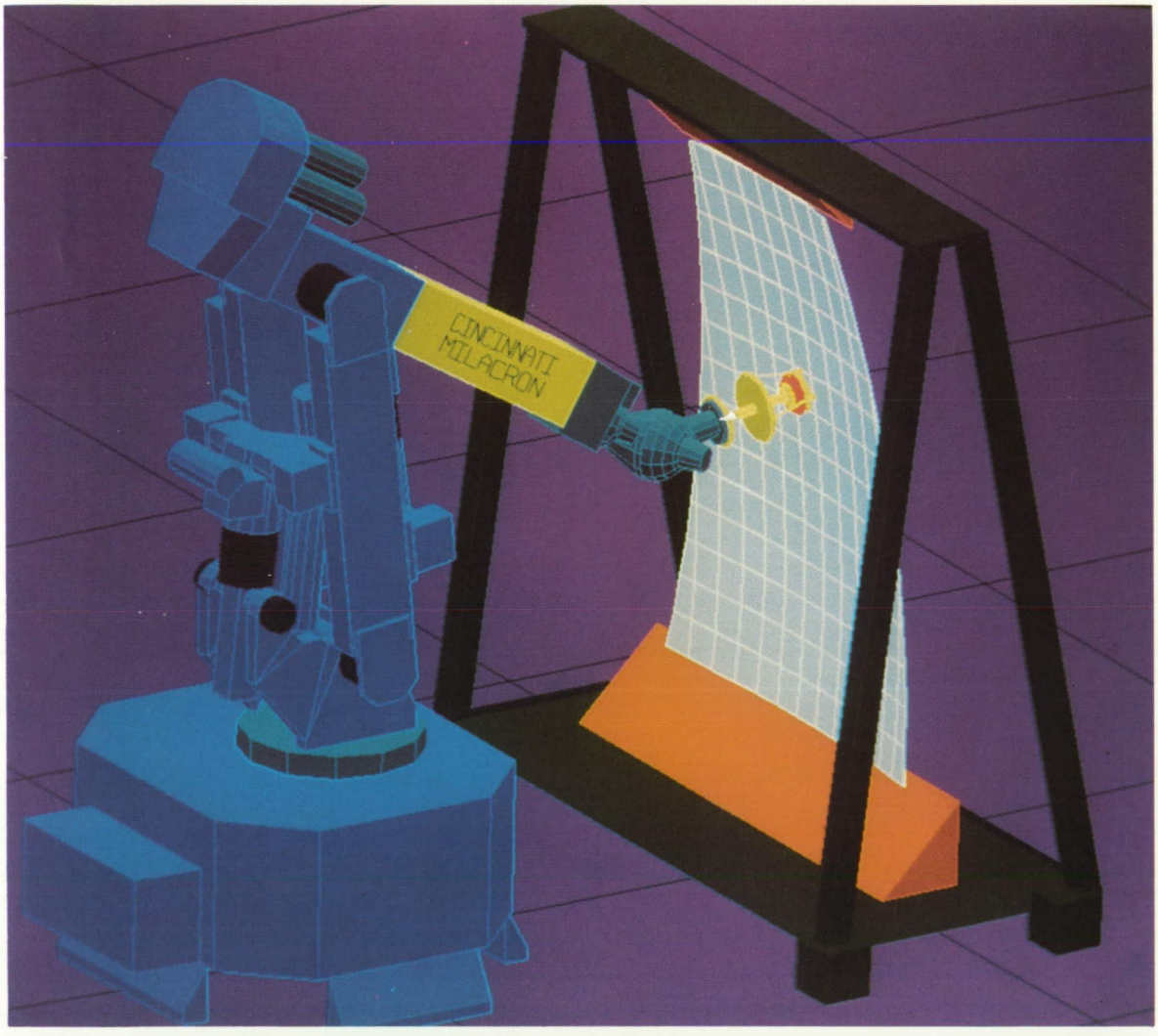

Figure 161. Deneb Robotics Gore Panel Off-Line Simulation

Robotic Eddy Current Inspection System

With the increased use of carbon-carbon and graphite-epoxy materials in the aerospace industry also comes a demand for more sophisticated methods of nondestructive evaluation (NDE) of these types of materials. The integration of computers into NDE equipment, coupled with automated methods of scanning hardware, allows both inspection and interpretation of results to be performed on-line in real time. The development of these types of "smart" systems also results in shorter inspection times and a more accurate interpretation of results.

Currently, under the direction of MSFC, the University of Alabama in Huntsville (UAH) has a contract to develop a "smart" system for eddy current inspection of both carbon-carbon and graphite-epoxy materials and hardware. This system will consist of a robotic manipulator arm to hold an inspection probe, a turntable to allow automated rotation of cylindrical hardware, and an eddy current instrument for test signal generation and display of results, all linked together by a supervisory computer, which will store and interpret all of the test results. At the completion of the contract, UAH will turn the system over to the NDE branch at MSFC.

Laboratory tests have indicated that digital eddy current testing may be an excellent method for in-process monitoring of composite components. The robotic eddy current inspection system will be used to perform in-process analyses of graphite epoxy and carbon-phenolic raw materials, in-process parts, and finished parts to identify general trends in processed materials, and localized changes in conductivity which might indicate changed mechanical or thermal properties. This information will be correlated with NDE data from other sources, such as computed tomography and ultrasonics through the Integrated NDE Data Evaluation and Reduction System.

A further contribution of digital eddy current testing is expected to be the extrapolation of ply-orientation from three-dimensional readings of directional conductivity. This technique provides critical orientation information in a quantitative format, which can then be used to support thermostructural analyses of as-built components. Preliminary testing with carbon-carbon indicates this information is critical in predicting the failure load of composite rings and cylinders. Efforts to extract ply-orientation effects in wrinkled carbon-carbon cylinders have shown promise, but require further development.

The information gained from this program will contribute to an increased understanding of the effects of processing on composite material properties and of the way composite materials fail.

C.C. Bryson/EH13
(205) 544-2553
Sponsor: Solid Propulsion Integrity Program

Fully Automated Variable Polarity Plasma Arc Welding

Computer-controlled variable polarity plasma arc (VPPA) welding has been used in the production of the Space Shuttle External Tank since 1981. This welding system provides control of critical welding parameters in addition to providing historical documentation of programmed and actual welding parameters for all welds. The welding operator, however, is still responsible for providing real-time adjustment to weld current, seam tracking, wirefeed entry, and plasma jet orientation. Therefore, the quality and repeatability of VPPA welds is still dependent on human judgement and skill.

MSFC has undertaken the design and development of a fully-automated VPPA system, independent of human intervention, in order to eliminate the possibility of weld defects caused by human error. The overall system architecture is shown in Figure 162. The system integrates multiple sensors (providing real time information on weld bead geometry, weld joint location, and wirefeed entry) with a weld model (describing weld geometry in relation to critical parameters) and computer-controlled VPPA equipment. This system provides real-time, closed-loop control of the weld as it is being made. A secondary benefit of this system is the potential of automated weld visual inspection, either during or after welding, of the weld dimensions, peaking, and mismatch for quality assurance requirements.

Presently, design and development of each individual component of the overall system is in work. Sensors based on stereo imaging and structured laser light are being evaluated for seam tracking. An optical laser sensor has been demonstrated for weld bead profiling and torch rotation. The wirefeed control sensor is under study as well as the host computer architecture. The weld model theoretical relations have been identified and a computer simulation of the VPPA process should be available within a year. NASA and NASA contractors are both involved because the complexity of the system requires a team approach, utilizing multiple engineering disciplines.

C. Kurgan/EH42
(205) 544-2705
Sponsor: Office of Space Flight

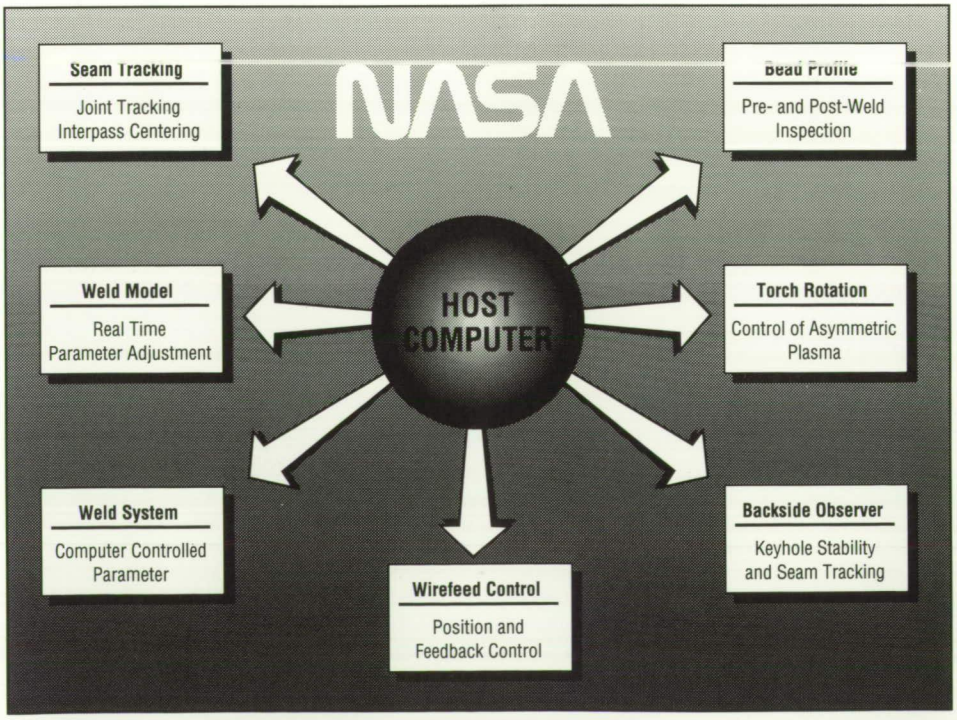

Figure 162. Automatic Weld System

Automated Rendezvous and Docking

With the development of the Orbital Maneuvering Vehicle and Space Station *Freedom*, and the upcoming needs of the Orbital Transfer Vehicle and the Mars Rover Sample Return mission, autonomous rendezvous and docking has become a practical necessity. This research has explored the use of a Charge Injection Device (CID) based tracker for use as the sensor to determine the relative states (range, roll, pitch, yaw, azimuth, and elevation) between a chase vehicle and a target vehicle for docking with the target vehicle within specifiable error and contact rate bounds. Further work is investigating the use of a Charge Coupled Device (CCD) as the sensor for the system.

A tracking system, consisting of laser diode illuminators in a CID-based tracker (the Retroreflector Field Tracker (RFT)) and a target with retroreflective tape mounted on an air-bearing vehicle, has been implemented. The system was tested on an air-bearing vehicle in the Flight Robotics Laboratory to evaluate autonomous rendezvous and docking under conditions similiar to those that will be encountered in space. A diagram of the system test configuration can be seen in Figure 163. The RFT was placed on a platform to one side of the flat floor, centered above grapple fixtures that represent two of the three fixtures in the Three Point Docking Mechanism. A Compaq 386 personal computer was

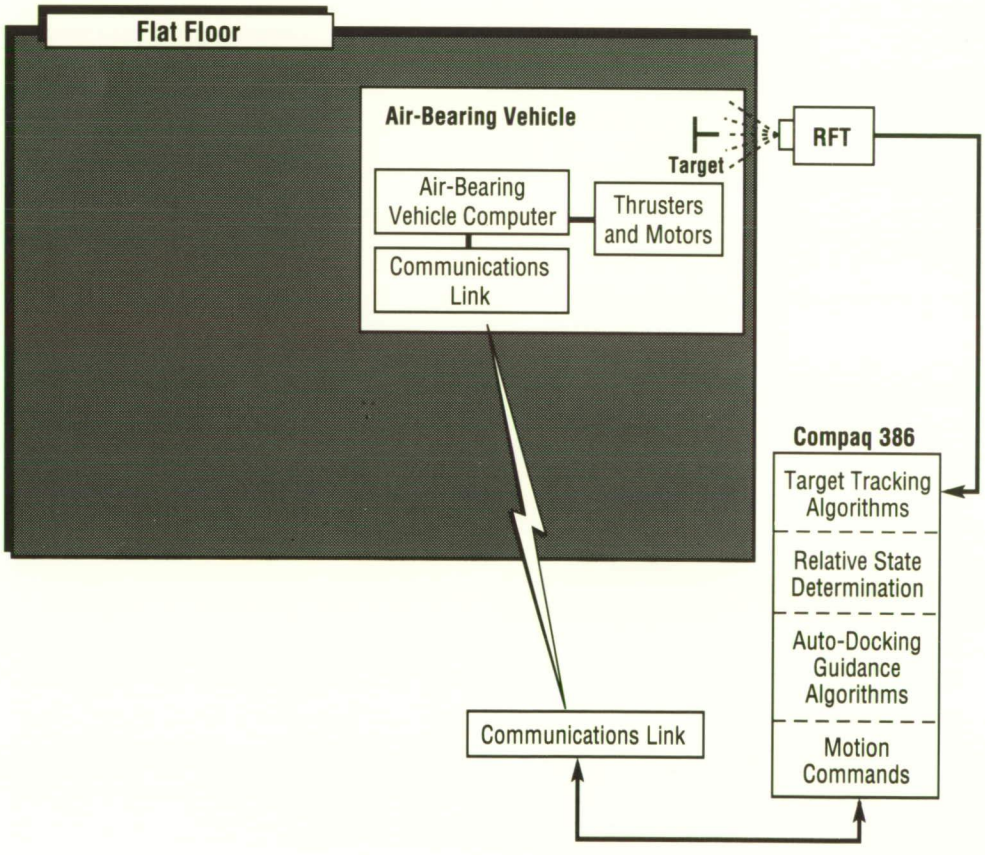

Figure 163. System Block Diagram

used to take data from the tracker, follow the reflections of interest (i.e., the ones that came from the target), calculate the relative states of the tracker and the vehicle, and send commands to the vehicle to bring it in to a hard dock with the grapple fixtures. The target was mounted on a 6 degree-of-freedom air-bearing vehicle in order to simulate as closely as possible the frictionless environment of space. A sample run can be seen in Figure 164. This figure shows an initial yaw position of +30 degrees and an initial yaw rate of +0.2 degrees per second.

Further work is continuing to replace the CID sensor with a CCD-based sensor, and to place the system onboard the air-bearing vehicle to provide a single integrated autonomous rendezvous and docking package — illumination, tracking, relative state determination, guidance, and propulsion.

From the previous and continuing work, numerous docking scenarios can be studied. The effects of initial position, lighting, orbital mechanics, and other areas can be explored in the Flight Robotics Laboratory Facility.

R. Howard/EB24
(205) 544-3536
Sponsor: Office of Aeronautics and Space Technology

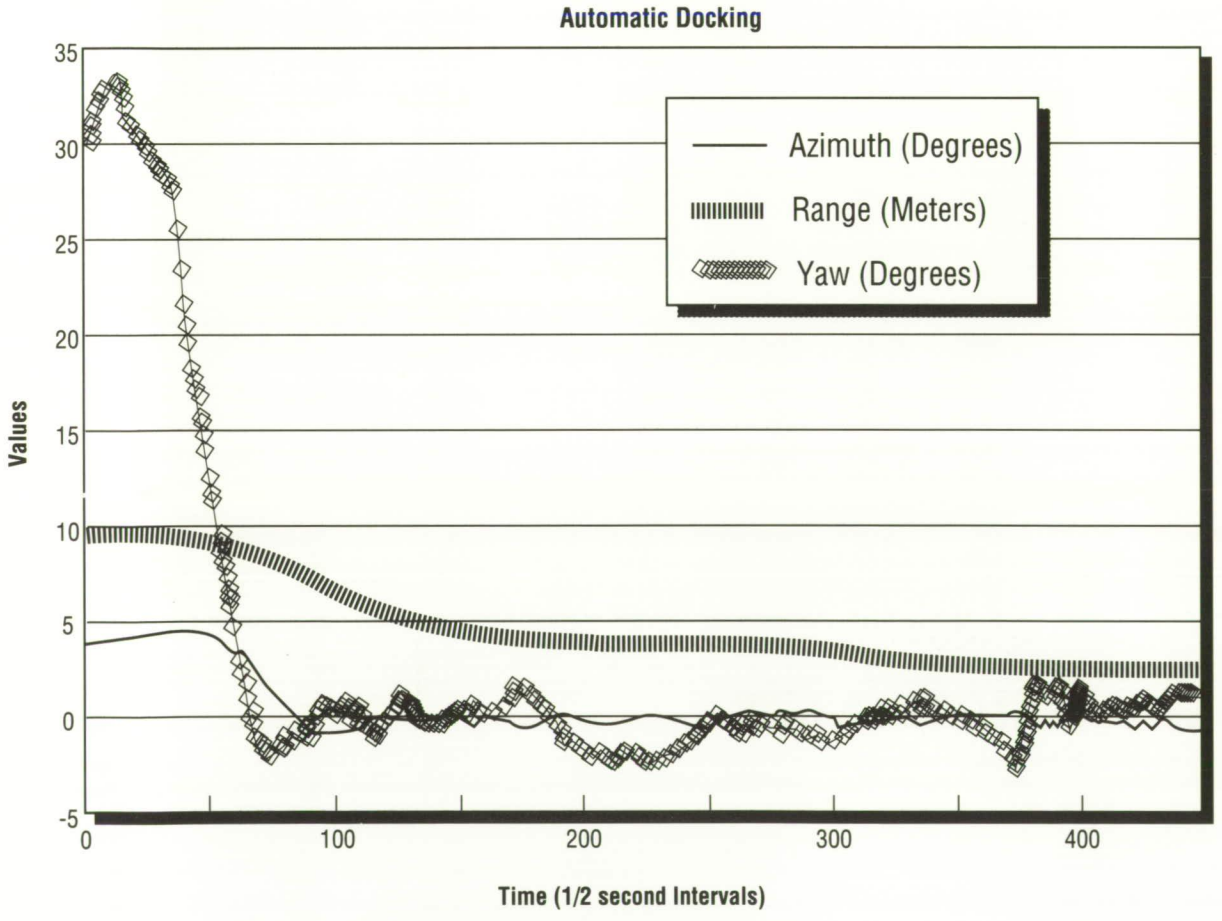

Figure 164. Sample Docking Run

Space Systems

Space Station Module Power Management and Distribution

The Space Station Module Power Management and Distribution (SSM/PMAD) breadboard models the power distribution within a Space Station *Freedom* Habitation or Laboratory module. Besides power hardware, the system includes computer control through a hierarchy of processors. At the lowest level is a fast, simple (from a computer standpoint) switch gear, capable of quickly safing the system. At the next level are local load center processors, called lowest level processors (LLP's), which execute scheduling, do redundant switching, and shed loads which pull more than scheduled power. Above the LLP's is a communication and algorithmic controller which coordinates communications with the highest level of control. At this highest level are three cooperating artificial intelligence (AI) systems which handle load prioritization, scheduling, load shedding, and fault recovery and management. The system, working together, provides an excellent venue for developing and examining advanced automation techniques.

The work which led to the SSM/PMAD breadboard began in 1984. The system, as it exists at this time, consists of the software, which was delivered December 17, 1988; 20 kHz power hardware; and the computer hardware shown in Figure 165. The configuration shown in this figure has been the baseline for demonstration and testing. Plans for the future involve modification of the system to keep it in line with plans for S.S. *Freedom*, and continuing research and development into the best way to automate the management and distribution of power in a space station module or similar structure. Modifications now in progress include a change from 208 V at 20 kHz to 150 Vdc throughout the breadboard. The topology for the power coming in to the breadboard will be changed from the current ring bus to a star bus. These changes, to keep the breadboard in line with current baselines, will require replacement of the switchgear and much of the wiring, and modification of other hardware and software. Figure 166 shows the evolved system.

To facilitate further development in automation, several efforts are under way. An upgrade to the computing and communications hardware is expected to remove some current bottlenecks. These changes are also shown in the second figure. A knowledge base management system (KBMS) is being designed. The KBMS will make the knowledge in the system more explicit, and will help in grouping the knowledge into modular groups of rules. It will also serve as an overall framework to expedite improvement of the cooperation between the three AI systems in the breadboard. An enhanced model will support an improved user interface, and provide a centralized repository of system-specific knowledge. An intermediate level of autonomy is planned, so that the system can assist the user. Also, a link is planned to the Lewis Research Center Autonomous Power System.

Walls, Bryan: Automation in the Space Station Module Power Management and Distribution Breadboard. Proceedings, Space Operations-Automation and Robotics Workshop, in press, 1989.

Walls, Bryan: Exercise of the SSM/PMAD Breadboard. Proceedings, 24th IECEC, in press, 1989.

B.K. Walls/EB12
(205) 544-3311
Sponsors: Office of Space Station
Office of Aeronautics and Space Technology

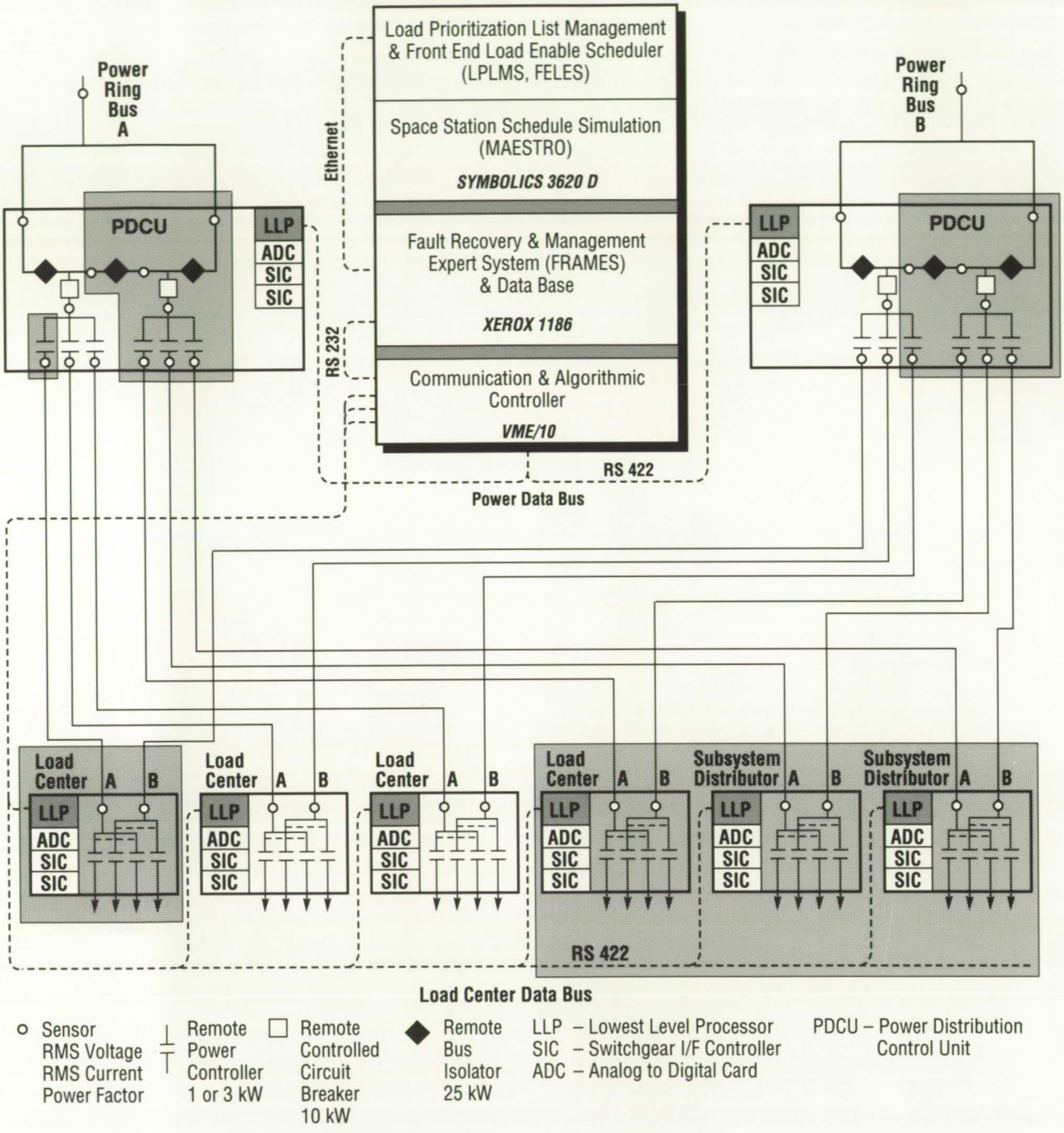

Figure 165. Current SSM/PMAD Configuration (20 kHz Ring Bus)

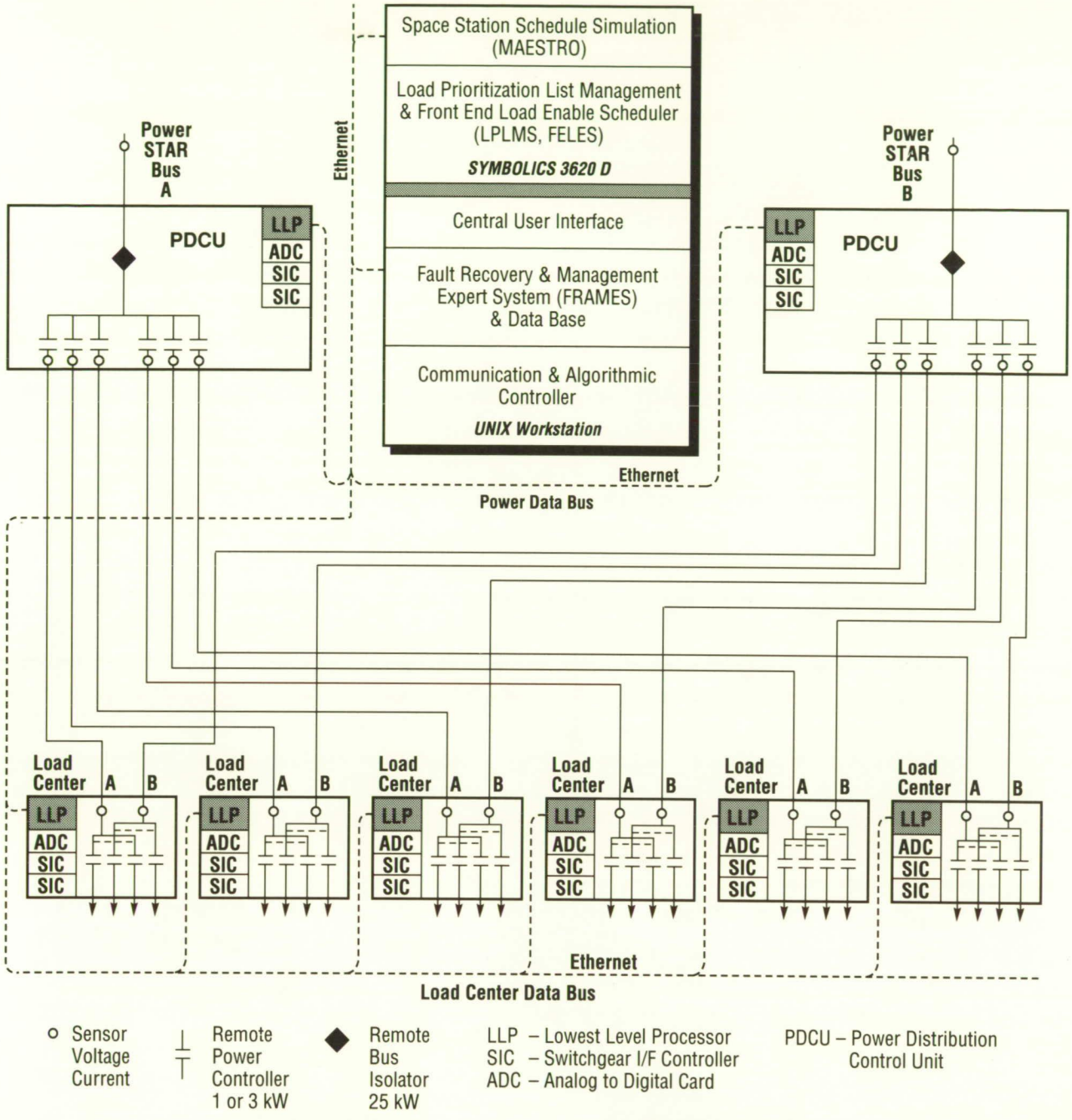

Figure 166. Planned SSM/PMAD Configuration (dc Star Bus)

Pathfinder In-Space Assembly and Construction

The objective of this project is to develop the technology required for assembling and constructing large structures in space. In-space assembly and construction is one of four key areas in Project Pathfinder. For this area of Pathfinder, the tasks are to develop methods for moving objects precisely into their proper position, assembling and disassembling major substructures, permanently joining structural elements, and assembling structures on-orbit with robotics. MSFC has the responsibility of defining the requirements for heavily-loaded, mechanically-fastened and welded truss joints. MSFC will also define the requirements for joining large components to major structures.

A personal computer version of NASTRAN was used to build and analyze a three-dimensional finite element model of a 37-m (120-ft) diameter tetrahedral aerotruss. A 3,591 N/m^2 (75 lb/ft^2) pressure load, found from a literature search, times 3 g's was converted to an equivalent axial load and applied at the node points of the aerotruss model to determine the maximum axial loads on the truss members. The results of this analysis showed that approximately 90 percent of the axial load was between 444.8 N (100,000 lb) tension and 444.8 N (100,000 lb) compression for both a four-point and an eight-point payload constraint. This load was chosen as the design load for a heavily loaded mechanical or welded truss joint.

A detailed mechanical truss joint concept is being designed and will be built to meet the requirements of a heavily-loaded truss joint. The selected joint design will allow the truss members to be easily assembled/disassembled via a robot that can place objects within a tolerance of ±0.0508 cm (0.020 in). In addition, the joint will be designed to allow truss elements to be assembled when there are large thermal distortions, assembly preloads, and tolerance build-ups.

Defining the technology necessary for large components to be assembled in-space involves determining the size, shape, weight, and thermal and radiation protection of the large masses that will be required for exploration missions. Examples of generic large components include pressurized modules, fuel tanks, cryogenic tanks, liquid storage tanks, and unpressurized storage tanks. A study will be performed to determine the optimum attachment scheme and loads for these large components. These large component loads will be placed on the aerotruss to determine the sensitivity of the large component loads on the aerotruss.

F.P. Thomas/ED52
(205) 544-4936
Sponsor: Office of Aeronautics and Space Technology

CO_2 Laser Research and Development

Effort is continuing in the investigation of candidate lasers for use in the space-based coherent Doppler lidar known as the Laser Atmospheric Wind Sounder (LAWS). Although LAWS is a facility instrument under the Office of Space Science and Application's Earth Observing System, this effort is funded under the Civil Space Technology Initiative. The effort consists of both theoretical and experimental investigations of lasers and laser subsystems to determine the optimum technology for LAWS.

The FY89 work encompassed investigations at MSFC, Langley Research Center (LaRC), the Jet Propulsion Laboratory (JPL), the National Oceanic and Atmospheric Administration's (NOAA's) Wave Propagation Laboratory, and Spectra Technology, Inc. Complementary investigations in the area of radio frequency discharge systems were undertaken at Qsource, Inc., by means of a phase I Small Business Innovative Research contract.

Investigations at Spectra Technology, Inc., have been pursued via a jointly funded effort with the Air Force Geophysical Laboratory. Work accomplished to date includes measurement of the small signal gain for the rare isotope $C^{12}O^{18}_2$ in an x-ray preionized discharge amplifier, and the determination of vibrational-relaxation rate constants for He, N_2, and $C^{12}O^{18}_2$ from the decay of small signal gain. A higher than expected small signal gain was obtained for the rare isotope, which will make the performance comparable to that of normal CO_2.

Investigations at the NOAA Wave Propagation Laboratory centered around a series of studies to understand system losses and increase frequency stability. Detailed modeling of the system has been completed and a number of experiments were performed to improve frequency stability by a change in locking methods. A self-filtered unstable resonator design was tested and found not to be satisfactory due to the overall system gain being too low.

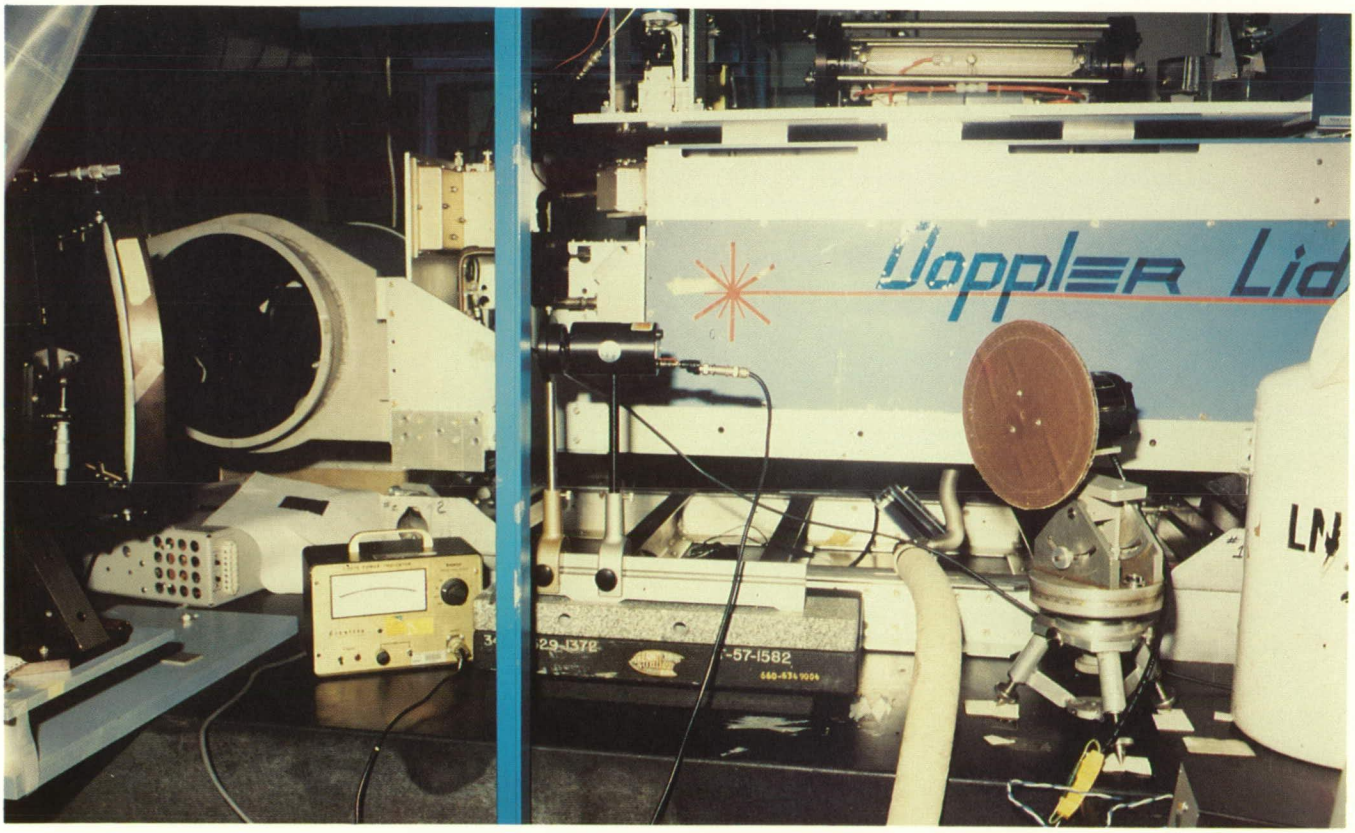

Figure 167. Set-up for Predetection Experiment

ORIGINAL PAGE
COLOR PHOTOGRAPH

LaRC investigations resulted in a better understanding of the role of water in the catalysis process. At LaRC, a process for pretreatment of the catalyst with a small amount of water was developed to prevent short-term decrease in catalyst efficiency. The catalyst was also successfully pretreated for rare isotope operation, and experiments were performed at elevated temperatures using the pretreated catalyst with the $C^{12}O^{18}_2$ isotope.

JPL and MSFC jointly investigated the Pulse Systems, Inc., LP-140 laser system. Initial investigations indicated that the laser was transverse-mode hopping and that cavity length instabilities were dominating system performance. Suggestions were made for improving the transverse-mode problem, but implementation must await successful stabilization of the cavity length.

In-house investigations have focused on modeling the self-filtered unstable resonator design and performing laboratory investigations into predetection amplification and stabilization of the cavity of the LP-140 laser. The results of the predetection amplification experiments showed improvement against a distributed target, as well as a hard target. The experimental setup for the predetection experiment is shown in Figure 167. Papers on the modeling and the predetection experiments were prepared for the Fifth Conference on Coherent Laser Radar.

Hamilton, C.E., Pindroh, A.L., Lawrence, T.R. and Fisher, C.H.: Small Signal Gain and Vibrational Relaxation for Rare Isotope $C^{12}O^{18}_2$. Presented at the Fifth Conference on Coherent Laser Radar, SPIE, Munich, West Germany, June 5–9, 1989.

Smithers, M.E.: Frequency Stability Using a Self-Filtering Unstable Resonator. Presented at the Fifth Conference on Coherent Laser Radar, SPIE, Munich, West Germany, June 5–9, 1989.

Johnson, S.C.: Laser Detector Preamplifier Experiments. Presented at the Fifth Conference on Coherent Laser Radar, SPIE, Munich, West Germany, June 5–9, 1989.

J.W. Bilbro/EB23
(205) 544-3467
Sponsor: Office of Aeronautics and Space Technology

Coherent Doppler Lidar Research and Development

Research and development into coherent Doppler lidars (laser radars) once again covered a broad region during FY89. Technical support was provided to Program Development in the evaluation of proposals for the Laser Atmospheric Wind Sounder (LAWS). Technical support is continuing in this area, supporting the two parallel study contracts awarded as a result of proposal evaluations to General Electric and Lockheed. Upgrade work continues on the ground-based lidar facility, backscatter measurements, system simulations, target calibration, and various system investigations including atmospheric effects and signal processing. In addition, the Fifth Coherent Laser Radar Conference was co-chaired in Munich, West Germany, June 5–9, 1989.

Software capabilities for display and processing of lidar data continue to be enhanced. Programs have been installed which allow collection and processing of data from the in-phase and quadrature processor system and which also allow the analysis of data for frequency chirp. Several experiments have been performed to obtain information on atmospheric effects on the lidar return and to simulate the conical scan expected from the space-based LAWS system.

Efforts in the measurement of backscatter have been concentrated in the area of calibration in the single particle mode of the continuous-wave backscatter (Beta) systems. Although the systems were designed to operate in either a volume mode or a single-particle mode, previous calibrations have concentrated on the more conventional volume mode. This effort has incorporated the use of a particle generator system developed by the Georgia Institute of Technology to map the sensitivity of the Beta systems as a function of particle size and location in the measurement beam. The experimental setup is shown in Figure 168. An example of the results of the calibration of the 10.6-μm system is

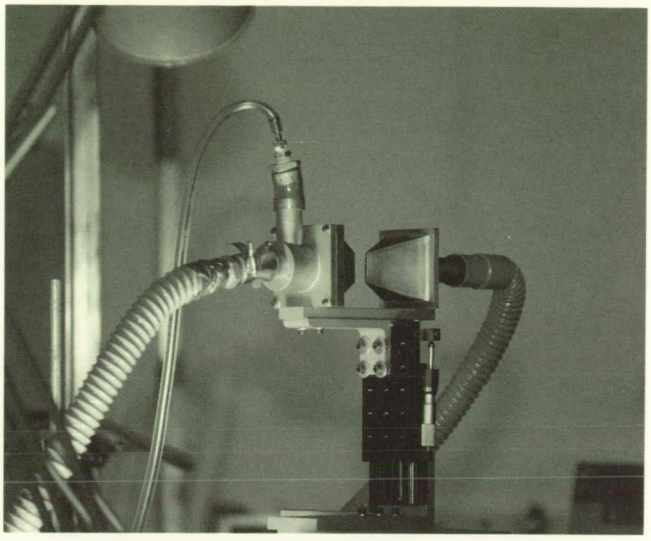

Figure 168. Experimental Set-Up for Coherent Doppler Lidar Research and Development

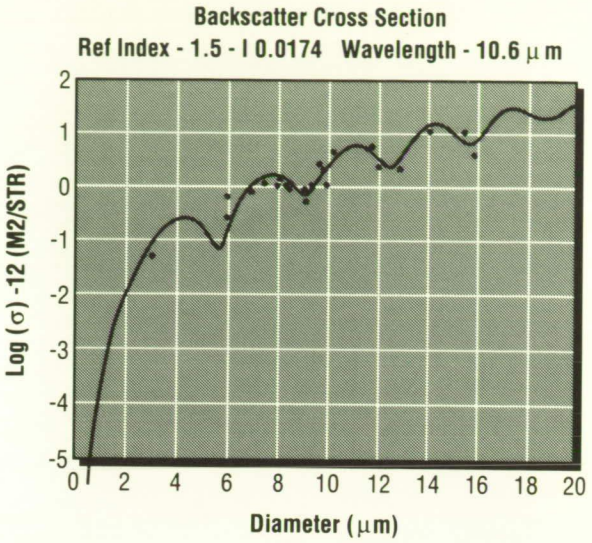

Figure 169. Backscatter Cross Section

shown in Figure 169. The pulsed system is also being modified to ascertain the effects of long-term pulse averaging. Both of the Beta systems (10.6 and 9.11 μm) will be flown aboard the Ames Research Center's DC–8 this fall as part of the Global Backscatter Experiment, which is intended to provide data on atmospheric backscatter for use in the design of LAWS.

In-house work is continuing in support of LAWS. Programs are being developed which will provide the capability of simulating the LAWS system from a variety of orbital and atmospheric conditions. A study was performed to establish the feasibility of using the LAWS system to provide topographic mapping.

Investigations are continuing to assess the feasibility of incorporating a new laser transmitter into the MSFC pulsed-lidar system for renewed airborne measurements.

Jones, W.D.: Calibrating a Continuous-Wave Focused CO_2 Lidar for Single-Particle Mode Backscatter Measurements. Presented at the Fifth Conference on Coherent Laser Radar, SPIE, Munich, West Germany, June 5–9, 1989.

Anderson, R.: A Correct Polarization Technique to Calibrate Hard Targets for Coherent Lidar Systems. Presented at the Fifth Conference on Coherent Laser Radar, SPIE, Munich, West Germany, June 5–9, 1989.

Bilbro, J.W.: Global Surface Mapping. Presented at the Fifth Conference on Coherent Laser Radar. Sponsored by SPIE, Munich, West Germany, June 5–9, 1989.

J.W. Bilbro/EB23
(205) 544-3467
Sponsor: Office of Space Science and Applications

Welding in Space

Welding processes produce strong, light, gas-tight joints easily and economically on the Earth's surface. Welding is also a potentially valuable process for fabrication and repair of metal structures in the environment of space. But the space environment imposes certain difficulties (and provides certain opportunities) for would-be welders: zero-g, vacuum, severe operator constraints due to the need to protect operators from the environment, limited available power, difficulty in dumping waste heat, etc.

The effects of zero-g are under study through the use of the NASA KC-135 aircraft. At present no significant effects of gravity upon weld quality have been identified.

Vacuum welding experiments are being designed to be implemented in a vacuum chamber with high gas load capability [six 81-cm (32-in) diffusion pumps] belonging to MSFC's Low-Density Flow Facility.

Two contracts for preliminary studies of space welding tests to be developed for shuttle flight are being monitored. One is an electron beam system; the other is a gas tungsten arc system which emits inert gas to maintain an arc in vacuum.

A.C. Nunes/EH42
(205) 544-2699
Sponsor: Office of Aeronautics and Space Technology

Expendable Lightweight Composite Intertank

The goal of this technology program is to research the use of composite materials in the primary structures of space launch vehicles, such as the Advanced Launch System, a joint NASA/U.S. Air Force project to inexpensively deliver heavy payloads to orbit. The composite intertank (Fig. 170) allows composite materials, design concepts, manufacturing processes, and nondestructive evaluation techniques to be brought together for the production of basic structures.

The baseline vehicle configuration has a 845.71-cm (333-in) diameter intertank with a length-to-diameter ratio of 0.8. Simultaneous trades for the intertank were based on weight, material, fabrication, and system cost effects. A honeycomb sandwich shell was selected as the best of 11 design concepts. Graphite/epoxy (T300/934) face sheets and a glass-phenolic honeycomb core (HFT-3/16-2.0) were the materials selected for construction of the sandwich.

A preliminary full-scale design analyzed the combined loads on the shell, around cutouts, and at the cryogenic propellant tank interface joint. Combined load conditions determined critical scaling parameters during design of a structural test article. Fabrication of the intertank involves both automated filament winding and tape laying to build up the shell around a removable mandrel. A manufacturing implementation plan has been developed for a detailed subscale design of a 200-cm (78.75-in) diameter cylindrical structural test article with the same failure mechanisms as the full-scale design.

Prior to manufacturing and testing the cylindrical article, a set of full-scale component panels and a set of subscale component panels were designed for fabrication and test. Identical materials and manufacturing techniques are being used for the component test panels as will be used for the cylindrical article. Fabrication started in June 1989. Ultrasound, computer tomography, and thermography will be used for nondestructive evaluation of the test panels. Testing will provide a correlation between full-scale and subscale characteristics.

D.B. Ford/ED52
(205) 544-2454
Sponsor: Office of Aeronautics and Space Technology

Accomplishments to Date

- Defined Generic Vehicle Loads and Environmental Requirements
- Traded Concepts Using Weight/Material/Fabrication/Systems Cost Effects
- Developed Preliminary Full-Scale Design and Analysis
- Determined Scaling Parameters and Manufacturing Processes
- Designed Detailed Cylindrical Structural Test Article
- Designed Component Test Panels
- Fabrication Initiated August 1989

Near Term Bench Marks

- Testing Initiated October 1989
- Phase I Complete November 1989

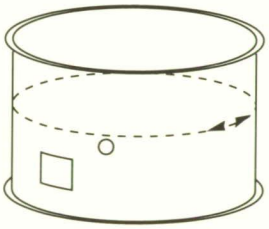

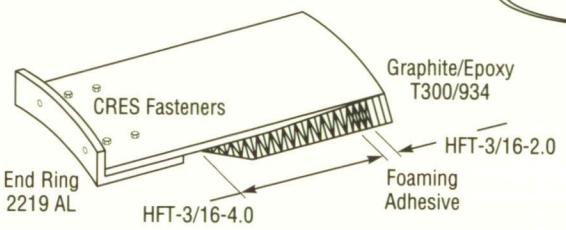

Figure 170. Composite Intertank Status

Computed Tomography for Shuttle Components

Computed tomography (CT) has become a viable method of evaluating the internal structure of shuttle components. CT utilizes highly-collimated x-ray fan beams to reconstruct a cross-sectional image of components. The Advanced Computed Tomography Inspection System (ACTIS), developed by Bio-Imaging Research under contract to MSFC, represents a significant milestone in the development of industrial CT scanners. Other industrial scanners have been built to perform evaluation of a particular component. The MSFC approach was to gain maximum flexibility with the simplest man-machine interface possible. This concept is beautifully demonstrated in ACTIS.

ACTIS employs three x-ray sources to allow adjustable beam energies between 50 keV and 2 MeV. The system geometry is uniquely designed to provide variable scan field diameters and magnifications. X-ray source and geometry selection are accomplished at the touch of a button. The detector system and operating software have also been designed to allow total system optimization for any part. MSFC has received two patents as a result of ACTIS development. The system is limited to objects 120-cm (47-in) diameter and of 1,000-kg (2,200-lb) weight.

An additional 320-keV x-ray tube source is currently being incorporated into ACTIS. This fine-

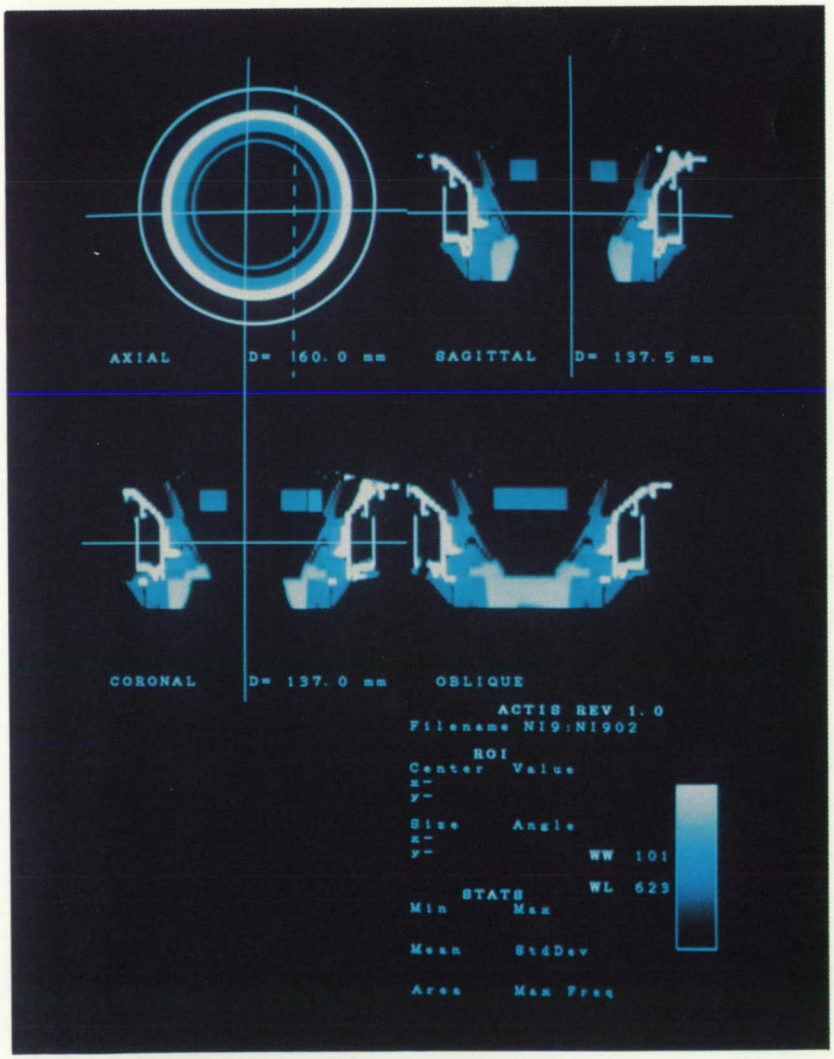

Figure 171. Multiplanar Reconstruction of PALAPA Nozzle CT Images

focused x-ray source will result in images of significantly higher spatial resolution, and will be used in the scanning of smaller hardware, particularly turbine blades from the Space Shuttle Main Engine (SSME).

The system incorporates a number of special image processing features, including image averaging, subtraction, statistical analysis, and color imaging. The system is capable of performing multiplanar reconstruction, a feature which allows the operator to view a data set from any of three mutually perpendicular planes.

MSFC has developed links which allow ACTIS images to be downloaded to any computer-aided design and analysis station which accepts the International Graphics Exchange Standard (IGES) format. Images can then be used to build three-dimensional models of as-fabricated components.

A variety of components from the solid rocket motor, external tank, SSME, and other hardware have been imaged successfully. ACTIS has also been used to scan several large carbon composite nozzles in support of various programs. Chief among these was a PALAPA nozzle, a component of a WESTAR satellite. This nozzle was fired in space and retrieved during a shuttle mission. ACTIS technology will contribute greatly to the development of acceptance criteria for composite materials and the analytical modeling of as-built components.

Figure 171 shows multiplanar reconstruction of CT images of a PALAPA nozzle. Side (sagittal) and end (coronal) views through a number of axial views are shown, as is an oblique view. The plane at which the oblique view is made is represented by the dashed line in the axial view.

L.H. Hediger/EH13
(205) 544-2544
Sponsor: Office of Space Transportation

Advanced X-Ray Astrophysics Facility's Technology Mirror Assembly

The Technology Mirror Assembly (TMA) consists of two mirrors which are approximately two-thirds the size of the innermost pair of mirrors of the Advanced X-Ray Astrophysics Facility (AXAF). The TMA program was designed to demonstrate an ability to fabricate optics to the level of precision required for AXAF. The original TMA program produced a set of mirrors that in x-ray testing at MSFC did not measure up to expected performance. Subsequent to the x-ray tests, the TMA was disassembled and refurbished to correct errors which were discovered in the disassembly process, as reported in last year's report. Although the original problems with the TMA mirrors were largely corrected, new problems arose which again provided valuable information for the program even though they resulted in somewhat decreased performance from what was desired. In addition to the problems reported last year, assembly of the mirrors uncovered an instability which could not be corrected prior to x-ray testing. Consequently, it was decided to align the TMA in the x-ray test chamber just prior to testing. It was felt that this was the only method that would ensure that the system would be in alignment for testing. In order to accomplish this, the laser alignment scanner had to be modified to perform the final alignment in the chamber, and several modifications to the optical bench had to be performed in order to accommodate the alignment system.

Alignment of the TMA was accomplished and a prediction of the results made based on metrology and alignment data. The TMA is shown in the x-ray chamber in Figure 172. During subsequent x-ray testing, x-ray data indicated that the alignment of the TMA was incorrect. On the basis of this data, the chamber was opened and a correction made. When x-ray testing resumed, it was found that the correction was not what was anticipated and that the system initially appeared to be unstable. The system eventually reached equilibrium and the x-ray tests

were completed. Aside from mount instabilities, the mirror performance was excellent. The results of the test data in contrast to the predictions are shown in Figure 173.*

The TMA is currently under investigation to determine the amount of contamination on the mirrors. This data will be used along with the results of the x-ray tests to evaluate the effects of contamination. Investigations to understand the mount instability problem are also in progress.

*Van Speybroeck, L., Reid, P., Schwartz, D. and Bilbro, J.: Predicted and Preliminary Evaluation of the X-Ray Performance of the AXAF Technology Mirror Assembly. Presented at SPIE 33rd Annual Inter. Symp. on Optical and Optoelectronic Appl. Science and Eng., San Diego, CA, August 6–11, 1989.

Slane, P., McLaughlin, E.R., Schwartz, D.A., Van Speybroeck, L.P., Bilbro, J.W. and Nerren, B.H.: Measurement of the Effects of Particulate Contamination on X-Ray Reflectivity. Presented at SPIE Conference, Orlando, FL, March 27–30, 1989.

J.W. Bilbro/EB23
(205) 544-3467
Sponsor: Office of Space Science and Applications

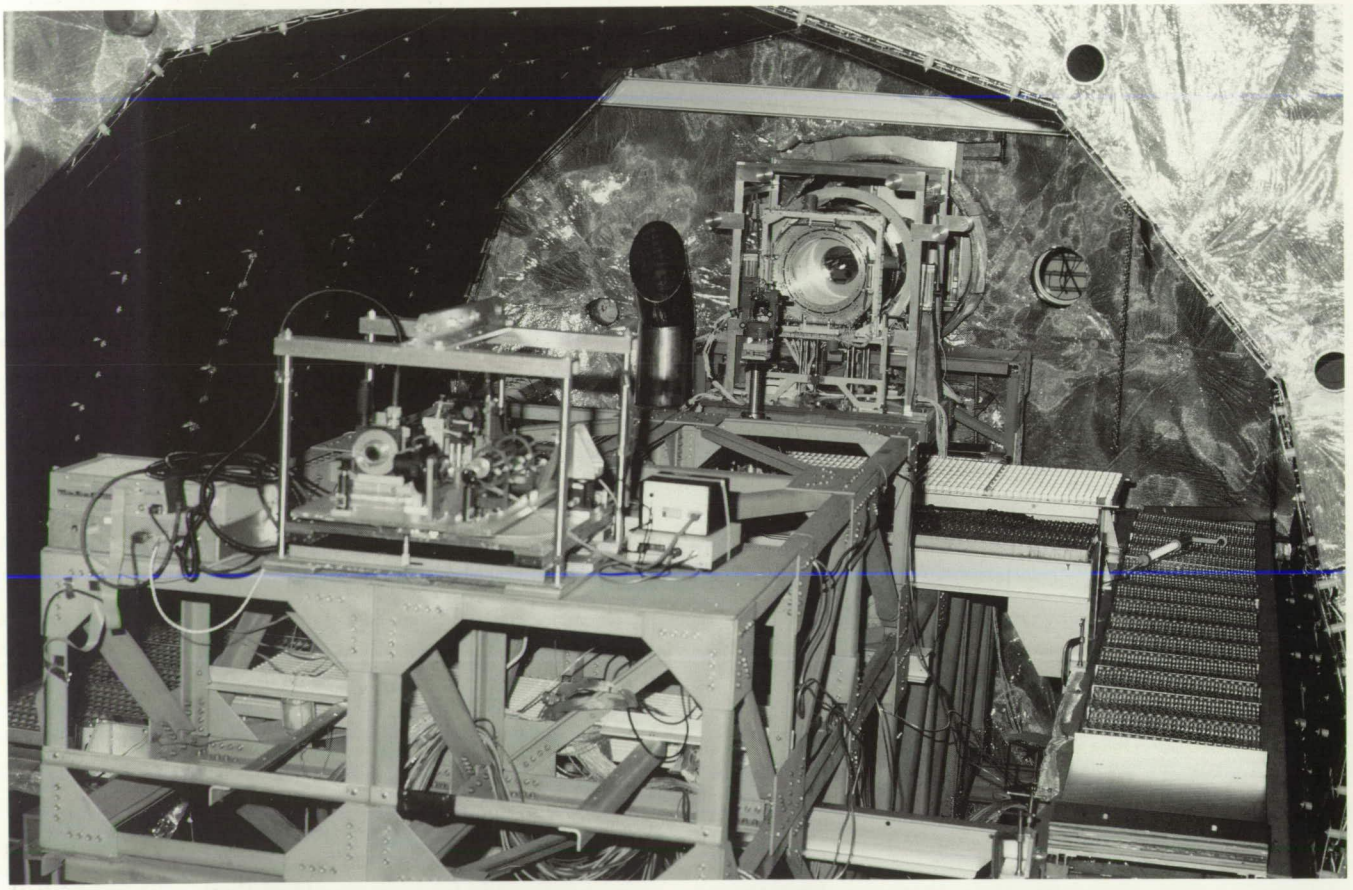

Figure 172. Technology Mirror Assembly Located in the X-Ray Chamber

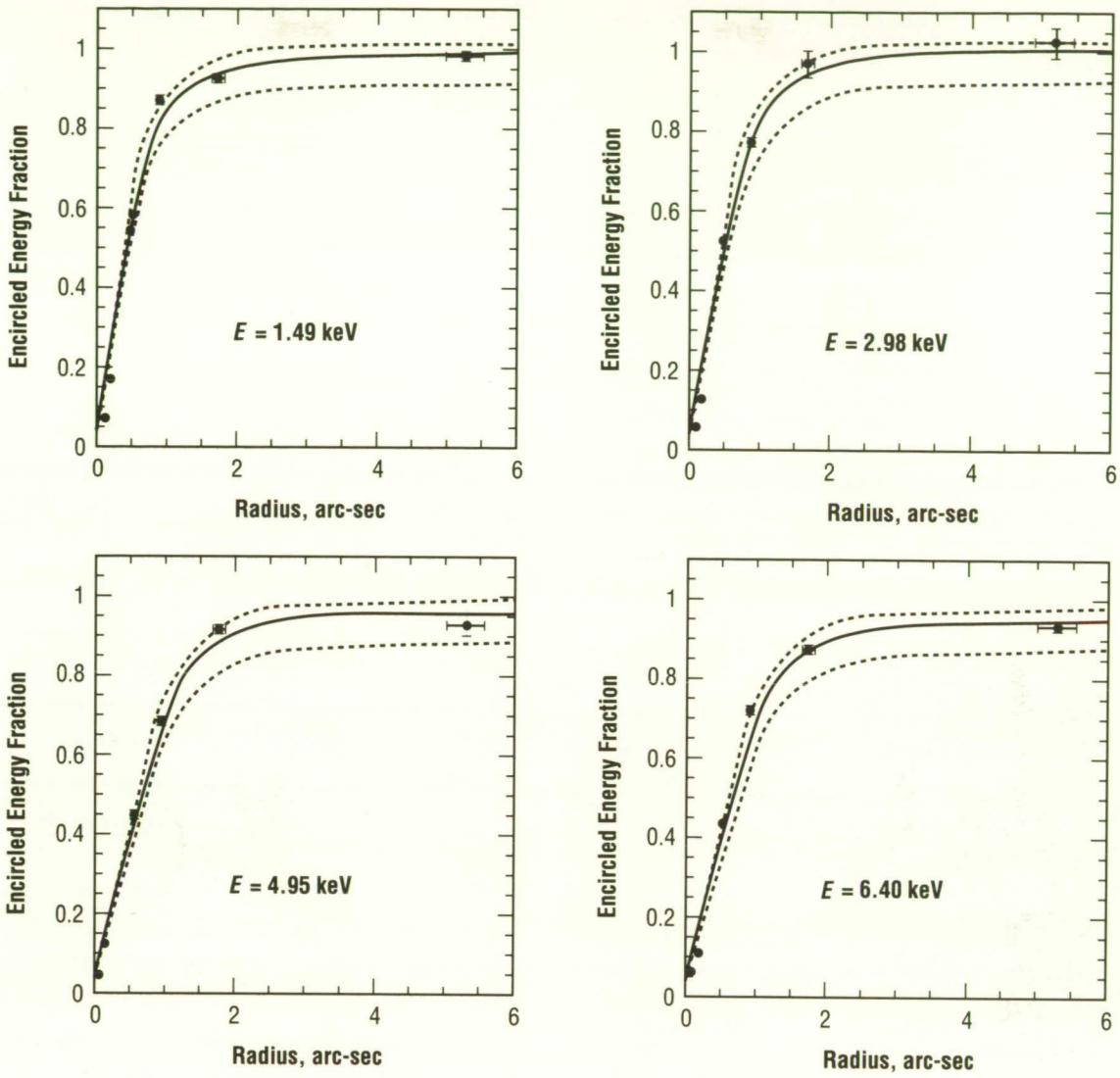

Figure 173. Results of Test Data Versus Predicted Results

Large Space Structure Control Verification

Since the establishment of the MSFC ground facility for large space structures (LSS) control verification in FY86, intensive ground testing, modeling, and control experiments have been conducted under a joint NASA/U.S. Air Force program called Active Control Evaluation for Spacecraft, Phase I (ACES-I). The intent is to compare controller design methodologies applicable for LSS's in terms of time domain performance improvements.

The primary design methodologies are the filter-accommodated model error sensitivity suppression, high-authority control/low-authority control, positivity, and classical decentralized frequency domain techniques.

The ACES-I test configuration (Fig. 174) includes a 13.7-m (45-ft) deployable mast, a 3-m (10.2-ft) antenna, and an antenna feed, providing the structural flexibility characteristics of the LSS, i.e., low frequency, low damping, closely-spaced vibration modes, and large generalized masses. The upper end of the mast is attached to a flight-quality 3 degree-of-freedom (DOF) pointing mount assembly, which in turn is attached to a hydraulically-driven shake table to simulate disturbances likely to be experienced in orbit. At two distinct locations on the mast, a pair of linear momentum exchange devices, along with a pair of quadrature accelerometers, are provided as additional control effectors and sensors. On the lower end of the mast is a flexible 3-m (10-ft) antenna-like structure mounted on a flexible boom. A mirror at the antenna vertex reflects a laser beam (originating from an "inertially fixed" source) to a 2-DOF turning mirror (antenna feed). The turning mirror is commanded to redirect the laser beam to a detector on the antenna, thereby providing image motion compensation (IMC) in a flexible structure representative of a large aperture, flexible offset feed antenna, or of a long focal length, Cassegrain-type telescope.

The ACES-II test configuration has the same features as the ACES-I test article with the addition of the Laser Motion Optical Detector (LaMOD) and an Array Processor Unit (APU). The LaMOD provides 12 times more area for IMC light motion detection, while the APU increases the computing capability of the ACES-I system by a factor of 3. With this increase in capability over the ACES-I test configuration, the ACES-II program will perform frequency, robustness, and failure analyses on the ACES-I controllers. The ACES-III program will examine three additional control techniques and will add three more effectors to the ACES-II test configuration. These effectors, whose locations are shown in the figure, will include bilinear thrusters and one roll torque motor, allowing investigation of complex multibody system interactions. This configuration will be called the ACES-IV test article and will be used to examine previous and additional control techniques that show promise relative to complex system interactions.

H.B. Waites/ED12
(205) 544-1441
Sponsor: Office of Aeronautics and Space Technology

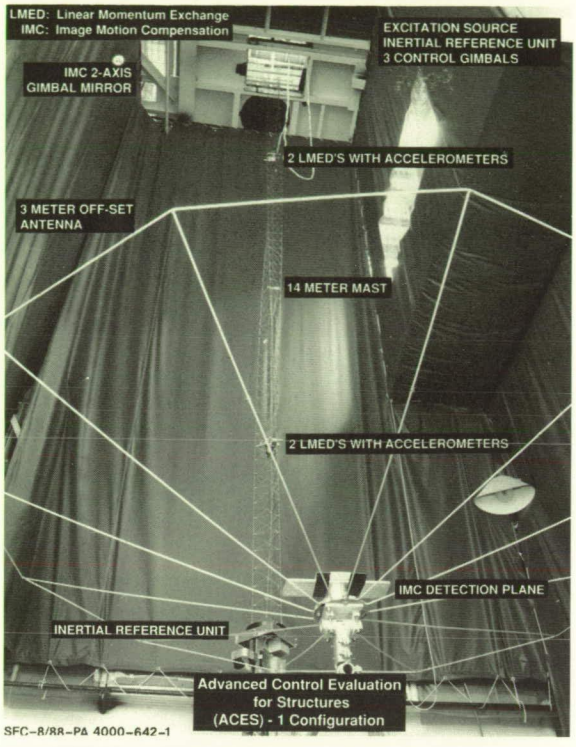

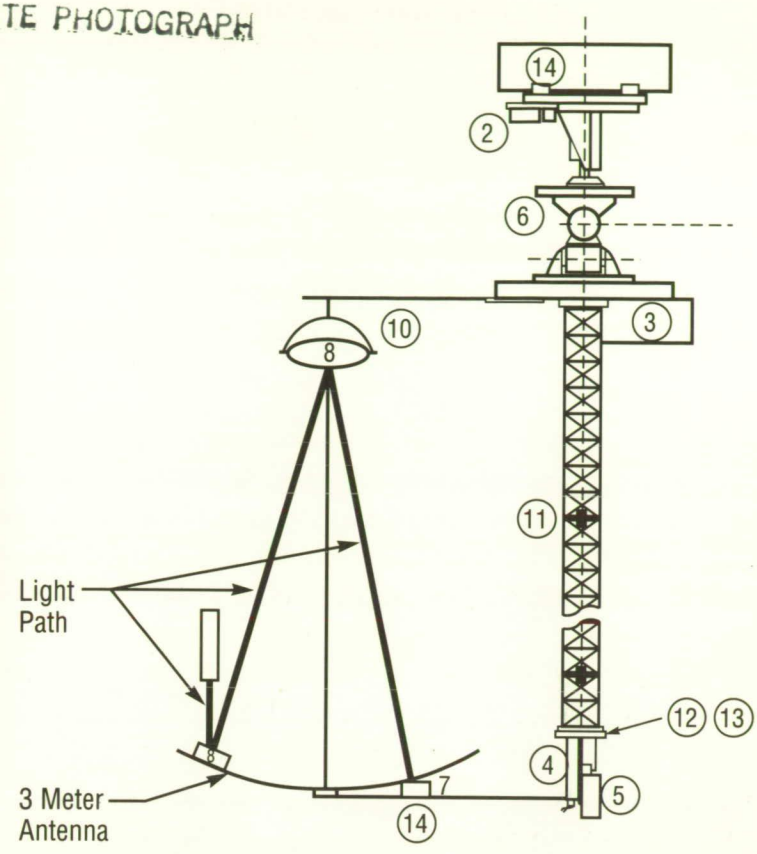

1. Shake Table
2. 3 Axis Base Accelerometers
3. 3 Axis Base Rate Gyros
4. 3 Axis Tip Rate Gyros
5. 3 Axis Tip Accelerometers
6. Advanced Gimbal System (AGS)
7. Optical Detector
8. Reflectors
9. Laser
10. 2 Gimbal System
11. Linear Momentum Exchange Device (LMED)
12. Bilinear Thrusters
13. Roll Tip Motor
14. Enlarged Optical Detector (15 x 15 in)

Figure 174. Side View of ACES-1 Configuration

Control Structures Interaction

With the development of large space structures, the study of control structures interaction (CSI) has become a necessity. Because of this, it is desirable to have a small-scale model which exhibits the approximate dynamics of a full-scale system. With a model, different control schemes can be studied without the expense and time of constructing a larger system.

In response to this need, MSFC has developed a CSI suitcase demonstrator. Figure 175 is a picture of the demonstrator outside of the suitcase. Figure 176 is a block diagram of the CSI demonstrator. The second figure shows the primary components of the demonstrator and the interconnections. The spring-loaded translator simulates a disturbance to the system. The light emitting diode (LED) and the optical detector electronics act together as a position-sensing device. The CSI suitcase demonstrator was designed to have two control loops. One of the control loops is a conventional controller consisting of position feedback from the optical sensor to the torque motor. The gain of this loop is variable for demonstrating its effect on stabilizing the cantilever beam. This loop has the basic problem of the cantilever beam adding dynamics to the system between the torque motor and the position sensor. This causes the stabilization of the cantilever beam to be difficult. To help resolve this additional difficulty, the second control loop can be used. The second control loop utilizes polyvinylidene fluoride film (piezoelectric film) to sense deflections in the beam and add damping to the system. This piezoelectric controller results in the conventional

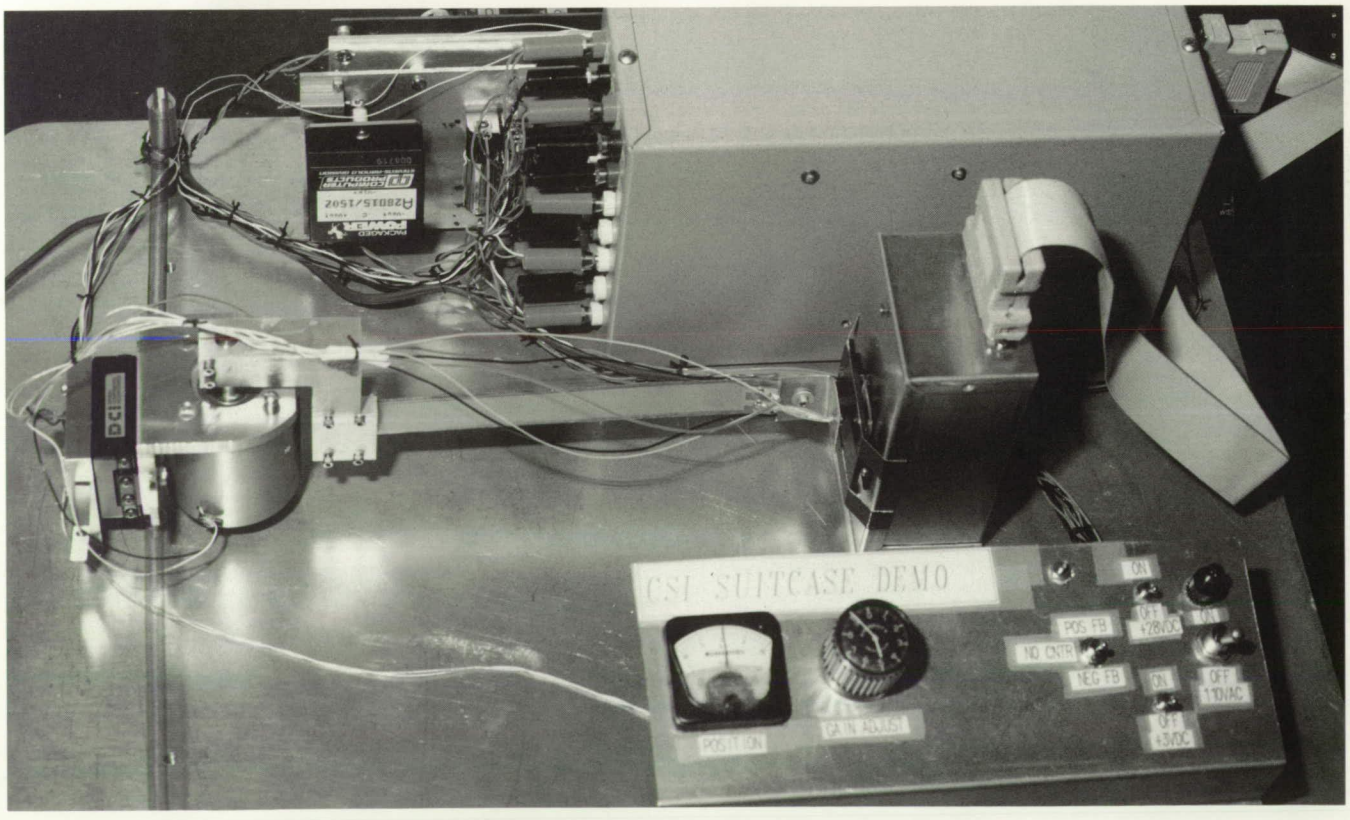

Figure 175. Control Structures Interaction Demonstrator

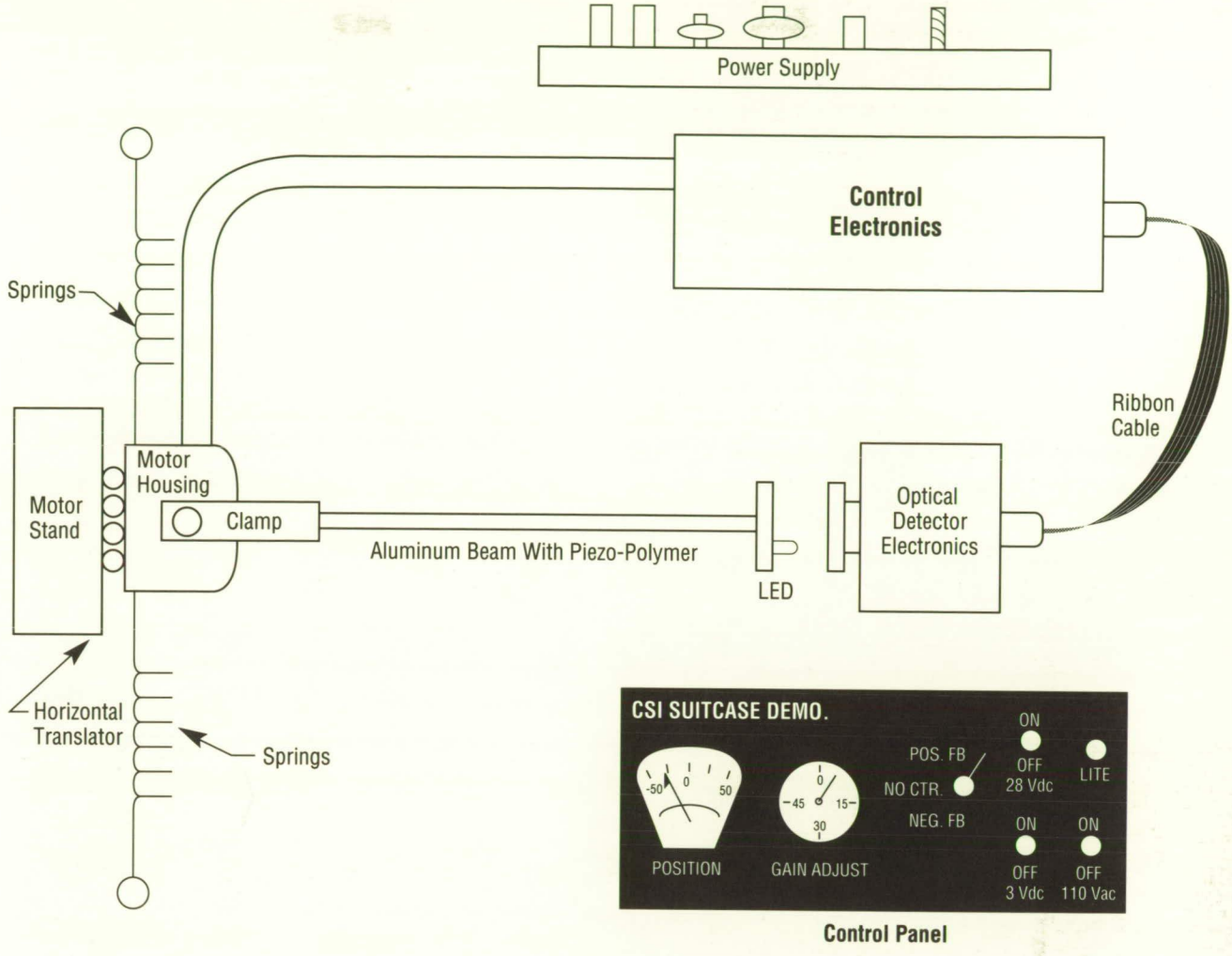

Figure 176. Control Structures Interaction Block Diagram

controller being relatively insensitive to the dynamics of the cantilever beam. The CSI suitcase demonstrator is rich in dynamics and can be very useful in the study of conventional and piezoelectric controllers as applied to CSI.

Further development plans include upgrading the CSI suitcase demonstrator to include an interface to a personal computer. This upgrade will allow more flexibility in studying different type controllers and in analyzing the interaction of these controllers with the flexible structural dynamics of the cantilevered beam (i.e., CSI).

D.E. Howard/EB24
(205) 544-8383
Sponsor: Office of Aeronautics and Space Technology

Avionics

Advanced Launch System Engine Controller

This effort was begun on May 1, 1989, when a contract was awarded to the Aerojet Techsystems Co. of Sacramento, CA, to define, develop, and demonstrate a highly reliable engine controller system with both low recurring cost and low life cycle cost. To validate the approach, a non-flight or brassboard engine controller system (Fig. 177) will be designed, fabricated, and tested. A cost model will also be developed and demonstrated that is applicable to flight hardware and software. The component and system design will be consistent with a low cost philosophy utilizing state-of-the-art hardware and software technology, design, manufacturing, assembly, testability, and maintainability techniques. Reliability will be a quantitized design requirement in the same context as cost and performance. Currently available engine controllers are complex and expensive, therefore a goal of this effort is to develop a simpler controller system with a cost consistent with reducing the cost of placing payloads into orbit by an order of magnitude.

Demonstration software will be written to run in the controller. An engine system model will be developed and software will be written to run the engine model in a Flight Simulation Lab (FSL) host computer. Simulations of sensors and effectors will also be developed. All of these items, along with interconnecting cabling and a power distribution system, will be delivered to the FSL where the system will be configured and demonstrated through a series of tests. The cost model will be used to predict the cost of a flight controller.

J.A. Ball/EB32
(205) 544-2468
Sponsors: Office of Space Flight
Strategic Defense Initiative Organization
U.S. Air Force/Space Division

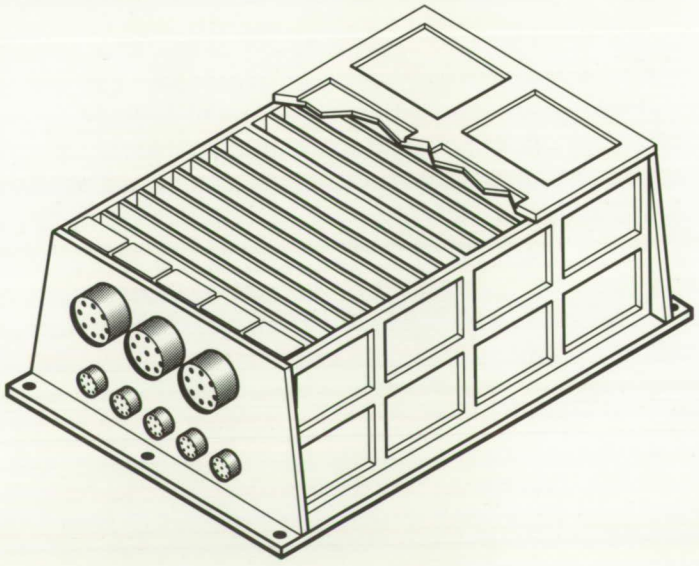

Figure 177. Advanced Launch System Engine Controller Hardware

Spacecraft Power System Automation

Since 1978 with the start of the Autonomously Managed Power System (AMPS) project, NASA/MSFC has been actively working on the problem of spacecraft power system automation. This work has progressed from reference power system studies to operating test beds employing both conventional and expert system computer controls.

The AMPS test facility (Fig. 178) features two power channels feeding into three power busses which in turn provide power to a load simulator. The 2 solar array simulators are rated at 75-kW and 17-kW capacity, respectively, while the 168 cell nickel-cadmium batteries are rated at 189 and 55 Ah. The smaller battery is left over from a Skylab project test bed and is a flight-type battery. The load simulator consists of nine resistive loads and one dynamic load that consume a total of 24 kW of power when operated at 200 Vdc. Finally, four Motorola 68000 microcomputer-based controllers provide data retrieval and low-level decision-making for the power system with an NCR tower-based host computer providing programmability and status display for flight power system simulations.

At present, four projects center on AMPS: STARR (a power system fault detection and recovery expert system), the AMPS Expertise Reinforcing Expert System (AMPERES), a graphical status and control display for AMPS, and a power quality load management study.

STARR is a fault detection/diagnosis/recovery expert system focused on AMPS. Implemented in

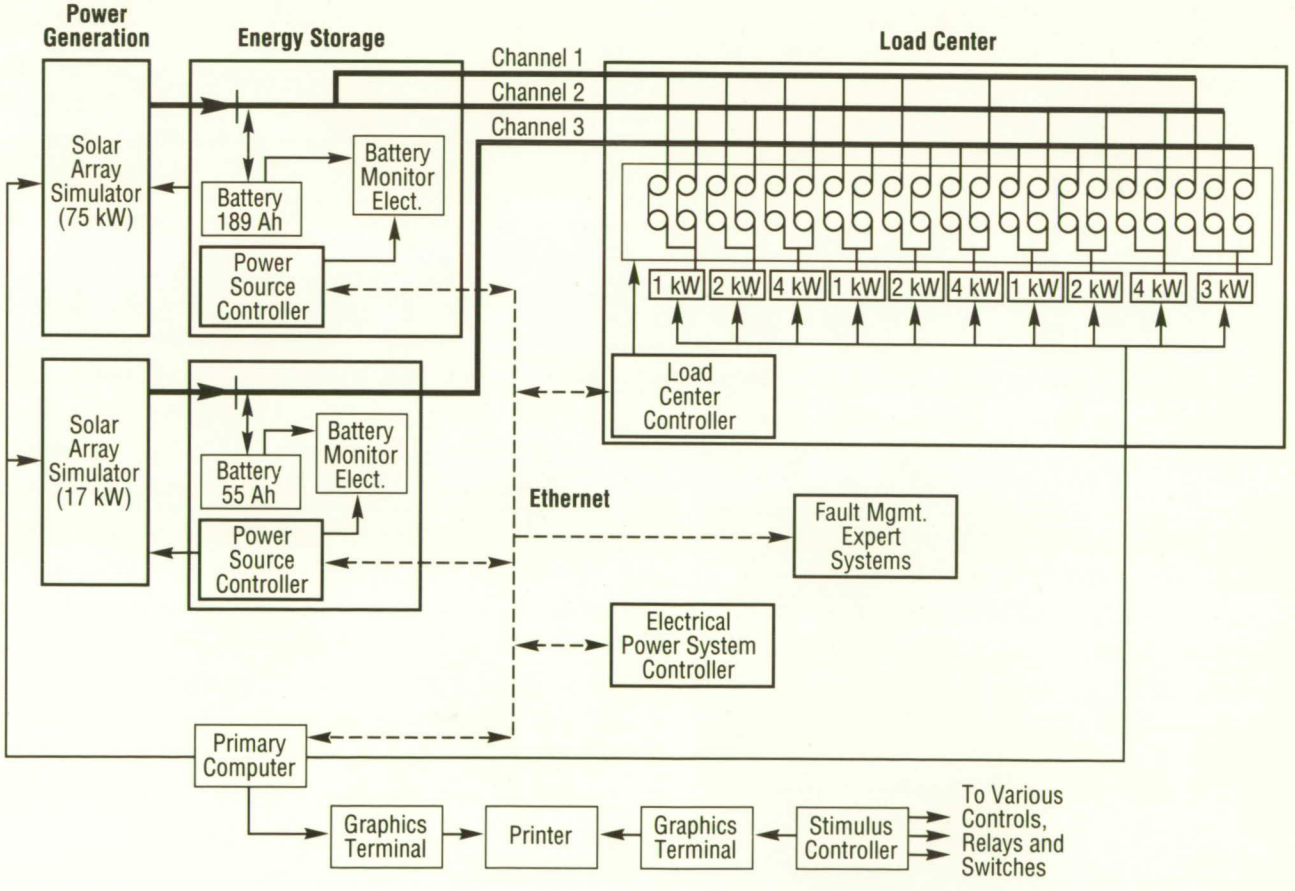

Figure 178. The Autonomously Managed Power System

the knowledge engineering environment on a Xerox 1109 artificial intelligence workstation, STARR models a representative portion of AMPS. The current phase of STARR involves connecting the expert system to AMPS via the Ethernet local area network which links the distributed processors and the host computer system of AMPS.

AMPERES, being developed under a grant to the University of Tennessee Space Institute, is an amplification of the STARR system. Like STARR, AMPERES will be a fault-monitoring and diagnosis-expert system for spacecraft power systems focused on AMPS. However, AMPERES will be a stand-alone expert system including a dedicated processor and additional data retrieval hardware. Thus, after completion, AMPERES will be a fault-monitoring/advisory expert system fully integrated into AMPS.

The University of Alabama in Huntsville is developing an integrated graphics and control program on the host computer for AMPS. This work involves installing additional levels to the AMPS Ethernet, developing the graphics software, and then integrating the software and hardware into AMPS. After completion, AMPS monitoring and control will be accomplished through the host computer using a pull-down menu type graphics display.

Various load management techniques for AMPS are being studied. One of these techniques is to relate particular loads to particular power busses based on power quality. This technique will require developing a "numerical" power quality, determining the power quality of various loads and busses, and then matching the correct loads to the correct buses. Finally, computer algorithms will be developed to load manage the AMPS power system based on these power qualities.

L.F. Lollar/EB12
(205) 544-3306
Sponsor: Office of Aeronautics and Space Technology

Optical Plume Anomaly Detector

During review of minor and major failures of the Space Shuttle Main Engine (SSME) during tests, there were frequent visual events which appeared to be precursors to the incidents. Thus, a program was undertaken to acquire spectral data by way of an optical monitor of the plume. Such data might provide a warning of impending component failure and make it possible to save an engine before a catastrophic incident occurred. The approach was an attempt to monitor certain metallic emission lines and to establish a normal background level for those chosen species. A significant increase above background levels would indicate impending failure.

The spectral region from about 200 nm to about 16 μm was studied with ultraviolet, visible, and infrared radiometers, spectrometers, cameras, and optical multichannel analyzers (OMA's). The radiometers and cameras (Fig. 179) provided continuous coverage; the OMA's provided higher-resolution data during certain sample periods. Instruments available in the laboratory were mounted on a test stand approximately 7.6 m (25 ft) from the plume center line.

The resulting studies showed the need for a high resolution instrument capable of resolving metallic lines above the high background noise. Some molecular species were also seen to be important, for example, CAOH proved to be important as a tracer for pump bearing cage wear. Ni and Cr are indicators of combustion chamber problems. Even with relatively low spectral resolution (as obtained with good filters), the above species can be detected if the problem is sufficiently severe. Detection of these would enable early shutdown decisions. The highest resolution system might permit more critical choices to be evaluated.

The first instrument designed, based on the above, was a 16-channel, grating spectrometer based system, covering the spectral range from 0.25 to 1 μm with a resolution of about 2 Å on some channels.

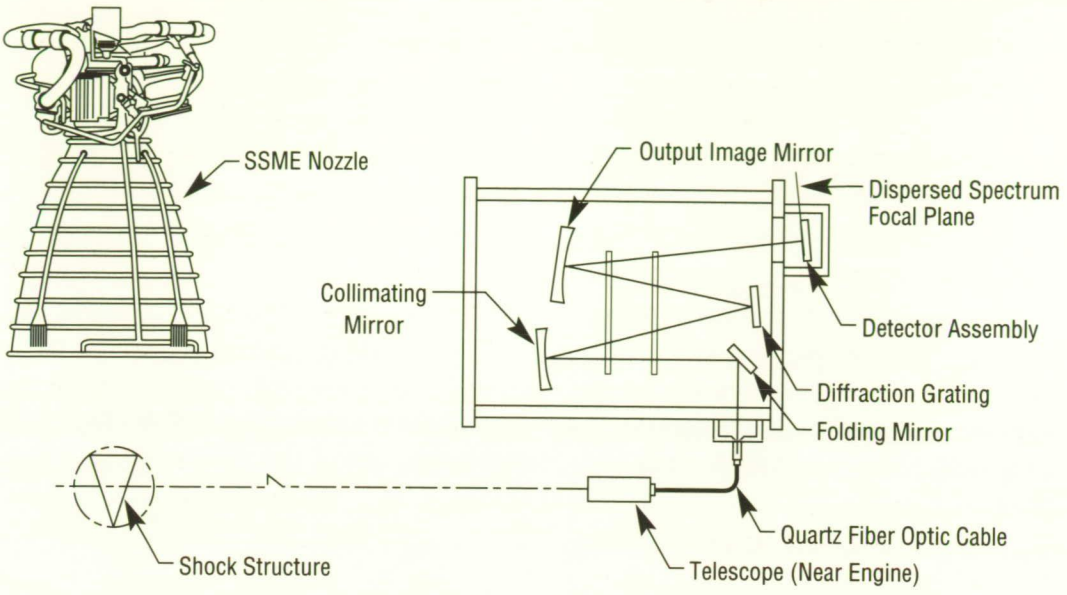

Figure 179. Optical Plume Anomaly Detector Configuration

The bandpass is adjustable on each channel, as is the sensitive wavelength. The silicon photodetectors, unintensified, are closely coupled to preamplifiers, and are cabled to fast auto-ranging electrometer amplifiers, which in turn are fed to a fast *A* to *D* conversion system which is computer interfaced. The computer can manipulate data as required and provide a display. A separate, but allied, computer archives the data on 20-megabyte Bernoulli removable discs. The optical input to the spectrometer is by telescope and quartz multifilament cable; the cable is round at the telescope end and linear at the spectrometer entry slit.

A second instrument, having a similar front optic assembly but having 8,192 self-scanning linear array diodes, functions as a super spectrometer. Data from this unit, scanned at about 15 to 20 times per second, is stored on optical discs for archiving.

These two instruments have been mounted on the SSME Technology Test Bed Engine stand at MSFC and are generating data which is to be correlated with that normally acquired during testing. Methods of using the information will become researched as more tests are serviced.

Powers, W.T. and Sherrell, F.C.: Plume Spectrometry for Liquid Rocket Engine Health Monitoring. Presented at the Symposium on Engine Health Monitoring, Quebec City, Canada, June 3, 1988.

McCoy, R.G., Zaccardi, V.A. and McGregor, W.K.: Sverdrup Technologies/AEDC; and Powers, W.T. and Cikanek, H.A., MSFC: Spectral Analysis of the SSME Plume. Presented at the 1988 Conf. on Adv. Earth-to-Orbit Technology, May 12, 1988.

W.T. Powers/EB22
(205) 544-3452
Sponsor: Office of Aeronautics and Space Technology

Nonintrusive Hot Gas Temperature Sensor

A method of measuring the temperature of hot gas flowing within the Space Shuttle Main Engine (SSME) is desired which does not use an intrusive sensor. A probe disturbs flow, presents mechanical/aerodynamic difficulties, and is slow in response. An instrument yielding the gas temperatures from sensing thermal radiation is being developed (Fig. 180). Detection of narrow-band, filtered radiation emitted from combustion unique molecules presents the best opportunity to accomplish the needed measurement. This program provides an optimized detector and electronics, a window assembly fitting a standard SSME instrumentation port, and the interface required to mate the device with the SSME. Several locations on the turbopumps and hot gas manifolds are being considered.

The system has a pressure-sealing window (Fig. 181) capable of withstanding temperature and heat-flux extremes and could possibly use coupled fiber optic cable to a remote mounted detector-electronic assembly, which could be mounted in an engine controller.

A system has been breadboarded and tested in the laboratory using a methane fueled flame (methane is easier to use in a lab than is H_2). A thermal profile of the flame was taken using an infrared camera and thermocouples. When properly thermally compensated, the system performed satisfactorily.

The window selected is of diamond, because of its strength and high thermal conductivity. Mounted at the end of a tube having the fiber optic rod/cable mounted in it, the assembly fits into the same ports on an SSME as does the existing resistance temperature sensors; a direct replacement is intended.

The completed system will permit fast temperature measurement (1 kHz or better) and high accuracy so that dynamic reactions may be monitored and closed-loop control may be effectively enhanced.

W.T. Powers/EB22
(205) 544-3452
Sponsor: Office of Aeronautics and Space Technology

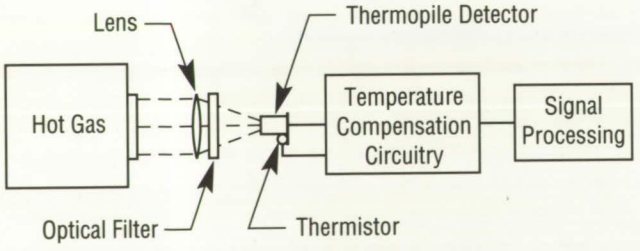

Figure 180. Basic Sensor Layout

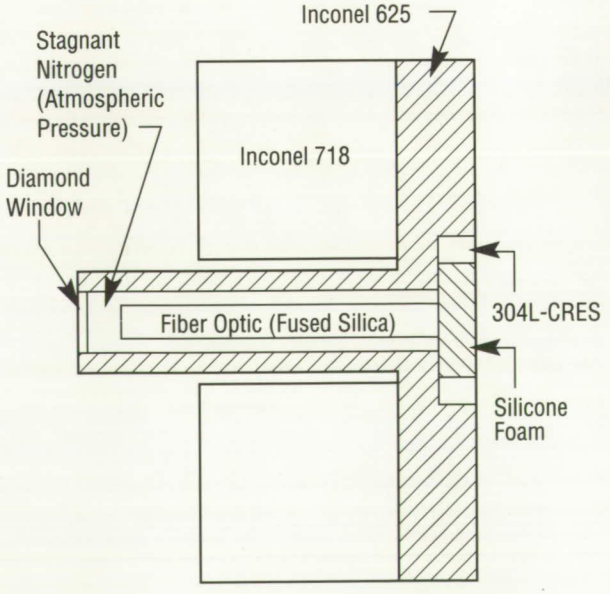

Figure 181. Conceptual Window Design

Intelligent Data Reduction Expert System

The Intelligent Data Reduction Expert System (I-DARE) is an expert system project. In most spacecraft subsystems, only a small fraction of the telemetry data are significant. The ideal situation would be to reduce the telemetry data to its significant components on-board so that enhanced fault management, incipient failure detection, and other trends analyses can be executed in real-time. Currently, data reduction is a labor-intensive operation.

The objective of the I-DARE project is to autonomously capture and intelligently reduce telemetry data from a spacecraft subsystem. The approach is to develop an artificial intelligence knowledge-based system that is able to emulate the specific reasoning that subsystem test bed personnel employ in reducing such data to its significant components.

The immediate application of I-DARE is the Hubble Space Telescope (HST) Nickel-Cadmium Battery Test Bed located at MSFC. The principal components of this test bed are six 23-cell flight-type nickel-cadmium batteries, along with associated protection and reconditioning electronics, and the solar array simulators for emulation of photovoltaic power generation in low-Earth orbit (LEO) conditions. Test bed engineers spend great amounts of time pouring over the telemetry data to determine system responses to various conditions and to determine developing trends. In order to accomplish these tasks, the data must first be reduced to its significant components, as up to 98 percent of the data are insignificant at any given time.

The telemetry data are also transmitted by way of the data bus at 9,600 bps to the I-DARE workstation located in a nearby building. There, a module of the I-DARE knowledge-based system, known as the data handler, continuously receives and files the raw data for up to 100 LEO orbits. The data handler also performs transmission error detection and correction to ensure the system is working with good data.

The expert function of I-DARE then reduces the data in order to allow near real time data trend analyses. Several timeframes within each orbit, such as battery end-of-discharge, battery end-of-charge, etc., are utilized to review and reduce the data. The knowledge engineer has interviewed the three principal test bed engineers and the manager to determine the heuristics, facts, and other guidelines employed in reducing this data. The current prototype knowledge-based system is a rule-based approach which begins to approximate the behavior and efficiency of test bed engineers in reducing this telemetry data. Recently, the system has been modified to allow context sensitivity so that the end-user is able to dynamically change the model of the data source to better meet his needs.

I-DARE currently resides on a Symbolics Lisp machine and is written in the Lisp computer language. It is hoped that the approaches and methodologies employed for intelligent reduction of the HST power system test bed telemetry data can be utilized for intelligent data reduction of other subsystem telemetry such as propulsion, thermal, environmental crew life support systems, etc., by changing only the man-machine interface and the knowledge base to support each particular subsystem.

The University of Alabama in Huntsville has supported this research effort under NASA grant NAG8-642. This grant is now nearing completion of the 2.5-year continuing award, originally jointly funded by the HST program and the MSFC Center Director's Discretionary Fund.

Ford, D.R. and Weeks, D.J.: Intelligent Data Reduction: a Preliminary Investigation. Proceedings, 23rd IECEC, Vol. 3, pp. 383–388, 1988.

Brady, M., Moody, G.E. and Scharnhorst, D.A.: A Symbolic Programming Approach to Intelligent Data Reduction. Proceedings, 24th IECEC, in press, 1989.

B.K. Walls/EB12
(205) 544-3311
Sponsor: Center Director's Discretionary Fund

Nickel-Cadmium Battery Expert System

During the testing of nickel cadmium batteries for the Hubble Space Telescope (HST), an urgent need for data management was observed. Testing of these batteries generates much needed data that is used for vital decision making, such as when to recondition, change the charging scheme, or adjust the workload of the batteries. In researching a solution to this problem, possible use of an expert system seemed viable. This expert system would be able to recognize a test bed anomaly, identify the malfunctioning component, recommend a course of action, evaluate battery status, and provide decision support.

The Nickel-Cadmium Battery Expert System (NICBES) was the product of this research. The HST Electrical Power System (EPS) Nickel Cadmium Six Battery test bed utilizes NICBES to predict certain anomalies by relaying battery status and trend information to the user. NICBES major functions are fault diagnosis, status and advice, and decision support graphics. Input to NICBES from the HST EPS test bed comes across a serial RS232 cable from the digital data acquisition system computer every minute. NICBES consists of two independent programs, the data handler (written in C) and the expert system (written in Arity Prolog 4). The data handler receives raw data from the HST EPS test bed, reduces the data, puts the data in the corresponding files, and sends the data to the expert system. The expert system takes this data and evaluates it for fault diagnosis, to predict anomalies or battery "health," give advice on battery maintenance, and aid in decision support. The NICBES functional block diagram is shown in Figure 182.

NICBES has been monitoring the HST EPS test bed since November 1986. An addition of a simple interactive rule editor (SIRE) has been made since that time. The need for user-friendly rule editing and display prompted this research. SIRE allows a user who has no knowledge of any programming language to modify the existing rule base of NICBES. NICBES and SIRE reside together on an IBM PC/AT.

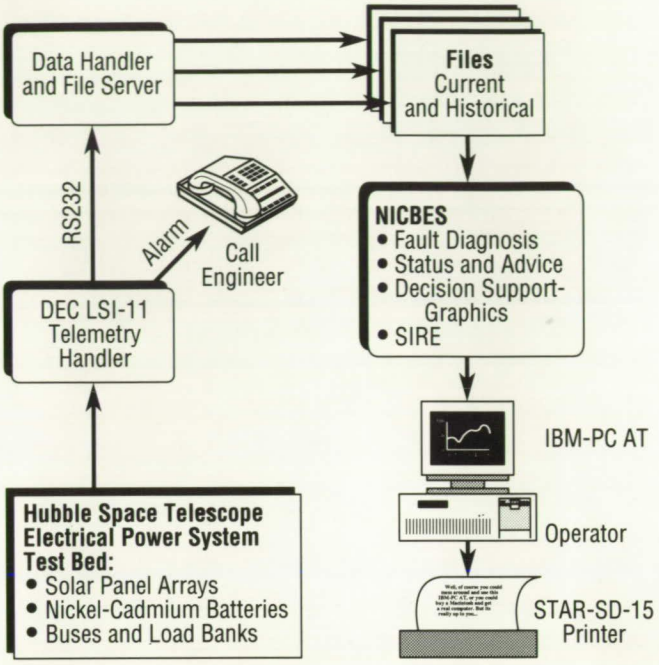

Figure 182. Nickel-Cadmium Battery Expert System Functional Diagram

A grant was awarded to the University of Tennessee at Chattanooga to upgrade the equipment for the expansion of NICBES. This upgrade will enable NICBES to operate in a multitasking mode, as well as provide the capability to store more orbits for more accurate trend analysis. Other enhancements include better graphics resolution and faster computation capability. It has been proposed that more equipment be obtained to implement these enhancements. The operating system selected, Unix, supports both a large memory model and multitasking with priority scheduling. Unix supports up to 4 gigabytes of virtual memory, has interrupt-driven device input/output, and a number of paradigms for interprocess communication. The Sun 386i/150x computer with a 4-megabyte random access memory expansion, 60-megabyte tape, development toolkit, and Quintus Prolog would be suitable to run the operating system and complete all of the other enhancement requirements.

Y.B. Johnson/EB12
(205) 544-3310
Sponsor: Office of Space Flight

Index of Contacts

☆ U.S. GOVERNMENT PRINTING OFFICE: 1990—732-549

NASA
National Aeronautics and
Space Administration

George C. Marshall Space Flight Center
Marshall Space Flight Center, Alabama 35812

MSFC Cover 42 (Rev. Dec 1989)